

Hawa Diallo

Gunnels Wood Road

Stevenage

Hertfordshire

SG1 2NY

United Kingdom

**Synthesis and optimisation of novel molecules to
probe epigenetic mechanisms with applications in
the treatment of inflammatory disorders**



8th of October 2014

GSK supervisor: Mr Jon Seal / Mr Robert Sheppard

Academic supervisor: Prof. Jonathan Percy

Abstract

Jumonji (Jmj) histone demethylases are Fe(II) and α -oxoglutarate dependent oxygenases that constitute essential components of regulatory transcriptional chromatin complexes. These enzymes demethylate lysine residues found in histones, in a methylation-state and sequence-specific context. This report is the first account of a structure-guided small molecule and chemoproteomics approach to elucidate the functional role of JmjD3. In an effort to discover suitable chemotypes for further optimisation against JmjD3, a focused screen and high throughput screen were performed. These screens identified a number of hits, of which the initial investigations of three are discussed in this report. The demonstration of SAR for the pyridyl-pyrimidine series, and confirmation of binding in the JmjD3 active site by X-ray crystallography, led to this template being selected for further optimisation by improving the interaction with a key residue in the active site. The optimisation of this series enabled the identification of the first small molecule inhibitor selective for JmjD3. This small molecule inhibitor was shown to successfully engage the endogenous JmjD3 using a chemoproteomics approach and reduce lipopolysaccharide-induced pro-inflammatory cytokine production in human primary macrophages. This report provides encouragement for designing small molecule inhibitors to enable selective pharmacological intervention across the Jmj family.

Acknowledgements

First of all, I would like to thank Patrick Vallance and Dave Allen for supporting the PhD programme.

Moreover I would like to thank Dr. Harry Kelly, Dr. David Wilson, Dr. Kevin Lee, Dr. Jason Witherington, Dr. Nigel Parr and Dr. Rab Prinjha for this great opportunity and the support from start to finish.

I am deeply indebted to my supervisors Professor Jonathan Percy, Jon Seal and Robert Sheppard for their guidance, support, the numerous corrections and patience during the writing of this thesis.

I would like to express my appreciation and thanks to Dr. Chun-Wa Chung, Dr. Paul Bamborough and Dr. Pamela Thomas for the Jmj crystallography data, the dockings and the help provided for the use of the different softwares.

Moreover, I would like to thank the other members of Jmj programmes: Dr. John Liddle, Mike Barker, Matt Campbell, Clement Douault, Tom Hayhow, Dr. Phil Humphreys, Tracy Shipley Emily Kiss, Katharina Reeh, Mike Perryman, Michaela Daubney, for the chemistry. People who run the assays: Laurie Gordon, Melanie Leveridge, Carl Haslam, Yugesh Sinah, Fiona Brown, Kate Simpson, Matthew Lochansky and John Martin. The biologists: Dr. Laurens Kruidenier, Dr. Pal Mander, Dr. Julia Smith, Catriona Sharp, Valerie Ludbrook, Cesar Ramirez-Molina and Richard Gregory.

I would like to thank colleagues at SGC especially Oleg Federov.

Furthermore, I am grateful to Dr. Richard Upton, Sean Lynn, Steve Richards (NMR specialists), and Bill Leavens for their help on my project.

I am very grateful to Dr. Jack Brown for our weekly chemistry tutorials.

I would like to say a big thank you to Robert Sheppard, Jon Seal, Dr. Jack Brown, Dr. Phil Humphreys, Dr. Steve Atkinson and Dr. Emmanuel Demont for reading my report and giving me a hard time during the mock viva.

I would like to say a special thank you to Dr. Laurens Kruidenier for the time spent explaining the biology around Jmj and epigenetics.

I would like to thank my friends Nadia, Sylviane, Marie-Elodie and Dr. Dominique Amans for their support.

And finally, I would like to thank a million times my parents, Binta and Bakary, brothers, Moussa and Abdoullaye, sister, Ténémedié, my cousin Fatoumata and my partner, M'Part for their support, understanding and patience.

This thesis is the result of the author's original research, except stated otherwise. It has been composed by the author and has not been previously submitted for examination which has led to the award of a degree.

The copyright of this thesis belongs to the author under the terms of the United Kingdom Copyright Acts as qualified by University of Strathclyde Regulation 3.50. Due acknowledgement must always be made of the use of any material contained in, or derived from, this thesis.

Signed:

Date:

Table of Contents

Abbreviations	3
I Introduction	9
I.1 Epigenetics.....	10
I.1.1 DNA	10
I.1.2 Chromatin	11
I.1.3 Histone modifications.....	12
I.1.4 JmjD3	24
I.1.5 Project aims	31
I.2 Assays	41
I.2.1 TR-FRET	41
I.2.2 MALDI/RapidFire	43
I.2.3 Cellular assay.....	44
I.2.4 Target Product Profile (TPP).....	44
I.3 HTS and focused screen hits	46
I.3.1 HTS and focused screen triage	46
I.3.2 Hits	51
I.4 C-C coupling reactions	56
I.4.1 Organozinc reagents in context	56
I.4.2 Preparation of organozinc reagents	58
I.4.3 Mechanism of the Negishi reaction.....	68
I.4.4 Scope of the Negishi coupling reaction.....	84
II Synthetic Chemistry, Results and Discussion.....	90
II.1 <i>Bis</i> -Aminoaryl series	90
II.1.1. Synthetic chemistry	91
II.1.2. Assay results and discussion	98
II.2. Pyridone series	108
II.2.1. Initial SAR	109

II.2.2. Synthetic chemistry	111
II.2.3. Assay results and discussion	117
II.3. Pyridyl-pyrimidine series	125
II.3.1. Synthetic chemistry	126
II.3.2. Assay results and discussion	183
III Experimental.....	269
IV Appendices	399
Appendix 1	400
Appendix 2	401
Appendix 3	412
Appendix 4.....	413
Appendix 5	414
Appendix 6	416
Appendix 7.....	419
Appendix 8.....	420
Appendix 9.....	422
Appendix 10.....	424
Appendix 11	427
Appendix 12.....	435
Appendix 13.....	441
References	446

Abbreviations

AcOH	Acetic acid
AIM	Atoms-in-Molecules
AOL	Amine oxidase-like
BINAP	2'-Bis(diphenylphosphino)-1,1'-binaphthyl
Boc	<i>tert</i> -Butyloxycarbonyl
BSA	bovine serum albumin
Cbz	Carbobenzyloxy
CCDC	Cambridge Crystallographic Data Centre
CHAPS	3-[(3-Cholamidopropyl)dimethylammonio]-1-propanesulfonate
CSC	Computational and structural chemistry
CSD	Cambridge Structural Database
CV	Column Volume
DavePhos	2-Dicyclohexylphosphino-2'-(<i>N,N</i> -dimethylamino)biphenyl
Dbp	Dibenzylideneacetone
DCM	Dichloromethane
DEAD	Diethyl azodicarboxylate
DIAD	Di- <i>iso</i> -propyl azodicarboxylate
DIPEA	<i>N,N</i> -Di- <i>iso</i> -propylethylamine
DMA	<i>N,N</i> -Dimethylacetamide
DMAP	4-Dimethylaminopyridine

CONFIDENTIAL – DO NOT COPY

DMF	<i>N,N</i> -Dimethylformamide
DMPU	1,3-Dimethyltetrahydropyrimidin-2(1 <i>H</i>)-one
DMSO	Dimethylsulfoxide
DMSO-d ₆	Deuterated dimethylsulfoxide
DNA	Deoxyribonucleic acid
DoM	Directed <i>ortho</i> -metallation
Dppf	Diphenylphosphinoferrrocene
ED ₃₀	Effective dose in mg/kg that lowers the blood pressure 30 mmHg
EGLN	Egg Laying-9
FAD	Flavin adenine nucleotide
FBS	Foetal bovine serum
FC	Fold cutoff
HDAC	Histone deacetylase
Hepes	4-(2-hydroxyethyl)-1-piperazineethanesulfonic acid
2-HG	2-Hydroxyglutarate
HL-60	Human promyelocitic leukaemia cells
HMBC	Heteronuclear multiple bond correlation
HPLC	High performance liquid chromatography
8-HQ	8-Hydroxyquinoline
HTS	High throughput screening
I	Isomerisation
γIFN	Interferon γ
IPent	Di- <i>iso</i> -pentylphenylimidazolium

<i>i</i> Pr	<i>iso</i> -Propyl
IPr	Di- <i>iso</i> -propylphenylimidazolium
Jmj	Jumonji
KDM	Lysine demethylase
KMT	Lysine methyltransferase
LAH	Lithium aluminium hydride
LC/MS	Liquid chromatography mass spectrometry
LE	Ligand efficiency
LLE	Lipophilic ligand efficiency
LiHMDS	Lithium hexamethyldisilazide
LPS	Lipopolysaccharide
LSD1	Lysine specific demethylase 1
Lys	Lysine
MDAP	Mass directed auto-preparative
MI	Migratory insertion
mRNA	Messenger ribonucleic acid
MW	Molecular weight
NHC	<i>N</i> -Heterocyclic carbene
NMP	<i>N</i> -Methyl-2-pyrrolidinone
NMR	Nuclear magnetic resonance
NOG	<i>N</i> -Oxalylglycine
OA	Oxidative addition
2-OG	2-Oxoglutarate

CONFIDENTIAL – DO NOT COPY

P	Pressure
PBMC	Peripheral blood mononuclear cell
PCR	Polymerase chain reaction
PDCA	2,4-Pyridinecarboxylic acid
PDE4D	Phosphodiesterase 4D
PEPPSI	Pyridine-enhanced precatalyst preparation, stabilization and initiation
PHD	Plant homeobox domain
PMA	Phorbol 12-myristate 13-acetate
PVDF	Polyvinylidene difluoride
RE	Reductive elimination
ROESY	Rotating-frame Overhauser effect spectroscopy
RNA	Ribonucleic acid
rt	Room Temperature
RuPhos	2-Dicyclohexylphosphino-2',6'-di- <i>iso</i> -propoxy-1,1'-biphenyl
SAH	<i>S</i> -Adenosyl-L-homocysteine
SAM	<i>S</i> -Adenosyl-L-methionine
SAR	Structure activity relationship
SBDD	Structure based drug design
SCX	Strong cation exchange
s.e.m.	Standard error of the mean
SET	Su(var)3-9 (suppressor of variegation 3-9), E (z) (enhancer of zeste) and tritorax
SGC	Structural Genomics Consortium

CONFIDENTIAL – DO NOT COPY

SM	Starting material
S _N 2	Bimolecular nucleophilic substitution
S _N Ar	Nucleophilic aromatic substitution
SPE	Solid phase extraction
shRNA	Short hairpin ribonucleic acid
S-Phos	2-Dicyclohexylphosphino-2',6'-dimethoxybiphenyl
SWIRM	Swi3p/Rsc8p/Moira
T	Temperature
TBDMSCl	<i>tert</i> -Butylchlorodimethylsilane
TBP	Tatabox binding protein
TCEP	<i>Tris</i> (2-carboxyethyl)phosphine
TEP	Tolman electronic parameter
TFA	Trifluoroacetic acid
THF	Tetrahydrofuran
THP	Tetrahydropyran
TLC	Thin layer chromatography
TM	Transmetallation
TMEDA	Tetramethylethylenediamine
TMP	2,2,6,6-Tetramethylpiperamidyl
TMS	Tetramethylsilane
TMSCl	Trimethylchlorosilane
TPP	Target product profile
TPR	Tetratricopeptide repeat

CONFIDENTIAL – DO NOT COPY

UPLC	Ultra-high performance liquid chromatography
UT	Untreated
UTX	Ubiquitously transcribed tetratricopeptide repeat X
UTY	Ubiquitously transcribed tetratricopeptide repeat Y
UV	Ultra Violet
X-Phos	2-Dicyclohexylphosphino-2',4',6'- <i>tri-iso</i> -propylbiphenyl
WT	Wild-type

I Introduction

Many of the signal transduction processes and transcription factors that regulate inflammatory responses have been well characterised, and a number are being actively explored as potential therapeutic drug targets. However, in recent years epigenetic tags or marks have been revealed as an additional level at which these processes are controlled. These marks take the form of reversible modifications (such as acetylation, phosphorylation and methylation) to the histone tails of nucleosomes in the region of gene promoters and coding regions, and can be either permissive or restrictive to efficient transcription.¹ Families of proteins have now been described which can write (*e.g.* histone acetyl transferases, lysine methyl transferases), read (*e.g.* Bromodomains, Tudor domains, Plant Homeobox Domains) and erase (*e.g.* histone deacetylases (HDACs), lysine demethylases) these marks.

The aim of this project is to design and synthesise potent and selective small molecules as probes to investigate the role of one histone modifying enzyme in modulating inflammatory processes.

I.1 Epigenetics

Deoxyribonucleic acid (DNA) is the hereditary material in humans and nearly all other organisms. In each individual, the same DNA sequence is located in the nucleus of all the hundreds of different cell types in the human body. Despite this identical genetic backbone, each cell type expresses a different set of genes and can adapt this transcriptome to its specific circumstances. Epigenetics refers to the heritable changes in how the genome is accessed in different cell types and during development and differentiation. Epigenetic processes do not change the DNA sequence but they allow the genes to be expressed differently due to various environmental factors.

I.1.1 DNA

Accommodating a DNA strand, which is about 1.6 m long, into the nucleus (20 μm) of each cell requires sophisticated ‘packaging’ machinery (Figure 1).

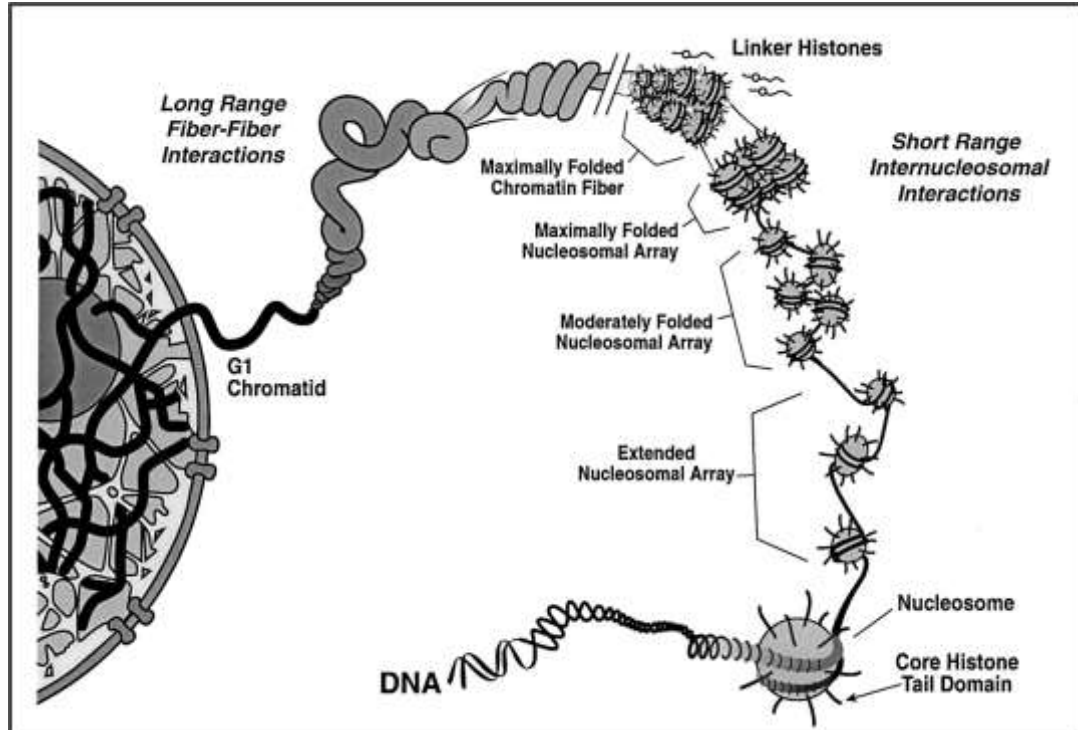


Figure 1. From DNA to chromatin.¹

Key components of this machinery are core histones, nucleosomes and chromatin. First, DNA is wrapped around a histone octamer (Figure 2) to create a nucleosome. In turn, the nucleosomes condense further to form chromatin.²

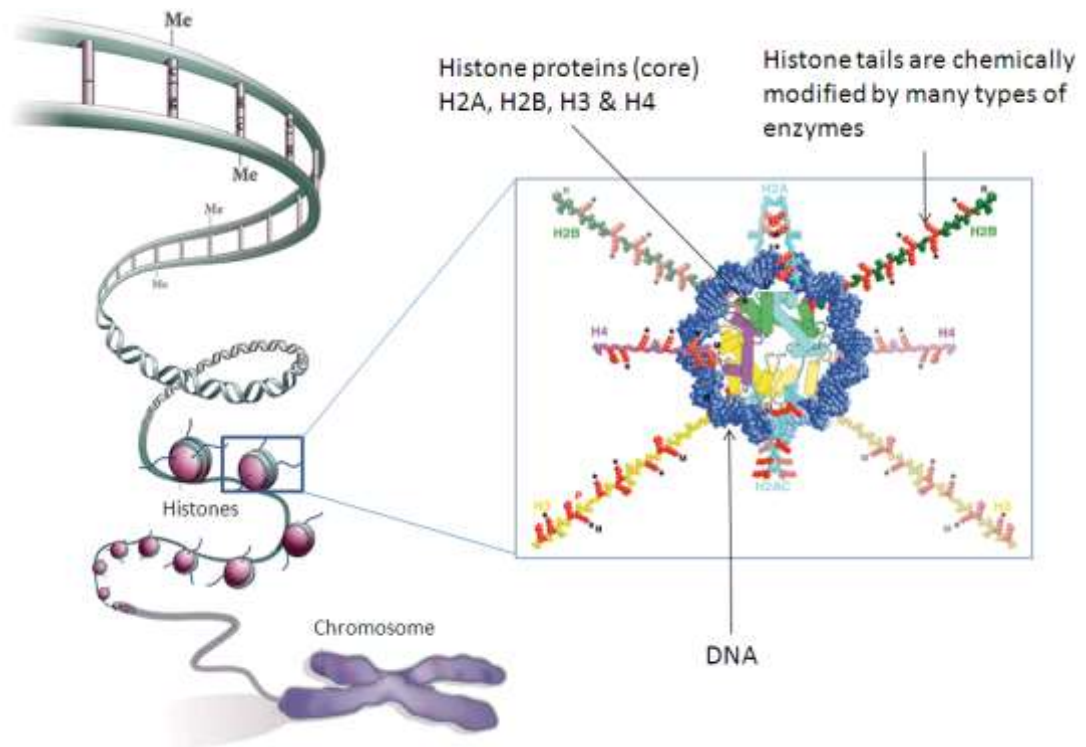


Figure 2. Nucleosome.³

I.1.2 Chromatin

Chromatin can exist in two states (Figure 3) called heterochromatin and euchromatin. Heterochromatin is a “closed, repressed” form, in which DNA is not accessible for transcription of genes. Euchromatin is an “opened, permissive” form, which allows RNA polymerase and transcription factors to access DNA sequences and facilitates the subsequent transcription and expression of genes.² The control of this dynamic conformation of chromatin, which has a major impact on gene transcription, is subject to a complex and

precise mechanism of regulation, the basic principles of which are only now beginning to be understood.

The state of the chromatin (euchromatin vs heterochromatin) is governed by the presence or absence of covalent modifications on the DNA or the core histones which make up the nucleosomes. By controlling the state of the chromatin, these epigenetic modifications control the expression of genes. Covalent modifications of DNA take the form of methylation of the cytosine and/or adenine bases. This will not be discussed further here but more can be found in the review by Kron *et al.*⁴ However, histone modification is more complex.

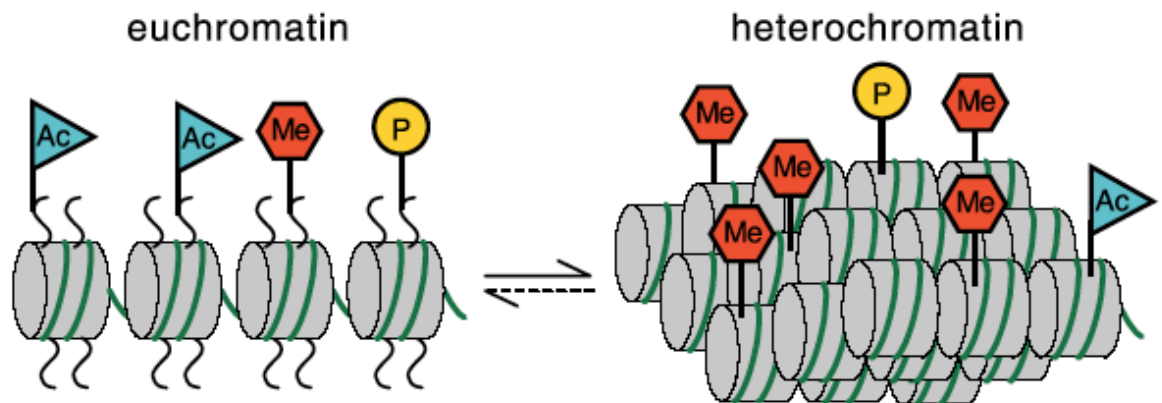


Figure 3. Chromatin and histone modifications. On the left, highly acetylated euchromatin, which can start DNA transcription; on the right heterochromatin with a high degree of methylation which is closed to transcription.⁵

I.1.3 Histone modifications

There are five main histone proteins. These are H1, H2A, H2B, H3 and H4, each of them participating in the packaging of the DNA. These histones are divided into two groups: these are the core histones (H2A, H2B, H3 and H4) which form the histone octamer (Figure 2), and the linker histone (H1) which mainly binds DNA to the nucleosome. The core histones

have similar structures based on a globular domain with *N* and *C*-terminal tails.² The *N*-terminal tails of these histones are mainly unstructured and protrude from nucleosomes and are the main sites at which histone modifications occur (Figure 2). There are four main alterations: acetylation, ubiquitylation and phosphorylation (which will not be discussed further here), and methylation, which will be the main subject of this report. The combination of these covalent markers on the *N*-terminal tails of histones is known as the “histone code”. This histone code controls the state of the chromatin and, therefore, gene transcription (Table 1). In order to function correctly, a cell requires the ability to alter which genes it expresses at which time. This necessitates that the state of the chromatin, and the covalent marks on the histones which control it, be dynamic. To achieve this, there are proteins responsible for writing, reading and removing these covalent marks.

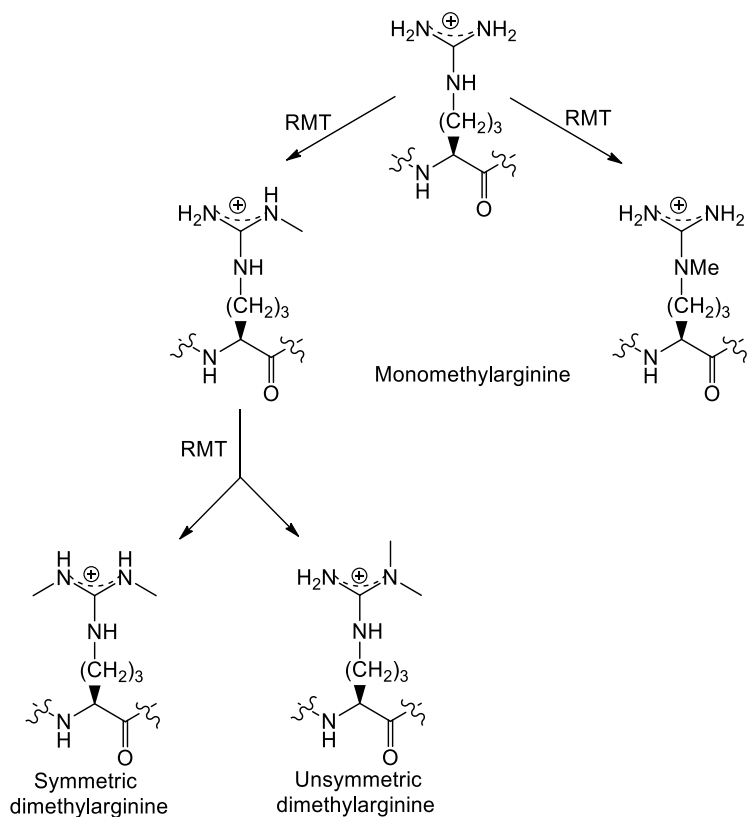
Modification	Histone	Residues	Effects on transcription
Acetylation	H2A	K5	Activation
	H2B	K5, K12, K15, K20	Activation
	H3	K4, K14, K18, K23, K27	Activation
	H4	K8, K16	Activation
Methylation	H3	K4, K79	Euchromatin
		K9, K27	Silencing
		R17	Activation
	H4	R3	Activation
		K20	Silencing
Phosphorylation	H2a	S1, T119	Mitosis
	H2AX	S139	DNA repair
	H3	T3, S10, T11, S28	Mitosis
	H4	S1	Mitosis
Ubiquitylation	H2A	K119	Silencing
	H2B	K120	Activation

Table 1. Histone modifications. K: lysine, R: arginine, S: serine, T: threonine.

I.1.3.1 Histone methylation

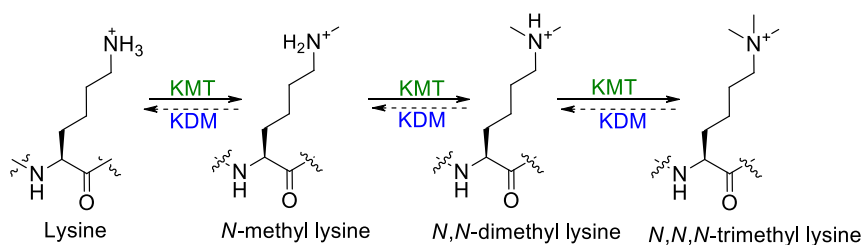
Histones can be methylated on the side chains of arginine and lysine residues by specific enzymes. These are arginine methyl transferases (RMTs) and lysine methyl transferases (KMTs), respectively. Arginine can be mono-methylated in one of two ways: either at the terminal guanidino nitrogen, or the internal guanidino nitrogen. It can also be di-methylated in two ways leading to unsymmetrical dimethylarginine or symmetric dimethylarginine

(Scheme 1). Arginine methylation will not be discussed further in this report but more information can be found in the reviews by Bedford.^{6,7}



Scheme 1. Possible arginine methylation.

Lysine, on the other hand, can be unsubstituted or mono-, di-, or trimethylated. The degree of methylation depends on different factors such as the number and the location of acetylated histones.² There are several families of lysine methyl transferases which catalyse these methylations (Scheme 2).



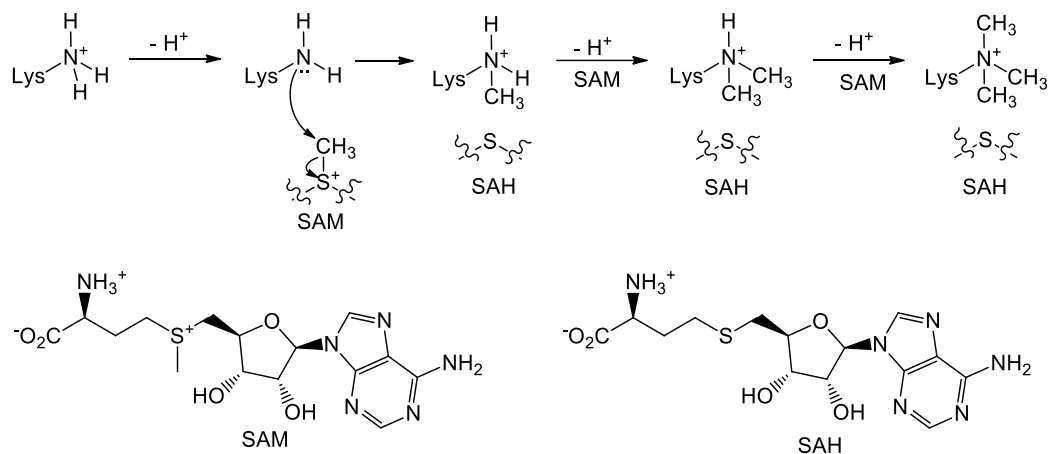
Scheme 2. Degree of lysine methylation.

A comprehensive discussion of these modes of methylation lies outside the scope of this dissertation, but more information can be found in the reviews by Wooster and Heightman.^{8,9} Some KMTs are specific for particular lysines, as can be seen with the examples in Table 2.

Lysine residue modified	Lysine Methyltransferases
H3K4	MLL1, 2, 3, 4 and 5 SET1A and 1B SET7/9 ASH1 SMYD3
H3K9	SUV39H1 and H2 SETDB1/ESET EHMT1/GLP EHMT2/G9a CLL8 RIZ1/PRDM2
H3K27	EZH2
H3K36	NSD1 SMYD2 SET2
H3K79	DOT1L
H4K20	SUV4-20H1 and 20H2 SET8/PreSET7

Table 2. Lysine methyl transferases and the residues modified.

Both the RMTs and KMTs utilise the same cofactor, *S*-adenosyl-L-methionine (SAM), which acts as the methyl group donor (Scheme 3). The methylation of lysine starts with the deprotonation of Lys-NH₃⁺ to form the neutral lysine which is then methylated by SAM to give Lys-N(Me)NH₂⁺ and SAH (*S*-adenosyl-L-homocysteine). The deprotonation and methylation steps are repeated to form di- and trimethyl lysine, respectively.¹⁰



Scheme 3. Mechanism of KMT.

I.1.3.2 Methylated histone reading

The various methylated states of histone lysine residues are read by specific proteins, such as members of the Royal superfamily, Chromodomains, Tudor domains and PHD (Plant Homeobox Domain) fingers. For a common mark (mono-, di-, or trimethylated lysine) the recognition domains of these reader proteins are similar in terms of binding surfaces. The recognition domains contain between two and four aromatic rings and often one or more acidic residues are also present.^{11,12} These aromatic rings, often referred to as the “aromatic cages”, engage the mono-, di-, or trimethylated ammonium group of the lysine in π -cation interactions.¹¹ Hughes *et al.* showed that the electrostatic component of the π -cation interaction plays an important role and that the polarized methyl groups interact with the aromatic rings (Figure 4).¹³

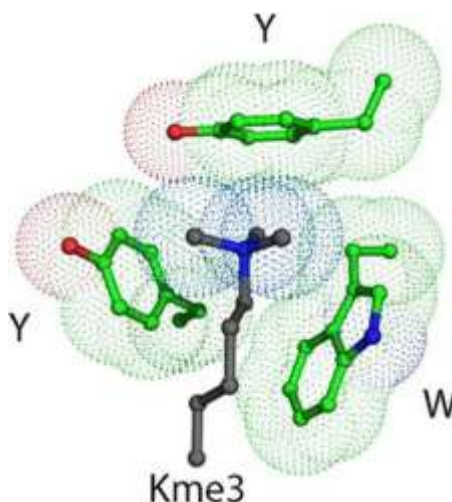


Figure 4. Trimethylated lysine H3K9 in an aromatic cage in HP1 Chromodomain (PDB: 1KNE). The aromatic cage is made of two tyrosines (Y) and one tryptophan (W) (green); trimethyl lysine is shown in grey.¹³

These reader proteins will not be covered in this report but more information can be found in some reviews.^{11,12}

I.1.3.3 Histone demethylation

In Section I.1.3.1, the process of histone methylation was discussed. However, a cell also requires the ability to demethylate histone residues, so that it can control gene expression efficiently by reversing any change in expression brought about by histone methylation. To fulfil this role there are enzymes responsible for the removal of histone methyl groups. Again, there are two superfamilies of enzymes involved in this process: these are the arginine demethylases and lysine demethylases, which demethylate arginine and lysine residues, respectively. Lysine specific demethylase 1 (LSD1) was the first histone lysine demethylase discovered in 2004.^{14,15} Later, in 2006, the Jumonji (Jmj) family proteins were also reported to demethylate lysine residues.³ These demethylases have different substrate specificities, which can be explained by their different mechanisms of action: LSD1 is an

amine oxidase flavoenzyme and the Jmj family is part of the iron(II)-dependent 2-oxoglutarate (2-OG) utilising family of oxygenases.

LSD1 demethylates mono- and dimethylated lysines. It has three main domains: a C-terminal amine oxidase-like (AOL) domain, a second central domain referred to as a “tower domain”, and an N-terminal domain (Figure 5). The LSD1 “tower domain” is not a real tower domain because a genuine tower domain includes two long helices and a three-helical domain situated at the end of the two helix stalk.¹⁶ The apparent “tower domain” described by the authors, Stavropoulos *et al.*, who first reported the LSD1 structure in July 2006, has the two extended helices but lacks the three-helical domain.¹⁷ The same authors described the two helices as packed against each other, with no coiling, but two months later, Chen *et al.*,¹⁸ described the LSD1 tower domain as two helices packed against each other in a typical antiparallel coiled coil, characterised by the repeat of seven residues (ABCDEFGF)_n. It is not clear if this domain is a coiled coil or not; however, it is definitively not a genuine tower domain.

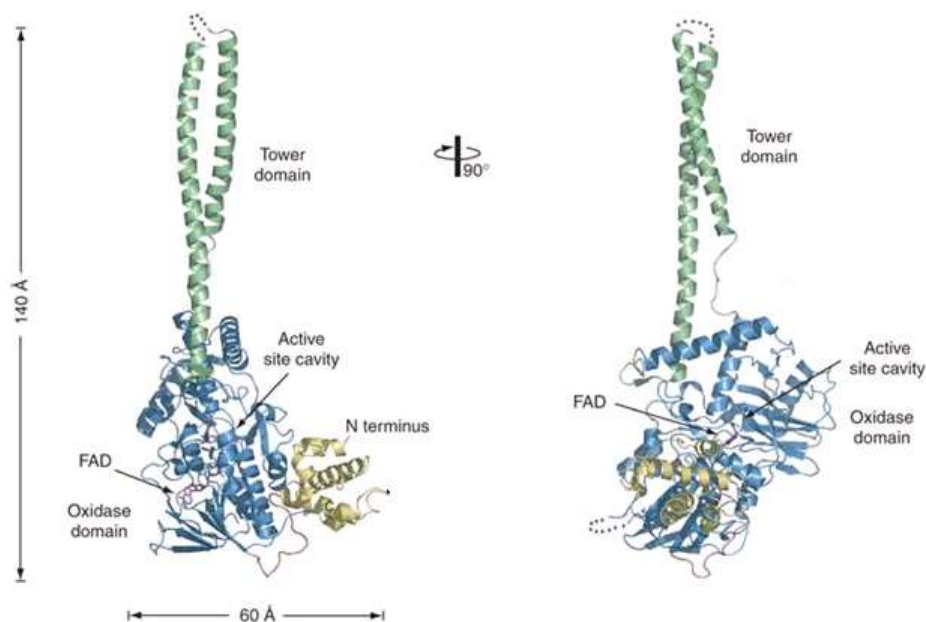
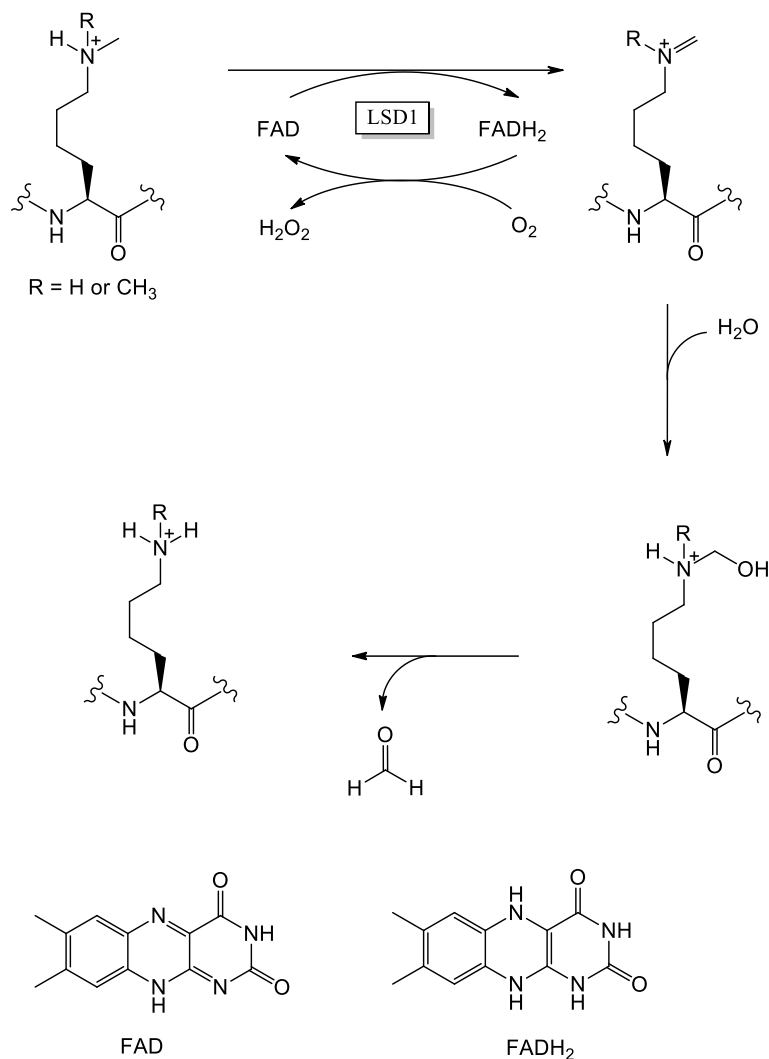


Figure 5. X-ray crystal structure of LSD1 in ribbon (PDB: 2H94). The oxidase domain is represented in blue, the tower domain in green and the *N*-terminal domain in yellow. On the right is represented a 90° rotated view.¹⁷

In LSD1, the substrate binds to one of the subdomains of the oxidase domain. This oxidase domain also contains another subdomain where the co-factor, flavin adenine nucleotide (FAD), binds.

Upon binding to LSD1 the protonated mono- or dimethyllysine is oxidised into an iminium ion, facilitated by the concomitant reduction of FAD to FADH₂ (Scheme 4). The resulting iminium ion is then attacked by water to give the hydroxymethyl intermediate. This hydroxymethyl intermediate is unstable and decomposes to give formaldehyde and the protonated lysine. To complete the catalytic cycle, the FADH₂ is then oxidised to FAD by reduction of dioxygen to hydrogen peroxide.⁸ The mechanistic necessity for a protonated lysine substrate explains why trimethyllysines are not demethylated by LSD1.

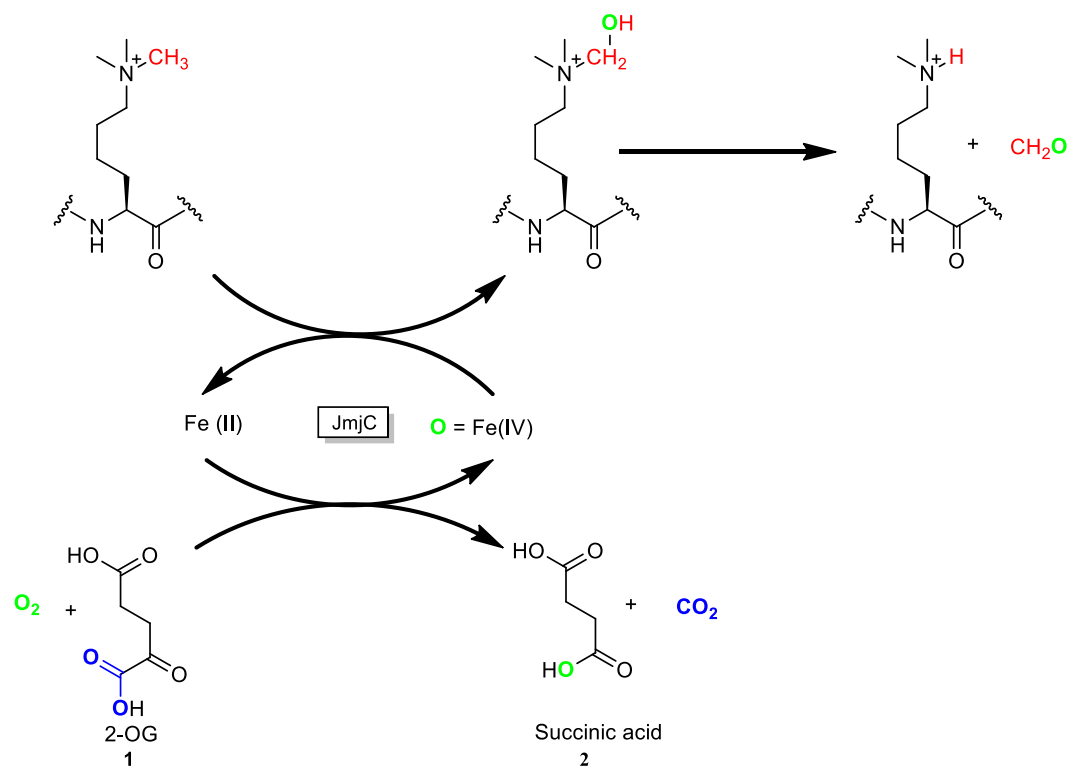


Scheme 4. Mechanism of demethylation by LSD1.⁸

Since LSD1 cannot demethylate trimethylated lysine residues, another class of enzymes is required. This role is fulfilled by the Jmj family of enzymes. The crystal structure of one member of this family, JmjD2a, was resolved by Chen *et al.* in 2006.¹⁹ Their structure revealed that the enzyme contains four main areas: a JmjN domain, a JmjC domain, corresponding to the catalytic domain, a β -hairpin domain and a C-terminal domain. The cupin-like JmjC domain binds the catalytic Fe(II), the co-factor 2-oxoglutarate (2-OG) and the methylated lysine. The Fe(II) ion is chelated by a glutamic acid and two histidine residues in most of the Jmj family members, although in some family members the glutamic

acid is replaced by an aspartic acid. A tetrahedrally coordinated Zn(II) ion is present in the C-terminal domain of most of the Jmj family members, and is believed to play a role in stabilising the structure of the protein.²⁰ Although all the members of the Jmj family demethylate methylated lysines and have similar architecture, there are differences in the residues present in the catalytic domain. It is these differences which give rise to the varied substrate specificities of the family members. Indeed, enzymes JmjD2a and JmjD3 show 15.8% overall sequence identity (*cf.* Appendix 1), whilst JmjD2a demethylates H3K9 and H3K36 and JmjD3 specifically demethylates H3K27.²¹

Unlike LSD1, the JmjC domain-containing enzymes can demethylate all three states of lysine residue methylation. They achieve this by using a highly reactive Fe(IV) oxo species to oxidise the methyl group to be removed. The Fe(IV) oxo species which is required for this process is formed in the reaction between the 2-OG co-factor, oxygen and the Fe(II) which is bound to the enzyme *via* the Glu or Asp and two His residues. In addition to the Fe(IV) oxo species the products of this reaction are carbon dioxide, succinic acid and the same hydroxymethyl intermediate as formed in the LSD1 catalytic cycle. Again, this intermediate decomposes to form the protonated lysine and formaldehyde (Scheme 5).



Scheme 5. Outline mechanism of lysine demethylation by JmjC domain-containing enzymes.¹⁵

LSD1 and JmjC domain-containing enzymes are lysine specific (Table 3); LSD1 only demethylates H3K4, whereas some members of the JmjC family of enzymes can demethylate multiple residues; for example, JmJD2a demethylates H3K9 and H3K36.²²

Lysine residues modified	State	Active or inactive genes	Lysine Demethylases
H3K4	Di-methylated	Active genes	LSD1
H3K9	Tri-methylated	Inactive genes	JmjD1a JmjD1b JmjD2a JmjD2b JmjD2c JmjD2d
H3K27	Tri-methylated	Inactive genes	JmjD3
H3K36	Tri-methylated	Active genes	JmjD2a JmjD2c

Table 3. Demethylases and residues they modify.²³

As shown in Table 1, the methylation state of the lysine residues on histones is linked to activation or inactivation of gene transcription. This is explained more fully in Table 3. For example, in some cases (*e.g.* H3K9 and H3K27), removal of one, two or three methyls from the lysine residue results in the activation of transcription of key genes such as pro-inflammatory genes.

I.1.4 JmjD3

JmjD3 or KDM6A is a member of the KDM6 family along with UTX/UTY. UTX and UTU contain a tetratricopeptide repeat (TPR) and a JmjC domain (Figure 6a). The TPR motif is

responsible for mediating protein-protein interactions, and consists of tandem repeats of 34 amino-acid residues (Figure 6b).²⁴

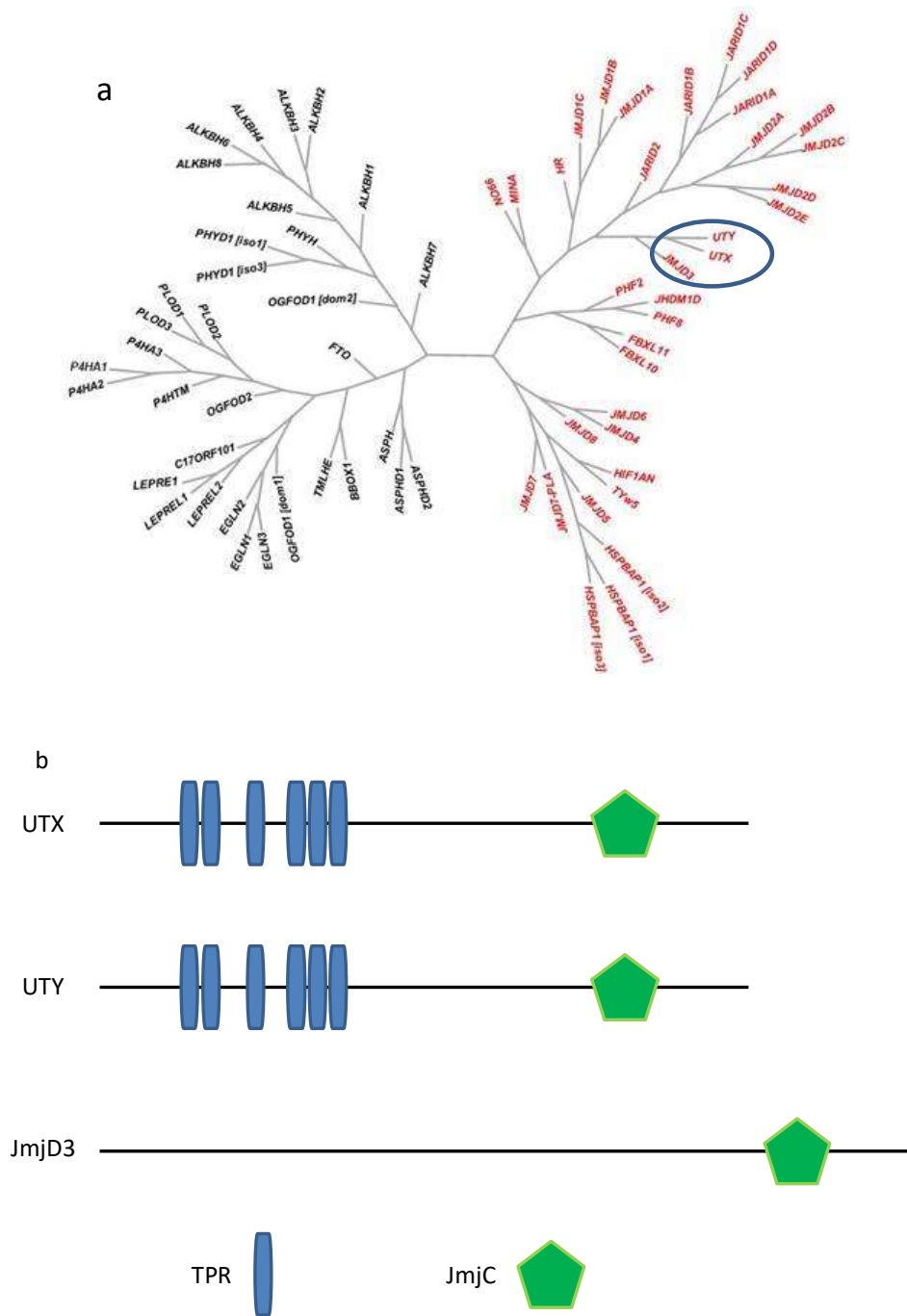


Figure 6. a. Jmj family phylogenetic tree;²⁵ b. KDM6 family.

CONFIDENTIAL – DO NOT COPY

Although JmjD3 lacks the TPR motif, it still belongs to this group of protein because of its high homology with UTX and UTY inside and outside the JmjC domain (Figure 7).²⁴

JMJD3	1175	REKLNPPPTPSIYLESKRDAFSPVLLQFCTDPRNPITVIRGLAGSLRLNLGLFSTKTLVEA
UTX	933	KDKLNPPPTPSIYLENKRDAFFPPLHQFCTNPNNPVTVIRGLAGALKLDLGLFSTKTLVEA
UTY	880	KDKLNPPPTPSIYLENKRDAFFPPLHQFCTNPKNPVTVIRGLAGALKLDLGLFSTKTLVEA
JMJD3	1235	SGEHTVEVRTQVQQPSDENWDLTGTRQIWPCESSRSHTTI AKYAQYQASSFQESLQEEK E
UTX	993	NNEHMVEVRTQLLQPADENWDPTGTTKIWHCESNRSHTTI AKYAQYQASSFQESLREENE
UTY	940	NNEHMVEVRTQLLQPADENWDPTGTTKIWRCESNRSHTTI AKYAQYQASSFQESLREENE
JMJD3	1295	SEDEESEEPDSTTGTTPSSAPDPKN-HHIKFGTNI DLSDAKRWKPKLQELLKLP AFMRV
UTX	1053	KRSHHKDHSDESSTSSDNSGRRRKGPFKTIKFGTNI DLSDDKKWKLLQLHELTKLP AFVRV
UTY	1000	KRTQHKDHSDNESTSSSENSGRRRKGPFKTIKFGTNI DLSDNKKWKLLQLHELTKLP AFARV
JMJD3	1354	TSTGNMLSHVGHITLGMNTVQLYMKVPGSRTPGHQENNNFCSVNI INI GPGDCEWFV VHEH
UTX	1113	VSAGNLLSHVGHITLGMNTVQLYMKVPGSRTPGHQENNNFCSVNI INI GPGDCEWFV VPEG
UTY	1060	VSAGNLLTHVGHITLGMNTVQLYMKVPGSRTPGHQENNNFCSVNI INI GPGDCEWFV VPED
JMJD3	1414	YWETISAFCDRHGVDYLTGSWWPI LDDLYASNIPVYRFVQRPGDLVWINAGTVHWVQATG
UTX	1173	YWGVLNDFCEKNNLNF LMGSSWWPNLEDLYEANVPVYRFIQRPGDLVWINAGTVHWVQAVG
UTY	1120	YWGVLNDFCEKNNLNF LMSWWPNLEDLYEANVPVYRFIQRPGDLVWINAGTVHWVQAVG
JMJD3	1474	WCNNIAWNVGPLTAYQYLALERYEWNKVKSVIPMIHVSWNVARTVKISDPDLFKMI
UTX	1233	WCNNIAWNVGPLTACQYKLAVERYEWNKLSVKSIVPMVHLSWNMARNIKVSDPKLFEMI
UTY	1180	WCNNIAWNVGPLTACQYKLAVERYEWNKLSVKSIVPMVHLSWNMARNIKVSDPKLFEMI
JMJD3	1534	KFCLLQSMKHCQVQRESLVRAGKKIAYQGRVKDEPAYYCNECDVEVFNI L FVTS ENGSRN
UTX	1293	KYCLLRTLKQCQTLREALIAAGKEI IWHGRTKEEPAHYCSICEVEVFDLL FVTNESNSRK
UTY	1240	KYCLLKI LKQYQTLREALVAAGKEVIWHGRTNDEPAHYCSICEVEVFNLL FVTNESNTQK
JMJD3	1594	TYLVHCEGRCARRSAGLQGVVLEQYRTEELAQA YDAFTL(AP)
UTX	1353	TYIVHCQDCARKTSGNLENFVLEQYKMEDLMQVYDQFTLAPPLPSASS
UTY	1300	TYIVHCHDCARKTSSKLENFVLEQYKMEDLIQVYDQFTLALSLSSSS

Figure 7. Homology levels in the UTX/UTY family in a section of the JmjC domain and the linker region. Fe(II) binding residues in red.

JmjD3 is specific to H3K27, which when methylated is associated with the silencing of genes.² Before 2007, very little was known about the function of JmjD3; then, during 2007, Natoli *et al.* showed that JmjD3 expression in macrophages was induced by lipopolysaccharide (LPS) stimulation.²⁶

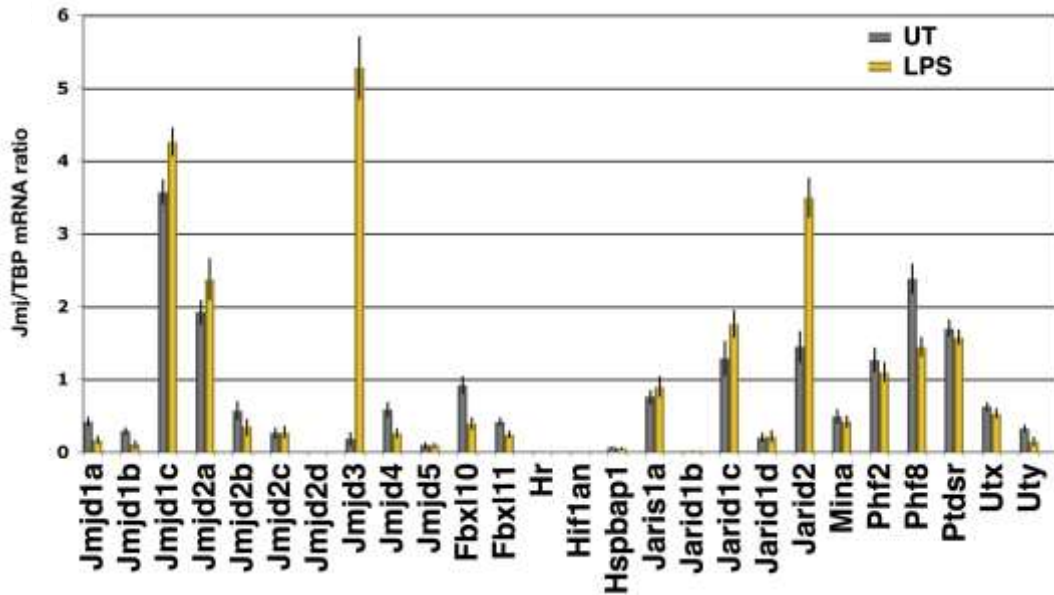


Figure 8. LPS induction of Jmj enzymes in mouse macrophages. Comparison of messenger RNA (mRNA) levels of various Jmj in unstimulated and stimulated Raw264.7 macrophages. The mRNA levels are relative to Tatabox binding protein (TBP). UT = untreated. The mean variations \pm are shown in the Figure.²⁶

Figure 8 shows that Jmjd3 was the only enzyme in the Jmj family significantly upregulated after LPS stimulation of macrophages. This induction was very rapid and reached its maximum between 60 and 120 min (Figure 9).

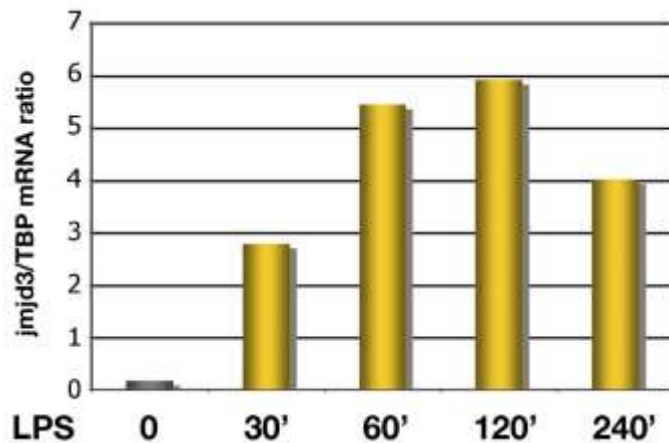


Figure 9. Kinetics of LPS induction of Jmjd3 in mouse macrophages. Raw264.7 cells were used for this experiment.²⁶

Natoli *et al.* showed that JmjD3 production was induced in various macrophages (Figure 10A) but not in non-macrophage cells such as fibroblasts and MCF10 (Figure 10B).²⁶

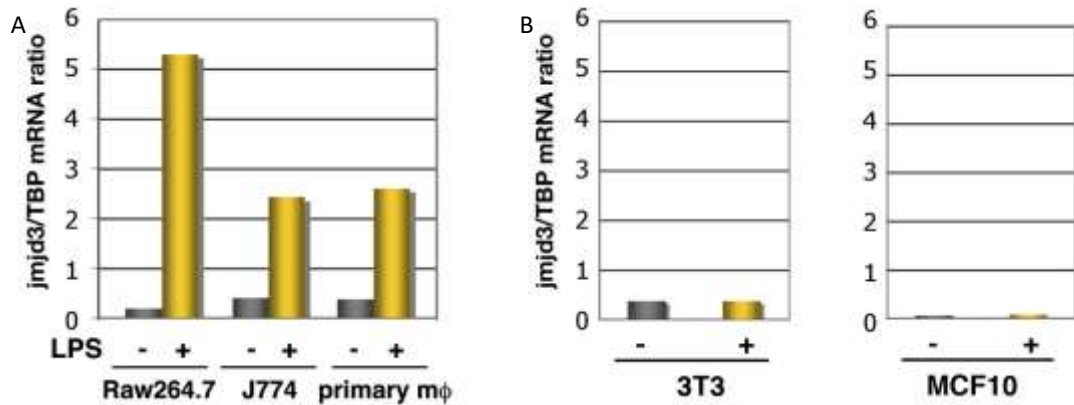


Figure 10. LPS induction of Jmj enzymes in mouse cells. (A) mRNA levels of JmjD3 after LPS stimulation in three mouse macrophages; (B) mRNA levels of JmjD3 after LPS stimulation in 3T3 fibroblasts and MCF10.²⁶

Natoli *et al.* stimulated macrophages using LPS and interferon γ (IFN- γ) and observed that JmjD3 protein level was also increased which was in agreement with the mRNA data (Figure 11).²⁶

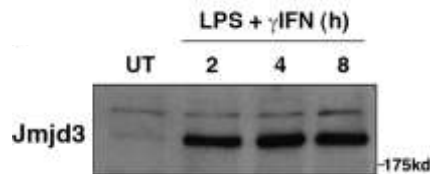


Figure 11. JmjD3 protein detection in mouse macrophages after LPS + IFN- γ stimulation.²⁶

At the time when Natoli *et al.* divulged these studies, little was known about JmjD3. In fact, the Jmj family had only been discovered just a year before this paper was published. Consequently, Natoli *et al.* carried out numerous experiments to identify the location of JmjD3, to understand more about its role and target genes, such as in the experiments described in Figures 12, 13 and 14.²⁶

Natoli *et al.* showed that Jmjd3 was exclusively located in the nucleus, as shown in Figure 12. They also showed that histone H3 was located in the nucleus.²⁶

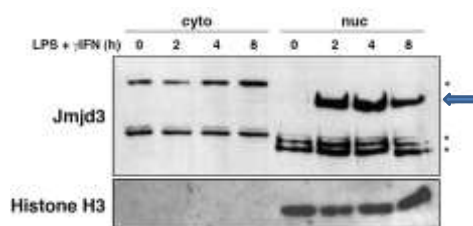


Figure 12. Localisation of Jmjd3 at the cell level. Raw264.7 macrophages were stimulated by LPS and IFN- γ . Western blot was utilised to analyse the cytoplasmic and nuclear fractions. Asterisks (*) indicate non-specific bands and the arrow indicates Jmjd3. Histone 3 analysed by western blot.²⁶

The specificity of Jmjd3 was demonstrated as shown in Figure 13.²⁶ The cells overexpressing Jmjd3 are in red. The cells containing the indicated lysine residues are in blue; these cells did not overexpress Jmjd3. The cells containing the indicated lysine residues after overexpression of Jmjd3 are in green. Only the H3K27me3 residue disappeared after overexpression of Jmjd3, demonstrating that Jmjd3 was specific to H3K27me3.

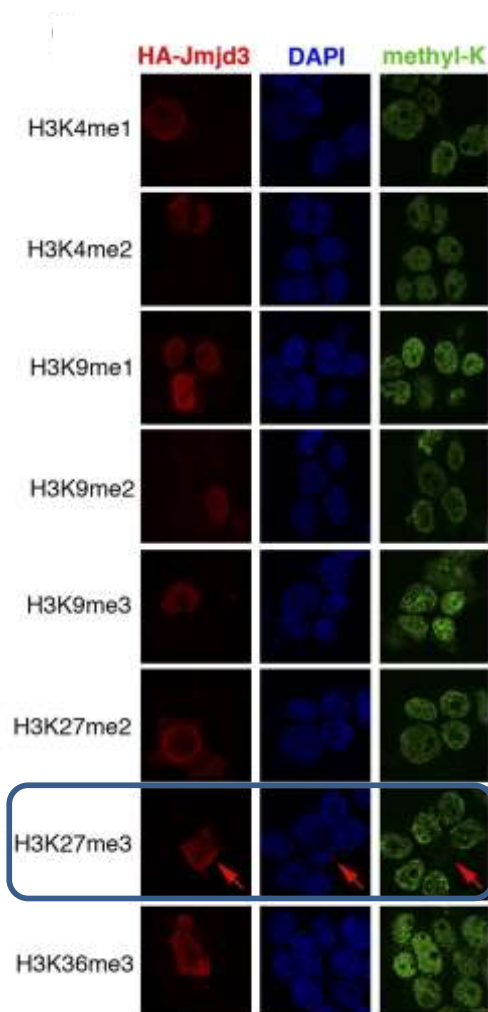


Figure 13. Specificity of Jmjd3. Analysis of the impact of overexpression of Jmjd3 in HEK293 cells on methylated histones. Cells were transfected with HA-tagged full-length Jmjd3. The analysis of the substrate specificity was carried out *in vivo* by double-indirect immunofluorescence with an anti-HA antibody and the indicated anti-methyl histone antibodies.²⁶

It was shown that overexpressed Jmjd3 could erase H3K27me3 from transfected HEK293 cells (Figure 13), but Jmjd3 produced after LPS + IFN- γ stimulation did not decrease the global level of H3K27me3 in macrophages (Figure 14).²⁶ Moreover, Jmjd3 knockdown did not increase the global level of H3K27me3 in macrophages before or after

LPS + IFN- γ stimulation (Figure 14). These results suggested that Jmjd3 potentially demethylates H3K27me3 on specific genes.

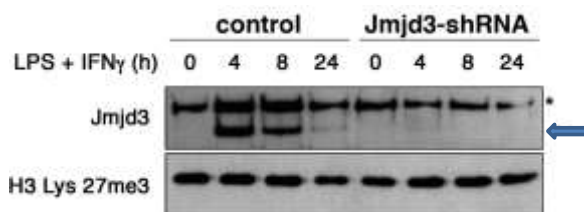


Figure 14. Impact of Jmjd3 knockdown on H3K27me3 levels. Asterisks (*) indicate non-specific bands and the arrow indicates Jmjd3. Jmjd3 knockdown was accomplished using short hairpin RNA (shRNA).²⁶

In 2009, Natoli *et al.* investigated the effect of Jmjd3 knockout on production of genes and the level of H3K27me3 in macrophages (Table 4).²⁷ They measured the levels of mRNA of more than 20000 genes in wild-type and Jmjd3 knockout in macrophages after LPS + IFN- γ stimulation and discovered that only 33 genes were expressed differently in Jmjd3 knockout macrophages for a two-fold cutoff.²⁷ Some of these genes were IL-12b, Ccl5 and Ccl9 which could potentially be important for treatment of inflammation.

Threshold (FC)	Number of genes
2	33
1.5	237
1.4	478

Table 4. Microarray results wild-type (WT) vs. Jmjd3 knockout in macrophages 4 h after LPS + IFN- γ stimulation. FC = fold cutoff.

I.1.5 Project aims

Preventing the removal of the repressive methyl marks, by inhibiting the activity of the demethylases, has the potential to control the transcription of pro-inflammatory genes and

thus control inflammation. It follows that, from a drug discovery point of view, finding small molecules which inhibit these epigenetic enzymes could be a very attractive way to modulate cellular mechanisms such as inflammation.²⁸ To test the hypothesis, a Jumonji enzyme selective to only one lysine was required to ensure that any biological response observed would be solely due to the inhibition of this particular enzyme. Table 3 shows that LSD1 is specific to H3K4 and JmjD3 specific to H3K27 and these specificities make them attractive potential targets. Natoli's work on JmjD3 regarding the specificity of this enzyme^{26,27} and the potential link with inflammation made this enzyme even more attractive. Therefore, JmjD3 was selected as the lysine demethylase enzyme to inhibit. In 2007, JmjD3 was surrounded by numerous questions which required a large amount of work to answer. These included solving the crystal structure of the enzyme, the effect of demethylation of H3K27me3 and the biological benefit of inhibiting this enzyme. This project describes efforts to identify and optimise JmjD3 inhibitors with a view to using these species as probes to elucidate the role of this enzyme in the regulation of inflammatory processes.

Control of epigenetic modification is an area of science in its infancy and few drugs on the market act by these mechanisms. The HDAC inhibitors Vorinostat and Romidepsin are successful examples for the treatment of cancer.²⁹ To date, there is no marketed demethylase inhibitor.

I.1.5.1 Inhibitors of JmjC domain containing enzymes

A limited number of inhibitors of JmjC domain-containing enzymes have been reported in the literature. Some of these are shown in Figure 15. *R*- and *S*-2-Hydroxyglutarate (2HG) (**3a** and **3b**, respectively) inhibit Jmj histone demethylases.³⁰ *N*-Oxalylglycine (NOG) (**4**) inhibits JmjD2c *in vitro*,³¹ and *N*-oxalyl-D-tyrosine (**5**) inhibits JmjD2e.³² 2,4-Pyridinedicarboxylic acid (2,4-PDCA) (**6**), a different type of structure, inhibits the JmjD2 family.³³ Related

heterocyclic carboxylic acids, 4'-((2-aminoethyl)carbamoyl)-[2,2'-bipyridine]-4-carboxylic acid (**7**) inhibits JmjD2e³⁴ and 8-hydroxyquinoline (8HQ) (**8**) inhibits the JmjD2 family.³⁵

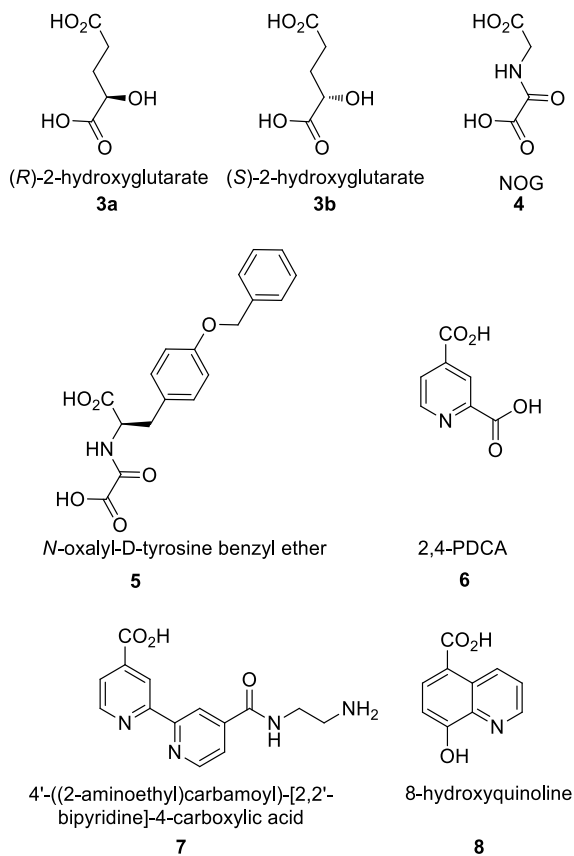


Figure 15. Structures of JmjD2 family enzyme inhibitors.

Understanding the mechanisms by which these compounds inhibit JmjC domain-containing enzymes has been helped greatly by the resolution of crystal structures of the target proteins with the inhibitors bound.

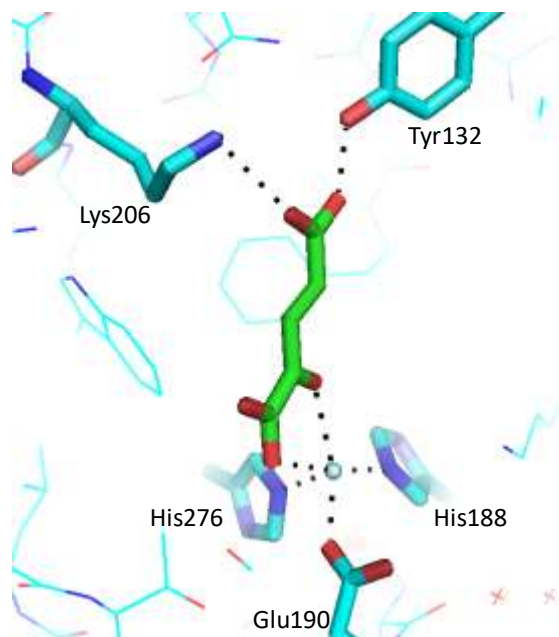


Figure 16. Crystal structure of 2-OG 1 (PDB: 2GP5) (in green) bound to Ni(II) (in silver) in JmjD2a (in cyan). Ni(II) is octahedrally coordinated to His188, His276, Glu190, water and 2OG.³⁰

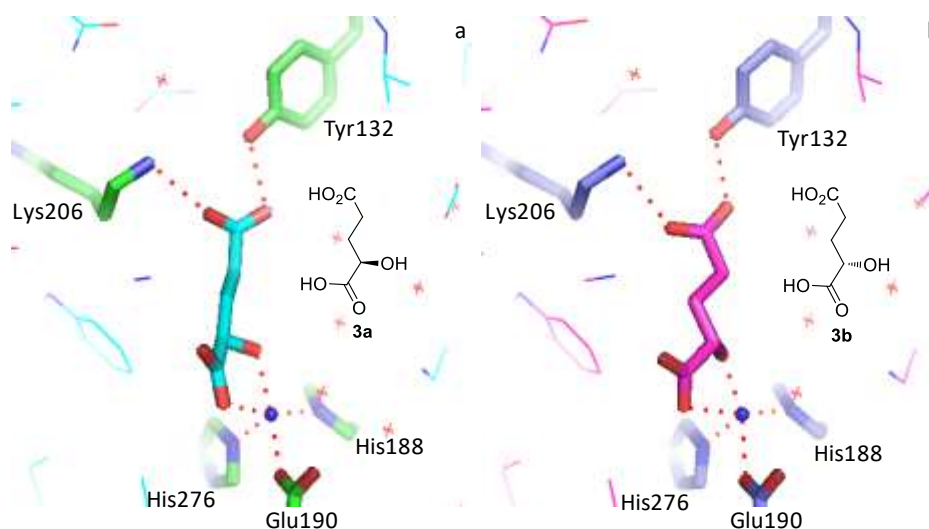


Figure 17. (a) Crystal structure of *R*-2HG **3a** (PDB: 2YBP) (in cyan) bound to Ni(II) (in blue) in JmjD2a (in green).³⁰ Ni(II) is octahedrally coordinated to His188, His276, Glu190, water and *R*-2HG. *R*-2HG is also involved in a hydrogen bond with Tyr132 and a salt bridge with Lys206. (b) Crystal structure of *S*-2HG **3b** (PDB: 2YBS) (in pink) bound to Ni(II) (in blue) in JmjD2a (in blue).³⁰ Bidentate interaction of *S*-2HG with Ni(II) and interactions with Tyr132 and Lys206 are displayed.

The crystal structures of *R*- **3a** and *S*-2HG **3b** (Figure 17), NOG **4** (Figure 18) and *N*-oxalyl-D-tyrosine **5** (Figure 19) are all closely related to the structure containing the natural co-factor (2-OG) **1** (Figure 16). All four structures show binding to the active site metal in ways similar to 2-OG **1**. Ni(II) is used as a substitute for Fe(II) for crystallography so that the demethylation mechanism is blocked. Each of these four inhibitors are involved in hydrogen bonding with Tyr132 and a salt bridge with Lys206 through one of their carboxylic acids. In addition to these interactions, all of the inhibitors bind to the active site metal *via* a bidentate interaction, although the moieties participating in this vary slightly. Indeed, NOG **4** and *N*-oxalyl-D-tyrosine **5** bind to the metal *via* the oxygen of C1-carboxylic acid and the oxalyl carbonyl, whereas *R*- and *S*-2HG bind through the oxygen of C1-carboxylic acid and the 2-hydroxyl group.

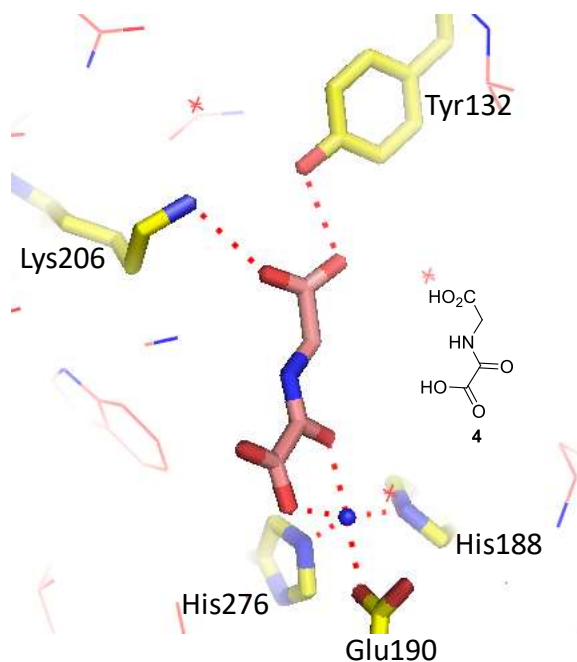


Figure 18. Crystal structure of NOG **4** (in pink) bound to Ni(II) (in blue) in JmjD2a (in yellow) (PDB: 2GP3).³⁶ NOG is also involved in a hydrogen bond with Tyr132 and a salt bridge with Lys206.

N-Oxalyl-D-tyrosine benzyl ether **5** was designed by the Schofield group, based upon NOG, with the aim of occupying the position of the co-factor and creating additional interactions with the enzyme. Indeed, the tyrosinyl side chain is involved in hydrophobic interactions with the methylene groups of Lys241, Phe185, Ile71, Tyr177 and Tyr132 (not shown). A comparison of the crystal structures of JmjD2a complexed with *N*-oxalyl-D-tyrosine benzyl ether **5** and JmjD2a complexed with H3K9Me3 shows that the benzylic ether of **5** sits in the same area as Gly12 and Thr11 of the H3K9Me3 substrate (not shown).

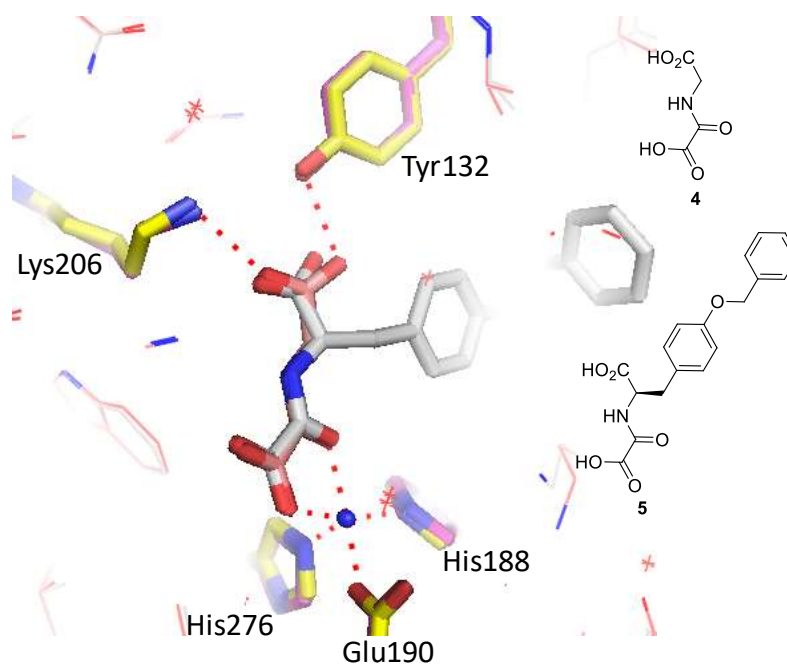


Figure 19. Crystal structures of **5** (in grey) bound to Ni(II) (in blue) in JmjD2a (in pink) (PDB: 2WWJ) and **4** (in pink) bound to Ni(II) (in blue) in JmjD2a (in yellow). The terminal carboxylic acid is involved in a bidentate interaction with Ni(II); the second carboxylic acid is involved in a hydrogen bond with Tyr 132 and a salt bridge with Lys276.³²

All four inhibitors, *R*- **3a** and *S*-2HG **3b**, NOG **4** and *N*-oxalyl-D-tyrosine benzyl ether **5**, compete with 2-OG for binding to the Fe(II) and, as a result, inhibit the enzyme. NOG **4**, since it is a stable mimetic of 2-OG **1**, has been widely used as a substitute for 2-OG **1** in structural studies. *N*-Oxalyl-D-tyrosine benzyl ether **5** and the two enantiomers of 2HG have been shown to inhibit the enzyme in more complicated ways. *N*-Oxalyl-D-tyrosine benzyl ether **5**, by disturbing the binding of the co-factor (2-OG) and the substrate in the active site, is a mixed inhibitor.³² In the case of 2HG, kinetic analyses of the binding of the two enantiomers carried out by Schofield *et al.* demonstrated that the inhibition modes were less simple. Indeed these analyses showed *R*-2HG **3a** to be a mixed inhibitor and *S*-2HG **3b** to act as an uncompetitive inhibitor.³⁰

Despite structural differences between 2,4-PDCA **6** and 2-OG **1**, the X-ray crystal structure of 2,4-PDCA **6** bound in the active site of JmjD2a shows there are similarities in the binding modes they adopt in the enzyme. Indeed, the two molecules bind to the catalytic metal *via* a bidentate interaction. In the case of 2,4-PDCA **6**, the binding to the catalytic metal is through the pyridyl nitrogen and the C-2 carboxylate, with the C-4 carboxylate being involved in an electrostatic interaction with Lys206 (Figure 20).³⁷ This binding mode showed that 2,4-PDCA **6** inhibited the enzyme by competing with 2-OG **1** for binding to the metal, and this was confirmed by kinetic studies.³³

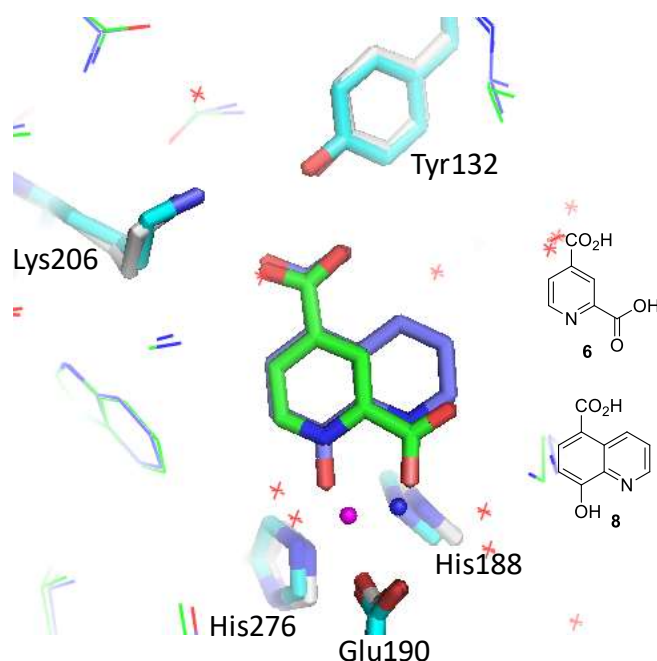


Figure 20. Overlay of JmjD2a crystal structures with 5-carboxy-8-hydroxyquinoline **8** (compound in blue, residues in grey and Ni(II) in blue) (PDB: 3NJY) and with 2,4-PDCA **6** (compound in green, residues in cyan and Ni(II) in magenta) (PDB: 2OQ6). Ni(II) occupies different positions in the two crystal structures.³⁵

Inhibitor 4'-((2-aminoethyl)carbamoyl)-[2,2'-bipyridine]-4-carboxylic acid **7** binds to the metal ion through two pyridyl nitrogens occupying the positions opposite His276 and Glu190 (Figure 21). In contrast, 2-OG **1** sits opposite Glu190 and His188 leaving the

position opposite His276 accessible for the binding of molecular oxygen (Figure 16). This led Schofield *et al.* to believe that bipyridyl derivatives inhibit JmjD2 enzymes not only by competing with 2-OG **1**, but also by taking the place of the oxygen in the active site.³⁴

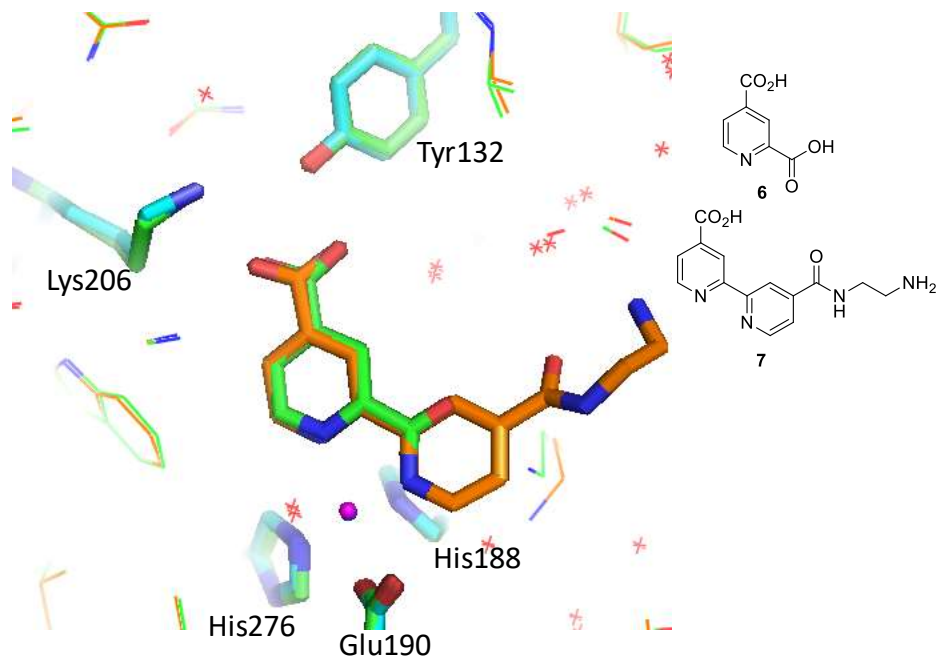


Figure 21. Overlay of JmjD2a crystal structures with bipyridyl derivative **7** (compound in orange, residues in green and Ni(II) ion in blue) (PDB: 3PDQ) and with 2,4-PDCA **6** (compound in green, residues in cyan and Ni(II) in magenta).^{33,34}

The co-crystal structure of 8HQ **8** in the JmjD2a active site showed that 8HQ binds to the metal through the quinoline nitrogen and C-8 hydroxyl, while the C-5 carboxyl is involved in an electrostatic interaction with Lys206 and Tyr132 (Figure 20).³⁵ 8HQ is a mixed inhibitor, competing with 2-OG for binding to the metal, and also disturbing the binding of the substrate in the active site. Furthermore, a shift in position of the Ni(II) in the active site was observed: in the JmjD2a - 2,4-PDCA (PDB: 2OQ6) co-crystal structure, the Ni(II) interacts with His276 whereas in JmjD2a - 8HQ (PDB: 3NJY) structure, the C-8 hydroxyl interacts with His276 and the Ni(II) has moved away from this residue. This movement of the metal

demonstrates that there is some flexibility in the positions of the residues and metal in the active site.

By using the increasing amount of structural information available across the Jmj family, these inhibitors could be optimised further to deliver potent and selective 2-OG competitive active site inhibitors. One of our strategies to obtain a potent JmjD3 inhibitor was to find a metal binder (monodentate or bidentate) and, using the resulting structural information, further optimise the emerging lead compound to engage residues in the catalytic domain in a manner similar to the reported inhibitors. Moreover, from X-ray crystal structures, we know that there are differences in the residues present in the catalytic domain which we could potentially exploit to obtain selective JmjD3 inhibitors.

I.2 Assays

Before any drug discovery programme can be pursued, it is essential to have a robust set of assays in place so that compound efficacy can be evaluated in a way that generates insight. The following assays of enzyme activity were used in order to evaluate the activity and selectivity of novel Jumonji inhibitors:

- time-resolved fluorescence resonance energy transfer (TR-FRET)
- matrix-assisted laser desorption/ionisation (MALDI) and RapidFire
- cellular assay.

I.2.1 TR-FRET

TR-FRET is a biochemical assay which uses homogeneous time-resolved fluorescence resonance energy transfer technology to measure the intensity of a signal (Appendix 2).^{38,39} This assay is based on the competition between monomethylated lysine peptide (produced in the assay by demethylation of trimethylated lysine peptide) and a tracer complex formed by monomethylated lysine peptide-Ulight for binding sites on specific antibodies labelled with Europium (Figure 22). Ulight is an acceptor dye used for the direct labelling of molecules of various sizes. The monomethylated lysine peptide-Ulight tracer complex is formed by the tight interaction between Biotin-monomethylated lysine peptide and streptavidin which is labelled with Ulight. When the Europium-labelled antibodies are bound to the monomethylated lysine peptide-Ulight tracer, excitation of the Eu-chelate at 340 nm causes TR-FRET Ulight molecules to emit light at 665 nm. The fluorescence intensity measured at 665 nm will decrease in the presence of monomethylated lysine peptide produced by JmjD3.³⁶

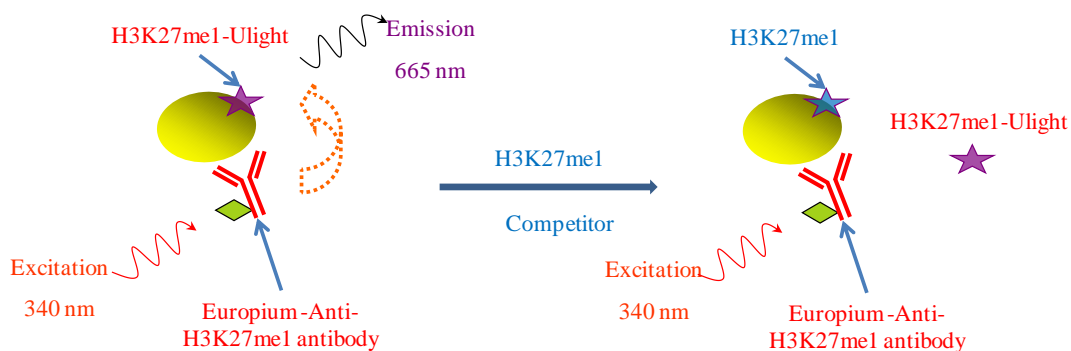


Figure 22. JmjD3 TR-FRET assay.

In this assay, a compound which acts as an inhibitor will reduce the ability of JmjD3 to produce monomethylated lysine peptide, and so the signal will remain high. In contrast, a compound which is inactive in this assay will not inhibit JmjD3 and the monomethylated lysine peptide concentration will increase, causing the signal to decrease. This type of assay, run in-house,⁴⁰ was also used for the other family members to assess the selectivity of the compounds. A potential issue with this assay is that some compounds could give the appearance of inhibiting the enzyme by interfering with the detection system rather than acting on the enzyme itself. Consequently, a second assay was used to discriminate the real inhibitors from the fluorescent interfering compounds. The analysis of TR-FRET data in combination with the secondary assay data would allow discrimination between inhibitors, interfering compounds and compounds which inhibit the enzyme and interfere with the detection system. In this interference assay, the TR-FRET assay is run without any inhibitor, and so monomethylated lysine peptide is produced by JmjD3 resulting in a low signal. The solution of the reaction products resulting from this TR-FRET assay (including TR-FRET components) is subsequently added to a solution of the compound to be assessed, so if a signal is produced, this could only be related to the presence of the compound. The signal arising from this assay is only a function of the interference degree.⁴¹ The compounds with TR-FRET data described in this report did not show any interference issues with the TR-FRET detection system.

TR-FRET assay was run by Laurie Gordon and Carl Haslam.

I.2.2 MALDI/RapidFire

The MALDI and RapidFire assays utilise mass spectrometry to measure the relative proportions of a trimethylated lysine peptide substrate and the dimethylated lysine peptide produced as a result of the action of JmjD3 (Appendices 2).^{33,42,43,44}

An inhibitor of JmjD3 will reduce the rate of conversion of the trimethylated lysine peptide substrate to the dimethylated lysine. Since this assay directly measures the function of the enzyme, it is not susceptible to the same limitations as the TR-FRET assay. The MALDI assay only became available six months after the TR-FRET assay was used to screen the first compounds made in-house. Once available, the MALDI assay was run in parallel to the TR-FRET assay for several months to ensure that the MALDI assay was robust. Once confidence in the MALDI assay was established, the TR-FRET assay was retired. The RapidFire assay became available one year after the MALDI assay was first used. The main difference between the two assays is the throughput; RapidFire allows higher throughput than MALDI, but is still not high enough to be used in HTS.

The MALDI assay was run bi-weekly with 120 compounds per screen, whilst RapidFire was run once a week with a capacity of six hundred compounds per screen. MALDI and RapidFire use different mass spectrometers, with RapidFire using a more sensitive technique. In addition, MALDI requires the use of costly special plates, which had to be spotted manually, whilst RapidFire does not require any spotting and the plates used are inexpensive making it cheaper to run. Moreover, RapidFire is set up to export data in an

automated manner that could be fed directly into the curve fitting software, whereas MALDI involved considerable data manipulation, which is not ideal for data integrity.

MALDI and RapidFire assays were run by Melanie Leveridge, Laurie Gordon and Sue Hutchinson

I.2.3 Cellular assay

As well as the biochemical assays already described, another system was developed to establish inhibitor efficacy in a cellular environment. The purpose of this assay was to identify compounds capable of penetrating a cell nucleus and inhibiting JmjD3 *in situ*. The results from this assay reflect both biochemical potency and cellular penetration, and therefore should be more closely related to the endogenous system. The level of histones containing trimethylated lysines in cells expressing a high level of JmjD3 is quantified. An inhibitor will reduce the activity of JmjD3, resulting in a higher concentration of histones containing trimethylated lysines, giving an intense signal. An inactive compound will not affect the enzymatic activity and so the histone lysines will be demethylated, causing a reduction of the level of trimethylated lysine histones and a concomitant reduction of the intensity of the signal.^{45,46}

Cellular assay was run by Carl Haslam, Fiona Brown and Becky Randle.

I.2.4 Target Product Profile (TPP)

As this programme was investigating a novel target JmjD3, about which little has been reported, the aim was to find a tool compound to understand the cellular phenotype associated with inhibition of the enzyme. This tool compound would have to be potent, showing the following activity across these three assays:

- TR-FRET pIC₅₀ ≥ 6

CONFIDENTIAL – DO NOT COPY

- MALDI/RapidFire pIC₅₀ ≥ 6
- Cellular assay pIC₅₀ ≥ 5.

In addition, it was desirable that the inhibitor would be more than 100-fold selective for JmjD3 over the other 2-OG utilising enzymes.

I.3 HTS and focused screen hits

In total, 1.9 million compounds were screened through the TR-FRET assay as part of a high throughput screen (HTS). A focused set, consisting of known inhibitors of 2-OG utilising enzymes, 2-OG mimetics, Lys mimetics and potential metal binders, such as 2,4-PDCA, was also screened. Initially, the focused set and HTS compounds were tested at single concentrations in the TR-FRET assay. Compounds which showed an acceptable percentage of inhibition at single concentration were selected for testing in a dose-response manner. Those which exhibited encouraging IC_{50} values of $\leq 20 \mu\text{M}$ were then taken through a stepwise triage.

I.3.1 HTS and focused screen triage

I.3.1.1 False-positives

A problem commonly encountered when performing a high throughput screen is how to distinguish genuine inhibitors from false-positives.⁴⁷ Such false-positives may be produced *via* a variety of different mechanisms, depending on the assay detection system, nature of the compounds, or catalytic machinery of the enzyme under study. Certain molecules form aggregates in solution which adsorb the protein of interest onto their surface resulting in inhibition.⁴⁸ There are also compounds discovered by HTS which show activity in multiple screens through undesirable mechanisms, which cannot be exploited from a drug discovery point of view.⁴⁹ These promiscuous inhibitors act by undergoing a chemical reaction such as acylation or alkylation with the protein. Numerous compounds can give false-positives because they interfere with the mechanism of the assay. Finally, there are also inhibitors which show redox reactivity, and which inhibit the protein indirectly by oxidising key residues in the active site (*e.g.* cysteine), redox cofactors (*e.g.* quinones and flavins) and

metals (Fe, Co, and Mn). Because the probability of having a significant number of promiscuous inhibitors in the HTS and focused screen was fairly high, nuisance assays were used to discriminate the real hits from the promiscuous inhibitors. For example, an interference assay was used to eliminate the false-positive compounds which acted by interfering with the fluorescence energy transfer used in the TR-FRET assay (*cf.* Section I.2.1.).

I.3.1.2 Redox reactivity

The knowledge that the Jumonji-C domain-containing demethylases utilise an Fe(IV) oxo species in their catalytic cycle (*cf.* Section I.1.3.3) raised a concern that enzyme function could be inhibited by compounds altering the oxidation state of the catalytic metal. When a compound is oxidised in the active site, one or two electrons are transferred and the iron is reduced. Since the Fe(IV) oxo species is essential for the demethylation catalytic cycle, its reduction results in a non-productive iron, blocking the demethylation process.

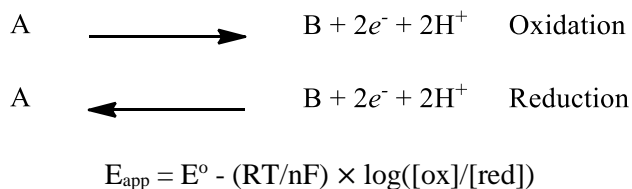
Compounds which act by altering the oxidation state of the catalytic metal were perceived to be less desirable than those displacing the co-factor or substrate, due to the prevalence of other oxidation state-sensitive enzymes in the body. It was considered that molecules acting in this way may be more likely to give rise to unwanted side effects if progressed further down the screening cascade.^{50,51}

Oxidation state	Reduction reactions	E° (mV)
Fe(III) → Fe(II)	$\text{Fe}_2\text{O}_3 + 3\text{H}_2\text{O} + 2\text{e}^- \rightarrow 2\text{Fe}(\text{OH})_2 + 2\text{OH}^-$	-0.86
	$[\text{Fe}(\text{CN})_6]^{3-} + \text{e}^- \rightarrow [\text{Fe}(\text{CN})_6]^{4-}$	+0.36
	$\text{Fe}^{3+} + \text{e}^- \rightarrow \text{Fe}^{2+}$	+0.77

Table 5. Iron reduction electropotentials.⁵²

Table 5 shows a variety of electropotentials at which Fe(III) is reduced to Fe(II). It is of note that the electropotential for this reduction varies depending upon the environment

surrounding the iron. For example, reduction of Fe(III) to Fe(II) can be carried out at three different electropotentials, -0.86 mV, +0.36 mV or +0.77 mV. This shows how much the ligands around the iron impact on the electropotential of reduction; it is therefore difficult to predict at which electropotential the Fe(IV) oxo species in the active site could be reduced. Although the electropotential of reduction of the Fe(IV) oxo species in the active site was not known, the propensity to undergo redox reactions was established for members of each series by measuring their oxidation potentials in an oxidative stability assay. The results from this assay could then be used to triage those compounds with undesirable profiles from those of greater oxidative stability. This assay was designed to measure oxidative stability by applying known voltages to the molecule in a series of electrochemical cells and measuring the current generated by the flow of electrons from the analyte. The standard potential, as defined by the Nernst equation (Equation 1), is observed by generating a hydrodynamic voltammogram and defining the voltage in which half the concentration has transformed to the oxidised form.



Equation 1. Nernst equation (at 25 °C). E° is the potential for which the concentrations of the oxidised and reduced forms are equal. R is the universal gas constant, F is the Faraday constant, T is the temperature in Kelvin, and n is the number of electrons transferred.

In practice, the sample is injected onto the system, initially passing through an HPLC column to ensure that the result is due to a single pure compound. Having passed through the HPLC column, the sample then moves through twelve cells in serial fashion, with each cell individually configured with potentials varying from 0 to 1320 mV (Δ of 120 mV between

each cells). As a compound passes through each cell, the current generated from the electron transfer is measured (Figure 23).

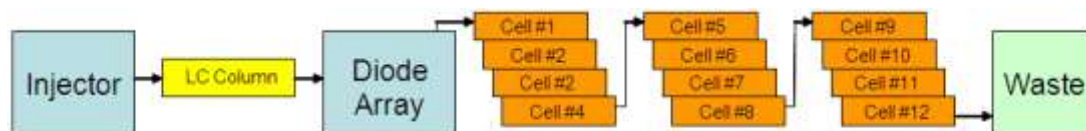


Figure 23. Oxidative stability assay.

This assay is run only when requested and not routinely. However, two hundred compounds can be run through this assay at a time. Depending on their oxidation potentials, the compounds were classified as having high, medium or low probability of reducing the iron with the most stable compound having the higher E° .

E°	Stability
< 699 mV	High risk
700 mV - 899 mV	Medium risk
> 900 mV	Low risk

Table 6. Electropotential and risks.

The classification of electrochemical risk shown on Table 6 was established in an historical GSK programme which looked at inhibitors of an enzyme containing a non-heme iron which undergoes reversible oxidation between Fe(II) and Fe(III).⁵³ By measuring the oxidative potential of a large number of compounds from this project it was discovered that a number of compounds showing moderate to good activity *in vitro* were actually having this effect by reducing the iron. Compounds which reduced the iron were oxidised below 699 mV in general, and classified as high risk. Compounds inhibiting the enzyme without reducing the iron were oxidised above 900 mV and classified as low risk. These empirical values are not fixed, and can be reviewed for each project. It should be noted that the redox reactivity assay

was only introduced to the HTS triage after inconsistencies were observed when attempts were made to optimise the earliest hits.

I.3.1.3 Summary of measures taken to obtain genuine hits

Eliminating the false-positives resulting from redox reactivity, chemical reaction with the target protein, or interference with the HTS assay detection system helps to reduce the number of hits and delivers higher quality leads for optimisation. An additional method to determine if the activity of the compounds is genuine, is to use another biochemical assay which is a direct measure of the activity of the enzyme. This role is fulfilled by MALDI and RapidFire assays, which became available later in the programme.

Compounds which showed an acceptable level of potency when tested from solution samples had to be re-tested from the same solution and also be tested through nuisance assays to confirm the data. Once these additional data confirmed that the hits were genuine, these compounds were re-tested as solids. Although all samples in the GSK compound bank have been through a quality control (QC) process, some samples may only be 80% pure resulting from degradation over time. As a consequence, it is important to ensure that active compounds are re-tested from pure solids.

I.3.1.4 LE and LLE

To prioritise and reduce the number of hits, several criteria were used; these included potency against TR-FRET, cellular assay, selectivity, ligand efficiency (LE) and ligand lipophilic efficiency (LLE).

The concepts of LE, LLE and binding efficiency have been introduced in the last few years to help medicinal chemists identify lead compounds and optimise them to safe and effective

clinical candidates.^{54,55,56} It is well known that highly lipophilic compounds are prone to fail before completing clinical evaluation. Highly lipophilic compounds are often poorly soluble and are more likely to be promiscuous binders. Indeed, lipophilicity is a major driver of the binding affinity of compounds. Anticipating the effect of lipophilicity on the activity of the compounds at an early stage can reduce failure rate and help prioritise lead compounds or small fragments for further development. In our current program, LE and LLE, which are calculated using Equations 2 and 3, are used most often.

$$LE = 1.37 \frac{pIC_{50}}{HVY}$$

Equation 2. Calculation of LE. HVY = number of heavy atoms.

$$LLE = pIC_{50} - cLogP$$

Equation 3. Calculation of LLE.

LE and LLE link compound potency to physical properties and lipophilicities. LE is defined as the potency normalised by the number of heavy atoms; it evaluates the strength of a binding interaction with respect to the size of the molecule. LLE is the difference between the potency and lipophilicity. An ideal lead compound would have a $LE \geq 0.3$ and an $LLE \geq 5.0$. A high value of LLE (≥ 5.0) is thought to decrease the risk of compound toxicity.

I.3.2 Hits

A variety of hits were identified from the triage of the HTS and focused screens using the various criteria described in the preceding Section. Three compounds of interest (**9**, **10** and **11**) are shown below (Figure 24).

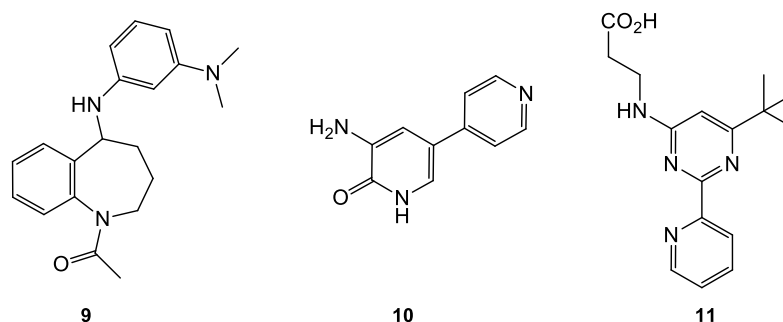


Figure 24. HTS and focused screening hits.

Assay data for compounds **9**, **10**, and **11** are summarised in Table 7.

Compound	JmjD3 TR-FRET pIC ₅₀	Cell assay pIC ₅₀	EGLN pIC ₅₀	LE	LLE	cLogP
9^a	6.0*	4.2	5.7‡	0.34	3.2	2.8
10	4.7	< 4.0	5.7	0.46	5.4	-0.7
11	4.8	< 4.0	< 4.3	0.30	1.9	2.9

Table 7. Lead compounds.

^a Compound tested as a racemate.

* Compound showed activity below the limit of detection on 4 test occasions.

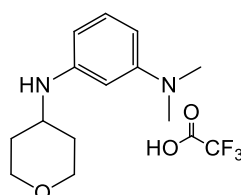
‡ Compound showed activity below the limit of detection on 2 test occasions.

Lead compounds **9**, **10** and **11** were interesting starting points in terms of ligand efficiency.

I.3.2.1 *Bis*-aminoaryl series

1-(5-((3-(Dimethylamino)phenyl)amino)-2,3,4,5-tetrahydro-1H-benzo[b]azepin-1-yl)ethanone **9** was identified as one of the most promising starting points due to the TR-FRET potency (pIC₅₀ = 6.0) and cellular activity (pIC₅₀ = 4.2). Additionally, its good ligand efficiency (LE = 0.34) and LLE (3.2) made this chemotype very attractive for further

exploration. Screening compound **9** against a range of other enzymes indicated that it also inhibited another 2-OG dependent Fe(II) utilising enzyme Egg Laying-9 (EGLN) ($pIC_{50} = 5.7$). As previously stated, the initial goal of the programme was the identification of a cellular probe with which the phenotypic response resulting from the inhibition of JmjD3 could be measured. In order to have confidence that any response observed was due to the inhibition of JmjD3, it was desirable to have the most selective probe possible. This objective meant that selectivity had to be monitored, and analogues designed to minimise any unwanted activity. Initial work was carried out to investigate Structure Activity Relationships (SAR) and simplify the core. From that initial work (data not shown) compound **12** was identified (Figure 25).⁵⁷



12

TR-FRET $pIC_{50} = 6.7$
 Cell assay $pIC_{50} < 4.3$
 LE = 0.57
 LLE = 5.30
 cLogP = 1.4

Figure 25. Compound **12**.

A number of factors made compound **12** more attractive than compound **9** as a starting point from which to optimise the series further. Compound **12** was more potent in the TR-FRET assay than **9** ($pIC_{50} = 6.7$ vs 6.0) and more selective (EGLN $pIC_{50} < 4.3$ vs 5.7). As a consequence of its increased potency and reduced size, compound **12** was more ligand efficient than **9** (LE 0.57 vs 0.34). Unfortunately compound **12**, unlike **9**, did not exhibit any detectable cellular activity. At this early stage this was not considered to be a major issue as

it was thought that increasing the cLogP during optimisation would help in obtaining a cellular penetrant compound.

I.3.2.2 Pyridone series

Despite displaying only moderate inhibition of JmjD3 in the TR-FRET assay ($pIC_{50} = 4.7$) and no detectable activity in the cellular assay, compound **10** was considered a good starting point for optimisation. The attraction of compound **10** lay in its good LE and LLE, driven by its small size (MW = 187) and very low lipophilicity (cLogP = -0.7). The aim of the follow up work was to increase the potency in the primary assays, increase the selectivity over other related enzymes and identify a compound which was active in the cell.

Suzuki cross-coupling, reductive amination, and BBr_3 deprotection were the key reactions for the optimisation of this template.

I.3.2.3 Pyridyl-pyrimidine series

Initial profiling of compound **11** showed it to have moderate activity against JmjD3 ($pIC_{50} = 4.8$) and no detectable cellular activity. Due to its relatively large size and lipophilic nature, compound **11** initially appeared to be less attractive than the other hits (**9** and **10**) when comparing LE and LLE. However, unlike **9** and **10**, **11** showed no detectable activity against EGLN. It was this selectivity profile which made compound **11** an attractive starting point for optimisation.

The pyridyl-pyrimidine template was optimised using a variety of methodologies such as Buchwald amination, Mitsunobu reaction, S_NAr , and Suzuki and Negishi palladium-catalysed cross coupling reactions. The Negishi cross-coupling reaction was a key step at

different stages of the construction of the pyridyl-pyrimidine series and will be discussed further in the next section.

I.4 C-C coupling reactions

The palladium-catalysed cross coupling between an organometal and an organic electrophile (Equation 4) has developed into probably the most general and selective way to form carbon-carbon bonds of the last 40 years.



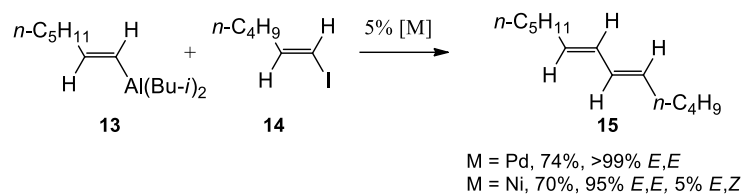
Equation 4.

Palladium-catalyzed cross coupling reactions to form bonds between two sp^2 carbons can use various organometals, based on ten or more different metals, including boron (Suzuki-Miyaura), tin (Stille), zinc, aluminium and zirconium (Negishi), silicon (Hiyama/Denmark), and magnesium (Kumada-Corriu).

This chapter will discuss aspects of the palladium-catalysed cross coupling reaction involving zinc organometals, which is known as the Negishi reaction, surveying key features and highlighting selected recent developments.

I.4.1 Organozinc reagents in context

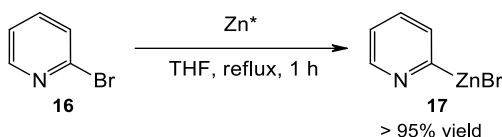
In 2010, Negishi was awarded the Chemistry Nobel Prize (along with Heck and Suzuki) for his work on palladium-catalyzed coupling. In 1977, he published the first stereoselective enyne synthesis using a palladium-catalysed coupling of an alkynylzinc nucleophile.⁵⁸ In the same period, Negishi's group described palladium- and nickel-catalysed cross coupling reactions to form aryl-aryl and benzyl-aryl bonds in seminal papers.^{59,60,61,62} Both nickel and palladium complexes are efficient catalysts, but the palladium-based species tend to be superior in terms of yields and stereoselectivity, as shown in Scheme 6.⁶³



Scheme 6. Stereoselectivities of Pd and Ni -catalysed synthesis of dienes.

While organometals based on the more electropositive metals, such as Li and Mg, are more reactive, they are less useful than Zn in catalytic cycles. Moreover, due to their high reactivity, they display poor chemoselectivity as they react with functionalities such as nitrile and carbonyl groups. Organozinc reagents are generally much more tolerant towards such functionalities than organomagnesium (*e.g.* Grignard) and organolithium reagents. They can tolerate nitrile, nitro, amino and various oxygen-containing functional groups, and the less reactive carbon halogen bonds (C-F, C-Cl and, in some cases, C-Br bonds).⁵⁸ Organolithium and Kumada-Corriu reagents are therefore rarely used in palladium-catalysed cross coupling reactions.⁶⁴ However, they are very useful for the preparation of other organometals containing metals of intermediate electropositivity such as Zn, B and Sn. Organometallic reagents of sp^3 carbon can be unstable and decompose readily by β -hydride elimination or protodemetalation.⁶⁵ Zn, being more electropositive than B and Sn, is less susceptible to β -hydride elimination, which makes the Zn-based methodology a better candidate for sp^3 - sp^3 C-C bond formation.

Organozinc reagents have been known for more than 150 years; the first well characterised organozinc compound, diethylzinc, was prepared by Frankland in 1849.^{66,67} Organozinc compounds can be very stable; for example, Coleridge *et al.* showed that a solution of 2-pyridylzinc bromide **17** in THF could be stored at room temperature for one year without significant degradation (Scheme 7).⁶⁸



Scheme 7. Preparation of 2-pyridylzinc bromide.

In addition, the C-Zn bond is highly covalent which gives access to configurationally stable organozinc reagents, whereas organolithium and Grignard reagents would potentially undergo racemisation at comparable temperatures;⁶⁹ organozincs would therefore be the reagents of choice for chiral organometallics. Despite the effectiveness and stability of organozinc reagents, they have not been fully used in synthesis because of perceived difficulties in their preparation. Recently methods have been developed to access these attractive organozinc reagents more easily and reliably.

I.4.2 Preparation of organozinc reagents

Organozinc reagents can be divided into three main types:

- Organozinc halides, RZnX
- Diorganozincs, R_2Zn
- Organo-zincates, R_3ZnM (M is, in general, Li or MgX).

The zincates are the most reactive due to the presence of negative charge on the zinc centre (Figure 26).



Figure 26. Reactivity order of organozinc reagents.

Various methods of preparation of organozinc reagents will be covered in this section, starting from the common preparation *via* organometals and halides and finishing with the recent direct metallation methods.

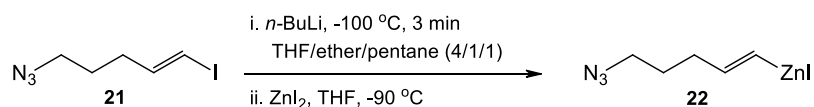
I.4.2.1 Preparation of organozinc reagents from Grignard and organolithium

Organozinc halides can be prepared from organolithium and Grignard reagents *via* transmetallation (Scheme 8).



Scheme 8. Preparation of an organozinc bromide from a Grignard reagent.

The scope of this method depends on the availability of the organolithium or Grignard reagents and their tolerance of various functionalities. Despite the low tolerance of organolithium reagents to many functionalities, halogen–lithium exchange at low temperature ($-100\text{ }^{\circ}\text{C}$ to $-90\text{ }^{\circ}\text{C}$) has been used to prepare organolithiums containing cyano⁷⁰ or nitro⁷¹ groups. These functionalised organolithiums could subsequently be transmetallated with zinc bromide. An example of this procedure is shown in Scheme 9, where an alkenylzinc bearing an azido group is prepared. Direct insertion of zinc into the organohalide was unsuccessful for this substrate. The alkenylzinc **22** was prepared by lithium-iodine exchange of alkenyl iodide **21** with *n*-BuLi at $-100\text{ }^{\circ}\text{C}$, followed by a transmetallation using zinc iodide at $-90\text{ }^{\circ}\text{C}$ in THF.



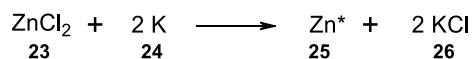
Scheme 9. Preparation of alkenylzinc.⁷²

In the earlier literature, demanding methods of preparation like this are relatively common. However, recent advances have made this class of reagents much easier to prepare.

I.4.2.2 Direct preparation of organozinc reagents from organohalides

I.4.2.2.1 Rieke's method

Rieke *et al.* developed a method to form organometallic reagents from powders of reactive metal.⁷³ This method covers metals such as Cd, Ni, Cu, Mg and Zn, and enabled the preparation of moderately to highly reactive metal powders by reducing metal salts (Scheme 10).



Scheme 10. Metal salt reduction.⁷⁴ K metal is the reducing agent and Zn* is the reactive Zn powder.

In the case of Zn, the reactive zinc powder reacts quickly with alkyl halides (iodides, bromides and chlorides) by oxidative addition to form the desired organozinc compounds. The activated zinc also reacts with vinyl bromides, aryl iodides and bromides. This method is compatible with nitriles, esters, ketones and chlorides (Table 8).

Organohalide	Product	Equiv Zn*	T	t (h)	Yield (%)
 27a	 28a	1.2	rt	4	100
 27b	 28b	1.0	rt	1	100
 27c	 28c	2.0	rt	3	100
 27d	 28d	2.0	reflux	1.9	100

Table 8. Zincation of organohalides with activated zinc.⁷³

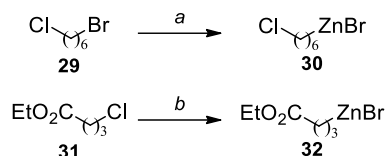
A large number of organozinc reagents (282) prepared by the Rieke method are commercially available from Rieke Metals at research scale and pilot plant quantities.⁷⁵ In addition, the Rieke Metals company converts specific halides on demand.

The organozinc reagents can be prepared as solutions in ethereal solvents such as THF, using Rieke's method. Coleridge *et al.* used this method to prepare a solution (1 M) of 2-pyridylzinc bromide **17** in THF (Scheme 7).⁶⁸ The solution was stable for one year without significant loss of activity.

I.4.2.2.2 Huo's method

Another method to prepare alkylzinc reagents was developed by Huo. This simple method enables the formation of alkylzinc compounds from unactivated alkyl halides (bromides and chlorides).⁷⁶ This zincation method uses zinc dust (powder, granule or shot can be used) and iodine. Potentially, the iodine may act by cleaning the metal surface (by reacting with the

zinc oxide film). Zincation of alkyl chlorides, which are less reactive than alkyl bromides, requires the presence of a bromide salt (LiBr or R₄NBr in a 1:1 ratio with the alkyl chloride) in addition to the iodine (Scheme 11). Dipolar aprotic polar solvents such as DMA, DMF, NMP, DMSO and DMPU gave the best results.



Scheme 11. Zincation of alkyl bromide and chloride. Conditions: (a) Zn (dust), I₂, DMA; (b) Zn (dust), I₂, Bu₄NBr, DMA.

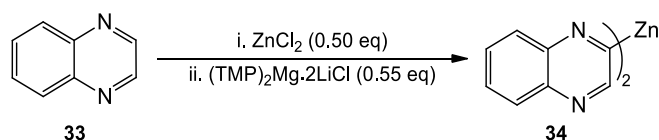
This method can tolerate various functionalities such as alkyl chlorides (**30**), esters (**32**), nitriles, alkenes, amides and acetals.

I.4.2.3 Preparation of organozinc reagents by direct metallation

In addition to the three methods described earlier, direct metallation is developing as a valuable alternative strategy for the preparation of organozinc compounds. Recently, methods for the metallation or transformation of a C-H bond to a C-metal bond have been developed by various groups. The direct metallation methods use mixtures of several components, often called “complex metallators”.⁷⁷

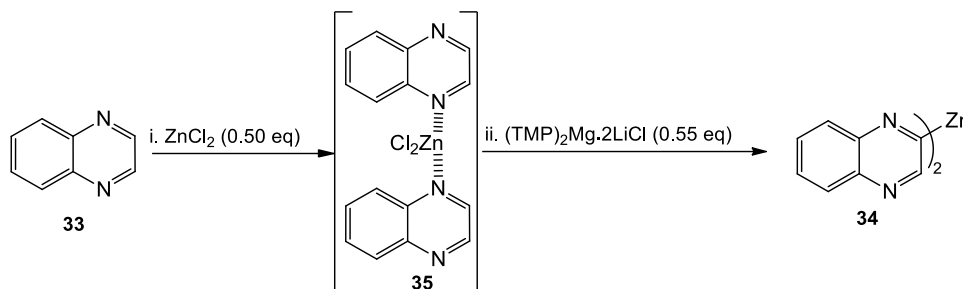
I.4.2.3.1 Knochel’s method

Knochel *et al.*⁷⁸ used the magnesium *bis*amide base (TMP)₂Mg·2LiCl, known as the Turbo Hauser base in the presence of ZnCl₂, to prepare diarylzinc **34** (Scheme 12).



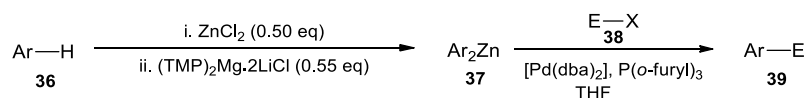
Scheme 12. Zincation of quinoxaline.⁷⁸

The Turbo Hauser base enables the direct zincation of a variety of interesting aryl and heteroaryl compounds including functionalised species. The very reactive quinoxaline **33** was zincated successfully using this method (Table 9). Knochel *et al.* showed by mechanistic studies that a Zn complex (**35**) is formed by reacting the hetero-arene with ZnCl_2 .⁷⁸ This Zn complex reacts with the magnesium base, $(\text{TMP})_2\text{Mg}\cdot 2\text{LiCl}$ to form the desired organozinc reagent after fast transmetalation (Scheme 13).



Scheme 13. Postulated metallation of quinoxaline.

The organozinc reagents formed by this method were used successfully in Negishi cross-coupling reactions (Scheme 14 and Table 9). 2-Bromopyrimidine was zincated using this method and the resulting organozinc product was used in an almost quantitative Negishi cross-coupling with 4-iodobenzonitrile with the nitrile function and the very reactive C-Br bond staying intact. The Negishi cross-coupling between the ethyl 4-chlorobenzoate with ethyl 4-iodobenzoate using these conditions is also remarkable. Indeed, the reaction was high yielding (90%) with the ester functionality and the Cl-C bond untouched under these conditions.



Scheme 14. Formation of organozinc reagents used in Negishi cross-coupling.

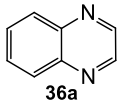
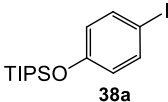
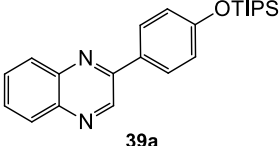

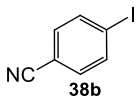
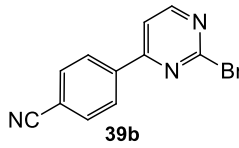
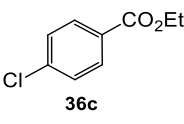
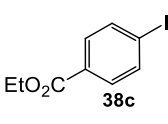
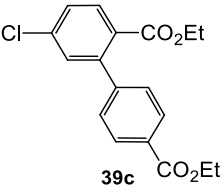
Aryls	t (h)	E-X	Product	Yield (%)
	2			71
	12			91
	12			90

Table 9. Products obtained after zincation using Turbo-Hauser metallation (ZnCl_2 (0.5 eq), $(\text{TMP})_2\text{Mg} \cdot 2\text{LiCl}$ at 25 °C) followed by a Negishi cross-coupling.⁷⁸

Knochel *et al.* have recently described the zincation of highly functionalised alkenes bearing various functionalities such as ester, nitrile, amine and nitro units, using the TMP bases.⁷⁹

Table 10 summarises some of the remarkable examples described in this recent paper.

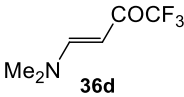
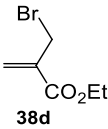
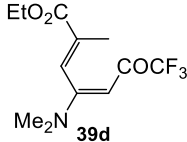
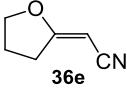
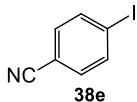
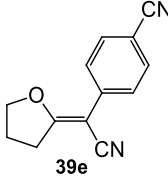
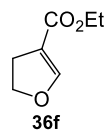
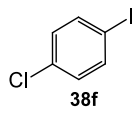
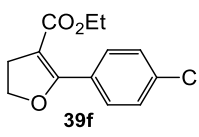
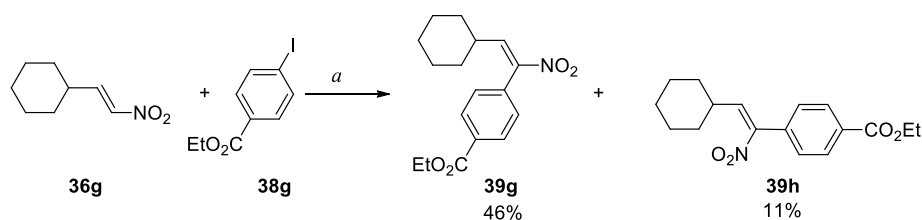
Alkenes	E-X	Conditions	Product	Yield (%)
		a		85
		b		62
		c		55

Table 10. Zincation of substituted alkenes using TMP bases followed by quenching with various electrophiles. Metallation conditions: (a) $\text{TMPZnCl}\cdot\text{LiCl}$; 5% $\text{CuCN}\cdot 2\text{LiCl}$ added; (b) $\text{TMPZnCl}\cdot\text{LiCl}$; $[\text{Pd}(\text{dba})_2]$ (3%), $\text{P}(2\text{-furyl})_3$ (6%); (c) $\text{TMP}_2\text{ZnCl}\cdot 2\text{LiCl}$; $[\text{Pd}(\text{dba})_2]$ (3%), $\text{P}(2\text{-furyl})_3$ (6%).⁷⁸

Compound **36d**, containing a sensitive trifluoroacetyl group, was successfully zincated and quenched with ethyl 2-(bromomethyl)acrylate to form compound **39d** after isomerisation of the double-bond during chromatographic purification. This paper showed that alkenes containing esters and nitriles could now be zincated at practical temperatures and, in general, TMP bases allowed smooth zincation. In addition, they demonstrated the first example of an α -zincation of a nitroalkene with the use of compound **36g** (Scheme 15).⁷⁹



Scheme 15. Alkene zincation using TMP base. Conditions: (a) i) $\text{TMPZnCl}\cdot\text{LiCl}$, $-50\text{ }^\circ\text{C}$, 0.5 h; ii) **38g** $[\text{Pd}(\text{dba})_2]$, $\text{P}(2\text{-furyl})_3$.

I.4.2.3.2 Mulvey's method

Mulvey *et al.* presented another complex metallator: [(TMEDA) . Na(μ -TMP)(μ -tBu)Zn(tBu)] (Figure 27), which can form organozinc compounds with high and sometimes unexpected regioselectivity.⁸⁰

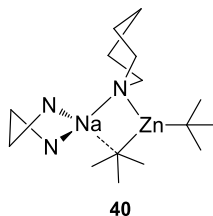
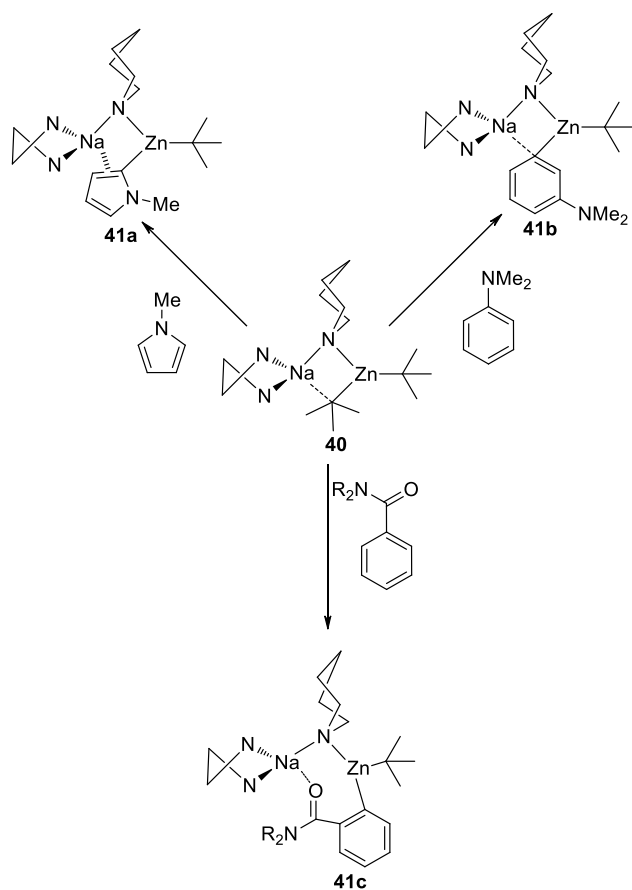


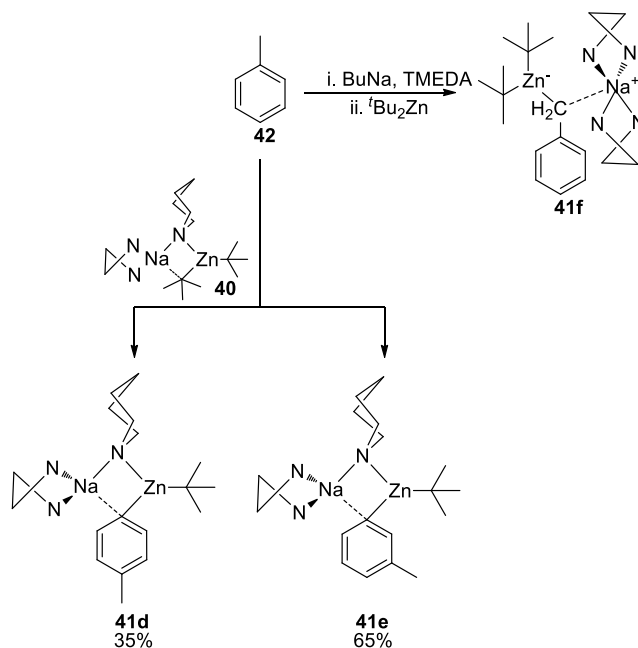
Figure 27. Complex metallator: [(TMEDA).Na(μ -TMP)(μ -tBu)Zn(tBu)]. Methyl groups omitted for clarity.

Metallation using this reagent is alkali-metal mediated and synergic. A proton is replaced by a zinc in the presence of an alkali metal; without the alkali metal, the reaction does not occur. This complex enables regioselective zincation of several benzene derivatives and a pyrrole, as exemplified in Scheme 16. *N,N*-Diisopropylbenzamide is monozincated at the *ortho*-position⁸¹ and 1-methylpyrrole at the α -position (crystal structure of compound and NMR spectra showing disappearance of 2- C^1H signal relative to the 1-methylpyrrole, suggesting a π -Na interaction);⁸² both results are identical to that expected from a DoM reaction. However, *N,N*-dimethylaniline is monozincated at the *meta*-position, whereas an *ortho*-zincation was expected.⁸³ The *meta*-zincated product **41b**, which is stabilised by coordination with Zn and Na, was isolated at room temperature as a crystalline solid.



Scheme 16. Examples of regioselective zincation. Methyl groups are omitted for clarity; R = *i*-Pr and ||| indicates a π -interaction between sodium and *N*-methylpyrrole.

Zincation of toluene **42** (Scheme 17) is another good example of unexpected regioselectivity. The complex metallator gave a mixture of *para*- **41d** and *meta*- **41e** regioisomers instead of the most thermodynamically stable benzyl isomer **41f** (obtained by indirect zincation/transmetallation).⁸⁴



Scheme 17. Toluene zincation by two methods leading to three regioisomer products.

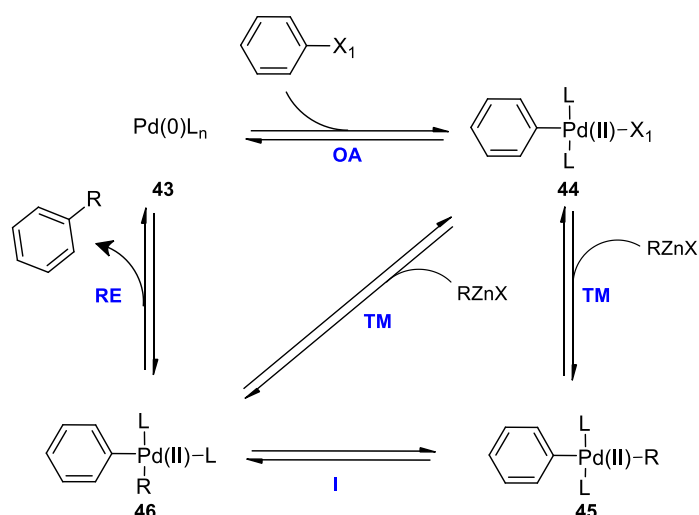
Newer methods of zincation appear to show considerable potential for the generation of unusual regiochemistries. The full value of these procedures will not be appreciated until considerably more work has been done.

Direct zincation or metallation is a developing area which is being explored by a number of groups around the world, and will probably expand furthermore in the near future. The approach avoids the use of costly halide substrates and complements existing patterns of regioselectivity.

I.4.3 Mechanism of the Negishi reaction

The Negishi reaction mechanism (Scheme 18) is related to those of the other palladium-catalyzed reactions such as Suzuki and Stille reactions.⁸⁵ The Pd(0) active species undergoes an oxidative addition of the organic electrophile to afford the Pd(II) species. This new species undergoes transmetalation with the organozinc halide reagent to give the *cis* or *trans*

Pd(II) intermediate. In the case of the *trans* Pd(II) intermediate, an isomerisation is required to give the productive *cis* intermediate. The transmetalation will be covered in more detail in the next section. The catalytic cycle finishes with a reductive elimination step which releases the product of C-C bond formation and regenerates the catalytic Pd(0) species. This final reductive elimination step is also under the control of palladium ligands, especially in the case of the sp^3 - sp^3 C-C bond formation. The reductive elimination competes with β -hydride elimination of the diorganopalladium complex, which leads to side products. To increase the rate of the reductive elimination relative to β -hydride elimination, the leaving partners must be in a *cis*-geometry preferentially. This is achieved by using bulky ligands (*e.g.* PPh₃ or P^tBu₃) or bidentate ligands with a wide bite angle, like dppf.⁸⁶

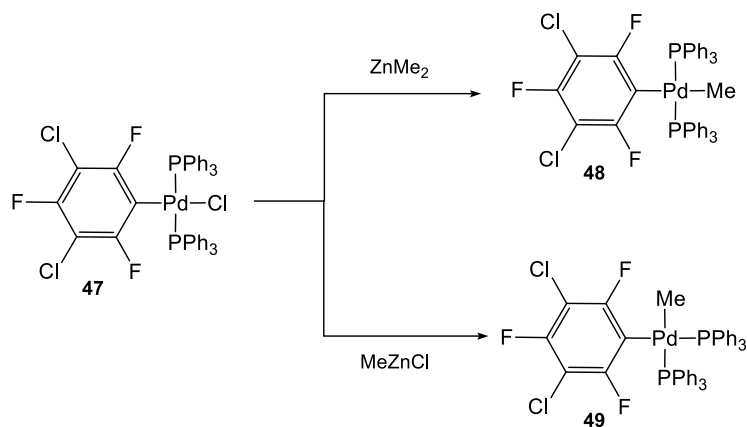


Scheme 18. Negishi reaction mechanism. OA = oxidative addition, TM = transmetalation, I = isomerisation, RE = reductive elimination

I.4.3.1 Transmetalation step

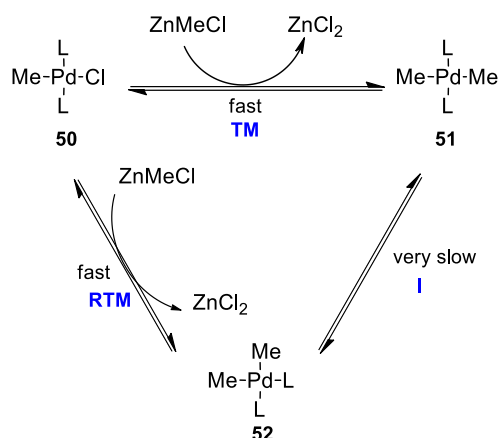
More complex aspects of the transmetalation step have begun to emerge, especially from the work of Espinet *et al.*^{87,88} They showed that in the case of the transmetalation of *trans*-[PdR_fCl(PPh₃)₂] (R_f = 3,5-dichloro-2,4,6-trifluorophenyl) **47** with ZnMe₂, the *trans*-

$[\text{PdR}_f\text{Me}(\text{PPh}_3)_2]$ **48** was formed initially, whereas the *cis*- $[\text{PdR}_f\text{Me}(\text{PPh}_3)_2]$ **49** was formed directly using MeZnCl (Scheme 19).



Scheme 19. Transmetalation of *trans*- $[\text{PdR}_f\text{Cl}(\text{PPh}_3)_2]$ ($\text{R}_f = 3,5\text{-dichloro-2,4,6-trifluorophenyl}$).

The same researchers studied the transmetalation of $[\text{PdMeCl}(\text{PPh}_3)_2]$ with MeZnCl and discovered that the direct isomerisation between the *cis* and *trans* Pd(II) intermediates was actually very slow, and that the *cis* intermediate could be produced by fast retrotransmetalation between **50** and **51**, followed by a transmetalation of **50** (Scheme 20). They studied the isomerisation of *trans*-isomer **51** to *cis*-isomer **52**: a reaction time of 10 h in solution in THF at 273 K was required for the isomerisation of *trans*-isomer **51**. Isomerisation of *cis*-isomer **52** to *trans*-isomer **51** at 223 K was negligible. However, addition of ZnCl_2 to solutions of *cis*- and *trans*-isomers **51** and **52** in THF at 223 K, produced **50** very rapidly showing that the transmetalation between **50** and MeZnCl to form either *cis*- or *trans*-isomers (**51** or **52**) is very fast. This result, combined with the observation that *trans*-isomer **51** appears to be produced faster than the *cis*-isomer, supports the hypothesis that the *cis* intermediate **52** could be produced by fast retrotransmetalation between **50** and **51**, followed by a transmetalation of **50**.



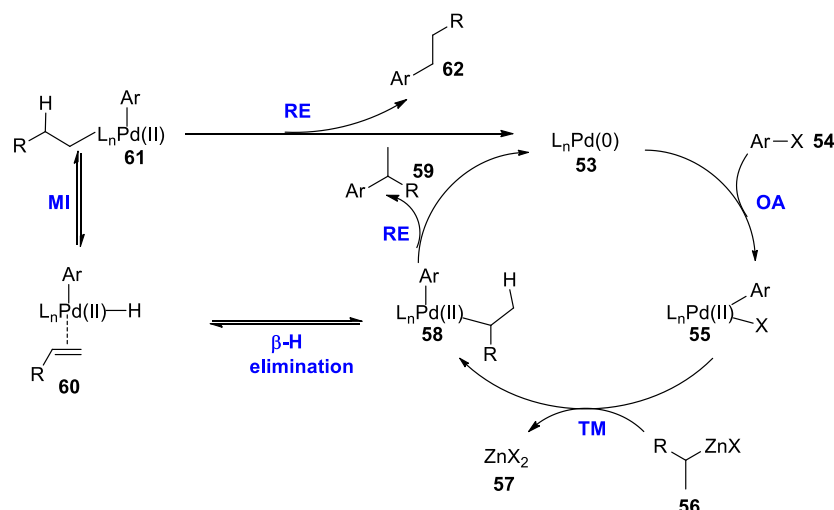
Scheme 20. Isomerisation vs retrotransmetallation. L = PMePh₂, solvent: THF; TM = transmetallation, I = isomerisation, RTM = retrotransmetallation.

Transmetallation and its reverse are faster than the reductive elimination, which may increase the chances of forming new intermediates and consequently potentially increase the extent of side product formation.⁸⁸ Controlling the transmetallation step to produce the *cis*-intermediate, and its rate relative to reductive elimination (to decrease the formation of side products), will be key to the improvement of the Negishi cross-coupling in terms of yield and rate. Other control measures, such as additives, have been studied to improve this reaction and will be covered in more detail.

I.4.3.2 Reductive Elimination

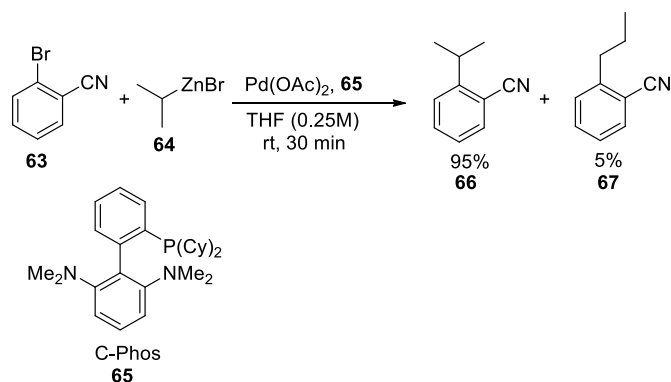
It is largely believed that reductive elimination is facilitated by bulky ancillary ligands. This is potentially due to the relief of steric hindrance by elimination of the product and by formation of a metal with a lower coordination number.⁸⁹ In addition to the steric effect, the reductive elimination is also governed by the electronic nature of the ligands. The reductive elimination process is favoured thermodynamically when the metal is electron-deficient. Complexes containing ligands with electron-donating groups are more electron-rich, and the reductive elimination of such complexes is slower than complexes containing ligands with weaker electron-donating groups.

The cross-coupling reactions involving sp^3 C-halides are more difficult than those involving sp^2 carbons. First the oxidative addition of sp^3 C-halides is much more difficult because sp^3 C-X bonds are less electron poor than sp^2 C-X bonds. Secondly, due to the absence of π -electrons in the alkyl group, the oxidative addition product cannot be stabilised by back-donation to the metal. Finally, the presence of C-H bonds β to the reaction centre in the alkyl group, in combination with the lower stability of alkyl-metal intermediates increases the possibility of side reactions such as β -hydride elimination/migratory insertion (Scheme 21). These side reactions can subsequently compete with transmetallation and reductive elimination steps.⁹⁰ One obvious way to suppress these β -hydride elimination/migratory insertion, would be to accelerate the reductive elimination step.



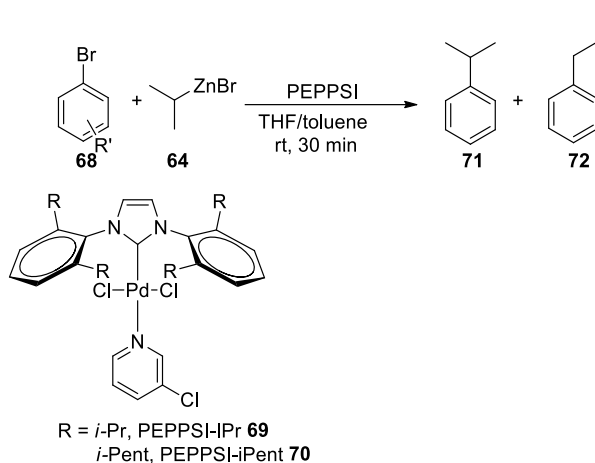
Scheme 21. Negishi reaction mechanism. OA = oxidative addition, TM = transmetallation, I = isomerisation, RE = reductive elimination, β -H = β -hydride, MI = migratory insertion.

One option to accelerate the rate of reductive elimination vs β -hydride elimination involves the use of sterically demanding ancillary ligands. Buchwald *et al.* demonstrated that near complete suppression of β -hydride elimination was achievable in the case of Negishi cross-couplings of aryl halides with secondary alkylzinc halides when a bulky C-Phos phosphine ligand was used (Scheme 22).⁹¹



Scheme 22. Negishi cross-coupling reaction with *iso*-propylzinc bromide.

Organ *et al.* successfully reduced the rate of β -hydride elimination vs reductive elimination by using the pyridine-enhanced precatalyst preparation, stabilization and initiation (PEPPSI) catalyst. They increased the bulk of the PEPPSI catalyst in order to accelerate the rate of the reductive elimination (Table 11).⁹²



Aryl bromide	Catalyst	Yield (%)	71 : 72
R' = 4-CHO	69	64	6 : 1
	70	78	39 : 1
R' = 4-COCH ₃	69	99	6 : 1
	70	98	30 : 1
R' = 4-CO ₂ CH ₃	69	83	5 : 1
	70	99	40 : 1
R' = 4-CN	69	85	3 : 1
	70	92	27 : 1
R' = 3-CN	69	77	1 : 1.4
	70	84	11 : 1
R' = 2-CN	69	99	1 : 8
	70	80	2.4 : 1

Table 11. Negishi cross-coupling reaction between *iso*-propylzinc bromide and arylbromides.

Table 11 shows that good yields were obtained with *i*Pent, likewise with the *IPr* and, most importantly, the selectivity for the branched product was maintained with the *i*Pent PEPPSI catalyst regardless of the position of the R' group on the phenyl substrate, whilst the selectivity was inverted in favour of the linear product with the *IPr* PEPPSI catalyst in the case of 2- and 3-cyano substituted bromophenyl units.

I.4.3.3 PEPPSI catalyst

The *N*-heterocyclic carbene (NHC) is a key component of the PEPPSI catalysts (Figure 28).

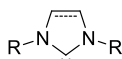


Figure 28. *N*-heterocyclic carbenes.

NHC ligands have been often referred to as phosphine analogs; they are σ -donors, but tend to be better donors than even the best σ -donor phosphines according to the Tolman electronic parameters (TEP) (Table 12).⁹³

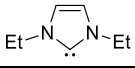
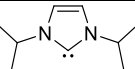
Ligands	$\nu(\text{CO}) \text{ cm}^{-1}$
$\text{P}(\text{Me})_3$	2064.1
$\text{P}(\text{tBu})_3$	2056.1
	2052.8
	2051.5

Table 12. Calculated TEP $\nu(\text{CO})$ for $\text{Ni}(\text{CO})_3\text{L}$ with $\text{L} = \text{PR}_3$ or NHC ligands.⁹⁴

TEP is a measure of the electronic-donating capability of a ligand (L), determined by measuring the stretching frequency of the CO bond ($\nu(\text{CO})$) in the $\text{Ni}(\text{CO})_3\text{L}$ complex. σ -Electron-donating ligands increase the electron density around the Ni metal which releases some of this electron density into the CO bond by π -back donation. Indeed, the metal and the CO can form a π bond with the metal donating *d* electrons into the empty anti-bonding π^* orbital of CO. By donating electrons to the CO, the metal strengthens the M-C bond and at the same time weakens the C-O bond, which is then translated by a reduced $\nu(\text{CO})$ frequency. Thus, the most electron-donating ligands are characterised by lower $\nu(\text{CO})$ frequencies. $\text{P}(\text{tBu})_3$ with a $\nu(\text{CO})$ of 2056.1 is considered one of the strongest σ -donors amongst the phosphines, and Et- or *iPr*-NHC with $\nu(\text{CO})$ of 2052.8 and 2051.5, respectively, are even stronger σ -donor than even the strongest σ -donor phosphines.

The bulky phosphine ligands increase the electron density around the palladium and also accept electrons from the metal by back-bonding into the P-R σ^* orbital.⁹⁵ The possibility of π -back donation by NHC ligands is a much discussed subject. For a long time NHC ligands were thought to act mainly as σ -donors with minimal π -back donation. Nolan and Meyer showed that the π -orbitals of the NHC ligands can accept electrons from metals.^{96,97}

The phosphine ligands are often described by their Tolman cone angles (θ) (Figure 29) which can be very large, but this descriptor cannot be used for the NHC ligands because of their “fan” or “fence”- type structure.^{96,98}

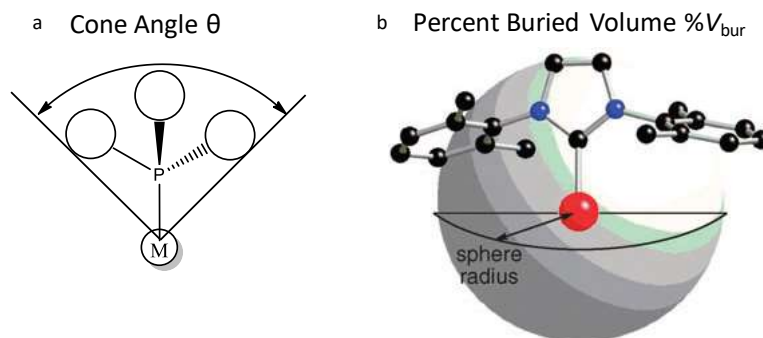


Figure 29. Tolman cone angle (θ) and Percent buried volume ($\%V_{bur}$). (a) Tolman cone angle (θ); Percent buried volume ($\%V_{bur}$) (b).⁹⁹

Nolan *et al.* introduced the percent buried volume ($\%V_{bur}$) concept so the relative sizes of phosphine and NHC ligands could be compared. In this model the metal is in the centre of a sphere which has a defined radius. The $\%V_{bur}$ represents the volume of the sphere potentially occupied by the ligand. Thus, the bulkier the ligand the more space it will occupy in the sphere, and so the greater the $\%V_{bur}$. Table 13 shows that certain NHC ligands (IPr) could occupy similar volume as some bulky phosphines (PCy_3).

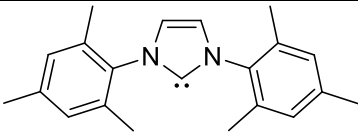
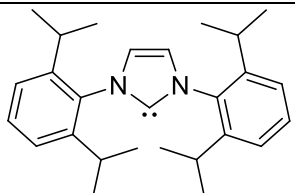
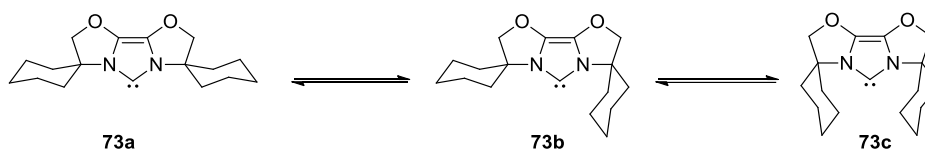
Ligands	% V_{bur}
PCy ₃	32
P ^t Pr ₃	32
	26
	28

Table 13. % V_{bur} values of NHC and phosphine ligands.¹⁰⁰

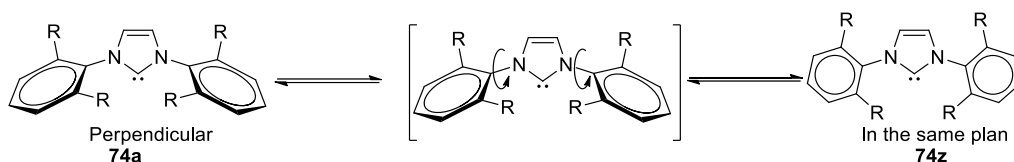
The NHC ligands can be described as ligands with flexible steric bulk, and this flexibility explains why the NHC ligands facilitate many steps of the Negishi cross-coupling reaction.¹⁰¹ Glorius *et al.* suggested that the presence of three conformers of the NHC was important in the case of Suzuki cross-couplings (Scheme 23).¹⁰¹



Scheme 23. NHC conformers.

Glorius suggested that the more open conformer **73a** could allow the oxidative addition step to proceed easily, and the more hindered conformers **73b** and **73c** could increase the rate of the reductive elimination step.¹⁰¹

In the PEPPSI catalyst, it is possible that the phenyl ring could rotate, which would allow the adoption of various conformers between the conformer in which the phenyl ring is perpendicular to the imidazole ring plane, and the conformer in which the phenyl ring is in the same plane as the imidazole ring (Scheme 24). These potential conformers could facilitate various steps of the Negishi cross-couplings.

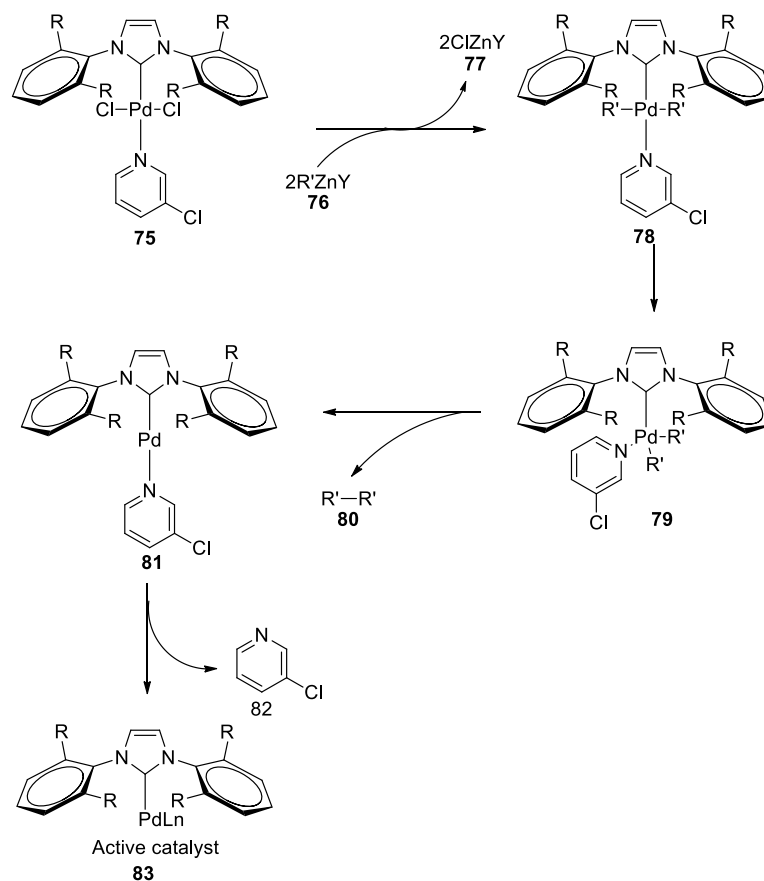


Scheme 24. Potential PEPPSI conformers.

The nature of R substituents on the phenyl ring has an almost negligible effect on the electronic properties of the system, but has significant impact on the steric environment around the metal.¹⁰² The best way to change the electronic properties of the ligand is to change the nature of the azole ring.¹⁰³

I.4.3.3.1 PEPPSI Mechanism

The 3-chloropyridyl ligand, referred as a “throw-away ligand”,¹⁰² helps in stabilising the whole complex, and also helps in the formation of the active species (Scheme 25). The first step in the formation of the active catalyst system could be a double transmetallation to form intermediate **78**. To facilitate the RE, an isomerisation would probably be required to form intermediate **79**. The last step to form the active species is the dissociation of the 3-chloropyridine ligand which is facilitated by the high *trans*-effect of the NHC ligands.¹⁰³ The pyridine ligand was shown to be very labile by Grubbs *et al.*¹⁰⁴



Scheme 25. Proposed mechanism for the formation of the active catalyst.

Organ *et al.* studied the mechanism of Negishi reactions which use the PEPPSI catalyst.¹⁰² Organ and co-workers have used computational methods to reveal a range of interactions between alkyl groups on the aryl and the Pd centre (between ~ 3.315 and 3.265 \AA).¹⁰⁵ These agostic interactions are not permanent and disappear and reappear during the catalytic cycle; they contribute to the stabilisation of the complex and coordinatively saturate the Pd. It was proposed that these interactions could potentially also hinder four positions within the Pd coordination sphere, allowing the reactants to coordinate only to the Pd *anti* to the NHC (Figure 30). In the case of the oxidative addition step of IPr-Pd with EtBr, they showed that the Et group was approaching *anti* to Pd whilst the Br atom was approaching through one of the four positions so that it could interact with two hydrogens of the *i*-Pr group instead of with the Pd metal centre.

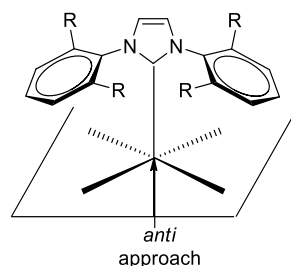
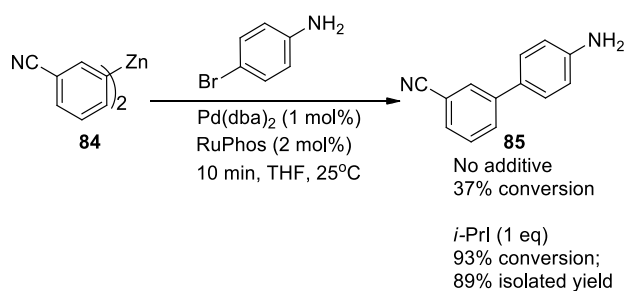


Figure 30. Potential reactant approach in the Pd coordination sphere.

Organ *et al.* proposed that the agostic C-H...Pd interactions between the NHC ligand and the Pd occur because they saturate the coordination sphere of the Pd; they potentially prevent agostic interactions between the hydrogen from the transferring alkyl substituent and the Pd, and subsequently reduce β -hydride elimination greatly.¹⁰⁵ This explains why PEPPSI catalysts are so efficient in the case of the formation of sp^3 - sp^3 and sp^3 - sp^2 (and *vice versa*) C-C bonds.

I.4.3.4 Additives

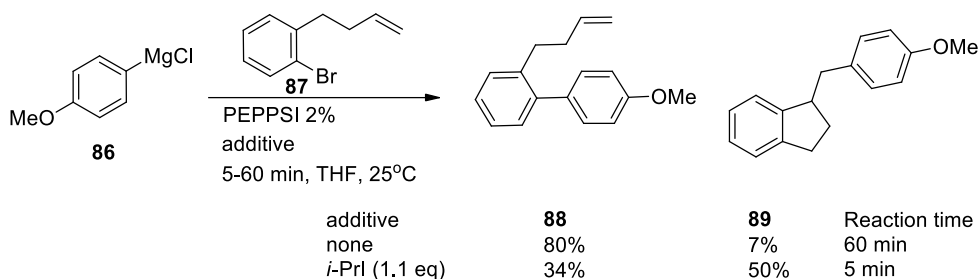
A number of groups have recently shown that additives can improve the rate and yield of Negishi coupling reactions. For example, Knochel *et al.*¹⁰⁶ have shown that the palladium catalysed cross-coupling of a zinc reagent is faster and gives higher yields in the presence of *i*-PrI than in the absence of the additive (Scheme 26).



Scheme 26. Acceleration of Negishi cross-coupling by *i*-PrI.

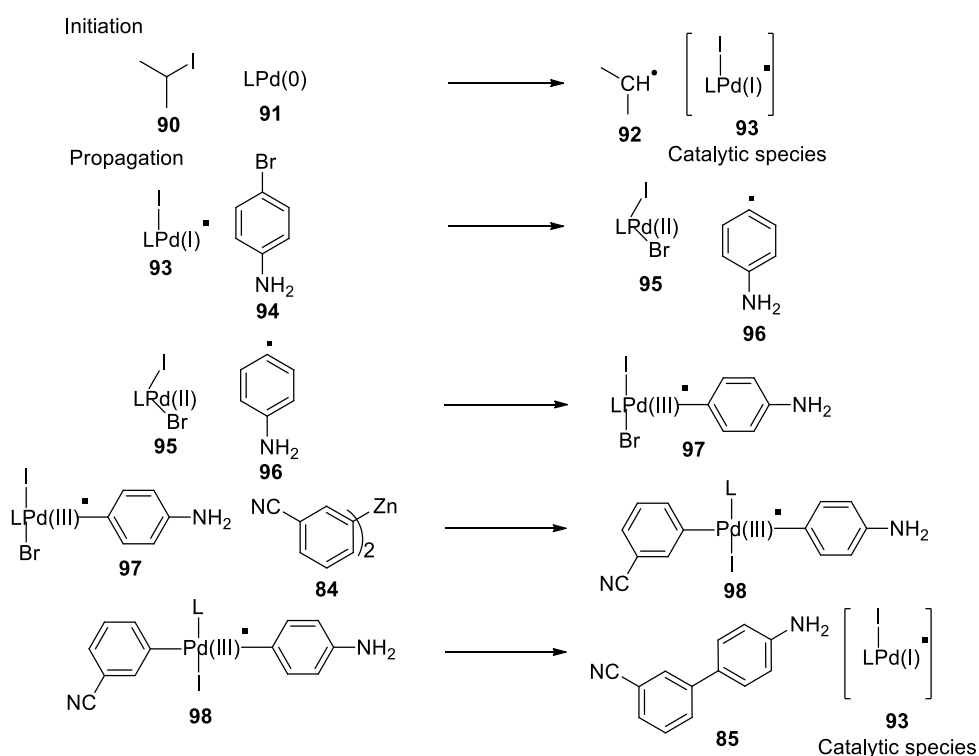
Knochel *et al.* used the *i*-PrI in the case of Kumada cross-coupling reaction and suggested that this cross-coupling reaction was occurring *via* a radical mechanism.¹⁰⁷ Osborn, Kochi

and Hegedus have all proposed this radical mechanism.^{108,109,110,111} In addition, Knochel showed that the reaction between **86** and **87** led to the formation of **88** and **89**, suggesting the formation of a radical intermediate, and so supporting further the radical cross-coupling mechanism (Scheme 27).



Scheme 27. Kumada cross-coupling of arylmagnesium chloride and aryl bromide containing a double bond.

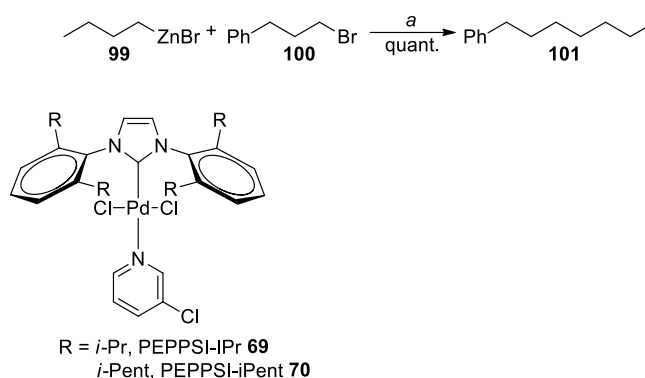
Potentially, the Negishi cross-coupling reaction shown in Scheme 26 could also occur *via* a radical mechanism; a proposed mechanism is shown in Scheme 28.



Scheme 28. Proposed mechanism for Negishi cross-coupling in the presence of *i*-PrI.

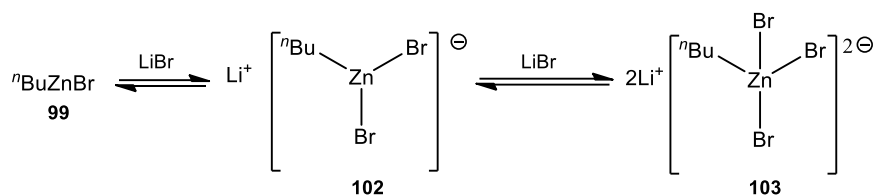
In this proposed mechanism, a radical Pd(I) intermediate **93** is formed in the initiation step. Subsequently in the presence of the aryl bromide **94** the radical Pd(I) **93** forms a dihalide Pd(II) **95** and an aryl radical **96**. This aryl radical is trapped by the dihalide Pd(II) **95** and forms a radical Pd(III) **97**, which after transmetalation provides the diaryl Pd(III) **98**. The cycle finishes by a reductive elimination resulting in the formation of the cross-coupling product **85** and regeneration the catalytic species radical Pd(I) **93**.

Organ *et al.*¹¹² studied the effect of organic and inorganic salts on sp^3 - sp^3 Negishi cross-coupling yields (Scheme 29).



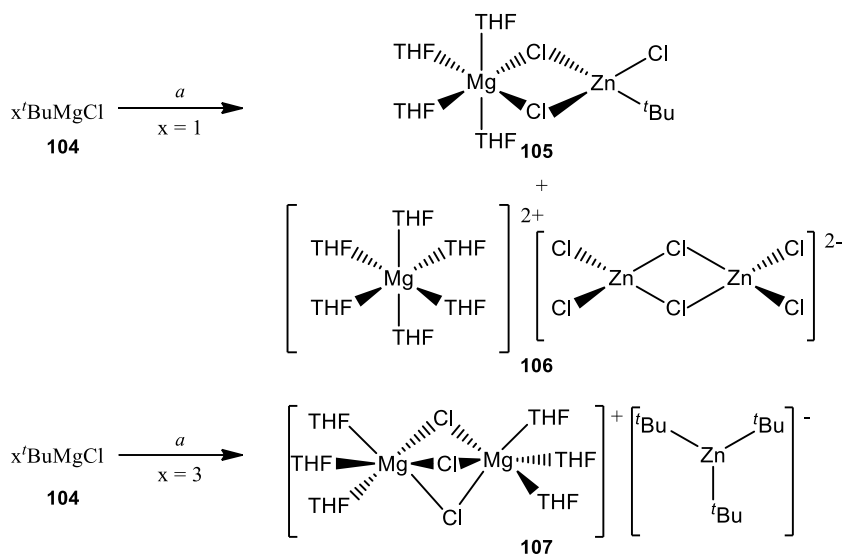
Scheme 29. Alkyl-alkyl cross-coupling. **Conditions:** (a) Pd-PEPPSI-IPr **69**, LiBr, THF-DMI, rt, 2 h.

Organ *et al.* have discovered that LiBr and LiCl additives (with LiBr being more effective than LiCl) improved the yield of difficult alkyl-alkyl cross-couplings catalysed by Pd-PEPPSI-IPr **69**. A slight excess of bromide salt (at least 1.4 eq relative to organozinc reagent) is required to obtain the best results. It was postulated that LiBr complexes with the organozinc reagent to form an organozincate of higher order such as $\text{Li}_m\text{Zn}^{(n)\text{Bu}}\text{Br}_3^{(2-m)}$ (**90**). This organozincate is believed to be the transmetallating reagent in the catalytic cycle (Scheme 30).



Scheme 30. Proposed formation of $\text{Li}_m\text{Zn}({}^n\text{Bu})\text{Br}_3^{(2-m)-}$.

Another group, that of Marder *et al.*,¹¹³ showed that adding MgCl_2 to phenylzinc reagents increased the rate of the Ni-catalysed cross-coupling by facilitating the transmetalation step. A bimetallic complex of MgCl_2 and zinc was characterised by X-ray crystallography. It is now believed that the structure of organozinc reagents entering the cross-coupling catalytic cycle is much more complex than a simple monomeric RZnX . Indeed, Hevia *et al.*¹¹⁴ revealed the structure of the products formed by reaction of ZnCl_2 with $x^t\text{BuMgCl}$ (x varying from 1 to 3) (Scheme 31).



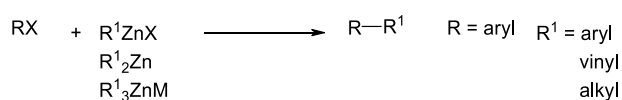
Scheme 31. Formation of various Mg-Zn complexes. Conditions: (a) ZnCl_2 , THF.

This simple reaction led to the formation of three different mixed metal complexes (depending on the amount of Grignard reagent); the structures were confirmed by X-ray crystallography. Tris(*tert*-butyl) magnesium zincate **107** successfully reacted with 4-

iodotoluene *via* Zn-I exchange at rt to afford a tris(aryl) magnesium zincate, which could potentially be a powerful reagent for the Negishi cross-coupling.¹¹⁴

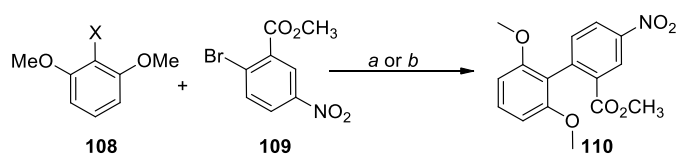
I.4.4 Scope of the Negishi coupling reaction

The Negishi cross-coupling reaction is being utilised more frequently as the methodology of choice for the formation of C-C bonds *via* coupling, due to the robustness of organozinc reagents, their high reactivity and compatibility with a wide range of functional groups. Organozinc halides, diorganozinc and zincate reagents can all be used to form the C-C bond (Scheme 32).^{59,115}



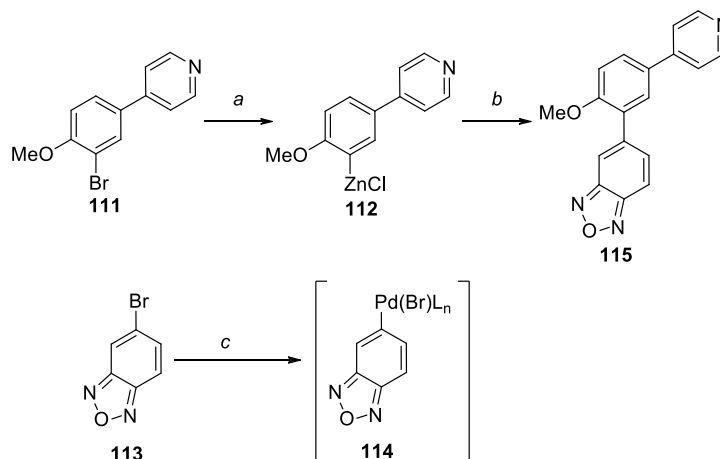
Scheme 32. Scope of Negishi reaction.

Ku *et al.*¹¹⁶ described an example in which Negishi cross-coupling was more effective than the Suzuki reaction (Scheme 33). Compound **110** was isolated in 75% yield, after a 24 h reaction at 100 °C using Suzuki conditions, whereas under Negishi conditions, **110** was isolated in 90% yield after 2 h reaction at 45 °C.



Scheme 33. Suzuki *vs* Negishi. Conditions: (a) X = B(OH)₂, PdCl₂(PPh₃)₂, Cs₂CO₃, DMF, 100 °C, 24 h, 75%; (b) X = ZnCl, PdCl₂(PPh₃)₂, THF, rt, 45 °C, 2 h, 90%.

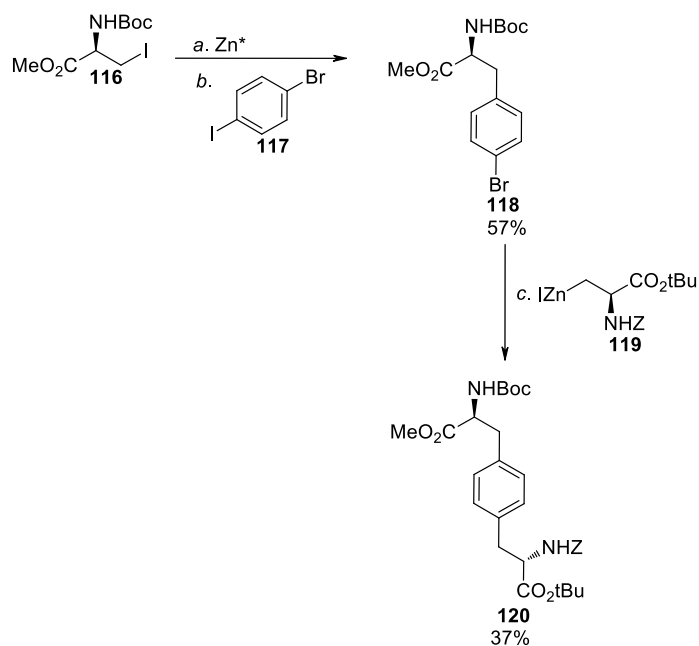
Manley *et al.*¹¹⁷ used the Negishi cross coupling in a scale up campaign to produce 4.5 kg of a selective PDE4D inhibitor **115** (Scheme 34).



Scheme 34. Scale up of **115**. Conditions: (a) i) HexLi, THF/pentane; ii) ZnCl_2 , THF; (b) **113/114** $\text{Pd}(\text{PPh}_3)_4$, DMF; (c) $\text{Pd}(\text{PPh}_3)_4$, DMF. L = PPh_3 .

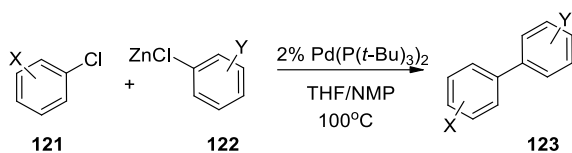
The yield of the Negishi key step was improved by pre-forming complex **114** from 5-bromo-2,1,3-benzoxadiazole **113** and $\text{Pd}(\text{PPh}_3)_4$, which was added to a solution of the zinc intermediate **112**. The initial low yield and slow reaction were attributed to complexation of palladium by 4-(4-methoxyphenyl)pyridine, which was assumed to be a good ligand for $\text{Pd}(0)$. This pre-complexation process enabled a faster (1 h instead of 16 h) Negishi reaction with a better yield (79% instead of 38%). Moreover, this procedure required a much lower loading of palladium catalyst (0.8% instead of 8%), which is less costly and meant less palladium residues were present in the product.

Jackson *et al.*¹¹⁸ used the Negishi cross-coupling for the synthesis of phenylene *bis*-alanine derivative **120** (Scheme 35). The synthesis of this enantiomerically pure and orthogonally protected phenylene *bis*-alanine derivative highlights the difference in reactivity between aromatic iodides and bromides.



Scheme 35. Synthesis of phenylene *bis*-alanine derivatives. Conditions: (a) Zn, cat. I₂, DMF; (b) Pd₂(dba)₃, P(*o*-Tol)₃, rt, 16 h; (c) Pd(OAc)₂, P(*o*-Tol)₃, DMF, 50 °C, 2 h.

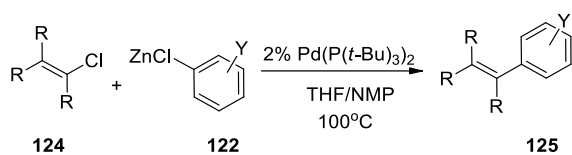
Fu *et al.* have developed a methodology for one particularly difficult Negishi cross-coupling based on bulky phosphine ligands.¹¹⁹ The issues they looked to resolve involved C-C bond formation from an aryl chloride. The low reactivity of aryl chlorides is potentially linked to the energy of the C-Cl bond dissociation (95 kcal/mol) which is high relative to the dissociation of C-Br (80 kcal/mol) and C-I (65 kcal/mol) bonds.¹²⁰ Therefore, the oxidative addition of Pd(0) into an aryl carbon-chlorine bond appears to be more difficult. Fu *et al.* showed that the Pd₂(dba)₃/P(*t*-Bu)₃ combination enabled Negishi cross-coupling of aryl and vinyl chlorides (Tables 14 and 15).¹¹⁹



Ar-Cl	Ar-ZnCl	Product	Yield (%)
 121a	 122a	 123a	96
 121b	 122b	 123b	76

Table 14. Negishi cross-coupling of aryl chlorides using $\text{Pd}_2(\text{dba})_3/\text{P}(t\text{-Bu})_3$.¹¹⁹

They successfully synthesised hindered biaryl systems and even the biaryl tetra-*ortho*-substituted **123b** in good yield using the $\text{Pd}_2(\text{dba})_3/\text{P}(t\text{-Bu})_3$ complex.¹¹⁹

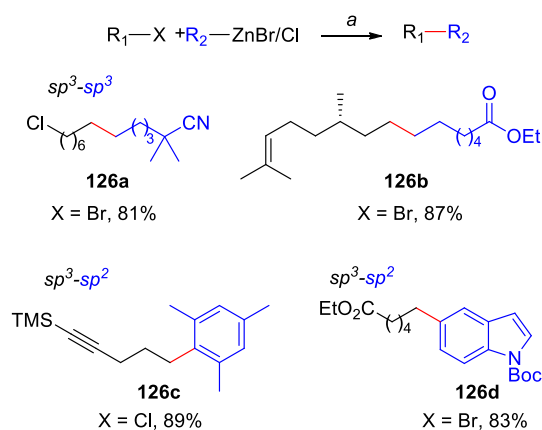


Ar-Cl	Ar-ZnCl	Product	Yield (%)
 124	 122c	 125a	81
 124	 122a	 125b	87
 124	 122d	 125c	92

Table 15. Negishi cross-coupling of vinyl chlorides using $\text{Pd}_2(\text{dba})_3/\text{P}(t\text{-Bu})_3$.¹¹⁹

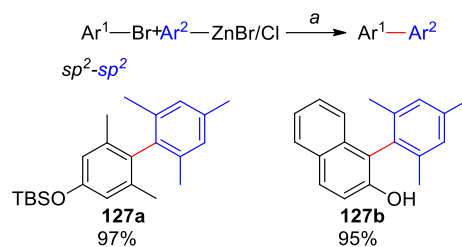
Fu *et al.* also showed that a variety of styrene compounds could be synthesised from vinyl chlorides using this methodology, even with very hindered examples such as example **125c** (92% yield).¹¹⁹

Organ *et al.* have used first and second generation PEPPSI catalysts. PEPPSI-IPr **69** and PEPPSI-IPent **70** for Negishi cross-coupling.^{121,122,123} These moisture and air stable complexes enable sp^3-sp^3 , sp^3-sp^2 (and *vice versa*) and sp^2-sp^2 C-C bond formation under mild conditions. For the formation of sp^3-sp^3 C-C bonds, LiBr additive is required to obtain good yields (Scheme 36).



Scheme 36. Negishi cross-coupling of sp^3 centres and reaction products. Conditions: (a) PEPPSI-IPr **69**, LiBr, THF/NMP or THF/DMI, rt, 2 h.

In the cross-coupling reaction of hindered aryls, the PEPPSI-IPent **70** catalyst is more efficient than PEPPSI-IPr **69**. Schemes 34 and 35 summarize the variety of products formed using the two catalysts. A variety of functionalities are tolerated such as nitrile (**126a**), ester (**126b**), amide, acetal, aniline, phenol (**127b**) and chloride (**126a**) (by using the appropriate set of conditions).

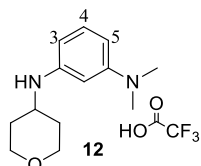


Scheme 37. Negishi cross-coupling of *sp*³-*sp*³, *sp*³-*sp*² and *sp*²-*sp*³. Conditions: (a) for **127a** PEPPSI-IPent **70**, THF/NMP, rt, 16 h; for **127b**, PEPPSI-IPent **70**, NaH, THF/NMP, 50 °C, 24 h.

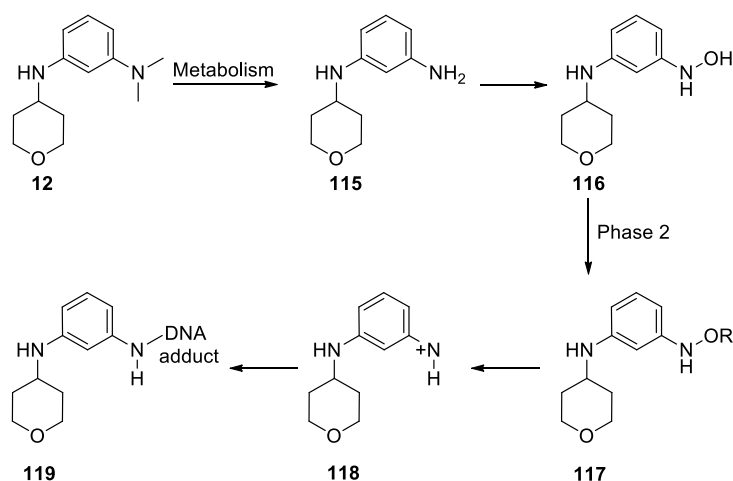
The preceding discussion represents significant recent developments in our understanding of the reaction, and in its implementation. The Negishi reaction has a number of features which make it attractive for use in the pharmaceutical industry, including its tolerance of a range of types of carbon centres (*sp*² and *sp*³), ease of access to reagents and mild reaction conditions. In our current medicinal chemistry programme the Negishi cross-coupling reaction was used to form *sp*²-*sp*³ and *sp*²-*sp*² C-C bonds in two series: the pyridone and pyridyl-pyrimidine series. In addition, the formation of aryl-aryl bonds with 2-pyridylzinc (a more effective reagent than the corresponding boronic ester), was also of interest. This will be covered in the section where each series will be discussed in terms of both synthetic and medicinal chemistry.

II Synthetic Chemistry, Results and Discussion

II.1 *Bis-Aminoaryl Series*



The synthesis of compounds belonging to the *bis-aminoaryl* series will be described here. The aim of this work was to investigate the potential of this series to deliver potent inhibitors of JmjD3, which were also selective over other Jmj-C domain containing oxygenases in the primary biochemical and cellular assays. At this stage of the programme, no X-ray crystal structure of the target enzyme had been solved, so compound design and optimisation was limited to traditional systematic medicinal chemistry. Inspection of the structure of compound **12** shows it to possess two anilinic nitrogen atoms. It is well known that anilines can be genotoxic; here nitrenium ion **118** (Scheme 36) produced by metabolic reactions, could react with DNA.¹²⁴



Scheme 36. Potential aniline metabolite of compound **12**.

As a consequence, removal of this functionality was investigated initially. Hence, replacement of the phenyl ring by various nitrogen-containing heterocyclic systems was explored.

The work plan also sought to explore the effect of substitution along different vectors, whilst maintaining the *meta*-diamine relationship, with a view to creating extra interactions with the enzyme and increasing potency. The planned programme is summarised in Figure 30.

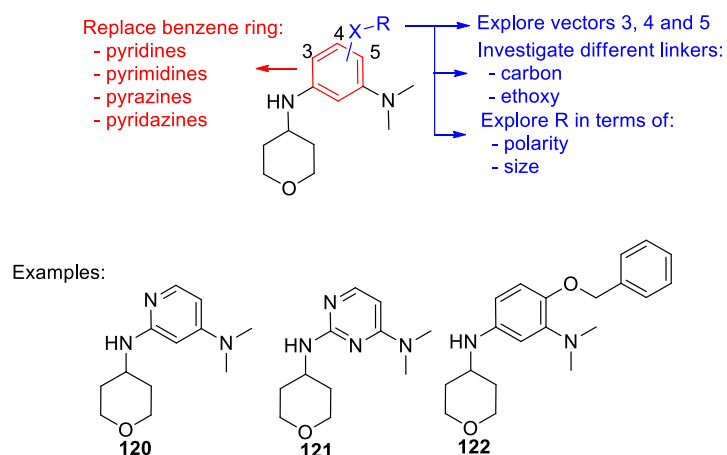
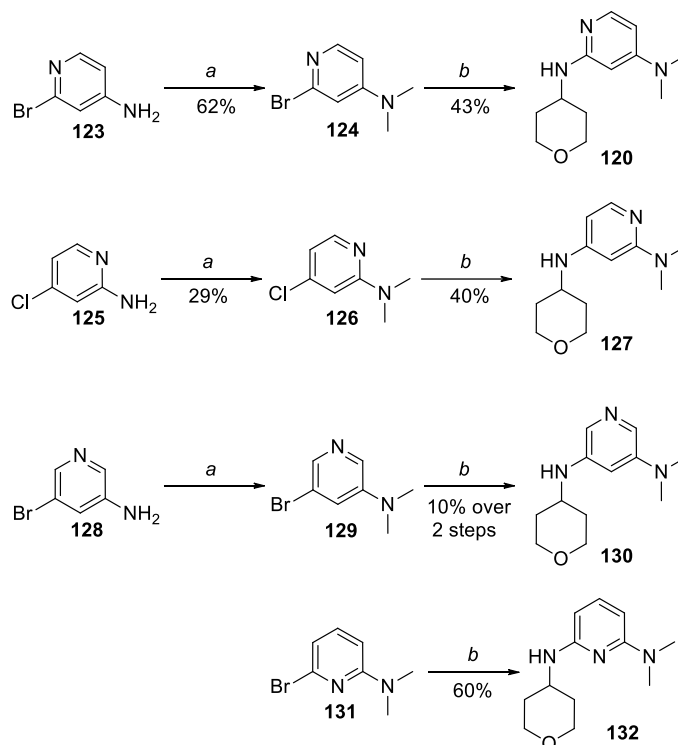


Figure 30. Work plan around the *bis*-aminoaryl series.

II.1.1 Synthetic chemistry

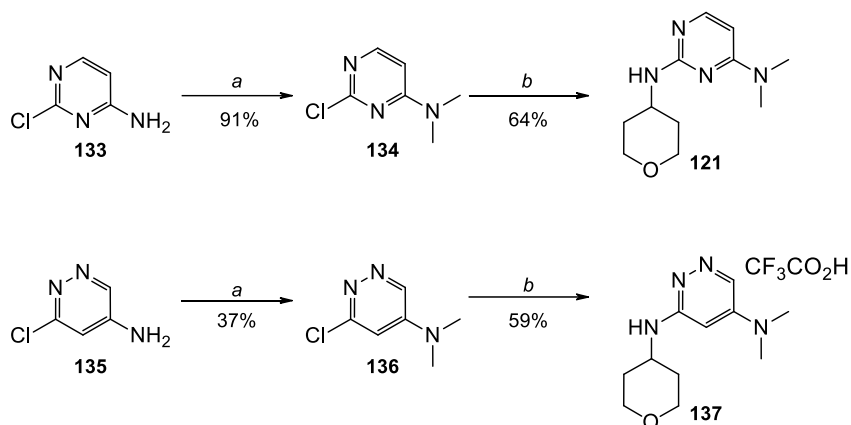
The first target compounds in the *bis*-aminoaryl series, described in Schemes 37, 38 and 39, were designed to find a replacement for the core phenyl group of **12**. Pyridyl analogues **120**, **127**, **130** and **132** were prepared according to Scheme 37 from the appropriate halopyridinamines. The dimethylamino compounds **124**, **126** and **129** were formed by dimethylation of the amines using sodium hydride and iodomethane. Attempts to synthesise and isolate the mono methyl analogues were unsuccessful. In the case of the synthesis of intermediate **126**, an excess (3.3 equivalents, added in three equal portions) of sodium hydride and iodomethane was used to consume the starting material. This reaction was one of the slowest and although all the starting material was consumed, the product was isolated

in only 29% yield. The 4-amino-THP was introduced by Buchwald-Hartwig amination to deliver final compounds **120**, **127**, **130** and **132**.¹²⁵



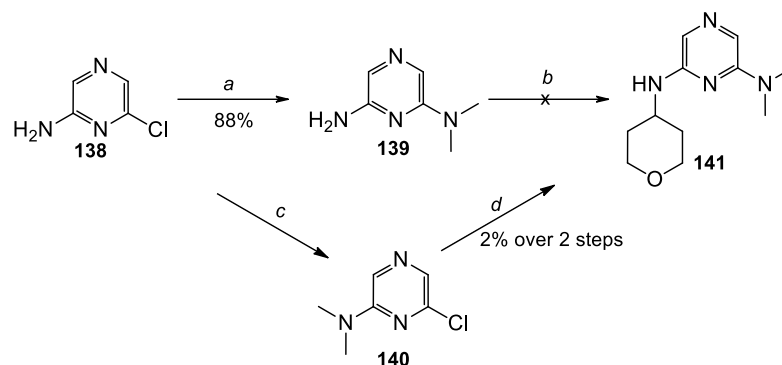
Scheme 37. Bis-aminopyridines **120**, **127**, **130** and **132**. Conditions: (a) MeI, NaH, DMF, rt; (b) 4-amino-THP, Pd₂(dba)₃, DavePhos, NaO^tBu, dioxane, microwave, 120 °C, 15 min.

Pyrimidine, pyridazine and pyrazine analogues **121**, **137** and **141** were prepared according to the methods described in Schemes 38 and 39. Dialkylation of pyrimidin- and pyridazin- amines (**133** and **135**) using iodomethane and sodium hydride gave *N,N*-dimethyl intermediates **134** and **136**, respectively. These intermediates were reacted with 4-amino-THP to give the final compounds **121** and **137** *via* a nucleophilic aromatic substitution (S_NAr), which occurs *via* an addition-elimination mechanism.



Scheme 38. Bis-amino pyrimidine (**121**) and pyridazine (**137**). Conditions: (a) MeI, NaH, DMF, rt; (b) 4-amino-THP, microwave, 190 °C.

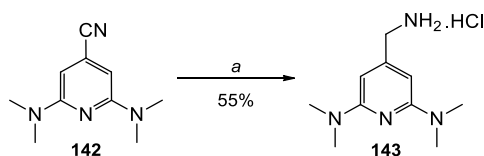
In the first approach to pyrazine analogue **141**, dimethylamine was used to substitute the chlorine atom of 6-chloropyrazin-2-amine (**138**) to give intermediate **139** in good yield. However, attempts to alkylate **139** with 4-iodotetra-2H-pyran failed to deliver the target compound (Scheme 39). An alternative route was therefore sought. It was considered that introduction of the 4-amino-THP group *via* an *S_NAr* reaction on an appropriately substituted chloride may offer a higher chance of success since this approach had been employed in the pyrimidine and pyridazine series. Compound **138** was first dialkylated to give crude intermediate **140**, which was then reacted with 4-amino-THP to give target **141** rapidly but in low yield.



Scheme 39. Bis-amino pyrazine (**141**). Conditions: (a) HNMe₂, microwave, 190 °C, 2 h; (b) 4-iodotetrahydro-2H-pyran, NaH, DMF, rt; (c) MeI, NaH, DMF, rt; (d) 4-amino-THP, microwave, 190 °C, 2 h.

The target compounds, of which the syntheses are described in Schemes 40, 41 and 42, were designed to probe the sensitivity of the enzyme to the introduction of substitution along the vectors presented by the core aromatic ring. Once vectors tolerant to substitution had been identified the aim was to further elaborate the core in these areas to increase potency, by making electrostatic or hydrophobic interactions with the enzyme. This work was performed with the pyridyl central ring as a replacement for the phenyl group.

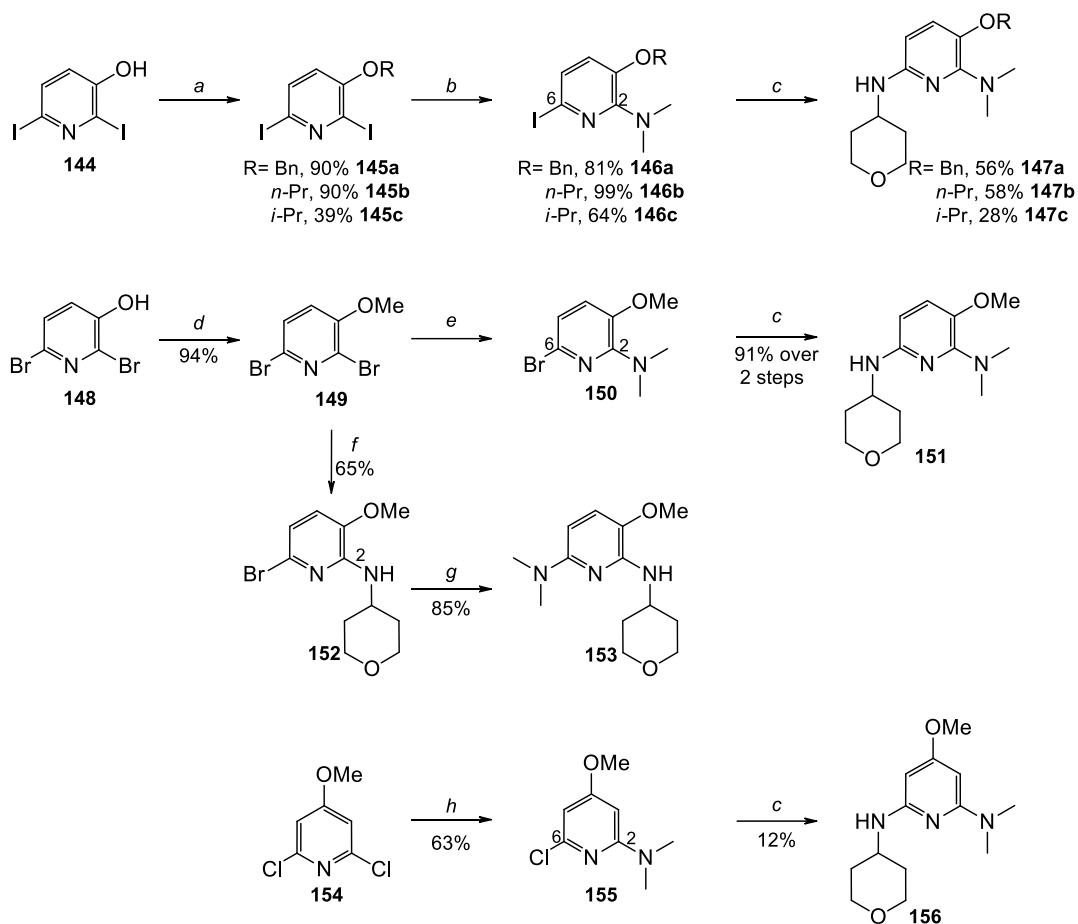
Compound **143** was designed as a consequence of the acceptable level of potency of a compound available in the compound data bank (**162**) (*cf.* Section II.1.2.2). Hydrogenation of the nitrile group of intermediate **142**, which had been synthesised elsewhere in our laboratory,¹²⁶ delivered the analogue **143** with an aminomethyl group in the 4-position (Scheme 40).



Scheme 40. Preparation of aminomethylpyridinediamine **143**. Conditions: (a) H₂, 10% Pd/C, MeOH, H-Cube, 25 °C.

Compounds **147a - 147c**, **151**, **153** and **156** were prepared according to Scheme 41. The alkoxy substituted analogues targeted (R = Bn, *n*-Pr and *i*-Pr) were obtained by Mitsunobu reaction of 2,6-diiodopyridin-3-ol (**144**) with the corresponding alcohols to form **145a**, **145b** and **145c**.¹²⁷ The Mitsunobu reactions were generally very rapid (complete in less than 1 h) and high yielding, except for the reaction involving the more hindered *iso*-propylalcohol which took 65 h and gave the desired product in 39% yield. Alkylation of 2,6-dibromopyridin-3-ol (**148**) using iodomethane and caesium carbonate proceeded to give methoxypyridine **149** in good yield.

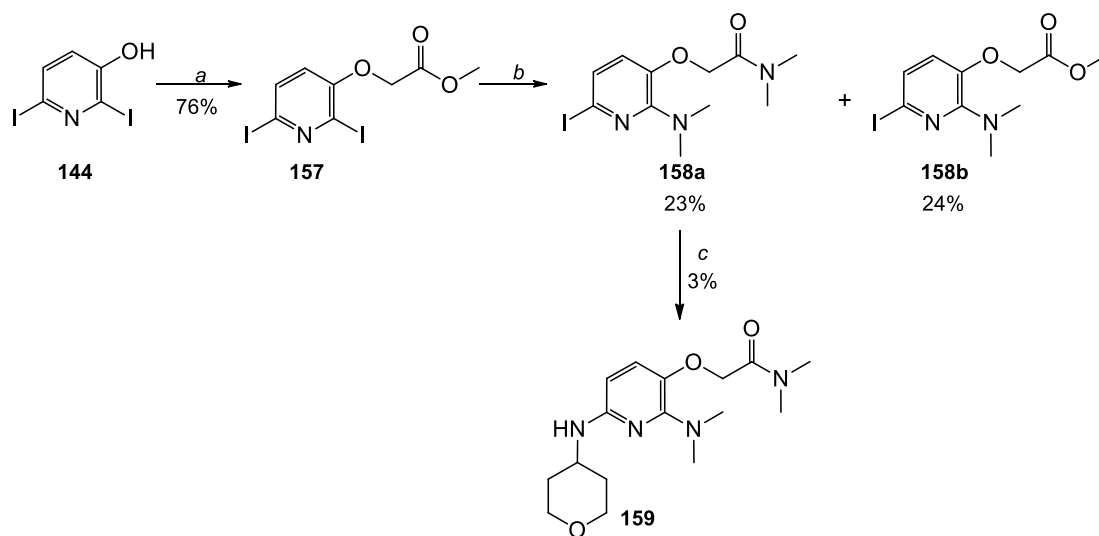
Once the appropriate alkoxy substituted pyridines were in hand, the first amine was introduced by S_NAr reaction to form **146a - 146c**, **150**, **152** and **155**. Attempts to introduce the second substituent *via* an S_NAr reaction proved unsuccessful. However, Buchwald-Hartwig amination was able to deliver the final compounds **147a - 147c**, **151**, **153** and **156**. The failure of the S_NAr reaction to introduce the second amine might be explained by the fact that the pyridine intermediates containing alkoxy and *N,N*-dimethylamino groups are more electron-rich than the dihalopyridin-3-ethers and so nucleophilic attack, the first step of an S_NAr , is much more difficult. The S_NAr reaction always occurred at position 2 (confirmed by NOE in the ¹H NMR spectra between dimethylamino and alkoxy groups) due to the inductive effect of the methoxy moiety which made position 2 more electrophilic than position 6.



Scheme 41. Alkoxy substituted analogues. Conditions: (a) ROH, DIAD, PPh₃, THF, rt, 1-65 h; (b) HNMe₂, microwave; (c) 4-amino-THP, Pd₂(dba)₃, DavePhos, NaO^tBu, dioxane, microwave, 120 °C, 15 min; (d) MeI, Cs₂CO₃, DMF, rt; (e) HNMe₂, microwave; (f) 4-amino-THP, microwave, 150 °C, 1 h; (g) HNMe₂, Pd₂(dba)₃, DavePhos, NaO^tBu, dioxane, microwave, 120 °C, 15 min; (h) HNMe₂, microwave, 100-190 °C, 1.5 h.

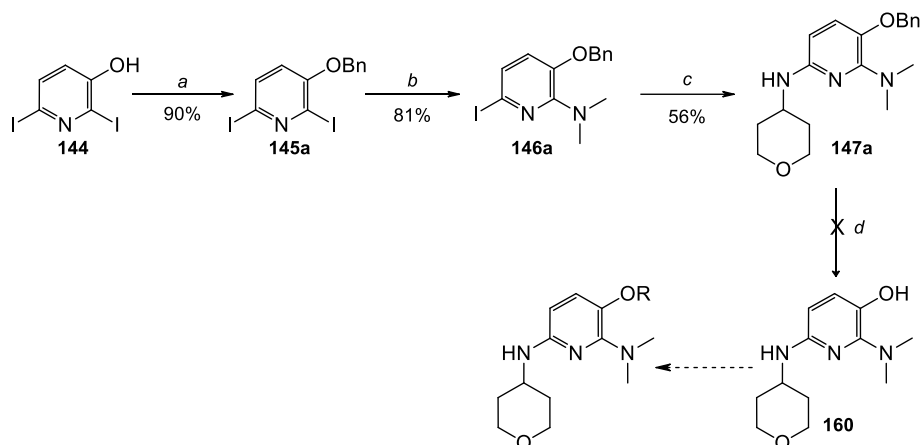
N,N-Dimethylamide **159** was made as described in Scheme 42. Alkylation of 2,6-diiodopyridin-3-ol (**144**) using Mitsunobu conditions gave intermediate **157** in good yield. This intermediate was reacted with a large excess of *N,N*-dimethylamine to form the *N,N*-dimethylamide and introduce the *N,N*-dimethylamino group in the same step, resulting in the formation of intermediate **158a**. Compound **158b** was also isolated in this reaction in 24% yield, showing that the S_NAr occurs more rapidly than the formation of *N,N*-dimethylamide.

Finally, the 4-amino-THP was introduced by Buchwald-Hartwig amination to give the final compound **159** in low yield due to difficulty in isolating the product.



Scheme 42. *O*-Linker compounds. Conditions: (a) methyl hydroxyacetate, DIAD, PPh₃, THF, rt, 40 min; (b) HNMe₂, dioxane, microwave, 180 °C, 0.5 h; (c) 4-amino-THP, Pd₂(dba)₃, DavePhos, NaO^tBu, dioxane, microwave, 120 °C, 15 min.

To probe the 3-*O* substitution pattern further, it was desirable to access a late stage intermediate which would allow introduction of diversity in the last step. Scheme 43 was designed with this in mind. The hydroxyl group was protected *via* Mitsunobu reaction to give the benzyl ether (**145a**), then the dimethylamino and tetrahydro-2*H*-pyran-4-amino groups were introduced consecutively by S_NAr and Buchwald-Hartwig reactions to form intermediate **147a**. All that remained to access the desired late stage intermediate **160** was removal of the benzyl protecting group by hydrogenation in acetic acid and water. Analyses at the end of the reaction showed the desired product (at 0.42 min). However, after neutralisation of the acetic acid with sodium hydroxide, analyses showed only a trace of the desired product **160** (Appendix 3) and a significant increase in the level of impurities. It was therefore concluded that this route could not be developed further due to the instability of the key intermediate **160**.



Scheme 43. Conditions: (a) PhCH₂OH, DIAD, PPh₃, THF, rt, 1 h; (b) HNMe₂, microwave, 190 °C, 1 h; (c) 4-amino-THP, Pd₂(dba)₃, DavePhos, NaO^tBu, dioxane, microwave, 120 °C, 15 min; (d) H₂, 10%Pd/C, acetic acid/water, rt.

II.1.2 Assay results and discussion

As described in Section I.3.1, compound **12** was identified from initial work carried out to simplify the hit **9**, which had been identified from a focused screen (Figure 31).

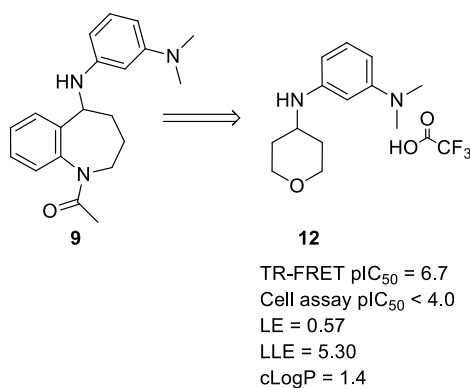


Figure 31. The relationship between compounds **9** and **12**, a simplified analogue of **9**.

This new core was then explored further within our laboratory as exemplified in Figure 32.¹²⁸ Substitution along different vectors of the phenyl ring was investigated to try to increase the potency, as was replacement of the dimethylamino group with other functionalities. Moving the dimethylamino group around the ring (**161a**, **12** and **161b**) led to the conclusion that

inhibitor potency was linked to the *meta* relationship between the two substituents. The dimethylamino group was then replaced with other alkylamino groups such as methylamino **161c**, *N*-pyrrolidinyl **161d** and *N*-piperidinyl **161e**, but all were less active than **12** (data not shown). Other replacements for the dimethylamino group, such as *N*-acetyl **161f**, *iso*-propyl **161g** and methoxy **161h** also delivered less potent inhibitors.

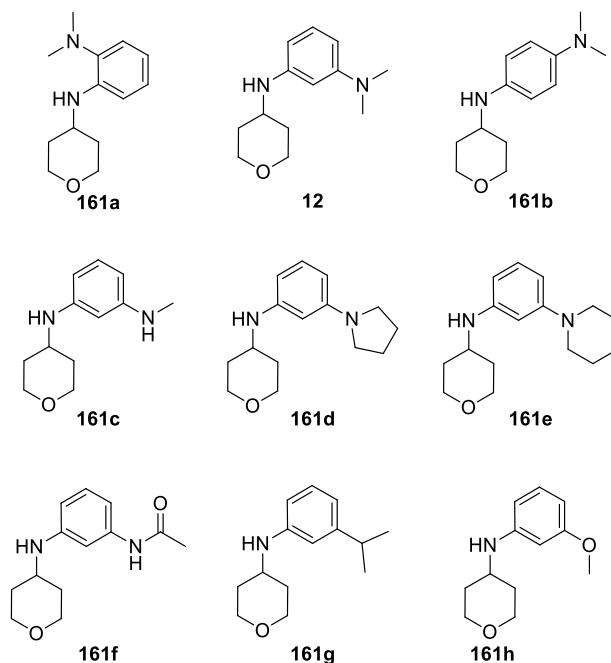


Figure 32. Initial modifications in the *bis*-aminoaryl series.

Once the SAR had shown that two amino groups in a *meta* relationship were necessary for enzyme potency, all further targets were designed bearing two amino groups in a *meta* relationship.

II.1.2.1 Pyridines, pyrimidines, pyrazines and pyridazines

The first part of the work was focused on replacement of the phenyl ring with pyridines and the results are summarized in Table 15. It was concluded that the position of the nitrogen in the ring was critical with only one position showing an acceptable level of activity (**132**, TR-FRET $pIC_{50} = 5.0$). All the other pyridyl analogues (**120**, **127** and **130**) had activities below

the detection limit of the assay. Introducing other heteroatoms to give pyrimidine **121**, pyridazine **137** and pyrazine **141** analogues resulted in compounds with activities below the limit of detection of the assay.

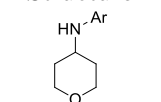
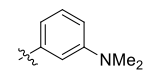
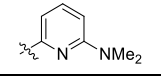
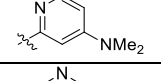
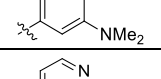
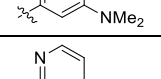
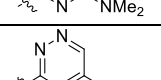
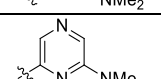
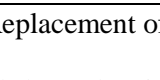
Structure 	Compound	JmjD3 TR-FRET pIC ₅₀	EGLN pIC ₅₀
	12	6.7	< 4.3
	132	5.0 ^a	4.5 ^b
	120	< 4.0	4.6 ^a
	130	< 4.0	< 4.3
	127	< 4.0	4.5 ^c
	121	< 4.0	< 4.3
	137	< 4.0	< 4.3
	141	< 4.0 ^d	< 4.3 ^a

Table 15. Replacement of the benzene ring with heteroarenes, and their assay performance.

^a Compound showed activity below the limit of detection on 2 test occasions.

^b Compound showed activity below the limit of detection on 4 test occasions.

^c Compound showed activity below the limit of detection on 1 test occasions.

^d Compound gave pIC₅₀ < 4 (n=10) and pIC₅₀ = 4.1 (n=2).

Although the pyridyl analogue **132** was almost 100-fold less potent than the parent compound **12**, it had a reduced risk of genotoxicity since it could not be metabolised to an aniline. Moreover, the pyridyl analogue **132** gave access to more tractable chemistry. This core was therefore used in the majority of further SAR explorations. It was hoped that forming additional interactions with the enzyme would raise the potency of this template.

II.1.2.2 SAR by catalogue and compound bank

At such an early stage of a programme, it is common to use commercially available or proprietary compounds to generate more SAR and increase confidence in a series, without using valuable chemistry resource. Compounds featuring a phenyl ring with a *meta* relationship between two amines were therefore selected from the GSK compound bank, and screened in the TR-FRET assay. Several compounds such as **162**, **163** and **164** were discovered in this fashion (Table 16).

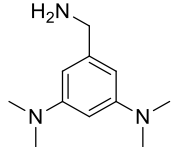
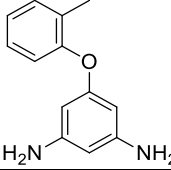
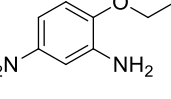
Structure	Compound	JmjD3 TR-FRET pIC ₅₀	MALDI pIC ₅₀	Cell assay pIC ₅₀	EGLN pIC ₅₀
	162	5.3	5.5	< 4.0	4.8
	163	6.3 ^a	< 4.0	4.8 ^b	5.2
	164	5.7	-	< 4.3	6.4

Table 16. Analogues containing *meta*-related amino groups.

^a Compound showed activity below the limit of detection on 4 test occasions.

^b Compound gave pIC₅₀ < 4 (n=12) and pIC₅₀ = 4.8 (n=1).

Though they lack the dimethylamino group, which had been demonstrated as being important for potency, the activities of **163** and **164** were encouraging. The activity of **162** also suggested that additional substitutions on a *meta* diamino phenyl core could be tolerated. It was therefore decided to apply the substitution patterns of these three compounds to the pyridyl core and study their effects on the biological activity (Tables 17 and 18). Though all three compounds displayed good potency against JmjD3, they also had activity against EGLN to varying degrees (pIC₅₀ 4.8 - 6.4). This was a concern, as was the

fact that the activity of **163** in the TR-FRET assay did not match the potency in the MALDI assay. This discrepancy was clearly something which needed to be monitored.

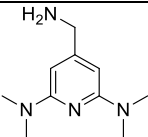
Structure	Compound	JmjD3 TR-FRET pIC ₅₀	MALDI pIC ₅₀	Cell assay pIC ₅₀	EGLN pIC ₅₀
	143	5.4	4.8	< 4.0	5.6

Table 17. Bis(dimethylamino) compound.

Compound **143** was the first of these to be synthesised; it showed a similar level of potency to **162** against JmjD3 (pIC₅₀ 5.4 vs 5.3) but was less selective (EGLN pIC₅₀ 5.6 vs 4.8). More targets around this template were planned but because of stability issues, which will be covered in more detail later in this section, this template was not investigated further.

II.1.2.3 Ether-linked analogues

Because ether-linked analogues **163** and **164** possessed significant activity against JmjD3, analogues based on lead molecule **12** were designed. It was hoped that the incorporation of all of the key potency-delivering moieties would be additive and would result in a marked improvement in enzyme inhibition. The activities of the 3-, 4-, or 5-methoxy substituted pyridines **153** (TR-FRET pIC₅₀ = 5.6), **156** (TR-FRET pIC₅₀ = 5.8) and **151** (TR-FRET pIC₅₀ = 5.7) (Table 18) were similar showing no preference for the different vectors.

Increasing the steric demand of the 5-alkoxy substituent by extending the carbon chain to *n*-propyl (**147b** TR-FRET pIC₅₀ = 4.8), or by increasing the bulk and lipophilicity of the substituent at the 5-position (**147c** TR-FRET pIC₅₀ = 5.3, **147a** TR-FRET pIC₅₀ = 5.5) failed to improve the potency. The observation that compound **147b** was less potent than compound **164** was particularly disappointing. It was expected that replacing the two primary amines of **132** with an *N,N*-dimethylamino group and a 4'-tetrahydropyranyl-amino

group would result in an increase in potency. Instead a 10-fold drop in potency was seen against JmjD3, whilst the EGLN activity was maintained.

As part of early exploration of SAR, it was decided to introduce H-bond acceptors off the 5-position of the pyridyl ring which resulted in the design of compound **159**. Compound **159** with the 5-dimethylamide glycol ether group showed the highest potency with a pIC₅₀ of 6.6 (TR-FRET), almost 100-fold more potent than compound **132**. Two hypotheses were postulated to try to explain this increase in potency. The first hypothesis was that introduction of the amide carbonyl enhanced the binding interaction between the inhibitor and the amino-acid side chains of the JmjD3. The second hypothesis was that the amide was forming an interaction with the catalytic iron, inhibiting the enzyme by preventing binding of the substrate or co-factor.¹²⁹ However, in the absence of the crystal structure, it was difficult to rationalise the activity of this compound. Although **159** showed enhanced potency against JmjD3 it was observed that it also had increased activity against EGLN relative to the 5-unsubstituted parent **132**. This finding was a concern but, by itself, would not have precluded further investigations of this substituent.

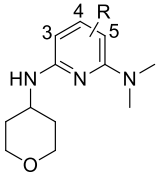
Structure		Compound	JmjD3 TR-FRET pIC ₅₀	Cell assay pIC ₅₀	EGLN pIC ₅₀
Position	R				
					
3	H	132	5.0 ^a	< 4.0	4.5 ^b
3	OMe	153	5.6	< 4.0 ^c	6.1
4	OMe	156	5.8	< 4.0	7.0
5	OMe	151	5.7	< 4.0	6.2
5	<i>Oi</i> -Pr	147c	5.3	< 4.0	6.0
5	<i>On</i> -Pr	147b	4.8	< 4.0 ^d	6.2
5	OBn	147a	5.5	4.8 ^b	-
5	OCH ₂ CONMe ₂	159	6.6	-	6.6

Table 18. Ether-linked analogues.

^a Compound showed activity below the limit of detection on 2 test occasions.

^b Compound showed activity below the limit of detection on 4 test occasions.

^c < 4.0 (n = 1) and pIC₅₀ = 4.4 (n = 1).

^d < 4.0 (n = 5) and pIC₅₀ = 4.5 (n = 1).

Though a number of compounds with biochemical potencies as high as pIC₅₀ of 6.7 had been synthesised, no significant measurable activity had been observed in the cellular assay (Table 18). A range of different explanations for this observation could be envisaged, but the low stability of intermediate **160** mentioned in Section II.1.1 raised some concerns around this series. To investigate this potential issue a stability study of compound **151** in cell assay conditions was initiated. The sample was dissolved in a mixture of fetal calf serum and DMSO (10.7:1) and heated at 37 °C. After less than one hour, compound **151** was found to decompose to multiple products, which could not be identified. This clearly called into question all other cell assay results for this series. After keeping **151** in the chemical store at room temperature for about three years, LCMS and NMR (Appendix 4) were run and these new data showed that the compound had completely decomposed with possibly only 6% of the product visible by LCMS. The unexpected behaviour of compound **151** in the cell assay

conditions and upon storage at room temperature for a long period of time (3 years) and the decomposition of compound **160** led to a literature search of small molecules containing substituted pyridines (Appendix 5). This investigation showed that none of the final compounds described in the *bis*-aminoaryl series were known in the literature (*cf.* Experimentals). However a very limited number of analogues were found in Sci-Finder (Figure 33).

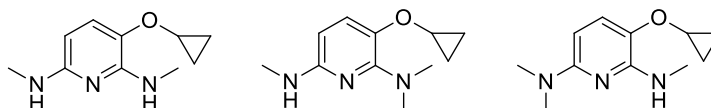


Figure 33. Analogues of *bis*-aminoaryls found in Sci-Finder.

There was neither literature reference nor experimental data available for these compounds. They are allegedly supplied by two companies Milestone Pharmtech¹³⁰ and FCH group.¹³¹ However when contacted, Milestone Pharmtech stated that the compounds had been discontinued and FCH group stated that they could supply these molecules in seven to eight weeks. The fact that the small molecules described in Figure 33 are supplied by only one company which does not have any in stock, and the lack of scientific literature related to analogues of *bis*-aminoaryl reinforced the concern around this series.

In parallel the evaluation of compounds from the *bis*-aminoaryl series against JmjD3, a number of examples were also screened in an assay to determine their redox potentials. The results are shown in Table 19 and should be put in context by referring to Section I.3. The four compounds in Table 19 were considered oxidatively unstable. This suggests that compounds from the *bis*-aminoaryl series could potentially reduce the Fe(IV) oxo species in the active site, resulting in a catalytically compromised iron, and so inhibiting JmjD3. This mechanism of action was undesirable for the reasons described in Section I.3.1.2.

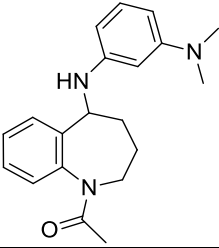
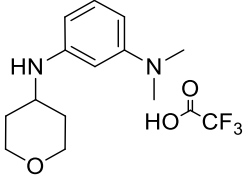
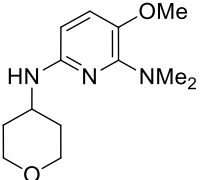
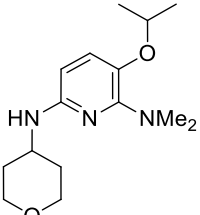
Structure	Compound	JmjD3 TR-FRET pIC ₅₀	E° Oxidation (mV)
	9	6.0 ^a	560
	12	6.7	519
	151	5.7	660
	147c	5.3	433

Table 19. Redox measurement. Assay run by Matthew Lochansky (Appendix 2).

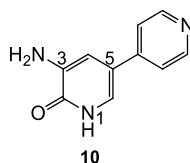
^a Compound showed activity below the limit of detection on 4 test occasions.

II.1.2.4 Summary

Development of the SAR around focused screening hit **9** delivered enhanced potency (*e.g.* compound **159**) and potentially reduced the genotoxicity risk through the replacement of the aniline core. However, several exemplars of the *bis*-amino aryl series were shown to be unstable in the cellular assay media and, in some instances, compounds were returned due to the fact the purity had fallen between submission and dissolution in DMSO and immediate processing quality control analysis. These pyridyls with *O*-alkyl, and two *N*-alkyls are very electron-rich and this could potentially explain the instability issue of these compounds. In

addition, some compounds were shown to exhibit a potential redox liability. The combination of these issues and the lack of X-ray crystal structure data with which to understand and optimise compound binding led to a decision to discontinue efforts on this series and focus on optimising alternative series.

II.2 Pyridone series



JmjD3 TR-FRET pIC₅₀ = 4.7
 Cell assay pIC₅₀ < 4.0
 LE = 0.46
 LLE = 5.39
 cLogP = -0.7

As described in Section I.3.2, compound **10** was identified from an HTS. Analysis of the properties of compound **10** showed that it had only moderate biochemical potency (pIC₅₀ = 4.7) in the TR-FRET. It was therefore recognised that biochemical potency would likely need to be increased to pIC₅₀ > 6 in order to allow for the expected drop-off when evaluating any effect in a cellular system. At this stage of the programme, the X-ray crystal structure of the target enzyme had not been solved, so systematic traditional medicinal chemistry was used in the optimisation of this pyridone series. It was also clear that **10** was a rather polar molecule (cLogP = -0.7) and that this property may hinder its ability to penetrate the cell and show a response in the cellular assay. In a review, Young *et al.* showed that membrane permeability increased as the lipophilicity (measured by Chrom log $D_{pH7.4}$) increased, up to a certain point (Chrom log $D_{pH7.4}$ = 5); after this point permeation decreased again.¹³² It was, therefore, decided to modulate the lipophilicity of the compounds primarily using vectors 1 and 3 (Figure 34).

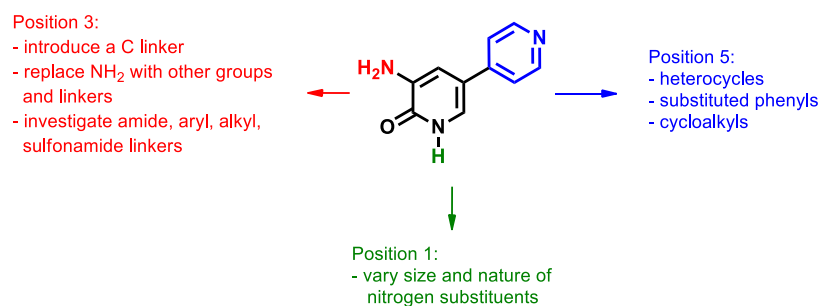


Figure 34. Work plan around the pyridone series.

The goal for this programme was to evaluate the potential of this series to deliver molecules which were potent and selective in both the primary biochemical and cell-based assays.

II.2.1 Initial SAR

II.2.1.1 Initial SAR development - vector 5

Initial work to identify the optimum position for the heteroatom in the aryl ring on position 5 of the pyridone was carried out by Bioduro.¹³³ The key results are summarised in Table 20. The 3'-pyridyl compound **165** was shown to be the most active substituent from this first iteration, with pIC₅₀ of 5.7 in TR-FRET assay and 4.7 in MALDI assay. Compound **165** was 6-times more potent than compound **10** and, more importantly, this compound showed activity in the MALDI assay whereas compound **10** showed activity below the limit of detection in this assay.

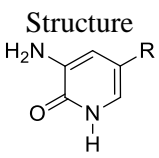
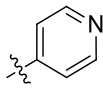
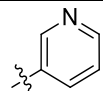
Structure 	Compound	JmjD3 TR-FRET pIC ₅₀	MALDI pIC ₅₀	EGLN
R				
	10	4.7	< 4.0	5.7
	165	5.7	4.7	5.7 ^a

Table 20. Replacement of 5-pyridyl.

^a Compound showed activity below the limit of detection on 1 test occasion.

It was therefore decided to use the more potent 3-pyridyl substituent in the 5-position of the pyridone when investigating the other vectors off the pyridone core. Starting with a more

active template would increase our ability to discern the fine details of the SAR we were seeking to examine.

II.2.1.2 Initial SAR development - vector 3

As described for the *bis*-aminoaryl series (*cf* Section II.1.2.2), the GSK compound bank was mined for analogues of pyridone lead **10** so that SAR around this template could be generated without the need to carry out much preparative chemistry. During the initial stages of these explorations, many pyridone analogues were selected and screened in the TR-FRET and MALDI assays. From this effort, compounds **166** and **167** were identified (Table 21).

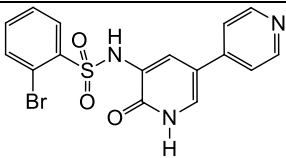
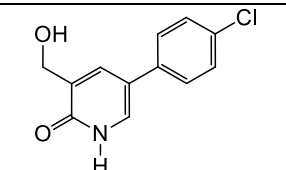
Structure	Compound	JmjD3 TR-FRET pIC ₅₀	MALDI pIC ₅₀	EGLN pIC ₅₀
	166	4.9	-	< 4.3
	167	5.1	4.6	5.8

Table 21. Enzyme assay data for compound solutions from GSK compound bank.

Despite lacking the potent 3'-pyridyl substituent, which had been shown to impart an increase in potency over the 4'-pyridyl analogue at position 5, both compounds showed encouraging levels of potency in the TR-FRET assay with pIC₅₀ of 4.9 and 5.1, respectively. In contrast to the 3-*N* unsubstituted parent molecule **10**, compound **166** was selective for JmjD3 over EGLN (pIC₅₀ of 4.9 *vs* < 4.3). The introduction of the bromobenzensulfonyl substituent onto the core **165** would be a priority in the search for more selective pyridones. Unlike **166**, **167** was more potent against EGLN (pIC₅₀ of 5.8) than JmjD3 (pIC₅₀ of 5.1). Although this was a concern, it was thought that it may be possible to increase selectivity as

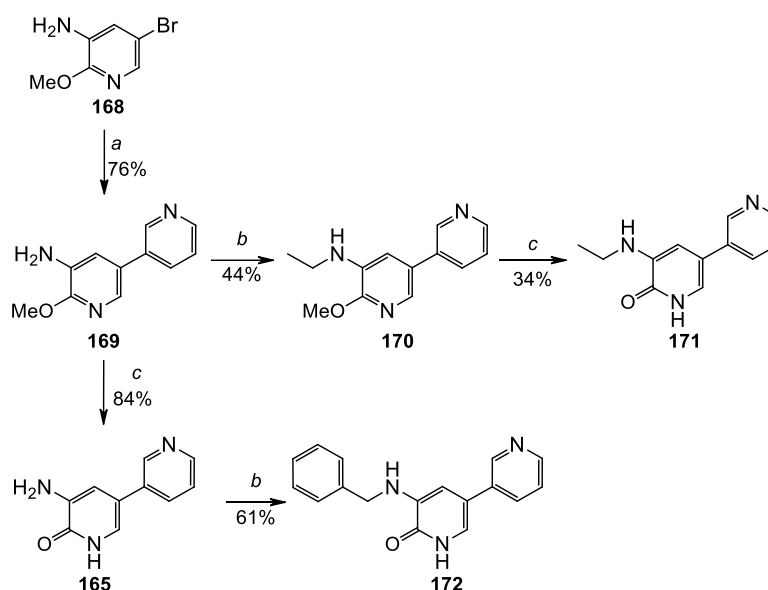
the SAR of the series was developed. It was therefore decided to explore the potential of these 3-substituents to enhance the potency and selectivity of partially optimised lead **165**. In addition to the two substituents already discussed, *N*-alkyl, (*N*-alkylamino)methyl and *N*-acetamido pyridones were also designed to further explore vector 3.

II.2.2 Synthetic chemistry

II.2.2.1 3-*N*-Alkyl pyridones

N-Alkylated compounds **171** and **172** were prepared according to the method described in Scheme 44. Cross-coupling of 5-bromo-2-(methoxy)-3-pyridinamine **168** and 3-pyridylboronic acid using a Suzuki reaction delivered the bi-aryl intermediate **169** in good yield. Reductive alkylation of aminopyridine **169** with acetaldehyde gave *N*-ethyl intermediate **170**. Subsequent deprotection of **170** using BBr₃ gave the target pyridone compound **171** in disappointing yield.

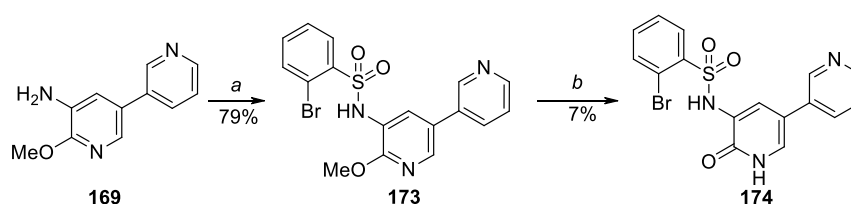
In an effort to establish whether the overall yield of the reaction sequence could be improved, and to allow introduction of diversity later on in the synthesis, a portion of methoxy pyridine **169** was deprotected using BBr₃ to give pyridone **165** in 84% yield. Reductive alkylation of aminopyridone **165** with benzaldehyde gave the targeted *N*-benzylaminopyridone **172** in 61% yield. Thus, the desired material was delivered in 58% overall yield from intermediate **169**. This compared very favourably to the initial route of reductive alkylation followed by deprotection which gave the target compound **171** in 15% overall yield. Since this sequence was not utilised to access any further analogues it is unclear to what extent the improved overall yield is due to the change in the order of the reactions or the use of an aryl vs alkyl aldehyde.



Scheme 44. Conditions: (a) 3-pyridylboronic acid, Pd(dppf)Cl₂, K₂CO₃, dioxane/water (4:1), reflux, 2 h; (b) MeCHO or PhCHO, NaBH(OAc)₃, AcOH, THF, reflux; (c) BBr₃, DCM, rt.

II.2.2.2 3-*N*-Sulfonamido pyridones

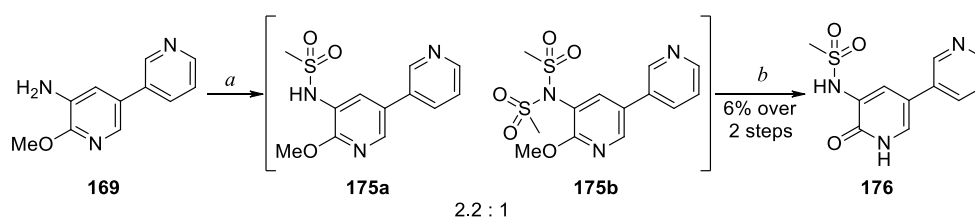
Compounds **174**, **176** and **178** with sulfonamido and amido moieties at position 3 were prepared as shown in Schemes 45, 46 and 47. Sulfonylation of 6-methoxy-[3,3'-bipyridin]-5-amine **169** with 2-bromobenzene-1-sulfonyl chloride delivered 2-bromobenzenesulfonamide **173** in moderate yield. Deprotection of methoxy pyridine **173** using BBr₃ afforded the final pyridone **174** in 7% yield, after a difficult purification.



Scheme 45. Conditions: (a) 2-bromobenzene-1-sulfonyl chloride, pyridine, DCM; (b) BBr₃, DCM.

In the case of the formation of compound **176**, the sulfonylation reaction was more troublesome (Scheme 46). Reaction of 6-methoxy-[3,3'-bipyridin]-5-amine **169** with

methanesulfonyl chloride at room temperature was slow and so an additional equivalent of methanesulfonyl chloride was used. The mixture was then heated to reflux to drive the reaction to completion. Analysis of the crude reaction mixture by LCMS revealed the formation of *bis*-sulfonylated side-product **175b** in addition to the desired mono-sulfonylated product **175a** in a ratio of (**175a** : **175b** = 2.2 : 1). Intermediate **175a** could not be separated from compound **175b**, so the mixture was taken on to the deprotection step. Given the low yield of the deprotection of the related molecule **173** (Scheme 45), it was decided to employ cyclohexyliodide which has been described as a milder reagent than BBr_3 .¹³⁴ Using this method the desired pyridone **176** was isolated in 6% (over 2 steps) after difficult purifications.

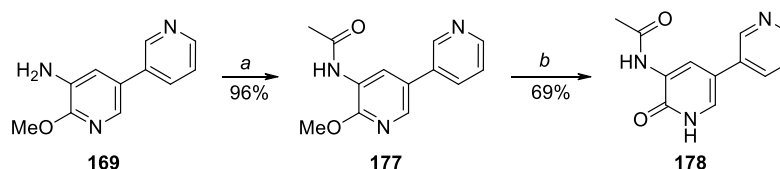


Scheme 46. Conditions: (a) MeSO_2Cl , pyridine, DCM, reflux; (b) cyclohexyliodide, DMF, reflux.

It is difficult to draw any firm conclusions about the relative merits of the two deprotection methods (BBr_3 vs cyclohexyliodide) because cyclohexyliodide was employed only once on a mixture of components **175a** and **175b** whilst BBr_3 was used on several occasions on different 2-methoxy pyridines giving a range of yields; **165** was isolated in 84% yield whilst **174** was isolated in only 7% yield.

II.2.2.3 3-*N*-Acyl pyridones

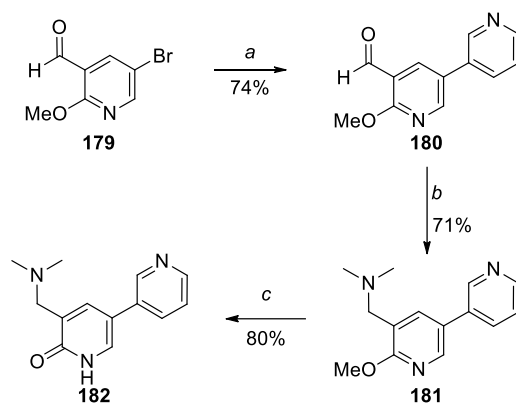
To access the *N*-acetylated analogue **178** (Scheme 47), 6-methoxy-[3,3'-bipyridin]-5-amine **169** was acylated with acetyl chloride to form *N*-acetamide intermediate **177** in 96% yield. Deprotection using BBr₃ gave *N*-acetylamino pyridone **178** in moderate yield.



Scheme 47. Conditions: (a) acetyl chloride, DIPEA, DCM, rt; (b) BBr₃, DCM.

II.2.2.4 3-Aminomethyl pyridones

To further our understanding of the SAR of this series it was desirable to explore the effect of introducing a methylene spacer between the 3-position nitrogen and the pyridone core of HTS hit **10**. Compound **182** was therefore targeted. Cross-coupling of 5-bromo-2-methoxynicotinaldehyde **179** and 3-pyridylboronic acid *via* a Suzuki reaction delivered bipyridyl intermediate **180** in good yield (Scheme 48). Subsequent reductive amination with dimethylamine delivered intermediate **181** in moderate yield. The reductive amination was slow, so excess dimethylamine and triacetoxyborohydride were used in an effort to drive the reaction to completion. Deprotection of methoxypyridine **181** using BBr₃ gave the final pyridone **182** in 80% yield.

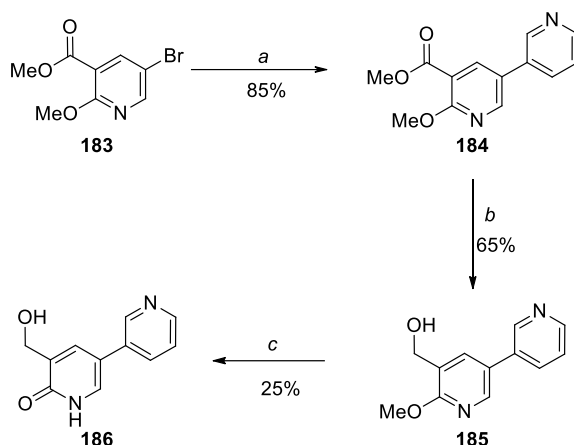


Scheme 48. Conditions: (a) 3-pyridylboronic acid, Pd(dppf)Cl₂, K₂CO₃, dioxane/water (4:1), microwave 100 °C, 30 min; (b) HNMe₂, NaBH(OAc)₃, AcOH, THF, rt; (c) BBr₃, DCM, rt.

II.2.2.5 3-Hydroxymethyl pyridones

As discussed in Section II.2.1.2, a sub-structure search looking for analogues of **10** identified the 3-hydroxymethyl group as being potentially interesting. To examine whether this group could be advantageous, compound **186** was designed.

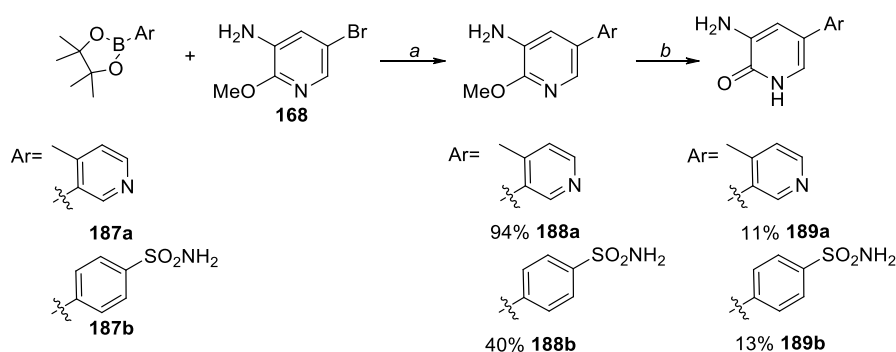
Cross-coupling of methyl 5-bromo-2-(methoxy)-3-pyridinecarboxylate **183** with 3-pyridylboronic acid *via* Suzuki reaction gave bi-aryl intermediate **184** in 85% yield (Scheme 49). Reduction of methyl ester **184** with lithium aluminium hydride gave (hydroxymethyl)pyridine **185** in moderate yield. Final deprotection using BBr₃ delivered the target pyridone **186** in 25% yield.



Scheme 49. Conditions: (a) 3-pyridylboronic acid, Pd(dppf)Cl₂, K₂CO₃, dioxane/water (4:1), microwave 100 °C, 30 min; (b) LiAlH₄, THF, rt; (c) BBr₃, DCM, rt.

II.2.2.6 5-Aryl pyridones

Compounds **189a** and **189b** were designed to build upon SAR generated by the initial array produced by Bioduro,¹³³ with the aim of increasing the potency by exploring vector 5. These two compounds were prepared by a two step route (Scheme 50). Reaction of 5-bromo-2-(methoxy)-3-pyridinamine **168** with the appropriate arylboronic acids (**187a** and **187b**) using Suzuki conditions gave biaryl intermediates **188a** and **188b**, respectively. The yield of intermediate **188b** was disappointing when compared with other Suzuki reactions described earlier. Deprotection of **188a** and **188b** using BBr₃ gave the final pyridones **189a** and **189b** in low yield after difficult purifications.



Scheme 50. Conditions: (a) arylboronate ester **187a** or **187b**, Pd(dppf)Cl₂, K₂CO₃, dioxane / water (4:1), microwave 100 °C, 30 min; (b) BBr₃, DCM, rt.

II.2.3 Assay results and discussion

II.2.3.1 SAR development - vector 3

Table 22 summarises the work carried out to follow up the encouraging data resulting from the screening of GSK compound bank (*cf.* Section II.2.1.2) and to explore vector 3 further.

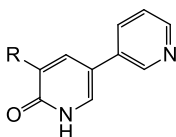
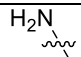
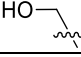
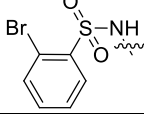
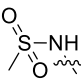
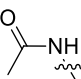
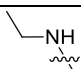
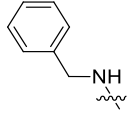
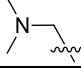
Structure 	Compound	JmjD3 TR-FRET pIC ₅₀	MALDI pIC ₅₀	cLogP
	165	5.7	4.7	-0.7
	186	< 4.0 ^a	< 4.0	-0.6
	174	< 4.4 ^b	< 4.0	1.2
	176	4.7	4.4	-0.8
	178	< 4.0	< 4.0	-0.5
	171	4.1 - 6.2 ^c	< 4.0 ^d	0.6
	172	5.4	4.3	1.5
	182	< 4.0 ^e	< 4.0	-0.2

Table 22. Enzyme assay data for compounds with various substituents at position 3.

^a < 4.0 (n = 5) and 4.6 (n = 1).

^b < 4.0 (n=3) and 4.3 (n=1).

^c < 4 (n=3) variable active data ranging from 4.1 - 6.2.

^d < 4.0 (n = 3) and 4.2 (n = 1).

^e < 4.0 (n = 5) and 4.3 (n = 1).

It was disappointing to find that the hydroxymethyl pyridone **186** (TR-FRET $pIC_{50} < 4.0$) and bromobenzenesulfonamido **174** (TR-FRET $pIC_{50} < 4.4$) displayed low activities. This was in marked contrast to the parent compounds **167** and **166** (Table 21) which showed moderate levels of activity. This discrepancy may be attributed to the fact that **166** and **167** had only been tested from old solution samples. It is possible that the samples may have degraded over time with the activity observed being due to impurities. Degradation of stored solution samples is an issue medicinal chemists are aware of and so where possible stored samples which show good activity in an assay are often re-synthesised, or re-purified and re-tested. Unfortunately, there were no solid samples available which could have been re-purified and re-tested.

Methylsulfonamide **176** was tolerated (TR-FRET $pIC_{50} = 4.7$, MALDI $pIC_{50} = 4.4$) whilst acetamide **178** (TR-FRET $pIC_{50} < 4.0$, MALDI $pIC_{50} < 4.0$) was not. In the absence of crystal structure data, these results are difficult to rationalise since there are several differences between these two compounds; these are the positions occupied by the Me group, the oxygens and the hydrogen.

The biochemical potency of *N*-ethyl pyridone **171** was variable and *N*-benzylamino pyridone **172** with pIC_{50} of 5.3 in TR-FRET assay, showed that potency was maintained with bulkier groups. In addition, *N*-benzylamino pyridone **172** with $cLogP$ of 1.5 showed that a 100-fold increase in lipophilicity over amino pyridone **165** ($cLogP$ -0.7) did not have a major impact on the potency (TR-FRET pIC_{50} of 5.4 vs 5.7 respectively).

A few compounds were screened in the MALDI assay, including compounds **182**, **172** and **178**. Only compound **172** showed any activity in this assay format, but was 10-fold weaker than in the TR-FRET assay.

At this point, the results could not be rationalised, and discrepancies between MALDI and TR-FRET assays led us to consider deprioritising this series.

II.2.3.2 SAR development - vector 5

As discussed in Section II.2.1.1 an array was designed to initially explore the SAR around the 5-position of the pyridone core with the work carried out by outsource partners Bioduro.¹³³ These analogues highlighted the role of the 3-pyridyl substituent in raising potency over the 4-pyridyl compounds (*eg* **165** vs **10**). The compounds in Table 23 were designed to fill the gaps of the first iteration (which was outsourced) and explore vector 5 further with various aryl groups.

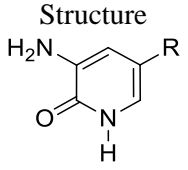
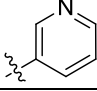
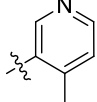
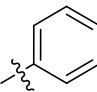
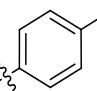
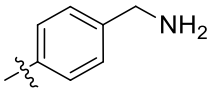
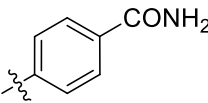
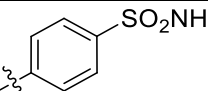
Structure  R	Compound	JmjD3 TR-FRET pIC ₅₀	MALDI pIC ₅₀
	165	5.7	4.7
	189a	5.1 ^a	< 4.0
	190	5.1	4.9
	191	5.3	4.8
	192	5.5	4.8
	193	5.6	4.6 ^b
	189b	5.5	4.5

Table 23. Enzyme assay data for compounds with various substituents at position 5.

^a < 4 (n=3) variable active data ranging from 4.0 - 5.6 (see Table 24).

^b < 4 (n=1).

Analysis of small molecule X-ray structures deposited in the Cambridge Database Crystallographic Centre (CDCC) revealed that biaryl systems such as **165** have solid-state conformations which are close to planar. To investigate the effect of twisting the 5-substituent aromatic ring out of plane an electronically-neutral substituent was introduced on the *ortho*-position of the 3-pyridyl ring. The *o*-methylpyridyl analogue **189a** was designed

with this in mind. Unfortunately, it is very difficult to draw any firm conclusions on the effect of twisting the ring out of the plane due to the high variability of the data (Table 24).

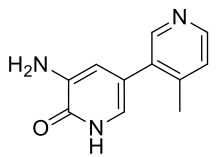
	Measurement dates	JmjD3 TR-FRET pIC ₅₀
		09/03/2010
	09/03/2010	< 4.0
	16/03/2010	5.4
	16/03/2010	< 4.0
	22/03/2010	4.8
	23/03/2010	5.0
	29/03/2010	5.2
	30/03/2010	5.2
	06/04/2010	< 4.0
	06/04/2010	< 4.0
	04/05/2010	5.1
	07/05/2010	5.6

Table 24. Compound **189a** TR-FRET data at various dates.

Analysis of the results of the outsourced 5-position array suggested that biochemical potency might be improved by elaborating the *para*-position of the 5-phenyl group.

On elaboration of the unsubstituted benzene ring to a benzylamine or benzamide, the potency was improved in the JmjD3 TR-FRET with the unsubstituted phenyl compound **190** (pIC₅₀ = 5.1) being less potent than the benzamide **193** (pIC₅₀ = 5.6). However, in the MALDI assay the differences in potency were less pronounced and the trend was going in the opposite direction, with the unsubstituted phenyl compound **190** (pIC₅₀ = 4.9) being more potent than the benzamide **193** (pIC₅₀ = 4.6). To complete the picture, it was decided to make the sulfonamide analogue **189b** which displayed a level of potency similar to the benzamide in the JmjD3 TR-FRET and MALDI assays (JmjD3 TR-FRET pIC₅₀ = 5.5, MALDI pIC₅₀ = 4.5). It was difficult to draw a firm conclusion from the data for the benzylamine, benzamide and sulfonamide compounds since there are several differences between them; these include the numbers of oxygens, positions of the oxygens, nitrogens and hydrogens, and the sizes of the substituents.

Unfortunately, in the absence of a crystal structure, and only with conflicting data from the two biochemical assays available, it was difficult to rationalise any of the SAR.

II.2.3.3 Oxidative stability

In parallel to the evaluation of the pyridone analogues against JmjD3, a number of examples were screened in an assay to measure their redox potentials and determine if pyridones were genuine inhibitors.

Table 25 contains some active pyridones synthesised by Bioduro (**190**, **192** and **193**).¹³³ The results showed that the pyridone series raised some concerns. All the compounds in this table were considered oxidatively unstable.

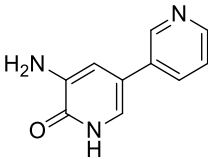
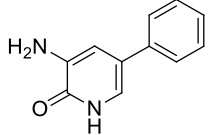
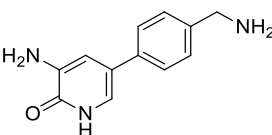
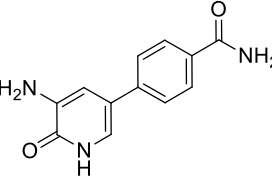
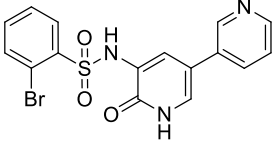
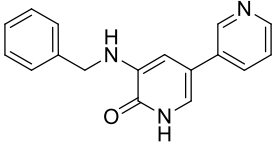
Structure	Compound	MALDI pIC ₅₀	E° Oxidation (mV)
	165	4.7	172
	190	4.9	422
	192	4.8	420
	193	4.6 ^a	420
	174	< 4.0	432
	172	4.3	444

Table 25. Redox measurement for compounds. Assay run by Matthew Lochansky (Appendix 2).

^a < 4 (n=1).

II.2.3.4 Summary

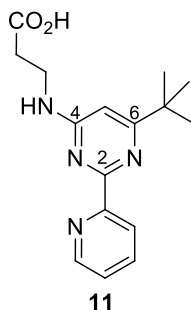
Development of the SAR around HTS hit **10** delivered up to a 6-fold enhanced potency in the TR-FRET assay. Although lipophilicity was increased by up to 100-fold (**172**), none of the analogues showed any cellular activity. Several compounds showed variable data, as exemplified by compound **189a**. Moreover, there were discrepancies between TR-FRET and MALDI data making it difficult to establish SAR. Since the MALDI assay directly measures the functional activity of the enzyme, as opposed to the TR-FRET assay which has additional fluorescence resonance energy transfer step (*cf.* Section I.2), it was considered that the MALDI data was more reliable. The compounds from the pyridone series which were tested in the MALDI assay all had $pIC_{50} < 5$, which was not high enough to justify putting any more effort on this series.

Moreover, this series was shown to exhibit redox liability issues, as also observed in the *bis*-aminoaryl series, and this could potentially explained the somewhat inconsistent SAR observed. Since enzyme function is reliant upon a change in the oxidation state of the catalytic iron, the redox stability of inhibitors is important for this class of enzymes, and will have to be monitored as early as possible in any new series. In addition, it was observed that examples of this series changed colour when stored as DMSO solutions (NMR samples), suggesting that they were not stable. Re-running the NMR samples after a week also showed a decrease in the purity of the sample confirming that the sample solutions in DMSO were degrading over time.

It was decided to discontinue work on the pyridone series based on all these observations.

II.3 Pyridyl-pyrimidine series

As described in Section I.3.2, compound **11** was identified from an HTS.



JmjD3 TR-FRET pIC₅₀ = 4.8

Cell assay pIC₅₀ < 4.0

EGLN pIC₅₀ < 4.3

E° oxidation (mV) > 900

LE = 0.30

LLE = 1.87

cLogP = 2.9

Pyridyl-pyrimidine **11** was an interesting starting point because of its moderate activity against JmjD3 (pIC₅₀ = 4.8), and its selectivity over EGLN (pIC₅₀ < 4.3). Because of the oxidative stability issues observed in the previous series (*cf.* Sections II.2.2.3 and II.1.2.3), this compound was run through the oxidative stability assay early in this portion of the programme and came back stable with E° oxidation > 900 mV. However, this compound showed no activity in the JmjD3 cell assay.

The aim of the work on this series was the identification of a probe molecule by improving potency of the compounds in both the primary biochemical and cell-based assays whilst maintaining the good selectivity over EGLN. The X-ray crystal structure of JmjD3 had not been solved when work was initiated on this series and so systematic traditional medicinal chemistry was used to drive the design of targets. Once the crystal structure data was available it was used to guide the investigation.

The synthesis and evaluation of pyridyl-pyrimidine compounds will be described in this section. The effort focused on vectors 2, 4 and 6, as shown in Figure 35.

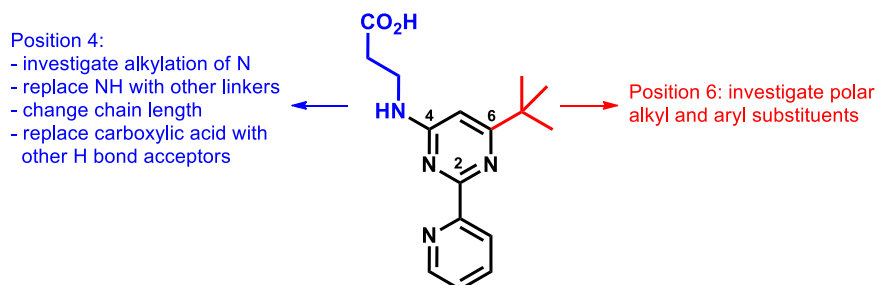


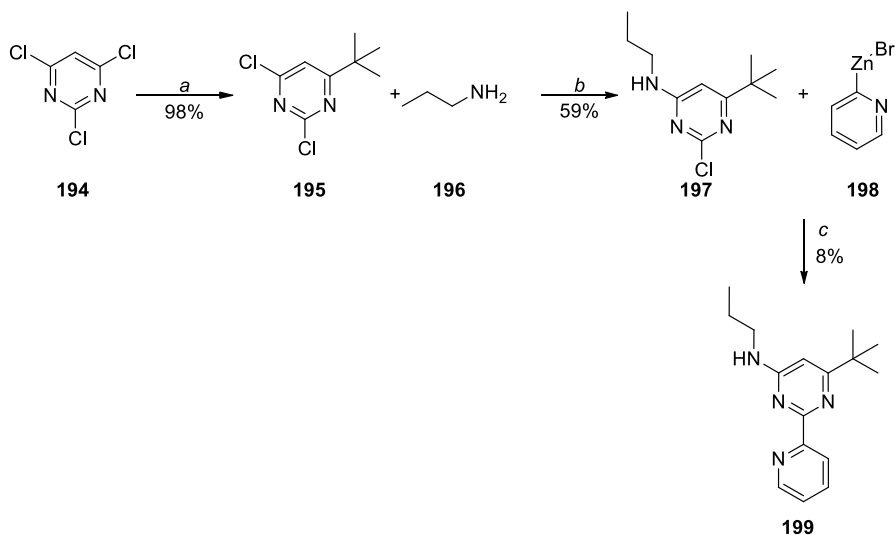
Figure 35. Work plan around the pyridyl-pyrimidine series.

II.3.1. Synthetic chemistry

II.3.1.1 Vector 4: primary modifications and carboxylic acid isosteres

II.3.1.1.1 Initial modifications

Through analysis of the X-ray structures of acid-containing compounds bound to other Jumonji enzymes (Section I.1.4.1), it was recognised that the carboxylic acid functionality of **11** may play an important role in the binding of **11** to JmjD3. To investigate whether or not this was the case, a compound in which the acid group had been removed, **199**, was targeted (Scheme 51). Copper-mediated cross-coupling of 2,4,6-trichloropyrimidine **194** with *tert*-butylmagnesium chloride gave 4-(*tert*-butyl)-2,6-dichloropyrimidine intermediate **195** in excellent yield.¹³⁵ The amine was introduced by regioselective S_NAr to form intermediate **197** in moderate yield. The final step employed a Negishi cross-coupling reaction to introduce the pyridyl ring.



Scheme 51. Conditions: (a) *tert*-butylmagnesium chloride (1.0 M in THF), CuI, THF, 0 °C; (b) K₂CO₃, DMA, rt; (c) Pd(OAc)₂, S-Phos, toluene, 100 °C.

It was found that a large excess (5 eq) of the (2-pyridyl)zinc(II) bromide was required to consume most of chloride **197**. Even when 5 eq of (2-pyridyl)zinc(II) bromide was used and the reaction heated at 100 °C, 8% of **197** still remained as determined by LC/MS. The crude material was purified initially by normal phase chromatography, but NMR analysis of **199** showed a broadening of signals which is characteristic of the presence of metal.¹³⁶ To remove the remaining traces of metal from the final compound, MDAP purification was employed. Analysis of a sample of **199** after MDAP purification showed the compound to be pure, with sharp peaks in the NMR (*cf.* Appendix 6).

Concurrent with this chemistry, it was discovered that compounds from this series were able to chelate transition metal ions and carry them through purification. Indeed, 2,2'-bipyridine and its analogues are known to be good metal-chelating ligands, a property which has been reviewed by Kaes *et al.*¹³⁷ To understand the effect metal contamination of final compounds could have on the activity against JmjD3, a sample of **200**¹³⁸ was submitted for test at two different levels of purifications. Compound **200** was made elsewhere in the lab using a

Negishi cross-coupling reaction employing $(\text{PdOAc})_2$, was purified by normal phase chromatography. A sample of **200** was submitted for test at this stage, whilst a portion was purified further by MDAP and subsequently submitted for test. The results are shown in Table 26. From this data it was clear that metal contamination was potentially a serious problem.

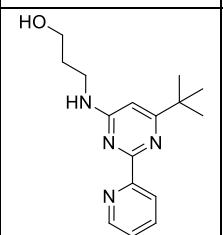
Structure	Compound	MALDI pIC ₅₀ batch 1 (before MDAP)	MALDI pIC ₅₀ batch (after MDAP)
	200	6.6	< 4.0

Table 26. Data for compound before and after MDAP purification.

It was, therefore, apparent that these transition metals were capable of inhibiting the Jumonji enzymes and giving rise to false positives in the biochemical assay. To investigate this further, a small number of transition metal salts were tested in the MALDI assay. The results in Table 27 demonstrate the magnitude and extent of this issue for the inhibition of JmjD3. $\text{Pd}(\text{OAc})_2$, used in the Negishi cross-coupling in the final step of Scheme 51, was active against JmjD3 with a pIC₅₀ of 5.9, showing a greater inhibition of the enzyme than lead compound **11**. Several other metal salts (Ni, Cu, Pd) also displayed higher inhibition of the enzyme than lead compound **11**.

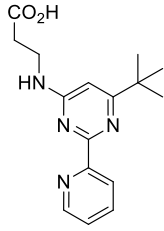
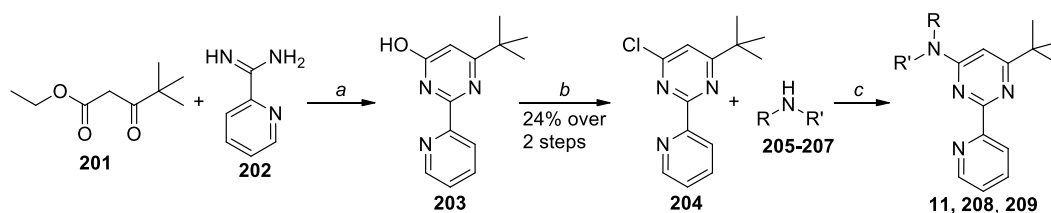
Inhibitors	MALDI pIC ₅₀
	5.0
MnCl ₂	< 4.0
NiCl ₂	5.7
CoCl ₂	5.9
CuSO ₄	5.0
ZnAc ₂	4.6
K ₂ PtCl ₄	4.2
Pd(OAc) ₂	5.9

Table 27. MALDI data for transition metals.

Schofield *et al.* in 2010 have reported similar observations in that a range of transition metals inhibit Jumonji enzymes JmjD2A and JmjD2E.¹³⁹ In their studies of inhibition of JmjD2E by various metals, it was discovered that the divalent metals from group 2 such as Ca(II) and Mg(II) did not inhibit the enzyme, whereas transition metals such as Co(II), Ni(II), Zn(II) and Cd(II) could inhibit the enzyme with IC₅₀ values close to the Fe(II) concentration required to reach 50% maximal activity.¹³⁹ The inhibition of the enzyme by these transition metals could be potentially explained if they are competing with the catalytic iron for the binding site characterised by two histidine residues and glutamic or aspartic acid residues (*cf.* Section I.1.3.3). However, other explanations could be considered such as binding competition with Zn(II) present in the C-terminal domain, present in most of the Jmj family members (*cf.* Section I.1.3.3), and also possible redox effects.

A metal-free route was devised to avoid any possibility of metal contamination interfering with the biochemical assay. The key to the metal-free route was the construction of the chloropyrimidine **204** from the amidine **202** (Scheme 52). Reaction of ethyl pivaloylacetate

201 with pyridinecarboxamide **202** gave the pyridyl-hydroxypyrimidine **203**. Subsequent reaction with POCl_3 gave chloro pyridyl-pyrimidine **204** in moderate yield.



Scheme 52. Conditions: (a) NaOEt, EtOH, reflux; (b) POCl_3 , reflux; (c) i. DIPEA, DMSO, microwave; ii. For **205** and **207** LiOH monohydrate, THF/water 3:1 or 1:1.

As well as avoiding the need for transition metal in the syntheses a significant benefit of chloro-pyridyl-pyrimidine **204** was the possibility of the introduction of diversity into position 4 in the last step of the synthesis, which greatly improved the efficiency of the medicinal chemistry investigation in this region. With the chloropyrimidine intermediate **204** now in hand, it was desirable to first remake the lead molecule **11** to confirm its data and, secondly, identify the optimum linker between the nitrogen attached to the pyrimidine ring and the carboxylate functional group. An $\text{S}_{\text{N}}\text{Ar}$ reaction of **204** with the amines **205** - **207** was therefore performed. The ethyl esters of **205** and **207** were subsequently hydrolysed to give the acids of interest (Table 28).

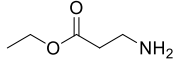
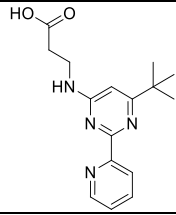
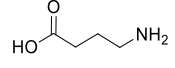
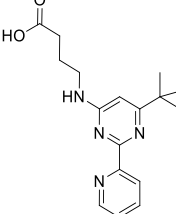
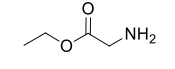
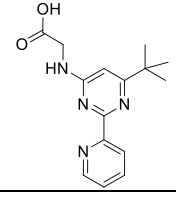
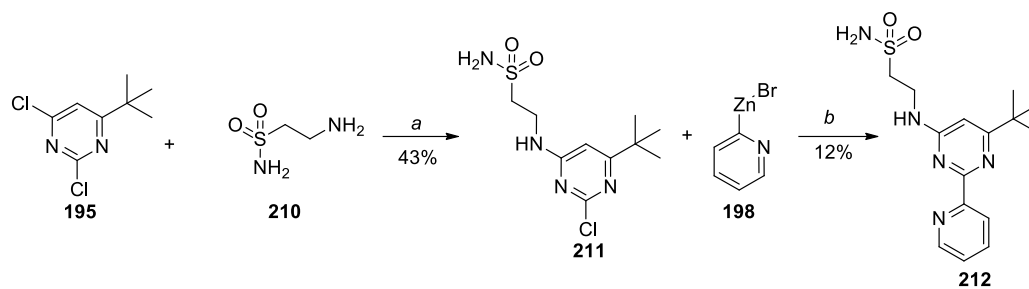
Amines		Product		Yield (%)
205		11		60*
206		208		8
207		209		50*

Table 28. S_NAr products.

* Overall yields over two steps.

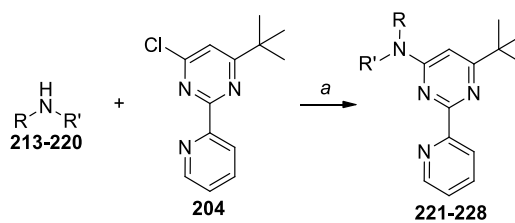
II.3.1.1.1 Replacement of carboxylic acid with alternative hydrogen bonding groups

Comparison of the biochemical assay results of 4-propyl analogue **199** with 4-(CH_2)₂CO₂H (Section II.3.2.3) demonstrated the importance of a hydrogen-bonding group to inhibitor efficacy. To explore the requirements in this region further, a variety of other hydrogen-bonding groups were investigated. The first of these hydrogen-bonding groups investigated as a carboxylic acid replacement was sulfonamide **212**. This compound was prepared before the discovery of the metal-free route, and so was accessed *via* S_NAr of amine **210** with 4-(*tert*-butyl)-2,6-dichloropyrimidine intermediate **195** to give intermediate **211** in moderate yield; subsequent Negishi reaction with (2-pyridyl)zinc(II) bromide **198** gave final compound **212** in low yield, after MDAP purification to remove residual metal (Scheme 53).



Scheme 53. Conditions: (a) K_2CO_3 , DMA, rt; (b) $Pd(OAc)_2$, S-Phos, toluene, 100 °C.

The remaining hydrogen-bonding groups investigated as carboxylic acid replacements were synthesised using the metal-free route as described in Scheme 54 and Table 29.



Scheme 54. Conditions: (a) DIPEA, DMSO, microwave or K_2CO_3 , DMA, 100 °C.

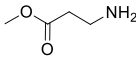
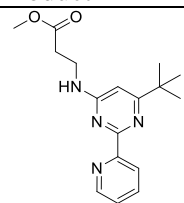
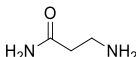
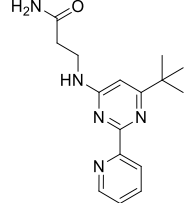
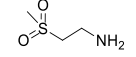
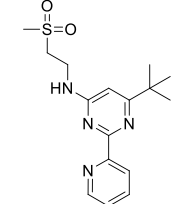
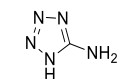
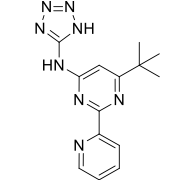
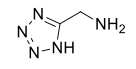
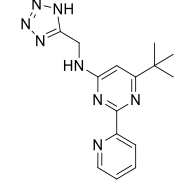
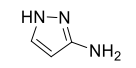
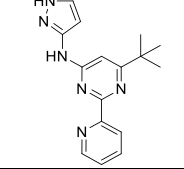
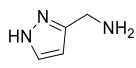
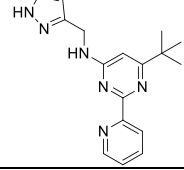
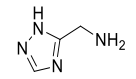
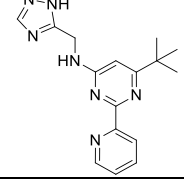
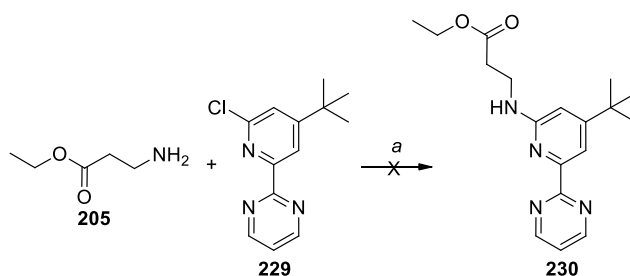
Amines		Product		Yield (%)
213		221		32
214		222		49
215		223		74
216		224		29
217		225		29
218		226		8
219		227		14
220		228		51

Table 29. S_NAr products.

The final products were isolated in yields varying from low to moderate. In the case of **226**, LC-MS analysis at the end of the reaction showed that starting material remained (10%) and twenty three side-products were also present explaining the low yield.

II.3.1.2 Pyrimidine replacement

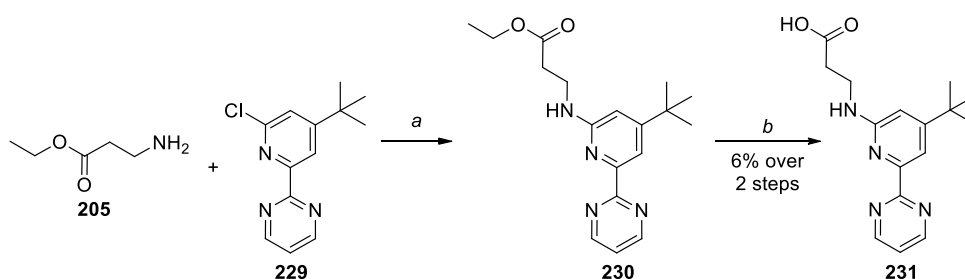
As discussed in section I.1.4.2, the published X-ray structures of JmjC domain containing enzymes demonstrated that inhibitors such as NOG and 2,4-PDCA bind in a similar way in the active sites of these enzymes. In all cases the inhibitors are involved in a bidentate interaction with the catalytic iron (*cf.* Section I.1.3.3). This observation led to the hypothesis that compound **11** was binding to JmjD3 through a bidentate interaction with the iron, the pyrimidine and pyridyl rings could be switched with no effect on the bidentate interaction or inhibitor efficacy. Compound **231** was designed to test this hypothesis (Scheme 56).



Scheme 55. Conditions: (a) Pd₂(dba)₃, DavePhos, NaO^tBu, 1,4-dioxane, microwave, 120 °C.

It was envisaged that the target compound **231** could be accessed from **229** (supplied by Bioduro)¹³³ using Buchwald-Hartwig methodology. Initially the reaction was attempted using Pd₂(dba)₃, DavePhos and NaO^tBu at 120 °C (Scheme 55). However no desired product was formed, instead significant amount of starting material (57% by LC-MS) remained. This result could potentially be explained by the oxidative addition not occurring. Another potential explanation would be the ester hydrolysis of ethyl β-alaninate by NaO^tBu

delivering the amino acid, consequently, the amine would be protonated preventing its participation in the Buchwald reaction. Therefore, the base, the ligand and the reaction temperature were changed as described in Scheme 56. Cs₂CO₃ was chosen because it is a milder base than NaO^tBu and so would be less likely to hydrolyse the ethyl ester. This new set of conditions afforded the impure intermediate **230** which gave **231** in poor yield after ester hydrolysis.

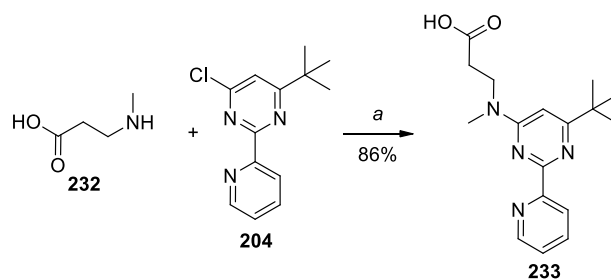


Scheme 56. Conditions: (a) Pd₂(dba)₃, (*S*)-BINAP, Cs₂CO₃, 1,4-dioxane, microwave, 150 °C; (b) LiOH monohydrate, THF/water 2:1.

II.3.1.3 NH linker replacement

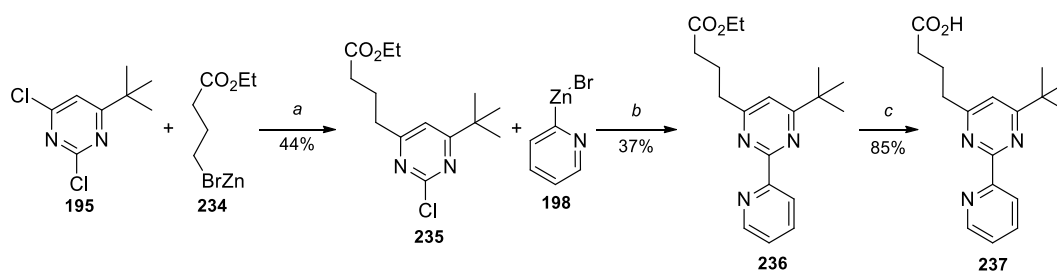
II.3.1.3.1 N-Me linked pyridyl-pyrimidine

In order to improve inhibitor potency, it was desirable to create additional interactions with the enzyme and so areas of the molecule suitable for functionalisation needed to be identified. One of the positions considered for substitution or replacement was the NH linker between the pyridyl-pyrimidine and the carboxylic acid containing side-chain. The tolerance to alkylation of the amino group of the nitrogen was the first modification to be investigated, with the design and synthesis of *N*-Me linked **233** (Scheme 57). As with previous examples, compound **233** was isolated in 86% yield following a microwave mediated S_NAr reaction.



Scheme 57. Conditions: (a) DIPEA, DMSO, microwave, 150 °C.

II.3.1.3.1 C-Linked pyridyl-pyrimidine



Scheme 58. Synthesis of **237**.¹⁴⁰ Conditions: (a) Pd(PPh₃)₂Cl₂, toluene, rt; (b) Pd(OAc)₂, S-Phos, toluene, rt; (c) LiOH monohydrate, THF/water 9:1.

An analogue of compound **11** in which the 4-NH linker was replaced with a 4-CH₂ linker, had been prepared elsewhere in our laboratory using palladium-catalysed cross-coupling chemistry (Scheme 58).¹⁴⁰ This compound **237** exhibited a JmjD3 pIC₅₀ of 5.5 in the MALDI assay suggesting that replacement of the 4-NH linker with a 4-CH₂ was beneficial for potency. Additionally the artificial membrane permeability of **237** was 13 nM sec⁻¹ at pH 7.4 which compared favourably to that of 4-NH linked compound **11** (< 10 nM sec⁻¹ at pH 7.4). However before synthesising any further 4-CH₂ linked analogues, it was desirable to obtain **237** via a metal-free route to eliminate any possibility that its potency could be due to metallic contamination of the sample.

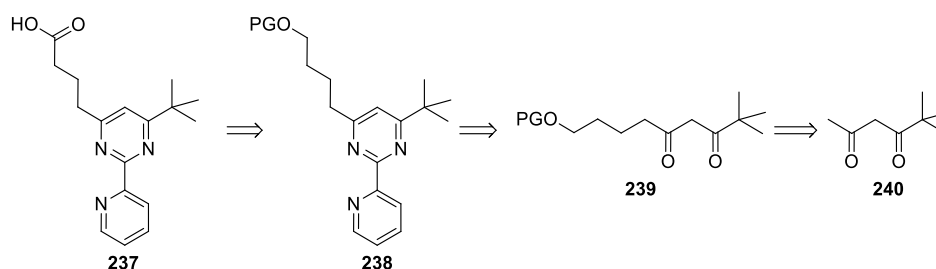
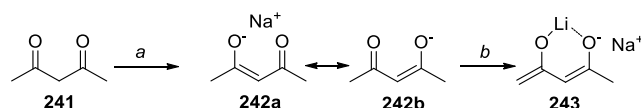


Figure 36. Retrosynthetic analysis of C-linked pyrimidine **237**.

From retrosynthetic analysis (Figure 36), **237** could be obtained from a protected alcohol containing pyridyl-pyrimidine **238**. This pyridyl-pyrimidine intermediate would be synthesised from diketone **239**, which would result from alkylation of diketone **240**. Alkylation of **240** at the terminal methyl group could be achieved *via* a dienolate. The difference in pK_a between the proton α to a single carbonyl group ($pK_a \sim 20$) and a proton between two carbonyl groups ($pK_a \sim 10$) enables regioselective alkylation of diketones. Consecutive treatment with strong bases such as NaH and *n*-BuLi, is required for the formation of the dienolate **243** (Scheme 59).

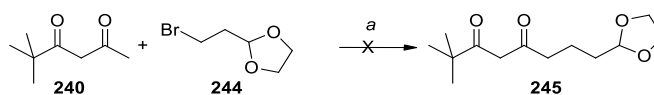


Scheme 59. Formation of dienolate **243**. Conditions: (a) NaH; (b) *n*BuLi.

Weiler and Huckin studied the formation and alkylation of β -ketoesters.^{141,142} They revealed that the temperature, reaction time, the base and the solvent were critical for the formation of the dienolate. When two equivalents of *n*-BuLi were used for the formation of the enolate, the enolate was not formed; in some cases, such as for phenylacetone or methyl acetoacetate, the use of two equivalents of *n*-BuLi resulted in the formation of products resulting from the addition of *n*-butyl nucleophile at the carbonyl group. This problem could be overcome by using one equivalent of *n*-BuLi in combination with another base such as NaH. Alkylation of the dienolate of a β -ketoester in high yield, required that the reaction be carried out in

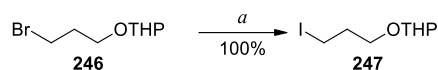
aprotic solvents such as ethers or hydrocarbons between 0 and 25 °C. At higher temperatures (25 °C and above), the reaction had to be closely monitored because the β-ketoester can be consumed quickly to form many side-products. All of this was taken into consideration in trying to find effective conditions for the formation of **245** (Scheme 60).

The first attempt to form **245** under Weiler conditions was unsuccessful: a mixture of sodium hydride and *n*-BuLi was used to generate the dienolate.^{143,144} The failure of the reaction was thought to be related either to the nature of the alkylating agent or failure to form the dienolate.



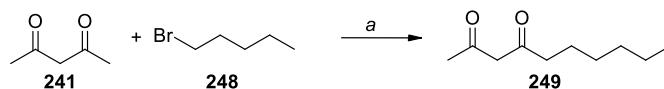
Scheme 60. Conditions: (a) i) NaH, THF, 5 °C, 10 min; ii) *n*-BuLi, -20 °C, 30 min; iii) **244**, 0 °C, 3 h.

Consequently, the alkylating agent was changed in case the bromide was not a good enough leaving group and/or the masked aldehyde was causing problems. A more reactive alkylating agent was therefore synthesised in which the bromide was exchanged for an iodide and the masked aldehyde was replaced with a protected hydroxyl group. The new alkylating agent bearing a THP-protected hydroxyl **247** was synthesised using a Finkelstein reaction as described in Scheme 61.¹⁴⁵

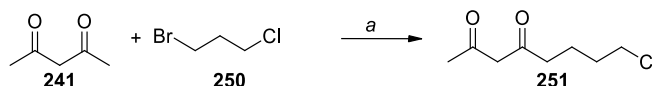


Scheme 61. Conditions: (a) NaI, acetone, rt.

At the time this work was performed there were a number of reports where acetylacetone had been successfully alkylated *via* the formation of the dienolate (Schemes 62 and 63).^{146,147}

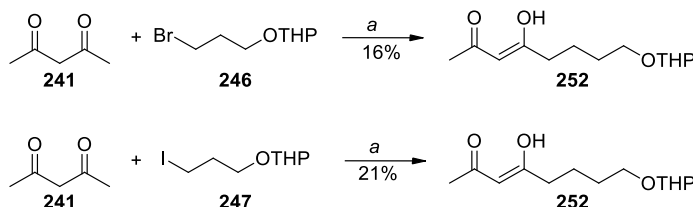


Scheme 62. Conditions: (a) i) NaH, THF, 0 °C, 10 min; ii) *n*-BuLi, 0 °C, 20 min; iii) **248**, rt.¹⁴⁶



Scheme 63. Conditions: (a) i) NaH, THF, 0 °C, 1 h; ii) *n*-BuLi, 0 °C, 10 min; iii) **250**, -50 °C to -30 °C, 18 h.¹⁴⁷

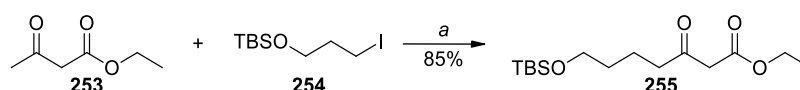
For this reason acetylacetone was chosen as model system to evaluate the ability of alkylating agents **246** and **247** to alkylate the derived dienolate (Scheme 64).^{146,147}



Scheme 64. Conditions: (a) i) NaH, THF, 0 °C, 30 min; ii) *n*-BuLi, -20 °C, 30 min; iii) 1,3-dimethyl-3,4,5,6-tetrahydro-2(1H)-pyrimidinone, -20 °C, 30 min; iv) **246** or **247**, T between -5 °C and 0 °C.

The mixture of acetylacetone, NaH and BuLi in THF was a suspension at the start, and so, 1,3-dimethyl-3,4,5,6-tetrahydro-2(1H)-pyrimidinone was added with the aim of obtaining a homogenous solution.¹⁴⁸ However, the addition of this co-solvent did not have the desired effect and the reaction mixture remained a suspension. Starting from the same amount of material (0.67mL of acetylacetone) both reactions delivered compound **252** successfully using either 2-[(3-iodopropyl)oxy]tetrahydro-2H-pyran **247** (244 mg) or 2-[(3-bromopropyl)oxy]tetrahydro-2H-pyran **246** (196 mg). Isolation of pure **252** was difficult, but **247** gave a slightly cleaner reaction. In both cases, the enol was observed instead of the diketone in NMR samples, and this was confirmed by characteristic proton signals for enolic

OH at 15.49 ppm (broad) and alkene CH at 5.50 ppm. Whilst it was encouraging to isolate the desired product **252**, the amounts of product obtained were disappointing. In an effort to improve the yield of this reaction the effect of concentration was investigated. Analysis of the literature showed that when Lee *et al.* alkylated the dianion of β -ketoester, using a similar alkylating agent **254** to that used in the current work, they performed the reaction at 0.17 M and they isolated the product in 85% yield (Scheme 65).¹⁴⁹



Scheme 65. Conditions: (a) i) NaH, THF, 0.17 M, 0 °C, 1 h; ii) *n*-BuLi, 0 °C, 1 h; iii) **254**, rt.¹⁴⁹

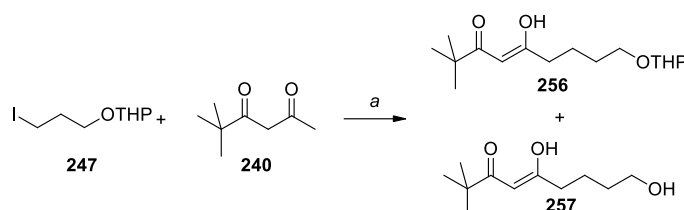
The alkylation of the dienolate of **241** was therefore performed at various concentrations using alkylbromide **246** and alkyl iodide **247**. Performing the reaction under conditions similar to those of Lee *et al.* (0.16 M) enable the isolation of a larger amount of crude product compare to the reaction performed at higher concentration (0.30 M) (440 mg vs 244 mg) (Table 30).

Alkylating agent	Concentration	Product	Amount (mg)
246	0.30 M	252	196
247	0.30 M	252	244
247	0.16 M	252	440

Table 30. Yields of synthesis of **252**. All three reactions carried out with the same amount of acetylacetone (0.67 mL).

Because of the improved yield, **240** was alkylated using similar conditions described in Scheme 63 and Table 30. The alkylation was undertaken with 1.5 mL of **240**, with alkyl iodide **247** in dilute conditions (0.16 M), at a higher temperature (between -10 °C and 0 °C), and calcium hydride was used to ensure that the reaction mixture was completely dry

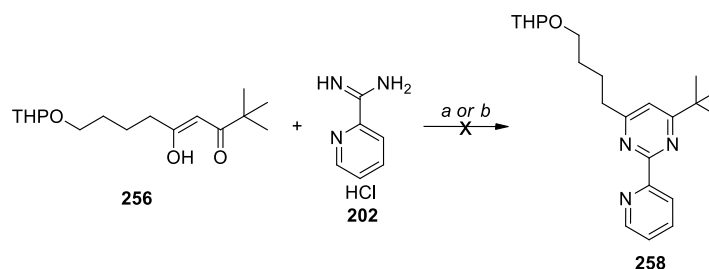
(Scheme 66).¹⁵⁰ The calcium hydride was added after addition of 5,5-dimethylhexane-2,4-dione **240** in the suspension of NaH in THF. These conditions delivered two products; these were the target **256** and related compound **257** from which the tetrahydropyranyl protecting group had cleaved. Neither compound could be isolated in high purity; however their structures were inferred by the detection of the characteristic signals of the enolic OH (15.8 ppm for **256** and 15.9 - 15.7 ppm for **257**) and alkene CH (5.7-5.6 ppm for **256** and 5.6 ppm for **257**) (*cf.* Experimental section).



Scheme 66. Conditions: (a) i) NaH, CaH₂, THF, -10 °C, 30 min; ii) *n*-BuLi, 0 °C; iii) **247**, 0 °C, 90 min.

With the required material **256** in hand, cyclisation with picolinimidamide to form the pyridyl-pyrimidine core could be attempted (Scheme 67). The reaction was performed at 50 °C with one equivalent of sodium ethoxide in ethanol (pK_a of 16). However, compound **258** was not formed and only picolinimidamide was present in the crude reaction mixture. The reaction was repeated with a non-nucleophilic base of similar basicity, DIPEA (pK_a ~11), so that the base could not react with the starting material. Two equivalents of base were used; one to form the free base of the amidine and one to drive the formation of the pyrimidine. To favour the formation of the pyrimidine ring the temperature was increased to 200 °C and no solvent was utilised. Disappointingly, despite these modifications **258** was not formed and picolinimidamide was consumed with multiple side-products being detected. Although a literature search showed that there were 47 hits for the formation of a pyrimidine ring from a

nitrogen containing 6-membered ring amidine and a diketone,¹⁵¹ it is unclear why the cyclisation failed and further studies are required.



Scheme 67. Conditions: (a) NaOEt, EtOH, 50 °C or (b) DIPEA, 200 °C.

As a result of the failure of this initial route, an alternative route to target molecule **237** was investigated (Figure 37).

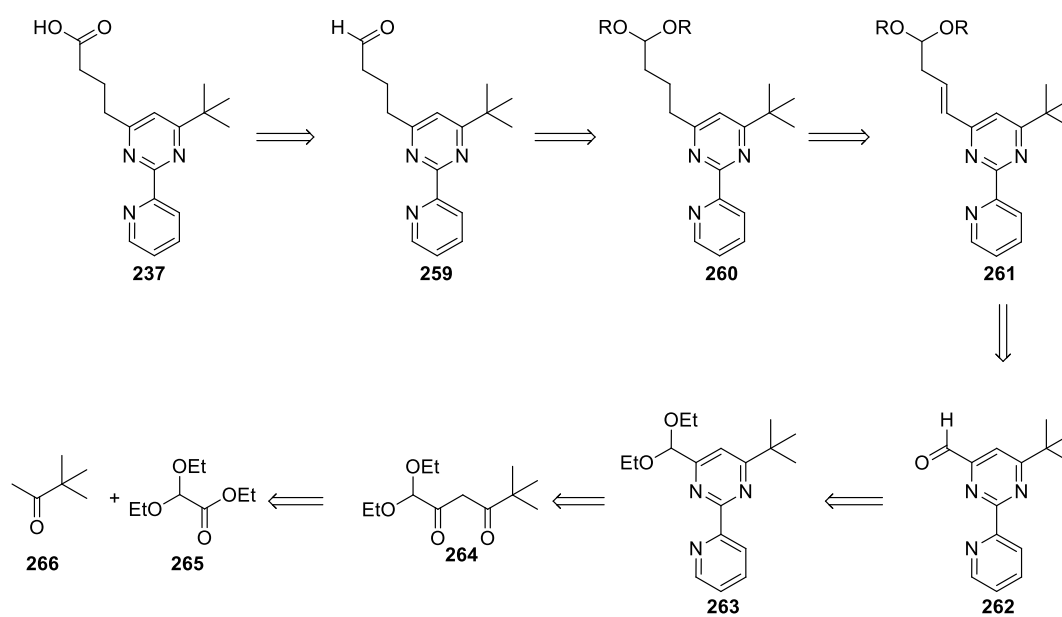
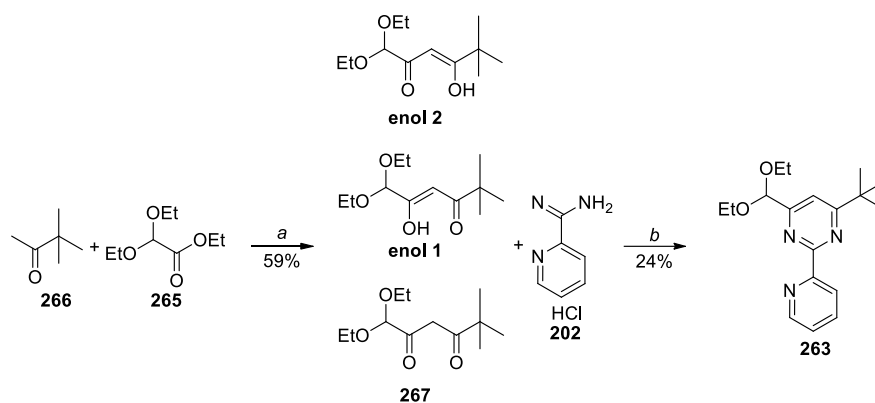


Figure 37. Retrosynthetic route analysis of **237**.

The desired product could result from oxidation of aldehyde **259** which could be released from acetal deprotection of **260**. Acetal **260** could be the result of reduction of the double bond of **261** which could be formed from Wittig reaction of aldehyde **262**.^{152,153} This

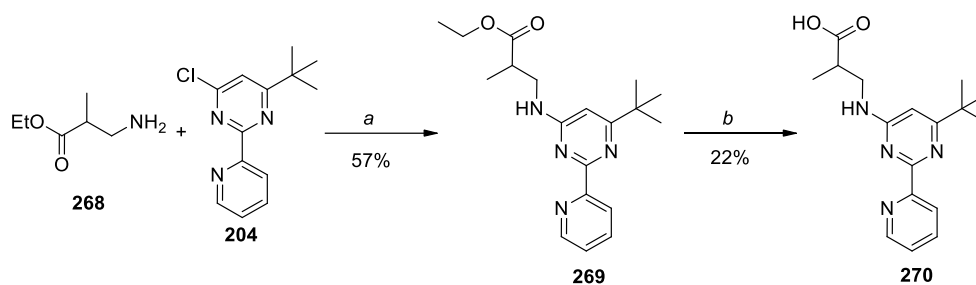
aldehyde **262** could be synthesised from acetal protected pyridyl-pyrimidine **263**, which could be formed by pyrimidine cyclisation with diketone possibly made by acylation of **266** with **265**. As shown in Figure 37, the synthesis involves seven steps (as opposed to four steps for the synthesis initially attempted), thus explaining why this was not attempted earlier. Acylation of 3,3-dimethyl-2-butanone **266** with ethyl *bis*(ethoxy)acetate **265** gave enol **267** in moderate yield (Scheme 68) as part of a mixture of tautomers. The presence of two enols and the diketone was inferred from the detection of characteristic signals of acetal CH (4.89 ppm for enol 1, 4.92 ppm for enol 2 and 4.65 ppm for the diketone) and alkene CH (6.00 ppm for enol 1 and 5.75 ppm for enol 2). Analysis of sample run in DMSO- d_6 by ^1H NMR showed that the tautomers were present with a ratio of enol 1:diketone:enol 2 = 5:1.5:1. Subsequent reaction of the enol **267** with **202** delivered the pyridyl-pyrimidine **263** in low yield. Having validated the chemistry to deliver 178 mg of **263** there remained a further five steps before the desired final product could be isolated; additional quantities of **263** would be required to achieve this. Completing this sequence would require investment of time so resources were re-directed to other areas of research.



Scheme 68. Second route to **237**. Conditions: (a) i) LiHMDS, THF, -70 °C, 30 min; ii) **265**, 5 °C, 2 h; (b) **202**, NEt₃, EtOH, 70 °C, 5 days.

II.3.1.4 α -Substituted acids

Compound **270** was designed to study the effect of branching in the linear side-chain (Scheme 69). Racemic amine ester **268** was introduced by S_NAr with chloropyrimidine **204** to give ester **269** in moderate yield. The ester was hydrolysed using lithium hydroxide and gave final compound **270**.



Scheme 69. Conditions: (a) DIPEA, DMSO, microwave, 150 °C; (b) LiOH monohydrate, THF/water 1:1, rt.

Two months after work on the pyridyl-pyrimidine series was initiated, the crystal structure of apo JmjD3 was solved by colleagues in Computational and Structural Chemistry (CSC).¹⁵⁴ Shortly afterwards, a soaking experiment enabled the structure of pyridyl-pyrimidine **11** bound to JmjD3 to be solved. This structure was used to guide the design of target compounds. One such example of structure based drug design (SBDD) was compound **271** (Figure 38) which was targeted in response to analysis of the overlay of the structures of 2-OG and **11** bound to JmjD3. The rationale behind the target will be covered more fully in Section II.3.2.5.

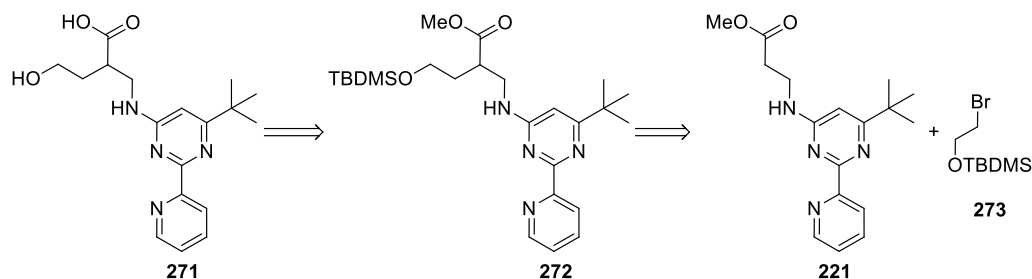
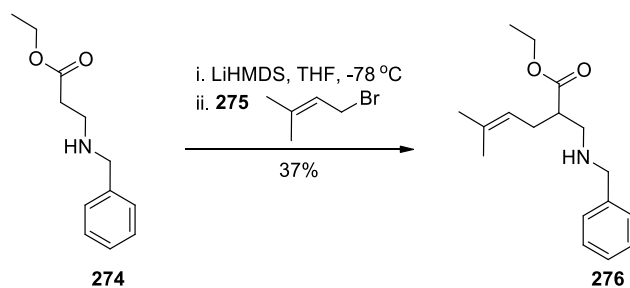


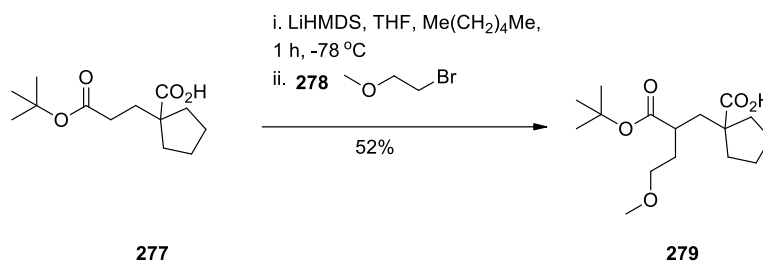
Figure 38. Retrosynthetic analysis of compound **271**.

Unfortunately compound **271** could not be obtained simply by using the S_NAr chemistry used for previous analogues since a suitably functionalised amine was not available. This left two options for the synthesis of **271**; synthesis of an appropriately functionalised amine or append a hydroxyethyl side chain onto a late-stage intermediate. Since the latter approach had the fewest steps count, it was attempted first. As shown in Figure 38, it was envisaged that **271** could be obtained by deprotection of **272**, which could be accessed by alkylation of **221**, which was readily available.



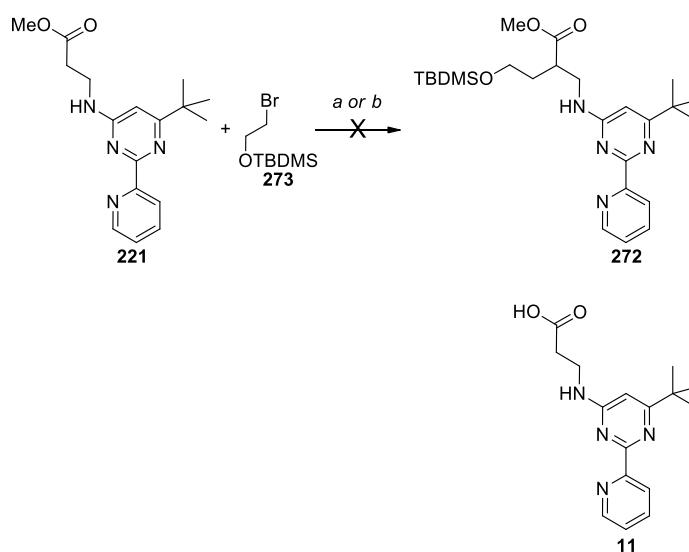
Scheme 70. Literature example of alkylation of β -aminoesters.¹⁵⁵

Literature precedent demonstrated that alkylation α - to an ester in the presence of an amine was possible using a combination of LiHMDS (as base) and powerful allylic electrophiles (Scheme 70).¹⁵⁵ Reports describing the use of weaker electrophiles for alkylation α to ester had also been reported (Scheme 71).¹⁵⁶



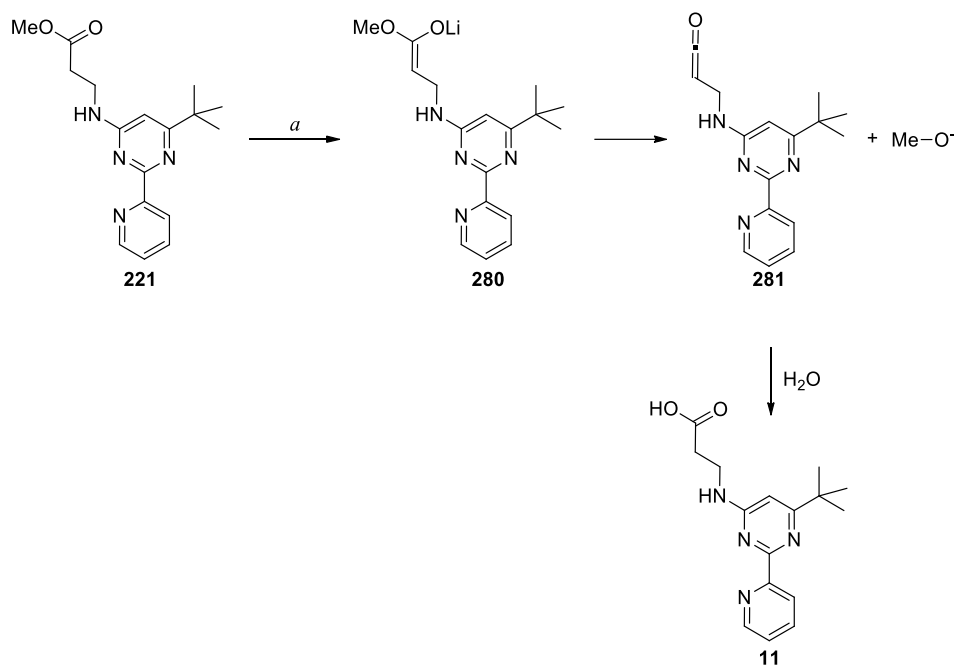
Scheme 71. Literature example of alkylation of β -aminoesters.

Following the literature precedent, LiHMDS ($pK_a \sim 36$) was added to ester **221** at $-70\text{ }^\circ\text{C}$ before addition of the protected bromoethanol **273** (Scheme 72). Analysis by LC/MS indicated that rather than the desired alkylated product **272**, by-product **11** was formed. The experiment was repeated, but this time using the stronger base *n*-BuLi ($pK_a \sim 50$) at $-70\text{ }^\circ\text{C}$. Compound **11** was again the major component observed in the LC/MS.



Scheme 72. Conditions: (a) *n*-BuLi, THF, $-70\text{ }^\circ\text{C}$ then **273**, rt or (b) LiHMDS, THF, $-70\text{ }^\circ\text{C}$ then **273**, rt.

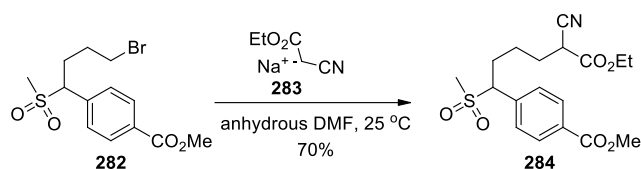
In both cases the ester **221** was hydrolysed, possibly *via* the ketene **281**,^{157,158} arising from the methoxide anion eliminating from the ester. If the ketene was formed it could react rapidly with water to give the carboxylic acid (**11**) (Scheme 73).



Scheme 73. Ester hydrolysis *via* ketene **281**. Conditions: (a) LiHMDS, THF, -70 °C or *n*-BuLi, THF, -70 °C then **273**, rt.

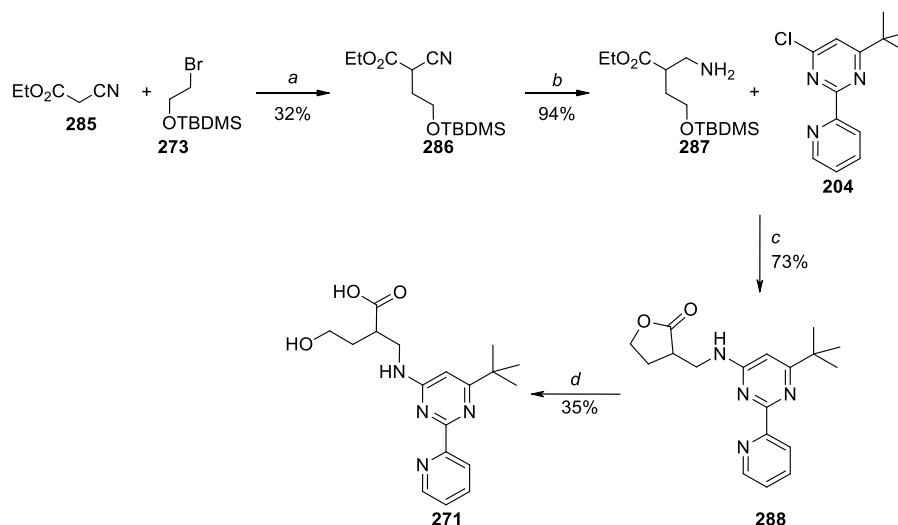
When this reaction was carried out with a much less reactive alkylating agent (like **273**) the formation of the ketene appeared to occur faster than the alkylation. This alkylation could have potentially delivered the desired product with a more powerful alkylating agent such as a protected iodoethanol, but this route was not pursued further.

Following the unsuccessful attempts to alkylate the late stage intermediate **221** an alternative approach to target **271**, involving the formation of the appropriate amine (Scheme 75), was investigated. The synthesis of the amine required the alkylation of ethylcyanoacetate which had been reported in the literature (Scheme 74).¹⁵⁹



Scheme 74. Literature example of alkylation of β -aminoesters.¹⁵⁹

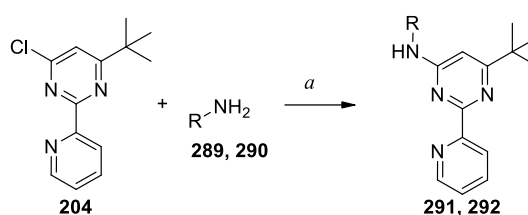
Alkylation of the sodium salt of ethyl cyanoacetate **285** using **273** gave intermediate **286** in moderate yield. The success of this reaction could be due to the high stability of the conjugate base of **285**. Hydrogenation of **286** using Raney nickel gave the required amine **287** in 94% yield.¹⁶⁰ During the S_NAr reaction between amine **287** and chloropyrimidine **204**, the *tert*-butyldimethylsilyl protecting group cleaved and the resulting hydroxyl group reacted with the ethyl ester *via* a lactonisation reaction to form the lactone **288**. Hydrolysis of this lactone gave the final compound **271** in moderate yield.



Scheme 75. Conditions: (a) NaH, DMF, 0 °C, then **273**; (b) Raney Ni, H₂, EtOH, 90 °C, 90 bar; (c) **204**, DIPEA, DMSO, microwave, 150 °C; (d) LiOH, THF/water 1:1, rt.

II.3.1.4 Vector 4: conformationally constrained linkers

Since compound **11** contained a flexible two-carbon chain, it was decided to investigate the effect of conformational constraint with the goal of locking the chain in a conformation which may give rise to enhanced potency. This will be discussed further in the Assay Results and Discussion Section. Two cyclobutanes and one cyclopropane were targeted. The *trans*- and *cis*-cyclobutane analogues **291** and **292** were synthesised using the methodology described in Section II.3.1.1.1 (Scheme 76 and Table 31).

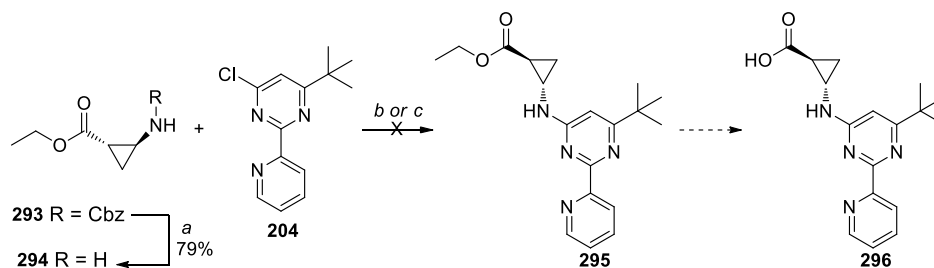


Scheme 76. Conditions: (a) DIPEA, DMSO, microwave, 150 °C.

Amines		Product		Yield (%)
289		291		32
290		292		20

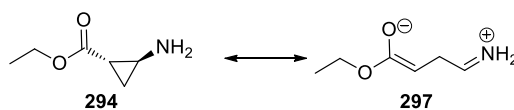
Table 31. S_NAr products.

The *trans*-cyclopropane **296** was also targeted (Scheme 77) to investigate an alternative conformational constraint.



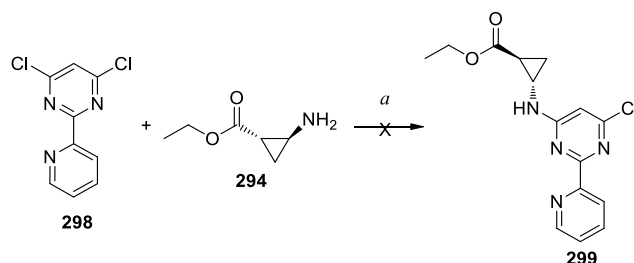
Scheme 77. Cyclopropyl constrained linker. Conditions: (a) H₂, Pd/C, MeOH; (b) **294**, DIPEA, DMSO, microwave, 150 °C, 4 h; or (c) NaH, DMF, rt, 24 h; NMP, 150 °C, 2 h.

The racemic *trans*-ethyl cyclopropanecarboxylate **294** formed by hydrogenation of **293**, was reacted with **204** using the standard S_NAr conditions but without success (only **204** was identifiable). Other conditions were attempted for the formation of intermediate **295**; these included deprotonating **294** with sodium hydride, or carrying out the S_NAr reaction in a different solvent such as NMP. None of these conditions led to the formation of the desired product. The failure of the reaction was thought to be related to the poor nucleophilicity of the amine, which may be reduced by the proximal electron-withdrawing ester. The cyclopropyl ring is known for its peculiar chemical properties and is often described as a ring with π character.¹⁶¹ The ethyl ester could, therefore, reduce the nucleophilicity of the amine either through the “π system” of the cyclopropyl or more probably through the resonance forms described in Scheme 78.



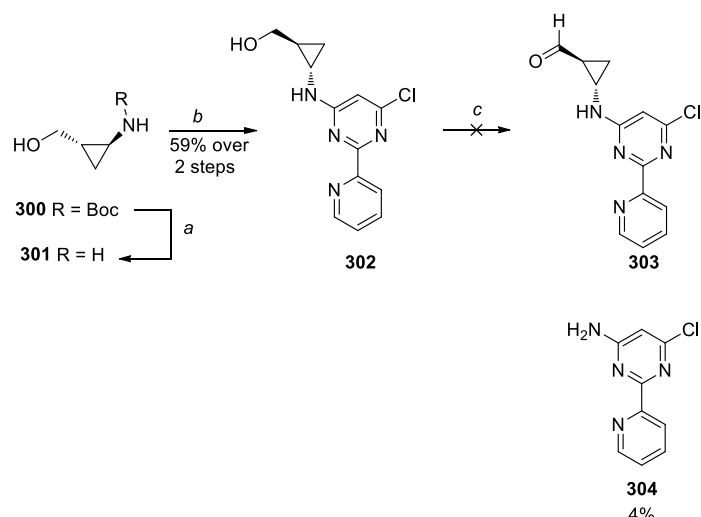
Scheme 78. Proposed explanation for relatively low nucleophilicity of ethyl 2-aminocyclopropanecarboxylate.

In an effort to compensate for the poor nucleophilicity of the amine **294** a reaction was attempted between amine **294** and the more electrophilic dichloropyrimidine **298** (Scheme 79).



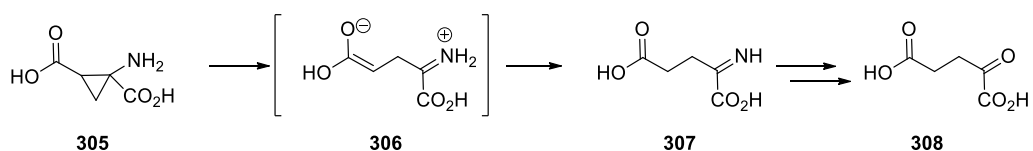
Scheme 79. Cyclopropyl constrained linker. Conditions: (a) DIPEA, dioxane, 90 °C, 72 h; DIPEA, dioxane, microwave, 150 °C, 2 h.

No reaction was observed after 72 h heated thermally at 90 °C, so the mixture was heated in the microwave for 2 h at 150 °C. Disappointingly, analysis of the LC/MS indicated that dichloride **298** remained along with side-products, probably resulting from decomposition of the starting material. It had now been shown that increasing the electrophilicity of the chloropyrimidine was insufficient to lead to productive reaction. This led to the investigation of the effect of increasing the nucleophilicity of the amine. With this in mind, it was decided to attempt a nucleophilic displacement using the amino alcohol **301** in which the ester functionality of **294** was replaced with a hydroxymethyl group, which could be oxidised at a later stage. The Boc protected amine **300** (available in our compound bank) was deprotected using hydrochloric acid in dioxane. The solution of **301** hydrochloride in dioxane was added to a mixture of **298** and DIPEA and stirred for 18 h at room temperature, the reaction was not complete and so, the reaction was then heated at 80 °C to drive the reaction to completion (Scheme 80).



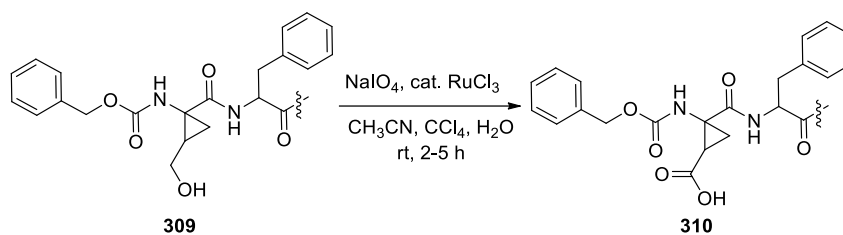
Scheme 80. S_NAr with 2-aminocyclopropylmethanol. Conditions: (a) HCl, dioxane, rt, 18 h; (b) **298**, DIPEA, dioxane, rt for 18 h then 80 °C for 4 h; (c) SO_3 .pyridine, NEt_3 , DMSO/DCM 1:1, 4 h.

Gratifyingly, compound **302** was successfully isolated in 59% yield, thus suggesting that the increase in nucleophilicity of the amine was the key to successful displacement. Disappointingly, however, attempted oxidation of alcohol **302** to the aldehyde **303**, using pyridine sulfur trioxide and triethylamine, failed to give the expected product. From the reaction mixture it was only possible to isolate a very small quantity of 6-chloro-2-(pyridin-2-yl)pyrimidin-4-amine **304**. In light of these results a detailed analysis of the literature was performed and revealed that 1-amino-2-carboxy cyclopropyl systems are unstable and the lone pair of the nitrogen (if available) can initiate the opening of the cyclopropane (Scheme 81).¹⁶²



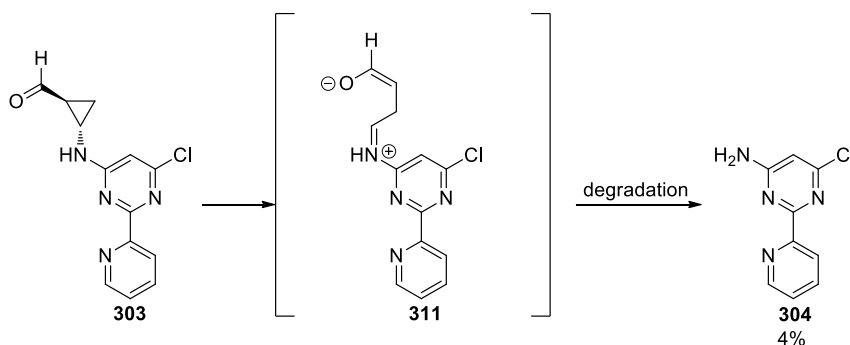
Scheme 81. Spontaneous ring opening of 1-aminocyclopropane-1,2-dicarboxylic acid.¹⁶²

When the nitrogen atom is acylated, the lone pair is much less available to participate in the reactions depicted in Schemes 80 and 81, making the formation of stable compounds such as **293** and **310** possible (Scheme 82). It is therefore probable that the extra stabilisation of the lone pair imparted by the carbamate group of **309** enables the hydroxymethyl group to be oxidised to deliver acid **310**.



Scheme 82. Example of formation of stable Cbz aminocyclopropanecarboxylic acid.¹⁶²

By analogy, the spontaneous ring opening of 1-aminocyclopropane-1,2-dicarboxylic acid **305** reported by Godier-Marc *et al.*¹⁶² suggests that **303** might degrade quickly leading to the formation of amino-pyrimidine **304** (Scheme 83).



Scheme 83. Proposed mechanism for the formation of **304**.

As a result of these findings it was acknowledged that the target compound **296** was unlikely to be stable so efforts in this area were terminated.

II.3.1.5 Vector 6: *tert*-butyl replacement

The X-ray crystal structure of **11** bound to JmjD3 was solved shortly before work to probe the pocket occupied by the *tert*-butyl group of **11** was initiated, so it was used to guide the design of the targets in this area of the molecule. Various substituents were introduced at position 6 to investigate the size of the pocket and create interactions with polar residues. The biochemical results of this work will be discussed more fully in Section II.3.2.6.

II.3.1.5.1 C-Linked substituents

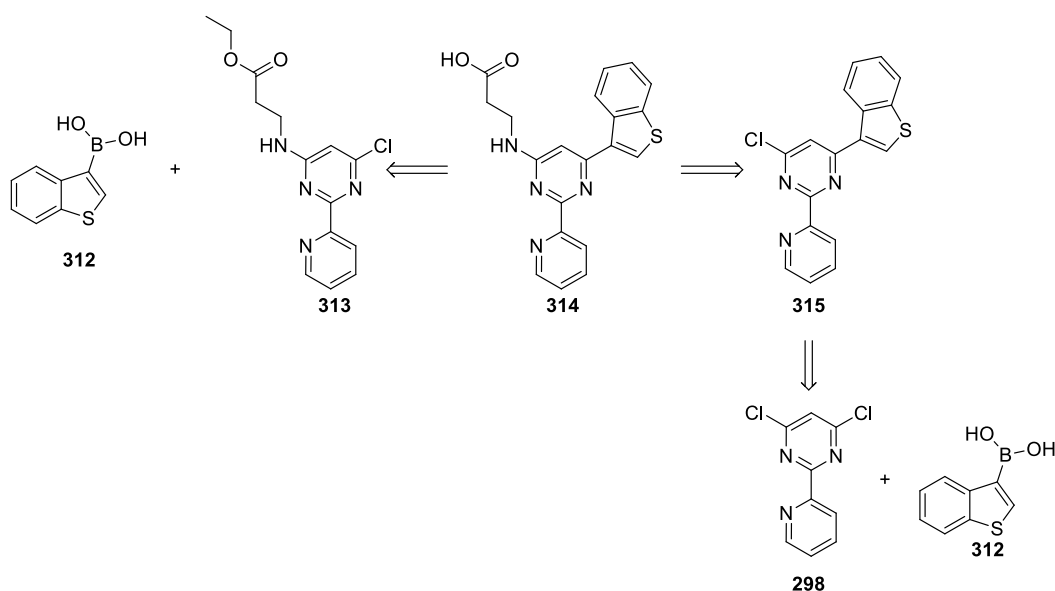
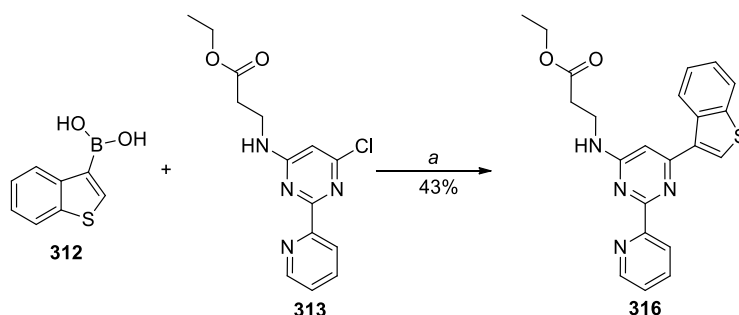


Figure 39. Retrosynthetic routes to compound **314**.

Benzothiophene was one of the aromatic rings considered for this position. Two routes were evaluated for this target as shown in Figure 39.

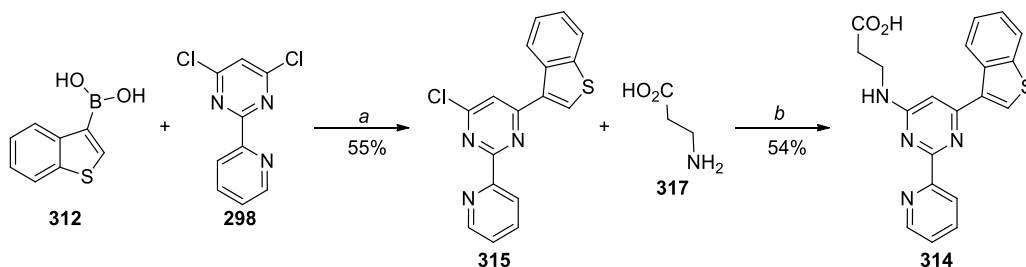
To explore the *tert*-butyl group pocket further, a late-stage intermediate was required to rapidly access final compounds *via* cross-coupling and/or S_NAr reactions. Intermediate **313** was made in gram quantities elsewhere in our laboratory¹⁶³ to support this overall effort.

It was envisaged initially that the desired material **316** could be accessed *via* a Suzuki cross-coupling of benzothiophen-3-ylboronic acid **312** with ethyl 3-((6-chloro-2-(pyridin-2-yl)pyrimidin-4-yl)amino)propanoate **313**. Compound **316** was isolated in 43% yield (Scheme 84). Concurrently with this work an alternative approach was employed in which a cross-coupling reaction was performed between **312** and dichloropyridyl-pyrimidine **298** to give intermediate **315** in 55% yield (Scheme 85).



Scheme 84. Benzothiophene target. Conditions: (a) Pd(PPh₃)₄, Cs₂CO₃, 1,4-dioxane/water 4:1, 100 °C, microwave, 30 min.

The Suzuki route with intermediate **298** was pursued because of its higher yield.



Scheme 85. Benzothiophene target. Conditions: (a) Pd(PPh₃)₄, Cs₂CO₃, 1,4-dioxane/water 4:1, 100 °C, microwave, 30 min; (b) DIPEA, DMSO, microwave, 150 °C, 2 h.

Since this scheme involved the use of palladium in the presence of the pyridyl-pyrimidine moiety there was a possibility that metal ions could be carried through the reaction sequence by chelation with the pyridyl-pyrimidine ring. The need to remove transition metals after cross-coupling reactions is not unique to this project, and approaches have been developed to

achieve this. Ferrari *et al.* have shown that silica gel containing a thiourea group can sequester Pd(II) from aqueous or organic media.¹⁶⁴ Thiourea-containing silica gel sorbent can also scavenge metals such as Ag and Au.¹⁶⁵

With this in mind, to reduce the risk of contamination intermediate **315** was purified by normal phase column chromatography followed by treatment with SiliaMetS® Thiourea (Figure 40) to remove residual palladium.¹⁶⁶

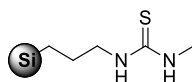
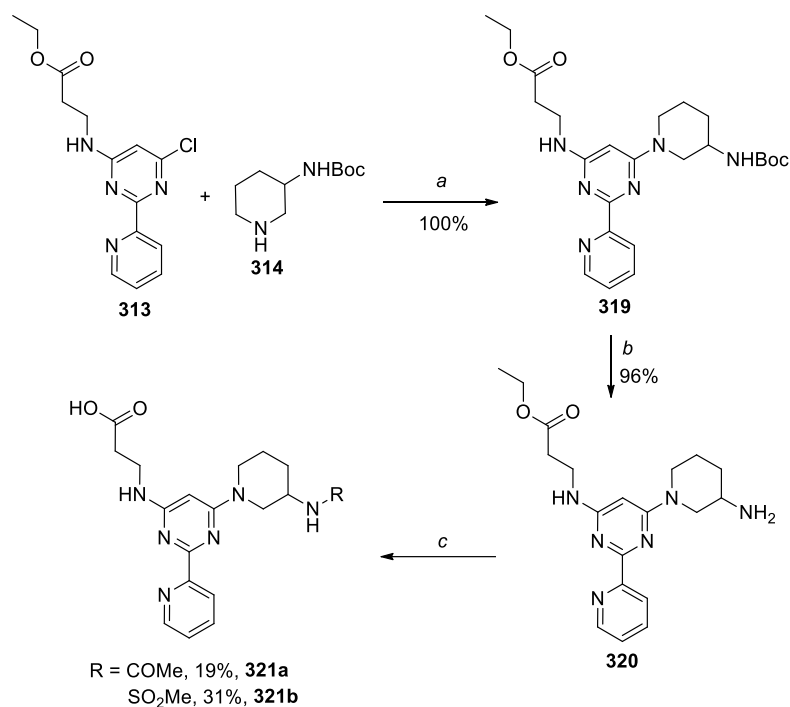


Figure 40. SiliaMetS® Thiourea

With **315** in hand an S_NAr reaction with 3-aminopropanoic acid **317** to deliver the final compound **314** in moderate yield after MDAP purification (which was also known to remove residual metal from products *cf.* Section II.3.1.1.1). A colleague demonstrated that after the use of thiourea resin, there was only 4 ppm of palladium left in the sample giving a compound pure enough to be tested.¹⁶⁷ Although thiourea resin and MDAP purification had been shown to remove metals from samples by a colleague, it was still preferable to avoid the use of transition metal ions as far as possible, so *N*-linked substituents, which could be accessed without the use of transition metals were investigated.

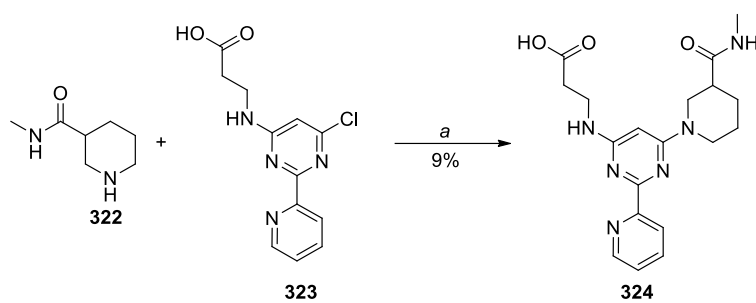
II.3.1.5.2 *N*-Linked substituents

The synthesis of the first set of 6-*N*-linked targets is described in Scheme 86. The Boc-protected 3-aminopiperidine was introduced by S_NAr reaction with chloropyrimidine **313**. After quantitative deprotection, the 3-aminopiperidine **320** was acylated and sulfonlated, followed by ester hydrolysis to give compounds **321a** and **321b**.



Scheme 86. 3-substituted aminopiperidine target. Conditions: (a) DIPEA, 1,4-dioxane, 150 °C; (b) TFA, rt; (c) i) acetyl chloride or methanesulfonyl chloride, DCM, rt; ii) LiOH, THF/water 1:1, rt.

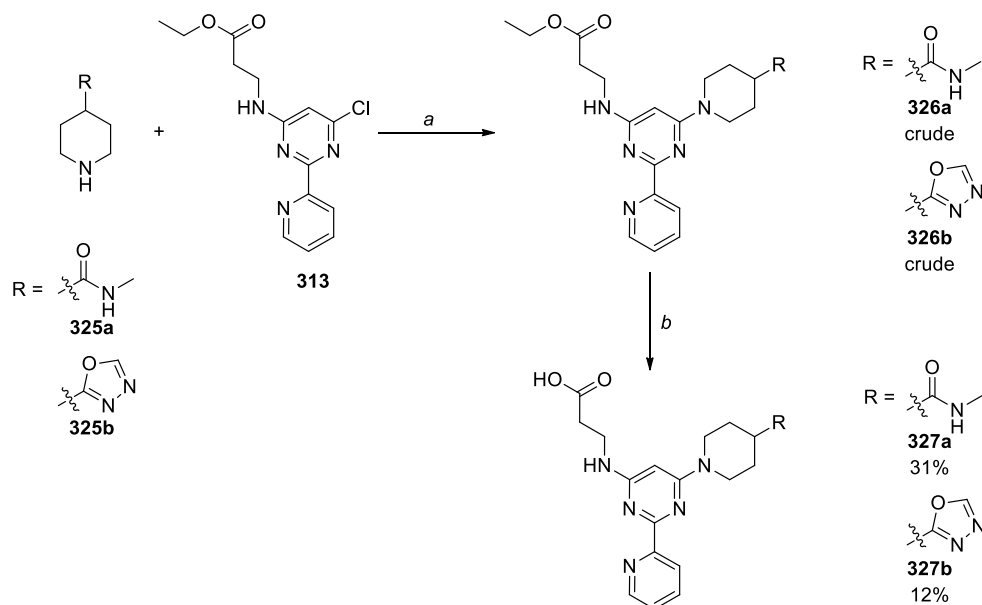
To explore the effect of reversing the amide of **321a**, *N*-methylpiperidine-3-carboxamide **322** was reacted with the carboxylic acid **323** (synthesised elsewhere in our laboratory)¹⁶⁸ to deliver final product **324** (Scheme 87).



Scheme 87. 3-Substituted aminopiperidine targets. Conditions: (a) DIPEA, DMSO, microwave, 160 °C.

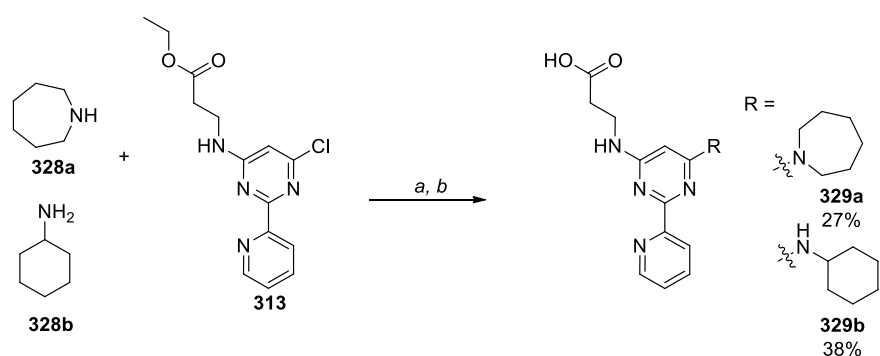
Compound **324** was isolated in a disappointing 9% yield; all of the starting material was consumed, but there were several side-products (51% in total) along with the desired product (49%). None of the side products were isolated. In addition, two MDAP purifications were required to obtain a product pure enough to be submitted for test. The combination of formation of side-products and the difficult purifications may explain the low yield of this reaction. It was shown in Scheme 86 that an S_NAr carried out in 1,4-dioxane in the presence of the ethyl ester intermediate **313** could be high yielding. It was therefore decided to carry out the remaining S_NAr reactions on the ethyl ester intermediate **313**.

The *N*-methylamide at position 4 of the piperidine (**327a**) was designed to investigate the effect of moving the acetamido group around the piperidine. The commercial piperidine **325a** was reacted with ethyl 3-((6-chloro-2-(pyridin-2-yl)pyrimidin-4-yl)amino)propanoate **313** to give a mixture of **326a** and DIPEA after partial purification (Scheme 88). This material was used in the next step, where hydrolysis of the ester followed by MDAP purification gave the final product **327a** in moderate yield. The oxadiazole at position 4 of the piperidine (**327b**) was designed as an isostere for the acetamide (**327a**). The commercial piperidine **325b** was reacted with intermediate **313** to form the 4-oxadiazole piperidine **326b** (Scheme 88). Hydrolysis of the ester gave the final product **327a** in moderate yield.



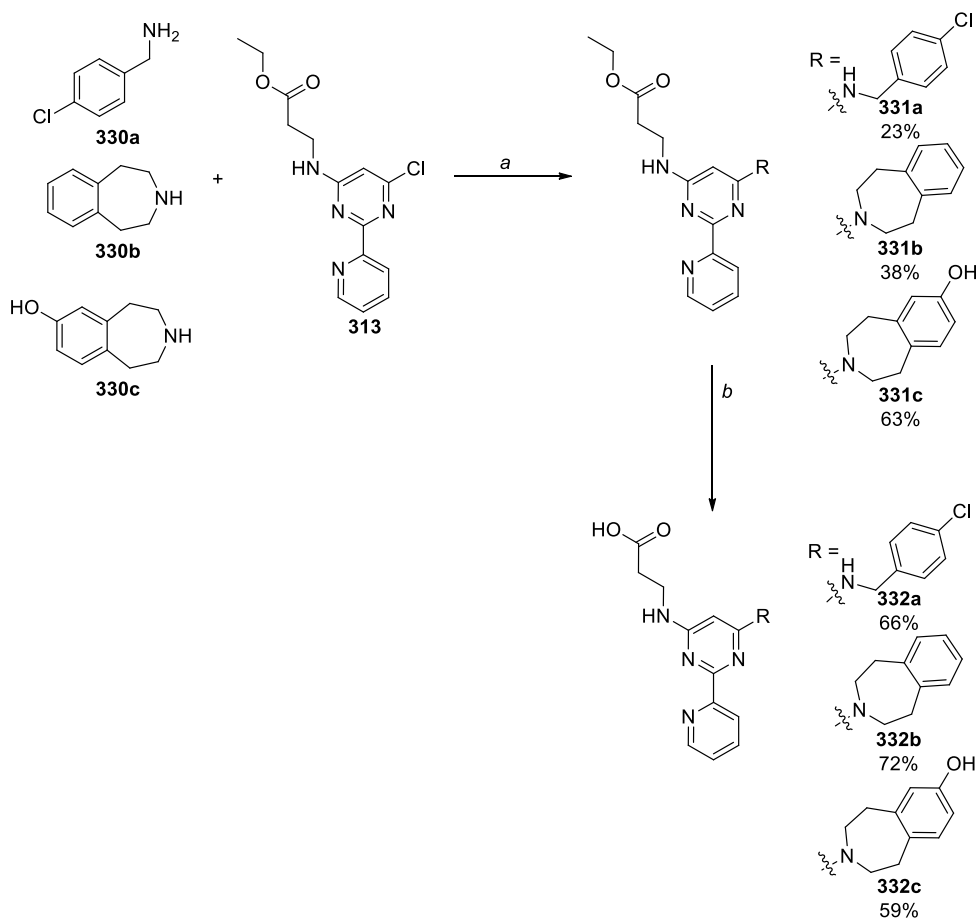
Scheme 88. 4-Substituted aminopiperidine targets. Conditions: (a) DIPEA, 1,4-dioxane, microwave, 160 or 200 °C; (b) LiOH, THF/water 1:1, rt.

Unsubstituted aliphatic amines such as azepane and cyclohexylamine were also investigated. These compounds were synthesised using the same methodology as the previously described analogues; S_NAr reaction followed by ester hydrolysis (Scheme 89).



Scheme 89. Aliphatic amine targets. Conditions: (a) DIPEA, 1,4-dioxane, microwave; (b) LiOH, THF/water 2:1, rt.

Next to be synthesised were analogues derived from amines containing aromatic rings. These targets were designed to probe for interactions with Arg1247 present in the pocket occupied by the *tert*-butyl group of **11**. This will be discussed further in Section II.3.2.6.



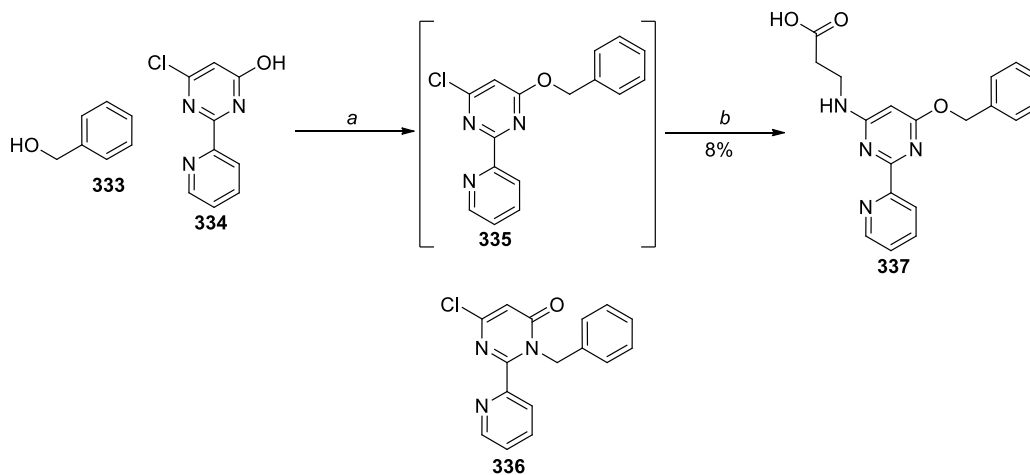
Scheme 90. Aromatic ring containing amine targets. Conditions: (a) DIPEA, 1,4-dioxane or DMSO, microwave; (b) LiOH, THF/water 1:1, rt.

The amines containing aromatic rings were introduced by S_NAr , giving intermediates **331a**, **b** and **c** in various yields (Scheme 90). Finally, the esters **331a**, **b** and **c** were hydrolysed to give the final compounds **332 a**, **b** and **c** in good yields.

II.3.1.5.3 6-*O*-Linked substituents

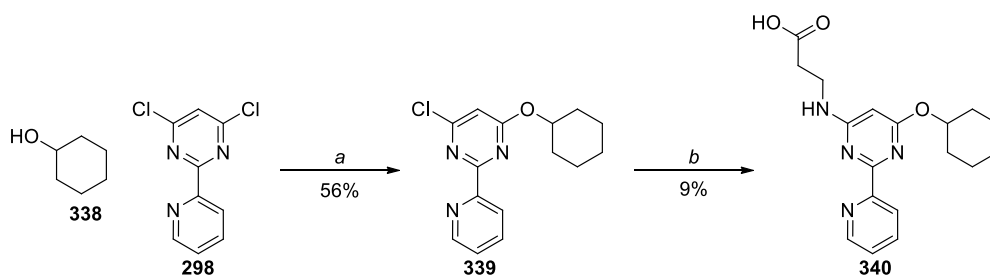
In parallel to the 6-*N*-linked compounds, an oxygen linker was investigated with aliphatic and aromatic substituents. These targets were designed essentially to evaluate the effect on inhibitor potency of having an *O*-linker compared to a *N*-linker.

The first approach to *O*-linked analogues utilised hydroxypyrimidine **334** which was made elsewhere in our laboratory (Scheme 91).¹⁶⁹ Alkylation of the hydroxyl of **334** was achieved using Mitsunobu methodology, and delivered two compounds of the same molecular weight in the ratio of 1.1:1. The less polar of these was partially isolated by automated chromatography (SP4), characterised and shown to be **335**. The more polar side product which had a molecular ion of mass 298 was also isolated from the purification. *N*-alkylation product **336** would have an $[M+H]^+$ ion of this mass, but no further evidence for structure **336** was obtained. Despite the purification on normal phase sample **335** contained DIAD in a 1:1 ratio. The impure **335** gave **337** after a S_NAr with a 8% yield over two steps.



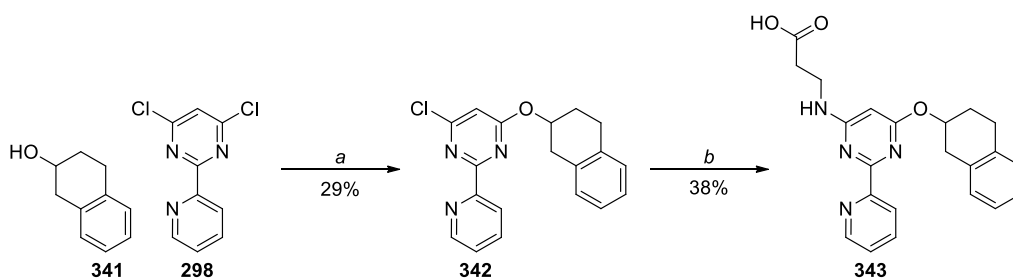
Scheme 91. *O*-Benzyl target. Conditions: (a) DIAD, PPh₃, THF, rt, 2 h; (b) β -alanine, DIPEA, DMSO, 150 °C, microwave.

Due to the limited availability of chloro-hydroxypyrimidine **334**, dichloropyrimidine **298** was used to pursue the exploration of this area. Compound **340** was formed by two consecutive S_NAr reactions. The cyclohexanol was introduced in a first in a moderate yield, followed by β -alanine to give **340** in low yield (Scheme 92). The S_NAr step with β -alanine gave a complex reaction mixture with more than twenty peaks observed by LC/MS, which explained the low yield for this step.



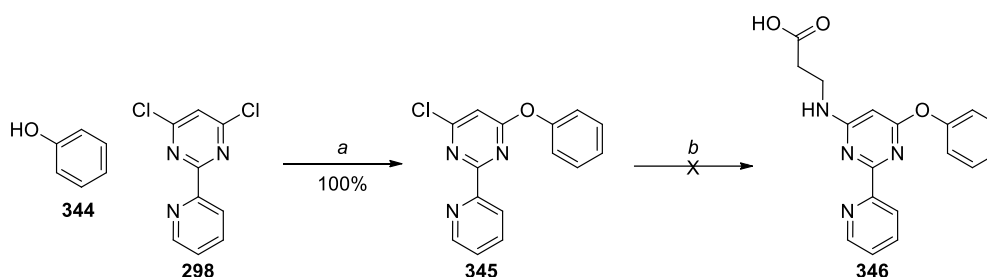
Scheme 92. *O*-Cyclohexyl target. Conditions: (a) NaH, DMF, rt; (b) β -alanine, DIPEA, DMSO, microwave, 200 °C, 2h.

Tetrahydronaphthalen-2-ol was introduced first to give intermediate **342** in 29% yield. Subsequent S_NAr at 150 °C instead for 200 °C, delivered compound **343** in 38% yield (Scheme 93). Carrying out the S_NAr at 150 °C, instead of at 200 °C, gave a much simpler product mixture compared to the formation of **340**.



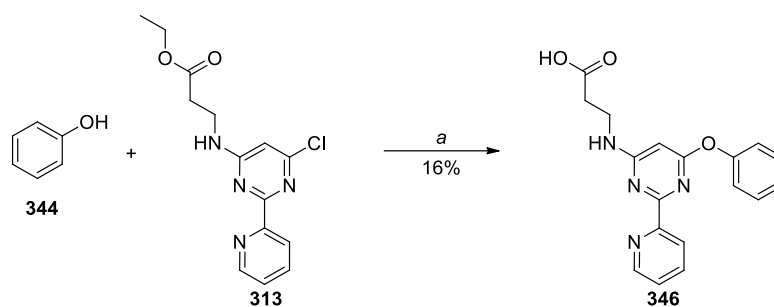
Scheme 93. Conditions: (a) NaH, DMF, rt; (b) β -alanine, DIPEA, 1,4-dioxane, microwave, 150 °C.

To provide a closely related analogue of **340** the 6-*O*-phenyl (**346**) was targeted, utilising the methodology employed for synthesis of **340**. Quantitative reaction of phenoxide ion with dichloropyrimidine **298** gave **345**. However, attempted introduction of the β -alanine side-chain *via* S_NAr reaction was problematic. Despite heating the mixture at 200 °C for two periods of two hours each, with an excess of β -alanine (2.4 eq) and DIPEA (6 eq). Only a trace (4%) of the desired product was observed by LC/MS, along with dichloropyrimidine **298** (37%) and a by-product (40%) which $[M+H]^+$ consistent with presence of 6-(phenyloxy)-2-(2-pyridinyl)-4-pyrimidinol, resulting from replacement of the chloride with hydroxide. The formation of this by-product could potentially be explained by the presence of water in one of the reagents. Due to the large amount of by-product and dichloropyrimidine **298** (almost 1:1 with **298**) after two runs at 200 °C, it was decided to employ another route to form the target **346** (Scheme 94).



Scheme 94. *O*-Phenyl target. Conditions: (a) CS_2CO_3 , DMF, rt; (b) β -alanine, DIPEA, 1,4-dioxane, microwave, 200 °C.

Scheme 94 showed that it was not possible to form **346** by introduction of phenol first, followed by β -alanine. An alternative approach was, therefore, investigated in which the order of introduction of the phenol and β -alanine substituents were reversed (Scheme 95). Intermediate **313** which contained the β -alanine substituent, was available in the laboratory, was reacted with phenol **344** to give the desired product as the ethyl ester. Subsequent ester hydrolysis delivered compound **346** in 16% overall yield (over two steps).



Scheme 95. *O*-Phenyl target. Conditions: (a) i. Cs₂CO₃, DMF, 95 °C; ii. LiOH, THF/water 2:1, rt.

The 6-*O*-linked substituted pyrimidine compounds were synthesised using three methodologies (Schemes 91, 94 and 96). The first method (Mitsunobu reaction followed by S_NAr), suffered from the main drawback of the formation of the *N*-alkylated product (Scheme 91). The second method showed that aliphatic alcohols should be introduced first *via* NaH mediated S_NAr with dichloropyrimidine **298**, followed by the β-alanine (Scheme 96), whilst in the third method the aromatic hydroxyls are introduced at the penultimate step *via* mild base mediated S_NAr reaction with the β-alaninate containing intermediate **313** (Scheme 94).

II.3.1.6 Design and synthesis of a chemoproteomic probe molecule

For reasons explained in section II.3.2.6, compound **332b** was selected as a tool molecule. In order to generate an immobilised probe for chemoproteomic studies a suitable attachment point needed to be introduced to **332b** in a way that did not affect its binding to the enzyme.

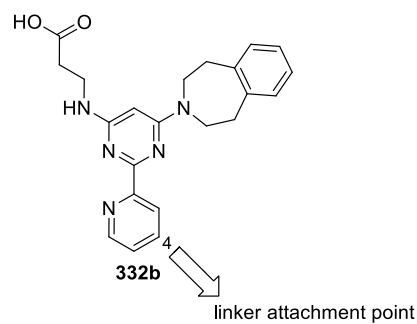


Figure 41. Linker attachment point.

The X-ray crystal structure of **332b** bound to JmjD3 showed that there was space around the 4-position of the pyridyl ring (Figure 41), suggesting that this was a good site for bead attachment. Additionally, a colleague had shown that substituents could be attached at this position *via* an O, an N and a C, resulting in the inhibition potency being maintained (Table 32).¹⁷⁰

Structure	Compound No.	MALDI pIC ₅₀
R		
	11	5.0
	347	5.3
	348	5.2*
	349	4.8

Table 32. Data for 4-substituted pyridyl. Compounds prepared elsewhere in our laboratory.¹⁷⁰

* 5.2 (n = 3) and < 4.0 (n = 1).

The encouraging result of the methoxy analogue in the biochemical assay led to an ether being selected as the functional group from which a tether to a linkable amine moiety could be introduced (Figure 42). This will be explained further in Section II.3.2.8.

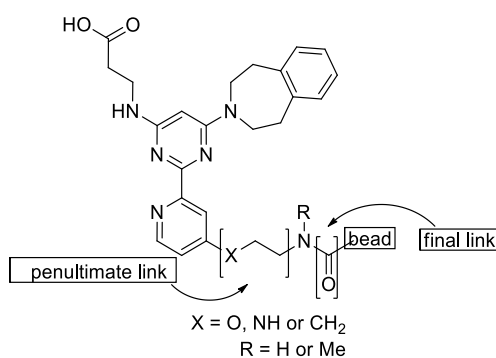


Figure 42. Immobilised inhibitor.

Thus, the immobilised version of **332b** was targeted, and the retrosynthesis of compound **355** is shown in Figure 43.

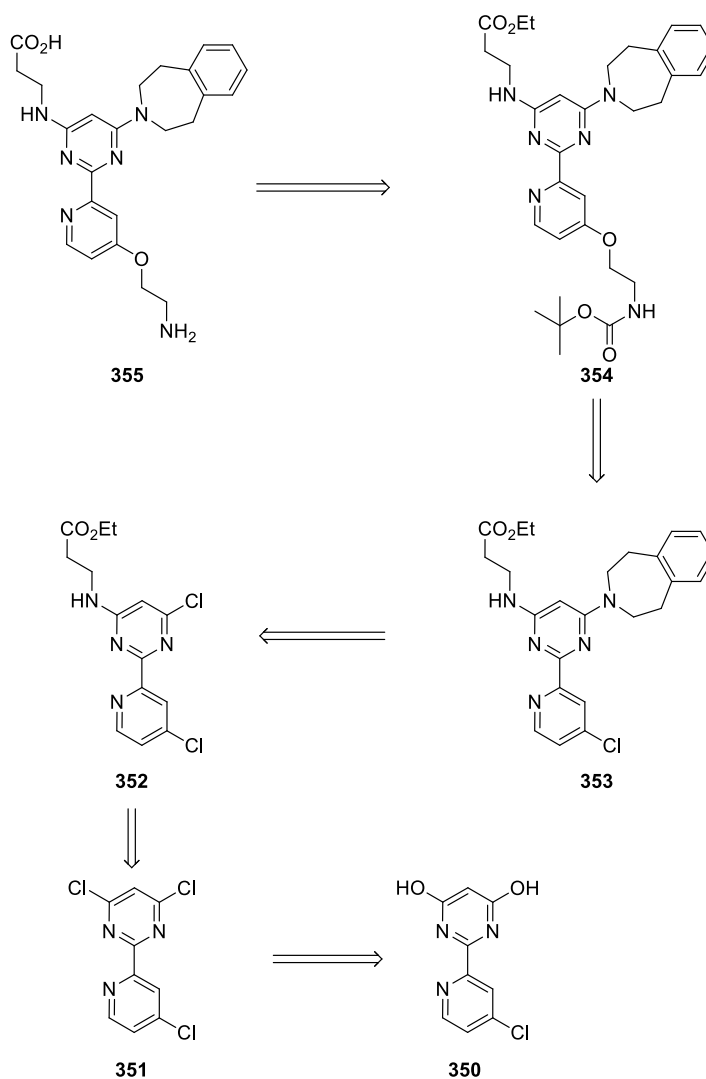
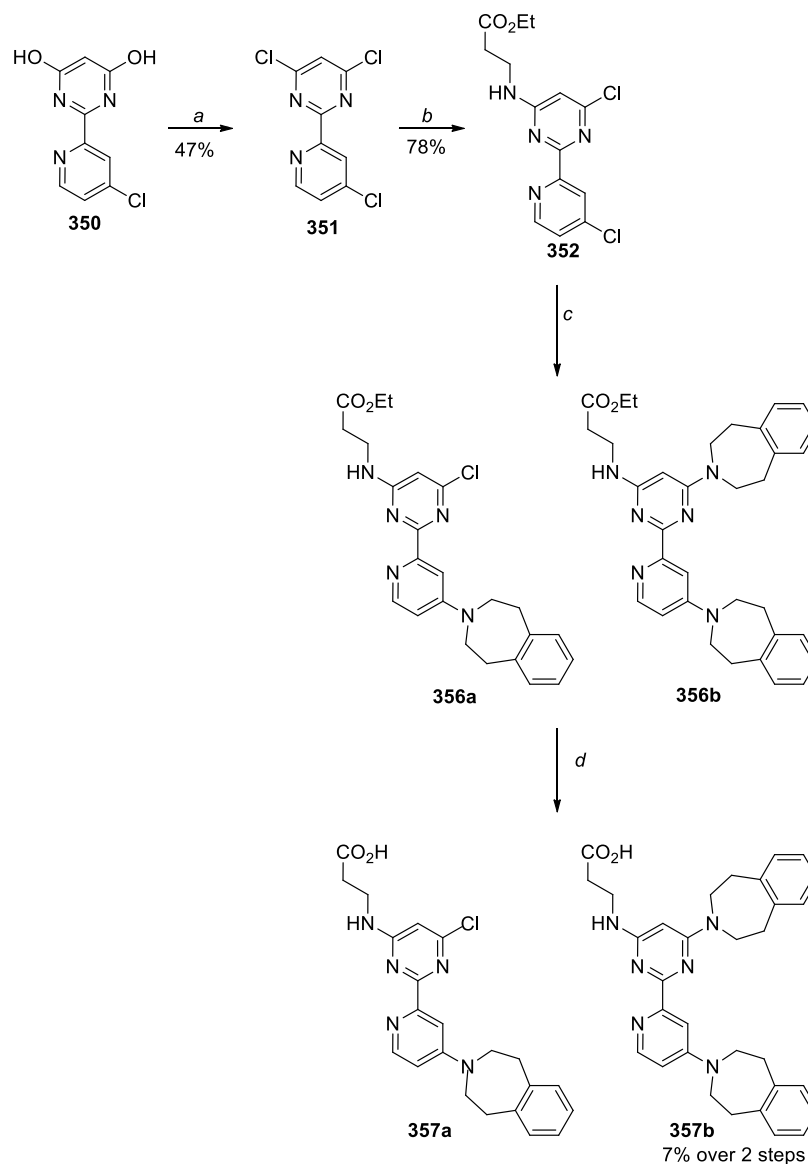


Figure 43. Target **355** retrosynthetic route.

2-(4-Chloropyridin-2-yl)pyrimidine-4,6-diol **350** was reacted with POCl_3 to give the trichloropyridyl-pyrimidine **351** in moderate yield (Scheme 97). Ethyl 3-aminopropanoate was introduced by regioselective $\text{S}_{\text{N}}\text{Ar}$ to give monochloropyrimidine **352** in 78% yield. On this occasion the $\text{S}_{\text{N}}\text{Ar}$ reaction was carried out in 1,4-dioxane instead of the usual DMSO, because of the ease of removing this solvent under reduced pressure. When designing the

synthesis it had been thought that the Cl-pyrimidine moiety of **352** would be more reactive than the Cl-pyridine moiety when subjected to an S_NAr reaction with tetrahydrobenzazepine. This was rationalised by the fact that the chlorine in the pyrimidine moiety of **352** has nitrogen atoms *para* and *meta* to it potentially making it more activated than the chlorine in the pyridine which is *para* to only one nitrogen. Disappointingly, compound **353** was not formed, and a mixture of **356a** and **356b** in a 1.2:1 ratio, was isolated instead.

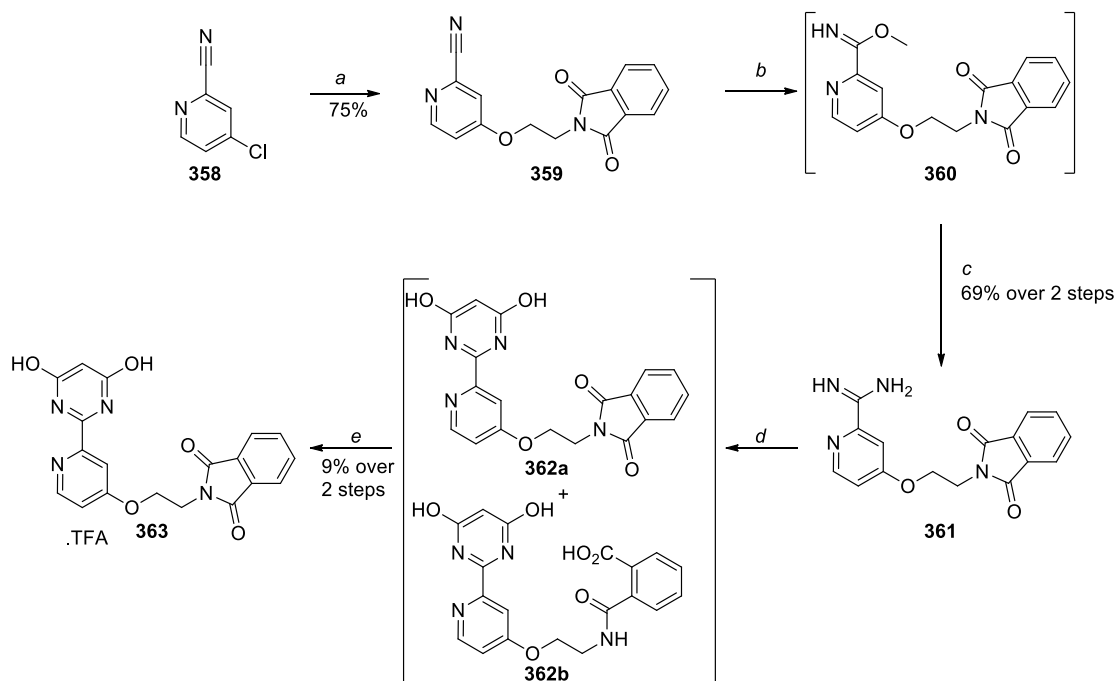


Scheme 97. First chemistry route to **355**. Conditions: (a) POCl₃, reflux; (b) ethyl 3-aminopropanoate, DIPEA, 1,4-dioxane, 100 °C; (c) 2,3,4,5-tetrahydro-1H-3-benzazepine, DIPEA, DMSO, 160 °C; (d) LiOH, THF / water 1:1.

Unfortunately, the mixture of **356a** and **356b** could not be separated. The formation of these two intermediates showed that in the S_NAr reaction of **352**, the chloropyridyl was more reactive than the chloropyrimidyl. The mixture of components was carried through to the hydrolysis step in the hope that the products would be separable by MDAP at this stage. The mixture was hydrolysed using lithium hydroxide monohydrate to give **357a** and **357b** after

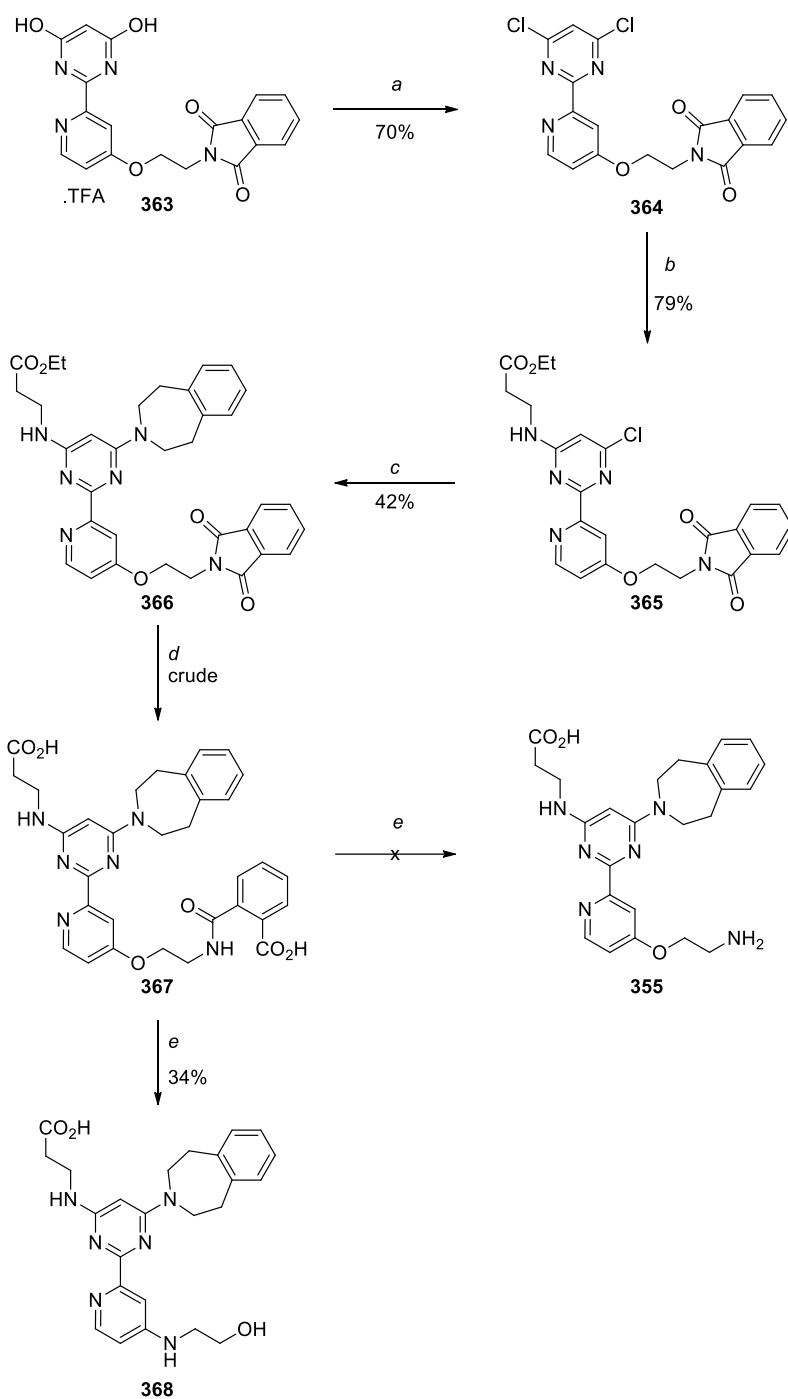
MDAP purification. Compound **357b** was not an intended target, but it was an interesting compound to investigate the space around the *para*-position of the pyridine ring.

As a result of the unexpected regioselectivity observed in the S_NAr reaction of **352** with tetrahydrobenzazepine an alternative route to **355** was investigated. The new route was designed so that the amine-containing side-chain was introduced in the first step. The amino group needed to be protected so as not to interfere with the reaction scheme, and the protecting group selected had to be stable to the acidic conditions of the $POCl_3$ reaction and the basic conditions of the ester hydrolysis. The phthalimido group was therefore selected as the protecting group for the terminal amine. 4-Chloropicolinonitrile **358** was reacted with the sodium salt of 2-(phthalimido)ethanol to give **359** in 75% yield. The picolinonitrile **359** was reacted with sodium methoxide to form the transient amidate **360**, which was then reacted with ammonium chloride to form the amidine **361**. The crude intermediate **361** was treated with diethyl malonate and sodium ethoxide to form the core pyrimidine ring. However, under these basic conditions, the phthalimide partially opened, affording a mixture of very polar compounds (**362a** and **362b**) which could not be separated at this stage. This mixture was reacted with hydrochloric acid to reform the phthalimide ring. Intermediate **363** was obtained as the trifluoroacetate salt in low yield after MDAP purification (Scheme 98).



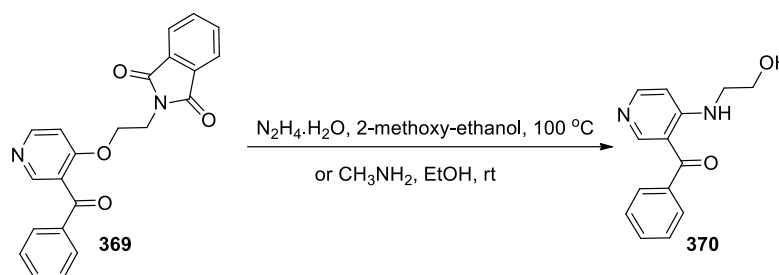
Scheme 98. Second synthetic route to **355**. Conditions: (a) 2-(phthalimido)ethanol, NaH, DMF, rt; (b) NaOMe, MeOH, rt; (c) NH₄Cl, MeOH, 55 °C then 65 °C; (d) diethyl malonate, NaOEt, 80 °C; (e) HCl, 90 °C.

Chlorination of dihydroxypyrimidine **363** with POCl₃ gave the dichloropyrimidine **364** in 70% yield. Ethyl 3-aminopropanoate and benzazepine were introduced by consecutive S_NAr reactions to give intermediate **366** in moderate yield.



Scheme 99. Second synthetic route to **355**. Conditions: (a) POCl₃, reflux; (b) ethyl 3-aminopropanoate, DIPEA, 1,4-dioxane, 100 °C; (c) 2,3,4,5-tetrahydro-1H-3-benzazepine, DIPEA, DMSO, 160 °C; (d) LiOH, THF / water 3:1, rt; (e) hydrazine monohydrate, 1,4-dioxane / DMF 2.5:1, 80 °C.

Basic ester hydrolysis gave the crude acid **367**, in which opening of the phthalimide had also occurred. Complete deprotection was achieved using an excess of hydrazine monohydrate at 80 °C. However, analysis of the product (obtained in 34% yield) by ¹H NMR did not show a signal for the expected primary amino group of **355** but, instead, two signals for two NH's at 6.76 and 6.67 ppm. Since the molecular weight of the material obtained was consistent with the desired product, but the ¹H NMR spectrum was not, it was concluded that a Smiles rearrangement had afforded the alcohol **368** instead of the desired terminal amine (Scheme 99). The Smiles rearrangement during phthalimide deprotection on pyridine rings has been reported previously in the literature.

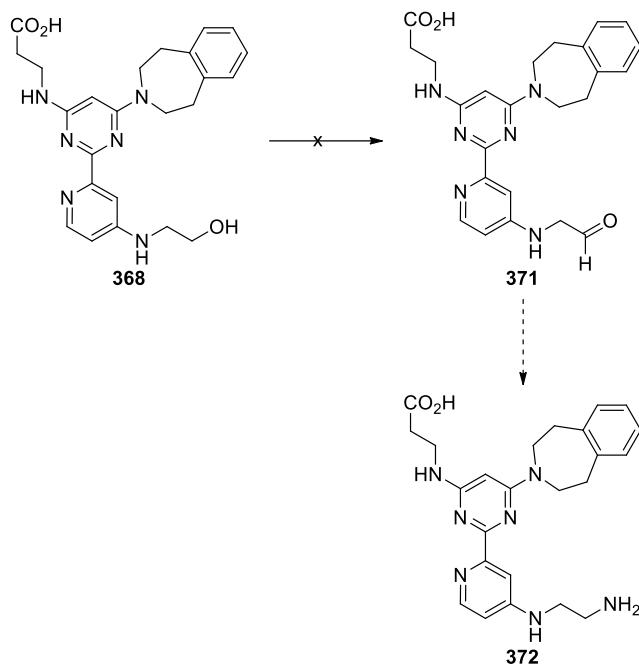


Scheme 100. Smiles Rearrangement.¹⁷¹

Radinove *et al.*¹⁷¹ showed that in the case of compound **369**, deprotection of the amine always led to Smiles rearrangement whatever conditions were used (Scheme 100) affording compound **370** in 85-90% yield.

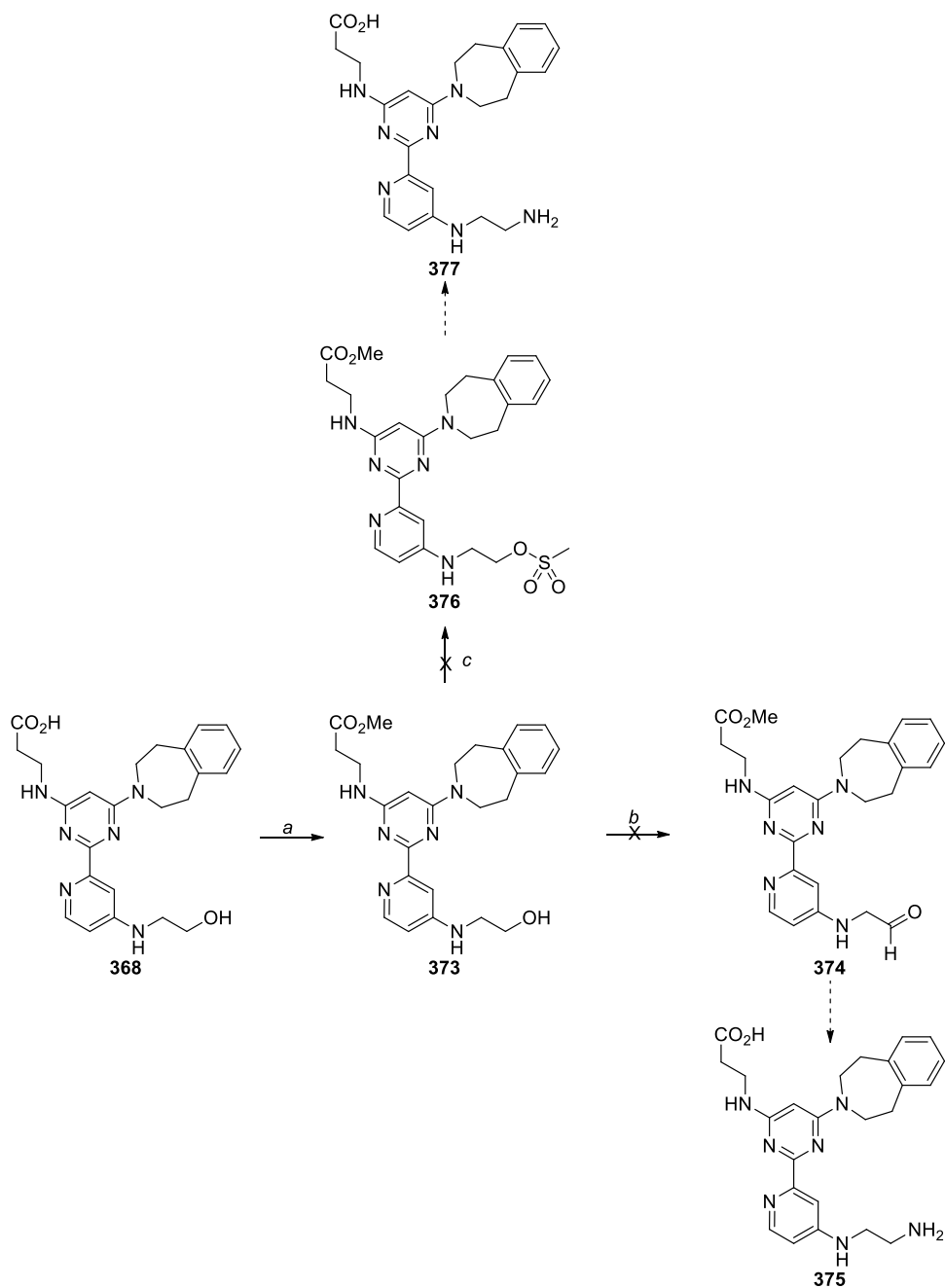
The synthesis of **368** had been relatively lengthy and had required a great effort but only a limited amount of material had been isolated. Unfortunately, this compound could not be used for the immobilisation since an amine was absolutely required to form an amide bond with the bead. Several attempts were therefore made to convert the hydroxyl group to an amine as shown in Schemes 101 and 102. Initial efforts to introduce an amino group involved oxidation of the hydroxyl group of **368** to an aldehyde, which would then be used

in a reductive amination reaction. Attempted oxidation of **368** using pyridine.sulfur trioxide failed, with only starting alcohol observed by LCMS analysis.¹⁷² To exclude the possibility that the carboxylate group of **368** was hindering the desired oxidation reaction, it was converted into a methyl ester using methyl iodide and potassium carbonate (Scheme 102).



Scheme 101. First attempt to hydroxyl group conversion. Conditions: pyridine sulfur trioxide, NEt₃, DCM/DMSO (1:1), rt.

A Swern oxidation was attempted on ester **373** (Scheme 102). Since the oxidation was unsuccessful it was decided to convert the hydroxyl group into a mesylate with a view to attempting a displacement with an amine in a subsequent step. However, attempted mesylation of intermediate **373** failed to deliver target **376**.



Scheme 102. Second and third attempts at hydroxyl group conversion. Conditions: (a) MeI, K_2CO_3 , DMF, rt; (b) oxalyl chloride, NEt_3 , DMSO, DCM, $-70\text{ }^\circ C$; (c) Methanesulfonic anhydride, DIPEA, DCM, rt.

Despite several attempts, it did not prove possible to convert the hydroxyl group of **368** to an amine suitable for linking. While other chemistries could have been attempted, efforts were halted at this stage due to the limited amount of **368** available. It was therefore decided to re-design the immobilised inhibitor to avoid any possibility of a Smiles rearrangement (Figure 44).

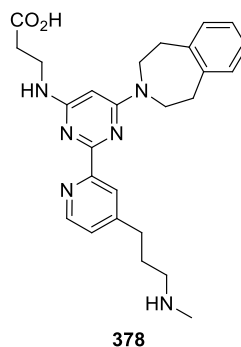
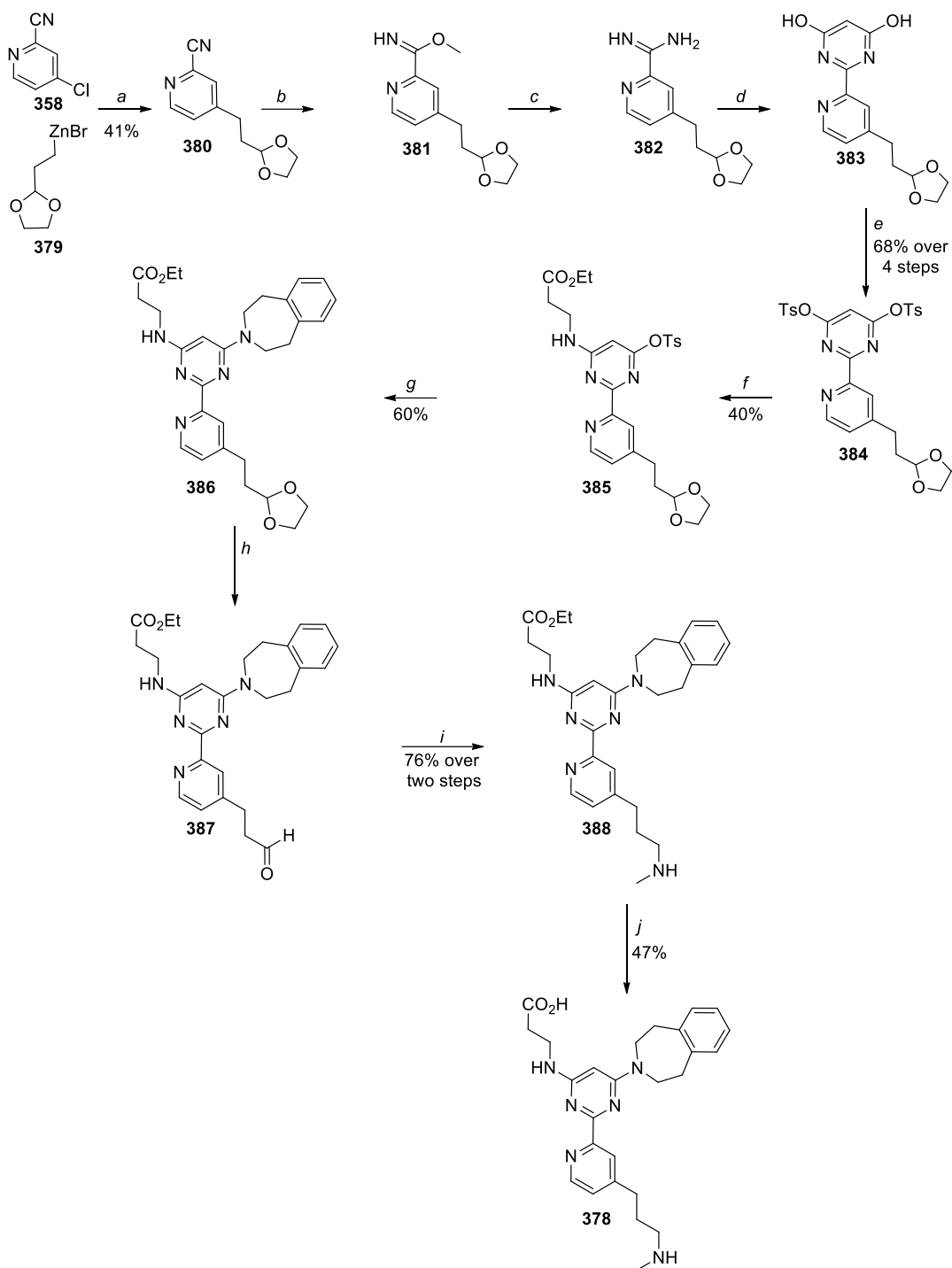


Figure 44. New inhibitor **378** for immobilisation.

The new methylene-linked target eliminated the issue of Smiles rearrangement entirely. The primary amino group first targeted was also changed to a secondary *N*-methylamino group for ease of chemistry. Chloropicolinonitrile **358** was cross-coupled with (2-(1,3-dioxolan-2-yl)ethyl)zinc(II) bromide **379** to introduce the flexible chain bearing a masked aldehyde (Scheme 103). Unlike the use of cross-coupling reactions late in the synthesis of pyridyl-pyrimidine series compounds discussed in Section II.3.1.1.1, the use of palladium for the synthesis of **380** was acceptable. This distinction is due to the fact that the cross-coupling reaction in the synthesis of **380** was the first step of a long synthesis, so any residual palladium should be eliminated through the subsequent purifications. Moreover, since the pyridyl-pyrimidine moiety was not yet formed there was no possibility of chelation of the palladium. Intermediate **380**, isolated in 41% yield, was reacted with sodium methoxide to form the amidate **381**. This amidate was not isolated, but was reacted *in situ* with ammonium chloride to give the amidine **382**, which was taken on directly to form the pyrimidine-4,6-

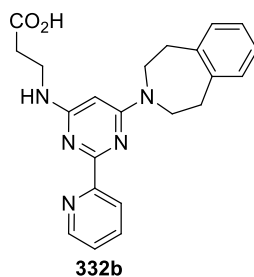
diol **383**. Concerns about potential instability of the acetal in the pyrimidine-4,6-diol **383** under the chlorination conditions used previously (POCl_3) led to the decision to employ a milder method of activation of the 4 and 6 positions. Thus, the crude intermediate **383** was reacted with tosyl chloride to give the *bis*-tosylated pyrimidine-4,6-diol intermediate **384** in 68% over four steps from **380**. Ethyl 3-aminopropanoate and tetrahydrobenzazepine were introduced consecutively by $\text{S}_{\text{N}}\text{Ar}$ reactions to give intermediate **386** in moderate yield. Deprotection of the aldehyde using acetic acid in water gave the crude aldehyde **387**. Reductive amination was carried out in a stepwise fashion, with MgSO_4 added to help the formation of the *N*-methyl iminium ion by acting as a chemical desiccant. Reduction to the *N*-methylamine **388** was achieved using sodium borohydride, delivering the amino ester in 76% yield (over two steps). Finally, hydrolysis of the ester using lithium hydroxide gave the target acid in 47%. The linkable molecule **378** was obtained from commercially available chloropyridine **379** in ten steps and 4% overall yield.



Scheme 103. Synthetic route to **378**. Conditions: (a) Pd(PPh₃)₄, microwave, 110 °C; (b) NaOMe, MeOH, rt; (c) NH₄Cl, MeOH, rt; (d) diethylmalonate, NaOMe, 80 °C; (e) TsCl, NEt₃, DMAP, DCM, rt; (f) ethyl 3-aminopropanoate, NEt₃, MeCN, microwave, 100 °C; (g) 2,3,4,5-tetrahydro-1H-3-benzazepine, *iso*-propanol, microwave, 150 °C; (h) acetic acid / water, 80 °C; (i) i. MgSO₄, MeNH₂; ii. NaBH₄, THF, rt; (j) LiOH, THF / water 1:1, rt.

This route delivered enough material to enable attachment to the bead which was used to study the inhibition of JmjD3 in cells.

II.3.1.7 Hybrid inhibitors

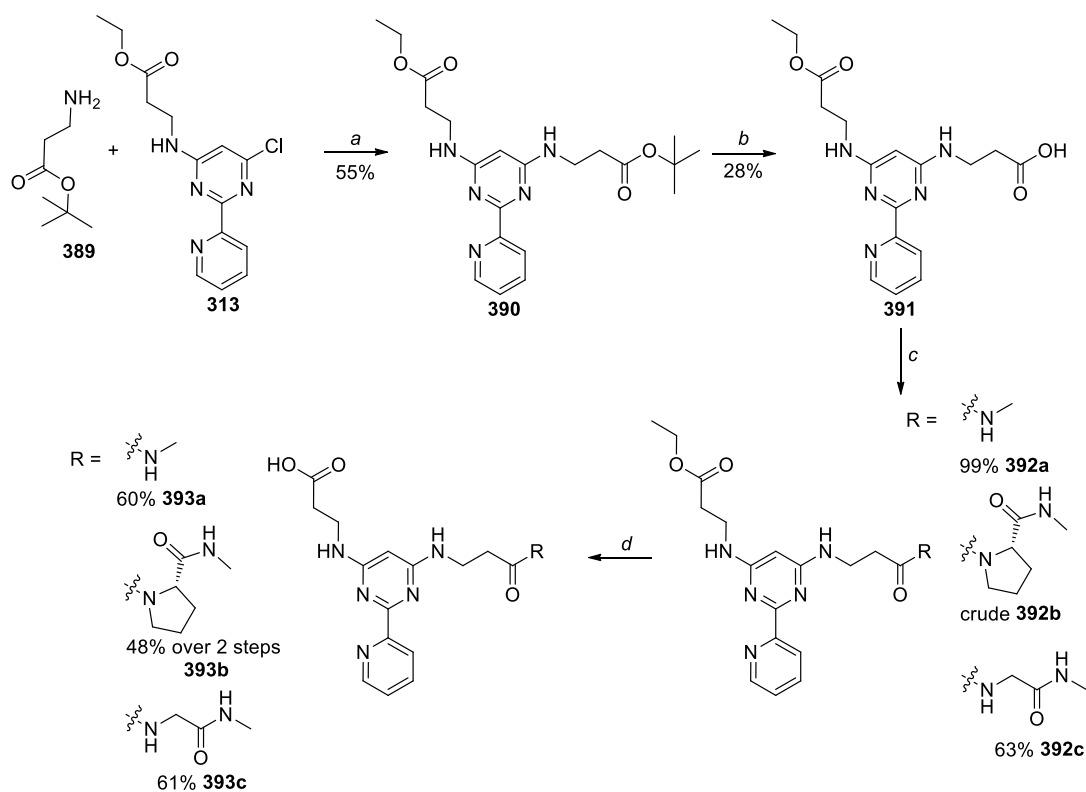


Shortly after **332b** was synthesised, the X-ray crystal structure of this compound bound to human JmjD3 (Figure 66) was solved. This was later followed by the structure of mouse JmjD3 in a complex with the peptide substrate (Figure 81). Taken together this information suggested the possibility of creating a hybrid molecule which would possess the best features of the pyridyl-pyrimidine and the substrate. It was hoped that combining these features in a single molecule would result in an increase in potency against JmjD3. The structure of mouse JmjD3 will be discussed in detail in Section II.3.2.6.4, but the key features relevant to the present work were hydrogen bond interactions between Arg1247 and the two carbonyls surrounding the Pro30 of the tri-methylated lysine substrate (Figure 81). The pyridyl-pyrimidine template was used to mimic these latter interactions. It was envisaged that introduction of a variety of amides in place of the tetrahydrobenzazepine ring may allow interaction with Arg1247 *via* hydrogen bond interactions. This will be discussed further in Section II.3.2.6.4

To access these amides, a carboxylic acid located a short distance from the 6-position of the pyrimidine was required. The requirements for an acid to bond to key residues in the protein and another to mimic the interactions of the peptide substrate necessitated an orthogonal

protection strategy. A *tert*-butyl ester was selected as the protecting group for the linking acid because it could be removed by use of trifluoroacetic acid, which would leave an ethyl ester untouched. The ethyl ester used to protect the acid key for potency, could then be hydrolysed under mild conditions at the end of the synthesis.

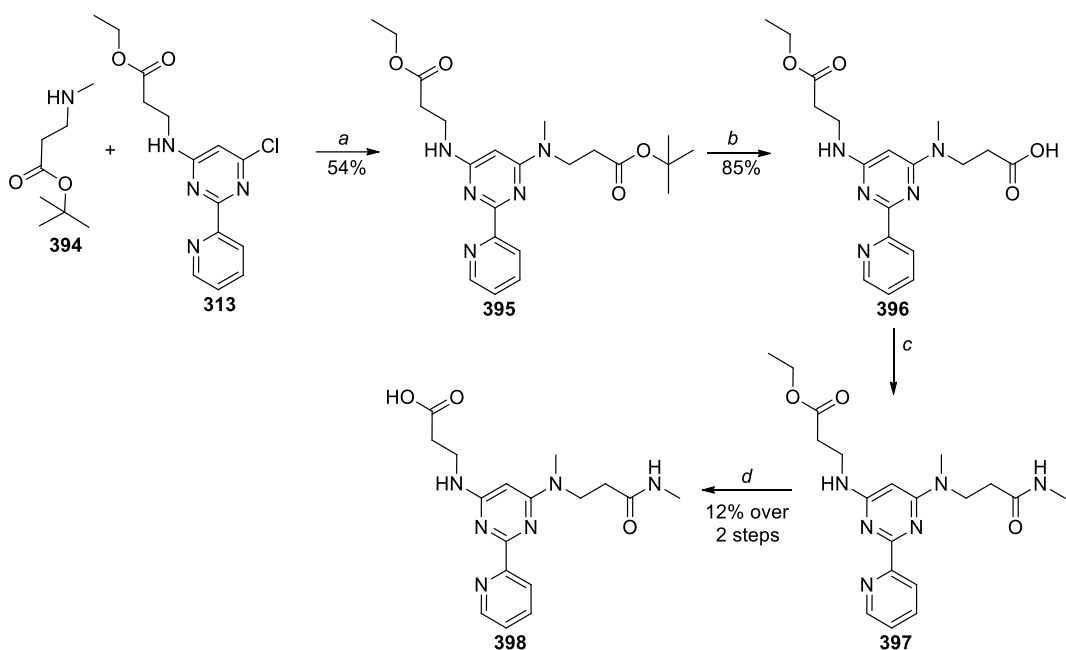
Starting with the chloropyrimidine **313**, *tert*-butyl 3-aminopropanoate **389** was introduced by a S_NAr reaction to give intermediate **390** in 55% yield. *Tert*-butyl ester cleavage using TFA afforded acid **391** in 28% yield. Amide **392a** was synthesised using HATU and methanamine which was used as the base and the reagent and so was used in excess. Amide coupling using HATU and DIPEA gave amide crude **392b** and **392c** in good yield. Final ester hydrolysis afforded the target compounds, also in good yields (ca. 60%) (Scheme 104). In the case of **393b** rotamers were visible by NMR, where one of the pyrrolidine proton was split into two signals at 4.37 ppm (0.33 H) and 4.23 ppm (0.67 H), this could be linked to the presence of pyrrolidine amide.



Scheme 104. Conditions: (a) DIPEA, 1,4-dioxane, 160 °C, microwave; (b) TFA, DCM 1:1, rt; (c) HATU, HNRR', DIPEA (except for MeNH₂), DMF, rt; (d) LiOH, THF/water 2:1, rt.

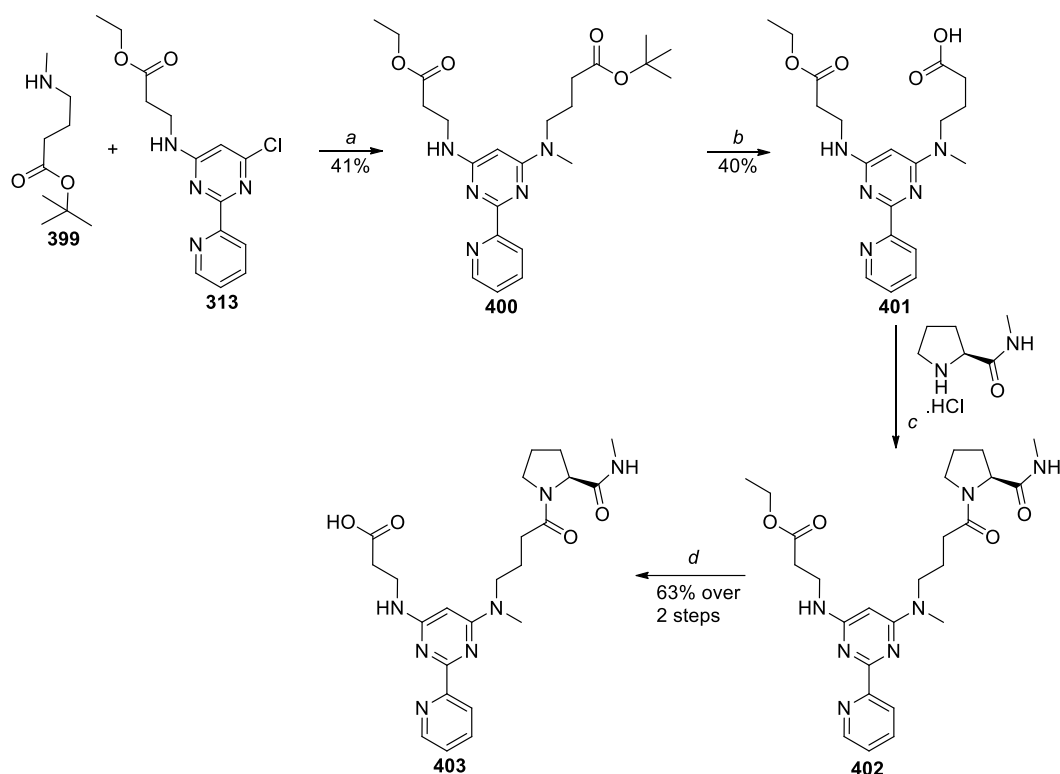
Compound **398**, the methylated analogue of **393a** was targeted to evaluate the impact on potency of a methylated linking nitrogen atom. As with the non-methylated analogue, *tert*-butyl 3-(methylamino)propanoate **394** was also introduced by S_NAr to give di-ester **395**. Subsequent removal of the *tert*-butyl ester by treatment with TFA afforded acid **396** in good yield. Standard amide coupling conditions utilising HATU failed to deliver the required product. The reaction was slow, with the reaction still incomplete even after three days. Less than one milligram of product was isolated which could not be characterised. New conditions were therefore required to form the amide more rapidly. It was decided to form the amide *via* an acid chloride, which was formed *in situ* from the acid by treatment with

oxalyl chloride. These conditions afforded the crude amide **397**, which was carried onto the final step to deliver acid **398** in 12% yield (over two steps) (Scheme 105).



Scheme 105. Conditions: (a) DIPEA, *iso*-propanol, 160 °C, microwave; (b) TFA, DCM 1:1, rt; (c) (i) oxalyl chloride, DMF, DCM (ii) MeNH₂, DIPEA, DCM rt; (d) LiOH, THF/water 6:1, rt.

Target **403** was designed to evaluate the impact on potency of a longer linker, to enable a comparison to be made with **393b** (Scheme 106). Intermediate **401** was synthesised using the same methodology described above, S_NAr and *tert*-butyl ester cleavage using TFA. HATU mediated amide coupling afforded **402** in low purity. This material was carried on to the next step. Although the reaction was successful, the compound was lost before being tested. However, due to the low biochemical potency of the other analogues (**393a – c** and **398**, cf. Section II.3.2.7.4) and a change of priority, compound **403** was not resynthesised.



Scheme 106. Conditions: (a) DIPEA, 1,4-dioxane, microwave; (b) TFA, DCM, rt; (c) HATU, DIPEA, DMF, rt; (d) LiOH, THF/water 6:1, rt.

II.3.2 Assay results and discussion

II.3.2.1 Bidentate interaction

As previously stated, the crystal structure of **11** bound to the active site of JmjD3 was not available when optimisation of the pyridyl-pyrimidine series was commenced. However, as discussed in Section I.1.3.3, a common binding mode observed with published inhibitors of Jumonji enzymes is a bidentate interaction between the inhibitor and the catalytic iron. This knowledge led to the hypothesis that **11** bound to JmjD3 *via* a bidentate interaction with the catalytic iron, employing nitrogen atoms from both the pyridyl and pyrimidine rings. It was

therefore postulated that replacement of either of these nitrogen atoms should result in a significant loss of inhibitor potency.

Three compounds were commissioned from Bioduro to test this hypothesis.¹³³ The design balanced synthetic accessibility with preservation of conformation, polarity and electronic character. These compounds are shown in Table 33.

Replacing the 2-pyridyl nitrogen with a C-H gave phenyl analogue **404** which showed very weak inhibition of JmjD3, a result which would seem to support our hypothesis. However whilst lacking the pyridyl nitrogen lone pair present in **11**, **404** is also significantly more lipophilic than **11**. It is possible that the increased lipophilicity of **404** is, in part, responsible for the weak inhibition observed in the biochemical assay since it is well known that lipophilic molecules are more prone to non-specific binding (*cf.* Section I.3.1 HTS and focused screen triage). To address concerns about lipophilicity, the pyridyl isomers **405** and **406** were also synthesised. These compounds have very similar cLogP values to compound **11**. Table 33 shows that both of these compounds have pIC₅₀ values < 4.0 in the MALDI assay, results which also support the hypothesis that a bidentate interaction with the metal is important.

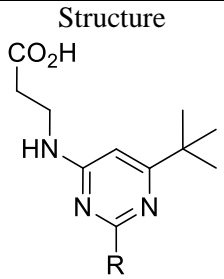
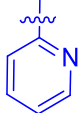
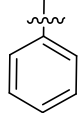
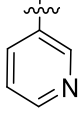
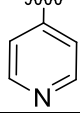
Structure	Compound No.	MALDI pIC ₅₀	cLogP
			
R			
	11	5.0	2.9
	404	4.1	4.1
	405	< 4.0	2.7
	406	< 4.0*	2.7

Table 33. Enzyme assay data for variation at position 2.

* < 4.0 (n = 1) and 4.5 (n = 1).

Potential effects on conformation were assessed using molecular modelling and verified using experimental data from the Cambridge Crystallographic Data Centre (CCDC). Molecular modelling of a 2-pyridyl-pyrimidine and a phenyl-pyrimidine suggested the two rings were coplanar in the lowest energy conformations for both systems (Figure 45).

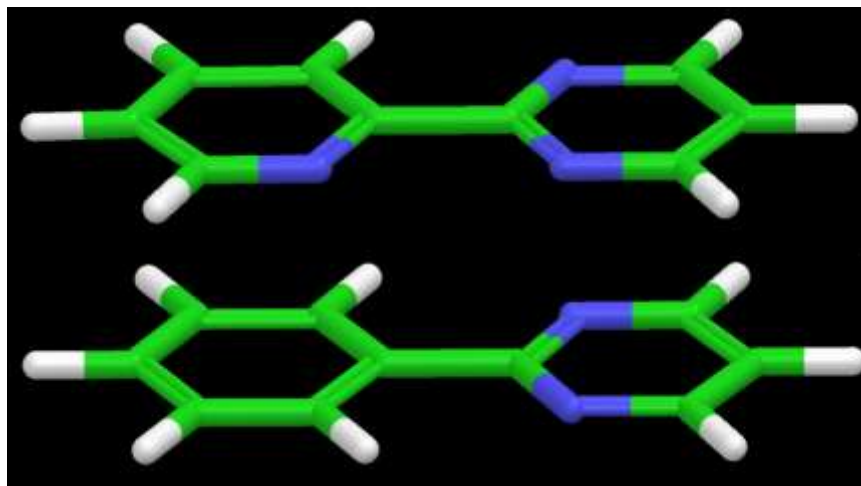


Figure 45. Pyridyl-pyrimidine (top structure) and phenyl-pyrimidine (bottom structure) in their minimal energy conformations. Minimisation performed by R. Sheppard, GSK (Appendix 7).

Analysis of CCDC structures allowed a comparison, based on experimental observations, of torsion angles between a pyrimidine and the four rings of interest (phenyl, 2-pyridyl, 3-pyridyl and 4-pyridyl). This showed that the distribution of torsion angles between a pyrimidine and a 2-pyridyl (Figure 46a) is similar to the distribution observed in the crystal structures of pyrimidines substituted with a phenyl (Figure 46b), 3-pyridyl (Figure 47a) or 4-pyridyl (Figure 47b) ring.¹⁷³ The analysis shows that the pyrimidine has a preference for coplanar geometry with the various aromatic rings. Care should be taken when interpreting the CCDC data for 2-pyridyl-pyrimidines, 3-pyridyl-pyrimidines and 4-pyridyl-pyrimidines due to the limited number of experimentally determined structures. Indeed, only three structures were found for 2-pyridyl-pyrimidines, one structure for 3-pyridyl-pyrimidines and two structures for 4-pyridyl-pyrimidines, whereas 123 structures were found for phenyl-pyrimidines. Considered together, molecular modelling information and CCDC data demonstrated that there were minimal conformational differences between **11** and **404** and therefore, strongly suggested that conformational differences were unlikely to be the cause of the reduction in enzyme inhibition on moving from **11** to **404**.

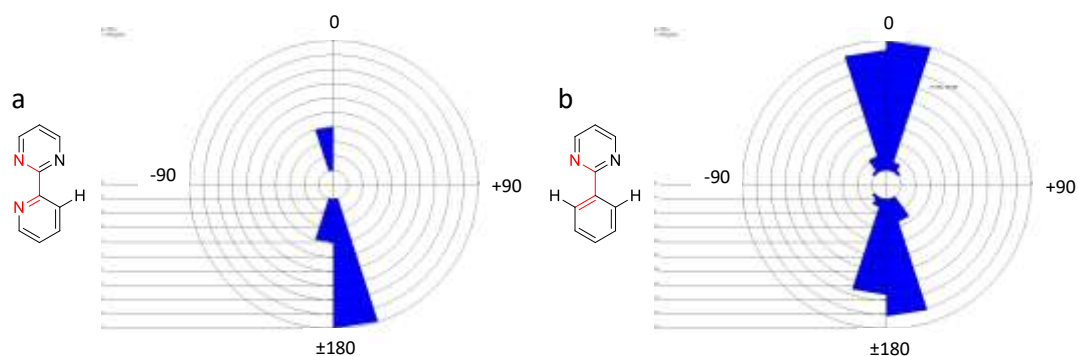


Figure 46. CCDC analysis of the torsion angles between the two rings in a) 2-pyridyl-pyrimidine; phenyl-pyrimidine, and b) phenyl-pyrimidine. Substructure search carried out with nitrogens bonded to only two other atoms (to exclude *N*-oxides). Substructure for which data was retrieved is shown, with the torsion angle measured highlighted in red. Data presented as a polar histogram, with the frequency of observation shown in the left-hand side of each histogram.

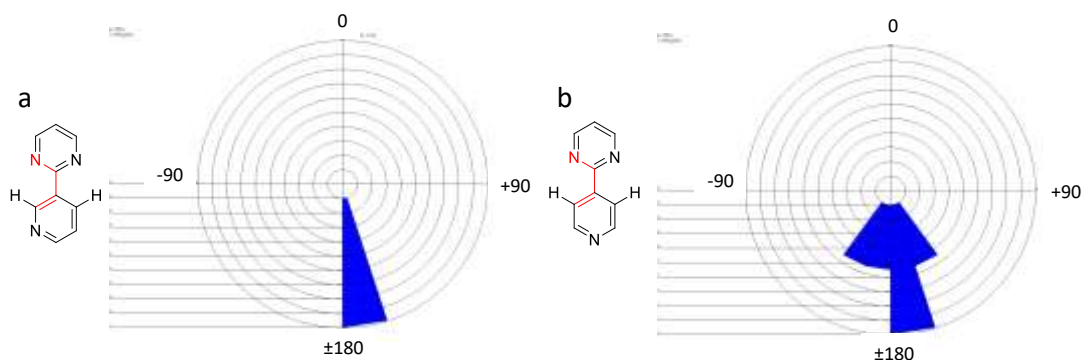


Figure 47. CCDC analysis of the torsion angles between the two rings in a) 3-pyridyl-pyrimidine, and b) 4-pyridyl-pyrimidine. Substructure search carried out with nitrogens bonded to only two other atoms (to exclude *N*-oxides). Substructure for which data was retrieved is shown, with the torsion angle measured highlighted in red. Data presented as a polar histogram, with the frequency of observation shown in the left-hand side of each histogram.

Taken as a whole, the results presented in the preceding paragraphs gave us confidence that **11** was indeed binding to the catalytic iron through the nitrogen atoms of both the 2-pyridyl and pyrimidine rings. The 2-pyridyl-pyrimidine core was therefore conserved while the SAR was developed around positions 4 and 6 of the pyrimidine.

II.3.2.2 Carboxylic acid isosteres investigation

Analysis of the binding of inhibitors of Jumonji enzymes disclosed in the literature revealed that many, if not all, have an acidic group which binds to a lysine residue in the co-factor binding region of the enzyme. In the absence of an X-ray structure of **11** bound to JmjD3 it seemed reasonable to assume that something similar was occurring in this case. A compound was synthesised in which the carboxylic acid group had been removed (**199**) (Table 34), in order to establish the importance of the acidic group of **11** for enzyme inhibition. The observation that **199** had a potency below the limit of detection in the MALDI assay confirmed that the carboxylic acid was critical for potency.

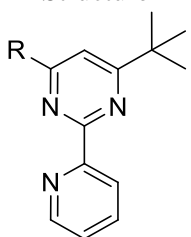
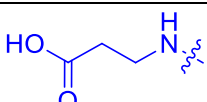
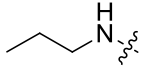
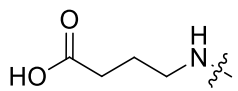
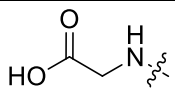
Structure	Compound	MALDI pIC ₅₀	cLogP	Permeability (nM/sec pH7.4)
				
R				
	11	5.0	2.9	< 10
	199	< 4.0 ^a	4.3	470
	208	< 4.0	3.3	14
	209	< 4.0 ^b	2.7	< 10

Table 34. Enzyme assay data for variation at position 4.

^a < 4.0 (n = 3) and 4.5 (n = 2).

^b < 4.0 (n = 2) and 4.7 (n = 2).

The length of the methylene chain between the carboxylic acid and the NH linker was investigated next. Compound **209** was synthesised twice using the two routes, *i.e.* the Pd-mediated route and the metal free route (*cf.* II.3.1.1 Vector 4: primary modifications and carboxylic acid isosteres). The first batch of compound **209** (Pd-mediated route) was active in the MALDI assay with a pIC₅₀ of 4.7, whilst the second batch displayed activity below the limit of the assay (pIC₅₀ < 4.0). The activity of the first batch could potentially be related to the presence of Pd contamination as for compound **200** (*cf.* II.3.1.1 Vector 4: primary modifications and carboxylic acid isosteres), and so compound **209** was considered as inactive in this assay. Compounds **208** (pIC₅₀ < 4.0) and **209** (pIC₅₀ < 4.0) were both less active than **11** showing that the ethyl chain was optimal.

Synthesis of **199** was also useful to address another question about **11**: its cellular permeability. Despite moderate biochemical potency compound **11** was inactive in the cellular assay and it was postulated that this may be due, in part, to its poor permeability (< 10 nM/sec at pH 7.4 in the artificial membrane permeability assay) which may prevent access of the compound to the interior of the cell and its nucleus where JmjD3 is located. This poor permeability was thought to be related to the carboxylic acid group of **11** and the associated polarity of the compound (cLogP = 2.9). The high permeability of **199** (Table 34) with its higher cLogP supported this hypothesis. A major challenge for the programme was the improvement of biochemical potency whilst obtaining cellular activity.

Although carboxylic acids are present in several marketed oral drugs, such as Zyrtec (Pfizer) and Daypro (Pharmacia) (Figure 48), medicinal chemists tend to avoid carboxylic acids in drug-like molecules because they often suffer from drawbacks such as poor permeability, poor pharmacokinetic properties and toxicity.¹⁷⁴

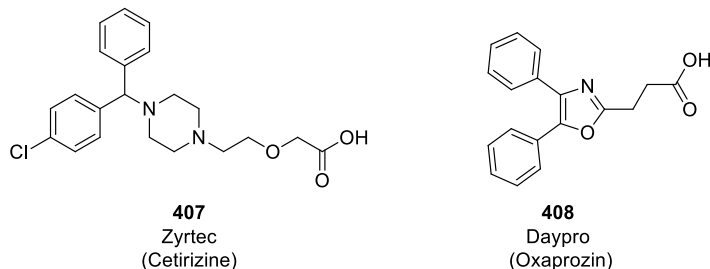


Figure 48. Marketed drugs containing carboxylic acid groups.

Carboxylic acid bioisosteres are often investigated to try and overcome these issues. These carboxylic acid bioisosteres are separated into two groups, classical and non-classical.¹⁷⁵

II.3.2.2.1 Classical carboxylic acid isosteres

A carboxylic acid usually acts as an hydrogen bond donor through its hydroxyl group and an hydrogen bond acceptor through its hydroxyl and/or carbonyl groups. However, at physiological pH (7.4) and when free in solution, a carboxylic acid (pK_a 3-4) exists as a carboxylate ion and so can only be involved in ionic interactions and/or act as a powerful hydrogen bond acceptor.

No crystal structure of the lead molecule **11** bound to JmjD3 was available at the time this work was performed, so the precise interactions involving the carboxylate were not yet known. However, the results already presented demonstrate that this carboxylate was critical for biochemical potency but potentially limiting to cellular activity. Carboxylic acid isosteres were therefore investigated to improve the permeability. In the first instance, classical carboxylic acid isosteres were designed to mimic the hydrogen bond acceptor properties of the carboxylate (Table 35). Initial targets in this area sought to investigate a variety of H-bonding characteristics and so the sulfonamide **212** (both H-bond donors and acceptors), as well as the methyl ester **221** (H bond acceptor), methyl sulfone **223** (*bis*-hydrogen bond acceptor) and amide **222** (both H-bond donors and acceptors) were synthesised and tested. Disappointingly, all were found to be inactive ($pIC_{50} < 4.0$). A number of electronic and steric factors could explain these observations. Whilst all of these isosteres possessed H-bond acceptors with which to mimic the carboxylate of **11** some, such as the amide and sulphonamide, also had the potential to act as H-bond donors. These H-bond donors may have the effect of disrupting other interactions in the active site and result in an increased energy penalty to binding. Additionally, the methyl ester **221**, sulfonamide **212** and methyl sulfone **223** have different steric characteristics to the carboxylic acid, potentially impeding the binding of the molecule in the active site of JmjD3. It will be noted that all of these carboxylic acid isosteres were designed with an ethylamine linker to the 4-position of the

pyrimidine. Whether improved activity could be obtained using a methylamine linker was not investigated with these groups.

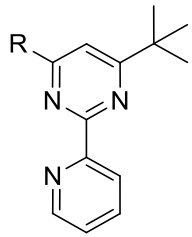
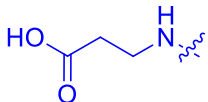
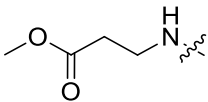
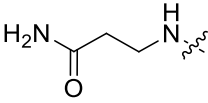
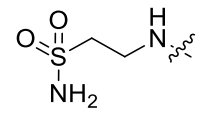
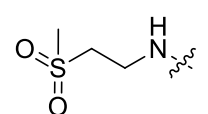
Structure	Compound	MALDI pIC ₅₀
R		
		
	11	5.0
	221	< 4.0 ^a
	222	< 4.0
	212	< 4.0
	223	< 4.0

Table 35. Enzyme assay data for classic carboxylic acid isosteres.

^a First Pd-mediated batch 4.7 (n = 2) and second metal-free batch < 4.0 (n = 1).

All of the SAR generated in this region of the molecule suggested that the carboxylate ion was probably involved in critical ionic interactions with residues in the active site of JmjD3.

II.3.2.2.2 Non-classical carboxylic acid isosteres

Several heterocycles have been used as carboxylic acid isosteres by other researchers.^{176,177}

The results are summarised in Table 36.

The tetrazolyl group is one of the most popular non-classical carboxylic acid isosteres. An NH tetrazole has a similar acidity to a carboxylic acid (pK_a of 4.5-4.9 for a NH tetrazole vs 3-4 for a carboxylic acid),¹⁷⁸ and so tetrazole is ionised at physiological pH. Tetrazoles are also planar in structure in common with the carboxylate group. In addition, it was demonstrated by Hansch that tetrazolyl anions are almost 10 times more lipophilic than carboxylate anions, so the permeability of compounds bearing an ionisable tetrazolyl group would normally be expected to be higher than the corresponding carboxylates.¹⁷⁴ Moreover, due to their more extended π -systems tetrazolyl anions are more delocalised, which could be beneficial for interactions with protein residues. An example of a successful drug containing tetrazolyl motifs is Losartan, a drug launched in 1994 by DuPont to treat high blood pressure. In this case, the tetrazolyl group enabled improvements in potency and in oral bioavailability (Figure 49) over the carboxylic acid-containing **367**.^{178,179}

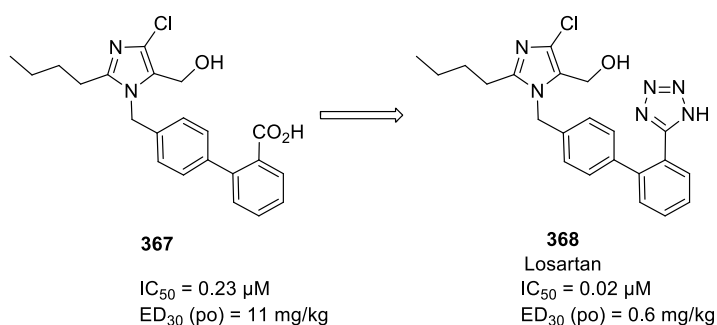


Figure 49. Losartan and less potent carboxylic acid **367**. ED_{30} is the effective dose in mg/kg that lowers the blood pressure 30 mmHg.

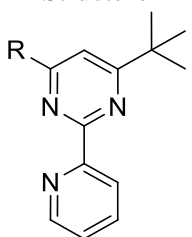
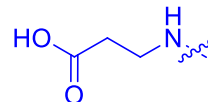
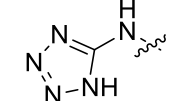
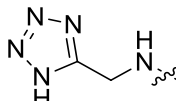
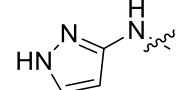
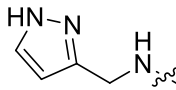
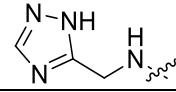
Structure	Compound	MALDI pIC ₅₀
		
R		
	11	5.0
	224	< 4.0
	225	< 4.0
	226	< 4.0
	227	< 4.0
	228	< 4.0

Table 36. MALDI data for heterocycles as potential carboxylic acid isosteres.

It therefore seemed logical to investigate this approach in the current work. Analogues containing heterocycles which have been used previously as carboxylic acid isosteres were synthesised. The results are summarised in Table 36. In our case, tetrazole **224** showed no activity (pIC₅₀ < 4.0). Compound **225** was designed to examine whether increased flexibility in the linker could restore activity, by allowing the tetrazole to adopt a more optimal position. Disappointingly, this analogue also displayed no detectable inhibition of JmjD3. This poor result could be explained by the difference in positions of the OH (CO₂H) and the NH (tetrazole), which was beneficial in terms of potency for Losartan.¹⁷⁸ The 3-substituted pyrazole was also tested with and without the methylene linker (**226** and **227**, respectively),

but neither displayed detectable activity. Analogues containing other heterocycles such as the triazole **228** also performed poorly.

II.3.2.3 Crystal structure of JmjD3

II.3.2.3.1 Crystal structure of 2-OG bound to JmjD3

The crystal structure of 2-OG bound to human JmjD3 was solved a few months after the optimisation of the pyridyl-pyrimidine series was initiated.¹⁵⁴ As observed in other members of the Jumonji family (*cf.* Section I.1.5.1) the structure showed that the co-factor bound the metal *via* a bidentate interaction. The metal is octahedrally coordinated with the co-factor occupying two sites, and His1390, Glu1392, His1470 and one water molecule occupying the remaining four (Figure 50). The C-5 carboxylate is involved in a hydrogen bond network with Lys1382, Thr1388 and Asn1401.

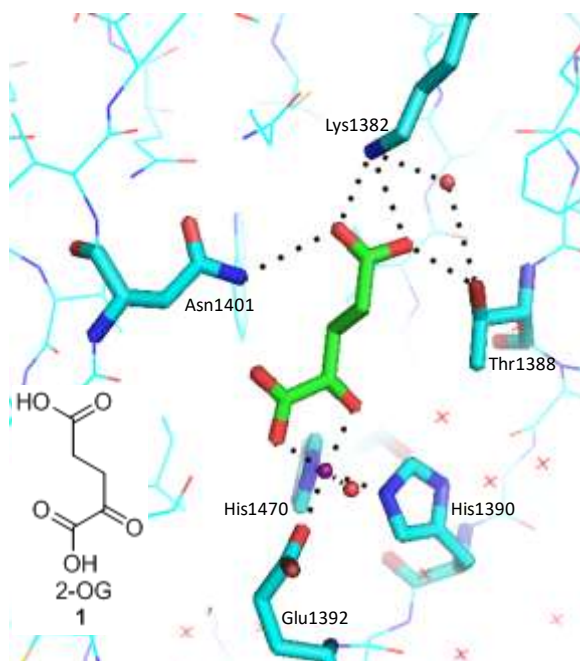


Figure 50. Crystal structure of 2-OG bound to JmjD3. The crystal structure was obtained with Co(II) (purple). Water molecules are represented by red spheres. Black dotted lines highlight the key interactions. PDB: 2XUE.

II.3.2.3.2 Crystal structure of **11** bound to JmjD3

The crystal structure of pyridyl-pyrimidine **11** became available soon after the crystal structure of 2-OG bound to human JmjD3 was solved (Figure 51).

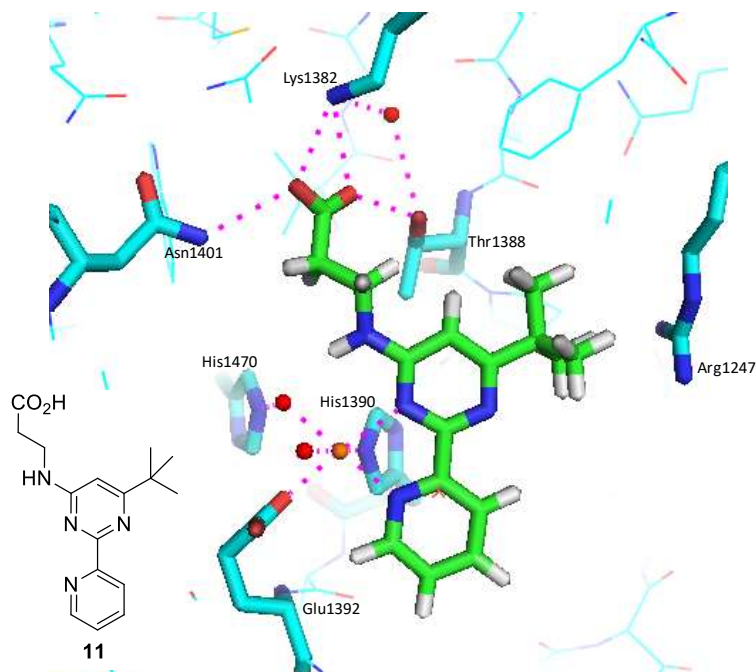


Figure 51. Crystal structure of pyridyl-pyrimidine **11** bound to human JmjD3. Crystal structure obtained with Co(II) (orange). Water molecules are represented by red spheres. Pink dotted lines indicate key polar interactions.

It was gratifying to observe that pyridyl-pyrimidine **11** is involved in a bidentate interaction with the catalytic metal through the 2-pyridyl nitrogen and one of the pyrimidine nitrogens, in agreement with our hypothesis based on the results shown in Table 33. The metal is octahedrally coordinated with the ligand occupying two sites, and His1390, Glu1392, and two water molecules occupying the remaining four (Figure 51).

The carboxylic acid is involved in a complex hydrogen bond network involving the same residues as those which interact with the C-5 carboxylate of 2-OG (Figure 52).

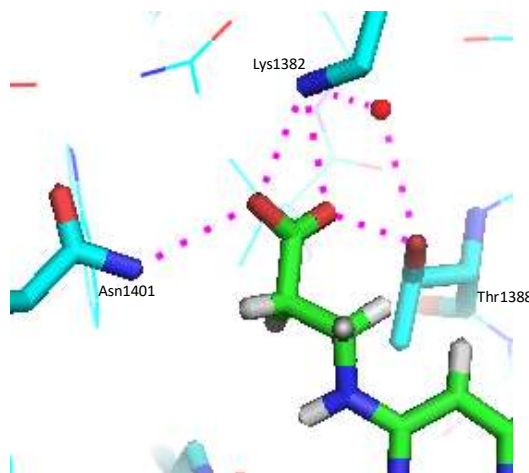


Figure 52. Hydrogen bond network between the carboxylate and Lys1382, Thr1388 and Asn1401.

It would appear that to satisfy the interactions of the carboxylate and the bidentate interaction of the pyridyl-pyrimidine with the catalytic metal a shift in the position of the metal by 2.1 Å is induced relative to its location in 2-OG structure (Figure 53). This change in position of the catalytic metal explains the difference observed in the coordination of His1470 with the metal (Figure 51), which now interacts through a bridging water molecule.

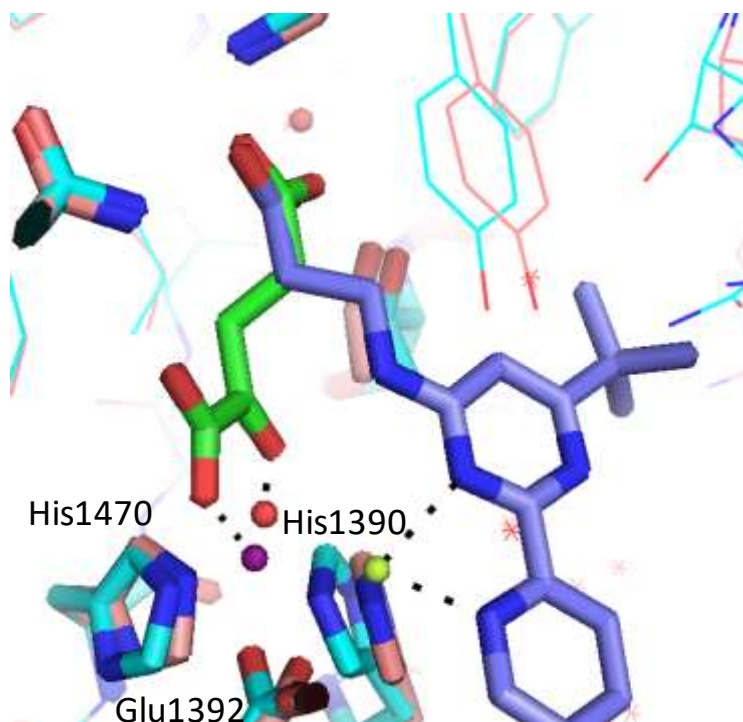


Figure 53. Overlay of 2-OG and **11** crystal structures in human JmjD3. Protein residues of 2-OG structure are in cyan; 2-OG is in green and Co(II) in purple. Protein residues of **11** are in pink, the apical water molecule in red, ligand **11** in blue and Co(II) in lime. Black dotted lines represent the bidentate interactions between 2-OG and Co(II); and ligand **11** and Co(II).

It is clear from the data presented in Tables 34-36 that the H-bond network between the carboxylate of ligand **11** and residues Lys1382, Thr1388 and Asn1401 (Figure 52) is critical and extremely hard to mimic. The space between the carboxylate and the various residues is limited, which makes it highly challenging to replace the carboxylate with other groups. As a result of this finding it was decided to shift the focus of the programme away from seeking acid isosteres and towards optimising inhibitor potency.

II.3.2.4 4-Linker analogues

In order to improve inhibition potency, it was desirable to create additional interactions with the enzyme. Sites from which these interactions could be introduced therefore needed to be identified. With this in mind replacement of the *N*-H group between the pyrimidine ring and the alkyl chain was therefore investigated. This exploration was initiated before the crystal structure of 2-OG bound to JmjD3 was resolved. It was hoped that incorporation of an *N*-Me group (Table 37) would be tolerated so that this vector could be used to grow the molecule with the aim of picking up new interactions. An increase in lipophilicity would also follow from the *N*-methylation, and this may have assisted cellular penetration.

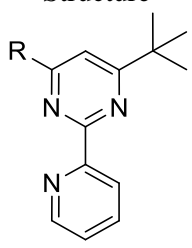
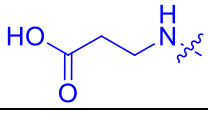
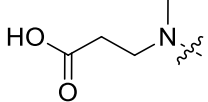
Structure	Compound	MALDI pIC ₅₀
		
R		
	11	5.0
	233	< 4.0

Table 37. MALDI data for NH linker replacement.

Disappointingly, methylation of the linker nitrogen to give **233** was not tolerated, suggesting that an H-bond donor may be required in this region (pIC₅₀ < 4.0). The crystal structure of **11** in the active site (Figure 51) offers a possible explanation for this observation. It may be that a hydrogen bond could exist between the *N*-H group and the apical water, and so the loss of this interaction would result in less active compound. Alternatively, with the apical water

being so close to the *N*-H group methylation could potentially introduced a steric clash with the bridging water molecule. Excluding this water molecule could potentially modify the coordination of His1470 with the iron and result in a drop in activity. Consequently this vector could not be used to obtain more lipophilic compounds.

II.3.2.5 SAR development: α -substituted carboxylic acids

Overlay of the X-ray crystal structures of 2-OG and **11** in JmjD3 suggested that substitution α - to the acid may be tolerated (Figure 53). Compounds were therefore designed to explore this hypothesis (Table 38). First, **270** was designed to determine whether or not substitution was tolerated at this position. Although **270** was not as potent as parent compound **11** (pIC_{50} = 4.6 vs 5.0) the biochemical data showed that the position α - to the acid could be substituted with a small penalty paid in terms of potency. Encouraged by this result compound **271** was designed to extend a hydroxyl group towards the water molecule which is involved in a binding interaction between His1470 and the catalytic iron (Figure 53). It was hoped that an H-bonding interaction could be picked up and go some way to compensate for the penalty paid for substituting at this position.

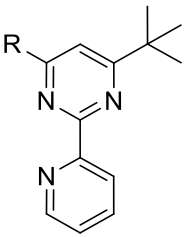
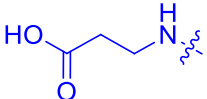
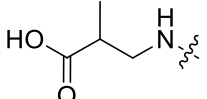
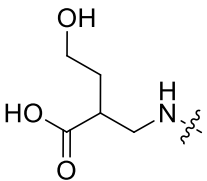
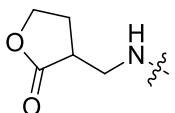
Structure	Compound	MALDI pIC ₅₀
		
R		
	11	5.0
	270	4.6
	271	< 4.0
	288	< 4.0 ^a

Table 38. MALDI data for α -substituted acids.

^a < 4.0 (n = 3) and 4.5 (n = 2).

En route to the target molecule **271**, the lactone **288** was also isolated and tested. Disappointingly, neither compound showed inhibition of JmjD3. In the light of these results, α -substituted acids were not investigated further.

II.3.2.6 Scoping constrained linkers

The finding that substitution α - to the carboxylate was tolerated provided encouragement for the investigation of conformationally restricted linkers.

It is a common medicinal chemistry strategy to try to preorganise a molecule in the conformation it would adopt once bound into the active site of a target protein. When a

flexible ligand binds, many internal rotations around flexible bonds must cease and this corresponds to an entropic loss which offsets the favourable enthalpy of binding. Restricting ligand conformation reduces the size of this entropic penalty while attempting to preserve the most favourable enthalpy.¹⁸⁰

New targets were therefore designed to investigate the effect of a variety of conformationally restricted linkers between the *N*-H and CO₂H groups of **11** (Figure 54).

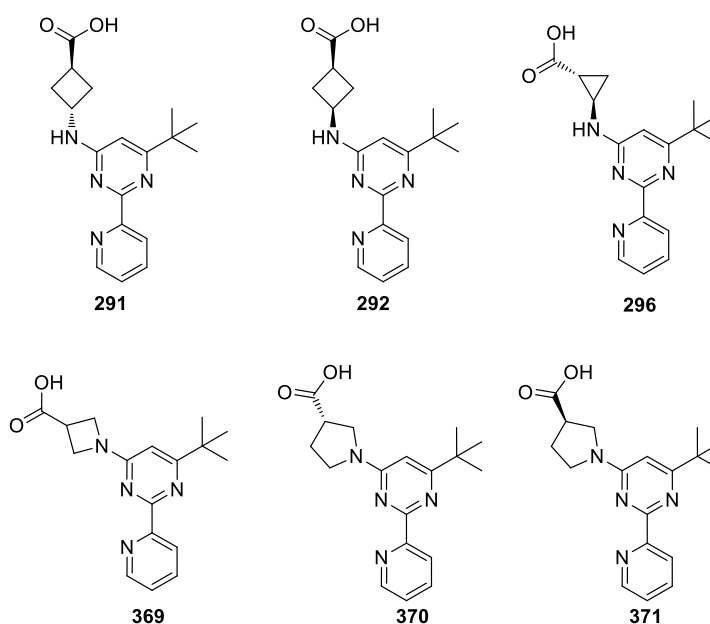


Figure 54. Conformationally restricted linker targets.

These potential targets were docked using Glide in Maestro (v 9.1) and prioritised using the scores from the dockings. The more negative the score the better the docking. Compound **296** came out with the most negative score (-9.16), placing it as high priority target; unfortunately it could not be synthesised because it was unstable (*cf.* Section II.3.1.4). Compounds **291** and **292** came out with less negative scores (-8.84 and -8.12, respectively) and were classified as medium priority. The docking of these targets was done such that the key interactions for potency were maintained, *i.e.* the bidentate interaction with the metal

and the H-bond network between the carboxylate and residues Lys1382, Thr1388 and Asn1401 (Figures 55, 56 and 57). The last three targets, azetidine **369** and pyrrolidines **370** and **371**, were classified as low priority because they each possessed a di-substituted nitrogen atom which the results for N-Me analogue **233** had showed was not tolerated (Table 37).

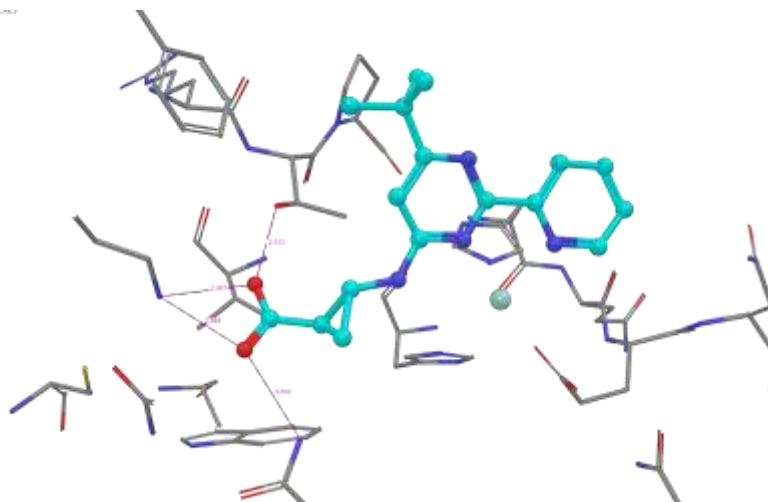


Figure 55. Docking of *trans*-cyclopropyl ring linked **296**. Glide docking score -9.16 (Appendix 8).

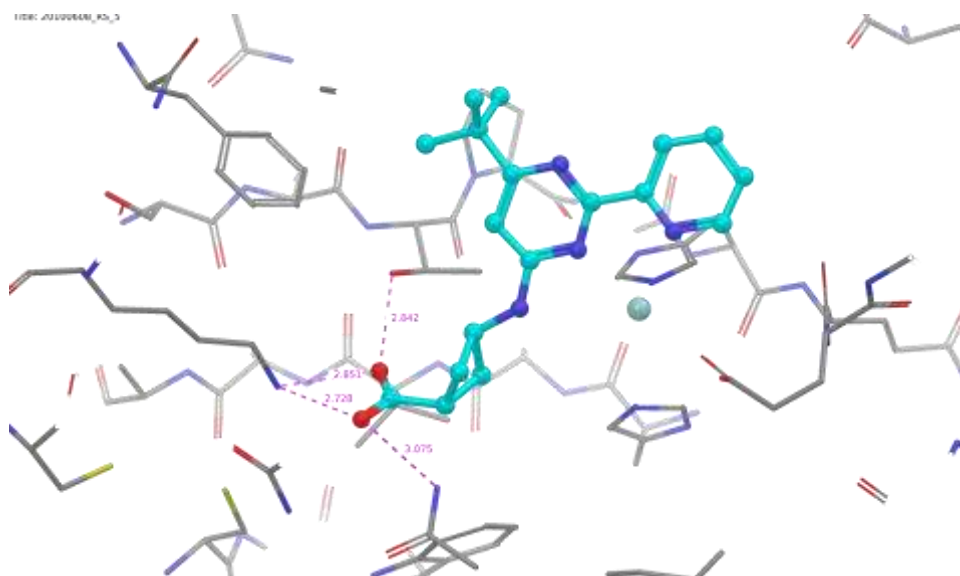


Figure 56. Docking of *trans*-cyclobutyl ring linked **291**. Glide docking score -8.84 (Appendix 8).

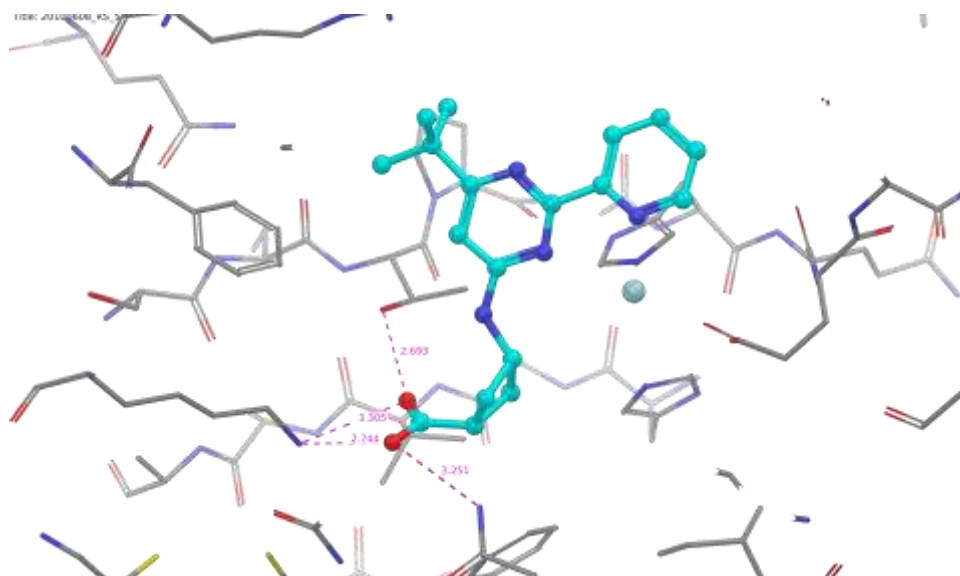


Figure 57. Docking of *cis*-cyclobutyl ring linked **292**. Glide docking score -8.12 (Appendix 8).

Compounds **291** and **292** were synthesised and their biochemical results are summarised in Table 39. Replacing the ethylene chain with a cyclobutyl ring gave less active compounds

291 ($pIC_{50} = 4.4$) and **292** ($pIC_{50} < 4.0$). It should be noted though that the *trans* cyclobutyl (**291**) was more potent than the *cis* (**292**), a trend which is in accordance with the docking scores and analysis of the conformations the ligands adopted in the dockings. Of particular note is the direction of the *N*-H bond in the poses of the two molecules. In the case of **291** the *N*-H bond was pointing down towards the bridging water molecule as seen in the X-ray structure of **11**, whilst in **292** the *N*-H bond was pointing in the opposite direction. If the *N*-H bond in **11** is involved in some interactions with the bridging water molecule, losing this interaction could potentially have an impact on potency and so could explain the loss of activity for compound **292**.

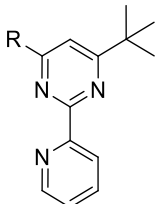
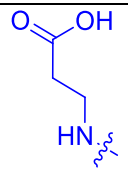
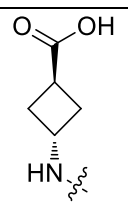
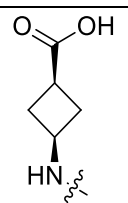
Structure	Compound	MALDI pIC_{50}
		
R		
	11	5.0
	291	4.4
	292	< 4.0

Table 39. MALDI data for constrained chains.

A number of modifications of the carboxylate-containing side chain were investigated in order to find more permeable analogues in a view of obtaining compounds active in the

cellular assay. These modifications mainly included carboxylic acid isosteres, but none could replace the carboxylate and this was confirmed by the crystal structure of **11**. In addition, improvement in biochemical potency was sought by creation of additional interactions with the enzyme through new vectors and use of constrained linkers to form more optimal conformations of the lead molecule. These modifications which included α -substitution to the critical carboxylate and conformationally restricted linkers such as cyclobutane did not deliver any improvement in potency. Subsequently it was decided to focus more effort on vector 6 to deliver more potent compounds.

II.3.2.7 SAR development: vector 6

II.3.2.7.1 'Bu pocket

Analysis of the environment surrounding the *tert*-butyl group revealed it to be sitting in a pocket made up of polar residues with Arg1247, Thr1331 and Asn1332 (Figure 58).

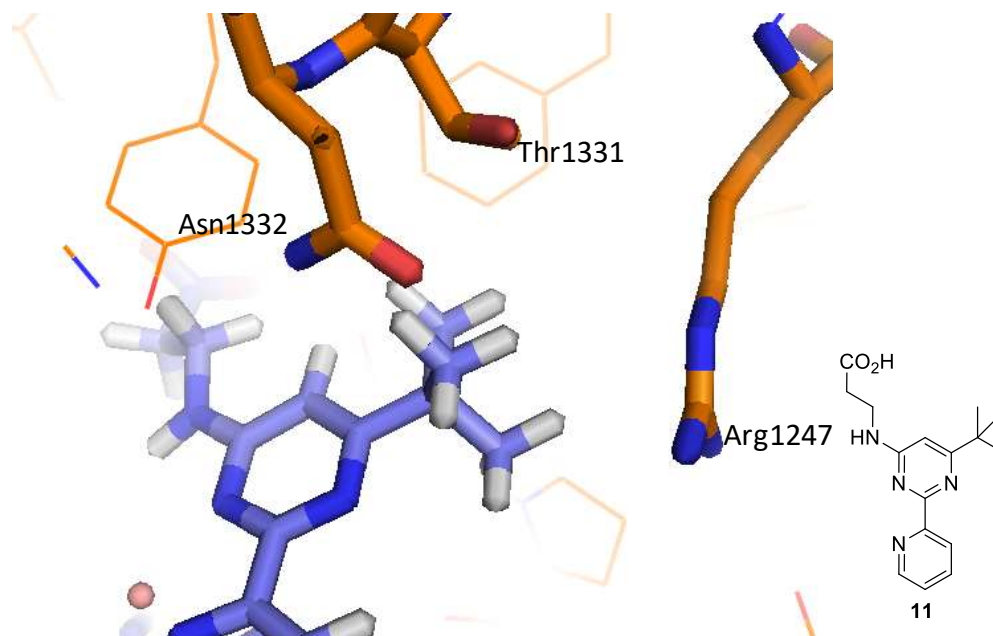


Figure 58. Crystal structure of **11** bound in the active site of JmjD3. Protein residues are in orange.

Figure 59 shows the good surface complementarity between the ligand and the active site.

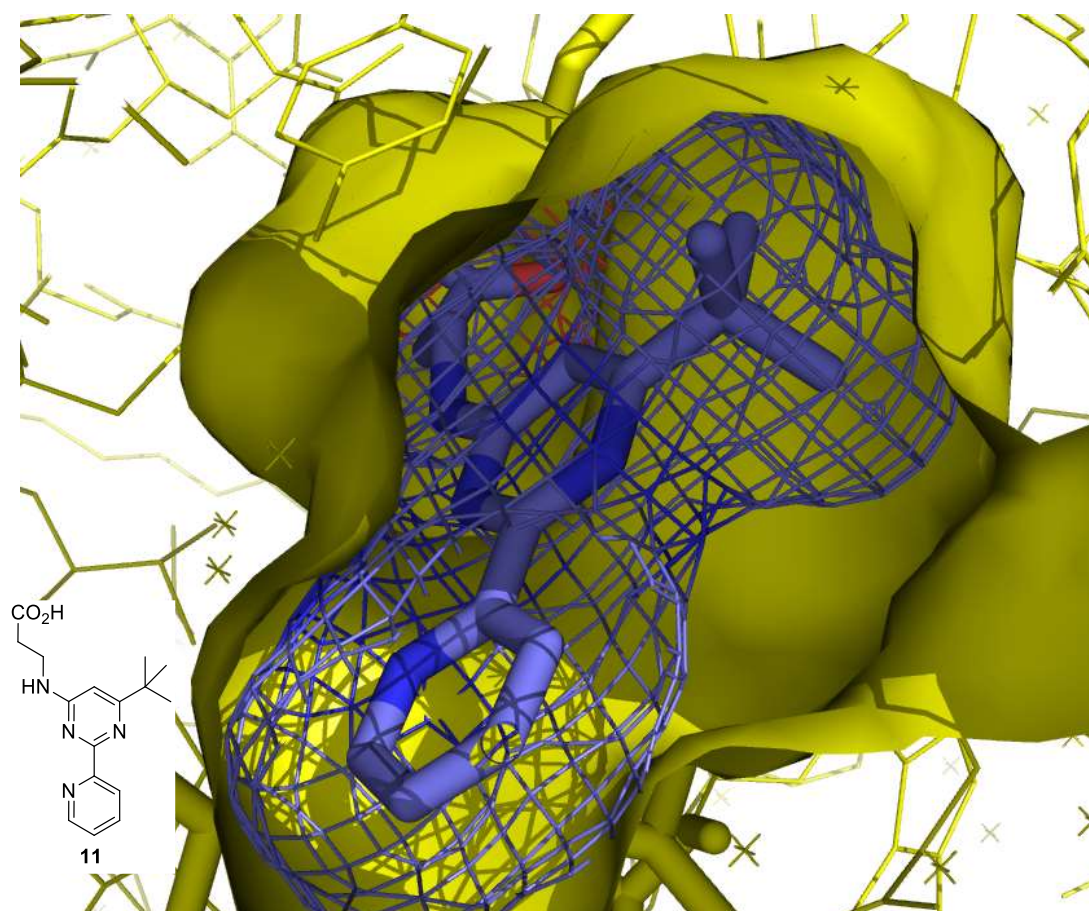


Figure 59. Surface of the active site of JmjD3. Compound **11** in blue and residues in yellow.

The overlay of the structures of 2-OG and **11** bound to JmjD3 is generally good. However, there are two significant differences, the change in position of the catalytic metal already discussed in Section II.3.2.3.1, and Figure 60 shows differences in the position of Arg1247 between the two crystal structures. In the case of ligand **11**, Arg1247 is now located to sit close to the *tert*-butyl group ($\sim 4 \text{ \AA}$ away), and this movement enabled the good surface complementarity between the ligand and the active site. This is another peculiarity of the active site of this enzyme; not only does the metal move in the active site, but also Arg1247 is flexible enough to move in or out depending on the nature of the bound ligand. Other polar

residues also sit in close proximity to the *tert*-butyl group though do not appear to be making any key interactions.

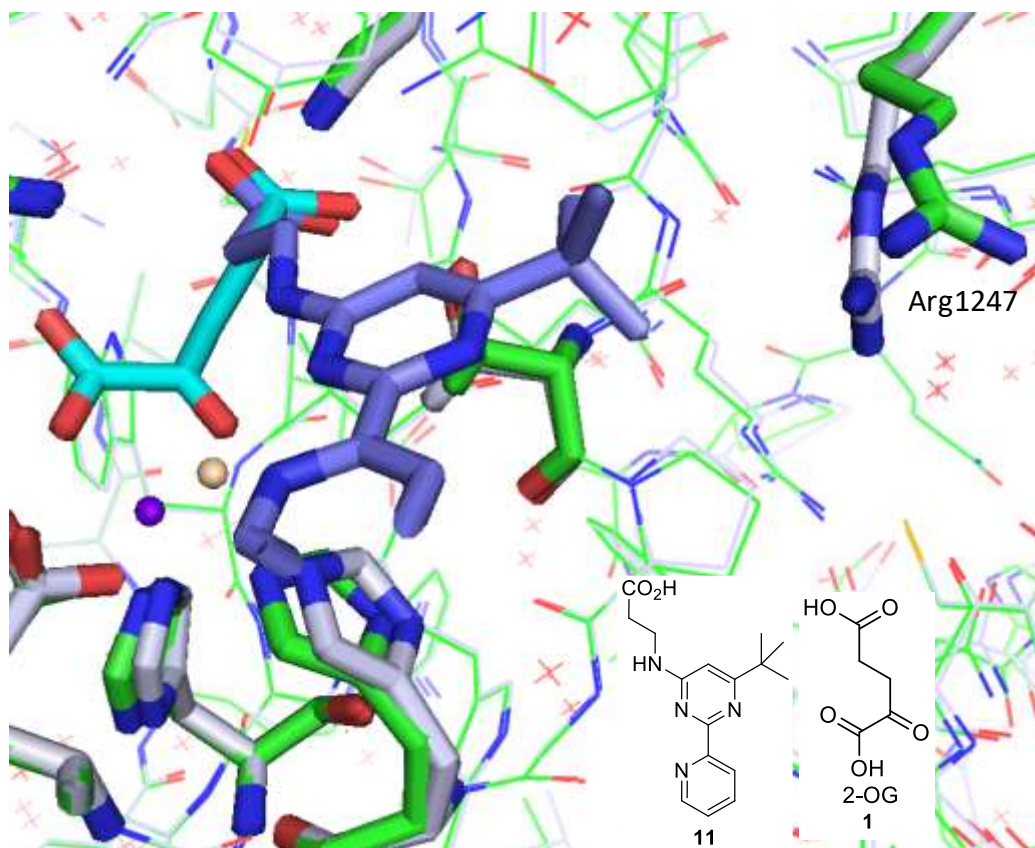


Figure 60. Overlay of crystal structures of 2-OG (compound in cyan, residues in green, Co(II) in purple) and **11** (compound in blue, residues in silver, Co(II) in beige) bound in the active site of JmjD3.

It was therefore decided to probe the space around the 6-position of the pyrimidine with substituents having a variety of steric demands and polarities in an effort to create interactions with residues of the active site to improve the potency.

II.3.2.7.2 C- and N-linked substituents

It was decided to explore the space around the 6-position of the pyrimidine with readily accessible aliphatic amine groups (Table 40). A colleague showed that substituting the *tert*-butyl group of **11** for a proton (**414**)¹⁸¹ resulted in a compound which lacked detectable activity against JmjD3 (Table 40). Though the *tert*-butyl group was not making polar interactions with the residues of the pocket, it was clearly contributing to the binding which resulted in inhibition. The piperidine **415** was synthesised elsewhere in our laboratory¹⁸² and was active with a similar potency to the parent compound **11**. A bigger cycloalkylamine such as the azepane **329a**, again displayed similar levels of potency (pIC₅₀ = 5.1).

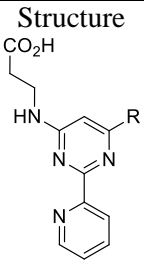

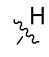
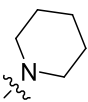
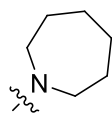
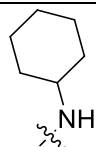
Structure	Compound	MALDI pIC ₅₀
		
R		
	11	5.0
	414	< 4.0
	415	5.2
	329a	5.1
	329b	< 4.0 ^a

Table 40. MALDI data for variation at position 6. Compound **414** and **415** were synthesised elsewhere in our laboratory.^{181,182}

^a < 4.0 (n =1) and 4 (n = 1).

The cyclohexylamine **329b**, which was expected to push further into the pocket and occupy a different position from the piperidine and azepane, was tested and displayed activity below the limit of the assay (pIC₅₀ < 4.0). This result could be due to a variety of reasons. One possibility considered was the H-bond donor, since compound **329b** was the only secondary amine in Table 40. In addition the position of the cyclohexyl ring as well as the ring size could also help explain this biochemical assay data. None of the amines in Table 40 could be crystallised in the JmjD3 active site either because they failed to crystallise or because they

gave poor quality crystals. However, comparing the lowest energy conformations of these amines (Figure 61) showed that the cyclohexylamine ring occupied different positions to the *tert*-butyl **11**, azepane **329a** and the piperidine **415**. One of the consequences of the cyclohexylamine being positioned differently is that this ring seems to push further in the pocket in certain directions (Figure 61a, 61b and 61c). If the space occupied by the cyclohexylamine in its lowest energy conformation is similar to the conformation adopted in the active site of JmjD3 and this conformation is not tolerated, this could potentially result in a reduction of potency and explain biochemical data obtained for compound **329b**.

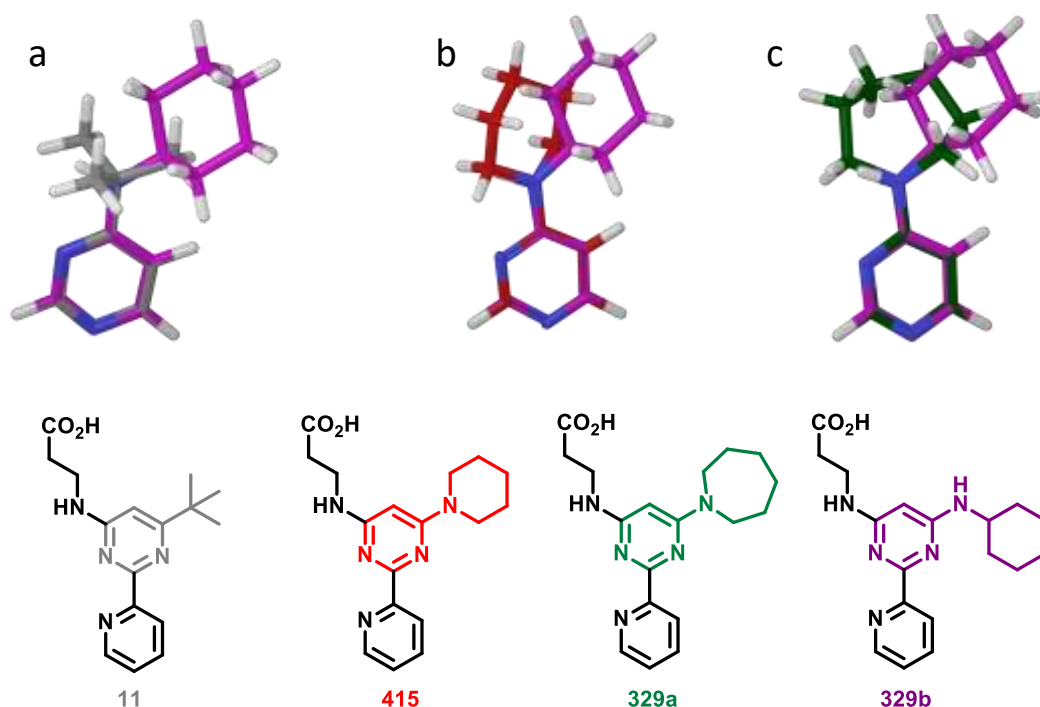


Figure 61. Lowest energy conformations of substructures of compounds **11**, **415**, **329a** and **329b**. Compound **11** is in grey, **415** in red, **329a** in green and **329b** in purple. (a) Overlay of lowest energy conformations of **11** and **329b**; (b) overlay of lowest energy conformations of **415** and **329b**; (c) overlay of lowest energy conformations of **329a** and **329b**. The lowest energy conformations were obtained using Maestro (v 9.1).

A substructure of compound **329b** in its lowest energy conformation was placed in the active site of JmjD3 (Figure 62). This Figure is not the results of a docking but at least gives an indication about compound **329b** fitting in the active site or not. Figure 62 clearly shows that the cyclohexylamine **329b** may not fit in the active site due to the potential clash with residues of the enzyme, and this could potentially result in a reduction of potency.

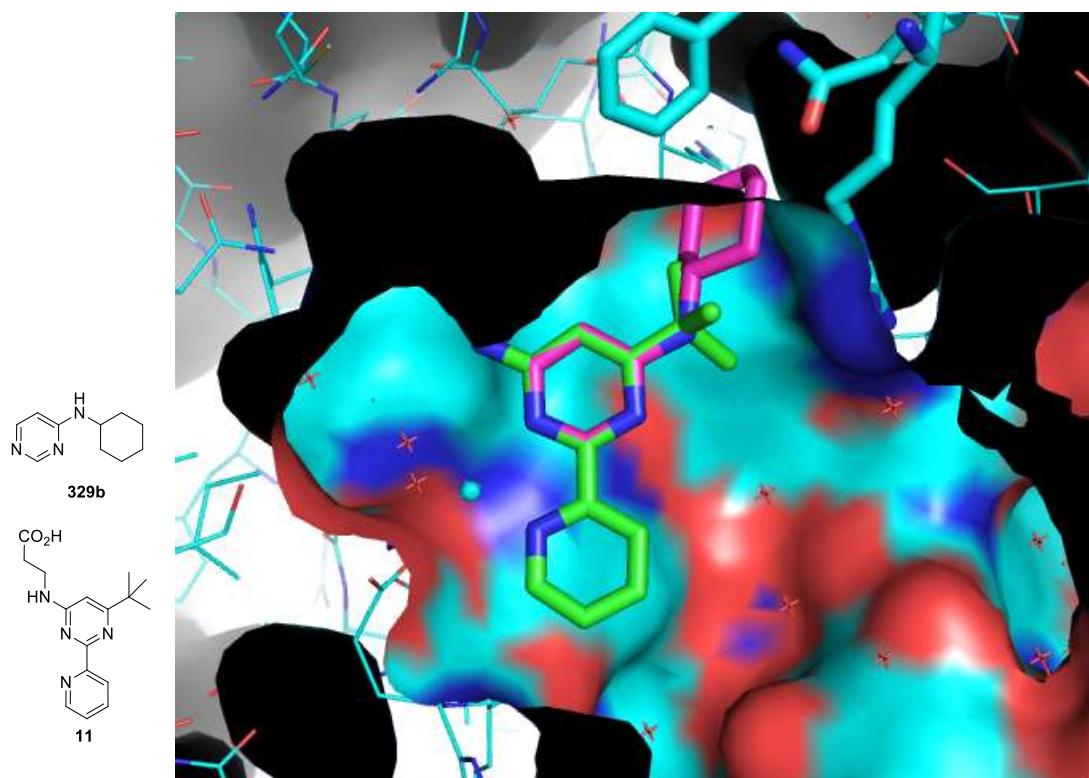


Figure 62. Overlay of lowest energy conformation of substructure of cyclohexylamine **329b** and **11** crystal structure in JmjD3. Protein residues of **11** structure are in cyan; **11** in green and Co(II) in cyan. Substructure of cyclohexylamine **329b** is in magenta. Substructure of cyclohexylamine **329b** was placed in the active site of JmjD3.

At physiological pH arginine residues (pK_a 12) are protonated and therefore act as H-bond donors which can interact with H-bond acceptor atoms such as N, O, F, Cl and S.¹⁸³ To explore the potential of increasing inhibitor potency by H-bonding to Arg1247, and also to

other residues such as Asn1332 and Gln1249 (Figure 63), a variety of H-bonding groups were introduced at position 6 of the pyrimidine.

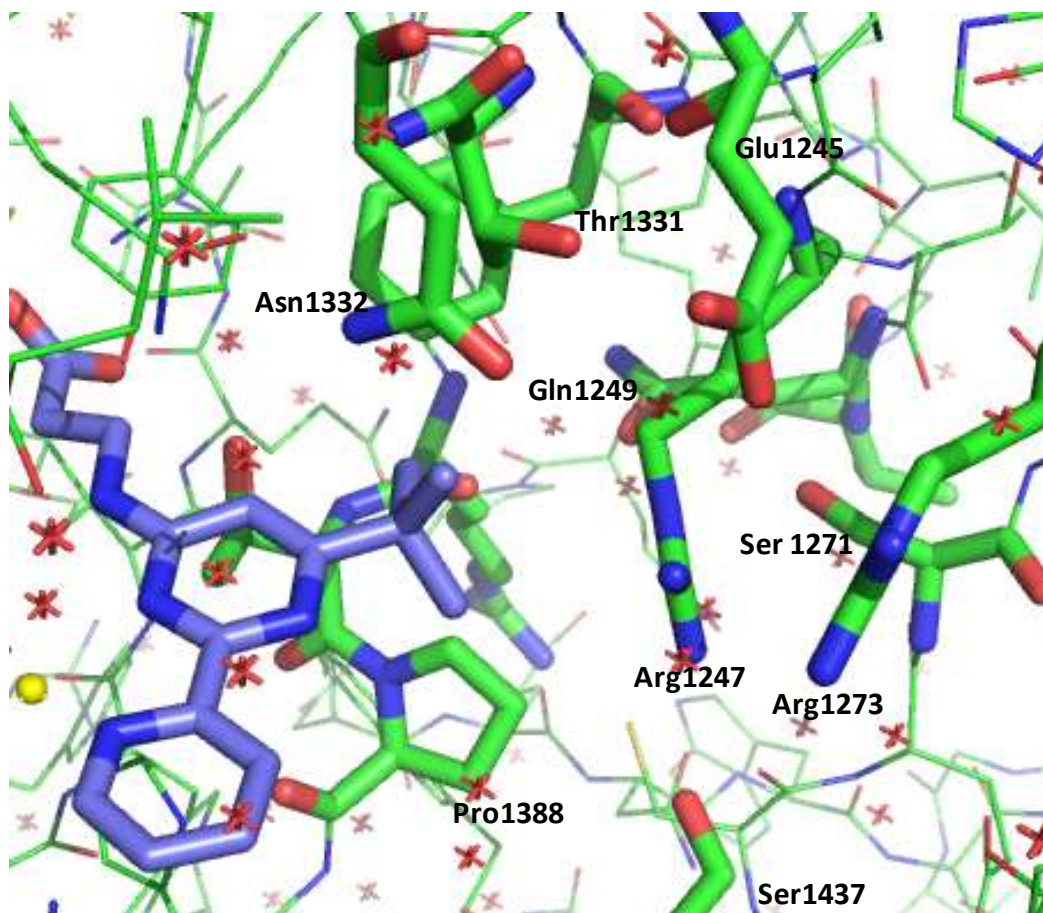


Figure 63. Crystal structure **11** bound in the active site of JmjD3. Protein residues are in green, **11** structure in blue and Co(II) in yellow.

The groups employed included amides, sulfonamides and heteroaryls as exemplified in Table 41. Some of the compounds in Table 41 contained substituents sterically larger than the *tert*-butyl group to investigate whether the pocket could be opened or a channel created. This kind of phenomenon has been observed in other proteins with flexible active sites, such as the glucocorticoid receptor (GR), as demonstrated by Biggadike *et al.*¹⁸⁴

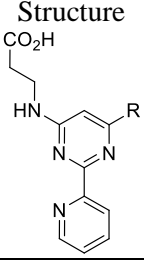

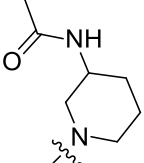
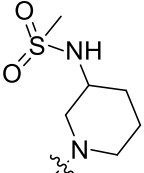
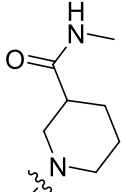
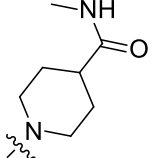
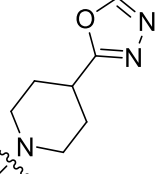
Structure 	Compound	MALDI pIC ₅₀
R		
	11	5.0
	321a	5.0
	321b	4.8
	324	5.1
	327a	5.0
	327b	5.0

Table 41. MALDI data for variation at position 6.

All of the 3-substituted piperidines examined, 3-acetamido piperidine (**321a**), reverse amide (**324**) and 3-methylsulfonamido piperidine (**321b**) showed a similar level of potency to the parent compound (**11**) (pIC₅₀ = 5.0, 5.1 and 4.8, respectively). This is despite these groups

possessing very different steric and electronic demands. Moving the *N*-methanamide to the 4-position of the piperidine to try to optimise potential H-bond interactions with residues in the enzyme also did not affect the potency (**327a**, $pIC_{50} = 5.0$). The oxadiazole **327b** was designed to increase the chances of interacting with the polar residues in this pocket through the two nitrogens and the oxygen; it was shown to be equipotent with parent compound **11** with pIC_{50} of 5.0. Although these results demonstrated that polar hydrogen-bonding groups were tolerated in the pocket, it was disappointing to find that none delivered an improvement in potency against JmjD3.

The results presented in Tables 40 and 41 show that substituents were required at position 6. The aliphatic amines were tolerated, as well as the substituted piperidines containing polar groups. As expected, the introduction of polar groups also did not help to improve the permeability (data not shown). For all these reasons, the exploration of the space around the 6-position of the pyrimidine with polar substituted piperidines was not pursued further and so effort was re-focused into engaging the Arg1247 with lipophilic aromatic rings by creating and optimising π -cation interactions.

The term “ π -cation interaction” was introduced by Dougherty in 1996 and was defined as the interaction of the π -face of an aromatic ring with a cation.¹⁸⁵ The π -cation interaction is a strong interaction which can be of a comparable magnitude, in some instances, to the interaction between a potassium cation and water, the energy of which is 18 kcal/mol (Table 42). This type of interaction is not limited to metal cations alone as shown by the interaction between NH_4^+ and benzene (19.3 kcal/mol). Alkylation of the ammonium ion decreases the energy of the π -cation interaction, but the energy of interaction between the tetrasubstituted nitrogen ion and benzene is still as high as 9.4 kcal/mol (Table 42).

Cation	Molecule	Binding energy (kcal/mol)
K ⁺	H ₂ O	18 ¹⁸⁶
K ⁺	C ₆ H ₆	19.2 ¹⁸⁶
Na ⁺	C ₆ H ₆	28.0 ¹⁸⁷
NH ₄ ⁺	C ₆ H ₆	19.3 ¹⁸⁸
CH ₃ NH ₃ ⁺	C ₆ H ₆	15.9 ¹⁸⁸
NMe ₄ ⁺	C ₆ H ₆	9.4 ¹⁸⁹

Table 42. Measurement of π -cation interaction energies in the gas-phase.

Burley and Petsko in 1986, examined thirty three high resolution crystal structures (≥ 2 Å) of proteins focusing on the interactions between aromatic amino-acids (Phe, Tyr and Trp) and adjacent residues with side chains containing nitrogen atoms (Lys, Arg, Asn, Gln and His). They demonstrated that the nitrogen atoms of arginine and lysine residues prefer to be between 3.4 and 6 Å of the centroids of aromatic rings (Figure 64).¹⁹⁰

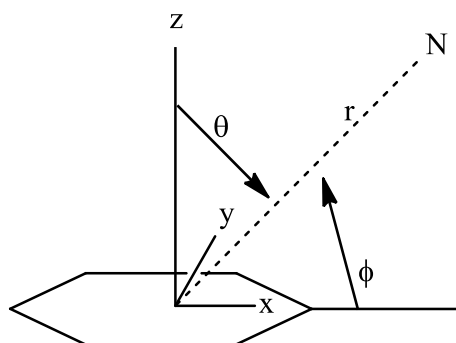


Figure 64. Coordinate axes for the definition of the polar coordinate (r , θ , and ϕ). The origin is placed at the centroid of the 6-membered ring.

At the time, Burley and Petsko referred to this interaction as an “amino-aromatic interaction”.¹⁹⁰ Moreover, they showed that 50% of the Arg residues were involved in this amino-aromatic interaction with an average of two aromatic amino acids. Gallivan and Dougherty analysed 593 proteins and revealed that about 70% of Arg residues were located close to aromatic amino acids.¹⁹¹ Arginine residues can interact with aromatic rings *via* two geometries (Figure 65); these are a perpendicular geometry in which the arginine NH’s make

the interaction with the aromatic ring by pointing into the ring and a stacked geometry in which the plane of the guanidinium group of the Arg is parallel to the face of the aromatic ring (Figure 65).¹⁹²

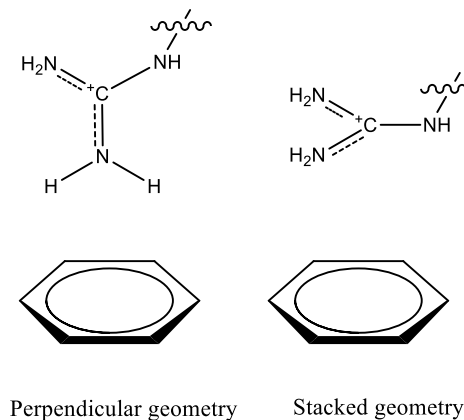


Figure 65. Limiting geometries of π -cation interaction between Arg residues and benzene ring.¹⁹²

Flocco and Mowbray analysed interactions between Arg residues and aromatic amino acids, and found a preference for the stacked geometry.¹⁹³ All the protons of the guanidinium are free to hydrogen bond to water and/or carbonyl groups in the protein backbone in this geometry.¹⁹⁴

The π -cation interaction between arginine residues and compounds containing aromatic groups have been studied and exploited in various medicinal chemistry programmes to improve the potency of compounds.^{195,196} Consequently it was decided to apply this strategy to our programme and try to identify an aromatic group to engage Arg1247 *via* a π -cation interaction. It was also envisaged that the presence of additional aromatic rings would increase the lipophilicity of the compounds to a level whereby cellular penetration would be facilitated. This work is summarised in Table 43.

Various aromatic systems were investigated. *C*-linked aromatic rings such as benzothiophene were considered because of their large π -faces which offer a greater area for interaction and allow more flexibility in the way the groups come together.¹⁹⁶ Additionally, *N*-linked amines containing aromatic rings were considered, for two main reasons. Firstly, non-aromatic amines had been demonstrated to be as potent as **11** (Tables 40 and 41), so adding a 6-membered aromatic ring could potentially improve the potency by forming a π -cation interaction. The second reason for choosing amines with pendant aromatic rings was more practical; the synthetic introduction of amines did not require the use of metal catalysts and associated risk of product contamination (cf. Section II.3.1.1.1), in contrast to the direct attachment of aromatic rings. It was shown in a review by Dougherty and Ma that an arginine residue interacts more strongly with the 6-membered ring than it does with the 5-membered ring of tryptophan.¹⁹²

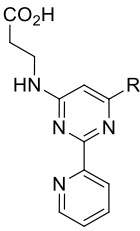

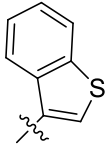
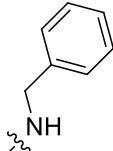
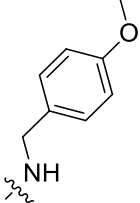
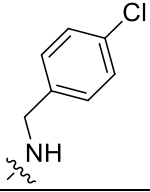
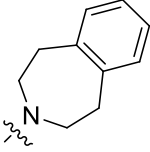
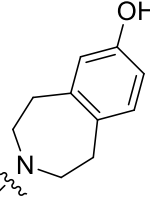
Structure  CO ₂ H HN R R	Compound	MALDI pIC ₅₀	EGLN	cLogP
	11	5.0	< 4.3	2.9
	314	5.1	4.8	4.3
	416	5.4	4.6 ^a	3.4
	417	5.1	< 4.3	3.3
	332a	5.3	5.0	4.1
	332b	5.6	< 4.3 ^b	3.8
	332c	6.0	4.7	3.1

Table 43. Biochemical assay data for variation at position 6.

^a < 4.3 (n=3) and 4.6 (n=2).

^b < 4.3 (n =3) and 4.7 (n=1).

Benzothiophene **314** and **11** (Table 43) were equipotent against JmjD3 in the MALDI assay, although **314** was less selective than **11**, with a pIC₅₀ of 4.8 against EGLN. The benzylamine **416** synthesised elsewhere in our laboratory¹⁹⁷ was more potent than **11** with a pIC₅₀ of 5.4 but showed the same issue of selectivity as **314** with a pIC₅₀ of 4.6 against EGLN. This increase in potency was very encouraging albeit with the loss of selectivity. Following this result it was decided to probe the pocket with substituted benzylamines and investigate different substituents which would affect the electronic character of the phenyl ring to assess their impact on potency. The *para*-methoxybenzylamine **417**, synthesised elsewhere in the laboratory, was more electron rich than **416** and showed initially that substituents at this position were tolerated (pIC₅₀ of 5.1).¹⁹⁸ Compound **417** showed similar potency to **11** and maintained the selectivity over EGLN (pIC₅₀ < 4.3). Whilst the *para* chlorobenzylamine **332a**, less electron rich than **416**, showed similar potency (pIC₅₀ of 5.3) it was less selective than **11** and **416** against EGLN with a pIC₅₀ of 5.0. The effect on selectivity could also be related to the differences in sizes between the two substituents OMe and Cl. This first set of data suggested that the nature and / or the size of the substituent at the *para*-position of the phenyl ring could be utilised to obtain more selective compounds over EGLN, albeit without an initial increase in potency against JmjD3. However more work would be required to validate this hypothesis with a wider range of substituents to fully explore electronic effects on potency.

Because azepane **329a** (Table 41) had been shown to be tolerated, it seems logical to investigate the introduction of an aromatic ring to this template in an effort to create a π -cation interaction with Arg1247. Thus, tetrahydrobenzazepine analogue **332b** was synthesised. Compound **332b** successfully delivered an appreciable improvement in potency with a pIC₅₀ of 5.6 against JmjD3 in the MALDI assay whilst maintaining good selectivity over EGLN (pIC₅₀ < 4.3) and other Jmj enzymes (data not shown). The fused phenyl ring offers further opportunities for the development of interactions with residues in the pocket.

Compound **332c** which was designed to interact with residue Gln1249 (Figure 63) through the phenolic OH was therefore synthesised. Compound **332c** was even more potent than the benzazepine **332b** with a pIC₅₀ of 6.0 against JmjD3 in the MALDI assay, but unfortunately this compound was not selective enough with a pIC₅₀ of 4.7 against EGLN.

Gratifyingly, these aromatic containing compounds presented in table 43 were more lipophilic than the parent compound **11** with cLogP varying from 3.1 for **332c** to 4.3 for **314**. However, only the benzothiophene **314**, which was the more lipophilic compound in this table, was weakly permeable (13 nM/sec at pH7.4).

An X-ray crystal structure of **332c** could not be obtained to confirm the interaction between the hydroxyl group and Gln1249. However, an X-ray crystal structure of **332b** bound to JmjD3 was obtained (Figure 66) and it shows that the key interactions for potency are maintained: these are a bidentate interaction with the metal ion and a hydrogen bond network between carboxylate and Lys1382, Thr1388 and Asn1401.¹⁵⁴ Additionally, a π -cation interaction between Arg1247 and the benzazepine ring can be observed.

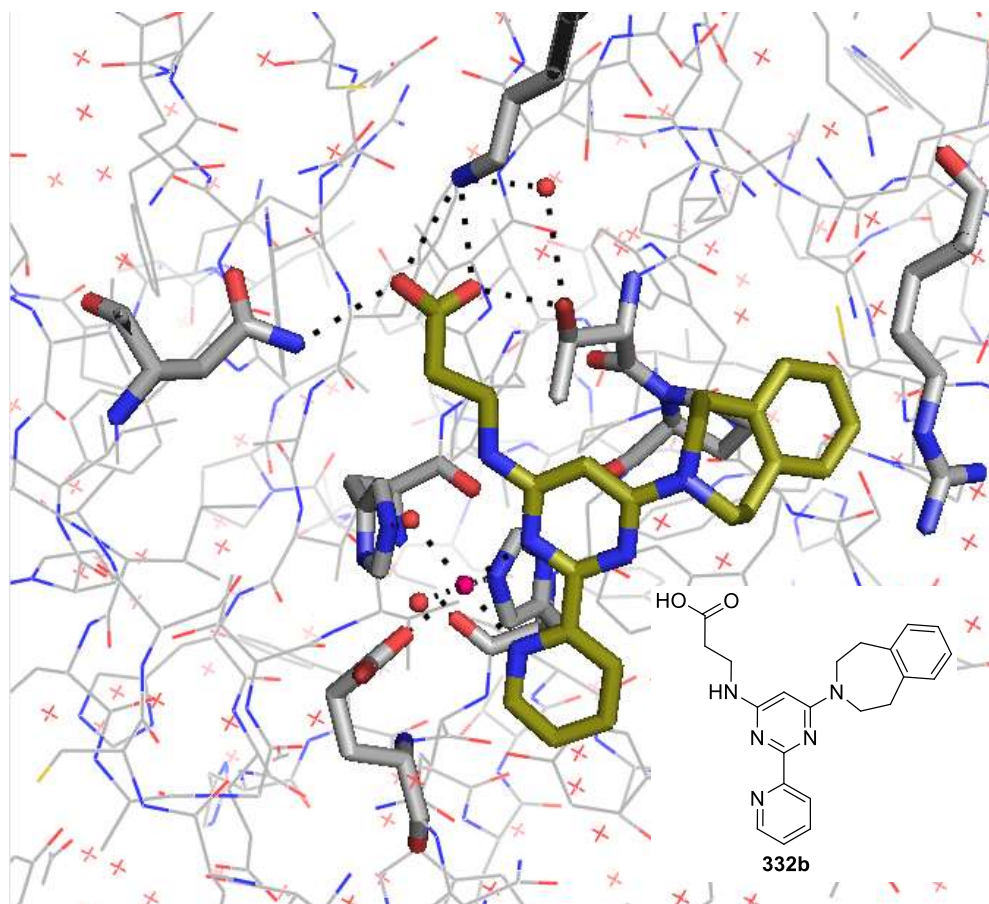


Figure 66. X-ray crystal structure of **332b** bound to JmjD3. PDB: 4ASK.

Although otherwise very similar, a comparison of the crystal structures of **11** and **332b** bound to JmjD3 reveals that Arg1247 occupies different positions in the two structures (Figure 67).

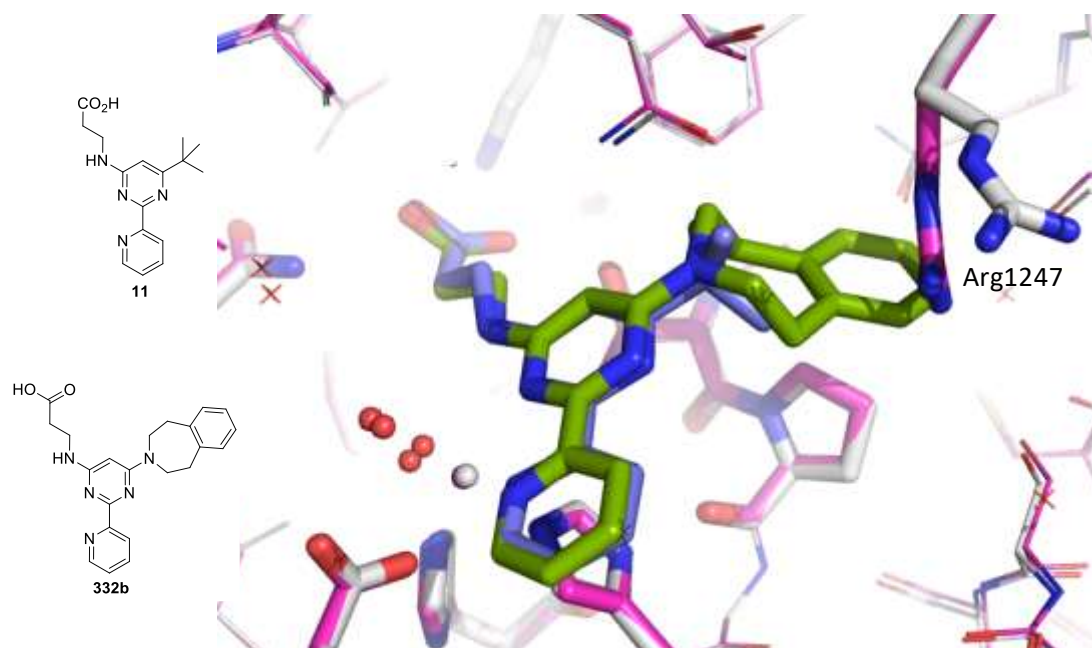


Figure 67. Overlay of crystal structures of **11** (compound in blue, residues in pink, Co(II) in purple) and **332b** (compound in khaki, residues in silver, Co(II) in silver) bound in the active site of JmjD3.

The overlay of the crystal structures with 2-OG and **332b** (Figure 68) shows that Arg1247 occupies the same position. In contrast the overlay of the crystal structures with 2-OG and **11** (Figure 60) shows that Arg1247 occupies different positions. It is also seen that the phenyl ring of **332b** sits comfortably between Arg1247 and Pro1388. If Arg1247 has a strong preference for the position observed in the 2-OG structure the fact that **332b** preserves this position and interacts with Arg1247 through a π -cation interaction could explain the improvement in potency.

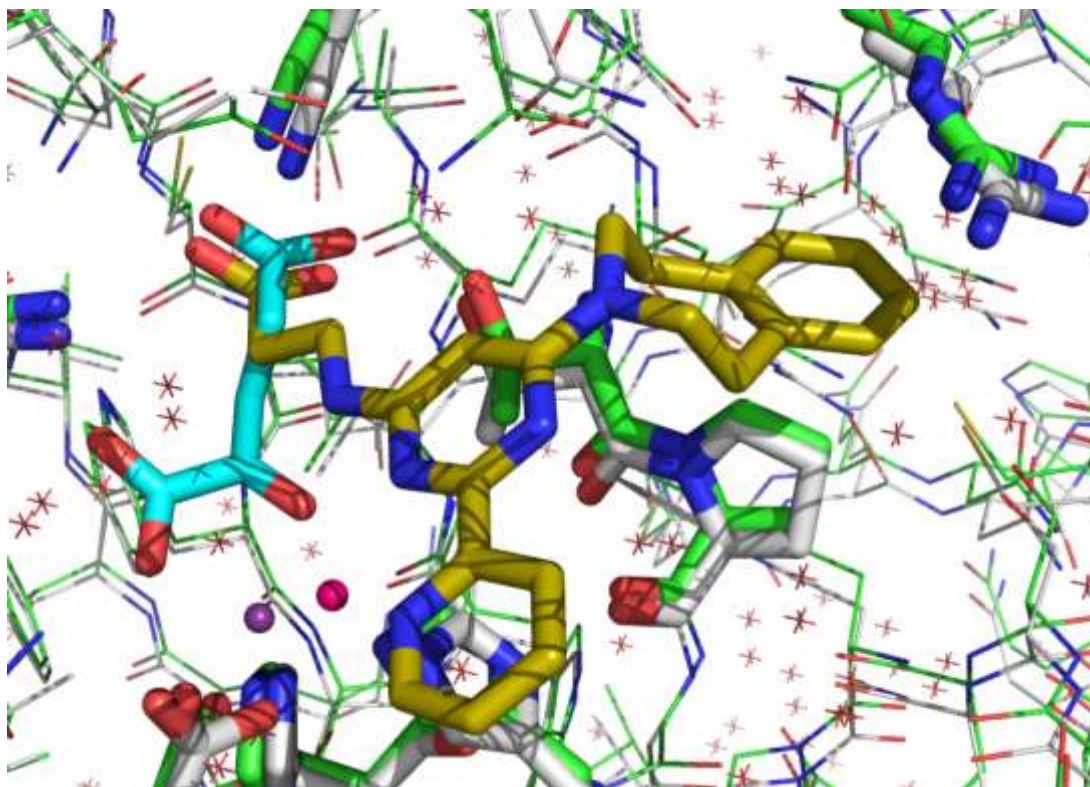


Figure 68. Overlay of crystal structures of 2-OG (compound in cyan, residues in green, Co(II) in purple) and **332b** (compound in khaki, residues in silver, Co(II) in pink) bound in the active site of JmjD3.

As expected Arg1247 is stacking above the aromatic 6-membered ring of the tetrahydrobenzazepine **332b** which enables the guanidinium residue to hydrogen bond to water.^{193,194} However Arg1247 does not stack directly above the ring; it is slightly shifted or at an angle (Figure 69).

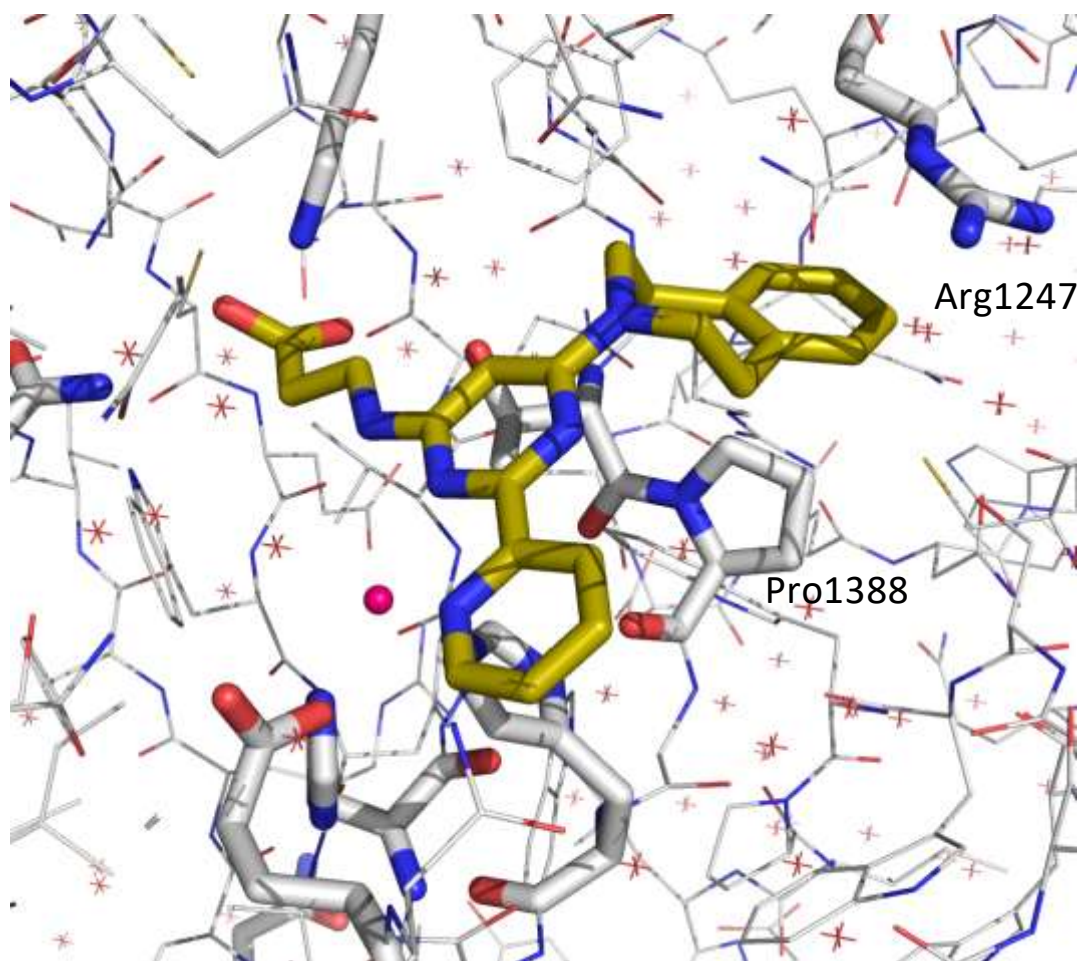


Figure 69. Tetrahydrobenzazepine group sits in a narrow cleft between Pro1388 and Arg1247 with which it interacts through a π -cation interaction.

Indeed, Figure 69 shows the angle of 18.6° between the plane of the phenyl from the tetrahydrobenzazepine ring and the plane of the guanidinium ion of Arg1247. Crowley and Golovin analysed the geometry of π -cation interaction involving Arg residue in protein-protein interfaces,¹⁹⁹ and found that 53% of the π -cation interactions between Arg and aromatic amino-acids Tyr, Phe and Trp involved a planar stacking geometry between the guanidinium ion and aromatic planes. These stacking interactions had an average angle of $17^\circ (\pm 8)$. Thus, the interaction observed between benzazepine group and Arg1247 could be considered as stacked.

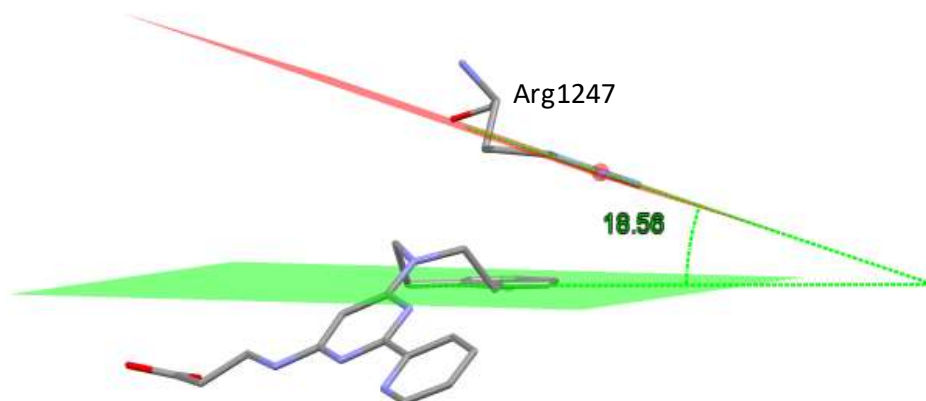


Figure 70. Planes of phenyl ring of benzazepine and Arg1247. Angle between planes of benzazepine phenyl ring and Arg1247 is represented in green.²⁰⁰

Moreover, the nitrogens of Arg1247 are close to the phenyl centroid ($r \leq 4.5 \text{ \AA}$) (Figure 71) in agreement with Burley and Petsko who demonstrated that nitrogen atoms of arginine and lysine residues prefer to be between 3.4 and 6 \AA of the centroids of aromatic rings.¹⁹⁰ Gallivan and Dougherty in 2000 refined the optimal distance for π -cation interaction further. They showed the existence of a strong π -cation interaction between methylammonium and benzene in water when the pair was 3.4-4.6 \AA apart, confirming that the distances between the nitrogens of Arg1247 and benzazepine are optimal to allow a π -cation interaction.²⁰¹

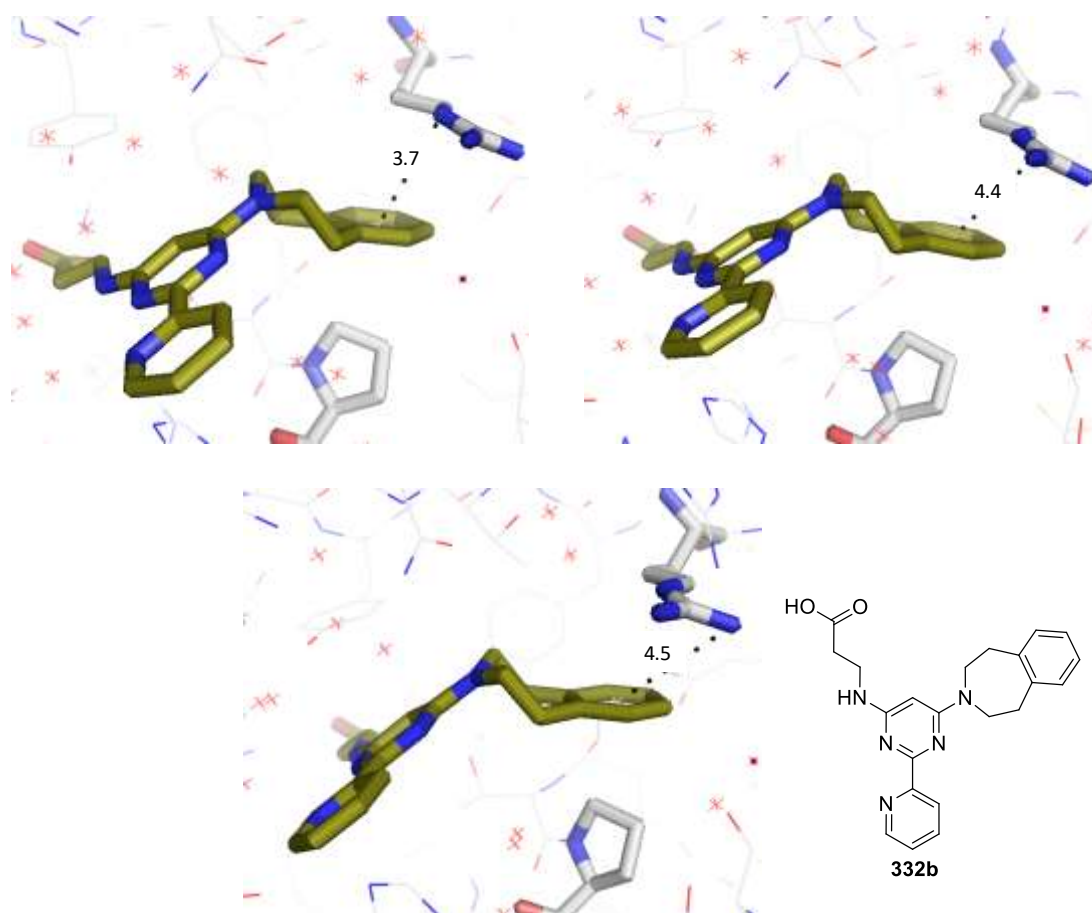


Figure 71. π -Cation interaction between benzazepine ring and Arg1247. Distances between the nitrogen atoms of the guanidinium ion and the centroid of the phenyl ring are represented by black dotted lines.

The improved potency of benzazepine **332b** relative to the *tert*-butyl substituted HTS hit **11** was an important result. The crystal structure confirmed that the benzazepine ring was involved in a π -cation interaction which rationalised this improvement in potency. The selectivity profile of **332b** was assessed using the Jmj mass spectrometric assays (Appendix 2) (Figure 72). Compound **332b** inhibits JmjD3 in a dose dependent manner whilst no dose response curves were obtained for inhibition of JmjD2a, D2c, D2d and D2e demonstrating that **332b** displayed the same good selectivity profile as **11**.

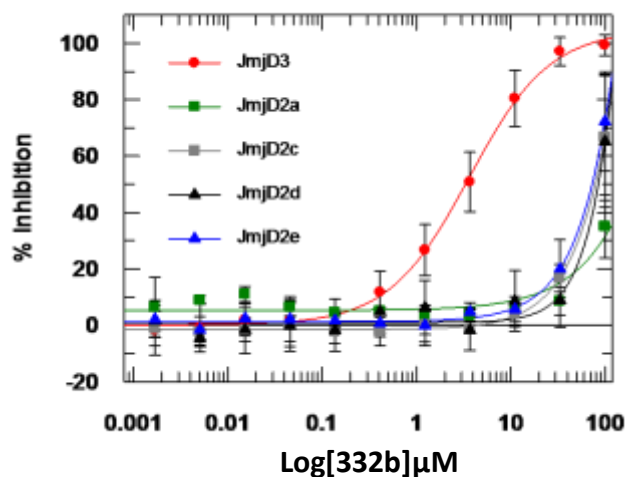


Figure 72. Selectivity profile of **332b** showing inhibition of JmjD3 whilst being inactive against JmjD2a, D2c, D2d and D2e. Evaluation of the selectivity of **332b** in Jmj mass spectrometric assays (Appendix 2). Data are presented as the mean \pm 10%.

II.3.2.7.3 *O*-Linked substituents

In parallel to the *N*-linked compounds, aromatic and aliphatic substituents were also investigated when attached with an ether linkage. These targets were designed to evaluate the effect of having an *O*-linker compared to an *N*-linker with respect to potency and which of the two is best suited to explore this region of the molecule (Table 44).

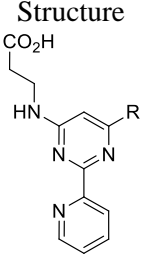
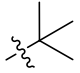
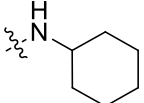
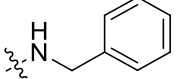
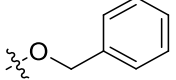
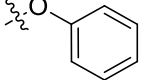
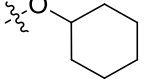
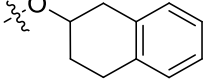
Structure	Compound	MALDI pIC ₅₀	EGLN
			
R			
	11	5.0	< 4.3
	329b	4.0 ^a	< 4.3
	416	5.4	4.6
	337	5.8	4.1 ^b
	346	< 4.0	< 4.0
	340	< 4.0	< 4.0
	343	4.9	4.5

Table 44. Biochemical assays data for *O*-linked substituents at position 6.

^a < 4.0 (n=1) and 4.0 (n=1).

^b < 4.3 (n=1) and 4.1 (n=1).

Compound **337**, which offer a direct comparison to benzylamine **416** was well tolerated and with a pIC₅₀ of 5.8 was more potent than both the hit **11** (pIC₅₀ of 5.0) and the benzylamine **416** (pIC₅₀ of 5.4). The *O*-phenyl **346** was not tolerated with pIC₅₀ values below the detection limit of the assay.

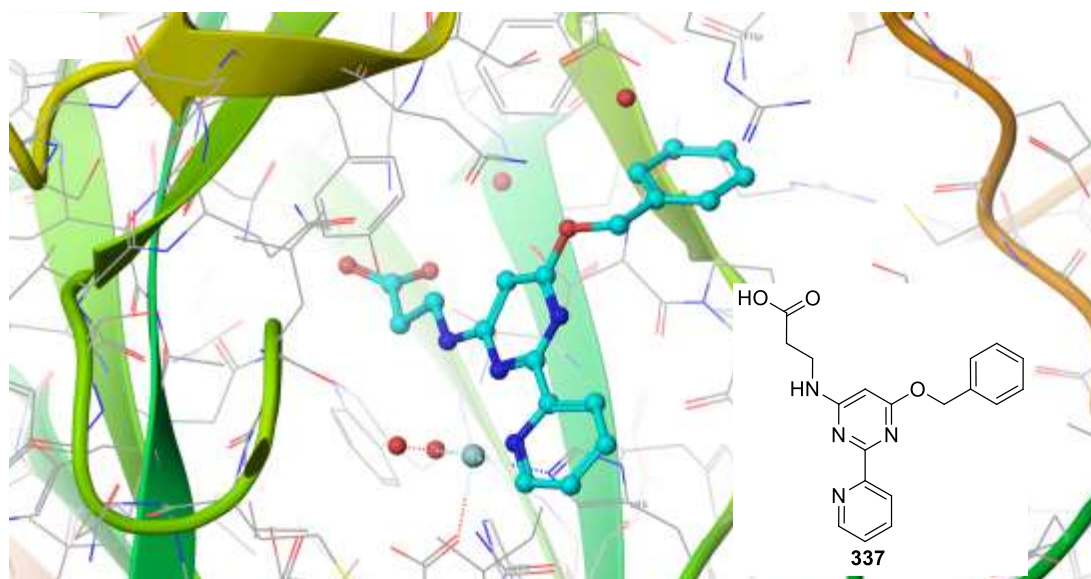


Figure 73. Docking of *O*-benzyl **337** in JmjD3 active site. Target docked in the active site using Glide in Maestro (v 9.3.515). Constraints applied (Appendix 9). Docking carried out by Pamela Thomas.

The docking of **337** in JmjD3 active site looked reasonable with a docking score of -9.3, the phenyl ring seemed to be tucked under the critical Arg1247 (Figure 73). However, the linker to the phenyl ring appears strained with a torsion angle between O, CH₂ and CH(phenyl) of 43.8°. This torsion angle was analysed with CCDC, only five compounds were found with dihedral angle values widely spread, but no hits around 40° (Figure 74).

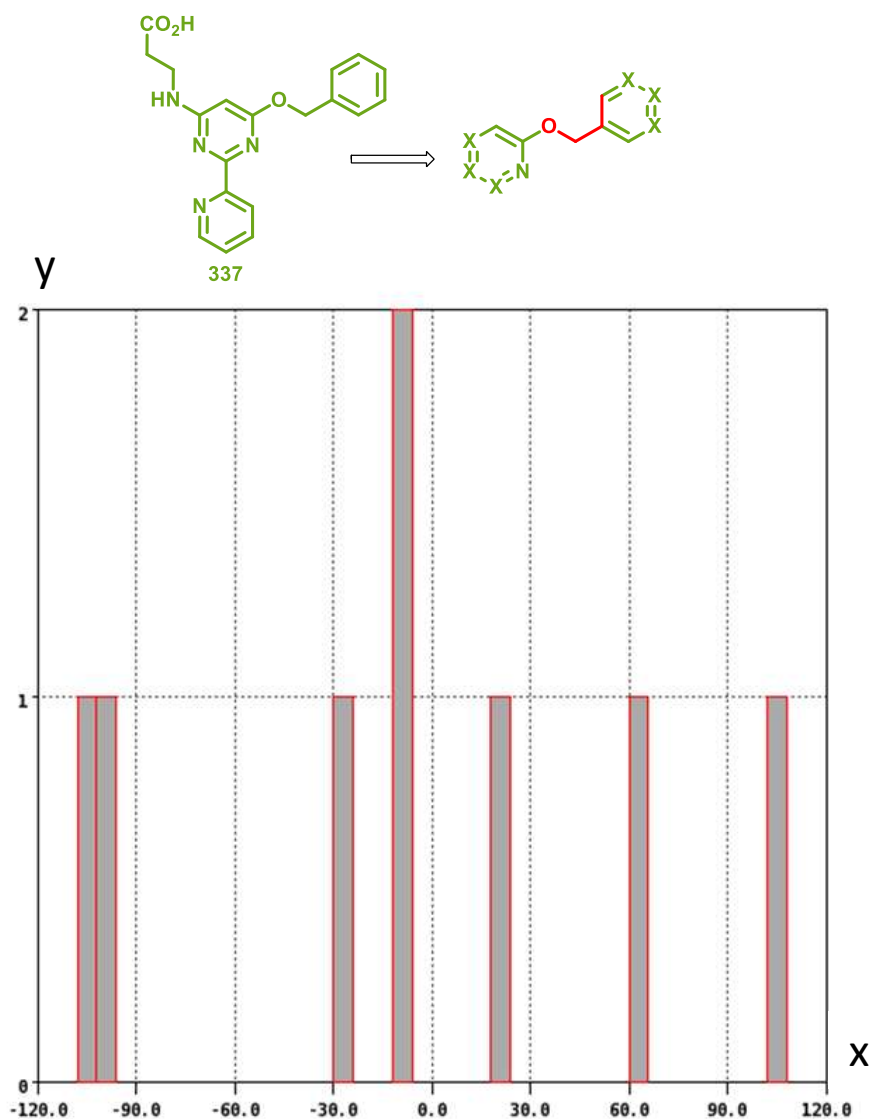


Figure 74. Torsion angle analysis of a substructure of **337** using CCDC data. This analysis was carried out with the nitrogen of the aromatic ring bonded to only two other atoms (to exclude N-oxides) and X = any atoms; torsion angle measured highlighted in red; y axis = number of hits, x axis = angle value.

The same analysis was repeated with a more generic structure (Figure 75). This time 260 structures were found and the dihedral angle values were also widely spread with low

number of hits around 40°. These analyses showed that the angle observed in the docking of **337** in JmjD3 active site was only plausible.

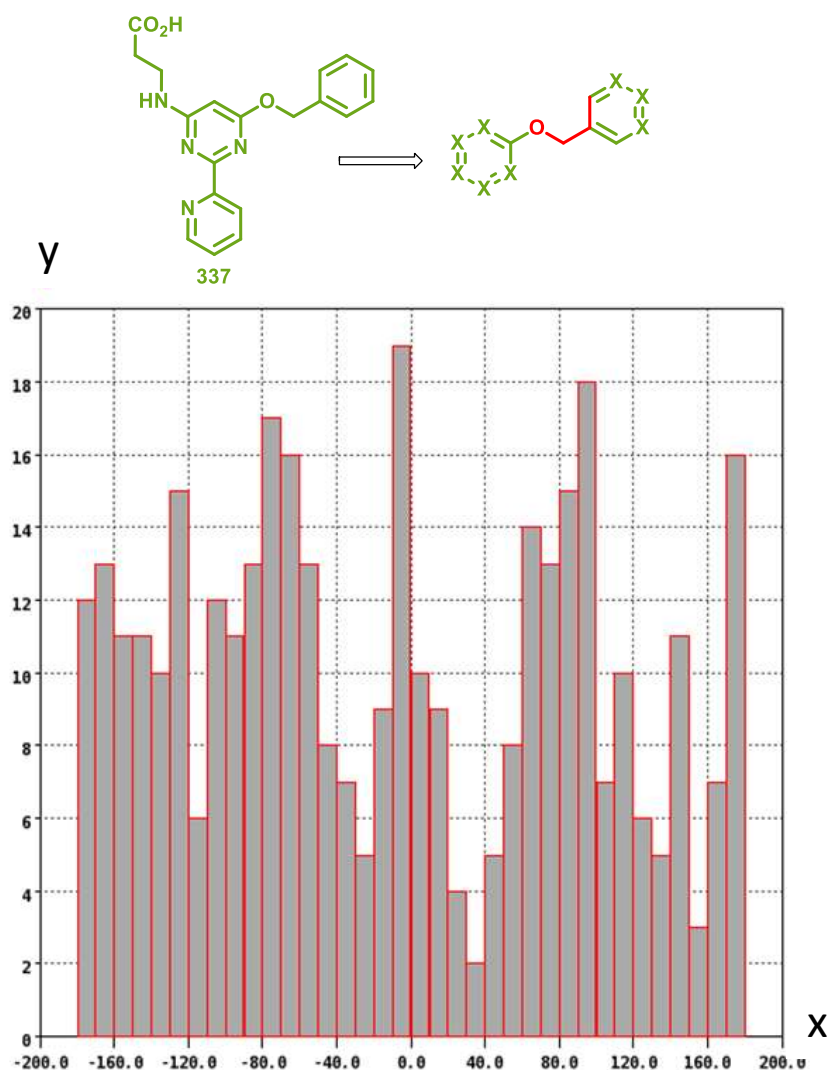


Figure 75. Torsion angle analysis of a generic substructure of **337** in CCDC. X = any atoms; torsion angle measured highlighted in red; y axis = number of hits, x axis = angle value.

The docking of **346** in the JmjD3 active site was less successful, none of the poses gave any good conformation for this molecule. In the best pose displayed in Figure 76, scored -8.3, the phenyl ring seemed to be too far from Arg1247 for positive interaction.

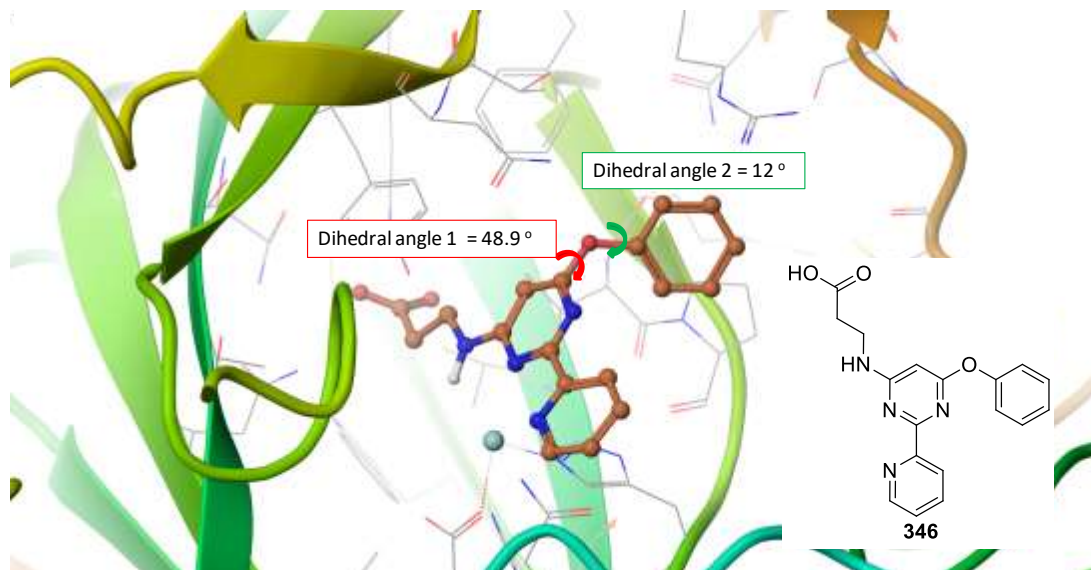


Figure 76. Docking of *O*-phenyl **346** in JmjD3 active site. Target docked in the active site using Glide in Maestro (v 9.3.515). Constraints applied (Appendix 9). Docking carried out by Pamela Thomas.

The analysis of the torsion angles 1 and 2 in the small molecule X-ray structures database showed that the dihedral angle values observed in the docking were not optimal. The substructure search gave 18 hits, with a preferred torsion angle 1 of 0° whilst 48.9° was observed in the docking (Figure 77).

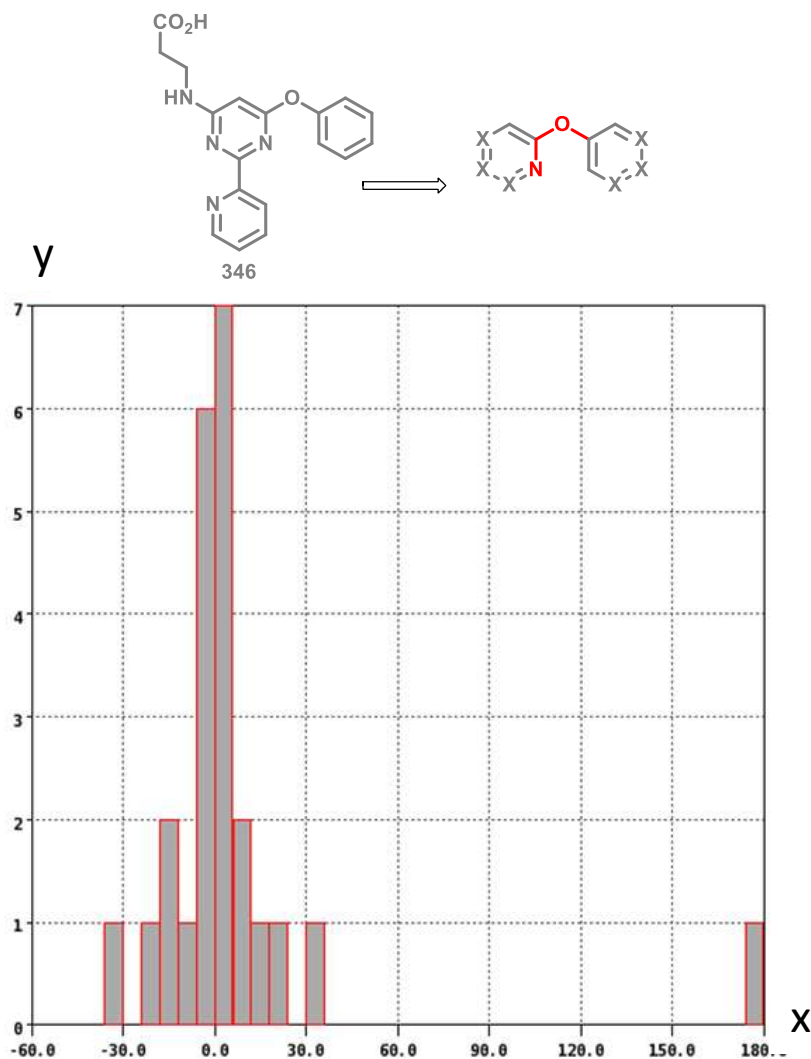


Figure 77. Torsion angle 1 analysis of a substructure of **346** in CCDC. This analysis was carried out with nitrogen ring bonded to only two other atoms (to exclude N-oxides) and X = any atoms; torsion angle measured highlighted in red; y axis = number of hits, x axis = angle value.

Figure 78 shows a preference for $\pm 90^\circ$ for torsion angle 2 indicating that the phenyl ring tends to sit in an orthogonal position to the nitrogen-containing ring, whilst 12° was observed in the docking (Figure 76).

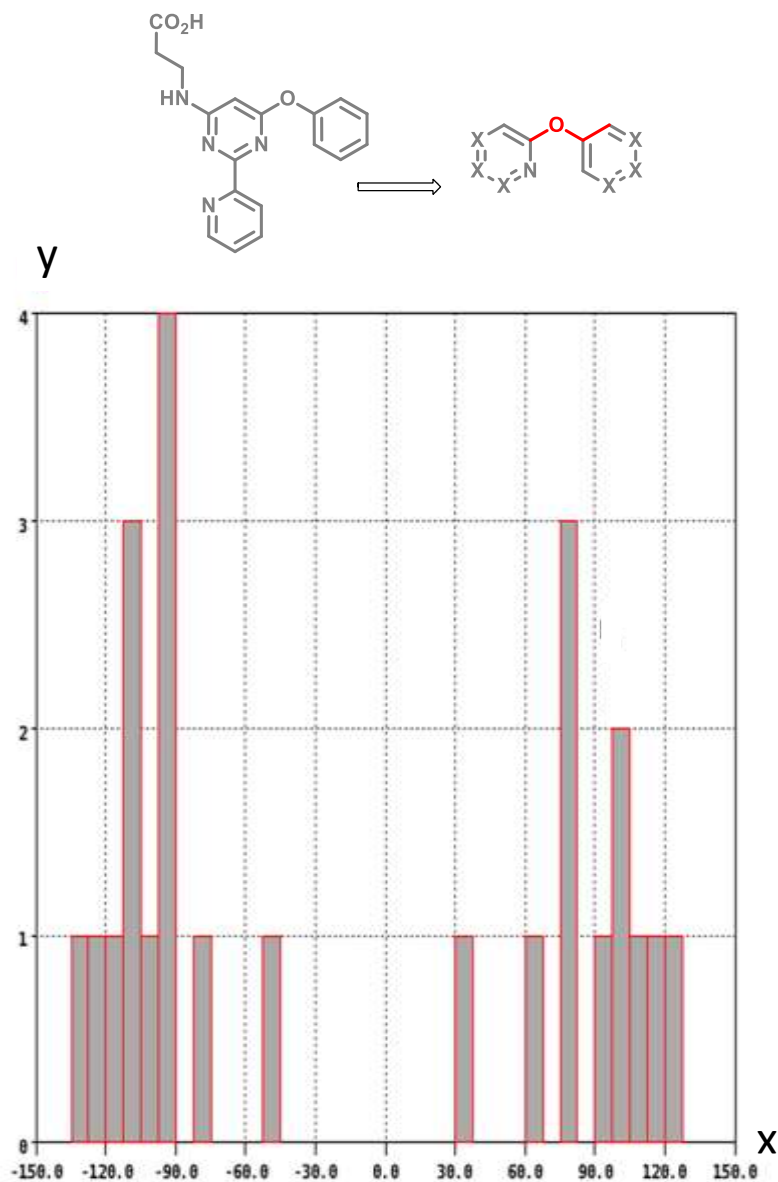


Figure 78. Torsion angle 2 analysis of a substructure of **346** in CCDC. This analysis was carried out with nitrogen ring bonded to only two other atoms (to exclude N-oxides) and X = any atoms; torsion angle measured highlighted in red; y axis = number of hits, x axis = angle value.

The docking scores of **337** and **346**, the divergent values for **346** torsion angles observed in the docking and the values obtained after analysis of torsion angle in CCDC may rationalise the good potency of **337** (pIC₅₀ of 5.8) relative to **346** (pIC₅₀ < 4.0) (Table 44).

The overlay of **337** docked in JmjD3 and crystal structure of **416** in JmjD3 showed few differences between the conformations of the two compounds such as the pyridyl rings not overlaid (Figure 79). Although the benzylic methylenes of these molecules pointed in opposite directions, the terminal phenyl rings were still stacking with Arg1247. The potency increased could potentially be explained by a better pose of the benzyl moiety in **337**. Compound **337** was also more selective than **416** with a pIC₅₀ of 4.1 vs 4.6 against EGLN.

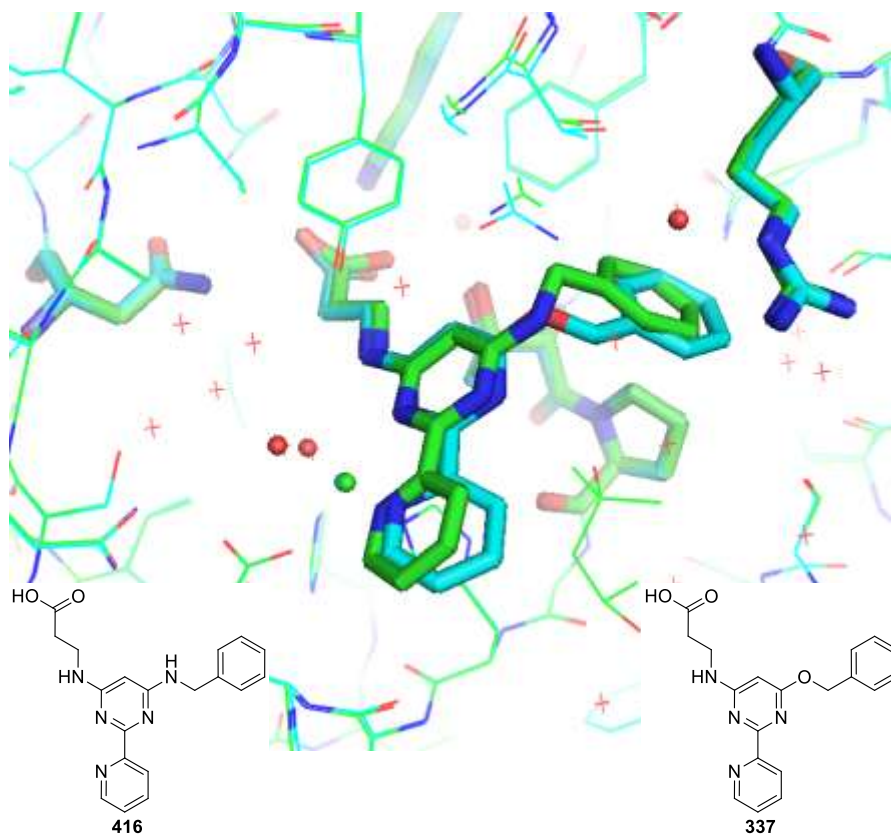


Figure 79. Overlay of **337** (compound, residues and Co(II) in cyan) docked in JmjD3 (Appendix 9) and crystal structure of **416** (compound, residues and Co(II) in green) in JmjD3.

This good result gave us confidence to further explore vector 6 with O-linked substituents. The cyclohexyl **340** ether was not tolerated with pIC₅₀ values below the detection limit of the assay. The result for **340** was not surprising considering that the cyclohexylamine analogue **329b** was also poor. In the tetrahydronaphthalenol **343**, there is probably not enough flexibility to allow the phenyl ring to sit close to Arg1247 since this compound is less potent than **337** with a pIC₅₀ of 4.9.

II.3.2.7.4 Hybrid inhibitors

The preceding sections have described how HTS hit **11** was optimised to deliver more potent analogues such as **332b**, **332c** and **337** with pIC₅₀ > 5.5. This was achieved by interacting with residues in the ^tBu pocket. In medicinal chemistry this strategy that is attempting to create interactions with residues in the active site is widely used. For targets where crystal structures exist, which contain the substrate bound to the enzyme a frequently used medicinal chemistry strategy is to incorporate some features of the natural substrate which could potentially mimic the interactions between the natural substrate and the enzyme with the aim of disturbing the binding of the natural substrate in the active site. This strategy was employed in the search of Jumonji C containing domain histone demethylase inhibitors by Wang *et al.*²⁰² The authors designed the molecule in which a methyllysine and a cofactor mimic were incorporated. These two groups were linked *via* a flexible carbon chain as shown in Figure 80.

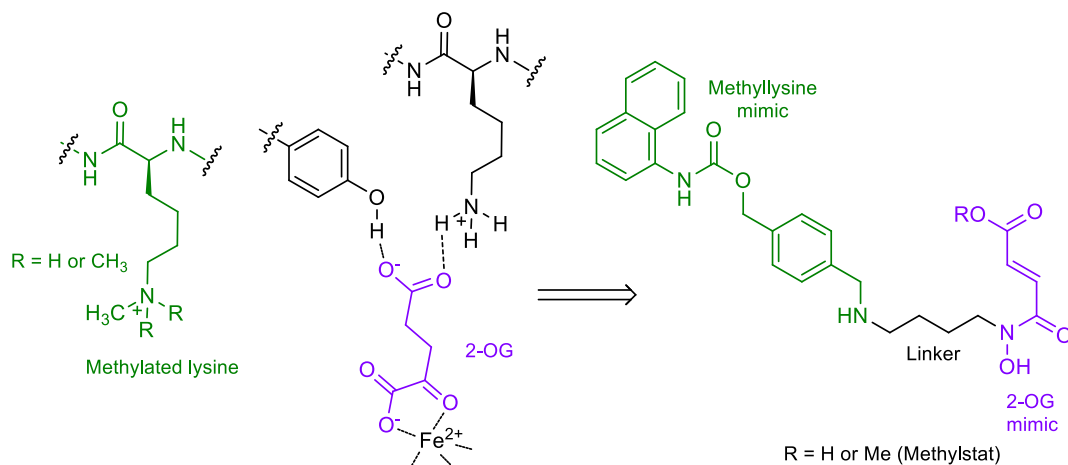


Figure 80. Structure-based design of Jumonji C-containing domain histone demethylase inhibitors.

This strategy enabled the identification of the methyl ester Methylstat, a pro-drug which selectively inhibits Jumonji C-containing domain histone demethylases in the cells. Since the hit **11** was a more selective 2-OG mimic than the hydroxyamide of Methylstat and there was a substantial amount of crystallographic data, it was decided to apply this strategy in order to identify a more potent and selective JmjD3 inhibitor.

Figure 81 shows the key interactions between the peptide substrate containing the trimethylated lysine and mouse JmjD3. The numbering system of the residues in the mouse is slightly different to the numbering system in man, so Arg1246 in the mouse corresponds to Arg1247 in man.

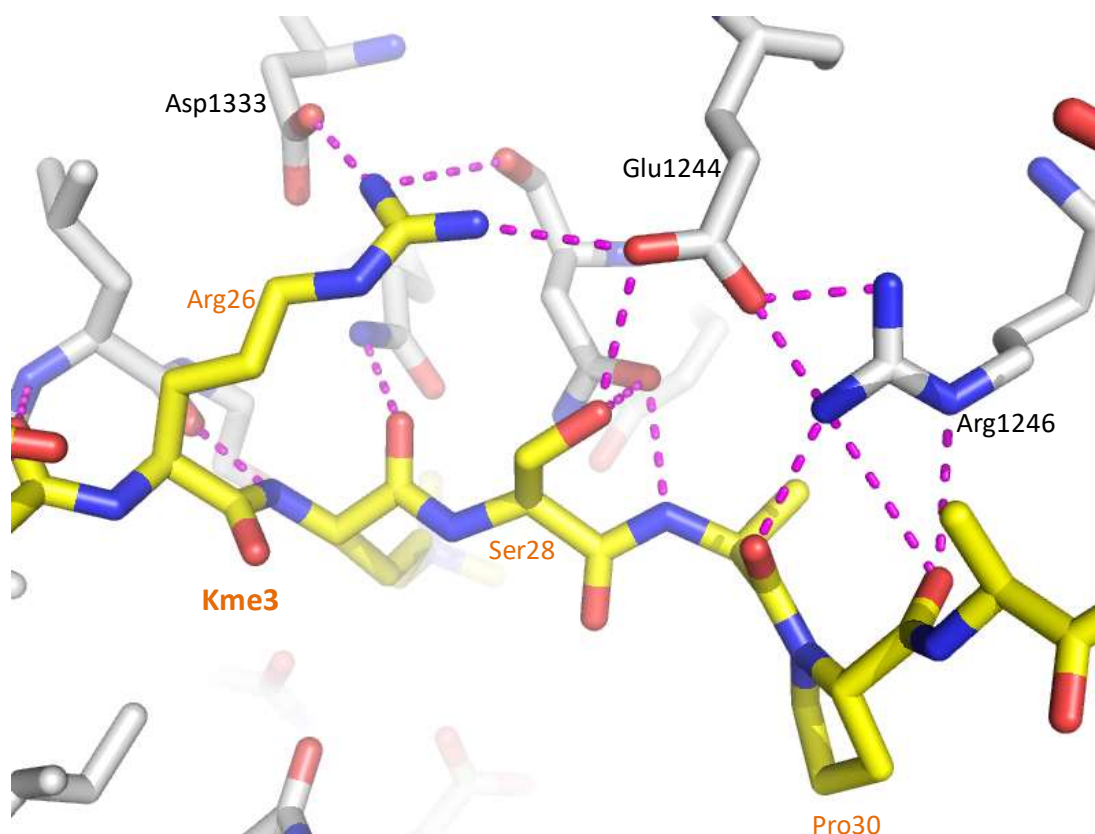


Figure 81. Tri-methylated lysine peptide bound to mouse JmjD3. Peptide in yellow, enzyme residues in silver and hydrogen bonds are represented in pink dashed lines.

Section II.3.2.7.2 focused on π -cation interactions between Arg1247 and various aromatic rings. However, the structure with the substrate bound shows that no amino acids containing aromatic groups are present in this region. Instead Arg1246 is involved in two hydrogen bonds with carbonyl groups either side of Pro30. Also, Arg26 of H3K27 is involved in ionic interaction with Asp1333 and Glu1244. The geometry of the hydrogen bonds between the guanidinium ion of Arg1246 and carbonyl groups surrounding Pro30 seemed non-optimal.

Analyses of H-bond interactions between a guanidino group and any O, C, N, S in Cambridge Structural Database (CSD), which analysed small molecules interactions, and PDB which analysed interaction between protein residues and bound small molecules,

showed a preference for a carbonyl in plane with the guanidino group (Figure 82). The interactions between Arg1246 and the carbonyl groups surrounding Pro30 lack this usual planarity, while the hydrogen bonds between the carbonyl group of Glu1244 and guanidinium ion of Arg26 appear more in plane. Consequently, the Arg1246 interactions could potentially be considered as weaker than the interactions between Glu1244 and guanidinium ion of Arg26.

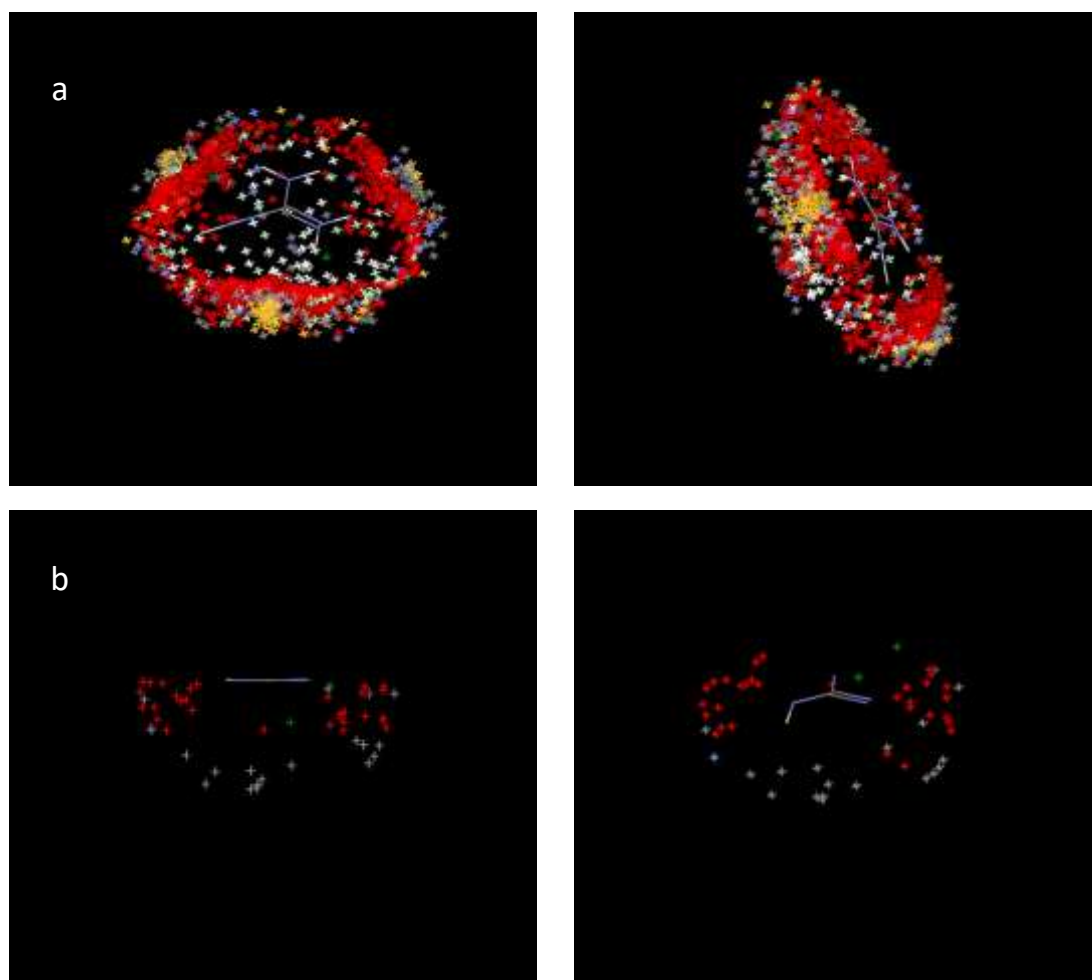


Figure 82. H-bond interactions between guanidino moiety and any O, C, N, S in CSD and PDB. (a) Interactions in CSD, 4867 hits; (b) Interactions in PDB, 197 hits.

However, these differences in geometry and distances are not sufficient to hypothesise on the relative importance of these interactions. To provide a more quantitative assessment of the interactions between the enzyme and the substrate, a study was performed in which key residues of the substrate were mutated and the rate of demethylation of the trimethylated lysine substrate was measured.¹⁵⁴ Replacement of Arg26 of the substrate with an Ala or a Lys greatly reduced the formation of K27me2 suggesting that Arg26 is important for recognition and / or the whole stability of the substrate (Figures 83a, b, c and 84a). Pro30 substitution had no major effect on the polarity, however, the substitution could have significant effect on conformation of substrate and positions of backbone carbonyls. It is likely this conformational change alters the ability to interact with Arg1246. Changing Pro30 for a Gly, Phe and Ser also had a detrimental effect on production of K27me2 suggesting that Pro30 is also important for recognition of the substrate and / or the whole stability of the substrate (Figure 83a, b, c and 84a).

(a) H3K27me3...AAR**K**me3SAPATG.

(b)

Entry	Shorthand	Sequence
1	H3 (20-36)	LATKAARK(Me3)SAPATGGVK
2	P30A	LATKAARK(Me3)SA A ATGGVK
3	P30S	LATKAARK(Me3)SA S ATGGVK
4	P30F	LATKAARK(Me3)SA F ATGGVK
5	P30G	LATKAARK(Me3)SA G ATGGVK
6	R26A	LATKAA A K(Me3)SAPATGGVK
7	R27K	LATKAA K K(Me3)SAPATGGVK
8	H3'	GKAPRKQLATKAARK(Me3)SAPATGGY

(c)

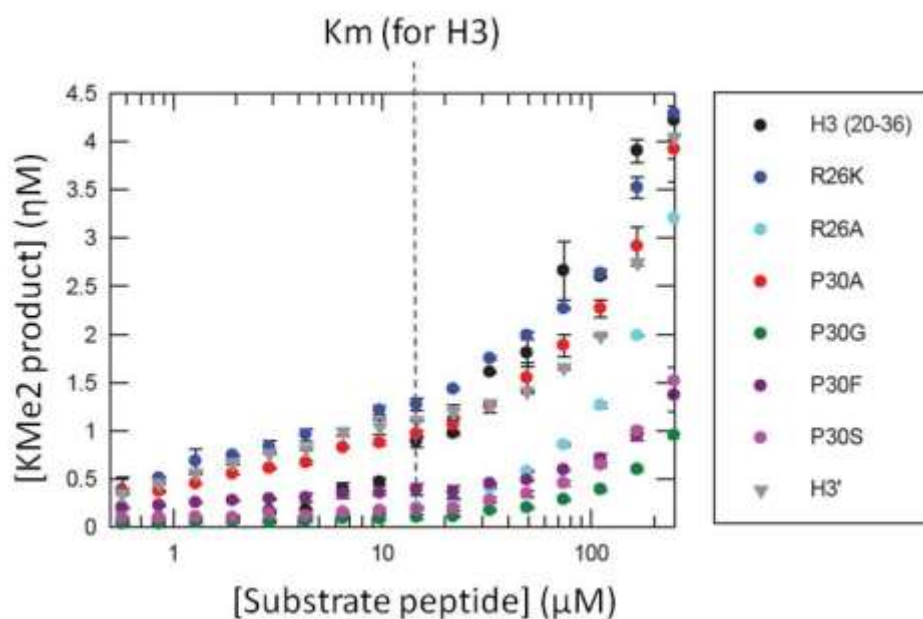
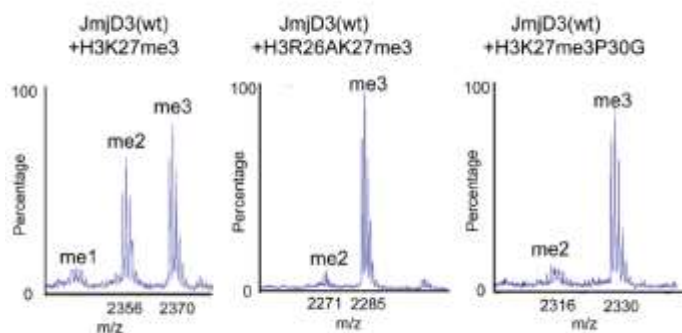


Figure 83. Rapidfire™ Mass spectrometry data for peptide substrate mutants. (a) Residues immediately around H3K27me3 substrate of JmjD3. Residues mutated to explore SAR of JmjD3 H3K27me3 recognition are highlighted in red. (b) Peptide sequences used for mass spectrometric experiments. (c) Effect of mutations at Arg26 and Pro30 of the native H3K27me3 substrate peptide (highlighted in red in a,) on turnover. Mass spectrometric quantitation of the K27me2 product was performed after a 6 minute reaction with concentrations of peptide spanning 250-0.6 μM . Km of standard H3K27me3 peptide is ~ 20 μM (marked by dashed line).¹⁵⁴

To further develop understanding of the importance of the various H-bonding interactions the enzyme JmjD3 was also mutated. Changing Arg1246 to an Ala residue, and so suppressing the H-bond interactions with the carbonyls surrounding P30, almost abolished the formation of K27me2 (Figure 84b). Replacing Asp1333 and Glu1244 with an Ala residue, and so suppressing the H-bond interactions with Arg26, also had a detrimental effect on production of K27me2 (Figure 84b). Here again, the data suggest that Arg1246, Asp1333 and Glu1244 are important for the demethylation of H3K27me3, but it is difficult to say at this stage if these residues are important for the recognition of the substrate or for the whole stability of the enzyme.

(a)



(b)

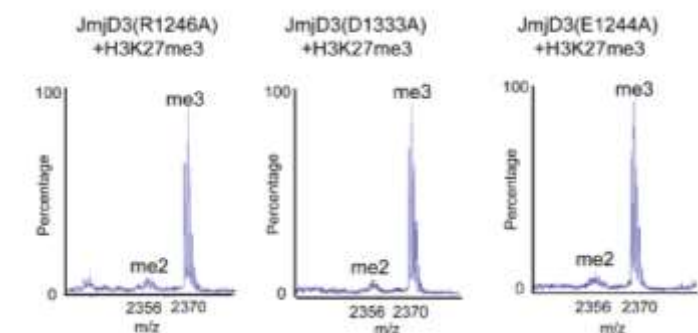


Figure 84. (a) Mass spectra (MALDI-TOF) of wild-type JmjD3 demethylation assays with modified histone H3K27me3 peptides; (b) Mass spectra (MALDI-TOF) of mutant JmjD3 demethylation assays with native H3K27me3 peptides.¹⁵⁴

Figure 85 shows that Pro30 from the substrate sits close to the location of the tetrahydrobenzazepine ring of **332b**.

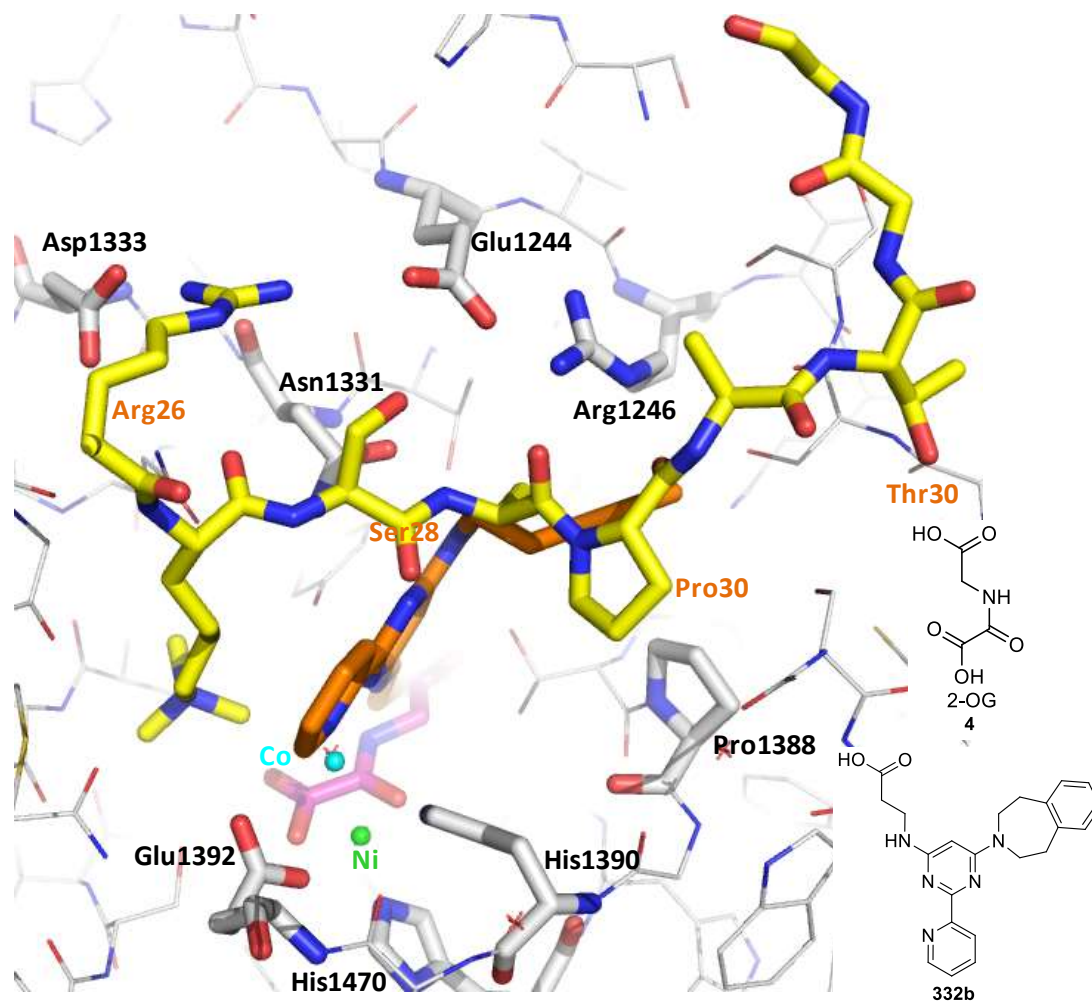


Figure 85. Superposition of the complexes of tri-methylated lysine substrate, and **332b** bound to JmjD3. Peptide in yellow, mouse enzyme residues in silver, NOG in magenta, Ni(II) in green. Inhibitor **332b** is in orange, and Co (II) in cyan; residues for the human JmjD3-**332b** complex are not shown.

In an attempt to improve the potency of pyridyl-pyrimidine analogues new targets were designed with the aim of mimicking the interactions between the carbonyls around Pro30 of the tri-methylated lysine substrate and Arg1246. The strategy employed was to introduce

amides in the ^tBu region. Compound **393b** was overlaid with the tri-methylated lysine peptide in the JmjD3 enzyme and showed a reasonable overlap of the proline residues (Figure 86).

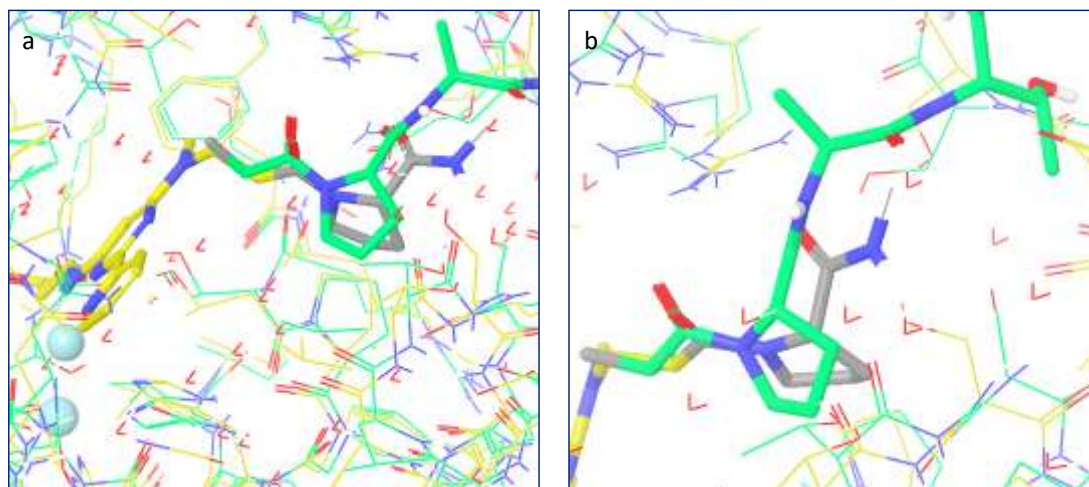
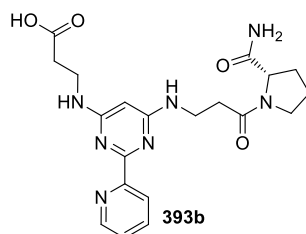


Figure 86. Overlay of tri-methylated lysine peptide bound to mouse JmjD3 and **393b** bound to human JmjD3. (a) Peptide and mouse enzyme residues in green, Ni(II) in blue. Inhibitor **393b** and human residues are in yellow, and Co (II) in blue. (b) Magnified section of (a).

This work is summarised in Table 45. In addition to the MALDI data (which has been presented in previous tables), Table 45 contains RapidFire Mass Spectrometry (RFMS) data. The RFMS was a new assay format designed to replace the MALDI assay (*cf.* Section I.2, p.42). By the time this assay was validated the programme was coming to an end so only a handful of compounds in the pyridyl-pyrimidine series have both MALDI and RFMS data. However analysis of the data from the two assays showed that the results were comparable.

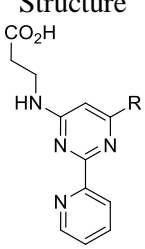

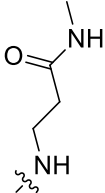
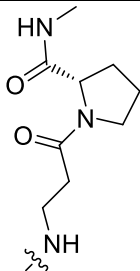
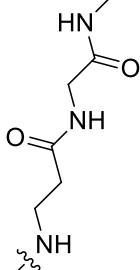
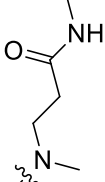
Structure	Compound	JmjD3 RFMS pIC ₅₀	EGLN pIC ₅₀
			
R			
	11	5.4	< 4.3
	393a	4.6	< 4.0
	393b	4.1 ^a	< 4.0
	393c	4.2	< 4.0
	398	5.2	< 4.3

Table 45. Hybrid inhibitors biochemical assay data.

^a < 4.0 (n = 2) and 4.1 (n = 2).

The hybrid inhibitors were tolerated but, disappointingly, they were less potent than the ^tBu analogue **11**. The proline-containing molecule was active with a pIC₅₀ of only 4.1, the

simpler *N*-Me amide was slightly more potent with a pIC₅₀ of 4.6. Interestingly, **398**, the *N*-methylated analogue of **393a**, showed a 0.6 log unit increase in potency. This increase in potency could potentially be explained by a change in conformation induced by the extra Me and/or the loss of a H-bond donor. Unfortunately no X-ray crystal structure was obtained with any of these hybrid inhibitors to help understand the binding of these molecules and the role of the extra Me in **398**.

In summary, exploiting vector 6 to increase inhibitor potency enabled the identification of several potent compounds with pIC₅₀ values up to 6 in the Jmjd3 MALDI assay. These potent inhibitors include benzylamine **416** (pIC₅₀ = 5.4, EGLN pIC₅₀ = 4.6), benzylether **337** (pIC₅₀ = 5.8, EGLN pIC₅₀ = 4.1), tetrahydrobenzazepine **332b** (pIC₅₀ = 5.6, EGLN pIC₅₀ <4.3) and hydroxyl-tetrahydrobenzazepine **332c** (pIC₅₀ = 6, EGLN pIC₅₀ = 4.7). The crystal structure of **332b** confirmed that the tetrahydrobenzazepine ring was involved in a π -cation interaction which rationalised this improvement in potency. Regarding the selectivity of these molecules compounds **332b** and **337** showed good selectivity against EGLN. Both compounds **332b** and **337** were considered as good potential probe molecules, but since compound **332b** was discovered first and more data were generated for this molecule, it was progressed towards being a tool molecule. Before compound **332b** could be declared as a probe molecule it had to pass the redox assay to make sure that the tetrahydrobenzazepine ring did not adversely affect the oxidative stability of this template.

II.3.2.8 Oxidative stability

To confirm that the new analogues retained the oxidative stability as opposed to the initial leads (pyridine and *bis*-aminorayl), several pyridyl-pyrimidine compounds were run through the redox assay and data for key compounds are summarised in Table 46. The most potent

compounds **314**, **332b** and **337** showed that the benzothiophene and tetrahydrobenzazepine rings did not affect the oxidative stability of this template.

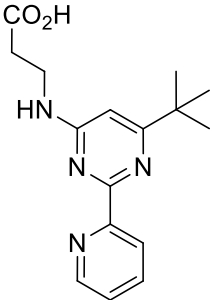
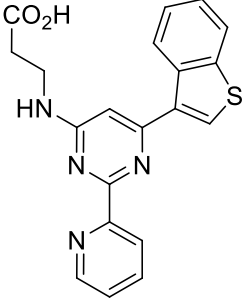
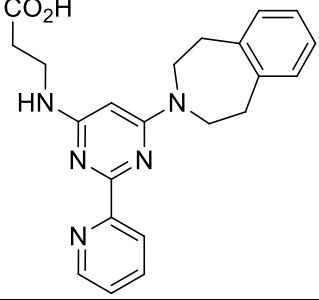
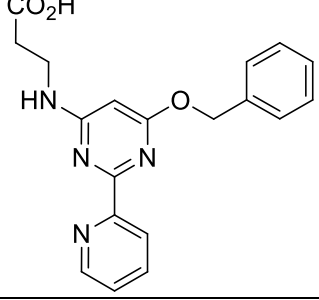
Structure	Compound	MALDI pIC ₅₀	E° Oxidation (mV)
	11	5.0	> 900
	314	5.1	> 900
	332b	5.6	> 900
	337	5.8	> 900

Table 46. Redox measurement. Assay run by Matthew Lochansky (Appendix 2).

Tetrahydrobenzazepine **332b** was therefore selected as a tool compound after confirmation of its good oxidative stability. It was used to determine endogenous target engagement and investigate the cellular phenotype.

II.3.2.9 Target engagement

All of the biochemical data discussed in the preceding sections was generated using a truncated JmjD3 construct (residues 1142 to 1682). A chemoproteomics approach was utilised to establish whether the inhibitors synthesised in the programme were able to engage full-length JmjD3 in a cellular environment.²⁰³ This approach required the covalent attachment of the tool molecule to beads through an amide bond. This meant that the structure of the tool molecule had to be modified to incorporate an amine or a carboxylic acid which would be reacted with beads containing a carboxylic acid / activated ester or an NH₂, respectively. Since **332b** already contained a carboxylic acid group which was critical for potency, it was decided to incorporate an amine. This modification had to be designed so that the overall profile (biochemical assay potency and selectivity) of the new compound was unchanged compared to the parent compound **332b**. Analysis of the crystal structure of **332b** bound to JmjD3 revealed that the position *para*- to nitrogen in the pyridine ring was pointing out towards solvent (Figure 87). It was therefore considered that this position was the most suitable one by which the molecule could be substituted for immobilisation without adversely affecting its potency.

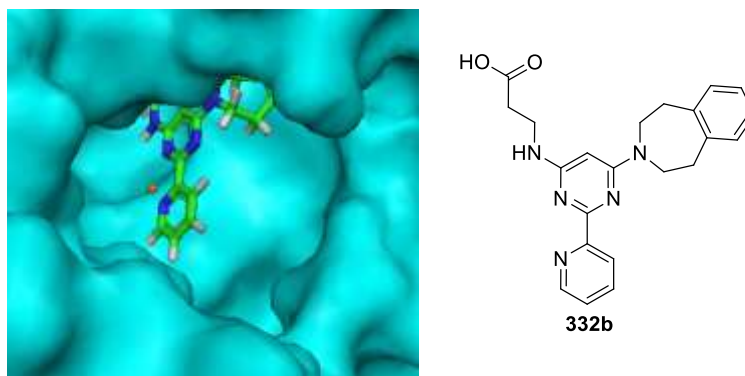


Figure 87. Crystal structure of **332b** bound into JmjD3.

The chemistry to deliver the appropriately substituted linkable analogues of **332b** was challenging. Early routes to linkable analogues resulted in the synthesis of **357b** and **368**. Although unsuitable for immobilisation these compounds did reveal useful information when they were tested in the biochemical assays (Table 46). In addition to the MALDI data Table 46 contains RFMS data. The biochemical assay results of **357b** and **368** confirmed that the 4-pyridyl position could be substituted with large groups with minimal impact on potency, and provided justification to continue with the effort to re-design the synthesis to deliver appropriately substituted linkable analogues of **332b**.

Structure		Compound	MALDI pIC ₅₀	JmjD3 RFMS pIC ₅₀	EGLN pIC ₅₀
R ₁	R ₂				
	H	332b	5.6	5.4	< 4.3 ^a
		357b	5.7	5.3	5.1
		368	5.6	5.8	4.8
		378	-	5.2	< 4.3

Table 46. Biochemical assays data for 4-substituted pyridyls.

^a < 4.3 (n=3) and 4.7 (n=1).

The *N*-methylamine **378** retained a good level of activity in the RFMS assay (pIC₅₀ = 5.2) and good selectivity (EGLN pIC₅₀ < 4.3). Encouraged by these results a crystal structure of **378** bound to JmjD3 was obtained and this confirmed that the *N*-methylamino group was pointing out into solvent as expected (Figure 88). The compound should therefore perform as desired upon immobilisation on Sepharose beads. With a potent JmjD3 inhibitor suitable for immobilisation now in hand a chemoproteomics investigation could now be initiated. Chemoproteomics utilises chemistry to identify the structure and functions of proteins.²⁰⁴ Over the last few years the scope of the chemoproteomics approach has been extended to

demonstrate the binding of small molecule inhibitors to proteins in relevant cellular contexts.²⁰³

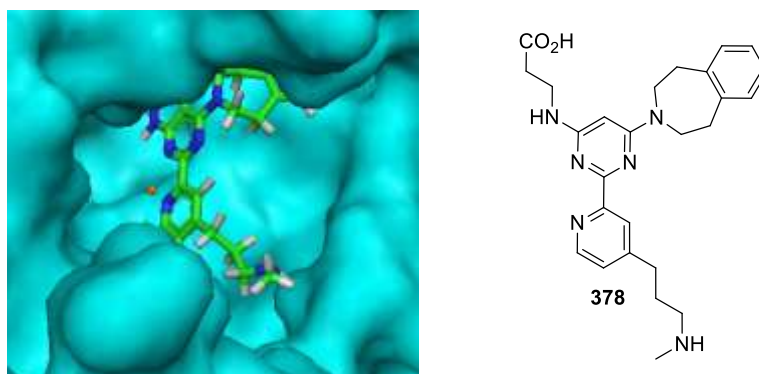


Figure 88. Crystal structure of **378** bound in JmjD3.

All the chemoproteomics work was carried out by colleagues at Cellzome, a company with whom GSK had an alliance. Before the immobilised compound could be used, an appropriate cell line with high expression of JmjD3 was required. The lysate from HL-60 cells was selected after screening numerous cell lines because JmjD3 is strongly expressed in phorbol 12-myristate 13-acetate (PMA) stimulated HL-60 cells (Figure 89a). With a suitable lysate identified, a series of experiments were performed using immobilised **378** and the results are summarised in Figure 89b. Incubation of the probe matrix **378** with PMA stimulated HL-60 lysate followed by removal and washing of the beads was shown to pull down full-length JmjD3 (vehicle box). In another experiment **332b** was first incubated with PMA stimulated HL-60 lysate then immobilised **378** was added. However, when the immobilised **378** was removed from the lysate and washed, it was observed that no JmjD3 had been pulled down as demonstrated by the absence of a band (image b) compared to the vehicle. This can be rationalised by **332b** fully engaging JmjD3, resulting in no enzyme available to be captured by immobilised **378**. The results of these experiments are fully

described in *Nature* by Kruidenier *et al.*¹⁵⁴ and the key finding was the demonstration that **332b** engages endogenous full length JmjD3.

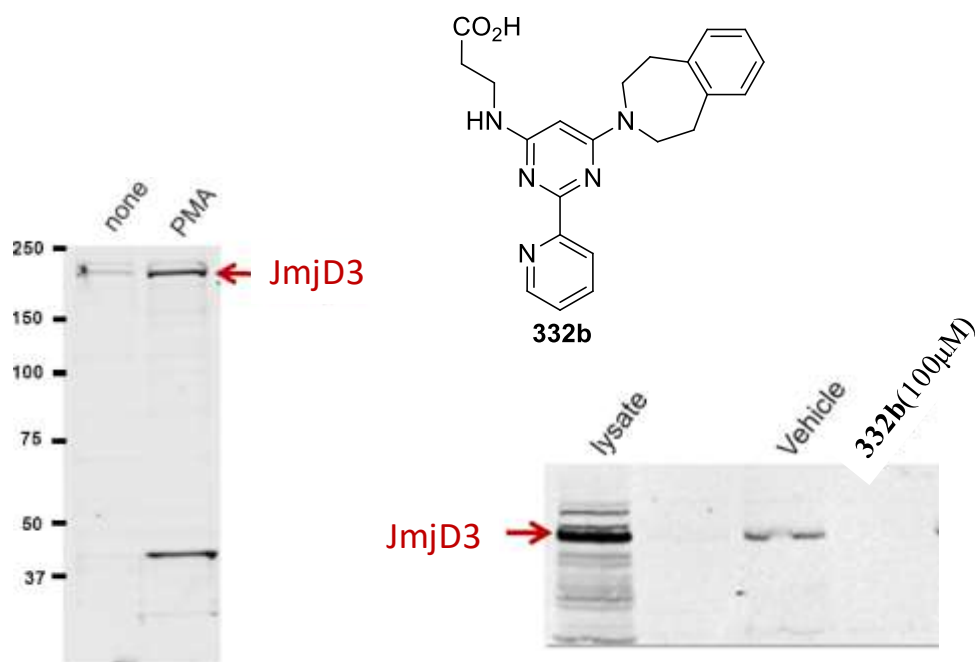


Figure 89. a) non-treated and PMA-stimulated HL-60 lysate. JmjD3 expressed in PMA-stimulated HL-60 lysate. b) PMA-stimulated HL-60 lysate with and without probe matrix **378**, is showed to bind JmjD3. Experiments carried out by colleagues at Cellzome (Appendix 10).

This was the first evidence that a small molecule could specifically inhibit full length JmjD3 in a cellular lysate. This encouraging result led to the next step where compound **332b** was used as a tool molecule to understand the phenotypic response to inhibition of JmjD3.

II.3.2.10 JmjD3 inhibition and cellular phenotype

The experiment described in the preceding section demonstrated that **332b** engaged the full length JmjD3 in a cellular lysate. Despite this **332b** was inactive in the cellular assay. This result was rationalised by consideration of the poor permeability of the molecule, and likely

poor intracellular concentration. Therefore, a method to deliver high intracellular concentration of **332b** was sought. Masking the polarity of the acid as an ester was selected as the most appropriate method to obtain a high concentration of the active compound in the cell. Once the ester had helped the molecule cross the phospholipid cell membrane, it can then be hydrolysed back to the active acid by esterases. Several esters were synthesised and only key esters are exemplified in Table 47. In Section II.3.2.2, importance of the carboxylic acid group was discussed. It therefore came as no surprise that ethyl ester **418** showed activity below the limit of detection in MALDI and cell assays. However, ester **331b** did show some activity ($pIC_{50} = 4.8$) in the MALDI assay. This result is difficult to rationalise and experiments were performed to measure the stability of the ester to the conditions used in the biochemical assay. It was postulated that the acid may be formed *in situ*, and then it was this acid that was inhibiting the enzyme. These studies suggested that the compound was indeed stable, so the reason why **331b** shows biochemical activity is unknown. Attempts to co-crystallise **331b** with JmjD3 failed, so no explanation for this result was forthcoming. In the cellular assay **331b** did show weak inhibition, unlike the parent acid suggesting that cellular penetration and subsequent ester hydrolysis had occurred.

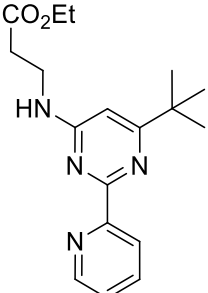
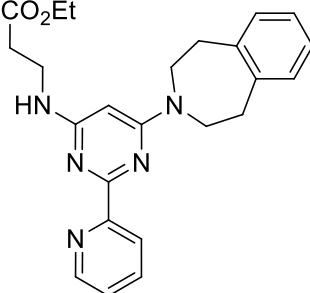
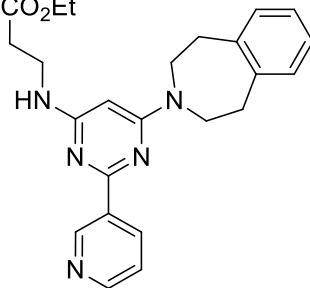
Structure	Compound	MALDI pIC ₅₀	Cell assay (Full) pIC ₅₀
	418	< 4.0	< 4.0
	331b	4.8	4.2
	419	< 4.0	< 4.0

Table 47. Data from MALDI and cell assays for pro-drug compounds. Compound **419**, essential as a negative control for the phenotypic assay was synthesised by a colleague.

In light of these results ester **331b** was used in a biological study to understand the cellular phenotype. To interpret the results of this study a negative control was required to demonstrate that any phenotypic response observed was the result of the selective inhibition of JmjD3 and not another mechanism. The 3-pyridyl analogue (**419**) of compound **331b** was selected as the negative control because although the physicochemical properties were almost identical to those of **331b** it could not bind to the catalytic iron through the bidentate interaction which has been demonstrated to be crucial for potency. The two esters, **331b** and **419**, were incubated with macrophages where they penetrated the cells and were then rapidly

hydrolysed by the macrophage esterases, delivering high concentrations of the acids of interest (Table 48). The corresponding acids, **332b** and **420** were also incubated with the macrophages. Table 48 shows that only a small amount of the acids dosed were detected in the cell (1.6 μM for **332b** and 7.8 μM for **420**) whilst the pro-drug approach enabled the delivery of higher concentrations of the acids (11.8 μM of acid **332b** from ester **331b** and 17.4 μM of acid **420** from ester **419**).

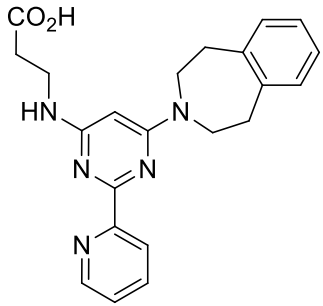
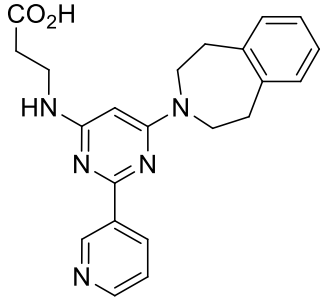
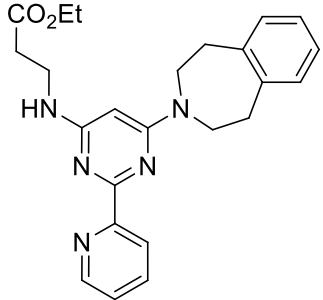
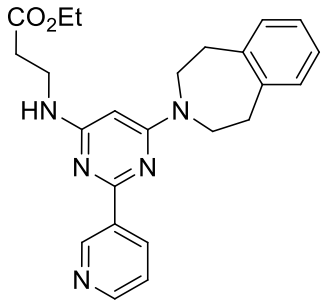
Structure	Compound	[332b]* in lysate (μM)	[420]* in lysate (μM)
	332b	1.6 ± 1.6	N/A
	420	N/A	7.8 ± 1.6
	331b	11.8 ± 0.6	N/A
	419	N/A	17.4 ± 1.5

Table 48. Intracellular concentration of **332b** and **420**. Compounds **332b** and **420** were detected in the lysates of human primary macrophages 1 h after the administration of the acids **332b** (30 μM) or **420** (30 μM) or the pro-drugs **331b** (30 μM) or **419** (30 μM). Experiments carried out by C. Molina, R. Gregory and V. Ludbrook.

* mean ± s.d. from n = 3 donors.

The efficacy of the active and inactive esters, **331b** and **419**, at inhibiting the response resulting from the activation of macrophages derived from healthy volunteers by lipopolysaccharide (LPS) was first assessed by a polymerase chain reaction (PCR) array. When a cell is stimulated, in this case by LPS, cytokines are the first genes to be produced by macrophages with the aim of fighting the infection. PCR allows the evaluation of expression of many genes by looking at the level of expression of the corresponding mRNAs in a cell. Hence this study was designed to assess cytokine production, more particularly profile the expression of 84 cytokine genes (Appendix 11). Figure 90 shows that 34 genes were highly expressed after LPS stimulation amongst which was tumor necrosis factor- α (TNF- α). The addition of compound **331b** prior to LPS stimulation resulted in a reduction in expression of 16 of these 34 LPS-driven cytokines, including TNF- α . Addition of **419** had almost no effect on these genes.

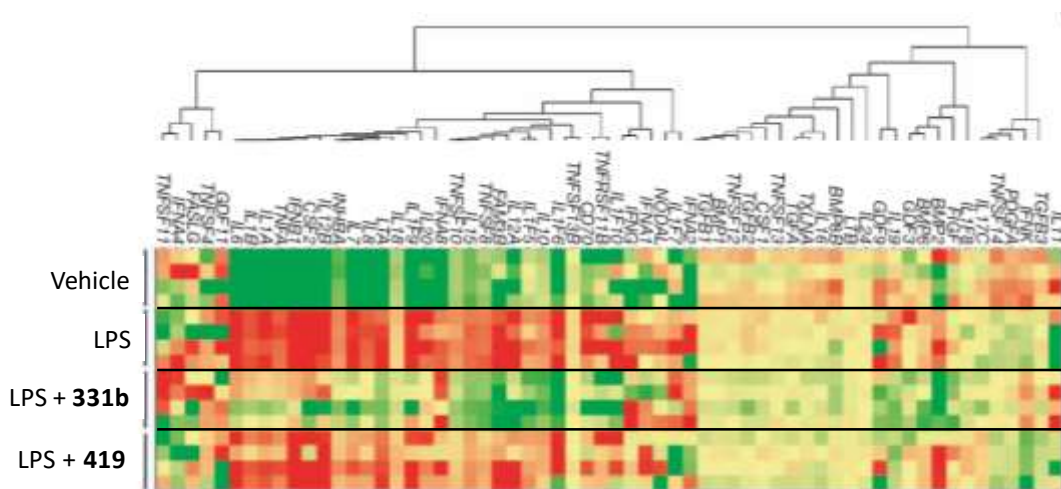


Figure 90. Heat map representation of cytokine expression by human primary macrophages activated with LPS (for 2 h) in the presence of 30 μ M of **331b** or **419** ($n = 4$ donors). Colour code: green means low expression and red high expression. Experiments run by J. Smith and C. Sharp (Appendix 11).

TNF- α is a pro-inflammatory cytokine, important in a variety of inflammatory disorders. Because of its high expression in human macrophages after LPS activation and its reduced expression due to addition of ester **331b** a study was set up to understand the effect of this molecule on the production of TNF- α . The effect of the compounds **419**, **332b** and **331b** on the production of TNF- α is displayed in Figure 91.¹⁵⁴ This graph shows that ester **331b** inhibits TNF- α production in a dose-dependent manner. The active acid **332b** cannot permeate into the cell and consequently had very little effect on the production of TNF- α . Increasing concentration of **419** also showed little effect on TNF- α production demonstrating that production of TNF- α is blocked by the action of potent inhibitor **331b**.

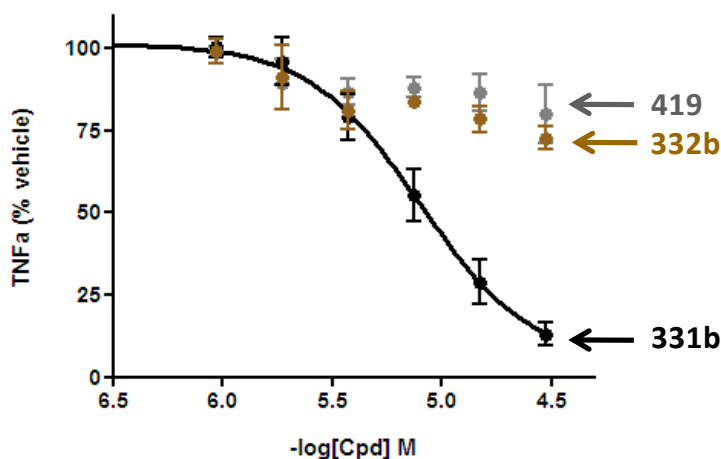


Figure 91. Inhibition of TNF- α production by **331b**. Experiments run by J. Smith (Appendix 11).

Kinetic analysis of inhibition of TNF- α production was also carried out. Figures 92 a and b show that production of TNF- α mRNA started 15 min after LPS activation and TNF- α protein after 60 min. These Figures show that **331b** had little effect on production of TNF- α at the mRNA and protein levels in the early phases. However, at later time-points post LPS stimulation the effect of **331b** was enhanced. For example after 15 min the production of

mRNA TNF- α was inhibited by 18% but after 1 h this was inhibited by 65%. TNF- α protein production was inhibited by 15% after 1 h and by 63% after 6 h showing the great effect of **331b** after a long period of time.

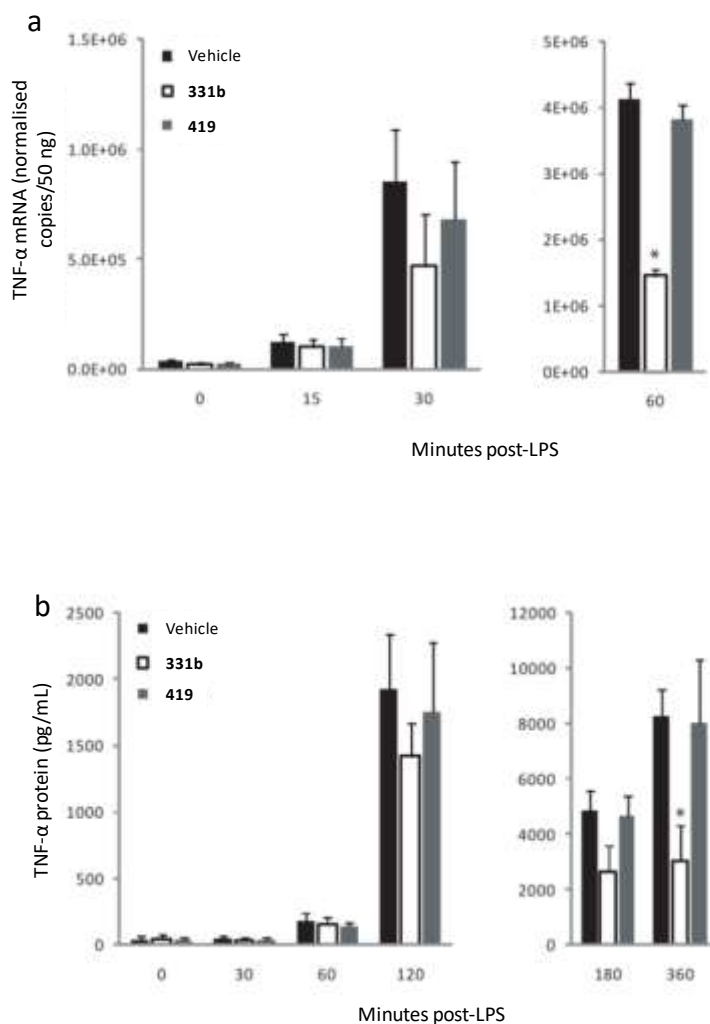


Figure 92. Kinetic analysis of the effects of **331b** and **419** on TNF- α production by primary human macrophages. LPS-induced mRNA expression (a) and protein production (b) of TNF- α at indicated time points, in the presence or absence of 10 μ M of **331b** or **419** ($n = 4$ donors). Data represent mean \pm s.e.m. Experiments run by J. Smith (Appendix 11).

Although TNF- α protein production was inhibited in a dose-dependent manner by **331b** (Figure 91) short interfering RNA (siRNA)-mediated knockdown of Jmjd3 in human macrophages had no effect on TNF- α production, with inhibition only occurring after addition of the inhibitor **331b** (Figure 93). This suggested that maybe another protein was inhibited by **331b** which resulted in prevention of the production of TNF- α .

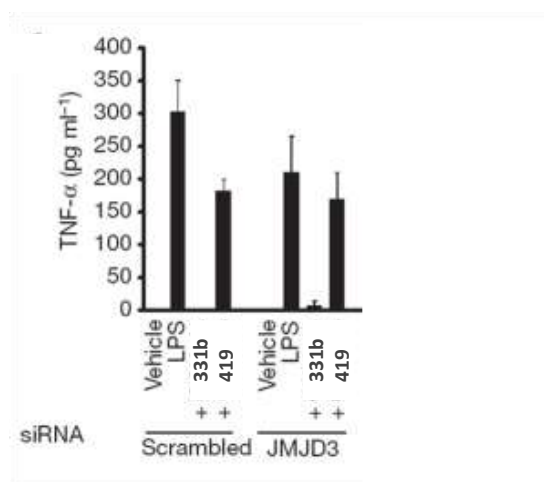


Figure 93. TNF- α production by LPS-stimulated human primary macrophages (1 h) transfected with scrambled, or JMJD3-directed siRNA, in the presence of 30 μ M **331b** or **419** (data are presented as the mean \pm s.d. from five transfection replicates from one representative experiment). Experiments run by P. Mander (Appendix 11).

Jmjd3 or KDM6A is part of the KDM6 sub-family and these proteins have similar structures (Cf. Section I.1.4). Yokoyama and Sengoku's paper published in 2011 reinforced the high structural similarity between UTX and Jmjd3.²⁰⁵ Subsequently the selectivity of **332b** against demethylases, especially those of the KDM6 subfamily, was re-evaluated. The selectivity profile of **332b** was studied using a melting point (T_m) shift assay (Figure 94). This assay is based on the fundamental observation that protein will denature at a certain temperature (T_m). It is assumed that when a ligand binds to a protein, it becomes more stable

than in the free state and this increase in stability is translated into an increase of temperature of denaturation of the protein. The difference of temperature measured for the denaturation of the protein determines the binding affinity. The phylogenetic tree in Figure 94 summarises the outcome of these assays. Of the 2-OG enzymes investigated, JmjD3 and UTX were the only two enzymes showing significant stabilisation ($T_m > 1\text{ }^{\circ}\text{C}$) indicating that **332b** could be binding to both JmjD3 and UTX. The aim of this project was to design and synthesise a selective JmjD3 inhibitor and actually, a UTX and JmjD3 inhibitor had been discovered serendipitously.

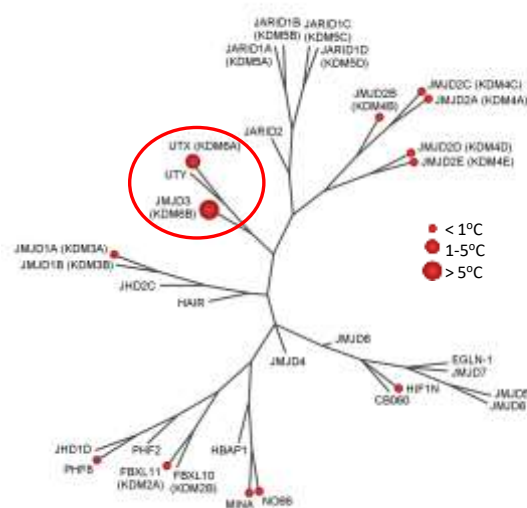


Figure 94. Wider selectivity profile of **332b**. Compound **332b** is selective for H3K27 demethylases of the KDM6 subfamily. Phylogenetic tree of human Jmj enzymes illustrating the selectivity of **332b** for demethylases of the KDM6 subfamily over other KDM subfamilies of methyl-lysine demethylases, as determined by melting point (T_m) shift screening. Temperature differences ($^{\circ}\text{C}$) are shown in red circles. Experiment carried out by Structural Genomics Consortium (SGC) colleagues.²⁰⁶

Because **332b** simultaneously inhibited both JmjD3 and UTX, a better understanding of the phenotypic response of **331b** was required. Figure 92 showed that TNF- α was produced in LPS stimulated human macrophages despite the siRNA-mediated knockdown of JmjD3 and inhibition of TNF- α only being possible after addition of the inhibitor **331b**. This inhibition could potentially have been due to the inhibition of UTX by **331b**. To test this hypothesis siRNA-mediated knockdowns of UTX, as well as UTX and JMD3 simultaneously, were carried out (Figure 95). siRNA-mediated knockdown of UTX alone in human macrophages had no effect on TNF- α production. Inhibition only occurred after addition of the inhibitor **331b**, akin to the results of siRNA-mediated knockdown of JmjD3 alone. However, TNF- α production after LPS activation was inhibited when both UTX and JmjD3 were simultaneously removed. This experiment showed that inhibition of TNF- α production was only possible after siRNA-mediated knockdown of both UTX and JmjD3.

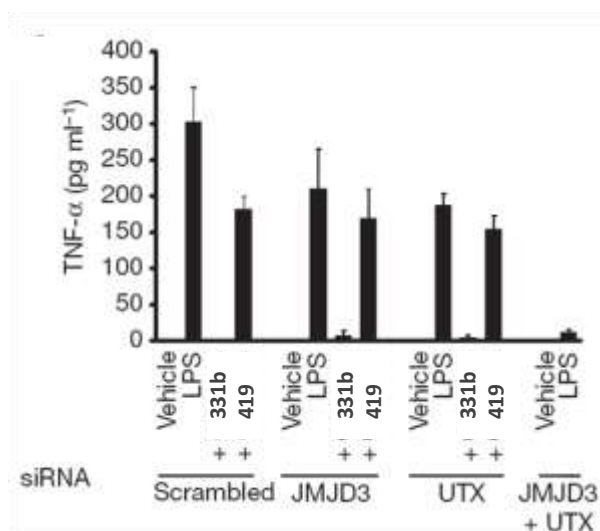


Figure 95. TNF- α production by LPS-stimulated human primary macrophages (1h) transfected with scrambled, or JmjD3-directed or UTX-directed siRNA, in the presence of 30 μ M **331b** or **419** (data are presented as the mean \pm s.d. from five transfection replicates from one representative experiment). Experiments run by P. Mander (Appendix 11).

Thus, the dose-dependent inhibition of TNF- α observed in human macrophages (Figure 91) was related to the inhibition of not only one but two enzymes, Jmjd3 and UTX.

Since the Jmjd3 programme was started, numerous 2-OG utilising enzyme assays were developed such as JARID1c. This enzyme is a member of the JARID1 sub-family of proteins which are implicated in transcriptional regulation. JARID1c is known to demethylate H3K4me3.^{24,207}

A small set of Jmjd3 inhibitors were screened against JARID1c by Cellzome colleagues in their binding assay (Table 49). The probe molecule **332b** which inhibited Jmjd3 and UTX was also shown to inhibit JARID1c with a pIC₅₀ of 5.8. The benzylamine **416** also a potent Jmjd3 inhibitor was inhibiting JARID1c with a pIC₅₀ of 5.3.

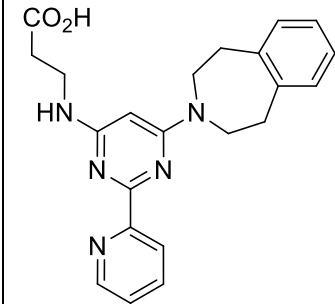
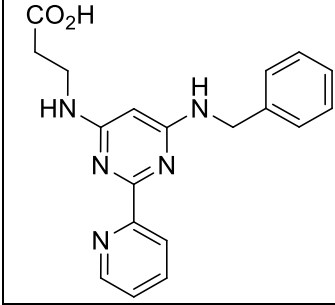
Structure	Compound	JARID1c pIC ₅₀
	332b	5.8
	416	5.3

Table 49. Cellzome JARID1c binding assay (Appendix 12). Assay run by colleagues at Cellzome.

Although **332b** was shown to inhibit JARID1c, it was still believed that the dose-dependent inhibition of TNF- α observed in human macrophages (Figure 90) was a consequence of the inhibition of JmjD3 and UTX as shown by the siRNA knockdown of these two enzymes (Figure 95). Additional experiments would be required to dispel any doubt regarding the non-involvement of JARID1c in inhibition of TNF- α production. These experiments could include studies of the effect of inhibition of JARID1c and siRNA-mediated knockdown of JARID1c on production of TNF- α in macrophages.

The purpose of this project was to identify potent, selective and cell penetrant probe molecules which inhibit JmjD3 with a view to modulating inflammation. It had been shown that it was possible to inhibit production of TNF- α in healthy human macrophages after LPS stimulation. It was therefore desirable to see if this inhibition was also observed in macrophages derived from patients suffering from inflammatory disorders such as rheumatoid arthritis. These macrophages were also stimulated using LPS, and the effects of compounds **331b** and **419** on production of TNF- α protein and mRNA were assessed at two concentrations, 3 and 10 μ M (Figure 96). These graphs show that **331b** inhibited the production of TNF- α protein and mRNA at 3 μ M concentration and had a more profound effect at 10 μ M. It was gratifying to show that the ester **331b** was also capable of inhibiting production of TNF- α protein and mRNA in primary macrophages derived from patients with rheumatoid arthritis after LPS stimulation. Compound **419** had little effect on production of TNF- α mRNA at 3 and 10 μ M but showed some partial inhibition of production of TNF- α protein at 10 μ M. However this observation might not be robust because Figure 96c shows that increasing the concentration of **419** from 3 to 10 μ M resulted in a reduction of the number of cells and so the inhibition of production of TNF- α protein observed at 10 μ M for **419** could potentially solely mirror the decrease of cell viability.

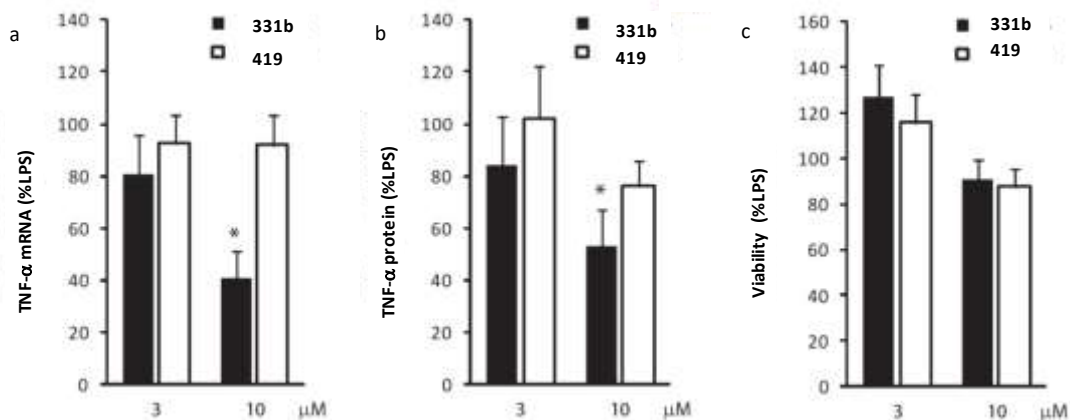
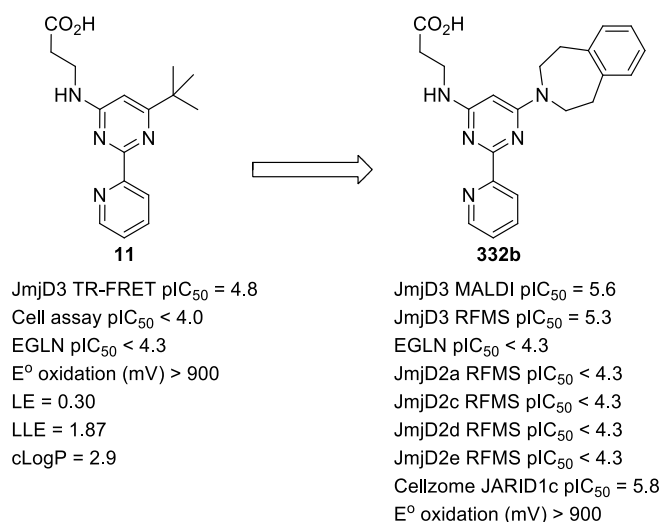


Figure 96. Inhibition of TNF- α production by **331b** in human primary macrophages derived from patients with rheumatoid arthritis. TNF- α mRNA production after 1h (a) protein production after 6 h and (b) and cellular viability (WST-1) after 6 h (c) of human primary macrophages activated with LPS in the presence of indicated concentrations of **331b** or **419** (n = 5 donors). Error bars represent s.e.m. Experiments run by biologist colleagues at GSK and at SGC (Appendix 11).

These experiments provided the first evidence that a small molecule inhibiting JmjD3 and UTX could inhibit the production of TNF- α , a pro-inflammatory cytokine, in healthy human macrophages and primary macrophages derived from patients with rheumatoid arthritis after LPS stimulation and thus could therefore potentially be used to modulate inflammation.¹⁵⁴

II.3.2.11 Conclusion

Pyridyl-pyrimidine **11** was a moderately potent and selective hit identified through a HTS and was the first in-house ligand crystallised in the JmjD3 active site. It was found that the active site of the JmjD3 enzyme was flexible with the catalytic Fe(II) occupying different positions in the crystal structures of **11** and 2-OG. Moreover this plasticity was also observed with Arg1247 occupying different positions in structures of JmjD3 with bound 2-OG and **11**. The flexibility of Arg1247 was exploited and key interactions were targeted with the aim of increasing the potency of the compounds whilst maintaining good selectivity. This effort led to the discovery of **332b** a potent JmjD3 inhibitor.



A crystal structure of **332b** in the JmjD3 active site again showed how elastic this active site could be with Arg1247 moving back to the position observed in the 2-OG crystal structure which was potentially its preferred position and interacting with the aromatic ring of **332b** resulting in an increase in potency. The inhibitor **332b** was shown to successfully engage the endogenous JmjD3 using a chemoproteomics approach. Ligand **332b** was designed to be a selective JmjD3 inhibitor, however, as additional selectivity assays became available, this compound was found to inhibit other members of the KDM6 family and JARID1c. Using a pro-drug approach compound **332b** could be delivered into cells to block the production of

TNF- α , a pro-inflammatory cytokine, in LPS-stimulated macrophages. This phenotypic response was confirmed by simultaneous siRNA knockdown of JmjD3 and UTX which suggested that the dual inhibition of JmjD3 and UTX by **332b** was necessary for the inhibition of the inflammatory response. In addition, compound **332b** was able to inhibit production of TNF- α in primary macrophages derived from patients with rheumatoid arthritis after LPS stimulation.

The discovery of the first potent small molecule inhibitor of the H3K27 demethylases and JARID1c has been presented in this report. This inhibitor brings us closer to delivering a new generation of drugs which treat inflammation through the inhibition of epigenetic processes such as histone demethylation. The work presented here enabled a chemoproteomics approach with the hypothesis and results detailed in *Nature*.¹⁵⁴ This was the first publication in the scientific community describing the X-ray crystal structure of JmjD3, the inhibition of JmjD3 with a small molecule, and the effect of inhibition of KDM6 demethylases on production of pro-inflammatory cytokines.

IV Experimental

All graphics showing ligand crystal structures were produced using PymolTM software.

All anhydrous solvents were supplied by Sigma Aldrich. All final compounds were characterised using NMR and mass spectrometry. ¹H NMR and ¹³C spectra were recorded in deuterated solvents using 400, 500 or 600 MHz Bruker Ultrashield spectrometers at ambient temperature unless stated otherwise. Chemical shifts are quoted in δ (ppm), measured relative to Me₄Si (TMS), with *J* values reported in Hertz. Multiplicities are described as: s = singlet, d = doublet, t = triplet, q = quartet, m = multiplet, dd = doublet of doublet, ddt = doublet of doublet of triplets, br.s = broad signal, app. = apparent, obs. = obscured. Thin layer chromatography was performed on precoated glass backed silica gel plates and the compounds were visualised using UV light ($\lambda = 254$ and 386 nm), potassium permanganate, ninhydrin or vanillin stains. Flash chromatography of crude products was performed on SNAP silica cartridges using a Biotage SP4 system. Aminopropyl and SCX cartridges were used to capture acidic or basic compounds from solutions. Microwave reactions were carried out using a Biotage InitiatorTM or EmrysTM Optimizer microwave synthesiser. Hydrogenation reactions were performed in an H-Cube[®] apparatus using disposable proprietary CatCarts[®]. Hydrogenation reactions were carried out with a solution flow rate of 1 mL min⁻¹ at various temperatures and pressures. Solutions of final compounds were evaporated using a Radleys blow-down apparatus.

LC-MS methodology

Method Formic

LC conditions: The UPLC analysis was conducted on an Acquity UPLC BEH C₁₈ column (50 mm x 2.1 mm, i.d. 1.7 µm packing diameter) at 40 °C. The solvents employed were: A = 0.1% v/v solution of formic acid in water; B = 0.1% v/v solution of formic acid in acetonitrile. The gradient (A:B) employed was from 97:3 to 3:97 over 2 min. The UV detection was a summed signal from wavelength of 210 nm to 350 nm.

MS conditions: The mass spectrometry was conducted on a Waters ZQ mass spectrometer, with an ionisation mode of alternate-scan positive and negative electrospray. The scan range was 100 to 1000 AMU, the scan time was 0.27 sec and the inter-scan delay was 0.10 sec.

Method TFA

The method was as for LC-MS (Formic), except the solvents employed were: A = 0.1% v/v solution of trifluoroacetic acid in water; B = 0.1% v/v solution of trifluoroacetic acid in acetonitrile.

Method high pH

The method was as for LC-MS (Formic), except the solvents employed were: A = ammonium hydrogen carbonate in water adjusted to pH 10 with ammonia solution; B = acetonitrile.

MDAP methodology

Method Formate

LC conditions: The HPLC analysis was conducted on either a Sunfire C18 column (100 mm x 19 mm, i.d 5µm packing diameter) or a Sunfire C18 column (150 mm x 30 mm, i.d. 5µm packing diameter) at ambient temperature.

The solvents employed were:

A = 0.1% v/v solution of formic acid in water

B = 0.1% v/v solution of formic acid in acetonitrile

Run as a gradient over either 15 or 25 min (extended run) with a flow rate of 20 mL/min (100 mm x 19 mm, i.d 5 µm packing diameter) or 40 mL/min (150 mm x 30 mm, i.d. 5µm packing diameter).

The UV detection was a summed signal from wavelength of 210 nm to 350 nm.

MS conditions

MS : Waters ZQ

Ionisation mode : Alternate-scan positive and negative electrospray

Scan range : 100 to 1000 AMU

Scan time : 0.50 sec

Inter scan delay : 0.20 sec

Method high pH

LC conditions: The HPLC analysis was conducted on either an Xbridge C18 column (100 mm x 19 mm, i.d 5µm packing diameter) or a Xbridge C18 column (100 mm x 30 mm, i.d. 5µm packing diameter) at ambient temperature.

The solvents employed were:

A = 10 mM ammonium bicarbonate in water, adjusted to pH10 with ammonia solution

B = acetonitrile

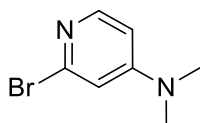
Run as a gradient over either 15 or 25 min (extended run) with a flow rate of 20 mL/min (100 mm x 19 mm, i.d 5µm packing diameter) or 40 mL/min (100 mm x 30 mm, i.d 5µm packing diameter).

The UV detection was a summed signal from wavelength of 210 nm to 350 nm.

MS conditions

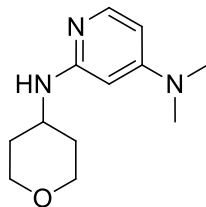
MS	:	Waters ZQ
Ionisation mode	:	Alternate-scan positive and negative electrospray
Scan range	:	100 to 1000 AMU
Scan time	:	0.50 sec
Inter scan delay	:	0.20 sec

None of the compounds from *bis*-amino aryl series were fully characterised because of stability issues described in Sections II.1. Further, for similar reasons, only two compounds in the pyridone series (Section II. 2) have been fully characterised.

2-Bromo-*N,N*-dimethylpyridin-4-amine 124²⁰⁸

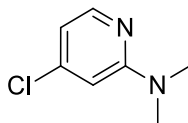
Sodium hydride (116 mg of a 60% w/w dispersion in mineral oil, 2.89 mmol) was added to a cold (0 °C) stirred solution of 2-bromo-4-pyridinamine (200 mg, 1.16 mmol) in DMF (7 mL). After stirring for 1 h at 0 °C, the reaction mixture was allowed to warm to rt. After stirring for 1 h at rt, iodomethane (0.18 mL, 2.89 mmol) was added and the reaction mixture was stirred under nitrogen for 69 h. The reaction mixture was concentrated under reduced pressure and the residue was loaded onto a Biotage silica (Si) 40+M column and purified by automated chromatography (SP4) using a 0-50% ethyl acetate in cyclohexane gradient (20 CV). The appropriate fractions were combined and concentrated under reduced pressure to give the impure product which was purified further. The residue was loaded onto a Biotage silica (Si) 12+S column and purified by automated chromatography (SP4) using a 0-100% ethyl acetate in cyclohexane gradient (15 CV). The appropriate fractions were combined and concentrated under reduced pressure to give **124** (144 mg, 62%) as a white solid.

¹H NMR (400 MHz, DMSO-d₆) δ 7.85 (d, *J* = 6.0 Hz, 1 H), 6.71 (d, *J* = 2.5 Hz, 1 H), 6.63 (dd, *J* = 6.0, 2.5 Hz, 1 H), 2.95 (s, 6 H); MS (ES+) *m/z* 202.79 [M + H]⁺.

General procedure for Buchwald-Hartwig amination***N*⁴,*N*⁴-Dimethyl-*N*²-(tetrahydro-2H-pyran-4-yl)pyridine-2,4-diamine **120****

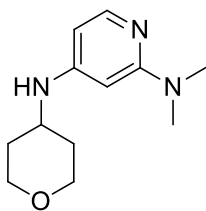
A mixture of 4-amino-THP (0.08 mL, 0.75 mmol), Pd₂(dba)₃ (22.8 mg, 0.03 mmol), DavePhos (29.4 mg, 0.08 mmol), **124** (100 mg, 0.50 mmol), sodium *tert*-butoxide (66.9 mg, 0.70 mmol) and 1,4-dioxane (1.5 mL) was degassed with nitrogen for 0.5 h and heated in an Emrys Optimizer microwave at 120 °C for 15 min. The reaction mixture was filtered under vacuum through a sinter funnel and the filtrate was concentrated under reduced pressure. The residue was loaded onto a SNAP silica cartridge (25 g) and partially purified by automated chromatography (SP4) using a 0-10% gradient of methanolic ammonia (2 M) in DCM (25 CV). The appropriate fractions were combined and concentrated under reduced pressure to give the impure product. The residue was further purified by MDAP on a Waters Xbridge C18 column using solution of ammonium bicarbonate (10 mM in methanol, adjusted to pH 10 with ammonia). Evaporation of the solvent under reduced pressure afforded **120** (47.1 mg, 43%).

¹H NMR (400 MHz, DMSO-*d*₆) δ 7.60 (d, *J* = 6.0 Hz, 1 H), 5.95 (dd, *J* = 6.0, 2.0 Hz, 1 H), 5.90 (d, *J* = 8.0 Hz, 1 H), 5.61 (d, *J* = 2.0 Hz, 1 H), 3.86 - 3.80 (m, 3 H), 3.41 - 3.32 (br. s, 2 H), 2.85 (s, 6 H), 1.85 - 1.78 (m, 2 H), 1.41 - 1.30 (m, 2 H); MS (ES+) *m/z* 226.86 [M + H]⁺.

4-Chloro-*N,N*-dimethylpyridin-2-amine 126²⁰⁹

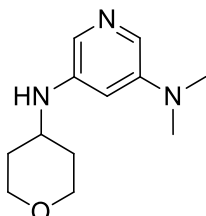
Sodium hydride (68.4 mg of a 60% w/w dispersion in mineral oil, 1.71 mmol) was added to a cold (0 °C) stirred solution of 4-chloro-2-pyridinamine (200 mg, 1.56 mmol) in DMF (7 mL). After stirring for 30 min, the reaction was allowed to warm to rt and iodomethane (0.11 mL, 1.71 mmol) was added. After stirring for a further 42 h at rt, the reaction mixture was cooled in an ice bath and sodium hydride (68.4 mg of a 60% w/w dispersion in mineral oil, 1.71 mmol) was added. The mixture was stirred for a further 30 min, then iodomethane (0.11 mL, 1.71 mmol) was added. After stirring for 4 h at rt, further iodomethane (0.11 mL, 1.71 mmol) and sodium hydride (68 mg of a 60% w/w dispersion in mineral oil, 1.71 mmol) were added and the reaction mixture was stirred for 66 h. The reaction mixture was partitioned between ethyl acetate (50 mL) and water (50 mL) and the organic layer was extracted and further washed with sodium bicarbonate (3 x 50 mL). The organic layer was dried over magnesium sulfate and filtered through a hydrophobic frit. The filtrate was concentrated under reduced pressure and the residue was loaded onto a Biotage silica (Si) 12+M column and purified by automated chromatography (SP4) using a 0-20% gradient of ethyl acetate in cyclohexane (10 CV). The appropriate fractions were combined and the solvent removed under reduced pressure to give the impure product which was purified further. The residue was loaded onto a Biotage silica (Si) 12+M column and purified by automated chromatography (SP4) using a 0-20% gradient of ethyl acetate in cyclohexane (20 CV). The appropriate fractions were combined and concentrated under reduced pressure to give **126** (70 mg, 29%) as a colourless oil.

¹H NMR (400 MHz, DMSO-*d*₆) δ 8.03 (d, *J* = 5.5 Hz, 1 H), 6.67 (d, *J* = 1.6 Hz, 1 H), 6.62 (dd, *J* = 5.5, 1.6 Hz, 1 H), 3.01 (s, 6 H); MS (ES⁺) *m/z* 156.78 [M + H]⁺.

***N*²,*N*²-Dimethyl-*N*⁴-(tetrahydro-2H-pyran-4-yl)pyridine-2,4-diamine 127**

Was prepared as for **120** from 4-amino-THP (0.07 mL, 0.67 mmol), Pd₂(dba)₃ (21 mg, 0.02 mmol), DavePhos (26 mg, 0.07 mmol), **126** (70 mg, 0.45 mmol) and sodium *tert*-butoxide (60.1 mg, 0.63 mmol). The usual purification afforded **127** (40 mg, 40%) as a white solid.

¹H NMR (400 MHz, CDCl₃) δ 7.85 (d, *J* = 5.8 Hz, 1 H), 5.89 (dd, *J* = 5.8, 1.9 Hz, 1 H), 5.62 (d, *J* = 1.9 Hz, 1 H), 4.00 (dt, ²*J* = 12.0, *J* = 3.4 Hz, 2 H), 3.95 - 3.88 (br. s, *J* = 7.5 Hz, 1 H), 3.61 - 3.46 (m, 3 H), 3.04 (s, 6 H), 2.07 - 1.99 (br. m, 2 H), 1.56 - 1.44 (m, 2 H); MS (ES⁺) *m/z* 221.99 [M + H]⁺.

***N*³,*N*³-Dimethyl-*N*⁵-(tetrahydro-2H-pyran-4-yl)pyridine-3,5-diamine 130**

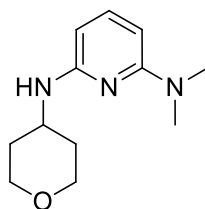
Intermediate **129** was prepared as for **124** from sodium hydride (87 mg of a 60% w/w dispersion in mineral oil, 2.17 mmol), 5-bromo-3-pyridinamine (150 mg, 0.87 mmol) and iodomethane (0.14 mL, 2.17 mmol). The usual purification afforded crude **129** (82 mg) as an orange solid. LCMS confirmed the presence of **129**, MS (ES⁺) *m/z* 202.8 [M + H]⁺.

A mixture of **129** (30.0 mg), 4-amino-THP (0.02 mL, 0.22 mmol), DavePhos (9 mg, 0.02 mmol), Pd₂(dba)₃ (7 mg, 7.46 μmol), sodium *tert*-butoxide (20.1 mg, 0.21 mmol) and 1,4-dioxane (1.5 mL) was degassed with nitrogen for 0.5 h and heated in an Emrys Optimizer microwave at 120 °C for 15 min. The reaction mixture was filtered under vacuum and the

solid was washed with methanol. The filtrate was concentrated under reduced pressure and the residue was loaded onto a SNAP silica cartridge (10 g) and purified by automated chromatography (SP4) using a 0-10% gradient of methanol in DCM (25 CV). The appropriate fractions were combined and the solvent removed under reduced pressure to give **130** (7 mg, 10% over 2 steps) as a yellow oil.

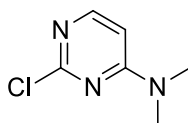
¹H NMR (250 MHz, DMSO-d₆) δ 7.39 - 7.34 (br. s, 2 H), 6.24 (s, 1 H), 5.44 (d, *J* = 8.2 Hz, 1 H), 3.85 (dt, ²*J* = 11.5, *J* = 3.3 Hz, 2 H), 3.5 - 3.34 (m, 3 H), 2.85 (s, 6 H), 1.91 - 1.81 (br. m, 2 H), 1.44 - 1.26 (m, 2 H); MS (ES+) *m/z* 229.9 [M + H]⁺.

N*²,*N*²-Dimethyl-*N*⁶-(tetrahydro-2H-pyran-4-yl)pyridine-2,6-diamine **132*



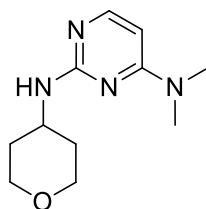
Was prepared as for **120** from 4-amino-THP (75 mg, 0.75 mmol), Pd₂(dba)₃ (22.8 mg, 0.03 mmol), DavePhos (29.4 mg, 0.08 mmol), **131** (100 mg, 0.50 mmol) and sodium *tert*-butoxide (66.9 mg, 0.70 mmol). The usual purification afforded **132** (66 mg, 60%) as a brown gum.

¹H NMR (400 MHz, DMSO-d₆) δ 7.11 (t, *J* = 7.9 Hz, 1 H), 5.99 (d, *J* = 7.3 Hz, 1 H), 5.70 (dd, *J* = 7.9 Hz, ⁴*J* = 2.6 Hz, 2 H), 3.85 (dt, ²*J* = 11.5, *J* = 3.3 Hz, 2 H), 3.82 - 3.75 (m, 1 H), 3.37 (td, ²*J* = 11.5, *J* = 11.5, 2.1 Hz, 2 H), 2.91 (s, 6 H), 1.91 - 1.83 (br. m, 2 H), 1.45 - 1.34 (m, 2 H); MS (ES+) *m/z* 221.96 [M + H]⁺.

2-Chloro-*N,N*-dimethylpyrimidin-4-amine 134

Was prepared as for **124** from sodium hydride (232 mg of a 60% w/w dispersion in mineral oil, 5.79 mmol), 2-chloro-4-pyrimidinamine **133** (300 mg, 2.32 mmol) and iodomethane (0.36 mL, 5.79 mmol). The usual purification afforded **134** (332 mg, 91%) as a white solid.

¹H NMR (400 MHz, DMSO-*d*₆) δ 8.03 (d, *J* = 6.3 Hz, 1 H), 6.66 (d, *J* = 6.3 Hz, 1 H), 3.05 (s, 6 H); MS (ES+) *m/z* 154.82 [M + H]⁺.

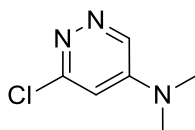
***N,N*-Dimethyl-*N*²-(tetrahydro-2H-pyran-4-yl)pyrimidine-2,4-diamine 121**

A mixture of 4-amino-THP (1.5 mL, 14.53 mmol) and **134** (100 mg, 0.64 mmol) was degassed with nitrogen for 0.5 h. The reaction mixture was heated in a Biotage Initiator microwave at 190 °C for 1 h. The solvent was removed under reduced pressure and the residue was loaded onto a SNAP silica cartridge (10 g) and partially purified by automated chromatography (SP4) using a 0-20% gradient of methanol in DCM (25 CV). The appropriate fractions were combined and evaporated under reduced pressure to give the impure product, which was purified further by MDAP on a Waters Xbridge C18 column using a solution of ammonium bicarbonate (10 mM in methanol, adjusted to pH 10 with ammonia). Evaporation of the solvent under reduced pressure afforded **121** (90 mg, 64%) as a yellow solid.

¹H NMR (400 MHz, DMSO-*d*₆) δ 7.75 (d, *J* = 5.8 Hz, 1 H), 6.44 - 6.32 (br. s, 1 H), 5.87 (d, *J* = 5.8 Hz, 1 H), 3.94 - 3.74 (m, 3 H), 3.39 - 3.29 (m, 2 H), 2.96 (s, 6 H), 1.83 - 1.75 (br. m,

2 H), 1.53 – 1.37 (m, 2 H); MS (ES+) m/z 222.93 [M + H]⁺.

6-Chloro-*N,N*-dimethyl-4-pyridazinamine 136

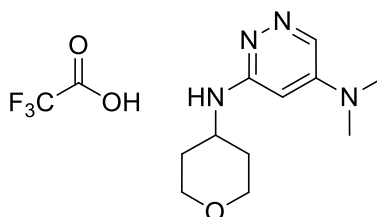


Was prepared as for **124** from sodium hydride (131 mg of a 60% w/w dispersion in mineral oil, 3.27 mmol), 6-chloro-4-pyridazinamine **135** (163 mg, 1.26 mmol) and iodomethane (0.20 mL, 3.27 mmol). The usual purification afforded **136** (73 mg, 37%) as a yellow solid.

¹H NMR (400 MHz, DMSO-*d*₆) δ 8.76 (d, *J* = 2.7 Hz, 1 H), 6.83 (d, *J* = 2.8 Hz, 1 H), 3.03 (s, 6 H); MS (ES+) m/z 158.07 [M + H]⁺.

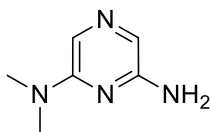
***N*⁵,*N*⁵-Dimethyl-*N*³-(tetrahydro-2H-pyran-4-yl)-3,5-pyridazinediamine trifluoroacetate**

137



A mixture of **136** (73 mg, 0.46 mmol) and 4-amino-THP (2 mL) was heated in a Biotage Initiator microwave at 190 °C for 6 h. The solvent was removed under reduced pressure and the residue was purified by MDAP on a Sunfire C18 column using a 5 - 99% gradient of acetonitrile (containing 0.1% v/v TFA) in water (containing 0.1% v/v TFA). Evaporation of the solvent under reduced pressure afforded **137** (91 mg, 59%) as a yellow solid.

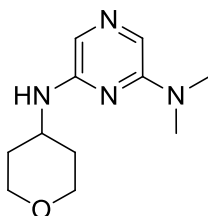
¹H NMR (400 MHz, DMSO-*d*₆) δ 13.52 (s, 1H) 8.34 (d, *J* = 2.5 Hz, 1 H), 8.13 (d, *J* = 8.0 Hz, 1 H), 6.02 (d, *J* = 2.5 Hz, 1 H), 3.93 - 3.85 (m, 1 H), 3.85 - 3.76 (m, 2 H), 3.46 - 3.33 (m, 2 H), 3.19 - 3.05 (br. s, 6 H), 1.89 - 1.82 (br. m, 2 H), 1.53 - 1.41 (m, 2 H); MS (ES+) m/z 223.25 [M + H]⁺.

***N,N*-Dimethylpyrazine-2,6-diamine 139²¹⁰**

Was prepared as for **121** from 6-chloro-2-pyrazinamine **138** (150 mg, 1.16 mmol) and dimethylamine (10 mL of a 2 M solution in THF, 20.0 mmol). The usual purification afforded **139** (140 mg, 88%) as a brown solid.

¹H NMR (400 MHz, DMSO-*d*₆) δ 7.19 (s, 1 H), 7.10 (s, 1 H), 5.87 (s, 2 H), 2.94 (s, 6 H);

MS (ES+) *m/z* 139.04 [M + H]⁺.

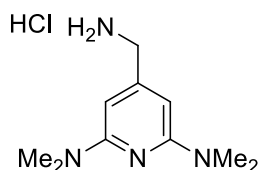
***N,N*-Dimethyl-*N'*-(tetrahydro-2H-pyran-4-yl)-2,6-pyrazinediamine 141**

Intermediate **140** was prepared as for **124** from sodium hydride (76 mg of a 60% w/w dispersion in mineral oil, 1.91 mmol) and 6-chloro-2-pyrazinamine (99 mg, 0.76 mmol). The usual purification afforded crude **140** (367 mg) as a brown solid which was used crude in the next step.

A mixture of crude **140** (122 mg) and 4-amino-THP (1 mL) was heated in an Emrys Optimizer microwave at 190 °C for 2 h. The solvent was removed under reduced pressure and the residue was purified by MDAP on a Waters Xbridge C18 column using a solution of ammonium bicarbonate (10 mM in methanol, adjusted to pH 10 with ammonia). Evaporation of the solvent under reduced pressure afforded **141** (4 mg, 2%) as a brown oil.

¹H NMR (400 MHz, DMSO-*d*₆) δ 7.15 (s, 1 H), 7.13 (s, 1 H), 6.52 (d, *J* = 7.3 Hz, 1 H), 3.93 - 3.73 (m, 3 H), 3.47 - 3.32 (m, 2 H), 2.95 (s, 6 H), 1.91 - 1.83 (br. m, 2 H), 1.54 - 1.29 (m, 2 H); MS (ES+) *m/z* 223.24 [M + H]⁺.

4-(Aminomethyl)-*N,N,N',N'*-tetramethyl-2,6-pyridinediamine hydrochloride 143

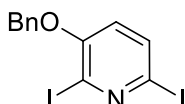


A solution of 2,6-bis(dimethylamino)-4-pyridinecarbonitrile **142** (22.6 mg, 0.12 mmol) in MeOH (2.4 mL) was hydrogenated using the H-Cube with a cat cart (10% Pd/C) at rt. The solvent was evaporated under reduced pressure and the residue was purified on a SCX column (5 g) using methanolic ammonia (3 CV of a 2 N solution). After evaporation of the solvent under reduced pressure, the product was treated with HCl (66 μ L of a 2 N solution in Et₂O). Evaporation of the solvent under reduced pressure afforded **143** (15 mg, 55%) as a brown solid.

¹H NMR (400 MHz, DMSO-d₆) δ 8.47 - 8.33 (br. s, 3 H), 6.02 (s, 2 H), 3.83 (q, *J* = 6.0 Hz, 2 H), 2.99 (s, 12 H); MS (ES+) *m/z* 195.0 [M + H]⁺.

General procedure for Mitsunobu reaction

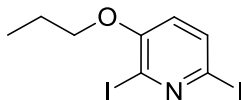
2,6-Diiodo-3-[(phenylmethyl)oxy]pyridine 145a



Benzyl alcohol (0.14 mL, 1.34 mmol) was added to a cold stirred solution (0-5 °C) of 2,6-diiodo-3-pyridinol **144** (233 mg, 0.67 mmol), triphenylphosphine (352 mg, 1.34 mmol) and diisopropylazodicarboxylate (0.27 mL, 1.34 mmol) in THF (5 mL). After stirring for 1 h, the solvent was removed under reduced pressure and the residue was loaded onto a SNAP silica cartridge (25 g), purified by automated chromatography (SP4) using a 0 - 30% gradient of ethyl acetate in cyclohexane (15 CV). Evaporation of the solvent under reduced pressure afforded **145a** (265 mg, 90%) as an off-white solid.

¹H NMR (400 MHz, DMSO-d₆) δ 7.74 (d, *J* = 8.4 Hz, 1 H), 7.51 - 7.46 (m, 2 H), 7.42 (t, *J* = 7.4 Hz, 2 H), 7.38 - 7.32 (m, 1 H), 7.20 (d, *J* = 8.4 Hz, 1 H), 5.24 (s, 2 H); MS (ES+) *m/z* 437.6 [M + H]⁺.

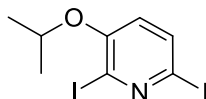
2,6-Diiodo-3-(propyloxy)pyridine 145b



Was prepared as for **145a** from 2,6-diiodo-3-pyridinol **144** (103 mg, 0.30 mmol), triphenylphosphine (156 mg, 0.59 mmol), diisopropylazodicarboxylate (0.12 mL, 0.59 mmol) and 1-propanol (0.05 mL, 0.59 mmol) for 1 h. The usual purification afforded **145b** (104 mg, 90%) as a colourless oil.

¹H NMR (400 MHz, DMSO-d₆) δ 7.71 (d, *J* = 8.4 Hz, 1 H), 7.10 (d, *J* = 8.4 Hz, 1 H), 4.02 (t, *J* = 6.7 Hz, 2 H), 1.73 (sxt, *J* = 6.7 Hz, 2 H), 1.01 (t, *J* = 6.7 Hz, 3 H); MS (ES+) *m/z* 389.6 [M + H]⁺.

2,6-Diiodo-3-isopropoxy pyridine 145c

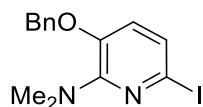


2-Propanol (0.06 mL, 0.72 mmol) was added to a cold stirred solution (0-5 °C) of **144** (250 mg, 0.72 mmol), triphenylphosphine (378 mg, 1.44 mmol) and diisopropylazodicarboxylate (0.28 mL, 1.44 mmol) in THF (4 mL). After 65 h, the solvent was removed under reduced pressure and the residue was loaded onto a SNAP silica cartridge (25 g), purified by automated chromatography (SP4) using a 0 - 40% gradient of ethyl acetate in cyclohexane (20 CV) followed by 40% ethyl acetate in cyclohexane (5 CV). The appropriate fractions were combined and evaporated under reduced pressure to give **145c** (109 mg, 39 %) as a colourless oil.

¹H NMR (400 MHz, DMSO-d₆) δ 7.69 (d, *J* = 8.5 Hz, 1 H), 7.15 (d, *J* = 8.5 Hz, 1 H), 4.68 (spt, *J* = 6.0 Hz, 1 H), 1.28 (d, *J* = 6.0 Hz, 6 H); MS (ES+) *m/z* 389.6 [M + H]⁺.

General procedure for nucleophilic aromatic substitution (S_NAr)

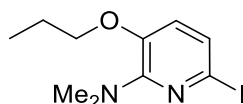
6-Iodo-*N,N*-dimethyl-3-[(phenylmethyl)oxy]-2-pyridinamine 146a



A mixture of **145a** (265 mg, 0.61 mmol) and dimethylamine (3.50 mL of a 2 M solution in THF, 7 mmol) was heated in an Emrys Optimizer microwave at 180 °C for 1 h. The solvent was removed under reduced pressure and the residue was loaded onto a SNAP silica cartridge (25 g) and purified by automated chromatography (SP4) using a 0 - 30% gradient of diethyl ether in cyclohexane (20 CV). Evaporation of the solvent under reduced pressure afforded **146a** (174 mg, 81%) as a colourless oil.

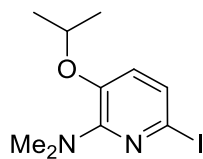
¹H NMR (600 MHz, DMSO-d₆) δ 7.46 - 7.43 (m, 2 H), 7.40 (t, *J* = 7.5 Hz, 2 H), 7.36 - 7.33 (m, 1 H), 7.10 (d, *J* = 8.1 Hz, 1 H), 7.01 (d, *J* = 8.1 Hz, 1 H), 5.08 (s, 2 H), 2.91 (s, 6 H); MS (ES+) *m/z* 354.8 [M + H]⁺.

6-Iodo-*N,N*-dimethyl-3-(propyloxy)-2-pyridinamine 146b



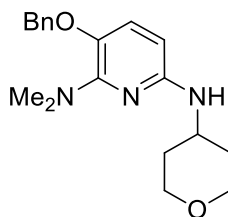
Was prepared as for **146a** from **145b** (104 mg, 0.27 mmol) and dimethylamine (2 mL of a 2 N solution in THF, 4.0 mmol) at 150 °C for 30 min then for two further periods of 60 min and at 180 °C for 60 min. The usual purification afforded **146b** (81 mg, 99%) as a brown oil.

¹H NMR (600 MHz, DMSO-d₆) δ 7.07 (d, *J* = 8.1 Hz, 1 H), 6.89 (d, *J* = 8.1 Hz, 1 H), 3.89 (t, *J* = 6.7 Hz, 2 H), 2.91 (s, 6 H), 1.75 (sxt, *J* = 6.7 Hz, 2 H), 0.98 (t, *J* = 6.7 Hz, 3 H); MS (ES+) *m/z* 306.8 [M + H]⁺.

6-Iodo-3-isopropoxy-*N,N*-dimethylpyridin-2-amine 146c

A mixture of **145c** (100 mg, 0.26 mmol) and dimethylamine (1.09 mL of a 2 N solution in THF, 2.18 mmol) was heated in an Emrys Optimizer microwave at 180 °C for 1 h. Additional dimethylamine (0.5 mL of a 2 N solution in THF, 1.0 mmol) was added and reaction mixture heated at 180 °C for 30 min further. Additional dimethylamine (0.5 mL of a 2 N solution in THF, 1.0 mmol) was added and reaction mixture heated at 180 °C for one hour further. The solvent was removed under reduced pressure and the residue was loaded onto a SNAP silica cartridge (10 g) and purified by automated chromatography (SP4) using a 0 - 50% gradient of ethyl acetate in cyclohexane (20 CV). Evaporation of the solvent under reduced pressure afforded **146c** (50 mg, 64 %) as a clear oil.

¹H NMR (400 MHz, DMSO-d₆) δ 7.07 (d, *J* = 8.0 Hz, 1 H), 6.91 (d, *J* = 8.0 Hz, 1 H), 4.54 (spt, *J* = 6.0 Hz, 1 H), 2.88 (s, 6 H), 1.25 (d, *J* = 6.0 Hz, 6 H); MS (ES+) *m/z* 306.98 [M + H]⁺.

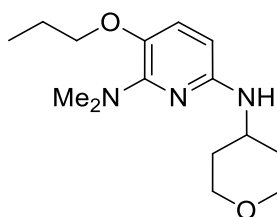
***N*²,*N*²-Dimethyl-3-[(phenylmethyl)oxy]-*N*⁶-(tetrahydro-2*H*-pyran-4-yl)-2,6-pyridinediamine 147a**

Was prepared as for **120** from 4-amino-THP (0.08 mL, 0.72 mmol), **146a** (171.0 mg, 0.48 mmol), sodium *tert*-butoxide (65.0 mg, 0.68 mmol), DavePhos (28.5 mg, 0.07 mmol) and Pd₂(dba)₃ (22.1 mg, 0.02 mmol). The usual purification afforded **147a** (88 mg, 56%) as a brown oil.

^1H NMR (400 MHz, DMSO- d_6) δ 7.44 - 7.35 (m, 4 H), 7.34 - 7.28 (m, 1 H), 7.05 (d, $J = 8.5$ Hz, 1 H), 5.83 (d, $J = 8.5$ Hz, 1 H), 5.80 - 5.75 (m, 1 H), 4.86 (s, 2 H), 3.85 (dt, $^2J = 11.4$, $J = 3.2$ Hz, 2 H), 3.77 - 3.66 (m, 1 H), 3.41 - 3.34 (m, 2 H), 2.87 (s, 6 H), 1.90 - 1.83 (br. m, 2 H), 1.44 - 1.31 (m, 2 H); MS (ES+) m/z 327.9 [M + H] $^+$.

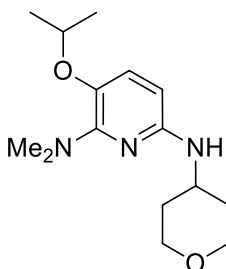
N^2,N^2 -Dimethyl-3-(propyloxy)- N^6 -(tetrahydro-2H-pyran-4-yl)-2,6-pyridinediamine

147b



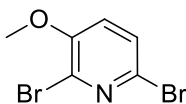
Was prepared as for **120** from 4-amino-THP (0.04 mL, 0.37 mmol), **146b** (76 mg, 0.25 mmol), sodium *tert*-butoxide (33.4 mg, 0.35 mmol), DavePhos (14.7 mg, 0.04 mmol), and Pd₂(dba)₃ (11.4 mg, 0.01 mmol). The usual purification afforded **147b** (40 mg, 58%) as a black solid.

^1H NMR (400 MHz, DMSO- d_6) δ 6.96 (d, $J = 8.4$ Hz, 1 H), 5.82 (d, $J = 8.4$ Hz, 1 H), 5.71 (d, $J = 7.2$ Hz, 1 H), 3.84 (dt, $^2J = 11.4$, $J = 3.4$ Hz, 2 H), 3.74 - 3.64 (m, 3 H), 3.37 - 3.35 (m, 2 H), 2.85 (s, 6 H), 1.90 - 1.82 (br. m, 2 H), 1.66 (sxt, $J = 7.2$ Hz, 2 H), 1.43 - 1.31 (m, 2 H), 0.96 (t, $J = 7.2$ Hz, 3 H); MS (ES+) m/z 279.9 [M + H] $^+$.

3-Isopropoxy-*N*²,*N*²-dimethyl-*N*⁶-(tetrahydro-2H-pyran-4-yl)pyridine-2,6-diamine 147c

Was prepared as for **120** from 4-amino-THP (0.02 mL, 0.22 mmol), Pd₂(dba)₃ (6.7 mg, 7.4 μmol), DavePhos (8.7 mg, 0.02 mmol), **146c** (45 mg, 0.15 mmol) and sodium *tert*-butoxide (19.8 mg, 0.21 mmol). The usual purification afforded **147c** (12 mg, 28 %) as a yellow oil.

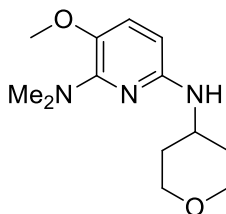
¹H NMR (600 MHz, DMSO-*d*₆) δ 6.91 (d, *J* = 8.4 Hz, 1 H), 5.82 (d, *J* = 8.4 Hz, 1 H), 5.73 (d, *J* = 7.3 Hz, 1 H), 4.16 (spt, *J* = 6.2 Hz, 1 H), 3.85 (dt, ²*J* = 11.4, *J* = 3.3 Hz, 2 H), 3.75 - 3.67 (m, 1 H), 3.39 - 3.30 (m, 2 H), 2.85 (s, 6 H), 1.90 - 1.83 (br. m, 2 H), 1.42 - 1.34 (m, 2 H), 1.16 (d, *J* = 6.2 Hz, 6 H); MS (ES+) *m/z* 280.1 [M + H]⁺.

2,6-Dibromo-3-(methoxy)pyridine 149

Cs₂CO₃ (108 mg, 3.31 mmol) was added to a cold stirred solution (0-5 °C) of 2,6-dibromo-3-pyridinol **148** (762 mg, 3.01 mmol) in DMF (3 mL). After stirring for 0.5 h, iodomethane (0.25 mL, 3.91 mmol) was added and the mixture was allowed to warm and stir at rt. After stirring for 3 h, the solvent was evaporated under reduced pressure and the residue was partitioned between DCM (50 mL) and water (50 mL). The organic layer was separated and dried using a hydrophobic frit and concentrated under reduced pressure to afford **149** (760 mg, 94%) as a white solid.

¹H NMR (400 MHz, DMSO-*d*₆) δ 7.66 (d, *J* = 8.5 Hz, 1 H), 7.52 (d, *J* = 8.5 Hz, 1 H), 3.90 (s, 3 H); MS (ES+) *m/z* 267.6 [M + H]⁺.

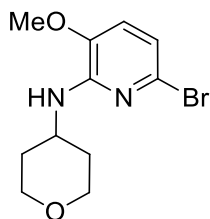
N*²,*N*²-Dimethyl-3-(methoxy)-*N*⁶-(tetrahydro-2*H*-pyran-4-yl)-2,6-pyridinediamine hydrochloride **151*



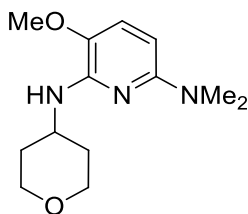
A mixture of dimethylamine (5 ml, 99 mmol) and 2,6-dibromo-3-(methoxy)pyridine **149** (360 mg, 1.35 mmol) was heated in a Biotage Initiator microwave at 150 °C for 1 h and then at 120 °C for a further 1 h. The solvent was removed under reduced pressure and the residue was loaded onto a SNAP silica cartridge (50 g), purified by automated chromatography (SP4) using a 0 - 40% gradient of Et₂O in cyclohexane (20 CV). The appropriate fractions were combined and evaporated under reduced pressure to afford crude **150** (330 mg) as a yellow oil. LCMS confirmed the presence of **150**, MS (ES+) *m/z* 232.99 [M + H]⁺.

A mixture of 4-amino-THP (0.22 mL, 2.14 mmol), **150** (330 mg), sodium *tert*-butoxide (192 mg, 2.0 mmol), DavePhos (84 mg, 0.21 mmol) and Pd₂(dba)₃ (65.4 mg, 0.07 mmol) was heated in a Biotage Initiator microwave at 120 °C for 15 min. The solvent was removed under reduced pressure and the residue was loaded onto a SNAP silica cartridge (100 g), purified by automated chromatography (SP4) using a 0 - 60% gradient of ethyl acetate in cyclohexane (15 CV). The appropriate fractions were combined and evaporated under reduced pressure to afford **151** (310 mg, 91% over 2 steps) as a black oil.

¹H NMR (400 MHz, DMSO-*d*₆) δ = 6.90 (d, *J* = 8.5 Hz, 1 H), 5.64 (d, *J* = 8.5 Hz, 1 H), 5.37 (d, *J* = 7.5 Hz, 1 H), 3.84 (dt, ²*J* = 11.4, *J* = 3.3 Hz, 2 H), 3.75 - 3.64 (m, 1 H), 3.66 (s, 3 H), 3.41 - 3.35 (m, 2 H), 2.86 (s, 6 H), 1.9 - 1.83 (br. m, 2 H), 1.43 - 1.31 (m, 2 H); MS (ES+) *m/z* 251.9 [M + H]⁺.

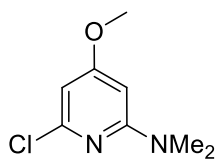
6-Bromo-3-(methoxy)-*N*-(tetrahydro-2*H*-pyran-4-yl)-2-pyridinamine 152

Was prepared as for **146a** from **149** (360 mg, 1.35 mmol) and 4-amino-THP (4 mL, 38.8 mmol) at 150 °C for 1 h. The usual purification afforded **152** (252 mg, 65%) as a white solid. ¹H NMR (600 MHz, DMSO-*d*₆) δ 6.92 (d, *J* = 7.7 Hz, 1 H), 6.60 (d, *J* = 7.7 Hz, 1 H), 6.14 (d, *J* = 7.7 Hz, 1 H), 4.01 - 3.91 (m, 1 H), 3.88 - 3.82 (br. m, 2 H), 3.77 (s, 3 H), 3.42 - 3.31 (m, 2 H), 1.79 - 1.73 (br. m, 2 H), 1.61 - 1.49 (m, 2 H); MS (ES+) *m/z* 288.9 [M + H]⁺.

***N*⁶,*N*⁶-Dimethyl-3-(methoxy)-*N*²-(tetrahydro-2*H*-pyran-4-yl)-2,6-pyridinediamine 153**

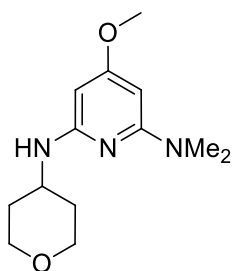
Was prepared as for **120** from **153** (54 mg, 0.19 mmol), dimethylamine (0.38 mL of a 2 N solution in THF, 0.75 mmol), sodium *tert*-butoxide (25.3 mg, 0.26 mmol), DavePhos (11.1 mg, 0.03 mmol) and Pd₂(dba)₃ (8.6 mg, 9.40 μmol). The usual purification afforded **153** (40 mg, 85%) as a brown oil.

¹H NMR (400 MHz, DMSO-*d*₆) δ 6.90 (d, *J* = 8.5 Hz, 1 H), 5.64 (d, *J* = 8.5 Hz, 1 H), 5.37 (d, *J* = 7.5 Hz, 1 H), 3.99 - 3.89 (m, 1 H), 3.88 - 3.83 (m, 2 H), 3.66 (s, 3 H), 3.41 - 3.35 (m, 2 H), 2.86 (s, 6 H), 1.89 - 1.82 (m, 2 H), 1.56 - 1.44 (m, 2 H); MS (ES+) *m/z* 252.0 [M + H]⁺.

6-Chloro-4-methoxy-*N,N*-dimethylpyridin-2-amine 155

A mixture of dimethylamine (0.28 mL of a 2 N solution in THF, 0.56 mmol), **154** (100 mg, 0.56 mmol) and THF (1.5 mL) was heated in a Biotage Initiator microwave at 100 °C for 0.5 h. Dimethylamine (0.28 mL of a 2 N solution in THF, 0.56 mmol) was added and the reaction mixture was heated at 100 °C for a further 0.5 h. A further portion of dimethylamine was added (1.4 mL of a 2 N solution in THF, 2.8 mmol) and the reaction mixture was heated at 190 °C for a further 0.5 h. The solvent was removed under reduced pressure and the residue was loaded onto a SNAP silica cartridge (25 g) and purified by automated chromatography (SP4) using a 0 - 50% gradient of ethyl acetate in cyclohexane (20 CV). Evaporation of the solvent under reduced pressure afforded **155** (66 mg, 63%) as a yellow solid.

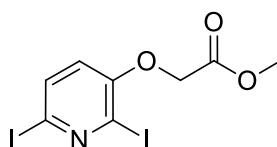
¹H NMR (400 MHz, DMSO-*d*₆) δ 6.26 (d, *J* = 1.7 Hz, 1 H), 6.01 (d, *J* = 1.7 Hz, 1 H), 3.79 (s, 3 H), 2.98 (s, 6 H); MS (ES+) *m/z* 188.8 [M + H]⁺.

4-Methoxy-*N*²,*N*²-dimethyl-*N*⁶-(tetrahydro-2H-pyran-4-yl)pyridine-2,6-diamine 156

Was prepared as for **120** from 4-amino-THP (0.03 mL, 0.24 mmol), Pd₂(dba)₃ (7.4 mg, 8.0 μmol), DavePhos (9.5 mg, 0.02 mmol), **155** (30 mg, 0.16 mmol) and sodium *tert*-butoxide (21.6 mg, 0.23 mmol) at 120 °C for 15 min. The solvent was evaporated under reduced pressure and the residue was loaded onto a SNAP silica cartridge (10 g), purified by

automated chromatography (SP4) using a 0 - 10% gradient of methanol in DCM (20 CV). The appropriate fractions were combined and evaporated under reduced pressure to give the impure product, which was purified further by MDAP on a Sunfire C18 column using acetonitrile water with a formic acid modifier. The solvent was evaporated under reduced pressure. The residue was eluted through a hydrogen carbonate column with methanol. Evaporation of the solvent under reduced pressure afforded **156** (5 mg, 12%) as a yellow oil. ¹H NMR (400 MHz, DMSO-d₆) δ 5.93 (d, *J* = 7.3 Hz, 1 H), 5.34 (d, *J* = 1.7 Hz, 1 H), 5.29 (d, *J* = 1.7 Hz, 1 H), 3.88 - 3.81 (m, 2 H), 3.81 - 3.74 (m, 1 H), 3.66 (s, 3 H), 3.41 - 3.34 (m, 2 H), 2.90 (s, 6 H), 1.9 - 1.82 (m, 2 H), 1.56 - 1.45 (m, 2 H); MS (ES+) *m/z* 251.95 [M + H]⁺.

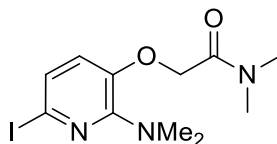
Methyl 2-((2,6-diiodopyridin-3-yl)oxy)acetate 157



Was prepared as for **145a** from **144** (400 mg, 1.15 mmol), triphenylphosphine (605 mg, 2.31 mmol), diisopropylazodicarboxylate (0.45 mL, 2.31 mmol) and methyl hydroxyacetate (0.18 mL, 2.31 mmol) at rt for 40 min. The usual purification afforded **157** (366 mg, 76 %) as a white solid.

¹H NMR (400 MHz, DMSO-d₆) δ 7.71 (d, *J* = 8.4 Hz, 1 H), 7.09 (d, *J* = 8.4 Hz, 1 H), 4.98 (s, 2 H), 3.69 (s, 3 H); MS (ES+) *m/z* 419.5 [M + H]⁺.

2-((2-(Dimethylamino)-6-iodopyridin-3-yl)oxy)-*N,N*-dimethylacetamide 158a

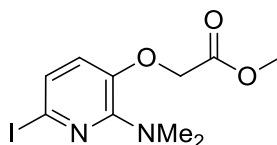


Was prepared as for **146a** from dimethylamine (3.5 mL, 69.10 mmol) and **157** (368 mg, 0.88 mmol) at 180 °C for 30 min. The usual purification afforded **158a** (71 mg, 23%) as a green

oil.

¹H NMR (400 MHz, CDCl₃) δ 7.02 (d, *J* = 8.0 Hz, 1 H), 6.68 (d, *J* = 8.0 Hz, 1 H), 4.65 (s, 2 H), 3.06 (s, 3 H), 3.03 (s, 6 H), 3.00 (s, 3 H); MS (ES+) *m/z* 349.73 [M + H]⁺.

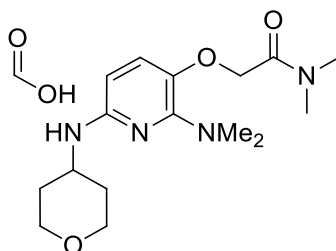
Methyl 2-((2-(dimethylamino)-6-iodopyridin-3-yl)oxy)acetate 158b



Compound **158b** was also isolated (71 mg, 24%) as an orange oil.

¹H NMR (400 MHz, CDCl₃) δ 7.02 (d, *J* = 8.0 Hz, 1 H), 6.59 (d, *J* = 8.0 Hz, 1 H), 4.59 (s, 2 H), 3.81 (s, 3 H), 3.04 (s, 6 H); MS (ES+) *m/z* 336.67 [M + H]⁺.

2-((2-(Dimethylamino)-6-((tetrahydro-2H-pyran-4-yl)amino)pyridin-3-yl)oxy)-*N,N*-dimethylacetamide formate 159

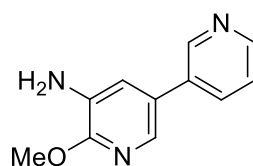


Was prepared as for **120** from 4-amino-THP (0.03 mL, 0.30 mmol), Pd₂(dba)₃ (7.3 mg, 8.02 μmol), DavePhos (11.8 mg, 0.03 mmol), **158a** (70 mg, 0.20 mmol) and sodium *tert*-butoxide (27.0 mg, 0.28 mmol). The solvent was evaporated under reduced pressure and the residue was loaded onto a SNAP silica cartridge (10 g), purified by automated chromatography (SP4) using a 0 - 60% gradient of ethyl acetate in cyclohexane. The appropriate fractions were combined and evaporated under reduced pressure to give the impure product, which was purified further by MDAP on a Sunfire C18 column using acetonitrile water with a

formic acid modifier. The solvent was evaporated under reduced pressure to give **159** (2 mg, 3 %) as an orange oil.

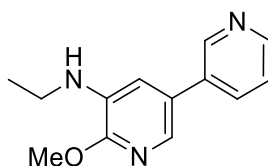
¹H NMR (400 MHz, CDCl₃) δ 8.21 (s, 1 H), 7.08 (d, *J* = 8.3 Hz, 1 H), 5.78 (d, *J* = 8.3 Hz, 1 H), 4.54 (s, 2 H), 4.00 (dt, ²*J* = 11.6, *J* = 2.7 Hz, 2 H), 4.0 – 3.82 (br. s, 1 H), 3.73 - 3.64 (m, 1 H), 3.51 (td, ²*J* = 11.6, *J* = 11.6, 2.7 Hz, 2 H), 3.03 (s, 3 H), 2.99 (s, 3 H), 2.98 (s, 6 H), 2.06 - 1.99 (br. m, 2 H), 1.56 - 1.45 (m, 2 H); MS (ES+) *m/z* 322.91 [M + H]⁺.

6-Methoxy-[3,3'-bipyridin]-5-amine **169**



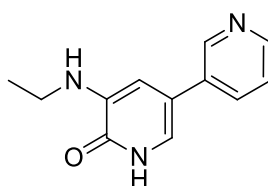
3-Pyridylboronic acid (1.45 g, 11.82 mmol), Pd(dppf)Cl₂ (1.08 g, 1.48 mmol) and K₂CO₃ (3.13 g, 22.66 mmol) were added to a solution of 5-bromo-2-(methoxy)-3-pyridinamine **168** (2 g, 9.85 mmol) in 1,4-dioxane (3 mL) and water (7.5 mL). The reaction mixture was refluxed for 2 h. The reaction mixture was cooled to rt and the solvent was removed under reduced pressure. The residue was loaded onto a SNAP silica cartridge (100 g), purified by automated chromatography (SP4) using a 0 - 100% gradient of ethyl acetate in cyclohexane. The appropriate fractions were combined and evaporated under reduced pressure to give **169** (1.5 g, 76 %) as a white solid.

¹H NMR (400 MHz, DMSO-d₆) δ 8.77 (d, ⁴*J* = 2.0 Hz, 1 H), 8.53 (dd, *J* = 4.8 Hz, ⁴*J* = 2.0 Hz, 1 H), 7.95 (dt, *J* = 8.0 Hz, ⁴*J* = 2.0 Hz, 1 H), 7.70 (d, ⁴*J* = 2.2 Hz, 1 H), 7.45 (dd, *J* = 8.0, 4.8 Hz, 1 H), 7.16 (d, ⁴*J* = 2.2 Hz, 1 H), 5.14 (s, 2 H), 3.34 (s, 3 H); ¹³C NMR (101 MHz, DMSO-d₆) δ 152.0, 148.1, 147.1, 133.6, 132.7, 130.4, 128.7, 127.0, 123.8, 116.7, 53.0; IR (cm⁻¹) 3360, 3302, 3192, 1584; 1473, 1397, 1228, 1022; HRMS (TOF): M + H calcd for C₁₁H₁₂N₃O 202.0975, found 202.0976; mp = 115 °C.

N-Ethyl-6-methoxy-[3,3'-bipyridin]-5-amine 170

Acetaldehyde (0.03 mL, 0.50 mmol) and acetic acid (0.57 mL, 9.94 mmol) were added to a solution of **169** (100 mg, 0.50 mmol) in THF (3 mL). Sodium triacetoxyborohydride (211 mg, 0.99 mmol) was added after stirring for 1 h at rt. The reaction mixture was stirred at rt for 19 h and refluxed for 20 h. The solvent was removed under reduced pressure and the residue was loaded onto a SNAP silica cartridge (10 g), purified by automated chromatography (SP4) using a 0 - 100% gradient of ethyl acetate in cyclohexane. The appropriate fractions were combined and evaporated under reduced pressure to give **170** (50 mg, 44 %) as a clear oil.

¹H NMR (400 MHz, DMSO-d₆) δ 8.86 (d, ⁴J = 2.0 Hz, 1 H), 8.53 (dd, J = 4.8 Hz, ⁴J = 2.0 Hz, 1 H), 8.04 (dt, J = 7.9 Hz, ⁴J = 2.0 Hz, 1 H), 7.68 (d, ⁴J = 2.2 Hz, 1 H), 7.45 (dd, J = 7.9, 4.8 Hz, 1 H), 7.02 (d, ⁴J = 2.2 Hz, 1 H), 5.23 (t, J = 5.6 Hz, 1 H), 3.92 (s, 3 H), 3.25 - 3.16 (m, 2 H), 1.18 (t, J = 7.2 Hz, 3 H); MS (ES+) *m/z* 230.2 [M + H]⁺.

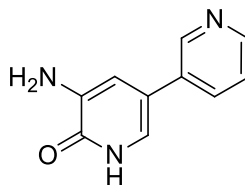
5-(Ethylamino)-[3,3'-bipyridin]-6(1H)-one 171

Boron tribromide (0.21 mL of a 1 M solution in DCM, 0.21 mmol) was added dropwise to a cold (0 °C) solution of **170** (47 mg, 0.21 mmol) in DCM (5 mL). After stirring for 2 h at rt, the reaction mixture was filtered through a 20 g silica SPE cartridge, and the product was eluted using 100% ethyl acetate (3 CV), 20% methanol in ethyl acetate (5 CV) and 20% methanolic ammonia (2 N) in ethyl acetate. The appropriate fractions were combined and

solvent was removed under reduced pressure to give the crude product, which was purified by automated chromatography (SP4). The residue was loaded onto a SNAP silica cartridge (10 g) and eluted with a 0 - 20% gradient of methanol in DCM. The appropriate fractions were combined and evaporated under reduced pressure to give the crude product. The residue was purified further by MDAP on a Sunfire C18 column using acetonitrile water with a formic acid modifier. The solvent was evaporated under reduced pressure giving **171** (15 mg, 34%) as a white solid.

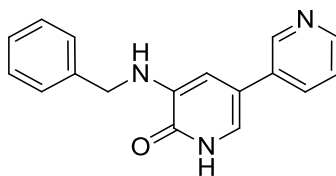
¹H NMR (400 MHz, DMSO-d₆) δ 11.81 - 11.65 (br. s, 1 H), 8.80 (d, ⁴J = 1.8 Hz, 1 H), 8.46 (dd, J = 4.8 Hz, ⁴J = 1.8 Hz, 1 H), 7.96 (dt, J = 8.0 Hz, ⁴J = 1.8 Hz, 1 H), 7.39 (dd, J = 8.0, 4.8 Hz, 1 H), 7.04 (d, ⁴J = 2.3 Hz, 1 H), 6.52 (d, ⁴J = 2.3 Hz, 1 H), 5.38 (t, J = 5.5 Hz, 1 H), 3.15 (qd, J = 7.2, 5.5 Hz, 2 H), 1.19 (t, J = 7.2 Hz, 3 H); MS (ES+) m/z 216.07 [M + H]⁺.

5-Amino-[3,3'-bipyridin]-6(1H)-one **165**



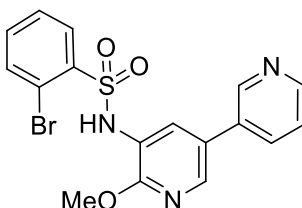
Was prepared as for **171** from **169** (100 mg, 0.50 mmol) and boron tribromide (0.50 mL of a 1 M solution in DCM, 0.50 mmol). The reaction mixture was loaded onto a SNAP silica cartridge (25 g), and purified by automated chromatography (SP4) using a 0 - 20% gradient of methanolic ammonia (2 N) in DCM. The appropriate fractions were combined and evaporated under reduced pressure to give **165** (78 mg, 84 %) as a yellow solid.

¹H NMR (400 MHz, DMSO-d₆) δ 11.73 - 11.63 (br. s, 1 H), 8.71 (d, ⁴J = 1.9 Hz, 1 H), 8.46 (dd, J = 4.8 Hz, ⁴J = 1.9 Hz, 1 H), 7.87 (dt, J = 8.0 Hz, ⁴J = 1.9 Hz, 1 H), 7.39 (dd, J = 8.0, 4.8 Hz, 1 H), 7.05 (s, 1 H), 6.80 (d, ⁴J = 2.3 Hz, 1 H), 5.23 (s, 2 H); MS (ES+) m/z 188.14 [M + H]⁺.

5-(Benzylamino)-[3,3'-bipyridin]-6(1H)-one 172

Benzaldehyde (0.04 mL, 0.42 mmol) was added to a solution of **165** (78 mg, 0.42 mmol) and acetic acid (0.48 mL, 8.33 mmol) in THF (3 mL). After stirring for 1 h at rt, sodium triacetoxyborohydride (177 mg, 0.83 mmol) was added. After stirring for 1 h at rt, the solvent was removed under reduced pressure and the residue was loaded onto a SNAP silica cartridge (25 g), and purified by automated chromatography (SP4) using a 0 - 10% gradient of methanol in DCM. The appropriate fractions were combined and evaporated under reduced pressure to give the crude product. The residue was purified further by automated chromatography (SP4), using a 0 - 10% gradient of methanol in DCM. The appropriate fractions were combined and the solvent was removed under reduced pressure to give **172** (70 mg, 61%) as a blue solid.

¹H NMR (400 MHz, DMSO-d₆) δ 11.78 - 11.68 (br. s, 1 H), 8.66 (d, ⁴J = 1.9 Hz, 1 H), 8.43 (dd, J = 4.6 Hz, ⁴J = 1.9 Hz, 1 H), 7.83 (dt, J = 8.0 Hz, ⁴J = 1.9 Hz, 1 H), 7.40 - 7.29 (m, 5 H), 7.25 - 7.18 (m, 1 H), 7.03 (s, 1 H), 6.46 (d, ⁴J = 2.3 Hz, 1 H), 6.18 (t, J = 6.4 Hz, 1 H), 4.40 (d, J = 6.4 Hz, 2 H); MS (ES+) *m/z* 278.2 [M + H]⁺.

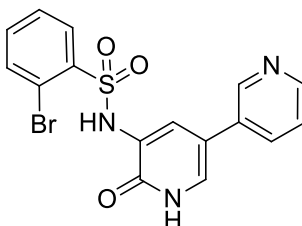
2-Bromo-N-(6-methoxy-[3,3'-bipyridin]-5-yl)benzenesulfonamide 173

2-Bromobenzenesulfonyl chloride (127 mg, 0.50 mmol) and DIPEA (0.09 mL, 0.50 mmol) were added to a solution of **169** (100 mg, 0.50 mmol) in DCM (5 mL). The reaction mixture

was stirred for 18 h at rt and refluxed for 4 h. 2-Bromobenzenesulfonyl chloride (127 mg, 0.50 mmol) and pyridine (0.04 mL, 0.50 mmol) were added to the reaction mixture which was stirred for 17 h at rt. The reaction mixture was concentrated under reduced pressure and the residue loaded onto a SNAP silica cartridge (25 g), purified by automated chromatography (SP4) using a 0 - 100% gradient of ethyl acetate in cyclohexane. The appropriate fractions were combined and evaporated under reduced pressure to give **173** (164 mg, 79%) as a clear oil.

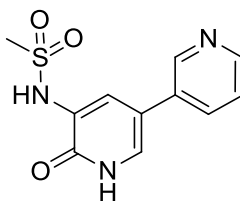
¹H NMR (400 MHz, DMSO-d₆) δ 10.09 (s, 1 H), 8.79 (d, ⁴J = 1.9 Hz, 1 H), 8.58 (dd, J = 4.7 Hz, ⁴J = 1.9 Hz, 1 H), 8.34 (d, ⁴J = 2.3 Hz, 1 H), 7.99 (dt, J = 8.0 Hz, ⁴J = 1.9 Hz, 1 H), 7.97 - 7.93 (m, 1 H), 7.89 - 7.86 (m, 1 H), 7.84 (d, ⁴J = 2.3 Hz, 1 H), 7.56 - 7.51 (m, 2 H), 7.49 (dd, J = 8.0, 4.7 Hz, 1 H), 3.67 (s, 3 H); MS (ES+) *m/z* 421.99 [M + H]⁺.

2-Bromo-N-(6-oxo-1,6-dihydro-[3,3'-bipyridin]-5-yl)benzenesulfonamide 174



Was prepared as for **171** from **173** (164 mg, 0.39 mmol) and boron tribromide (0.39 mL of a 1 M solution in DCM, 0.39 mmol). The usual purification afforded **174** (11 mg, 7 %) as a white solid.

¹H NMR (400 MHz, DMSO-d₆) δ 12.5 - 12.24 (br. s, 1 H), 9.52 - 9.36 (br. s, 1 H), 8.67 (s, 1 H), 8.50 (d, J = 4.8 Hz, 1 H), 8.17 (dd, J = 7.9 Hz, ⁴J = 1.9 Hz, 1 H), 7.9 - 7.79 (br. s, 2 H), 7.63 - 7.50 (m, 4 H), 7.43 (dd, J = 7.9, 4.8 Hz, 1 H); MS (ES+) *m/z* 405.95 [M + H]⁺.

***N*-(6-Oxo-1,6-dihydro-[3,3'-bipyridin]-5-yl)methanesulfonamide 176**

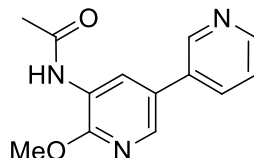
Methanesulfonyl chloride (0.04 mL, 0.50 mmol) and DIPEA (0.09 mL, 0.50 mmol) were added to a solution of **169** (100 mg, 0.50 mmol) in DCM (5 mL). The mixture was stirred for 17 h at rt, then refluxed for 2 h. Methanesulfonyl chloride (0.04 mL, 0.50 mmol) and pyridine (0.04 mL, 0.50 mmol) were added to the reaction mixture. After refluxing for 2 h, methanesulfonyl chloride (0.04 mL, 0.50 mmol) and pyridine (0.04 mL, 0.50 mmol) were added. After refluxing for 16 h, the solvent was removed under reduced pressure. The residue was loaded onto a SNAP silica cartridge (25 g), and purified by automated chromatography (SP4) using a 0 - 10% gradient of methanol in DCM. The appropriate fractions were combined and evaporated under reduced pressure to give a mixture of **175a** and **175b** (2.2 : 1) (129 mg) as a yellow oil.

The mixture of products (80 mg) was taken up in DMF (5 mL) and treated with cyclohexyl iodide (0.06 mL, 0.49 mmol). After refluxing for 2 h, the solvent was removed under reduced pressure and the residue was loaded onto a SNAP silica cartridge (10 g), and partially purified by automated chromatography (SP4) using a 0 - 20% gradient of methanol in DCM. The appropriate fractions were combined and evaporated under reduced pressure to give the crude product. The residue was taken up in methanolic DMSO (1 mL of a 1:1 mixture) and purified by MDAP on a Waters Xbridge C18 column using ammonium bicarbonate (10 mM in methanol, adjusted to pH 10 with ammonia). The solvent was removed under reduced pressure to give **176** (5 mg, 6% over 2 steps) as a white solid.

¹H NMR (400 MHz, DMSO-*d*₆) δ 12.55 - 12.0 (br. s, 1H), 9.5 - 9.0 (br. s, 1H), 8.78 (d, ⁴*J* = 1.8 Hz, 1 H), 8.51 (dd, *J* = 4.8 Hz, ⁴*J* = 1.8 Hz, 1 H), 7.95 (d, *J* = 8.0 Hz, 1 H), 7.67 (s, 1 H),

7.63 (s, 1 H), 7.44 (dd, $J = 8.0, 4.8$ Hz, 1 H), 3.12 (s, 3 H); MS (ES+) m/z 266.08 [M + H]⁺.

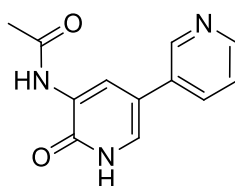
***N*-(6-Methoxy-[3,3'-bipyridin]-5-yl)acetamide 177**



Acetyl chloride (0.04 mL, 0.50 mmol) and DIPEA (0.09 mL, 0.50 mmol) were added to a solution of **169** (100 mg, 0.50 mmol) in DCM (5 mL). After stirring for 17 h at rt, the solvent was removed under reduced pressure. The residue was loaded onto a SNAP silica cartridge (10 g), purified by automated chromatography (SP4) using a 0 - 10% gradient of methanol in DCM. The appropriate fractions were combined and evaporated under reduced pressure to give **177** (116 mg, 96 %) as an off-white solid.

¹H NMR (400 MHz, DMSO-*d*₆) δ 9.55 (s, 1 H), 8.83 (d, ⁴ $J = 1.8$ Hz, 1 H), 8.64 (d, ⁴ $J = 2.3$ Hz, 1 H), 8.58 (dd, $J = 4.8$ Hz, ⁴ $J = 1.8$ Hz, 1 H), 8.25 (d, ⁴ $J = 2.3$ Hz, 1 H), 8.01 (dt, $J = 7.9$, ⁴ $J = 1.8$ Hz, 1 H), 7.49 (dd, $J = 7.9, 4.8$ Hz, 1 H), 3.99 (s, 3 H), 2.14 (s, 3 H); MS (ES+) m/z 244.13 [M + H]⁺.

***N*-(6-Oxo-1,6-dihydro-[3,3'-bipyridin]-5-yl)acetamide 178**

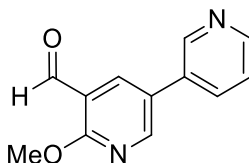


Was prepared as for **171** from **177** (116 mg, 0.48 mmol) and boron tribromide (0.48 mL of a 1 M solution in DCM, 0.48 mmol). The usual purification afforded **178** (75 mg, 69%)

¹H NMR (400 MHz, DMSO-*d*₆) δ 9.41 (s, 1 H), 8.74 (d, ⁴ $J = 1.9$ Hz, 1 H), 8.62 (d, ⁴ $J = 2.5$ Hz, 1 H), 8.50 (dd, $J = 4.8, ^4J = 1.9$ Hz, 1 H), 7.90 (dt, $J = 8.0, ^4J = 1.9$ Hz, 1 H), 7.55 (d, ⁴ J

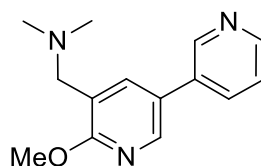
= 2.5 Hz, 1 H), 7.44 (dd, $J = 8.0, 4.8$ Hz, 1 H), 7.25 - 6.50 (br. s, 1H), 2.15 (s, 3 H); MS (ES+) m/z 230.09 [M + H]⁺.

6-(Methoxy)-3,3'-bipyridine-5-carbaldehyde **180**



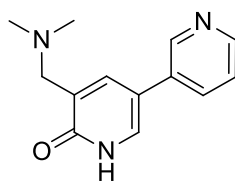
A mixture of K₂CO₃ (1.35 g, 9.75 mmol), 3-pyridylboronic acid (625 mg, 5.09 mmol), 5-bromo-2-methoxynicotinaldehyde (916 mg, 4.24 mmol), Pd(dppf)Cl₂ (465 mg, 0.64 mmol) in 1,4-dioxane (3 mL) and water (0.75 mL) was degassed with nitrogen for 0.5 h and then heated in an Emrys Optimizer microwave at 100 °C for 0.5 h. The solvent was evaporated under reduced pressure and the residue was loaded onto a SNAP silica cartridge (100 g) and purified by automated chromatography (SP4) using a 0 - 5% gradient of methanol in DCM (15 CV). The appropriate fractions were combined and evaporated under reduced pressure to give **180** (669 mg, 74%) as a yellow solid.

¹H NMR (400 MHz, DMSO-d₆) δ 10.30 (s, 1 H), 8.96 (d, ⁴ $J = 1.9$ Hz, 1 H), 8.88 (d, ⁴ $J = 2.6$ Hz, 1 H), 8.61 (dd, $J = 4.8, ^4J = 1.9$ Hz, 1 H), 8.42 (d, ⁴ $J = 2.6$ Hz, 1 H), 8.17 (dt, $J = 8.0$ Hz, ⁴ $J = 1.9$ Hz, 1 H), 7.52 (dd, $J = 8.0, 4.8$ Hz, 1 H), 4.08 (s, 3 H); ¹³C NMR (101 MHz, DMSO-d₆) δ 188.8, 163.3, 150.9, 148.9, 147.4, 136.4, 134.1, 131.6, 127.0, 123.9, 118.2, 54.2; IR (cm⁻¹) 3060, 2864, 1685, 1471, 1288, 999; HRMS (TOF): M + H calcd for C₁₂H₁₁N₂O₂ 215.0815, found 208.0814; mp = 133.9 °C.

***N,N*-Dimethyl-1-[6-(methoxy)-3,3'-bipyridin-5-yl]methanamine 181**

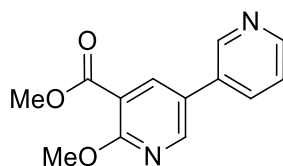
Dimethylamine (0.38 mL of a 2 M solution in THF, 0.76 mmol) and acetic acid (0.54 mL, 9.45 mmol) were added to a solution of 6-(methoxy)-3,3'-bipyridine-5-carbaldehyde **180** (81 mg, 0.38 mmol) in THF (3 mL). The mixture was stirred for 2 h before the addition of sodium triacetoxyborohydride (80 mg, 0.38 mmol). The mixture was stirred for 20 h at rt, then more dimethylamine (0.38 mL of a 2 M solution in THF, 0.76 mmol) and sodium triacetoxyborohydride (160 mg, 0.76 mmol) were added. After stirring for 16 h at rt, the reaction mixture was diluted with ethyl acetate (5 mL), and the pH was adjusted to 7 with a saturated solution of sodium hydrogen carbonate. The aqueous and organic phases were separated, the organic phase was dried through hydrophobic frit and concentrated under reduced pressure. The residue was loaded onto a SNAP silica cartridge (25 g) purified by automated chromatography (SP4) using a 0 - 20% gradient of methanolic ammonia (2 M) in DCM (20 CV). The appropriate fractions were combined and evaporated under reduced pressure to give **181** (65 mg, 71%) as a yellow oil.

^1H NMR (400 MHz, DMSO- d_6) δ 8.89 (d, $^4J = 1.9$ Hz, 1 H), 8.58 (dd, $J = 4.8$ Hz, $^4J = 1.9$ Hz, 1 H), 8.49 (d, $^4J = 2.2$ Hz, 1 H), 8.08 (dt, $J = 8.0$ Hz, $^4J = 1.9$ Hz, 1 H), 8.03 (d, $^4J = 2.2$ Hz, 1 H), 7.50 (dd, $J = 8.0, 4.8$ Hz, 1 H), 3.94 (s, 3 H), 3.62 - 3.51 (br. s, 2 H), 2.28 (s, 6 H); MS (ES+) m/z 244.0 $[\text{M}+\text{H}]^+$.

5-[(Dimethylamino)methyl]-3,3'-bipyridin-6(1H)-one **182**

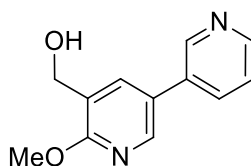
Was prepared as for **171** from boron tribromide (0.27 mL of a 1 M solution in DCM, 0.27 mmol) and **181** (65 mg, 0.27 mmol). The usual purification afforded **182** (49 mg, 80%) as a white solid.

^1H NMR (400 MHz, DMSO- d_6) δ 8.84 (d, $^4J = 1.8$ Hz, 1 H), 8.52 (dd, $J = 4.5$, $^4J = 1.8$ Hz, 1 H), 8.13 (d, $^4J = 2.4$ Hz, 1 H), 8.01 (dt, $J = 8.0$, $^4J = 1.8$ Hz, 1 H), 7.99 (d, $^4J = 2.4$ Hz, 1 H), 7.46 (dd, $J = 8.0$, 4.5 Hz, 1 H), 3.99 (s, 2 H), 3.47 - 3.25 (br. s, 1H), 2.67 (s, 6 H). MS (ES+) m/z 230.17 $[\text{M}+\text{H}]^+$.

Methyl 6-(methoxy)-3,3'-bipyridine-5-carboxylate **184**

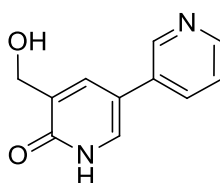
Was prepared as for **180** from K_2CO_3 (402 mg, 2.91 mmol), 3-pyridylboronic acid (186 mg, 1.52 mmol), methyl 5-bromo-2-(methoxy)-3-pyridinecarboxylate **183** (311 mg, 1.26 mmol) and $\text{Pd}(\text{dppf})\text{Cl}_2$ (139 mg, 0.19 mmol). The usual purification afforded **184** (262 mg, 85%) as a yellow solid.

^1H NMR (400 MHz, DMSO- d_6) δ 8.93 (d, $^4J = 1.8$ Hz, 1 H), 8.77 (d, $^4J = 2.5$ Hz, 1 H), 8.60 (dd, $J = 4.8$ Hz, $^4J = 1.8$ Hz, 1 H), 8.44 (d, $^4J = 2.5$ Hz, 1 H), 8.14 (dt, $J = 8.0$ Hz, $^4J = 1.8$ Hz, 1 H), 7.51 (dd, $J = 8.0$, 4.8 Hz, 1 H), 3.98 (s, 3 H), 3.85 (s, 3 H); MS (ES+) m/z 244.9 $[\text{M}+\text{H}]^+$.

[6-(Methoxy)-3,3'-bipyridin-5-yl]methanol 185

Lithium aluminium hydride (0.74 mL of a 1 M solution in Et₂O, 0.74 mmol) was added to a stirred solution of **184** (151 mg, 0.62 mmol) in THF (5 mL) under nitrogen at rt. After stirring for 3 h at rt, the reaction mixture was quenched with methanol (3 mL). The mixture was stirred for one hour further and allowed to stand overnight. The solvent was evaporated under reduced pressure, the residue was loaded onto a SNAP silica cartridge (25 g) and purified by automated chromatography (SP4) using a 0 - 75% gradient of ethyl acetate in cyclohexane (15 CV). The appropriate fractions were combined and evaporated under reduced pressure to give **185** (87 mg, 65%) as a white solid.

¹H NMR (400 MHz, DMSO-d₆) δ 8.88 (d, ⁴J = 2.0 Hz, 1 H), 8.57 (dd, J = 4.8 Hz, ⁴J = 2.0 Hz, 1 H), 8.43 (d, ⁴J = 2.4 Hz, 1 H), 8.06 (dt, J = 8.0, ⁴J = 2.0 Hz, 1 H), 8.03 (d, ⁴J = 2.4 Hz, 1 H), 7.49 (dd, J = 8.0, 4.8 Hz, 1 H), 5.31 (t, J = 5.6 Hz, 1 H), 4.53 (d, J = 5.6 Hz, 2 H), 3.93 (s, 3 H); MS (ES+) *m/z* 217.05 [M+H]⁺.

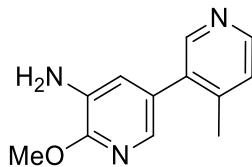
5-(Hydroxymethyl)-3,3'-bipyridin-6(1H)-one 186

Was prepared as for **171** from boron tribromide (0.37 mL of a 1 M solution in DCM, 0.37 mmol) and **185** (53 mg, 0.25 mmol). The usual purification afforded **186** (12.4 mg, 25%) as a white solid.

¹H NMR (600 MHz, DMSO-d₆) δ 12.08 - 11.82 (br. s, 1H), 8.79 (d, ⁴J = 1.9 Hz, 1 H), 8.49 (dd, J = 4.8 Hz, ⁴J = 1.9 Hz, 1 H), 7.93 (dt, J = 8.0, ⁴J = 1.9 Hz, 1 H), 7.80 (d, ⁴J = 2.6 Hz, 1

H), 7.73 (d, $^4J = 2.6$ Hz, 1 H), 7.43 (dd, $J = 8.0, 4.8$ Hz, 1 H), 5.22 - 5.05 (br. s, 1H), 4.37 (s, 2 H); MS (ES+) m/z 203.11 [M+H]⁺.

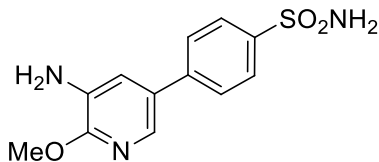
6-Methoxy-4'-methyl-[3,3'-bipyridin]-5-amine 188a



Was prepared as for **180** from **168** (110 mg, 0.54 mmol), Pd(dppf)Cl₂ (59.6 mg, 0.08 mmol), K₂CO₃ (172 mg, 1.25 mmol) and (4-methyl-3-pyridinyl)boronic acid **187a** (89 mg, 0.65 mmol). The usual purification afforded **188a** (110 mg, 94%) as a yellow oil.

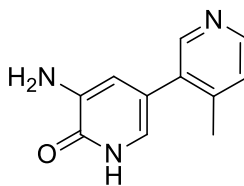
¹H NMR (400 MHz, DMSO-d₆) δ 8.40 (d, $J = 5.0$ Hz, 1 H), 8.32 (s, 1 H), 7.35 (d, $^4J = 2.2$ Hz, 1 H), 7.31 (d, $J = 5.0$ Hz, 1 H), 6.88 (d, $^4J = 2.2$ Hz, 1 H), 5.09 (s, 2 H), 3.91 (s, 3 H), 2.26 (s, 3 H); MS (ES+) m/z 215.8 [M+H]⁺.

4-(5-Amino-6-methoxypyridin-3-yl)benzenesulfonamide 188b



Was prepared as for **180** from **168** (110 mg, 0.54 mmol), Pd(dppf)Cl₂ (59.6 mg, 0.08 mmol), K₂CO₃ (172 mg, 1.25 mmol) and [4-(aminosulfonyl)phenyl]boronic acid **187b** (131 mg, 0.65 mmol). The usual purification afforded **188b** (60 mg, 40%) as a brown solid.

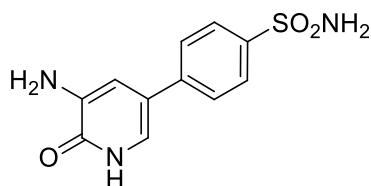
¹H NMR (400 MHz, DMSO-d₆) δ 7.86 (d, $J = 8.3$ Hz, 2 H), 7.76 - 7.71 (m, 3 H), 7.43 - 7.34 (br. s, 2 H), 7.19 (d, $^4J = 2.3$ Hz, 1 H), 5.15 (s, 2 H), 3.91 (s, 3 H); MS (ES+) m/z 280.01 [M+H]⁺.

5-Amino-4'-methyl-[3,3'-bipyridin]-6(1H)-one 189a

Boron tribromide (0.47 mL of a 1 M solution in DCM, 0.47 mmol) was added to a cold solution (5 °C) of **188a** (100 mg, 0.47 mmol) in DCM. The reaction mixture was stirred for 6 h at rt and refluxed for 16 h. The reaction mixture was cooled to 0 °C and quenched by the dropwise addition of water (7 mL). The organic and aqueous layers were separated. The aqueous layer was loaded onto an Oasis column (6 g) which had been previously conditioned with methanol and water, and eluted with 5% methanol in water. The appropriate fractions were combined and evaporated under reduced pressure to give the crude product. The residue was loaded onto a SNAP silica cartridge (10 g) and purified by automated chromatography (SP4) using a 0 - 100% gradient of ethyl acetate in cyclohexane, followed by a 0 - 20% gradient of methanolic ammonia (2 M) in DCM. The appropriate fractions were combined and evaporated under reduced pressure to give the crude product which was purified further. The residue was taken up in methanolic DMSO (1 mL of a 1:1 mixture) and purified by MDAP on a Waters Xbridge C18 column using ammonium bicarbonate (10 mM in methanol, adjusted to pH 10 with ammonia). The solvent was removed under reduced pressure to give **189a** (10 mg, 11%)

¹H NMR (400 MHz, DMSO-d₆) δ 11.70 - 11.44 (br. s, 1 H), 8.36 (d, *J* = 4.9 Hz, 1 H), 8.31 (s, 1 H), 7.27 (d, *J* = 4.9 Hz, 1 H), 6.65 (d, ⁴*J* = 2.3 Hz 1 H), 6.47 (d, ⁴*J* = 2.3 Hz, 1 H), 5.17 (s, 2 H), 2.27 (s, 3 H); MS (ES+) *m/z* 202.09 [M+H]⁺.

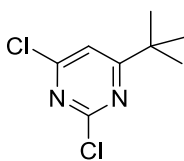
4-(5-Amino-6-oxo-1,6-dihydropyridin-3-yl)benzenesulfonamide 189b



Boron tribromide (0.20 mL of a 1 M solution in DCM, 0.20 mmol) was added to a cold solution (5 °C) of **188b** (55 mg, 0.20 mmol) in DCM (5 mL). The mixture was refluxed for 20 h, then loaded onto a silica column (10 g), flushed through with ethyl acetate, then 20% ethanol in ethyl acetate. The appropriate fractions were combined and evaporated under reduced pressure to give the crude product which was purified further. The residue was taken up in methanolic DMSO (1 mL of a 1:1 mixture) and purified by MDAP on a Sunfire C18 column using acetonitrile water with a formic acid modifier. The solvent was removed under reduced pressure to give **189b** (7 mg, 13%).

¹H NMR (400 MHz, DMSO-d₆) δ 11.81 - 11.61 (br. s, 1 H), 7.80 (d, *J* = 8.4 Hz, 2 H), 7.66 (d, *J* = 8.4 Hz, 2 H), 7.35 (s, 2 H), 7.08 (d, ⁴*J* = 2.2 Hz, 1 H), 6.84 (d, ⁴*J* = 2.2 Hz, 1 H), 5.24 (s, 2 H); MS (ES+) *m/z* 264.17 [M+H]⁺.

2,4-Dichloro-6-(1,1-dimethylethyl)pyrimidine 195¹³²

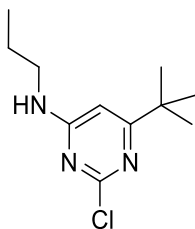


tert-Butylmagnesium chloride (45.7 mL of a 1 M solution in THF, 45.7 mmol) was added dropwise (over 50 min) to a cold stirred solution (0 °C) of 2,4,6-trichloropyrimidine (5 mL, 43.5 mmol) and copper(I) iodide (0.41 g, 2.17 mmol) in THF (40 mL). The reaction was stirred for 1 h at 0 °C, then the reaction was quenched with an excess of ammonium chloride (80 mL of a saturated solution). The resulting mixture was diluted with ethyl acetate (50

mL). The aqueous and organic phases were separated and the organic layer was dried through a hydrophobic frit and concentrated under reduced pressure. The residue was loaded onto a SNAP silica cartridge (100 g) and purified by automated chromatography (SP4) using a 0 - 40% gradient of DCM in cyclohexane (15 CV). The appropriate fractions were combined and evaporated under reduced pressure to give the required product **195** (8.71 g, 98%) as a yellow solid.

^1H NMR (400 MHz, DMSO- d_6) δ 7.81 (s, 1 H), 1.29 (s, 9 H); ^{13}C NMR (101MHz, DMSO- d_6) δ 183.2, 161.8, 158.7, 116.9, 38.1, 28.7; HRMS (TOF): M + H calcd for $\text{C}_8\text{H}_{11}\text{N}_2\text{Cl}_2$ 205.0299, found 205.0295; IR (cm^{-1}) 2967, 1554, 1519, 1257, 826; mp = 61 °C.

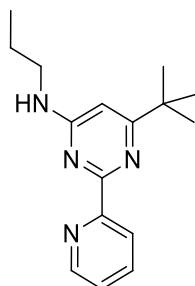
2-Chloro-6-(1,1-dimethylethyl)-*N*-propyl-4-pyrimidinamine **197**



n-Propylamine **196a** (0.06 mL, 0.73 mmol) and K_2CO_3 (152 mg, 1.10 mmol) were added to a solution of **195** (150 mg, 0.73 mmol) in *N,N*-dimethylacetamide (5 mL). After stirring for 4 h at rt, water (5 mL) was added to the reaction mixture, followed by ethyl acetate (10 mL). The aqueous and organic phases were separated and the organic layer was dried through a hydrophobic frit and concentrated under reduced pressure. The residue was loaded onto a SNAP silica cartridge (25 g) and purified by automated chromatography (SP4) using a 0 - 20% gradient of ethyl acetate in cyclohexane (20 CV). The appropriate fractions were combined and evaporated under reduced pressure to give the required product **197** (98 mg, 59%) as a colourless oil.

^1H NMR (400 MHz, DMSO- d_6) δ 7.77 (s, 1 H), 6.36 (s, 1 H), 3.21 (d, J = 6.1 Hz, 2 H), 1.58 - 1.43 (m, 2 H), 1.21 (s, 9H), 0.89 (t, J = 7.5 Hz, 3 H); MS (ES+) m/z 228.0 $[\text{M}+\text{H}]^+$.

6-(1,1-Dimethylethyl)-*N*-propyl-2-(2'-pyridyl)-4-pyrimidinamine 199

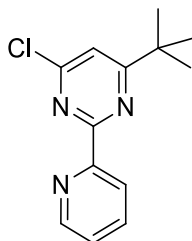


(2-Pyridyl)zinc bromide (0.88 mL of a 0.5 M solution in THF, 0.44 mmol), S-Phos (34.3 mg, 0.08 mmol) and palladium(II) acetate (9.4 mg, 0.04 mmol) were added to a suspension of **197** (95 mg, 0.42 mmol) in toluene (5 mL). The resulting mixture was degassed with nitrogen for 0.5 h, and then stirred at 100 °C for 18 h under nitrogen. Further (2-pyridyl)zinc bromide (4.20 mL of a 0.5 M solution in THF, 2.1 mmol) was added and the reaction mixture was stirred at 100 °C for 4 h under nitrogen. After cooling to rt, the solvent was evaporated under reduced pressure, and the residue was loaded onto a SNAP silica cartridge (25 g) and partially purified by automated chromatography (SP4), using a 0 - 50% gradient of ethyl acetate in cyclohexane (15 CV). The appropriate fractions were combined and evaporated under reduced pressure to give the impure product, which was purified further by MDAP on a Waters Xbridge C18 column using ammonium bicarbonate (10 mM in methanol, adjusted to pH 10 with ammonia). The solvent was evaporated under a stream of nitrogen in the Radleys blowdown apparatus to give **199** (4 mg, 8%) as a colourless oil.

^1H NMR (400 MHz, DMSO- d_6) δ 8.69 (d, J = 4.0 Hz, 1 H), 8.27 (d, J = 7.5 Hz, 1 H), 7.93 - 7.86 (m, 1 H), 7.44 (dd, J = 7.5, 4.8 Hz, 1 H), 7.44 - 7.34 (br. s, 1 H), 6.48 - 6.39 (br. s, 1 H),

3.34 (s, 2 H), 1.63 - 1.54 (m, 2 H), 1.28 (s, 9 H), 0.93 (t, $J = 7.5$ Hz, 3 H); MS (ES+) m/z 271.0 [M+H]⁺.

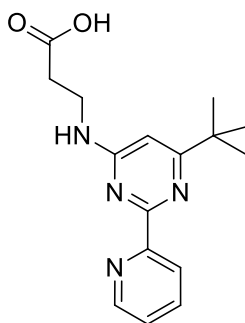
4-Chloro-6-(*tert*-butyl)-2-(2'-pyridyl)pyrimidine 204



Sodium ethoxide in ethanol (2.44 mL, 6.54 mmol) and ethyl 4,4-dimethyl-3-oxopentanoate **169** (1.16 mL, 6.54 mmol) were added to a solution of 2-pyridinecarboximidamide hydrochloride **202** (1.03 g, 6.54 mmol) in ethanol (10 mL). The reaction mixture was heated under reflux for 64 h. After cooling to rt, the solid was collected by filtration, and dried under reduced pressure to give the crude **203** (1.1 g) as a white solid.

Phosphorus oxychloride (2 mL, 21.46 mmol) was added to **203** (386 mg, 1.684 mmol) and the mixture was heated at 107 °C for 4 h. After cooling to rt, the reaction was cautiously quenched by dropwise addition of a saturated aqueous sodium acetate solution (until the pH reached 6-7). The aqueous solution was extracted with DCM (2 x 30 mL). The combined organic extracts were dried through a hydrophobic frit and concentrated under reduced pressure to give **204** (139 mg, 24 % over 2 steps) as a beige solid.

¹H NMR (400 MHz, DMSO-d₆) δ 8.78 (d, $J = 4.0$ Hz, 1 H), 8.40 (d, $J = 7.8$ Hz, 1 H), 8.01 (td, $J = 7.8, 1.8$ Hz, 1 H), 7.72 (s, 1 H), 7.59 - 7.55 (m, 1 H), 1.39 (s, 9 H); ¹³C NMR (126 MHz, DMSO-d₆) δ 180.2, 162.9, 161.5, 153.4, 149.8, 137.3, 125.6, 123.9, 116.6, 37.9, 28.9; IR (cm⁻¹) 2974, 1555, 1522, 1369, 1299, 827, 768, 679; HRMS (TOF): M + H calcd for C₁₃H₁₄ClN₃ 248.0955, found 248.0944; mp = 244.8 °C.

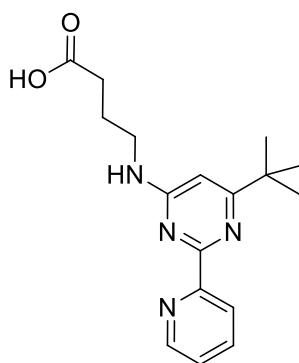
3-((6-(*Tert*-butyl)-2-(pyridin-2-yl)pyrimidin-4-yl)amino)propanoic acid 11

Ethyl 3-aminopropanoate hydrochloride **205** (113 mg, 0.74 mmol) and DIPEA (0.21 mL, 1.23 mmol) were added to a solution of **204** (152 mg, 0.61 mmol) in DMSO (0.5 mL). The mixture was heated at 150 °C in a Biotage Initiator microwave for 2 h. Ethyl 3-aminopropanoate hydrochloride (47.1 mg, 0.31 mmol) and DIPEA (0.11 mL, 0.61 mmol) were added to the reaction mixture which was heated at 150 °C in the microwave for 1 h. The reaction mixture was purified by MDAP on a Waters Xbridge C18 column using ammonium bicarbonate (10 mM in methanol, adjusted to pH 10 with ammonia) as eluant. The solvent was removed under reduced pressure to give the crude ethyl ester intermediate (204 mg). The residue was taken up in a mixture of THF/water (4 mL of a 3:1 mixture), lithium hydroxide monohydrate (25.7 mg, 0.61 mmol) was added and reaction mixture was stirred at rt for 20 h. The reaction mixture was concentrated under reduced pressure and the residue was purified by MDAP on a Waters Xbridge C18 column using ammonium bicarbonate (10 mM in methanol, adjusted to pH 10 with ammonia). The appropriate fractions were combined and concentrated under reduced pressure to give **11** (115 mg, 60%) as an off-white solid.

¹H NMR (400 MHz, DMSO-d₆) δ 8.69 (d, *J* = 4.6 Hz, 1 H), 8.28 (d, *J* = 7.8 Hz, 1 H), 7.89 (td, *J* = 7.8, 1.5 Hz, 1 H), 7.43 (ddd, *J* = 6.8, 4.6, 1.5 Hz, 1 H), 7.39 - 7.27 (br. s, 1 H), 6.46 (s, 1 H), 5.59 - 5.21 (br. s, 1H), 3.66 - 3.49 (br. s, 2 H), 2.44 (t, *J* = 6.8 Hz, 2 H), 1.28 (s, 9 H); ¹³C NMR (126 MHz, DMSO-d₆) δ 173.8, 163.4, 162.2, 156.3, 149.1, 136.5, 124.1,

123.3, 99.2 (br.), 59.8, 37.0, 36.6 (br.), 35.2, 29.1; IR (cm⁻¹) 2954, 1586, 1539, 1385, 1103, 746; HRMS (TOF): M + H calcd for C₁₆H₂₀N₄O₂ 301.1665, found 301.1652; mp = 183 °C (decomp).

4-((6-(*Tert*-butyl)-2-(pyridin-2-yl)pyrimidin-4-yl)amino)butanoic acid **208**

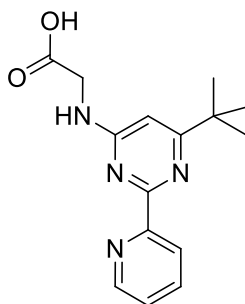


4-Aminobutanoic acid **206** (62.4 mg, 0.61 mmol) and DIPEA (0.32 mL, 1.82 mmol) were added to a solution of **204** (150 mg, 0.61 mmol) in DMSO (0.5 mL). The mixture was heated at 150 °C in a Biotage Initiator microwave for 2 h. The reaction mixture was purified by MDAP on a Waters Xbridge C18 column using ammonium bicarbonate (10 mM in methanol, adjusted to pH 10 with ammonia). The solvent was removed under reduced pressure to give the crude product. The residue was eluted through an aminopropyl cartridge (1 g) with 20% HCl (2M) in MeOH (3 CV of a 2 N solution). Evaporation of the solvent under reduced pressure afforded the crude product which was purified further by MDAP on a Waters Xbridge C18 column using ammonium bicarbonate (10 mM in methanol, adjusted to pH 10 with ammonia). The appropriate fractions were combined and concentrated under reduced pressure to give **208** (15 mg, 8 %) as a yellow solid.

¹H NMR (400 MHz, DMSO-d₆) δ 8.72 - 8.66 (br. s, 1 H), 8.29 (d, *J* = 7.8 Hz, 1 H), 7.90 (td, *J* = 7.8, 1.7 Hz, 1 H), 7.47 - 7.40 (m, 2 H), 6.44 (s, 1 H), 3.47 - 3.23 (m, 2 H) masked by water peak, 2.31 (t, *J* = 6.8 Hz, 2 H), 1.85 - 1.74 (m, 2 H), 1.29 (s, 9 H); MS (ES⁺) *m/z*

315.11 [M+H]⁺. The signal arising from the CO₂H proton could not be observed, either because of exchange on the NMR timescale, or masking by the water peak (3.47 - 3.23).

2-((6-(*Tert*-butyl)-2-(pyridin-2-yl)pyrimidin-4-yl)amino)acetic acid **209**

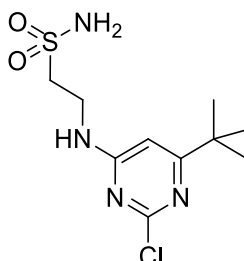


Ethyl glycinate hydrochloride **207** (60.9 mg, 0.44 mmol) and DIPEA (0.23 mL, 1.31 mmol) were added to a solution of **204** (108 mg, 0.44 mmol) in DMSO (0.5 mL). The mixture was heated at 150 °C in a Biotage Initiator microwave for 2 h. The reaction mixture was purified by MDAP on a Waters Xbridge C18 column using ammonium bicarbonate (10 mM in methanol, adjusted to pH 10 with ammonia). The appropriate fractions were combined and concentrated under reduced pressure to give the ethyl ester product (83 mg) as a yellow oil. The ester was taken up in aqueous THF (6 mL of a 1:1 mixture) and lithium hydroxide monohydrate (48.7 mg, 1.16 mmol) was added. After stirring for 3 h at rt, the solvent was removed under reduced pressure. The residue was purified by MDAP on Xbridge column using ammonium bicarbonate (10 mM in methanol, adjusted to pH 10 with ammonia). The solvent was removed under reduced pressure to give **209** (63 mg, 50%) as a yellow oil.

¹H NMR (500 MHz, DMSO-d₆) δ 8.69 (d, *J* = 4.3 Hz, 1 H), 8.27 (d, *J* = 8.0 Hz, 1 H), 7.96 - 7.85 (br. s, 1 H), 7.70 - 7.54 (br. s, 1 H), 7.48 - 7.41 (br. s, 1 H), 7.32 - 6.96 (br. s, 1 H), 6.65 - 6.51 (br. s, 1H), 4.19 - 4.04 (br. s, 2 H), 1.29 (s, 9 H); ¹³C NMR (126 MHz, DMSO-d₆) δ 174.5 (br.), 172.1, 163.4 (br.), 161.9, 157.8, 156.0, 149.1, 136.6, 124.3, 123.3, 99.4 (br.),

36.7, 29.1; IR (cm⁻¹) 3200 (br.), 2962, 1664, 1589, 1126; HRMS (TOF): M + H calcd for C₁₅H₁₉N₄O₂ 287.1503, found 287.1507; mp = 115 °C.

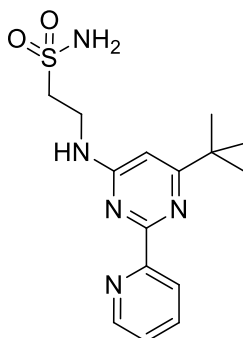
2-[2-Chloro-6-(1,1-dimethylethyl)-4-pyrimidinyl]amino}ethanesulfonamide 211



Was prepared as for **197** from **195** (150 mg, 0.73 mmol), K₂CO₃ (152 mg, 1.10 mmol) and 2-aminoethanesulfonamide **196b** (91 mg, 0.73 mmol). The usual work up and purification afforded **211** (91 mg, 43%) as a colourless oil.

¹H NMR (400 MHz, DMSO-d₆) δ 7.28 - 6.92 (br. s, 1H), 6.52 (s, 1 H), 3.77 (t, *J* = 6.9 Hz, 2 H), 3.45 (s, 2 H), 3.34 (t, *J* = 6.9 Hz, 2 H), 1.31 (s, 9 H); MS (ES+) *m/z* 293.1 [M+H]⁺.

2-[6-(1,1-Dimethylethyl)-2-(2'-pyridyl)-4-pyrimidinyl]amino}ethanesulfonamide 212

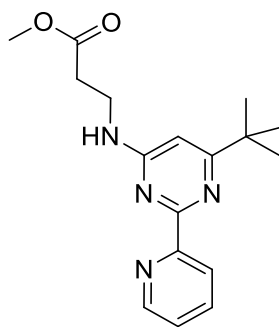


Was prepared as for **199** from **211** (91 mg, 0.31 mmol), (2-pyridyl)zincbromide (3.11 mL of a 0.5 M solution in THF, 1.55 mmol), S-Phos (38.3 mg, 0.09 mmol) and palladium(II)

acetate (10.5 mg, 0.05 mmol). The usual work up and purification afforded **212** (12 mg, 12%) as a colourless oil.

¹H NMR (400 MHz, DMSO-d₆) δ 8.68 (d, *J* = 4.3 Hz, 1 H), 8.35 (d, *J* = 7.7 Hz, 1 H), 7.92 (t, *J* = 7.7 Hz, 1 H), 7.52 (t, *J* = 5.8 Hz, 1 H), 7.47 (dd, *J* = 7.7, 4.3 Hz, 1 H), 7.19 - 7.07 (br. s, 2 H), 6.47 (s, 1 H), 3.87 - 3.76 (br. s, 2 H), 3.55 - 3.26 (m, 2 H) (partially masked by the water peak), 1.29 (s, 9 H), the signal arising from the NH₂ proton could not be observed, either because of exchange on the NMR timescale, or masking by the water peak (3.55 - 3.15); MS (ES+) *m/z* 336.0 [M+H]⁺.

Methyl 3-((6-(*tert*-butyl)-2-(pyridin-2-yl)pyrimidin-4-yl)amino)propanoate 221

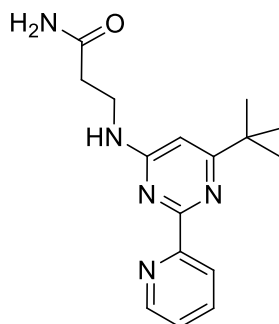


Was prepared as for **208** from methyl β-alaninate **213** (62.4 mg, 0.61 mmol), 4-chloro-6-(1,1-dimethylethyl)-2-(2'-pyridyl)pyrimidine **204** (150 mg, 0.61 mmol) and DIPEA (0.32 mL, 1.82 mmol). The usual work up and purification afforded **221** (60 mg, 32%) as an off-white solid.

¹H NMR (400 MHz, DMSO-d₆) δ 8.53 (d, *J* = 4.0 Hz, 1 H), 8.11 (d, *J* = 7.8 Hz, 1 H), 7.73 (td, *J* = 7.8, 1.9 Hz, 1 H), 7.31 - 7.24 (m, 2 H), 6.29 (s, 1 H), 3.53 - 3.43 (m, 2 H), 3.17 (s, 3 H), 2.49 (t, *J* = 6.7 Hz, 2 H), 1.11 (s, 9 H); ¹³C NMR (101 MHz, DMSO-d₆) δ 173.9 (br.), 172.0, 163.3, 162.2, 156.2, 149.1, 136.5, 124.2, 123.3, 51.4, 36.7, 36.3 (br.), 36.1 (br.), 33.5,

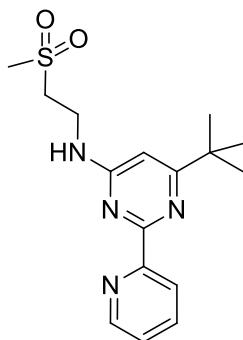
29.1; IR (cm⁻¹) 3280, 2959, 1733, 1603, 1363, 1198; HRMS (TOF): M + H calcd for C₁₇H₂₃N₄O₂ 315.1816, found 315.1816; mp = 128.6 °C.

3-((6-(*Tert*-butyl)-2-(pyridin-2-yl)pyrimidin-4-yl)amino)propanamide 222



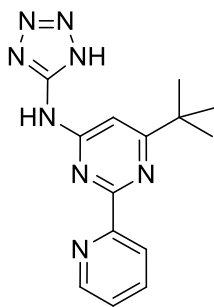
4-Chloro-6-(1,1-dimethylethyl)-2-(2'-pyridyl)pyrimidine **204** (150 mg, 0.61 mmol) and K₂CO₃ (126 mg, 0.91 mmol) were added to a solution of β-alaninamide **214** (53.4 mg, 0.61 mmol) in DMA (5 mL). The reaction was stirred at rt under nitrogen for 1 hour and heated at 100 °C for 19 h. Water and diethyl ether were added to the reaction mixture, the layers were separated and organic layer was extracted with water (x 3). The combined aqueous layer was concentrated under reduced pressure and loaded onto a SNAP silica cartridge (25 g), purified by automated chromatography (SP4), using a 0 - 20% gradient of methanol in DCM (15 CV). The appropriate fractions were combined and concentrated under reduced pressure to give **222** (88 mg, 49%) as a white solid.

¹H NMR (400 MHz, DMSO-d₆) δ 8.56 (d, *J* = 4.3 Hz, 1 H), 8.17 (d, *J* = 7.8 Hz, 1 H), 7.77 (td, *J* = 7.8, 1.9 Hz, 1 H), 7.34 - 7.29 (m, 2 H), 7.22 (t, *J* = 5.5 Hz, 1 H), 6.74 (br. s, 1 H), 6.34 (s, 1 H), 3.45 (br. s, 2 H), 3.26 - 3.21 (m, 2 H), 2.25 (t, *J* = 6.9 Hz, 1 H), 1.15 (s, 9 H); ¹³C NMR (126 MHz, DMSO-d₆) δ 174.4, 173.2, 163.9, 162.7, 156.7, 149.5, 136.9, 124.5, 123.6, 99.7 (br.), 37.1 (br. for 2C), 35.5, 29.6; IR (cm⁻¹) 3380, 3187, 2958, 1663, 1588, 1500, 1370, 1213, 672; HRMS (TOF): M + H calcd for C₁₆H₂₁N₅O 300.1824, found 300.1819; mp = 164.8 °C.

6-(Tert-butyl)-N-(2-(methylsulfonyl)ethyl)-2-(pyridin-2-yl)pyrimidin-4-amine 223

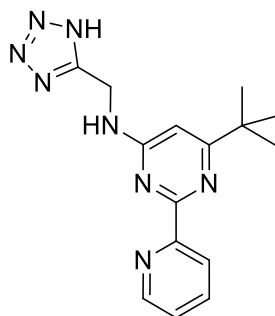
Was prepared as for **208** from [2-(methylsulfonyl)ethyl]amine hydrochloride **215** (97 mg, 0.61 mmol), 4-chloro-6-(1,1-dimethylethyl)-2-(2'-pyridyl)pyrimidine **204** (150 mg, 0.61 mmol) and DIPEA (0.32 mL, 1.82 mmol). The usual purification afforded **223** (150 mg, 74%) as a white solid.

^1H NMR (500 MHz, DMSO- d_6) δ 8.70 (d, $J = 4.4$ Hz, 1 H), 8.32 (d, $J = 7.7$ Hz, 1 H), 7.91 (td, $J = 7.7, 1.7$ Hz, 1 H), 7.57 (t, $J = 5.5$ Hz, 1 H), 7.45 (ddd, $J = 6.2, 4.4, 1.7$ Hz, 1 H), 6.51 (s, 1 H), 3.86 - 3.76 (br. s, 2 H), 3.44 (t, $J = 6.7$ Hz, 2 H), 3.08 (s, 3 H), 1.29 (s, 9 H); ^{13}C NMR (126 MHz, DMSO- d_6) δ 174.6 (br.), 163.1, 162.1, 156.0, 149.2, 136.6, 124.3, 123.4, 99.4 (br.), 52.8, 41.0, 36.7, 34.3 (br.), 29.1; IR (cm^{-1}) 3261, 2965, 1599, 1509, 1352, 1275, 1127, 975, 773; HRMS (TOF): $M + H$ calcd for $\text{C}_{16}\text{H}_{22}\text{N}_4\text{O}_2\text{S}$ 335.1542, found 335.1530; mp = 221 °C.

6-(Tert-butyl)-2-(pyridin-2-yl)-N-(1H-tetrazol-5-yl)pyrimidin-4-amine 224

A mixture of 4-chloro-6-(1,1-dimethylethyl)-2-(2'-pyridyl)pyrimidine **204** (150 mg, 0.61 mmol), 1H-tetrazol-5-amine **216** (51.5 mg, 0.61 mmol) and DIPEA (0.32 mL, 1.82 mmol) in DMSO (0.5 mL) was heated in Biotage Initiator microwave at 120 °C for 2, 2 and 5 h consecutively. The reaction mixture was taken up in methanolic DMSO (1.5 mL of a 2:1 mixture) and was purified by MDAP on a Waters Xbridge C18 column using ammonium bicarbonate (10 mM in methanol, adjusted to pH 10 with ammonia). The appropriate fractions were combined and concentrated under reduced pressure to give **224** (52 mg, 29%) as a white solid.

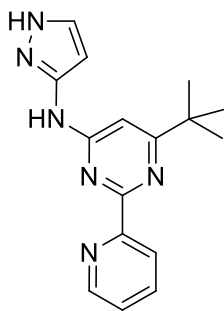
^1H NMR (400 MHz, DMSO- d_6) δ 16.15 - 14.95 (br. s, 1 H), 11.90 - 11.56 (br. s, 1 H), 8.97 (d, $J = 4.9$ Hz, 1 H), 8.62 (d, $J = 7.8$ Hz, 1 H), 8.17 (td, $J = 7.8, 1.8$ Hz, 1 H), 7.72 (dd, $J = 6.9, 4.9$ Hz, 1 H), 7.52 - 7.39 (br. s, 1 H), 1.52 (s, 9 H); MS (ES+) m/z 297.12 $[\text{M}+\text{H}]^+$.

N*-((1H-tetrazol-5-yl)methyl)-6-(*tert*-butyl)-2'-pyridylpyrimidin-4-amine **225*

A mixture of 4-chloro-6-(1,1-dimethylethyl)-2-(2'-pyridyl)pyrimidine **204** (150 mg, 0.61 mmol), (1H-tetrazol-5-ylmethyl)amine **217** (60 mg, 0.61 mmol) and DIPEA (0.32 mL, 1.82 mmol) in DMSO (0.5 mL) was heated in Biotage Initiator microwave at 150 °C for 2 x 2 h.

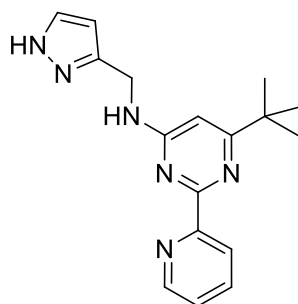
The reaction mixture was taken up in methanolic DMSO (1.5 mL of a 2:1 mixture) and was purified by MDAP on a Waters Xbridge C18 column using ammonium bicarbonate (10 mM in methanol, adjusted to pH 10 with ammonia). The appropriate fractions were combined and concentrated under reduced pressure to give **225** (55 mg, 29%) as a white solid.

¹H NMR (400 MHz, DMSO-d₆) δ 8.64 (d, *J* = 4.3 Hz, 1 H), 8.27 (d, *J* = 7.8 Hz, 1 H), 7.85 (td, *J* = 7.8, 1.5 Hz, 1 H), 7.52 - 7.44 (br. s, 1 H), 7.44 - 7.38 (m, 1 H), 7.33 - 6.96 (br. s, 1 H), 6.61 - 6.54 (br. s, 1 H), 4.72 - 4.55 (br. s, 2 H), 1.22 (s, 9 H); ¹³C NMR (126 MHz, DMSO-d₆) δ 174.8, 163.1, 161.4, 155.6, 149.1, 137.4, 124.9, 123.2, 41.4, 36.8, 29.1, 17.9, 13.0, IR (cm⁻¹) 1590, 1509, 1367, 677; HRMS (TOF): *M* + *H* calcd for C₁₅H₁₈N₈ 311.1733, found 311.1736; mp = 220.4 °C.

6-(1,1-Dimethylethyl)-N-1H-pyrazol-3-yl-2-(2'-pyridyl)-4-pyrimidinamine 226

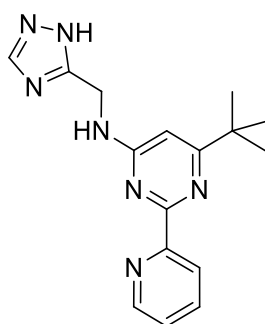
Was prepared as for **208** from **204** (101 mg, 0.41 mmol), DIPEA (0.21 mL, 1.22 mmol) and 1H-pyrazol-3-amine **218** (39.6 mg, 0.41 mmol). The MDAP was carried on Supelcosil ABZ+Plus column eluting with solvents A/B (A: water + 0.1% formic acid, B: MeCN:water 95:5 + 0.05% formic acid). The solvent was removed under reduced pressure to give a white solid. The solid was dissolved in methanol and passed through a hydrogen carbonate column which had been previously conditioned with methanol. The solution was dried under a stream of nitrogen in the Radleys blowdown apparatus to give **226** (9 mg, 8%) as a yellow oil.

^1H NMR (400 MHz, DMSO- d_6) δ 8.78 (d, $J = 4.0$ Hz, 1 H), 8.53 - 8.42 (m, 2 H), 7.99 (d, $J = 7.7$ Hz, 1 H), 7.58 - 7.50 (m, 2 H), 5.94 (d, $J = 2.8$ Hz, 1 H), 5.66 - 5.60 (br. s, 2 H), 1.45 - 1.34 (m, 9 H); MS (ES+) m/z 295.1 $[\text{M}+\text{H}]^+$.

6-(1,1-Dimethylethyl)-N-(1H-pyrazol-3-ylmethyl)-2-(2'-pyridyl)-4-pyrimidinamine 227

Was prepared as for **208** from **204** (101 mg, 0.41 mmol), DIPEA (0.21 mL, 1.22 mmol) and (1H-pyrazol-3-ylmethyl)amine **219** (39.6 mg, 0.41 mmol). The usual purification afforded **227** (17 mg, 14%) as a white solid.

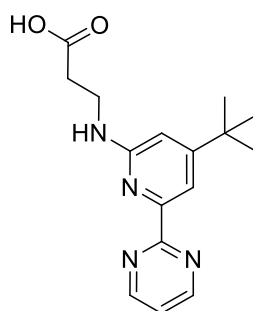
^1H NMR (400 MHz, DMSO- d_6) δ 13.20 - 12.63 (br. s, 1 H), 8.73 (d, $J = 4.3$ Hz, 1 H), 8.35 (app. d, $J = 7.7$ Hz, 1 H), 7.94 (td, $J = 7.7, 1.6$ Hz, 1 H), 7.84 - 7.73 (br. s, 1 H), 7.56 - 7.44 (m, 2 H), 6.53 (s, 1 H), 6.26 - 6.22 (m, 1 H), 4.59 - 4.50 (br. s, 2 H), 1.33 - 1.21 (s, 9 H); MS (ES+) m/z 309.1 $[\text{M}+\text{H}]^+$.

6-(1,1-Dimethylethyl)-2-(2'-pyridyl)-N-(1H-1,2,4-triazol-3-ylmethyl)-4-pyrimidinamine 228

Was prepared as for **208** from **204** (103 mg, 0.42 mmol), DIPEA (0.22 mL, 1.25 mmol) and (1H-1,2,4-triazol-3-ylmethyl)amine hydrochloride **220** (71.1 mg, 0.42 mmol). The usual purification afforded **228** (66 mg, 51%) as a white solid.

¹H NMR (400 MHz, DMSO-d₆) δ 14.47 - 13.98 (br. s, 1 H), 8.66 (d, *J* = 4.0 Hz, 1 H), 8.26 (d, *J* = 7.7 Hz, 1 H), 8.13 - 7.94 (br. s, 1 H), 7.91 - 7.83 (m, 2 H), 7.43 (t, *J* = 7.7 Hz, 1 H), 6.49 (s, 1 H), 4.57 (d, *J* = 4.0 Hz, 2 H), 1.21 (s, 9 H); ¹³C NMR (101 MHz, DMSO-d₆) δ 174.8 (br.), 163.8, 161.4, 156.0, 155.5, 149.2, 148.0 (br.), 137.1, 124.7, 123.1, 99.4 (br.), 37.0 (br.), 36.7, 29.1; IR (cm⁻¹) 3290, 2967, 1586, 1504, 887; HRMS (TOF): *M* + *H* calcd for C₁₆H₂₀N₇ 310.1775, found 310.1774; mp = 211.7 °C.

3-((4-(*Tert*-butyl)-6-(pyrimidin-2-yl)pyridin-2-yl)amino)propanoic acid 231

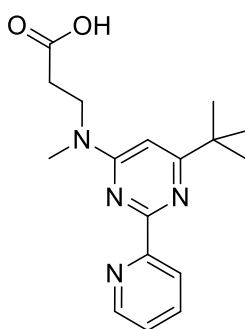


A mixture of ethyl β-alaninate hydrochloride (25.4 mg, 0.17 mmol), 2-[6-chloro-4-(1,1-dimethylethyl)-2-pyridinyl]pyrimidine (41 mg, 0.17 mmol), (*s*)-Binap (5.2 mg, 8.28 μmol), Cs₂CO₃ (135 mg, 0.41 mmol), and Pd₂(dba)₃ (1.5 mg, 1.66 μmol) in 1,4-dioxane (2 mL) was stirred at 100 °C for 20 h. The reaction mixture was transferred in a microwave vial, ethyl β-alaninate hydrochloride (25.4 mg, 0.17 mmol), (*s*)-Binap (5.2 mg, 8.28 μmol), Cs₂CO₃ (135 mg, 0.41 mmol), and Pd₂(dba)₃ (1.5 mg, 1.66 μmol) were added. The reaction mixture was heated in the Biotage initiator microwave at 150 °C for 2 x 60 min. Ethyl β-alaninate hydrochloride (25.4 mg, 0.17 mmol), (*s*)-Binap (5.2 mg, 8.28 μmol), Cs₂CO₃ (135 mg, 0.41 mmol), and Pd₂(dba)₃ (1.5 mg, 1.66 μmol) were added to the reaction mixture which was heated in the Biotage initiator microwave at 150 °C for 60 min. The solvent was removed under reduced pressure and the residue was loaded onto a SNAP silica cartridge (10 g) and partially purified by automated chromatography (SP4) using a 0-6% gradient of methanolic ammonia (2 M) in DCM (15 CV). The appropriate fractions were combined and evaporated

under reduced pressure, the residue was taken up in DCM (3 mL), to which SiliaMetS® Thiourea (0.2 g) was added. After stirring for 1 h at rt, the silica was filtered off using a hydrophobic frit, under *vacuum*. The filtrate was concentrated under reduced pressure to give the crude ester **230** (20 mg). The residue was taken up in a mixture of THF/water (3 mL of a 2:1 mixture), lithium hydroxide monohydrate (2.4 mg, 0.06 mmol) was added and reaction mixture was stirred at rt for 1 h. The reaction mixture was concentrated under reduced pressure and the residue was purified by MDAP on a Waters Xbridge C18 column using ammonium bicarbonate (10 mM in methanol, adjusted to pH 10 with ammonia). The appropriate fractions were combined and concentrated under reduced pressure to give **231** (3 mg, 6 % yield over 2 steps) as a yellow solid.

¹H NMR (400 MHz, CDCl₃) δ 8.88 (d, *J* = 4.8 Hz, 2 H), 7.87 (s, 1 H), 7.32 - 7.24 (m, 2 H), 6.58 (s, 1 H), 3.77 - 3.68 (br. s, 2 H), 2.81 - 2.71 (br. s, 2 H), 1.36 (s, 9 H); MS (ES+) *m/z* 301.1 [M+H]⁺. The signals arising from the CO₂H could not be observed, either because of exchange on the NMR timescale, or masking by the water peak (5.58 - 4.35 ppm).

3-((6-(*Tert*-butyl)-2-(pyridin-2-yl)pyrimidin-4-yl)(methyl)amino)propanoic acid 233

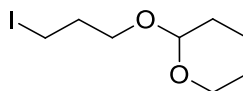


A mixture of *N*-methyl-β-alanine **232** (250 mg, 2.42 mmol), 4-chloro-6-(1,1-dimethylethyl)-2-(2'-pyridyl)pyrimidine **204** (600 mg, 2.42 mmol) and DIPEA (1.27 mL, 7.27 mmol) in DMSO (4 mL) was heated at 150 °C in a Biotage Initiator microwave for two periods of 2 h each. Reaction mixture was concentrated under reduced pressure and the residue was loaded

onto a SNAP silica cartridge (100 g), purified by automated chromatography (SP4) using a 0 - 20% gradient of methanolic ammonia (2N) in DCM (10 CV), followed by a 0 - 20% gradient of MeOH in DCM. The appropriate fractions were combined and evaporated under reduced pressure to give **233** (655 mg, 86%) as a yellow solid.

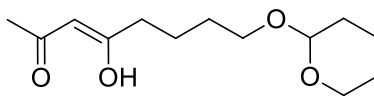
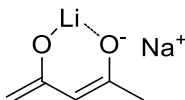
¹H NMR (400 MHz, DMSO-d₆) δ 8.70 (d, *J* = 3.8 Hz, 1 H), 8.30 (d, *J* = 7.8 Hz, 1 H), 7.91 (td, *J* = 7.8, 1.8 Hz, 1 H), 7.48 - 7.43 (m, 1 H), 6.56 (s, 1 H), 3.90 - 3.79 (br. s, 2 H), 2.38 (t, *J* = 7.3 Hz, 2 H), 1.82 (s, 9 H), 1.32 (s, 3 H); ¹³C NMR (126 MHz, DMSO-d₆) δ 175.3 (br.), 174.3 (br.), 162.3, 161.7, 156.3, 149.1, 136.6, 124.2, 123.4, 96.1, 37.1, 35.2 (br.), 33.8, 29.3, 22.2; IR (cm⁻¹) 3200 (br.), 2952, 1716, 1585, 1373, 1247; HRMS (TOF): M + H calcd for C₁₇H₂₃N₄O₂ 315.1816, found 315.1816; mp = 135 °C. The signal arising from the CO₂H proton could not be observed, either because of exchange on the NMR timescale, or masking by the water peak (3.69 - 3.03 ppm).

2-[(3-Iodopropyl)oxy]tetrahydro-2H-pyran **247²¹¹**



Sodium iodide (6.62 g, 44.2 mmol) was added to a stirred solution of commercially available 2-[(3-bromopropyl)oxy]tetrahydro-2H-pyran **246** (5 mL, 29.4 mmol) in acetone (140 mL). After stirring at rt under nitrogen for 18 h, the solvent was removed under reduced pressure and the residue was partitioned between water (50 mL) and diethyl ether (50 mL). The aqueous layer was extracted with diethyl ether (50 mL). The extract and the original organic layers were combined, dried through a hydrophobic frit and concentrated under reduced pressure to give crude **247** (8 g, 100%) as a yellow oil.

¹H NMR (400 MHz, DMSO-d₆) δ 4.61 - 4.53 (m, 1 H), 3.75 (m, 1 H), 3.67 (m, 1 H), 3.47 - 3.41 (m, 1 H), 3.37 (m, 1 H), 3.34 - 3.27 (m, 3 H), 2.00 (m, 2 H), 1.77 - 1.67 (m, 1 H), 1.66 - 1.57 (m, 1 H), 1.53 - 1.40 (m, 3 H).

8-(Tetrahydro-2H-pyran-2-yloxy)-2,4-octanedione 252**Preparation of dienolate 243**

Acetylacetone (2 mL, 19.42 mmol) was added to a stirred suspension of NaH (1.55 g of a 60% w/w dispersion in mineral oil, 38.8 mmol) in THF (40 mL) at 0 °C under nitrogen over 10 min (with gas evolution). The resulting white suspension was stirred at 0 °C for 0.5 h, then cooled to -30 °C and *n*BuLi (12.14 mL of a 1.6 M solution in hexane, 19.42 mmol) was added dropwise to form a pale yellow suspension. The mixture was stirred for 0.5 h at -20 °C, then 1,3-dimethyl-3,4,5,6-tetrahydro-2(1H)-pyrimidinone (4 mL) was added. The mixture was stirred at -20 °C for 10 min to allow completion of dienolate **243** formation.

Method A for preparation of 252

The dienolate solution (11 mL) was added to a stirred solution of 2-[(3-bromopropyl)oxy]tetrahydro-2H-pyran **246** (0.82 mL, 4.85 mmol) in THF (5 mL) containing molecular sieves at -5 °C. The mixture was maintained between -5 °C and 0 °C with stirring for 1 h, then ammonium chloride (20 mL of a saturated aqueous solution) was added followed by ethyl acetate (20 mL). The layers were separated and the aqueous layer was extracted with ethyl acetate (20 mL). The extract and the original organic layers were combined, dried through a hydrophobic frit and concentrated under reduced pressure. The residue was loaded onto a SNAP silica cartridge (50 g) and purified by automated chromatography (SP4), eluting with a 5 - 50% gradient of ethyl acetate in cyclohexane (15

CV). The appropriate fractions were combined and concentrated under reduced pressure to give crude diketone **252** (196 mg) as a yellow oil.

Method B for preparation of **252**

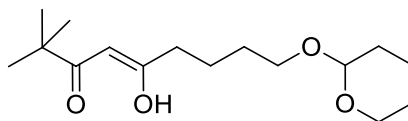
Same procedure as for method A from the dienolate solution (11 mL) and **247** (1.3 g, 4.85 mmol). The usual work up and purification afforded crude diketone **252** (244 mg) as a yellow oil.

Method C for preparation of **252**

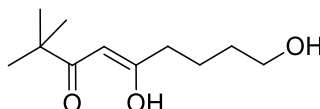
The dienolate solution (11 mL) was maintained between -5 °C and 0 °C with stirring for 90 min, cooled at -20 °C, diluted with THF (20 mL) and treated with **247** (1.3 g, 4.85 mmol). The mixture was stirred 5 °C for 1 h. The usual work up and purification afforded crude diketone crude **252** (0.44 g) as a yellow oil.

¹H NMR (400 MHz, CDCl₃), the spectrum recorded from crude material contains following significant peaks, δ 15.49 (s, 1 H), 5.50 (s, 1 H), 4.60 - 4.54 (m, 1 H), 3.91 - 3.82 (m, 1 H), 3.80 - 3.72 (m, 1 H), 3.55 - 3.47 (m, 1 H), 3.44 - 3.35 (m, 1 H), 2.35 - 2.28 (m, 2 H), 2.06 (s, 3 H), 1.87 - 1.48 (m, 10 H).

2,2-Dimethyl-9-(tetrahydro-2H-pyran-2-yloxy)-3,5-nonanedione 256



(4Z)-5,9-dihydroxy-2,2-dimethyl-4-nonen-3-one 257

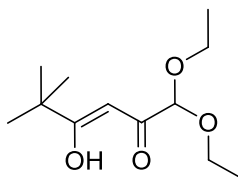


A solution of 2,2-dimethyl-3,5-hexanedione **240** (1.5 mL, 9.61 mmol) in THF (5.8 mL) was added to a stirred suspension of NaH (769 mg of a 60% w/w dispersion in mineral oil, 19.22 mmol) and calcium hydride (405 mg, 9.61 mmol) in THF (53 mL) at -10 °C under nitrogen, over 10 min (with gas evolution). After stirring at -10 °C for 0.5 h, *n*BuLi (6.01 mL, 9.61 mmol) was added dropwise to form a pale yellow suspension. 2-[(3-Iodopropyl)oxy]tetrahydro-2H-pyran **247** (2.60 g, 9.61 mmol) was added after 30 min of stirring at 0 °C. After stirring at 0 °C for 90 min, reaction was quenched with the addition of an aqueous solution of NH₄Cl (100 mL), followed by diethylether (100 mL). The layers were separated and the aqueous layer was extracted with diethylether (100 mL). The extract and the original organic layers were combined, dried through a hydrophobic frit and concentrated under reduced pressure. The residue was loaded onto a SNAP silica cartridge (100 g) and purified by automated chromatography (SP4), eluting with a 0 - 40% gradient of ethyl acetate in cyclohexane (15 CV). The appropriate fractions were combined and concentrated under reduced pressure to give crude **256** (0.99 g) as a yellow oil and crude **257** (447 mg) as a yellow oil. The yields could not be calculated because the compounds were impure.

The ¹H NMR (400 MHz, CDCl₃) spectrum recorded from crude material contains the following significant peaks for **256**, δ 15.84 (br. s, 1 H), 5.65 - 5.57 (m, 1 H), 4.62 - 4.54 (m, 1 H), 3.88 (m, 1 H), 3.82 - 3.73 (m, 1 H), 3.55 - 3.48 (m, 1 H), 3.46 - 3.37 (m, 1 H), 2.40 - 2.33 (m, 1 H), 1.90 - 1.79 (m, 1 H), 1.78 - 1.49 (m, 7 H), 1.39 - 1.28 (m, 2 H), 1.18 (s, 9 H).

The ¹H NMR (400 MHz, CDCl₃) spectrum recorded from crude material contains the following significant peaks for **257**, δ 15.94 - 15.69 (br. s, 1 H), 5.61 (s, 1 H), 3.67 (t, *J* = 6.3 Hz, 2 H), 2.40 - 2.31 (m, 2 H), 1.76 - 1.69 (m, 2 H), 1.62 (dd, *J* = 8.4, 6.6 Hz, 2H), 1.17 (s, 9 H).

(Z)-1,1-diethoxy-4-hydroxy-5,5-dimethylhex-3-en-2-one **235**²¹²



LiHMDS (4 mL of a 1 M solution in toluene, 4.0 mmol) was added to a stirred solution of 3,3-dimethyl-2-butanone **233** (0.5 mL, 4.0 mmol) in THF (20 mL) at -70 °C under nitrogen. The mixture was stirred at -70 °C for 0.5 h, then ethyl *bis*(ethoxy)acetate **265** (0.71 mL, 4.0 mmol) was added. The reaction mixture was stirred at 5 °C for 2 h, then warmed to rt; ammonium chloride (20 mL of a saturated aqueous solution) was added, followed by ethyl acetate (20 mL). The phases were separated, the organic extract was dried through a hydrophobic frit and concentrated under reduced pressure. The residue was loaded on a SNAP silica cartridge (25 g), purified by automated chromatography (SP4), eluting with a 0 - 50% gradient of DCM in cyclohexane (15 CV). The appropriate fractions were combined and evaporated under reduced pressure to give **235** (540 mg, 59%) as a colourless oil.

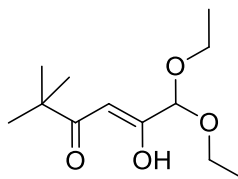
The ¹H NMR spectrum showed the presence of a number of components which were distinguished *via* integration of the spectrum.

The major component **235**:

¹H NMR (400 MHz, DMSO-d₆) δ 15.46 - 15.29 (br. s, 1 H), 6.00 (s, 1 H), 4.89 (s, 1 H), 3.67 - 3.44 (m, 4 H), 1.17 - 1.11 (m, 15 H).

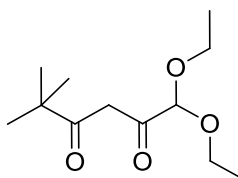
Minor components were identified as

(Z)-6,6-diethoxy-5-hydroxy-2,2-dimethylhex-4-en-3-one



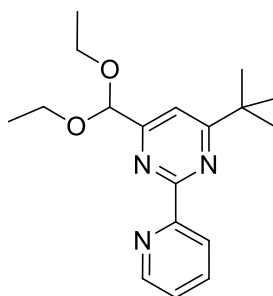
$^1\text{H NMR}$ (400 MHz, DMSO-d_6) δ 5.75 (s, 1 H), 4.92 (s, 1 H), 3.67 - 3.44 (m, 4 H), 1.17 - 1.11 (m, 15 H); and

1,1-Diethoxy-5,5-dimethylhexane-2,4-dione



$^1\text{H NMR}$ (400 MHz, DMSO-d_6) δ 4.65 (s, 1 H), 3.82 (s, 2 H), 3.67 - 3.44 (m, 4 H), 1.17 - 1.11 (m, 15 H).

4-[Bis(ethoxy)methyl]-6-(1,1-dimethylethyl)-2-(2'-pyridyl)pyrimidine 263

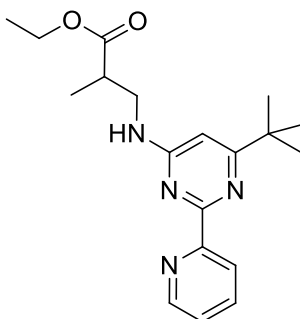


Intermediate **235** (540 mg, 2.35 mmol) was added to a suspension of 2-pyridinecarboximidamide **202** (370 mg, 2.35 mmol) in EtOH (15 mL), followed by triethylamine (0.65 mL, 4.70 mmol). The reaction mixture was stirred 50 °C for 16 h, at 90

°C for 7 h and at 70 °C for 88 h. After cooling at rt, the solvent was removed under reduced pressure and the residue was loaded on a SNAP silica cartridge (50 g) and partially purified by automated chromatography (SP4), eluting with a 0 - 60% gradient of ethyl acetate in cyclohexane (15 CV). The appropriate fractions were combined and evaporated under reduced pressure. The residue was taken up in methanolic DMSO (1 mL of a 1:1 mixture) and purified by MDAP on Xbridge column using ammonium bicarbonate (10 mM in methanol, adjusted to pH 10 with ammonia). The solvent was evaporated under reduced pressure to give **263** (178 mg, 24%) as a yellow oil.

¹H NMR (400 MHz, DMSO-d₆) δ 8.77 (d, *J* = 3.8 Hz, 1 H), 8.39 (d, *J* = 7.8 Hz, 1 H), 7.99 (t, *J* = 7.8 Hz, 1 H), 7.56 - 7.49 (m, 2 H), 5.48 (s, 1 H), 3.76 - 3.59 (m, 4 H), 1.39 (s, 9 H), 1.18 (t, *J* = 7.0 Hz, 6 H); MS (ES+) *m/z* 316.2 [M+H]⁺.

(±)-3-((6-(*Tert*-butyl)-2-(pyridin-2-yl)pyrimidin-4-yl)amino)-2-methylpropanoic acid
269

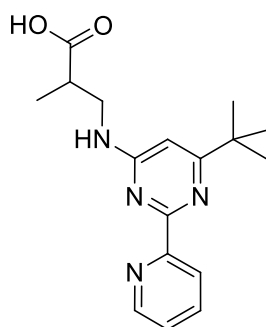


Was prepared as for **208** from ethyl 3-amino-2-methylpropanoate hydrochloride **268** (102 mg, 0.61 mmol), 4-chloro-6-(1,1-dimethylethyl)-2-(2'-pyridyl)pyrimidine **204** (150 mg, 0.61 mmol) and DIPEA (0.32 mL, 1.82 mmol). The reaction mixture was taken up in methanolic DMSO (1.5 mL of a 2:1 mixture) and was partially purified by MDAP on a Waters Xbridge C18 column using ammonium bicarbonate (10 mM in methanol, adjusted to pH 10 with ammonia). The appropriate fractions were combined and concentrated under reduced

pressure to give the crude product. The residue was taken up in methanolic DMSO (1 mL of a 1:1 mixture) and purified by MDAP on a Supelcosil ABZ+Plus column eluting with solvents A/B (A: water + 0.1% formic acid, B: MeCN:water 95:5 + 0.05% formic acid). The appropriate fractions were combined, passed through a hydrogen carbonate column and evaporated under reduced pressure to give **269** (119 mg, 57%) as an off-white solid.

¹H NMR (400 MHz, DMSO-d₆) δ 8.70 (d, *J* = 4.3 Hz, 1 H), 8.28 (d, *J* = 7.8 Hz, 1 H), 7.90 (td, *J* = 7.7, 1.8 Hz, 1 H), 7.48 - 7.42 (m, 2 H), 6.48 (s, 1 H), 4.02 (qd, *J* = 7.1, 2.1 Hz, 2 H), 3.70 - 3.58 (br. s, 1 H), 3.55 - 3.42 (br. s, 1 H), 2.86 - 2.75 (m, 1 H), 1.28 (s, 9 H), 1.13 (app. t, *J* = 7.1 Hz, 3 H), 1.14 (app. d, *J* = 7.1 Hz, 3 H); MS (ES+) *m/z* 343.2 [M+H]⁺.

(±)-3-((6-(*Tert*-butyl)-2-(pyridin-2-yl)pyrimidin-4-yl)amino)-2-methylpropanoic acid
270

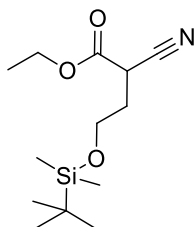


Lithium hydroxide (26.2 mg, 1.10 mmol) was added to a solution of ethyl 3-[[6-(1,1-dimethylethyl)-2-(2'-pyridyl)-4-pyrimidinyl]amino]-2-methylpropanoate **269** (75 mg, 0.22 mmol) in aqueous THF (2 mL of a 1:1 mixture). After stirring for 1 h at rt, the reaction mixture was concentrated using the blowdown apparatus. The residue was taken up in methanolic DMSO (2 mL of a 1:1 mixture) and partially purified by MDAP on a Waters Xbridge C18 column using ammonium bicarbonate (10 mM in methanol, adjusted to pH 10 with ammonia). The appropriate fractions were combined and concentrated under reduced pressure to give crude product. The residue was loaded onto an SCX cartridge (1 g) and

eluted with methanolic ammonia (2 N) (3 CV). The appropriate fractions were combined and concentrated using the blowdown apparatus to give **270** (15 mg, 22%) as a white solid.

¹H NMR (400 MHz, DMSO-d₆) δ 8.69 (d, *J* = 4.3 Hz, 1 H), 8.29 (d, *J* = 7.8 Hz, 1 H), 7.90 (td, *J* = 7.8, 1.8 Hz, 1 H), 7.48 - 7.38 (m, 2 H), 6.50 (s, 1 H), 3.67 - 3.53 (br. s, 1 H), 3.54 - 3.37 (br. s, 1 H), 2.72 - 2.61 (m, 1 H), 1.28 (s, 9 H), 1.11 (d, *J* = 7.1 Hz, 3 H); the signal arising from the CO₂H proton could not be observed, either because of exchange on the NMR timescale, or masking by the water peak (4.90 - 3.07 ppm); MS (ES+) *m/z* 315.15 [M+H]⁺.

(±)-Ethyl 2-cyano-4-[[[(1,1-dimethylethyl)(dimethyl)silyl]oxy]butanoate 286

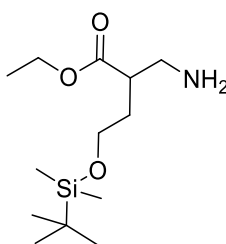


Ethyl cyanoacetate **285** (1.0 mL, 9.38 mmol) was added to a stirred suspension of sodium hydride (0.45 g of a 60% w/w dispersion in mineral oil, 11.26 mmol) in DMF (10 mL) at 0 °C under nitrogen. Gas evolution occurred after the addition. The mixture was stirred for 60 min at 0 °C, then [(2-bromoethyl)oxy](1,1-dimethylethyl)dimethylsilane **273** (2.01 mL, 9.38 mmol) was added. The mixture was stirred for a further 3 h at 0 °C, then allowed to stand for 16 h. The reaction was cooled to 0 °C and quenched with water (50 mL); ethyl acetate (50 mL) was added and the phases were separated. The aqueous phase was extracted with ethyl acetate (50 mL) and the extract and original organic phases were combined, dried through a hydrophobic frit and concentrated under reduced pressure. The residue was loaded on a SNAP silica column (100 g) and purified by automated chromatography (SP4), eluting with a 0 - 30% gradient of ethyl acetate in cyclohexane (10 CV). The appropriate fractions were

combined and evaporated under reduced pressure to give **286** (805 mg, 32%) as a colourless oil.

¹H NMR (400 MHz, CDCl₃) δ 4.19 (q, *J* = 7.2 Hz, 2 H), 3.77 - 3.64 (m, 3 H), 2.20 - 2.08 (m, 1 H), 2.05 - 1.92 (m, 1 H), 1.25 (t, *J* = 7.2 Hz, 3 H), 0.82 (s, 9 H), 0.01 (s, 3 H), 0.00 (s, 3 H).

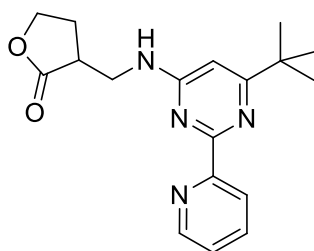
(±)-Ethyl 2-(aminomethyl)-4-[[[(1,1-dimethylethyl)(dimethyl)silyl]oxy]butanoate 287



A solution of **286** (495 mg, 1.82 mmol) in ethanol (35 mL) was hydrogenated in the H-Cube, using a Raney Ni catalyst cartridge at 90 °C under 90 bar. The solvent was removed under reduced pressure and the residue was loaded on a SNAP silica column (50 g), purified by automated chromatography (SP4), eluting with a 0 - 8% gradient of methanolic ammonia (2N) in DCM (15 CV). The appropriate fractions were combined and evaporated under reduced pressure to give **287** (474 mg, 94%) as a colourless oil.

¹H NMR (400 MHz, DMSO-d₆) δ 4.04 (q, *J* = 7.1 Hz, 2 H), 3.55 (d, *J* = 6.3 Hz, 2 H), 3.45 - 3.18 (br. s, 2 H) (masked by the water peak), 2.73 - 2.60 (m, 2 H), 2.46 - 2.37 (m, 1 H), 1.75 - 1.57 (m, 2 H), 1.21 - 1.13 (m, 3 H), 0.84 (s, 9 H), 0.01 (s, 3 H), 0.00 (s, 3 H). An additional signal (two protons) could not be observed, either because of exchange on the NMR timescale, or masking by the water peak (3.45 - 3.18).

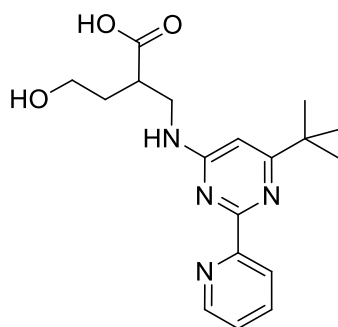
(±)-3-({[6-(1,1-Dimethylethyl)-2-(2'-pyridyl)-4-pyrimidinyl]amino}methyl)dihydro-2(3H)-furanone **288**



Was prepared as for **208** from **204** (145 mg, 0.59 mmol), DIPEA (0.20 mL, 1.17 mmol) and **287** (161 mg, 0.59 mmol). The solvent was removed under reduced pressure and the residue was loaded on a SNAP silica cartridge (25 g) and purified by automated chromatography (SP4), washed with 100% ethyl acetate (5 CV) and eluted with a 0 - 5% gradient of MeOH in DCM (10 CV). The appropriate fractions were combined and concentrated under reduced pressure to give **288** (140 mg, 73%) as a yellow oil, which solidified on standing.

¹H NMR (400 MHz, DMSO-d₆) δ 8.70 (d, *J* = 4.2 Hz, 1 H), 8.30 (d, *J* = 7.7 Hz, 1 H), 7.91 (td, *J* = 7.7, ⁴*J* = 1.2 Hz, 1 H), 7.49 (t, *J* = 5.7 Hz, 1 H), 7.45 (ddd, *J* = 7.7, 4.2, ⁴*J* = 1.2 Hz, 1 H), 6.53 (s, 1 H), 4.32 (td, *J* = 8.6 Hz, ²*J* = 2.8 Hz, 1 H), 4.21 - 4.15 (m, 1 H), 3.99 - 3.80 (br. s, 1 H), 3.50 (ddd, *J* = 13.6, 7.7, 5.7 Hz, 1 H), 3.09 - 2.98 (m, 1 H), 2.41 - 2.30 (m, 1 H), 2.14 - 2.03 (m, 1 H), 1.29 (s, 9 H); MS (ES+) *m/z* 327.2 [M+H]⁺.

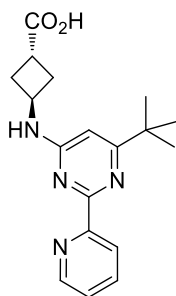
(±)-2-({[6-(1,1-Dimethylethyl)-2-(2'-pyridyl)-4-pyrimidinyl]amino}methyl)-4-hydroxybutanoic acid **271**



Lithium hydroxide monohydrate (13.0 mg, 0.31 mmol) was added to a stirred solution of **288** (101 mg, 0.31 mmol) in aqueous THF (6 mL of a 1:1 mixture). The reaction mixture was allowed to stand at rt for 16 h. The solvent was removed under reduced pressure to afford the lithium salt (80 mg). Of this, 57 mg was taken up in methanolic DMSO (1 mL of a 1:1 mixture) which was purified by MDAP on Xbridge column using ammonium bicarbonate (10 mM in methanol, adjusted to pH 10 with ammonia). The solvent was removed under reduced pressure to give **271** (37 mg, 35%) as a colourless oil.

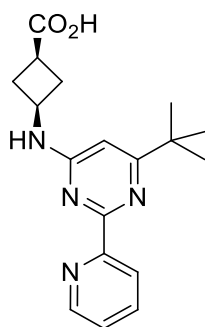
^1H NMR (400 MHz, DMSO- d_6) δ 8.68 (d, $J = 4.0$ Hz, 1 H), 8.32 (d, $J = 7.7$ Hz, 1 H), 7.91 (td, $J = 7.7$, $^4J = 1.8$ Hz, 1 H), 7.46 (dd, $J = 7.7$, 4.0 Hz, 1 H), 7.48 - 7.38 (br. s, 1 H), 6.55 (s, 1 H), 3.62 - 3.50 (m, 2 H), 3.50 - 3.42 (m, 2 H), 2.74 - 2.63 (br. s, 1 H), 1.79 - 1.69 (m, 1 H), 1.67 - 1.57 (m, 1 H), 1.28 (s, 9 H); MS (ES+) m/z 345.2 $[\text{M}+\text{H}]^+$.

Trans*-3-((6-(*tert*-butyl)-2-(pyridin-2-yl)pyrimidin-4-yl)amino)cyclobutanecarboxylic acid **291*



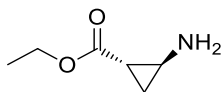
Was prepared as for **208** from *trans*-3-aminocyclobutanecarboxylic acid **289** (69.7 mg, 0.61 mmol), 4-chloro-6-(1,1-dimethylethyl)-2-(2'-pyridyl)pyrimidine **204** (150 mg, 0.61 mmol) and DIPEA (0.32 mL, 1.82 mmol). The usual purification afforded **291** (64 mg, 32%) as a yellow solid.

^1H NMR (500 MHz, DMSO- d_6) δ 8.69 (d, $J = 3.6$ Hz, 1 H), 8.25 (d, $J = 7.9$ Hz, 1 H), 7.90 (td, $J = 7.9$, $^4J = 1.9$ Hz, 1 H), 7.74 - 7.58 (br. s, 1 H), 7.46 - 7.42 (m, 1 H), 6.43 - 6.30 (br. s, 1 H), 4.83 - 4.51 (br. s, 1 H), 3.04 - 2.94 (m, 1 H), 2.57 - 2.51 (m, 2 H), 2.26 - 2.18 (m, 2 H), 1.28 (s, 9 H); ^{13}C NMR (126 MHz, DMSO- d_6) δ 176.6, 174.2 (br.), 162.6 (br.), 162.3, 156.2, 149.1, 136.5, 124.2, 123.3, 99.4 (br.), 43.6 (br.), 36.7, 33.0 (br.), 32.4 - 32.1 (m), 29.1; IR (cm^{-1}) 2956, 1586, 1371, 1129, 1036, 746; HRMS (TOF): $M + H$ calcd for $\text{C}_{18}\text{H}_{22}\text{N}_4\text{O}_2$ 327.1821, found 327.1814; mp = 165 $^\circ\text{C}$.

Cis*-3-((6-(*tert*-butyl)-2-(pyridin-2-yl)pyrimidin-4-yl)amino)cyclobutanecarboxylic acid*292**

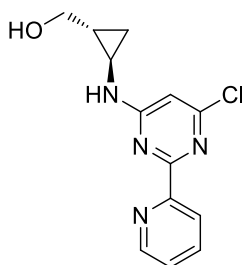
Was prepared as for **208** from *cis*-3-aminocyclobutanecarboxylic acid **290** (69.7 mg, 0.61 mmol), 4-chloro-6-(1,1-dimethylethyl)-2-(2'-pyridyl)pyrimidine **204** (150 mg, 0.61 mmol) and DIPEA (0.32 mL, 1.82 mmol). The usual purification afforded **292** (40 mg, 20%) as a yellow solid.

^1H NMR (400 MHz, 393 K, DMSO- d_6) δ 8.68 (d, $J = 3.8$ Hz, 1 H), 8.26 (d, $J = 7.8$ Hz, 1 H), 7.85 (td, $J = 7.8$, $^4J = 1.8$ Hz, 1 H), 7.41 - 7.35 (m, 1 H), 7.19 - 6.99 (br. s, 1 H), 6.44 (s, 1 H), 4.51 - 4.37 (m, 1 H), 2.83 (quin, $J = 8.8$ Hz, 1 H), 2.68 - 2.58 (m, 2 H), 2.25 - 2.14 (m, 2 H), 1.33 (s, 9 H); ^{13}C NMR (126 MHz, DMSO- d_6) δ 176.1, 174.1 (br.), 162.6 (br.), 162.2, 156.2, 149.1, 136.5, 124.2, 123.3, 99.0 (br.), 40.8 (br.), 36.6, 34.1 (br.), 31.6, 29.1; IR (cm^{-1}) 2958, 1587, 1372, 1203, 1130, 1040; HRMS (TOF): $M + H$ calcd for $\text{C}_{18}\text{H}_{23}\text{N}_4\text{O}_2$ 317.1816, found 317.1823; mp = 222.7 °C. The signal arising from the CO_2H proton could not be observed, either because of exchange on the NMR timescale, or masking by the water peak (3.74 - 3.08 ppm).

(±)-*Trans*-Ethyl 2-aminocyclopropanecarboxylate 294

A solution of ethyl *trans*-2-(Cbz)cyclopropanecarboxylate **293** (305 mg, 1.16 mmol) in MeOH (23 mL) was hydrogenated in the H-Cube using a 10% Pd-C catalyst cartridge at 30 °C. The solvent was removed under reduced pressure and the residue was loaded on a SCX column (10 g), washed with MeOH (3 CV) and eluted with methanolic ammonia (4 CV of a 2 M solution). The appropriate fractions were combined and evaporated under reduced pressure to give **294** (118 mg, 79%) as a yellow oil.

¹H NMR (400 MHz, DMSO-*d*₆) δ 4.03 (q, *J* = 7.0 Hz, 2 H), 3.17 (s, 2H), 2.45 (t, *J* = 6.9 Hz, 1 H), 2.34 - 2.28 (m, 1 H), 1.66 - 1.54 (m, 2 H), 1.17 (t, *J* = 7.0 Hz, 3 H).

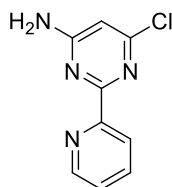
(±)- (*Trans*-2-((6-chloro-2'-(pyridyl)pyrimidin-4-yl)amino)cyclopropyl)methanol 302

HCl (0.88 mL of a 4M solution in dioxane, 3.52 mmol) was added to a stirred solution of Boc-[*trans*-2-aminocyclopropyl]methanol **300** (330 mg, 1.76 mmol) in 1,4-dioxane (1 mL). More HCl (0.44 mL of a 4M solution in dioxane, 1.76 mmol) was added after stirring at rt for 18 h. After stirring for 4 h at rt, the solution of [*trans*-2-aminocyclopropyl]methanol **301** was diluted with 1,4-dioxane (1 mL) and treated with DIPEA (1.54 mL, 8.84 mmol). 4,6-Dichloro-2-(2'-pyridyl)pyrimidine **298** (400 mg, 1.77 mmol) was added after 5 min of stirring at rt. The reaction mixture was stirred at rt for 18 h and at 80 °C for 5 h. After cooling to rt, the solvent was removed under reduced pressure, the residue was loaded on a

SNAP silica column (50 g) and purified by automated chromatography (SP4), eluting with a 0 - 5% gradient of MeOH in DCM (20 CV). The appropriate fractions were combined and evaporated under reduced pressure to give **302** (290 mg, 59% based on **300**) as an orange gum.

¹H NMR (400 MHz, 393 K, DMSO-d₆) δ 8.68 (d, *J* = 4.8 Hz, 1 H), 8.25 (d, *J* = 7.7 Hz, 1 H), 7.91 (t, *J* = 7.7 Hz, 1 H), 7.90 - 7.67 (br. s, 1 H), 7.47 (dd, *J* = 7.7, 4.8 Hz, 1 H), 6.80 (s, 1 H), 4.65 - 4.25 (br. s, 1 H), 3.63 (dd, ²*J* = 11.2, *J* = 5.3 Hz, 1 H), 3.28 (dd, ²*J* = 11.2, *J* = 7.4 Hz, 1 H), 2.61 - 2.53 (m, 1 H), 1.22 - 1.12 (m, 1 H), 0.84 - 0.74 (m, 2 H); MS (ES+) *m/z* 277.0 [M+H]⁺.

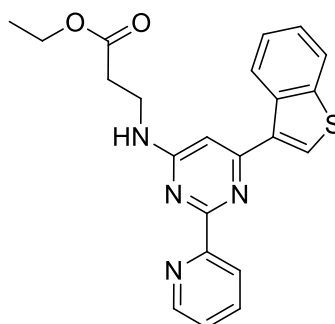
6-Chloro-(pyridin-2-yl)pyrimidin-4-amine 304



Triethylamine (0.31 mL, 2.20 mmol) and pyridine sulfur trioxide (281 mg, 1.76 mmol) were added to a solution of **302** (122 mg, 0.44 mmol) in a mixture of DCM and DMSO (4 mL of a 1:1 mixture) at rt. After stirring for 4 h at rt, brine (20 mL) and DCM (20 mL) were added. The layers were separated and the aqueous layer was extracted with further DCM (2 x 20 mL). The aqueous layer was concentrated under reduced pressure and the residue was purified by MDAP on Xbridge column using ammonium bicarbonate (10 mM in methanol, adjusted to pH 10 with ammonia). The appropriate fractions were combined and concentrated under reduced pressure to give **304** (4 mg, 4%).

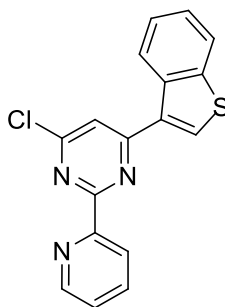
¹H NMR (400 MHz, DMSO-d₆) δ 8.69 (d, *J* = 4.4 Hz, 1 H), 8.22 (d, *J* = 7.8 Hz, 1 H), 7.93 (td, *J* = 7.8, ⁴*J* = 1.5 Hz, 1 H), 7.50 (ddd, *J* = 7.8, 4.4, ⁴*J* = 1.5 Hz, 1 H), 7.49 - 7.34 (br. s, 2 H), 6.49 (s, 1 H); MS (ES+) *m/z* 207.0 [M+H]⁺.

Ethyl 3-((6-(benzo[b]thiophen-3-yl)-2-(pyridin-2-yl)pyrimidin-4-yl)amino)propanoate
316



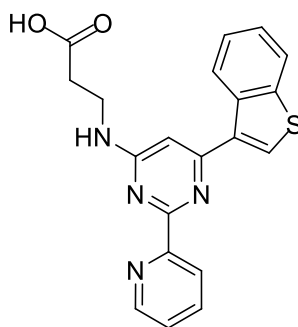
A mixture of 1-benzothien-2-ylboronic acid **312** (183 mg, 1.030 mmol), ethyl N-[6-chloro-2-(2'-pyridyl)-4-pyrimidinyl]-β-alaninate **313** (158 mg, 0.515 mmol), *tetrakis* (triphenylphosphino)palladium (60 mg, 0.052 mmol) and cesium carbonate (336 mg, 1.030 mmol) in 1,4-dioxane (0 mL) and water (0.5 mL) was degassed with nitrogen for 20 min and heated in a Biotage Initiator microwave at 100 °C for 0.5 h. The reaction mixture was concentrated under reduced pressure, the residue was loaded onto a SNAP silica column (50 g), purified by automated chromatography (SP4), eluting with 50-100% ethylacetate in cyclohexane (20 CV). The appropriate fractions were combined and evaporated under reduced pressure to give the required product (120 mg). The residue was taken up in EtOH (10 mL), to which SiliaMetS® Thiourea (0.6 g) was added. After stirring for 1 h at rt, the silica was filtered off using a hydrophobic frit, under gravity. The filtrate was concentrated under reduced pressure to give **316** (90 mg, 43%) as a yellow oil.

¹H NMR (400 MHz, DMSO-d₆) spectrum contained the following significant peaks δ 8.75 (d, *J* = 4.0 Hz, 1 H), 8.38 (d, *J* = 7.8 Hz, 1 H), 8.09 (d, *J* = 7.8 Hz, 1 H), 7.97 (td, *J* = 7.8, ⁴*J* = 1.8 Hz, 1 H), 7.70 - 7.59 (m, 2 H), 7.58 - 7.43 (m, 4 H), 6.97 (s, 1 H), 4.08 (q, *J* = 7.1 Hz, 2 H), 3.72 (br. s., 2 H), 2.70 (t, *J* = 6.6 Hz, 2 H), 1.18 (t, *J* = 7.1 Hz, 3 H); MS (ES+) *m/z* 405.3 [M+H]⁺.

4-(Benzo[b]thiophen-3-yl)-6-chloro-2-(pyridin-2-yl)pyrimidine 315

Was prepared as for **316** from *tetrakis*(triphenylphosphino)palladium (109.0 mg, 0.09 mmol), 1-thiophenyl-3-ylboronic acid **312** (201.0 mg, 1.13 mmol), 4,6-dichloro-2-(2'-pyridyl)pyrimidine **258** (213.0 mg, 0.94 mmol) and Cs₂CO₃ (614.0 mg, 1.88 mmol). The usual purification gave **315** (167 mg, 55%) as a colourless oil.

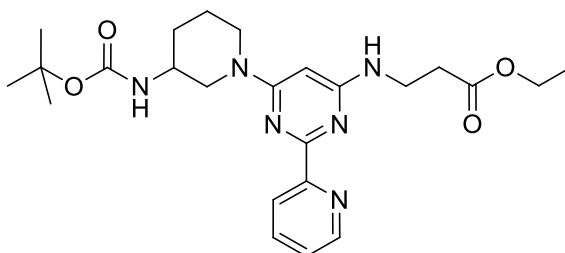
¹H NMR (400 MHz, DMSO-d₆) δ 9.06 (d, *J* = 8.1 Hz, 1 H), 8.90 (s, 1 H), 8.78 (d, *J* = 3.8 Hz, 1 H), 8.40 (d, *J* = 7.8 Hz, 1 H), 8.24 (s, 1 H), 8.07 (d, *J* = 7.8 Hz, 1 H), 8.00 (td, *J* = 7.8, 1.9 Hz, 1 H), 7.57 - 7.48 (m, 2 H), 7.46 - 7.40 (m, 1 H); ¹³C NMR (126 MHz, DMSO-d₆) δ 163.6, 162.9, 161.2, 153.4, 150.1, 140.2, 137.5, 136.3, 133.9, 131.7, 125.8, 125.5, 125.2, 125.2, 123.8, 123.1, 117.4; IR (cm⁻¹) 3067 (br.); 1549; 1520; 1368; 1249; HRMS (TOF): M + H calcd for C₁₇H₁₁ClN₃S 324.0357, found 324.0357; mp = 136 °C.

3-((6-(Benzo[b]thiophen-3-yl)-2-(pyridin-2-yl)pyrimidin-4-yl)amino)propanoic acid 314

Was prepared as for **208** from DIPEA (0.07 mL, 0.42 mmol), β -alanine **317** (14.9 mg, 0.17 mmol) and 4-(1-benzothien-3-yl)-6-chloro-2-(2'-pyridyl)pyrimidine **315** (45.0 mg, 0.14 mmol). The usual purification afforded **314** (28 mg, 54%) as a yellow solid.

^1H NMR (400 MHz, 393 K, DMSO- d_6) δ 8.75 (d, $J = 6.8$ Hz, 2 H), 8.36 (d, $J = 7.8$ Hz, 1 H), 8.30 (s, 1 H), 8.05 - 8.01 (m, 1 H), 7.92 (td, $J = 7.8$, $^4J = 1.8$ Hz, 1 H), 7.51 - 7.42 (m, 3 H), 6.99 (s, 1 H), 3.75 (t, $J = 6.8$ Hz, 2 H), 2.66 (t, $J = 6.8$ Hz, 2 H); MS (ES+) m/z 377.17 $[\text{M}+\text{H}]^+$. The signals arising from the CO_2H or NH protons could not be observed, either because of exchange on the NMR timescale, or masking by the water peak (3.91 - 3.03 ppm).

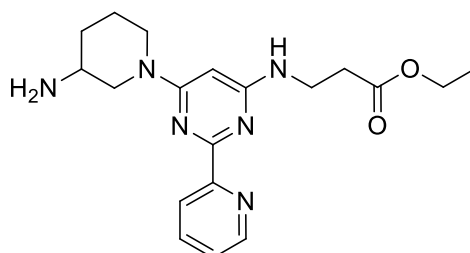
(±)-Ethyl 3-((6-(3-((tert-butoxycarbonyl)amino)piperidin-1-yl)-2-(pyridin-2-yl)pyrimidin-4-yl)amino)propanoate **319**



Was prepared as for **208** from 3-(tert-butyloxycarbonyl)aminopiperidine (0.67 g, 3.33 mmol), DIPEA (0.58 mL, 3.33 mmol), **313** (1.02 g, 3.33 mmol) in 1,4-dioxane (4 mL). The usual purification afforded **319** (1.6 g, 100%) as an orange oil.

¹H NMR (400 MHz, DMSO-d₆) δ 8.66 (d, *J* = 3.8 Hz, 1 H), 8.24 (d, *J* = 7.7 Hz, 1 H), 7.86 (td, *J* = 7.7, 1.8 Hz, 1 H), 7.47 - 7.38 (m, 1 H), 6.94 (d, *J* = 7.7 Hz, 1 H), 6.88 (t, *J* = 4.0 Hz, 1 H), 5.67 (s, 1 H), 4.23 - 4.6 (br. s, 1 H), 4.06 (q, *J* = 7.1 Hz, 2 H), 3.60 - 3.50 (br. s, 2 H), 2.95 - 2.84 (br. s, 1 H), 2.85 - 2.73 (br. s, 1 H), 2.61 (t, *J* = 6.8 Hz, 2 H), 1.92 - 1.81 (br. s, 1 H), 1.78 - 1.68 (br. s, 1 H), 1.49 - 1.39 (m, 4 H), 1.40 (s, 9 H), 1.18 (t, *J* = 7.1 Hz, 3 H); MS (ES+) *m/z* 471.4 [M+H]⁺.

(±)-Ethyl 3-((6-(3-aminopiperidin-1-yl)-2-(pyridin-2-yl)pyrimidin-4-yl)amino)propanoate **320**

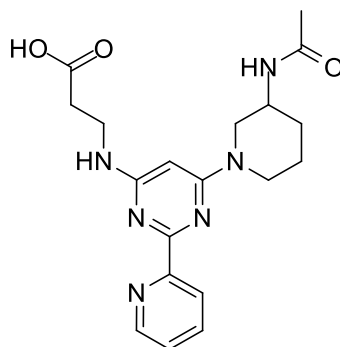


Ethyl N-[6-[3-(((1,1-dimethylethyl)oxy)carbonyl)amino]-1-piperidinyl]-2-(2-pyridinyl)-4-pyrimidinyl]-β-alaninate **319** (1.6 g, 3.40 mmol) was taken up in TFA (3 mL, 38.9 mmol). After stirring at rt for 30 min, and standing at the same T without stirring for 16 h, the

reaction mixture was concentrated under reduced pressure. The residue was loaded onto an SCX cartridge (50 g) and eluted with methanolic ammonia (2 N) (3 CV). The appropriate fractions were combined and concentrated under reduced pressure to give 320 (1.21 g, 96 %) as an orange gum.

¹H NMR (400 MHz, DMSO-d₆) δ 8.66 (d, *J* = 4.3 Hz, 1 H), 8.23 (d, *J* = 7.7 Hz, 1 H), 7.87 (td, *J* = 7.7, ⁴*J* = 1.8 Hz, 1 H), 7.43 (ddd, *J* = 7.7, 4.3, ⁴*J* = 1.4 Hz, 1 H), 6.82 (t, *J* = 5.7 Hz, 1 H), 5.66 (s, 1 H), 4.31 - 4.15 (m, 2 H), 4.07 (q, *J* = 7.2 Hz, 2 H), 3.54 (d, *J* = 5.8 Hz, 2 H), 2.87 - 2.77 (m, 1 H), 2.70 - 2.55 (m, 4 H), 1.93 - 1.83 (m, 1 H), 1.75 - 1.66 (m, 1 H), 1.48 - 1.35 (m, 1 H), 1.29 - 1.14 (m, 1 H), 1.18 (t, *J* = 7.2 Hz, 3 H); MS (ES+) *m/z* 371.3 [M+H]⁺. The signal arising from the NH₂ protons could not be observed, either because of exchange on the NMR timescale, or masking by the water peak (3.46 – 3.15 ppm).

(±)-3-((6-(3-Acetamidopiperidin-1-yl)-2-(pyridin-2-yl)pyrimidin-4-yl)amino)propanoic acid 321a

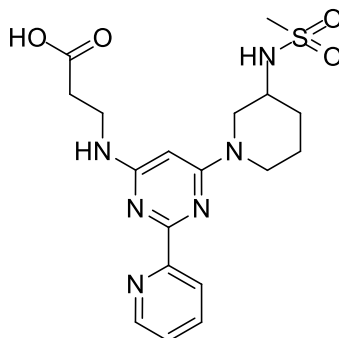


Acetyl chloride (0.02 mL, 0.30 mmol) was added to a suspension of ethyl *N*-[6-(3-amino-1-piperidinyl)-2-(2'-pyridyl)-4-pyrimidinyl]-β-alaninate **320** (100 mg, 0.27 mmol) in DCM (3 mL). After stirring for 18 h at rt, the reaction mixture was concentrated under reduced pressure. The residue was taken up in aqueous THF (2 mL of a 1:1 mixture) and lithium hydroxide monohydrate (22.7 mg, 0.54 mmol) was added. After stirring for 2 h at rt the reaction mixture was concentrated using the blow down unit. The residue was taken up in methanolic DMSO (1 mL of a 1:1 mixture) and purified by MDAP on a Waters Xbridge C18

column using ammonium bicarbonate (10 mM in methanol, adjusted to pH 10 with ammonia). The appropriate fractions were combined and concentrated under reduced pressure to give **321a** (20 mg, 19%) as a yellow solid.

¹H NMR (400 MHz, DMSO-d₆) δ 8.65 (d, *J* = 4.3 Hz, 1 H), 8.23 (d, *J* = 7.7 Hz, 1 H), 7.92 - 7.84 (m, 2 H), 7.42 (ddd, *J* = 7.7, 4.3, ⁴*J* = 1.1 Hz, 1 H), 6.88 - 6.79 (br. s, 1 H), 5.68 (s, 1 H), 4.19 - 4.02 (br. s, 2 H), 3.71 - 3.61 (m, 1 H), 3.54 - 3.42 (br. s, 2 H), 3.04 (m, 1 H), 2.84 (dd, *J* = 12.5, 9.5 Hz, 1 H), 2.51 - 2.45 (m, 2 H), 1.89 - 1.84 (m, 1 H), 1.81 (s, 3 H), 1.79 - 1.73 (m, 1 H), 1.53 - 1.38 (m, 2 H); MS (ES+) *m/z* 385.1 [M+H]⁺. The signal arising from the CO₂H proton could not be observed, either because of exchange on the NMR timescale, or masking by the water peak (3.86 - 2.92 ppm).

(±)-3-((6-(3-(Methylsulfonamido)piperidin-1-yl)-2-(pyridin-2-yl)pyrimidin-4-yl)amino)propanoic acid 321b

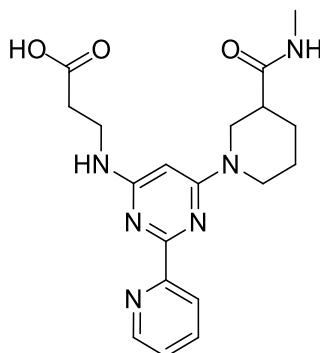


Methanesulfonyl chloride (0.02 mL, 0.30 mmol) was added to a suspension of ethyl *N*-[6-(3-amino-1-piperidinyl)-2-(2'-pyridyl)-4-pyrimidinyl]-β-alaninate **320** (100 mg, 0.27 mmol) in DCM (3 mL). After stirring at rt for 18 h, pyridine (0.02 mL, 0.27 mmol) was added to the reaction mixture. Reaction mixture was concentrated under reduced pressure, after standing without stirring for 4 days. The residue was taken up in aqueous THF (2 mL of a 1:1 mixture) and lithium hydroxide monohydrate (22.7 mg, 0.54 mmol) was added. After stirring for 4 h at rt, reaction mixture was concentrated using the blow down unit. The residue was taken up in methanolic DMSO (1 mL of a 1:1 mixture) and purified by MDAP on a Waters

Xbridge C18 column using ammonium bicarbonate (10 mM in methanol, adjusted to pH 10 with ammonia). The appropriate fractions were combined and concentrated under reduced pressure to give **321b** (35 mg, 31%) as a yellow solid.

¹H NMR (400 MHz, 393 K, DMSO-d₆) δ 8.64 (d, *J* = 4.3 Hz, 1 H), 8.22 (d, *J* = 7.7 Hz, 1 H), 7.82 (td, *J* = 7.7, ⁴*J* = 1.8 Hz, 1 H), 7.37 (dd, *J* = 7.7, 4.3 Hz, 1 H), 5.72 (s, 1 H), 4.30 (dd, *J* = 12.8, 4.0 Hz, 1 H), 4.08 - 3.99 (m, 1 H), 3.58 (t, *J* = 6.8 Hz, 2 H), 3.42 - 3.31 (m, 1 H), 3.11 - 3.03 (m, 2 H), 2.99 (s, 3 H), 2.56 (t, *J* = 6.9 Hz, 2 H), 2.09 - 1.97 (br. s, 1 H), 1.83 - 1.75 (m, 1 H), 1.64 - 1.51 (m, 2 H); the signals arising from the two NH and CO₂H protons could not be observed, either because of exchange on the NMR timescale, or masking by the water (3.33 ppm) and DMSO (2.5 ppm) peaks; MS (ES+) *m/z* 421.3 [M+H]⁺.

(±)-3-((6-(3-(Methylcarbamoyl)piperidin-1-yl)-2-(pyridyl)pyrimidin-4-yl)amino)propanoic acid 324

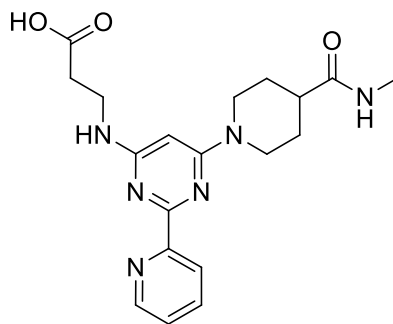


Was prepared as for **208** from *N*-[6-chloro-2-(2'-pyridyl)-4-pyrimidinyl]-β-alanine **323** (100 mg, 0.36 mmol), DIPEA (0.13 mL, 0.72 mmol) and *N*-methyl-3-piperidinecarboxamide **322** (63.2 mg, 0.44 mmol). Usual purification gave **324** (13 mg, 9%) as a yellow solid.

¹H NMR (400 MHz, DMSO-d₆) δ 8.65 (d, *J* = 4.9 Hz, 1 H), 8.21 (d, *J* = 7.3 Hz, 1 H), 7.93 - 7.84 (m, 2 H), 7.42 (dd, *J* = 7.3, 4.9 Hz, 1 H), 6.81 - 6.72 (br. s, 1 H), 5.71 (s, 1 H), 4.43 - 4.25 (br. s, 2 H), 3.56 - 3.44 (br. s, 2 H), 2.93 (dd, *J* = 12.8, 11.3 Hz, 1 H), 2.85 - 2.77 (m, 1 H), 2.58 (d, *J* = 4.5 Hz, 3 H), 2.53 - 2.47 (m, 2 H), 2.34 - 2.24 (m, 1 H), 1.89 - 1.81 (m, 1 H),

1.73 - 1.58 (m, 2 H), 1.47 - 1.34 (m, 1 H); MS (ES+) m/z 385.2 [M+H]⁺. The signal arising from the CO₂H proton could not be observed, either because of exchange on the NMR timescale, or masking by the water peak (4.04 - 2.98 ppm).

3-((6-(4-(methylcarbamoyl)piperidin-1-yl)-2-(pyridin-2-yl)pyrimidin-4-yl)amino)propanoic acid 327a



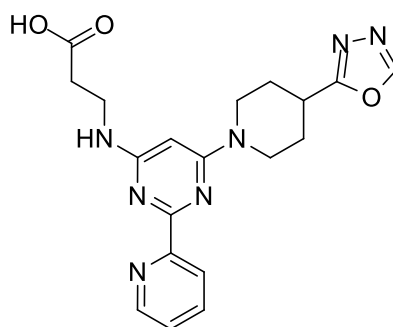
A mixture of ethyl *N*-[6-chloro-2-(2'-pyridyl)-4-pyrimidinyl]-β-alaninate **313** (150 mg, 0.49 mmol), DIPEA (0.17 mL, 0.98 mmol), *N*-methyl-4-piperidinecarboxamide **325a** (83 mg, 0.59 mmol) and DMSO (0.5 mL) was heated at 200 °C in a Biotage Initiator microwave for 2 h. A further portion of *N*-methyl-4-piperidinecarboxamide **325a** (83 mg, 0.59 mmol) was added and reaction mixture was heated at 200 °C in a Biotage Initiator microwave for a further 2 h. The reaction mixture was concentrated under reduced pressure, the residue was loaded onto a SNAP silica column (25 g) and purified by automated chromatography (SP4), eluting with a 8% gradient of MeOH in DCM (20 CV). The appropriate fractions were combined and evaporated under reduced pressure to give the crude **326a** (188 mg) as a brown gum.

Crude **326a** (188 mg) was taken up in aqueous THF (2 mL of a 1:1 mixture) and lithium hydroxide monohydrate (16.8 mg, 0.40 mmol) was added. After stirring for 1 h at rt, the reaction mixture was concentrated under reduced pressure. The residue was taken up in methanolic DMSO (1 mL of a 1:1 mixture) and purified by MDAP on a Waters Xbridge C18 column using ammonium bicarbonate (10 mM in methanol, adjusted to pH 10 with

ammonia). The appropriate fractions were combined and concentrated under reduced pressure to give **327a** (58 mg, 31%) as a yellow solid.

¹H NMR (400 MHz, DMSO-d₆) δ 8.66 (d, *J* = 4.3 Hz, 1 H), 8.23 (d, *J* = 7.8 Hz, 1 H), 7.87 (td, *J* = 7.8, 1.8 Hz, 1 H), 7.78 (q, *J* = 4.5 Hz, 1 H), 7.43 (ddd, *J* = 7.8, 4.3, 1.3 Hz, 1 H), 6.85 - 6.77 (br. s, 1 H), 5.69 (s, 1 H), 4.45 - 4.34 (br. s, 2 H), 3.54 - 3.42 (br. s, 2 H), 2.83 (t, *J* = 12.0 Hz, 2 H), 2.57 (d, *J* = 4.8 Hz, 3 H), 2.51 - 2.46 (m, 2 H), 2.42 - 2.32 (m, 1 H), 1.78 - 1.69 (m, 2 H), 1.51 (qd, *J* = 12.0, 3.9 Hz, 2 H); ¹³C NMR (126 MHz, DMSO-d₆) δ 174.4, 173.6, 163.9, 162.6, 161.8, 156.3, 148.9, 136.4, 124.1, 123.1, 80.6 (br.), 43.5, 42.2, 37.1, 34.7, 27.9, 25.5; HRMS (TOF): *M* + *H* calcd for C₁₉H₂₄N₆O₃ 385.1988, found 385.1974; IR (cm⁻¹) 3285, 2928, 1640, 1584, 1556, 1375, 1207, 786; mp = 246 °C (decomp.). The signal arising from the CO₂H proton could not be observed, either because of exchange on the NMR timescale, or masking by the water peak (3.81 - 3.03 ppm).

3-((6-(4-(1,3,4-oxadiazol-2-yl)piperidin-1-yl)-2-(pyridyl)pyrimidin-4-yl)amino)propanoic acid 327b

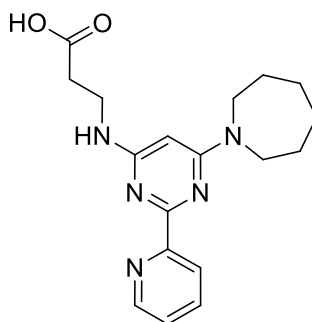


A mixture of ethyl *N*-[6-chloro-2-(2-pyridyl)-4-pyrimidinyl]-β-alaninate **313** (204.3 mg, 0.67 mmol), DIPEA (0.35 mL, 2.0 mmol), 4-(1,3,4-oxadiazol-2-yl)piperidine **325b** (122 mg, 0.80 mmol) and DMSO (0.5 mL) was heated at 160 °C in a Biotage Initiator microwave for 2 h. The reaction mixture was loaded onto a SNAP silica column (50 g) and partially purified by automated chromatography (SP4), eluting with a 0 - 10% gradient of MeOH in DCM (20 CV). The appropriate fractions were combined and evaporated under reduced pressure. The

residue was taken up in methanolic DMSO (1 mL of a 1:1 mixture) and purified by MDAP on a Waters Xbridge C18 column using ammonium bicarbonate (10 mM in methanol, adjusted to pH 10 with ammonia). The appropriate fractions were combined and evaporated under reduced pressure to give the crude **326b** (109 mg) as a dark yellow oil.

Crude **326b** (100 mg) was taken up in aqueous THF (2 mL of a 1:1 mixture) and lithium hydroxide monohydrate (9.9 mg, 0.24 mmol) was added. The reaction mixture was stirred at rt for 1 h and 50 °C for 20 h before more lithium hydroxide monohydrate (9.9 mg, 0.24 mmol) was added. After stirring at 50 °C for 3 h, the reaction mixture was concentrated using the blow-down unit. The residue was taken up in methanolic DMSO (1 mL of a 1:1 mixture) and purified by MDAP on a Waters Xbridge C18 column using ammonium bicarbonate (10 mM in methanol, adjusted to pH 10 with ammonia). The appropriate fractions were combined and evaporated under reduced pressure to give **327b** (30 mg, 12%) as an off-white solid.

¹H NMR (500 MHz, DMSO-d₆) δ 9.15 (s, 1 H), 8.65 (d, *J* = 4.3 Hz, 1 H), 8.23 (d, *J* = 7.9 Hz, 1 H), 7.87 (td, *J* = 7.9, ⁴*J* = 1.4 Hz, 1 H), 7.42 (ddd, *J* = 7.9, 4.3, ⁴*J* = 1.4 Hz, 1 H), 6.87 - 6.78 (br. s, 1 H), 5.74 (s, 1 H), 4.35 (d, *J* = 12.0 Hz, 2 H), 3.54 - 3.45 (br. s, 2 H), 3.32 (tt, *J* = 10.9, 3.9 Hz, 1 H), 3.10 (t, *J* = 12.0 Hz, 2 H), 2.53 - 2.50 (m, 2 H), 2.09 (dd, *J* = 13.0, 2.6 Hz, 2 H), 1.75 - 1.66 (m, 2 H); ¹³C NMR (126 MHz, DMSO-d₆) δ 173.4, 168.1, 163.9, 162.5, 161.8, 156.2, 154.3, 149.0, 136.4, 124.1, 123.1, 80.2 (br.), 43.0, 36.9, 34.5, 32.4, 28.3; HRMS (TOF): *M* + *H* calcd for C₁₉H₂₂N₇O₃ 369.1784, found 369.1790; IR (cm⁻¹) 3309, 1703, 1585, 1562, 1230, 1090, 970, 790; mp = 187 °C (decomp.). The signal arising from the CO₂H proton could not be observed, either because of exchange on the NMR timescale, or masking by the water peak (3.91 - 3.17 ppm).

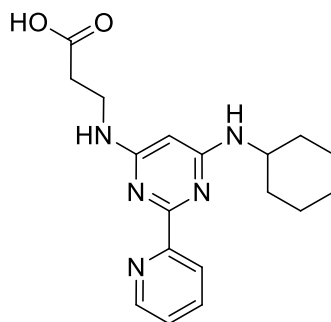
3-((6-(Azepan-1-yl)-2-(pyridin-2-yl)pyrimidin-4-yl)amino)propanoic acid 329a

A mixture of ethyl N-[6-chloro-2-(2-pyridinyl)-4-pyrimidinyl]-b-alaninate (200 mg, 0.65 mmol), azepane (0.09 mL, 0.78 mmol) and DIPEA (0.34 mL, 1.96 mmol) in 1,4-dioxane (2 mL) was heated at 150 °C in a Biotage Initiator microwave for 2 h. A further portion of azepane (0.09 mL, 0.78 mmol) was added to the reaction mixture which was heated at 150 °C in a Biotage Initiator microwave for 2 h. The solvent was removed under reduced pressure and the residue was loaded onto a SNAP silica cartridge (50 g) and partially purified by automated chromatography (SP4) using a 0-15% gradient of methanolic ammonia (2 M) in DCM (20 CV). The appropriate fractions were combined and evaporated under reduced pressure, to give the crude ester (284 mg, > 100 % yield) as a yellow oil.

A portion of the ester (194 mg, 0.525 mmol) was taken up in a mixture of THF/water (2 mL of a 1:1 mixture), lithium hydroxide monohydrate (44.1 mg, 1.05 mmol) was added and reaction mixture was stirred at rt for 20 min. The reaction mixture was concentrated under reduced pressure and the residue was purified by MDAP on a Waters Xbridge C18 column using ammonium bicarbonate (10 mM in methanol, adjusted to pH 10 with ammonia). The appropriate fractions were combined and evaporated under a stream of nitrogen in the Radleys blowdown apparatus and the residue was further purified by MDAP on a Waters Xbridge C18 column using ammonium bicarbonate (10 mM in methanol, adjusted to pH 10 with ammonia). The appropriate fractions were combined and concentrated under reduced pressure to give **329a** (41.2 mg, 27 %) as an off-white solid.

¹H NMR (400 MHz, DMSO-d₆) δ 8.64 (d, *J* = 4.5 Hz, 1 H), 8.19 (d, *J* = 7.8 Hz, 1 H), 7.81 (td, *J* = 7.8, 1.9, Hz, 1 H), 7.35 (ddd, *J* = 7.8, 4.5, 1.9 Hz, 1 H), 5.56 (s, 1 H), 3.71 - 3.64 (m, 4 H), 3.57 (t, *J* = 6.8 Hz, 2 H), 2.56 (t, *J* = 6.8 Hz, 2 H), 1.83 - 1.73 (br. s, 4 H), 1.60 - 1.52 (m, 4 H); ¹³C NMR (126 MHz, DMSO-d₆) δ 173.7, 163.5, 161.7, 156.6, 148.9, 136.4, 124.0, 123.0, 79.2 (br.), 46.6 (br.), 37.1, 34.8, 27.2 (br.), 26.6; IR (cm⁻¹) 3285, 2916 (br.), 1562, 1371; HRMS (TOF): *M* + *H* calcd for C₁₈H₂₄N₅O₂ 342.1925, found 342.1925; mp = 261.7. The signals arising from the NH and CO₂H protons could not be observed, either because of exchange on the NMR timescale, or masking by the water peak (3.11 - 2.78 ppm).

3-((6-(Cyclohexylamino)-2-(pyridin-2-yl)pyrimidin-4-yl)amino)propanoic acid 329b



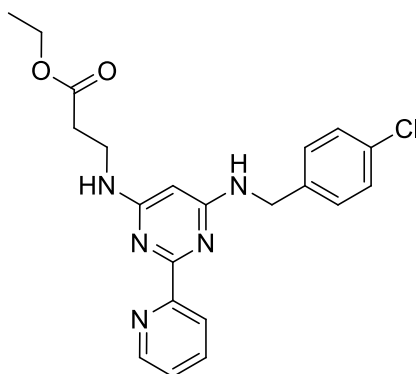
A mixture of ethyl *N*-[6-chloro-2-(2-pyridinyl)-4-pyrimidinyl]-β-alaninate (144.2 mg, 0.47 mmol), cyclohexanamine (0.07 mL, 0.56 mmol) and DIPEA (0.25 mL, 1.41 mmol) in 1,4-dioxane (1.5 mL) was heated in a Biotage Initiator microwave at 170 °C for 2 h. Cyclohexanamine (0.07 mL, 0.56 mmol) and DIPEA (0.08 mL, 0.47 mmol) were added and the reaction mixture was heated in a Biotage Initiator microwave at 200 °C for 1+ 2 +2 h. The reaction mixture was concentrated under reduced pressure and the residue was on a SNAP silica cartridge (25 g), purified by automated chromatography (SP4), eluting with a 0 - 7% gradient of methanolic ammonia (2M) in DCM (15 CV). The appropriate fractions were combined and evaporated under reduced pressure to give the crude ester as an orange oil (142 mg). MS (ES+) *m/z* 307.1 [*M*+*H*]⁺.

A portion of the crude ester (103 mg) was taken up in aqueous THF (2 mL of a 1:1 mixture)

and lithium hydroxide monohydrate (23.4 mg, 0.56 mmol) was added. After stirring for 1 h at rt, the reaction mixture was concentrated under a stream of nitrogen in the Radleys blowdown apparatus. The residue was taken up in methanolic DMSO (2 mL of a 1:1 mixture) and purified by MDAP on a Waters Xbridge C18 column using ammonium bicarbonate (10 mM in methanol, adjusted to pH 10 with ammonia). The appropriate fractions were combined and concentrated under reduced pressure to give **329b** (45 mg, 38%) as an orange solid.

^1H NMR (400 MHz, DMSO- d_6 , 393 K) δ 8.62 (d, $J = 4.0$ Hz, 1 H), 8.17 (d, $J = 7.8$ Hz, 1 H), 7.80 (td, $J = 7.8$, $^4J = 1.6$ Hz, 1 H), 7.34 (ddd, $J = 7.8$, 4.7, $^4J = 1.6$ Hz, 1 H), 5.94 - 5.86 (br. s, 1 H), 5.48 (s, 1 H), 3.73 - 3.62 (m, 1 H), 3.51 (t, $J = 6.9$ Hz, 2 H), 2.55 - 2.47 (m, 2 H), 1.99 - 1.90 (m, 2 H), 1.82 - 1.71 (m, 2 H), 1.66 - 1.57 (m, 1 H), 1.46 - 1.18 (m, 5 H). The signals arising from the NH and CO₂H protons could not be observed, either because of exchange on the NMR timescale, or masking by the water peak (3.4 – 3.28 ppm). ^{13}C NMR (126MHz, DMSO- d_6) δ 173.6, 163.0 (br.), 162.3 (br.), 162.1, 156.4, 148.8, 136.4, 124.0, 122.9, 79.9 (br.), 48.9 (br.), 37.1, 34.7, 32.6, 25.4, 24.7; IR (cm⁻¹) 3261 (br.), 2928, 2853, 1651, 1565, 1373; HRMS (TOF): M + H calcd for C₁₈H₂₄N₅O₂ 342.1925, found 342.1931; mp = 141.7 °C.

Ethyl 3-((6-((4-chlorobenzyl)amino)-2-(pyridin-2-yl)pyrimidin-4-yl)amino)propanoate
331a

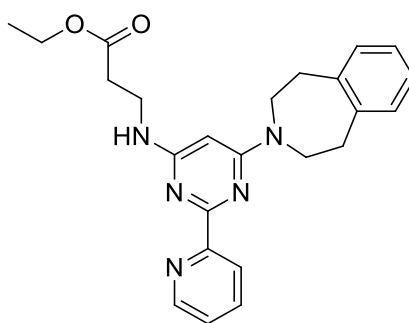


Was prepared as for **208** from DIPEA (0.17 mL, 0.10 mmol), [(4-

chlorophenyl)methyl]amine **330a** (0.07 mL, 0.60 mmol), **313** (152.7 mg, 0.5 mmol). The usual work up and purification afforded **331a** (47 mg, 23 %) as a pale orange solid.

¹H NMR (400 MHz, CDCl₃) δ 8.79 (d, *J* = 4.5 Hz, 1 H), 8.38 (d, *J* = 7.8 Hz, 1 H), 7.81 (td, *J* = 7.8, ⁴*J* = 1.6 Hz, 1 H), 7.40 - 7.29 (m, 5 H), 6.07 - 5.81 (br. s, 1 H), 5.62 - 5.45 (br. s, 1 H), 5.28 (s, 1 H), 4.49 (d, *J* = 5.8 Hz, 2 H), 4.17 (q, *J* = 7.1 Hz, 2 H), 3.70 - 3.56 (br. s, 2 H), 2.61 (t, *J* = 6.3 Hz, 2 H), 1.27 (t, *J* = 7.1 Hz, 3 H); MS (ES+) *m/z* 412.2 [M+H]⁺.

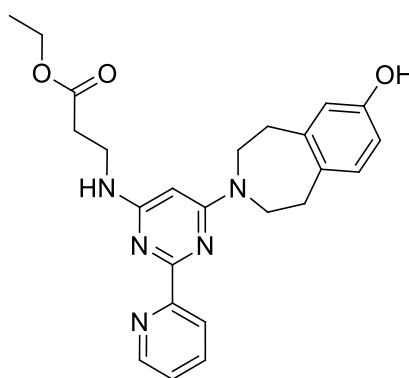
Ethyl 3-((6-(4,5-dihydro-1H-benzo[d]azepin-3(2H)-yl)-2-(pyridin-2-yl)pyrimidin-4-yl)amino)propanoate 331b



A mixture of DIPEA (0.30 mL, 1.70 mmol), ethyl 3-((6-chloro-2-(pyridin-2-yl)pyrimidin-4-yl)amino)propanoate **313** (208 mg, 0.68 mmol) and 2,3,4,5-tetrahydro-1H-benzo[d]azepine **330b** (200 mg, 1.36 mmol) in DMSO (2 mL) was heated in a Biotage Initiator microwave at 160 °C for 2 h and then allowed to stand at rt for 11 h. The solution was diluted with EtOAc (20 mL) and saturated aqueous NH₄Cl (20 mL) and the separated aqueous phase was then extracted with EtOAc (2 x 30 mL). The combined organic extracts were passed through a hydrophobic frit and evaporated under reduced pressure to give an orange oil. The residue was taken up in methanolic DMSO (4 mL of a 1:1 mixture) and purified by MDAP on a Sunfire C18 column using acetonitrile water with a formic acid modifier. The solvent was evaporated under reduced pressure to give a yellow oil. The oil was taken up in EtOH (10 mL), loaded onto an aminopropyl SPE column (5 g) and eluted with EtOH (3 CV). The appropriate fractions were combined and evaporated under reduced pressure to give **331b** (107 mg, 38%) as a yellow oil.

^1H NMR (400 MHz, DMSO- d_6) δ 8.67 (d, J = 4.8 Hz, 1H), 8.25 (d, J = 7.9 Hz, 1H), 7.88 (dt, J = 7.9, 1.5 Hz, 1H), 7.43 (ddd, J = 7.9, 4.8, 4J = 1.5 Hz, 1H), 7.19 - 7.08 (m, 4H), 6.83 (t, J = 5.6 Hz, 1H), 5.72 (s, 1H), 4.07 (q, J = 7.1 Hz, 2H), 3.86 - 3.80 (m, 4H), 3.57 (q, J = 6.6 Hz, 2H), 2.96 - 2.90 (m, 4H), 2.62 (t, J = 6.6 Hz, 2H), 1.18 (t, J = 7.1 Hz, 3H); MS (ES+) m/z 418.3 [M+H] $^+$.

Ethyl 3-((6-(7-hydroxy-4,5-dihydro-1H-benzo[d]azepin-3(2H)-yl)-2-(pyridin-2-yl)pyrimidin-4-yl)amino)propanoate 331c

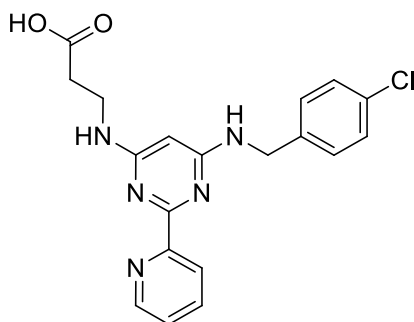


A mixture of 2,3,4,5-tetrahydro-1H-3-benzazepin-7-ol **330c** (84 mg, 0.51 mmol), **313** (157 mg, 0.51 mmol) and DIPEA (0.18 mL, 1.02 mmol) in 1,4-dioxane (1 mL) was heated in a Biotage initiator microwave at 160 °C for 4 h. A further portion of 2,3,4,5-tetrahydro-1H-3-benzazepin-7-ol **330c** (24 mg, 0.15 mmol) was added and the reaction mixture was heated in a Biotage initiator microwave at 180°C for 2 h. The reaction mixture was concentrated under reduced pressure and the residue was taken up in methanolic DMSO (3 mL of a 1:1 mixture) and purified by MDAP on a Waters Xbridge C18 column using ammonium bicarbonate (10 mM in methanol, adjusted to pH 10 with ammonia). The solvent was evaporated under reduced pressure to give **331c** (139 mg, 63 %) as a yellow oil.

^1H NMR (600 MHz, DMSO- d_6) δ 9.25 - 8.97 (br. s, 1 H), 8.67 (d, J = 3.7 Hz, 1 H), 8.24 (d, J = 7.7 Hz, 1 H), 7.88 (td, J = 7.7, 4J = 1.8 Hz, 1 H), 7.43 (ddd, J = 7.7, 5.1, 4J = 1.8 Hz, 1 H),

6.94 (d, $J = 8.1$ Hz, 1 H), 6.82 (t, $J = 5.7$ Hz, 1 H), 6.58 (d, $^4J = 2.2$ Hz, 1 H), 6.49 (dd, $J = 8.1$, $^4J = 2.2$, Hz, 1 H), 5.69 (s, 1 H), 4.07 (q, $J = 7.1$ Hz, 2 H), 3.79 (br. s, 4 H), 3.56 (br. s, 2 H), 2.83 - 2.78 (m, 4 H), 2.61 (t, $J = 6.8$ Hz, 2 H), 1.18 (t, $J = 7.1$ Hz, 3 H); MS (ES+) m/z 434.3 [M+H]⁺.

3-((6-((4-Chlorobenzyl)amino)-2-(pyridin-2-yl)pyrimidin-4-yl)amino)propanoic acid
332a

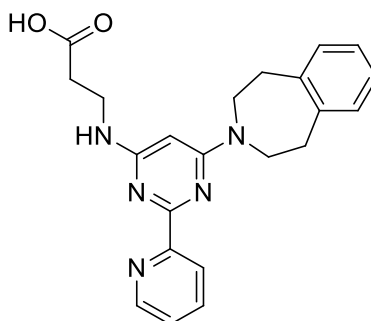


Ethyl *N*-[6-{{(4-chlorophenyl)methyl}amino}-2-(2-pyridinyl)-4-pyrimidinyl]-β-alaninate (20 mg, 0.05 mmol) was taken up in a mixture of THF (2 mL) and water (1 mL) and lithium hydroxide monohydrate (4.1 mg, 0.1 mmol). After stirring at rt for 80 min, the reaction mixture was concentrated under reduced pressure. The crude was taken up in *iso*-propanol (3 mL) and the mixture was acidified with an aqueous solution of HCl (2 M) (0.7 mL).

The solution was loaded onto an SCX cartridge (0.5 g) and eluted with a solution of 10% ammonia (aqueous) in *iso*-propanol (4 CV). The appropriate fractions were combined and concentrated under reduced pressure to give **332a** (12.3 mg, 66 %) as a yellow solid.

¹H NMR (400 MHz, DMSO-*d*₆) δ 12.25 - 12.10 (br. s, 1 H), 8.60 (d, $J = 4.0$ Hz, 1 H), 8.14 (d, $J = 7.8$ Hz, 1 H), 7.82 (td, $J = 7.8$, $^4J = 1.8$ Hz, 1 H), 7.41 - 7.28 (m, 6 H), 6.80 - 6.73 (br. s, 1 H), 5.38 (s, 1 H), 4.44 (d, $J = 4.5$ Hz, 2 H), 3.40 (d, $J = 4.5$ Hz, 2 H); MS (ES+) m/z 384.1 [M+H]⁺. The signals arising from the CO₂H or NH protons could not be observed, either because of exchange on the NMR timescale, or masking by the water peak (3.81 - 3.03 ppm).

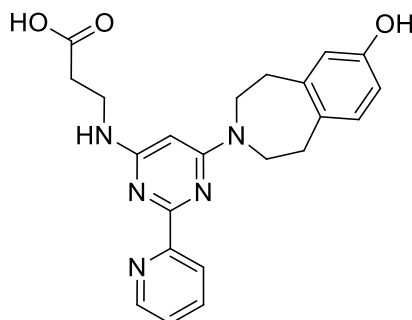
3-((6-(4,5-Dihydro-1H-benzo[d]azepin-3(2H)-yl)-2-(pyridin-2-yl)pyrimidin-4-yl)amino)propanoic acid 332b



Ethyl 3-((6-(4,5-dihydro-1H-benzo[d]azepin-3(2H)-yl)-2-(pyridin-2-yl)pyrimidin-4-yl)amino)propanoate **331b** (135 mg, 0.323 mmol) was taken up in a mixture of THF (2 mL) and water (1 mL) and lithium hydroxide monohydrate (13.6 mg, 0.32 mmol) was added. The resulting mixture was stirred at rt for 16 h, then solvent was removed under reduced pressure. The residue was taken up in methanolic DMSO (1:1) (2 mL) and purified by MDAP on a Waters Xbridge C18 column using ammonium bicarbonate (10 mM in methanol, adjusted to pH 10 with ammonia). The appropriate fractions were combined and concentrated under reduced pressure to give **332b** (90 mg, 72%) as a yellow solid.

^1H NMR (400 MHz, 393K, DMSO- d_6) δ 8.66 (d, $J = 4.6$ Hz, 1H), 8.22 (d, $J = 7.8$ Hz, 1H), 7.83 (dd, $J = 7.8$, $^4J = 1.3$ Hz, 1H), 7.37 (ddd, $J = 7.8$, 4.6, $^4J = 1.3$ Hz, 1H), 7.20 - 7.07 (m, 4H), 6.62 - 5.96 (br. s, 1H), 5.72 (s, 1H), 3.91 - 3.86 (m, 4H), 3.59 (t, $J = 6.8$ Hz, 2H), 3.04 - 3.00 (m, 4H), 2.57 (t, $J = 6.8$ Hz, 2H); ^{13}C NMR (600 MHz, 303K, DMSO- d_6) δ 173.3, 163.8, 162.0, 161.6, 156.4, 148.9, 140.9, 136.3, 129.7, 126.1, 124.0, 123.0, 80.6 (br), 46.5, 36.9, 35.9, 34.5. HRMS ($\text{M}+\text{H}$) $^+$ calculated for $\text{C}_{22}\text{H}_{23}\text{N}_5\text{O}_2$ 390.1925; found 390.1919. The signal arising from the CO_2H proton could not be observed, either because of exchange on the NMR timescale, or masking by the water peak (4.05 - 3.03 ppm).

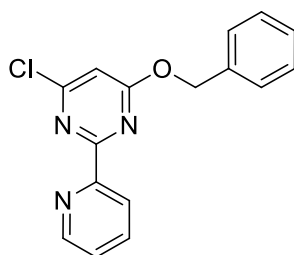
3-((6-(7-Hydroxy-4,5-dihydro-1H-benzo[d]azepin-3(2H)-yl)-2-(pyridin-2-yl)pyrimidin-4-yl)amino)propanoic acid 332c



Was prepared as for **332b** from **331c** (139 mg, 0.32 mmol) and lithium hydroxide monohydrate (13.5 mg, 0.32 mmol). The usual purification afforded (76.4 mg, 59%) as an off-white solid.

¹H NMR (400 MHz, DMSO-*d*₆) δ 12.57 - 12.04 (br. s, 1 H), 9.45 - 8.98 (br. s, 1 H), 8.67 (d, *J* = 4.0 Hz, 1 H), 8.25 (d, *J* = 7.8 Hz, 1 H), 7.89 (td, *J* = 7.8, ⁴*J* = 1.8 Hz, 1 H), 7.48 - 7.40 (m, 1 H), 6.94 (d, *J* = 8.1 Hz, 1 H), 6.82 (t, *J* = 5.6 Hz, 1 H), 6.58 (d, ⁴*J* = 2.5 Hz, 1 H), 6.49 (dd, *J* = 8.0, ⁴*J* = 2.5 Hz, 1 H), 5.70 (s, 1 H), 3.88 - 3.70 (br. s, 4 H), 3.58 - 3.48 (br. s, 2 H), 2.86 - 2.78 (m, 4 H), 2.55 (t, *J* = 6.9 Hz, 2 H); MS (ES⁺) *m/z* 406.2 [M+H]⁺.

4-(Benzyloxy)-6-chloro-2-(pyridin-2-yl)pyrimidine 335

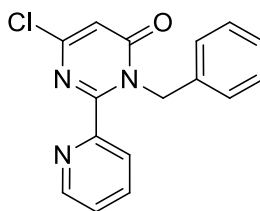


Triphenylphosphine (551 mg, 2.1 mmol) and di-*iso*-propylazodicarboxylate (0.41 mL, 2.1 mmol) were added to a cold (0°C) solution of 6-chloro-2-(2-pyridinyl)-4(1H)-pyrimidinone **334** (218 mg, 1.05 mmol) in THF (5 mL). Then, phenylmethanol (0.22 mL, 2.1 mmol) was added to the reaction mixture. After stirring at rt for 2 h, the reaction mixture was

concentrated under reduced pressure. The residue was loaded onto a SNAP silica cartridge (25 g) and partially purified by automated chromatography (SP4) using a 0-30% gradient of EtOAc in cyclohexane (15 CV). The impure product containing fractions were combined and concentrated under reduced pressure. The residue was loaded onto a SNAP silica cartridge (25 g) and partially purified by automated chromatography (SP4) using a 5-30% gradient of EtOAc in cyclohexane (15 CV). The appropriate fractions were combined and concentrated under reduced pressure to give crude **335** (270 mg) as a yellow solid.

MS (ES+) m/z 298.1 [M+H]⁺.

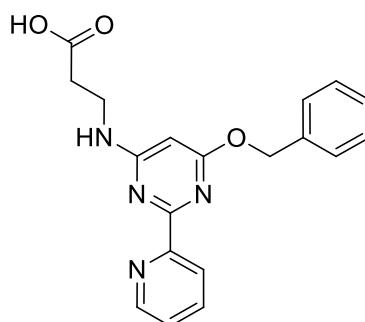
3-Benzyl-6-chloro-2-(pyridin-2-yl)pyrimidin-4(3H)-one 336



Compound **336** was also isolated but with low level of purity.

MS (ES+) m/z 298.1 [M+H]⁺.

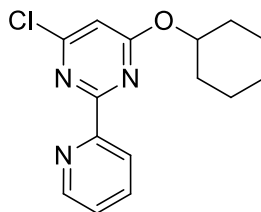
3-((6-(Benzyloxy)-2-(pyridin-2-yl)pyrimidin-4-yl)amino)propanoic acid 337



β -Alanine (113 mg, 0.74 mmol) and DIPEA (0.21 mL, 1.23 mmol) were added to a solution of **335** (221 mg, 0.74 mmol) in DMSO (0.5 mL). The mixture was heated at 150 °C in a Biotage Initiator microwave for 2 h.

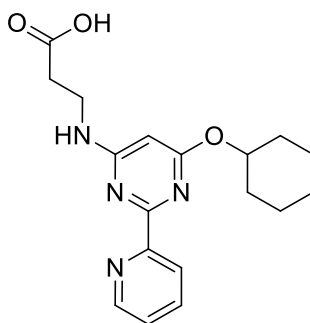
The reaction mixture was partially purified by MDAP on a Waters Xbridge C18 column using ammonium bicarbonate (10 mM in methanol, adjusted to pH 10 with ammonia) as eluant. The appropriate fractions were combined and concentrated under reduced pressure to give the impure product. The residue was further purified by MDAP on a Sunfire C18 column using acetonitrile water with a formic acid modifier. The residue was eluted through a hydrogen carbonate column with methanol. The product was eluted with methanolic HCl (1M) and was shown to be the methylester of the desired acid. The solvent was removed under reduced pressure and the residue was taken up in a mixture of THF/water (2 mL of a 1:1 mixture), lithium hydroxide monohydrate (62.3 mg, 1.49 mmol) was added and reaction mixture was stirred at rt for 2 h. The reaction mixture was concentrated under reduced pressure and the residue was purified by MDAP on a Waters Xbridge C18 column using ammonium bicarbonate (10 mM in methanol, adjusted to pH 10 with ammonia). The appropriate fractions were combined and concentrated under reduced pressure to give **337** (25 mg, 8% over 2 steps) as a white solid.

^1H NMR (400 MHz, DMSO- d_6) δ 8.70 (d, $J = 4.0$ Hz, 1 H), 8.29 (d, $J = 7.8$ Hz, 1 H), 7.92 (td, $J = 7.8$, $^4J = 1.8$ Hz, 1 H), 7.52 - 7.45 (m, 3 H), 7.41 - 7.29 (m, 4 H), 5.85 (s, 1 H), 5.43 (s, 2 H), 3.62 - 3.25 (br. s, 2 H), 2.48 - 2.40 (br. s, 2 H); MS (ES+) m/z 351.2 $[\text{M}+\text{H}]^+$. The signal arising from the CO_2H proton could not be observed, either because of exchange on the NMR timescale, or masking by the water peak (3.9 - 3.1 ppm).

4-Chloro-6-(cyclohexyloxy)-2-(pyridin-2-yl)pyrimidine 339

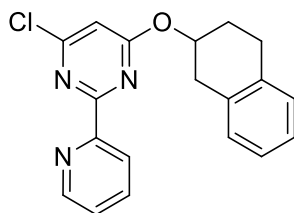
Cyclohexanol (0.12 mL, 1.11 mmol) was added to a cold (0 °C) solution of sodium hydride (48.7 mg, 1.22 mmol) in DMF (10 mL). After stirring for 30 min at 0 °C, 4,6-dichloro-2-(2-pyridinyl)pyrimidine **298** (250 mg, 1.11 mmol) was added. After stirring for 16 h at rt, the reaction mixture was cooled at 0 °C, sodium hydride (24 mg) was added. After stirring for 2 h at rt, water (50 mL) was added, followed by EtOAc (50 mL). The aqueous layer was further extracted with EtOAc (50 mL), the combined organic layers were dried through a hydrophobic frit and concentrated under reduced pressure. The residue was loaded onto a SNAP silica cartridge (25 g) and purified by automated chromatography (SP4) using a 0-50% gradient of EtOAc in cyclohexane (15 CV). The appropriate fractions were combined and concentrated under reduced pressure to give **339** (180 mg, 56%) as a yellow oil.

¹H NMR (400 MHz, DMSO-*d*₆) δ 8.77 (d, *J* = 3.8 Hz, 1 H), 8.33 (d, *J* = 7.8 Hz, 1 H), 8.01 (td, *J* = 7.8, ⁴*J* = 1.8 Hz, 1 H), 7.60 - 7.55 (m, 1 H), 7.16 (s, 1 H), 5.32 - 5.23 (m, 1 H), 2.06 - 1.96 (m, 2 H), 1.81 - 1.69 (m, 2 H), 1.62 - 1.50 (m, 2 H), 1.51 - 1.38 (m, 2 H), 1.38 - 1.22 (m, 2 H); MS (ES+) *m/z* 290.1 [M+H]⁺.

3-((6-(Cyclohexyloxy)-2-(pyridin-2-yl)pyrimidin-4-yl)amino)propanoic acid 340

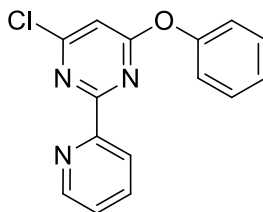
DIPEA (0.16 mL, 0.93 mmol) and β -alanine (33.2 mg, 0.37 mmol) were added to a solution of **339** (90 mg, 0.31 mmol) in DMSO (0.5 mL). The reaction mixture was heated in a Biotage initiator microwave at 200 °C for 2 h. The reaction mixture was purified by MDAP on a Waters Xbridge C18 column using ammonium bicarbonate (10 mM in methanol, adjusted to pH 10 with ammonia) as eluant. The appropriate fractions were combined and concentrated under reduced pressure to give **340** (10 mg, 9%) as an orange solid.

^1H NMR (400 MHz, DMSO- d_6) δ 8.68 (d, $J = 3.8$ Hz, 1 H), 8.23 (d, $J = 7.8$ Hz, 1 H), 7.90 (td, $J = 7.8$, $^4J = 1.8$ Hz, 1 H), 7.48 - 7.43 (m, 1 H), 7.26 - 7.18 (br. s, 1 H), 5.74 (s, 1 H), 5.12 - 5.02 (br. s, 1 H), 3.56 - 3.39 (br. s, 2 H), 2.44 (t, $J = 6.8$ Hz, 2 H), 2 - 1.91 (br. s, 2 H), 1.77 - 1.67 (br. s, 2 H), 1.58 - 1.22 (m, 6 H); MS (ES+) m/z 343.1 $[\text{M}+\text{H}]^+$. The signal arising from the CO_2H proton could not be observed, either because of exchange on the NMR timescale, or masking by the water peak (4 – 2.9 ppm).

4-Chloro-2-(pyridin-2-yl)-6-((1,2,3,4-tetrahydronaphthalen-2-yl)oxy)pyrimidine 342

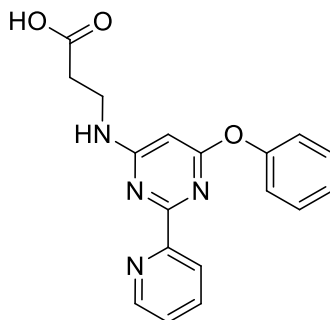
1,2,3,4-Tetrahydro-2-naphthol (164 mg, 1.11 mmol) was added to a cold (0 °C) solution of sodium hydride (48.7 mg, 1.22 mmol) in DMF (10 mL). After stirring for 30 min under nitrogen, **298** (250 mg, 1.11 mmol) was added. After stirring for 16 h at rt, the reaction was cooled at 0 °C, sodium hydride (24 mg) was added. After stirring for 2 h at rt, water (50 mL) was added to the reaction mixture, followed by EtOAc (50 mL). The aqueous layer was further extracted with EtOAc (50 mL). The combined organic layers were dried through a hydrophobic frit and concentrated under reduced pressure. The residue was loaded onto a SNAP silica cartridge (25 g) and purified by automated chromatography (SP4) using a 0-50% gradient of EtOAc in cyclohexane (15 CV). The appropriate fractions were combined and concentrated under reduced pressure to give the impure product (278 mg). A portion of the product (168 mg) was purified by MDAP on a Waters Xbridge C18 column using ammonium bicarbonate (10 mM in methanol, adjusted to pH 10 with ammonia). The appropriate fractions were combined and concentrated under reduced pressure to give **342** (64 mg, 29%) as a yellow oil. The yield was calculated based on pure **342** recovered from the purified portion.

¹H NMR (400 MHz, DMSO-d₆) δ 8.77 (d, *J* = 3.8 Hz, 1 H), 8.38 (d, *J* = 7.8 Hz, 1 H), 8.00 (td, *J* = 7.8, ⁴*J* = 1.8 Hz, 1 H), 7.60 - 7.55 (m, 1 H), 7.19 (s, 1 H), 7.15 - 7.10 (m, 4 H), 5.79 - 5.73 (m, 1 H), 3.40 - 3.31 (m, 2 H), 2.95 - 2.82 (m, 2 H), 2.22 - 2.08 (m, 2 H); MS (ES⁺) *m/z* 338.1 [M+H]⁺.

4-Chloro-6-phenoxy-2-(pyridin-2-yl)pyrimidine 345

Cs₂CO₃ (396 mg, 1.22 mmol) was added to a solution of phenol (104 mg, 1.11 mmol) in DMF (10 mL). After stirring at rt for 30 min under nitrogen, **298** (250 mg, 1.11 mmol) was added. After stirring at rt for 16 h, the reaction mixture was concentrated under reduced pressure to give **345** (317 mg, 100%) as a yellow oil which solidified over time.

¹H NMR (400 MHz, DMSO-d₆) δ 8.72 (d, *J* = 4.0 Hz, 1 H), 8.07 (d, *J* = 7.8 Hz, 1 H), 7.94 (td, *J* = 7.8, ⁴*J* = 1.8 Hz, 1 H), 7.57 - 7.47 (m, 3 H), 7.39 - 7.29 (m, 4 H); ¹³C NMR (126 MHz, DMSO-d₆) δ 171.5 (br.), 170.3, 163.3, 161.6, 152.6, 152.0, 149.8, 137.3, 130.0, 126.0, 125.8, 123.8, 121.4, 107.0, 91.3 (br.); IR (cm⁻¹) 3051, 1544, 1379, 1195; HRMS (TOF): *M* + *H* calcd for C₁₅H₁₁ClN₃O 284.0585, found 284.0588; mp = 96.5 °C.

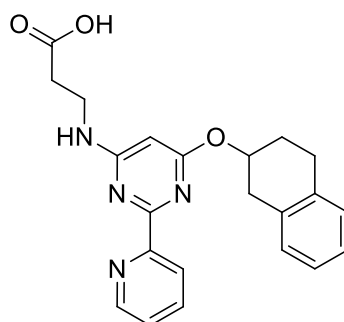
3-((6-Phenoxy-2-(pyridin-2-yl)pyrimidin-4-yl)amino)propanoic acid 346

Cs₂CO₃ (212 mg, 0.65 mmol) was added to a solution of phenol (61.4 mg, 0.65 mmol) in DMF (10 mL). After stirring at rt for 30 min, **313** (200 mg, 0.65 mmol) was added. After stirring at 95 °C for 18 h the reaction mixture was cooled at rt, and concentrated under reduced pressure. The residue was loaded onto a SNAP silica cartridge (25 g) and purified by automated chromatography (SP4) using a 0-7% gradient of MeOH in DCM (15 CV). The

appropriate fractions were combined and concentrated under reduced pressure to give the impure ethylester product. The residue was taken up in a mixture of THF/water (3 mL of a 2:1 mixture), lithium hydroxide monohydrate (54.7 mg, 1.30 mmol) was added and reaction mixture was stirred at rt for 1 h. The reaction mixture was concentrated under a stream of nitrogen in the Radleys blowdown apparatus. The residue was purified by MDAP on a Waters Xbridge C18 column using ammonium bicarbonate (10 mM in methanol, adjusted to pH 10 with ammonia). The appropriate fractions were combined and concentrated under reduced pressure to give **346** (36 mg, 16 % over 2 steps) as a white solid.

¹H NMR (400 MHz, DMSO-d₆) δ 8.66 (d, *J* = 3.3 Hz, 1 H), 8.21 - 8.08 (m, 1 H), 7.88 (t, *J* = 7.5 Hz, 1 H), 7.59 - 7.50 (m, 1 H), 7.49 - 7.42 (m, 3 H), 7.30 - 7.23 (m, 1 H), 7.21 (d, *J* = 7.5 Hz, 2 H), 5.83 - 5.76 (br. s, 1 H), 3.58 - 3.55 (m, 1 H), 3.64 - 3.49 (br. s, 2 H), 2.44 (t, *J* = 6.5 Hz, 2 H); ¹³C NMR (126 MHz, DMSO-d₆) δ 173.8, 169.7 (br.), 165.2, 163.0 (br.), 155.1, 152.9, 149.2, 136.7, 129.9, 125.0, 124.7, 123.3, 121.3, 86.8 (br.), 37.3 (br.), 35.1; IR (cm⁻¹) 3296, 2983 (br.), 1584, 1383, 1225; HRMS (TOF): M + H calcd for C₁₈H₁₇N₄O₃ 337.1295, found 337.1299; mp = 262.6 °C.

3-((2-(Pyridin-2-yl)-6-((1,2,3,4-tetrahydronaphthalen-2-yl)oxy)pyrimidin-4-yl)amino)propanoic acid **343**

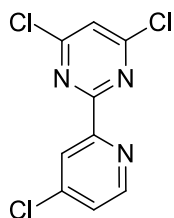


DIPEA (0.10 mL, 0.57 mmol) and β-alanine (20.3 mg, 0.23 mmol) were added to a solution of **342** (64 mg, 0.19 mmol) in DMSO (0.5 mL). The reaction mixture was heated at 150 °C in

a Biotage Initiator microwave for 2 h. β -Alanine (10 mg) and DIPEA (66 μ L) were added and the reaction mixture was heated at 150 $^{\circ}$ C in a Biotage Initiator microwave for 1 h. The reaction mixture was partially purified by MDAP on a Waters Xbridge C18 column using ammonium bicarbonate (10 mM in methanol, adjusted to pH 10 with ammonia) as eluant. The appropriate fractions were combined and concentrated under reduced pressure to give the impure product. The residue was purified further by MDAP on a Sunfire C18 column using acetonitrile water with a formic acid modifier. The appropriate fractions were combined and concentrated under reduced pressure and the residue was taken up in ethanol, loaded on a 2 g SCX column, washed with ethanol (4 CV) and eluted with 20% ammoniumhydroxide in ethanol (4 CV). The appropriate fractions were combined and concentrated under reduced pressure to give **345** (28 mg, 38%) as a yellow solid.

^1H NMR (600 MHz, DMSO- d_6) δ 8.68 (d, $J = 4.6$ Hz, 1 H), 8.27 (d, $J = 7.9$ Hz, 1 H), 7.90 (td, $J = 7.9$, $^4J = 1.8$ Hz, 1 H), 7.48 -7.44 (m, 1 H), 7.27 (t, $J = 5.5$ Hz, 1 H), 7.14 - 7.08 (m, 4 H), 5.77 (s, 1 H), 5.60 - 5.53 (m, 1 H), 3.51 - 3.19 (m, 3 H), 2.95 - 2.87 (m, 2 H), 2.87 - 2.80 (m, 1 H), 2.52 - 2.44 (m, 2 H), 2.13 - 2.07 (br. s, 1 H), 2.07 - 2.00 (m, 1 H); MS (ES+) m/z 391.2 $[\text{M}+\text{H}]^+$. The signal arising from the CO_2H proton could not be observed, either because of exchange on the NMR timescale, or masking by the water peak (3.57 – 2.95 ppm).

4,6-Dichloro-2-(4-chloropyridin-2-yl)pyrimidine 351

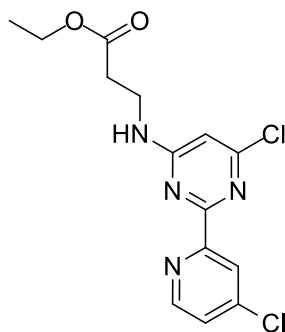


A suspension of 2-(4-chloro-2'-pyridyl)-6-hydroxy-4(1H)-pyrimidinone **313** (307 mg, 1.37 mmol) in phosphorus oxychloride (2 mL, 21.46 mmol) was heated under reflux for 1.5 h.

The reaction mixture was concentrated under reduced pressure and the resulting black tar was carefully treated with a saturated aqueous solution of NaOAc. The aqueous solution was then taken to pH 9 by addition of a saturated solution of NaHCO₃, and extracted with DCM (2 x 50 mL). The combined organic extracts were dried through a hydrophobic frit and concentrated under reduced pressure to give **351** (168 mg, 47%) as a brown solid.

¹H NMR (400 MHz, DMSO-d₆) δ 8.78 (d, *J* = 5.1 Hz, 1 H), 8.35 (d, *J* = 2.0 Hz, 1 H), 8.17 (s, 1 H), 7.80 (dd, *J* = 5.1, 2.0 Hz, 1 H); MS (ES+) *m/z* 262.0 [M+H]⁺.

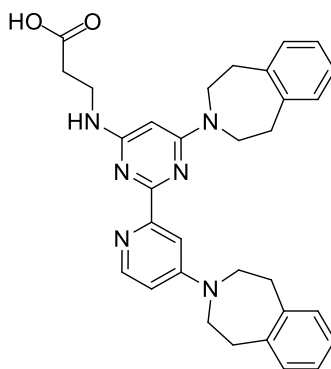
Ethyl 3-((6-chloro-2-(4-chloropyridin-2-yl)pyrimidin-4-yl)amino)propanoate 352



A mixture of DIPEA (0.34 mL, 1.94 mmol), ethyl β-alaninate hydrochloride (99.0 mg, 0.65 mmol) and 4,6-dichloro-2-(4-chloro-2'-pyridyl)pyrimidine **351** (168.0 mg, 0.65 mmol) in 1,4-dioxane (4 mL) was heated at 100 °C in a Biotage Initiator microwave for 45 min. DIPEA (0.03 mL, 0.19 mmol) and ethyl β -alaninate hydrochloride (10.0 mg, 0.07 mmol) were added and the reaction mixture was heated at 100 °C in a Biotage Initiator microwave for 30 min. The reaction mixture was concentrated under reduced pressure, and the residue was loaded onto a SNAP silica column (25 g) and purified by automated chromatography (SP4), eluting with a 0 - 60% gradient of ethyl acetate in cyclohexane (15 CV). The appropriate fractions were combined and evaporated under reduced pressure to give **352** (172 mg, 78%) as a brown gum.

¹H NMR (400 MHz, DMSO-d₆) δ 8.70 (d, *J* = 5.0 Hz, 1 H), 8.33 - 8.22 (br. s, 1 H), 8.07 - 7.97 (br. s, 1 H), 7.69 (dd, *J* = 5.0, 2.1 Hz, 1 H), 6.60 (s, 1 H), 4.06 (q, *J* = 7.1 Hz, 2 H), 3.70 (d, *J* = 5.9 Hz, 2 H), 2.65 (t, *J* = 5.9 Hz, 2 H), 1.16 (t, *J* = 7.1 Hz, 3 H); MS (ES+) *m/z* 341.0 [M+H]⁺.

3-(((6-(4,5-Dihydro-1H-benzo[d]azepin-3(2H)-yl)-2-(4-(4,5-dihydro-1H-benzo[d]azepin-3(2H)-yl)pyridin-2-yl)pyrimidin-4-yl)amino)propanoic acid 357b

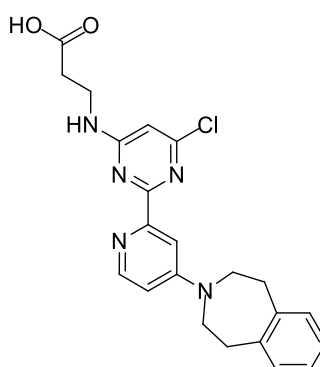


A mixture of DIPEA (0.11 mL, 0.64 mmol), 2,3,4,5-tetrahydro-1H-3-benzazepine (31.5 mg, 0.21 mmol) and ethyl *N*-[6-chloro-2-(4-chloro-2'-pyridyl)-4-pyrimidinyl]-β-alaninate **352** (73.0 mg, 0.21 mmol) in DMSO was heated at 160 °C in a Biotage Initiator microwave for 2 h. The reaction mixture was concentrated under reduced pressure, the residue was loaded onto a SNAP silica column (25 g) and partially purified by automated chromatography (SP4), eluting with a 0 - 10% gradient of MeOH in DCM (15 CV). The appropriate fractions were combined and evaporated under reduced pressure to give the crude product. The residue was loaded onto a SNAP silica column (10 g) and purified by automated chromatography (SP4), washing with a 0 - 100% gradient of ethyl acetate in cyclohexane (5 CV) and eluting with a 2 - 12% gradient of MeOH in DCM (15 CV). The appropriate fractions were combined and evaporated under reduced pressure to give an impure mixture of **356a** and **356b** (34 mg).

The mixture of **356a** and **356b** (34 mg) was taken up in aqueous THF (4 mL of a 1:1 mixture) and lithium hydroxide monohydrate (3.0 mg, 0.07 mmol) was added. After stirring for 1 h at rt, the reaction mixture was concentrated under reduced pressure and the residue was purified on a XBridge C18 column (100 mm x 30 mm i.d. 5 μ m packing diameter), eluting with 10 mM ammonium bicarbonate in water adjusted to pH 10 with ammonia solution (solvent A) and acetonitrile (solvent B) using an elution gradient of 5 to 80% over 15.5 min. The appropriate fractions were combined and evaporated under reduced pressure to give **357a** (8 mg, 7 % from **352**) as a yellow solid.

^1H NMR (400 MHz, DMSO- d_6) δ 8.26 (d, $J = 5.9$ Hz, 1 H), 7.73 (d, $J = 2.5$ Hz, 1 H), 7.22 - 7.15 (m, 4 H), 7.14 - 7.09 (m, 4 H), 6.89 (dd, $J = 5.9, 2.7$ Hz, 1 H), 6.81 - 6.71 (br. s, 1 H), 5.71 (s, 1 H), 3.87 - 3.79 (br. s, 4 H), 3.77 - 3.70 (m, 4 H), 3.57 - 3.48 (br. s, 2 H), 2.96 (m, 8 H), 2.57 - 2.50 (m, 2 H); MS (ES+) m/z 535.4 $[\text{M}+\text{H}]^+$. The signal arising from the CO_2H proton could not be observed, either because of exchange on the NMR timescale, or masking by the water peak (4.24 - 3.34 ppm); and

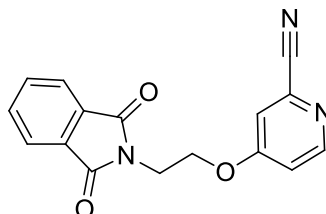
3-((6-Chloro-2-(4-(4,5-dihydro-1H-benzo[d]azepin-3(2H)-yl)pyridin-2-yl)pyrimidin-4-yl)amino)propanoic acid 357a



^1H NMR (600 MHz, DMSO- d_6) δ 8.26 (d, $J = 5.6$ Hz, 1 H), 7.90 - 7.85 (m, 1 H), 7.75 - 7.69 (br. s, 1 H), 7.18 - 7.14 (m, 2 H), 7.12 - 7.09 (m, 2 H), 6.93 (dd, $J = 5.6, ^4J = 2.4$ Hz, 1 H),

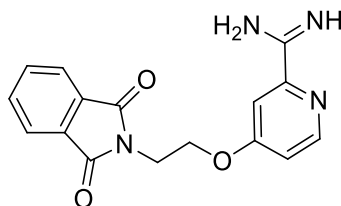
6.57 - 6.51 (br. s, 1 H), 3.74 - 3.70 (m, 4 H), 3.68 - 3.63 (m, 2 H), 2.97 - 2.93 (m, 4 H), 2.63 - 2.54 (br. s, 2 H); MS (ES+) m/z 424.16 $[M+H]^+$. The signal arising from the CO₂H proton could not be observed, either because of exchange on the NMR timescale, or masking by the water peak (3.8 - 3.27 ppm)

4-(2-(*N*-Phthalimido)-ethanol)picolinonitrile **359**



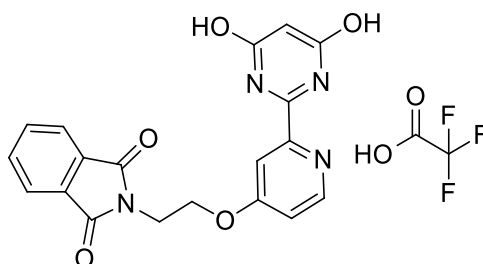
2-(2-Hydroxyethyl)*iso*indoline-1,3-dione (4.15 g, 21.65 mmol) was added to a cold solution (0 °C) of sodium hydride (0.95 g, 23.82 mmol) in DMF (80 mL). After stirring for 0.5 h at 0 °C, 4-chloropicolinonitrile **358** (3.0 g, 21.65 mmol) was added. After stirring for 6 h at rt, reaction mixture was concentrated under reduced pressure. Ethyl acetate (100 mL) and water (100 mL) were added to the residue; a precipitate formed, which was filtered off and washed with ethyl acetate. The aqueous layer from the filtrate was extracted with ethyl acetate (100 mL). The combined organic layers were dried through a hydrophobic frit and concentrated under reduced pressure to give a yellow solid. The yellow solid was combined with the solid from the precipitate and washed with methanol (3 x 20 mL) to give **359** (4.77 g, 75%) as a cream solid.

¹H NMR (400 MHz, DMSO-*d*₆) δ 8.50 (d, J = 5.8 Hz, 1 H), 7.91 - 7.83 (m, 4 H), 7.65 (d, J = 2.5 Hz, 1 H), 7.26 (dd, J = 5.8, 2.5 Hz, 1 H), 4.41 (t, J = 5.4 Hz, 2 H), 3.99 (t, J = 5.4 Hz, 2 H); MS (ES+) m/z 294.1 $[M+H]^+$.

4-(2-(*N*-phthalimido)-ethanol)picolinimidamide **361**

Sodium methoxide (3.41 mL, 14.90 mmol) was added to a suspension of 4-(2-(*N*-phthalimido)-ethanol)picolinonitrile **359** (4.37 g, 14.90 mmol) in MeOH (220 mL). After stirring for 23 h at rt, ammonium chloride (0.80 g, 14.90 mmol) was added to the reaction mixture. After stirring for 23 h at 55 °C, more ammonium chloride (0.40 g, 7.45 mmol) was added to the reaction mixture which was heated at 65 °C for 8 h. The reaction mixture was left to cool to rt, and then concentrated under reduced pressure. The residue was washed with EtOH (30 mL) then MeOH (30 mL) to give **361** (3.21 g, 69% from **359**) as a white solid.

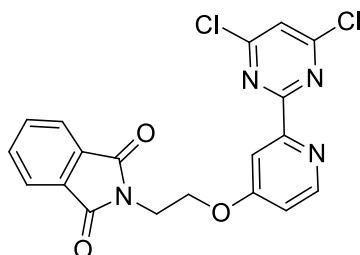
¹H NMR (400 MHz, DMSO-*d*₆) δ 9.56 - 9.37 (br. s, 3 H), 8.59 (d, *J* = 5.7 Hz, 1 H), 7.98 - 7.91 (br. s, 1 H), 7.92 - 7.84 (m, 4 H), 7.31 (dd, *J* = 5.7, 2.0 Hz, 1 H), 4.46 (t, *J* = 5.2 Hz, 2 H), 4.04 (t, *J* = 5.2 Hz, 2 H); MS (ES+) *m/z* 310.9 [M+H]⁺.

2-(2-((2-(4,6-Dihydroxypyrimidin-2-yl)pyridin-4-yl)oxy)ethyl)isoindoline-1,3-dione trifluoroacetate **363**

Sodium ethoxide (3.86 mL, 10.34 mmol) was added to a suspension of 4-(2-(*N*-phthalimido)-ethanol)picolinimidamide **361** (1.07 g, 3.45 mmol) in dry EtOH (40 mL). After

stirring for 45 min at rt, diethyl malonate (0.79 mL, 5.17 mmol) was added to the reaction mixture. After stirring for 14 h at 80 °C, reaction mixture was cooled to rt and filtered under vacuum. The solid was dissolved in MeOH, mixed with the filtrate and the resulting mixture was concentrated under reduced pressure. EtOH (40 mL) was added to the residue, and the suspension was acidified with aqueous HCl (2 M) until the pH reached 6. The solvent was removed under reduced pressure and the residue was suspended in ethanol (70 mL), treated with HCl (1.72 mL of a 4 M in dioxane, 6.90 mmol). After stirring for 2 h at 90 °C, reaction mixture was concentrated under reduced pressure. Et₂O (30 mL) was added to the residue; the solid which formed was filtered off, and the filtrate was concentrated under reduced pressure. The residue (550 mg) was loaded onto a SNAP silica column (25 g) and partially purified by automated chromatography (SP4), eluting with a 0 - 20% gradient of MeOH in DCM (10 CV). The appropriate fractions were combined and concentrated under reduced pressure to give the impure product. The crude product was taken up in methanolic DMSO (2 mL of a 1:1 mixture) dissolved in 1:1 MeOH:DMSO and purified by MDAP on a Sunfire C18 column using a 5 – 99% gradient of acetonitrile (containing 0.1% v/v TFA) in water (containing 0.1% v/v TFA). The solvent was evaporated under reduced pressure to give **363** (150 mg, 9% from **361**) as a white solid (as TFA salt).

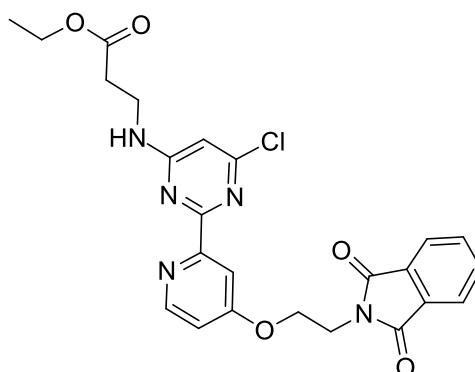
¹H NMR (400 MHz, DMSO-d₆) δ 12.0 - 11.33 (br. s, 1 H), 8.55 (d, *J* = 5.8 Hz, 1 H), 7.93 - 7.88 (m, 2 H), 7.88 - 7.83 (m, 2 H), 7.75 (d, *J* = 2.5 Hz, 1 H), 7.26 (dd, *J* = 5.8, ⁴*J* = 2.5 Hz, 1 H), 5.47 (s, 1 H), 4.43 (t, *J* = 5.2 Hz, 2 H), 4.04 (t, *J* = 5.2 Hz, 2 H); MS (ES+) *m/z* 379.0 [M+H]⁺. The signal arising from the OH protons could not be observed, either because of exchange on the NMR timescale, or masking by the water peak (4.34 - 3.24 ppm).

2-(2-((2-(4,6-Dichloropyrimidin-2-yl)pyridin-4-yl)oxy)ethyl)isoindoline-1,3-dione 364

A suspension of 2-(2-((2-(4,6-dihydroxypyrimidin-2-yl)pyridin-4-yl)oxy)ethyl)isoindoline-1,3-dione **363** (342 mg, 0.90 mmol) in phosphorus oxychloride (8 ml, 86.0 mmol) was refluxed for 1 h. The reaction mixture was concentrated under reduced pressure. The resulting black tar was loaded onto a SNAP silica column (50 g) and partially purified by automated chromatography (SP4), eluting with a 0 - 10% gradient of MeOH in DCM (15 CV), followed by a 10 - 20% gradient of MeOH in DCM (10 CV). The appropriate fractions were combined and evaporated under reduced pressure to give the impure product. The residue was partitioned between a saturated solution of sodium hydrogen carbonate (40 mL) and DCM (40 mL). The aqueous layer was extracted with DCM (40 mL). The organic extract and the original organic layer were combined and dried through a hydrophobic frit and concentrated under reduced pressure to give **364** (264 mg, 70%) as an off-white solid.

$^1\text{H NMR}$ (400 MHz, DMSO-d_6) δ 8.57 (d, $J = 5.8$ Hz, 1 H), 8.10 (s, 1 H), 7.91 - 7.87 (m, 2 H), 7.87 - 7.82 (m, 2 H), 7.76 (d, $J = 2.5$ Hz, 1 H), 7.18 (dd, $J = 5.8, 2.5$ Hz, 1 H), 4.42 (t, $J = 5.4$ Hz, 2 H), 4.03 (t, $J = 5.4$ Hz, 2 H); $\text{MS (ES}^+)$ m/z 414.9 $[\text{M}+\text{H}]^+$.

Ethyl 3-((6-chloro-2-(4-(2-(1,3-dioxoisindolin-2-yl)ethoxy)pyridin-2-yl)pyrimidin-4-yl)amino)propanoate 365

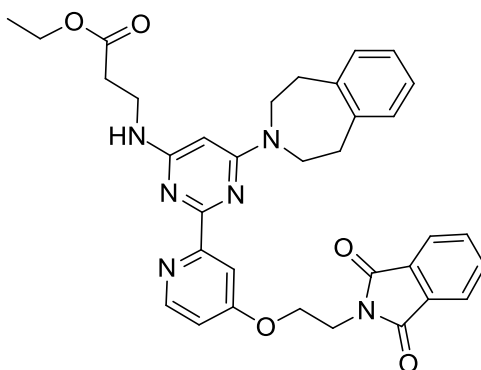


A mixture of 2-(2-((2-(4,6-dichloropyrimidin-2-yl)pyridin-4-yl)oxy)ethyl)isoindoline-1,3-dione **364** (271 mg, 0.65 mmol), DIPEA (0.34 mL, 1.96 mmol) and ethyl 3-aminopropanoate hydrochloride (120 mg, 0.78 mmol) in 1,4-dioxane (4 mL) was heated at 100 °C in a Biotage Initiator microwave for 1 h and then a further 20 min at 100 °C. Ethyl 3-aminopropanoate hydrochloride (25.1 mg, 0.16 mmol) and DIPEA (0.114 mL, 0.65 mmol) were added to the mixture, and the system was heated at 100 °C in a Biotage Initiator microwave for 0.5 h. The reaction mixture was concentrated under reduced pressure, and the crude material was loaded onto a SNAP silica column (50 g) and partially purified by automated chromatography (SP4), eluting with a 0 - 5% gradient of MeOH in DCM (15 CV). Fractions containing impure product were combined and concentrated under reduced pressure. The residue was loaded onto a SNAP silica column (50 g) and partially purified by automated chromatography (SP4), washing with a 0 - 100% gradient of ethyl acetate in cyclohexane (10 CV) and eluting with a 0 - 3% gradient of MeOH in DCM (15 CV). The appropriate fractions were combined and evaporated under reduced pressure to give **365** (257 mg, 79%) as a yellow gum.

¹H NMR (400 MHz, DMSO-d₆) δ 8.47 (d, *J* = 5.5 Hz, 1 H), 7.89 - 7.80 (m, 4 H), 7.73 (d, *J* = 2.5 Hz, 1 H), 7.41 (br. s, 1 H), 7.01 (dd, *J* = 5.5, 2.5 Hz, 1 H), 6.57 (s, 1 H), 4.45 (t, *J* = 5.8

Hz, 2 H), 4.10 (q, $J = 7.2$ Hz, 2 H), 4.05 (t, $J = 5.8$ Hz, 2 H), 3.68 (q, $J = 6.6$ Hz, 2 H), 2.64 (t, $J = 6.8$ Hz, 2 H), 1.19 (t, $J = 7.2$ Hz, 3 H); MS (ES+) m/z 496.2 $[M+H]^+$.

Ethyl 3-((6-(4,5-dihydro-1H-benzo[d]azepin-3(2H)-yl)-2-(4-(2-(1,3-dioxoisindolin-2-yl)ethoxy)pyridin-2-yl)pyrimidin-4-yl)amino)propanoate 366



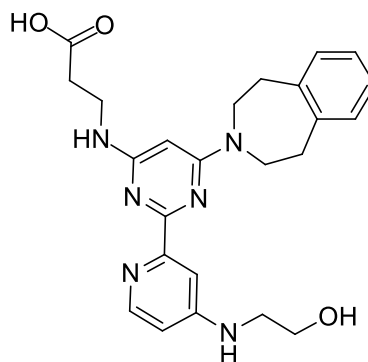
A mixture of ethyl 3-((6-chloro-2-(4-(2-(1,3-dioxoisindolin-2-yl)ethoxy)pyridin-2-yl)pyrimidin-4-yl)amino)propanoate **365** (238 mg, 0.48 mmol), DIPEA (0.25 mL, 1.44 mmol) and 2,3,4,5-tetrahydro-1H-3-benzazepine (94 mg, 0.58 mmol) in DMSO (1 mL) was heated at 160 °C in a Biotage Initiator microwave for 2 h. 2,3,4,5-Tetrahydro-1H-3-benzazepine (23.6 mg, 0.14 mmol) and DIPEA (62.0 mg, 0.48 mmol) were added and reaction mixture was heated at 160 °C in a Biotage Initiator microwave for 1 h. The reaction mixture was concentrated under reduced pressure. The residue was loaded onto a SNAP silica column (25 g) and partially purified by automated chromatography (SP4), eluting with a 0 - 5% gradient of methanolic ammonia (2M) in DCM (20 CV). The appropriate fractions were combined and concentrated under reduced pressure to give the impure product. The residue was loaded onto a SNAP silica column (50 g) and partially purified by automated chromatography (SP4), eluting with a 0 - 5% gradient of MeOH in DCM (20 CV).

The appropriate fractions were combined and concentrated under reduced pressure to afford the impure product which was dried under vacuum over 18 h. The residue was loaded onto a SNAP silica column (50 g) and partially purified by automated chromatography (SP4),

eluting with a 0 - 5% gradient of methanolic ammonia (2 M) in DCM (15 CV). Fractions containing impure product were combined and concentrated under reduced pressure. The residue was loaded onto a SNAP silica column (25 g) and purified by automated chromatography (SP4), eluting with a 0 - 4% gradient of methanolic ammonia (2 M) in DCM (20 CV). The appropriate fractions were combined and evaporated under reduced pressure to give **366** (123 mg, 42%) as a yellow solid.

¹H NMR (400 MHz, DMSO-d₆) δ 8.46 (d, *J* = 5.7 Hz, 1 H), 7.91 - 7.87 (m, 2 H), 7.87 - 7.83 (m, 2 H), 7.73 (d, ⁴*J* = 2.6 Hz, 1 H), 7.19 - 7.14 (m, 2 H), 7.14 - 7.09 (m, 2 H), 7.00 (dd, *J* = 5.7, 2.6 Hz, 1 H), 6.81 (t, *J* = 5.7 Hz, 1 H), 5.70 (s, 1 H), 4.39 (t, *J* = 5.7 Hz, 2 H), 4.10 - 4.01 (m, 4 H), 3.86 - 3.79 (m, 4 H), 3.55 (q, *J* = 6.6 Hz, 2 H), 2.96 - 2.89 (m, 4 H), 2.60 (t, *J* = 6.6 Hz, 2 H), 1.17 (t, *J* = 7.1 Hz, 3 H); MS (ES+) *m/z* 607.5 [M+H]⁺.

3-((6-(4,5-Dihydro-1H-benzo[d]azepin-3(2H)-yl)-2-(4-((2-hydroxyethyl)amino)pyridin-2-yl)pyrimidin-4-yl)amino)propanoic acid 368

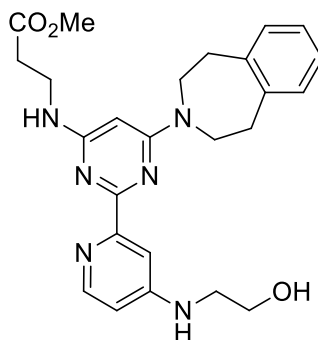


Lithium hydroxide monohydrate (8.5 mg, 0.20 mmol) was added to a solution of ethyl 3-((6-(4,5-dihydro-1H-benzo[d]azepin-3(2H)-yl)-2-(4-(2-(1,3-dioxoisindolin-2-yl)ethoxy)pyridin-2-yl)pyrimidin-4-yl)amino)propanoate **366** (123 mg, 0.20 mmol) in a mixture of THF and water 3:1. After stirring for 1 h at rt, lithium hydroxide monohydrate (8.5 mg, 0.20 mmol) was added to the reaction mixture. After stirring for 90 min at rt, the reaction mixture was concentrated using the blow-down unit. The residue was taken up in

water (1 mL) and solid carbon dioxide was added to the stirred solution. The reaction mixture was then concentrated under reduced pressure. The residue **276** (138 mg) was taken up 1,4-dioxane / DMF (3.5 mL of a 2.5:1 mixture) and hydrazine hydrate (0.06 mL, 0.93 mmol) was added, followed by MeOH (0.5 mL). After stirring for 4 h at 80 °C, MeOH (0.5 mL) and water (0.5 mL) were added. After stirring for 1 h at 80 °C, hydrazine hydrate (0.06 mL, 0.93 mmol) was added. The reaction mixture was then stirred at 80 °C for 7 h, at rt for 72 h and hydrazine hydrate (0.56 mL, 11.54 mmol) was added. After stirring for 8 h at 80 °C, reaction mixture was concentrated under reduced pressure. The residue was purified on a XBridge C18 column (100 mm x 19 mm i.d. 5 µm packing diameter) at rt, eluting with 10 mM ammonium bicarbonate in water adjusted to pH 10 with ammonia solution (solvent A) and acetonitrile (solvent B) using an elution gradient of 10 to 38% over 15 min. The appropriate fractions were combined and concentrated under reduced pressure to give **368** in 2 batches (31mg, 30% and 4 mg, 4%) as yellow solids.

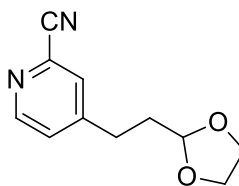
¹H NMR (600 MHz, DMSO-d₆) δ 8.10 (d, *J* = 5.8 Hz, 1 H), 7.49 (d, ⁴*J* = 2.2 Hz, 1 H), 7.17 - 7.14 (m, 2 H), 7.12 - 7.09 (m, 2 H), 6.79 - 6.73 (br. s, 1 H), 6.69 - 6.63 (br. s, 1 H), 6.55 (dd, *J* = 5.8, 2.4 Hz, 1 H), 5.66 (s, 1 H), 3.84 - 3.79 (m, 4 H), 3.58 (t, *J* = 6.0 Hz, 2 H), 3.51 - 3.43 (m, 2 H), 3.20 (q, *J* = 6.0 Hz, 2 H), 2.91 (m, 4 H), 2.37 (t, *J* = 6.6 Hz, 3 H); MS (ES+) *m/z* 449.2 [M+H]⁺. The signal arising from the CO₂H proton could not be observed, either because of exchange on the NMR timescale, or masking by the water peak (3.47 - 3.20)

Methyl 3-((6-(4,5-dihydro-1H-benzo[d]azepin-3(2H)-yl)-2-(4-((2-hydroxyethyl)amino)pyridin-2-yl)pyrimidin-4-yl)amino)propanoate 373



K_2CO_3 (12.0 mg, 0.09 mmol) was added to a solution of **368** (26 mg, 0.06 mmol) in DMF (1.5 mL). MeI (3.97 μ L, 0.064 mmol) was added after stirring for 30 min at rt, and the reaction mixture was stirred for 15 h at rt. The reaction mixture was concentrated under reduced pressure and the residue was purified by MDAP on a Sunfire C18 column using acetonitrile water with a formic acid modifier. The solvent was evaporated under reduced pressure to give **373** (13 mg) as an impure yellow solid. The presence of the product was confirmed by LCMS MS (ES+) m/z 463.2 $[M+H]^+$ with 89% purity so NMR was not recorded.

4-[2-(1,3-Dioxolan-2-yl)ethyl]-2-pyridinecarbonitrile 380

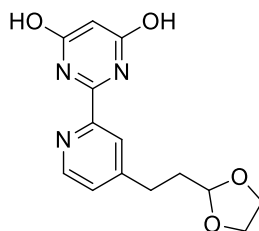


Nitrogen was bubbled through a mixture of (2-(1,3-Dioxolan-2-yl)ethyl)zinc(II) bromide **379** (5.77 mL of a 0.5 M solution in THF, 2.89 mmol) and 4-chloropicolinonitrile **358** (250 mg, 1.80 mmol) for 5 min. *Tetrakis*(triphenylphosphino)palladium (104 mg, 0.09 mmol) was added and nitrogen was bubbled through the brown suspension for a further 2 min. The reaction mixture was then heated in a microwave at 110 °C and stirred for 1 h. The reaction

mixture was cooled and quenched by the addition of NH₄Cl solution (20 mL) and water (20 mL). The mixture was diluted with Et₂O (30 mL) and the layers were separated. The aqueous layer was further extracted with Et₂O (2 x 20 mL) and the combined organic layers were dried (Na₂SO₄) and concentrated under reduced pressure to afford the crude product as a yellow oil. The crude product was loaded onto a SNAP silica column (25 g) and purified by automated chromatography (SP4), eluting with a 0 - 100% gradient of ethyl acetate in cyclohexane. The appropriate fractions were collected and concentrated under reduced pressure to afford **380** (151 mg, 41%).

¹H NMR (400 MHz, DMSO-d₆) δ 8.62 (d, *J* = 5.1 Hz, 1 H), 7.95 (d, ⁴*J* = 1.1 Hz, 1 H), 7.62 (dd, *J* = 5.1, ⁴*J* = 1.1 Hz, 1 H), 4.84 (t, *J* = 4.6 Hz, 1 H), 3.94 - 3.84 (m, 2 H), 3.83 - 3.73 (m, 2 H), 2.79 - 2.73 (m, 2 H), 1.97 - 1.90 (m, 2 H); MS (ES+) *m/z* 205.07 [M+H]⁺.

2-(4-(2-(1,3-Dioxolan-2-yl)ethyl)pyridin-2-yl)pyrimidine-4,6-diol **383**

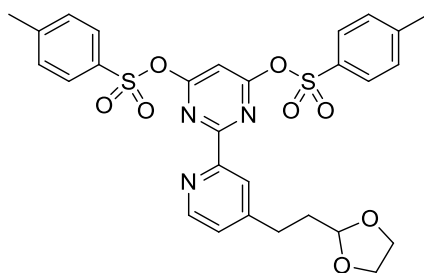


Sodium methoxide (0.28 mL of a 25% w/w in MeOH, 1.20 mmol,) was added to a solution of 4-(2-(1,3-dioxolan-2-yl)ethyl)picolinonitrile **380** (1.22 g, 5.99 mmol) in methanol (11.6 mL) and the reaction was stirred at rt for 1.5 h. Ammonium chloride (0.48 g, 8.98 mmol) was added and the reaction mixture was stirred at rt. Diethyl malonate (4.56 ml, 29.90 mmol) and sodium methoxide (10.95 mL of a 25% w/w in MeOH, 47.90 mmol) were added and the reaction was heated to reflux (80 °C) for 8.5 h. Further sodium methoxide (10.95 mL of a 25% w/w in MeOH, 47.90 mmol) and diethyl malonate (4.56 ml, 29.90 mmol) were added and heating was continued for a further 16 h. The reaction was then allowed to cool to rt and concentrated under reduced pressure. EtOH (50 mL) was added and the reaction mixture was

sonicated for 5 min. The resultant suspension was filtered and the residue was washed with further portions of EtOH (3 x 40 mL). The combined filtrate and washings were concentrated under reduced pressure to afford **383** (8.31 g). The purity of the product was estimated to 20%, it was used without further purification.

The ¹H NMR (400 MHz, DMSO-d₆) spectrum contained the following significant peaks δ 8.60 (d, *J* = 4.8 Hz, 1 H), 8.12 (s, 1 H), 7.52 (dd, *J* = 4.8, ⁴*J* = 1.5 Hz, 1 H), 5.35 - 5.27 (br. s, 1 H), 4.85 (t, *J* = 4.8 Hz, 1 H), 3.93 - 3.86 (m, 2 H), 3.83 - 3.76 (m, 2 H), 2.84 - 2.77 (m, 2 H), 1.97 - 1.91 (m, 2 H); MS (ES+) *m/z* 290.0 [M+H]⁺.

2-{4-[2-(1,3-Dioxolan-2-yl)ethyl]-2'-pyridyl}-4,6-pyrimidinediyl bis(4-methylbenzenesulfonate) 384

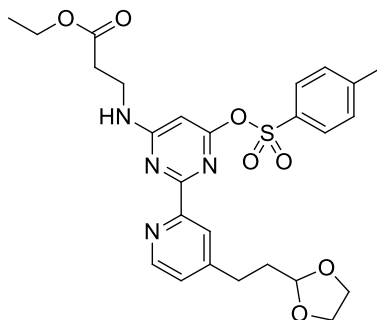


Triethylamine (5.29 mL, 37.9 mmol), *p*-toluenesulfonyl chloride (5.26 g, 27.6 mmol) and DMAP (0.14 g, 1.15 mmol) were added to a solution of 2-(4-(2-(1,3-dioxolan-2-yl)ethyl)pyridin-2-yl)pyrimidine-4,6-diol **383** (8.31 g, 20% purity) in DCM (40 mL) and the resultant solution was stirred at rt for 16 h. Further triethylamine (5.29 mL, 37.9 mmol) and *p*-toluenesulfonyl chloride (5.26 g, 27.6 mmol) were added and the reaction was stirred for a further 2 h. The reaction mixture was then quenched by the addition of water (50 mL), further DCM (30 mL) was added and the layers were separated. The aqueous phase was further extracted with DCM (2 x 40 mL) and the combined organic phase was dried (Na₂SO₄), filtered and concentrated under reduced pressure to give a brown oil. The crude product was loaded onto a SNAP silica column (100 g) and purified by automated

chromatography (SP4), eluting with a 10 - 100% gradient of ethyl acetate in cyclohexane. The appropriate fractions were combined and evaporated under reduced pressure to give **384** (2.35 g, 68% over 4 steps) as a pale cream foam.

¹H NMR (400 MHz, DMSO-d₆) δ 8.78 (d, *J* = 5.1 Hz, 1 H), 8.19 (d, *J* = 8.6 Hz, 4 H), 7.63 (s, 1 H), 7.56 - 7.49 (m, 5 H), 7.29 (s, 1 H), 4.90 (t, *J* = 4.6 Hz, 1 H), 3.99 - 3.91 (m, 2 H), 3.89 - 3.81 (m, 2 H), 2.81 - 2.74 (m, 2 H), 2.43 (s, 6 H), 1.97 - 1.90 (m, 2 H); MS (ES+) *m/z* 598.4 [M+H]⁺.

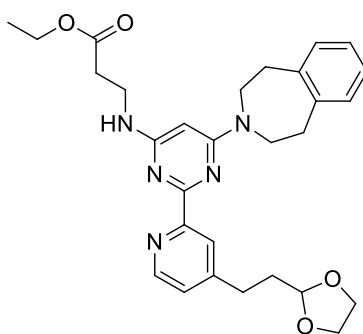
Ethyl 3-((2-(4-(2-(1,3-dioxolan-2-yl)ethyl)pyridin-2-yl)-6-(tosyloxy)pyrimidin-4-yl)amino)propanoate 385



Ethyl 3-aminopropanoate hydrochloride salt (265 mg, 1.72 mmol) and triethylamine (688 μL, 4.94 mmol) were added to a solution of 2-{4-[2-(1,3-dioxolan-2-yl)ethyl]-2'-pyridyl}-4,6-pyrimidinediyl bis(4-methylbenzene-sulfonate) **384** (1.0 g, 1.67 mmol) in MeCN (15 mL). The reaction mixture was heated at 100 °C for 20 min using a Biotage Initiator microwave. Three additional batches of **384** were reacted the same way, two of the same amount and one slightly smaller (857 mg, 1.43 mmol). The mixtures were combined and concentrated under reduced pressure to give a viscous orange liquid. The liquid was loaded onto a SNAP silica column (100 g) and purified by automated chromatography (SP4), eluting with a 0 - 5% gradient of MeOH in ethyl acetate. The appropriate fractions were combined and concentrated under reduced pressure to give **385** (1.4 g, 40%) as a colourless waxy oil.

¹H NMR (400 MHz, DMSO-d₆) δ 8.58 (d, *J* = 4.9 Hz, 1 H), 8.03 (d, *J* = 8.0 Hz, 2 H), 7.99 - 7.88 (br. s, 1 H), 7.82 - 7.68 (br. s, 1 H), 7.51 (d, *J* = 8.0 Hz, 2 H), 7.36 (dd, *J* = 4.9, ⁴*J* = 1.5 Hz, 1 H), 6.23 (s, 1 H), 4.86 (t, *J* = 4.6 Hz, 1 H), 4.05 (q, *J* = 7.1 Hz, 2 H), 3.96 - 3.88 (m, 2 H), 3.86 - 3.78 (m, 2 H), 3.74 - 3.59 (m, 2 H), 2.77 - 2.69 (m, 2 H), 2.67 - 2.58 (m, 2 H), 2.44 (s, 3 H), 1.95 - 1.87 (m, 2 H), 1.15 (t, *J* = 7.1 Hz, 3 H); MS (ES⁺) *m/z* 543.3 [M+H]⁺.

Ethyl 3-((2-(4-(2-(1,3-dioxolan-2-yl)ethyl)pyridin-2-yl)-6-(4,5-dihydro-1H-benzo[d]azepin-3(2H)-yl)pyrimidin-4-yl)amino)propanoate 386

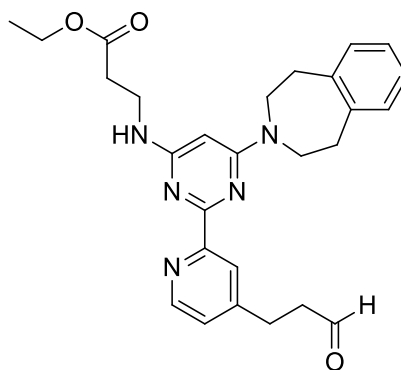


2,3,4,5-Tetrahydro-1H-benzo[d]azepine (522 mg, 3.55 mmol) was added to a solution of ethyl 3-((2-(4-(2-(1,3-dioxolan-2-yl)ethyl)pyridin-2-yl)-6-(tosyloxy)pyrimidin-4-yl)amino)propanoate **385** (385 mg, 0.71 mmol) in *isopropanol* (12 mL). The resultant solution was heated at 150 °C for 1 h. The reaction mixture was then diluted with EtOAc (10 mL) and concentrated under reduced pressure to give the crude product as a yellow oil. The crude product was loaded onto a SNAP silica column (50 g) and purified by automated chromatography (SP4), eluting with a 0 - 8% gradient of MeOH in DCM. The appropriate fractions were combined and concentrated under reduced pressure to give **386** (219 mg, 60%) as a yellow oil.

¹H NMR (400 MHz, CDCl₃) δ 8.65 (d, *J* = 5.1 Hz, 1 H), 8.26 (d, ⁴*J* = 1.3 Hz, 1 H), 7.19 (dd, *J* = 5.1, ⁴*J* = 1.3 Hz, 1 H), 7.18 - 7.12 (m, 4 H), 5.70 - 5.40 (br. s, 2 H), 4.95 (t, *J* = 4.6 Hz, 1 H), 4.17 (q, *J* = 7.2 Hz, 2 H), 4.06 - 3.99 (m, 2 H), 3.99 - 3.92 (m, 4 H), 3.92 - 3.84 (m, 2 H),

3.63 (q, $J = 6.3$ Hz, 2 H), 3.07 - 2.99 (m, 4 H), 2.89 - 2.82 (m, 2 H), 2.66 (t, $J = 6.6$ Hz, 2 H), 2.11 - 2.03 (m, 2 H), 1.27 (t, $J = 7.2$ Hz, 3 H); MS (ES+) m/z 518.3 [M+H]⁺.

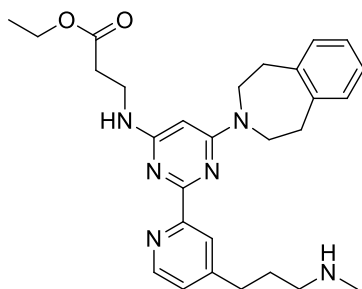
Ethyl 3-((6-(4,5-dihydro-1H-benzo[d]azepin-3(2H)-yl)-2-(4-(3-oxopropyl)pyridin-2-yl)pyrimidin-4-yl)amino)propanoate 387



A solution of ethyl 3-((2-(4-(2-(1,3-dioxolan-2-yl)ethyl)pyridin-2-yl)-6-(4,5-dihydro-1H-benzo[d]azepin-3(2H)-yl)pyrimidin-4-yl)amino)propanoate **386** (219 mg, 0.423 mmol) in acetic acid (6.4 mL) / water (1.6 mL) was heated at 80 °C and stirred for 16 h. The mixture was diluted with DCM (20 mL) and then quenched by the addition of NaHCO₃ solution. The mixture was stirred until the effervescence ceased, then the layers were separated. The aqueous layer was extracted further with DCM (2 x 20 mL) and the combined organic layers and extracts were washed with NaHCO₃ solution (20 mL), and then brine (20 mL). The organic layer was dried (Na₂SO₄) and concentrated under reduced pressure to give **387** as a yellow-green oil (162 mg) which was used directly in the subsequent reaction.

¹H NMR (400 MHz, CDCl₃) δ 9.89 (s, 1 H), 8.68 (d, $J = 5.1$ Hz, 1 H), 8.26 (s, 1 H), 7.22 - 7.09 (m, 5 H), 5.55 (s, 1 H), 5.33 - 5.23 (br s, 1 H), 4.18 (q, $J = 7.1$ Hz, 2 H), 4.0 - 3.90 (m, 4 H), 3.64 (q, $J = 6.3$ Hz, 2 H), 3.11 - 2.98 (m, 6 H), 2.89 (t, $J = 7.6$ Hz, 2 H), 2.66 (t, $J = 6.6$ Hz, 2 H), 1.28 (t, $J = 7.1$ Hz, 3 H); MS (ES+) m/z 474.2 [M+H]⁺.

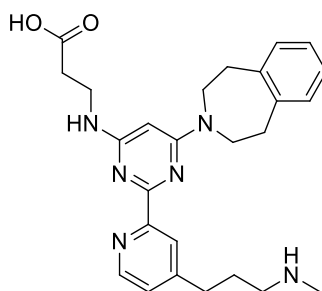
Ethyl 3-((6-(4,5-dihydro-1H-benzo[d]azepin-3(2H)-yl)-2-(4-(3-(methylamino)propyl)pyridin-2-yl)pyrimidin-4-yl)amino)propanoate 388



MgSO₄ (515 mg, 4.28 mmol) and methylamine (0.43 mL of a 2 M solution in THF, 0.86 mmol) were added to a solution of ethyl 3-((6-(4,5-dihydro-1H-benzo[d]azepin-3(2H)-yl)-2-(4-(3-oxopropyl)pyridin-2-yl)pyrimidin-4-yl)amino)propanoate **387** (81 mg, 0.17 mmol) in THF (4 mL). The mixture was stirred for 16 h. Sodium borohydride (6.47 mg, 0.17 mmol) was then added and the reaction mixture stirred at rt for 50 min. The reaction was quenched by the addition of water (20 mL) and DCM (20 mL). The layers were separated and the aqueous layer further extracted with DCM (2 x 20 mL). The combined organic layers and extracts were dried (Na₂SO₄) and concentrated under reduced pressure to afford the crude product as a yellow oil. LCMS showed a significant amount of a BH₃-coordinated by-product. To free the amine from the aminoborate complex, the crude product was taken up in EtOH (2 mL) and HCl (0.2 mL of a 1.0 M solution in Et₂O, 0.20 mmol) was added. The reaction mixture allowed to stand for 1 h, then a further portion of HCl (0.4 mL of a 1.0 M solution in Et₂O, 0.40 mmol) was added and the reaction mixture allowed to stand for a further 30 min. The reaction was concentrated under reduced pressure to afford the crude product as a yellow oil. The crude product was loaded onto a SNAP silica column (10 g) and purified by automated chromatography (SP4), eluting with a 0 - 20% gradient of methanolic ammonia (2 M) in DCM. The appropriate fractions were collected and concentrated under reduced pressure to afford **388** (58 mg, 76% over two steps) as a yellow oil.

¹H NMR (400 MHz, DMSO-d₆) δ 8.86 - 8.63 (br. s, 1 H), 8.59 (d, *J* = 4.8 Hz, 1 H), 8.09 (s, 1 H), 7.32 (d, *J* = 4.0 Hz, 1 H), 7.20 - 7.09 (m, 4 H), 6.82 (app. t, *J* = 5.1 Hz, 1 H), 5.73 (s, 1 H), 4.08 (q, *J* = 7.2 Hz, 2 H), 3.91 - 3.79 (m, 4 H), 3.57 (q, *J* = 6.3 Hz, 2 H), 2.99 - 2.87 (m, 6 H), 2.78 (t, *J* = 7.6 Hz, 2 H), 2.62 (t, *J* = 6.8 Hz, 2 H), 2.55 (s, 3 H), 2.04 - 1.93 (m, 2 H), 1.19 (t, *J* = 7.2 Hz, 3 H); MS (ES+) *m/z* 489.4 [M+H]⁺.

3-((6-(4,5-dihydro-1H-benzo[d]azepin-3(2H)-yl)-2-(4-(3-(methylamino)propyl)pyridin-2-yl)pyrimidin-4-yl)amino)propanoic acid 378

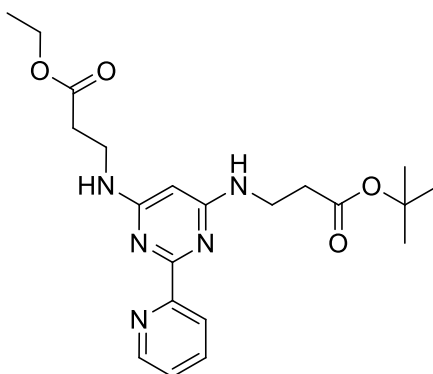


Lithium hydroxide monohydrate (4.7 mg, 0.11 mmol) was added to a solution of ethyl 3-((6-(4,5-dihydro-1H-benzo[d]azepin-3(2H)-yl)-2-(4-(3-(methylamino)propyl)pyridin-2-yl)pyrimidin-4-yl)amino)propanoate **388** (55 mg, 0.11 mmol) in aqueous THF (1 mL of a 1:1 mixture) and the reaction mixture was stirred for 30 min. Further lithium hydroxide monohydrate (4.7 mg, 0.11 mmol) was added and the reaction stirred for a further 1 h. The solvent was removed under a stream of nitrogen, then evaporated to dryness under reduced pressure to afford the lithium salt of **378** (51 mg, 97%) as a yellow solid. A portion of the lithium salt (25 mg) was purified further by MDAP on a Waters Xbridge C18 column using ammonium bicarbonate (10 mM in methanol, adjusted to pH 10 with ammonia). The pooled fractions were concentrated under reduced pressure to afford **378** (12 mg, 47%) as a white solid.

¹H NMR (400 MHz, DMSO-d₆) δ 8.53 (d, *J* = 5.1 Hz, 1 H), 8.19 (s, 1 H), 7.26 (dd, *J* = 4.8, 1.3 Hz, 1 H), 7.18 - 7.08 (m, 4 H), 6.81 - 6.73 (br. s, 1 H), 5.69 (s, 1 H), 3.87 - 3.77 (m, 4 H),

3.57 - 3.47 (m, 2 H), 2.96 - 2.87 (m, 4 H), 2.72 (t, $J = 7.3$ Hz, 2 H), 2.63 (t, $J = 7.1$ Hz, 2 H), 2.43 (t, $J = 6.8$ Hz, 2 H), 2.36 (s, 3 H), 1.94 - 1.83 (m, 2 H); ^{13}C NMR (150 MHz, 303K, DMSO- d_6) δ 174.3, 163.6, 162.0, 161.6, 156.5, 150.5, 148.8, 140.9, 129.7, 126.1, 124.1, 123.0, 80.6 (br.), 46.3, 46.5, 37.4, 35.9, 35.8 (br.), 34.3, 31.6, 27.8; HRMS (TOF): $M + H$ calcd for $\text{C}_{26}\text{H}_{32}\text{N}_6\text{O}_2$ 461.2660; found 461.2635; IR (cm^{-1}) 3303, 1582, 1530, 1357, 1033, 768; mp = 168.5 °C. The signals arising from one of the NH proton and the CO_2H could not be observed, either because of exchange on the NMR timescale, or masking by the water peak (4.92 - 4.07 ppm).

***Tert*-butyl 3-((6-((3-ethoxy-3-oxopropyl)amino)-2-(pyridin-2-yl)pyrimidin-4-yl)amino)propanoate 390**



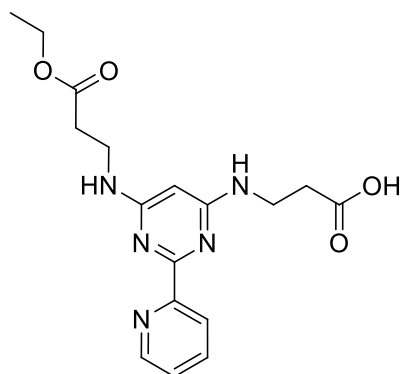
Tert-butyl 3-aminopropanoate hydrochloride (1.14 g, 6.25 mmol) was taken up in MeOH (5 mL) and eluted through an aminopropyl cartridge (20 g) with MeOH (4 CV). The appropriate fractions were combined and evaporated under reduced pressure to give the free base *tert*-butyl 3-aminopropanoate (916 mg) as a white oil.

DIPEA (0.43 mL, 2.43 mmol) and *tert*-butyl 3-aminopropanoate (706 mg, 4.86 mmol) were added to a solution of **313** (746 mg, 2.43 mmol) in *iso*-propanol (8 mL). The reaction mixture was heated in a Biotage Initiator microwave at 160 °C for 2 h. *Tert*-butyl 3-aminopropanoate (210 mg, 1.45 mmol) and DIPEA (0.26 mL, 1.46 mmol) were added and the reaction mixture was heated in a Biotage Initiator microwave at 160 °C for 2 h. The

reaction mixture was concentrated under reduced pressure and the residue was loaded onto a SNAP silica cartridge (100 g), partially purified by automated chromatography (SP4), using a 0 - 5% gradient of methanolic ammonia (2N) in DCM (15 CV). The appropriate fractions were combined and concentrated under reduced pressure to give the impure product. The residue was loaded onto a SNAP silica cartridge (100 g), purified by automated chromatography (SP4), using a 0 - 5% gradient of methanolic ammonia (2N) in DCM (20 CV). The appropriate fractions were combined and concentrated under reduced pressure to give **390** (555 mg, 55%) as a brown oil.

^1H NMR (400 MHz, DMSO- d_6) δ 8.64 (d, $J = 4.0$ Hz, 1 H), 8.20 (d, $J = 7.8$ Hz, 1 H), 7.86 (td, $J = 7.8$, $^4J = 1.8$ Hz, 1 H), 7.44 - 7.38 (m, 1 H), 6.79 - 6.68 (m, 2 H), 5.44 (s, 1 H), 4.07 (q, $J = 7.1$ Hz, 2 H), 3.55 - 3.41 (m, 4 H), 2.69 (t, $J = 6.8$ Hz, 4 H), 1.40 (s, 9 H), 1.18 (t, $J = 7.1$ Hz, 3 H); MS (ES+) m/z 416.2 $[\text{M}+\text{H}]^+$.

3-(((6-((3-Ethoxy-3-oxopropyl)amino)-2-(pyridin-2-yl)pyrimidin-4-yl)amino)propanoic acid 391



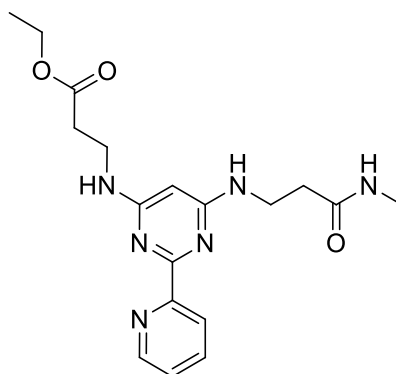
TFA (2.06 mL, 26.7 mmol) was added to a solution of **390** (555 mg, 1.34 mmol) in DCM (20 mL). After stirring at rt for 2 h and left ageing without stirring for 16 h, the reaction mixture was concentrated under reduced pressure. Water (20 mL) was added to the residue followed by DCM (30 mL). The layers were separated, the aqueous layer was further extracted with DCM (2x30 mL). The combined organic layers were concentrated under

reduced pressure to give the impure product. The residue was taken up in methanolic DMSO (2 mL of a 1:1 mixture) and purified by MDAP on a Supelcosil ABZ+Plus column eluting with solvents A/B (A: water + 0.1% formic acid, B: MeCN:water 95:5 + 0.05% formic acid). The appropriate fractions were combined and concentrated under reduced pressure to give **391** (126 mg, 23%) as a yellow oil.

The aqueous layer was acidified to pH 5 and extracted with DCM (10*30 mL). Aqueous layer was spotted on TLC plate after each extraction and showed product. The combined organic layers were concentrated under reduced pressure. Aqueous layer was concentrated under reduced pressure. Both residues were combined loaded on a SNAP C18 cartridge (120 g), purified by automated chromatography (CombiFlash), using a 3 - 30 % gradient of MeCN (+0.01% formic acid) in water (+0.01% formic acid) (15 CV). The residue was. Product was eluted with 3-30 MeCN (+0.01% formic acid) in water (+0.01% formic acid). The appropriate fractions were combined and concentrated under reduced pressure to give a further portion of **391** (23 mg, 5%) as a yellow oil.

^1H NMR (400 MHz, DMSO- d_6) δ 8.71 (d, $J = 4.0$ Hz, 1 H), 8.28 (d, $J = 7.9$ Hz, 1 H), 7.96 (td, $J = 7.9$, $^4J = 1.8$ Hz, 1 H), 7.53 (dd, $J = 6.7$, 4.9 Hz, 1 H), 7.20 - 7.01 (br. s, 1 H), 5.61 (s, 1 H), 4.11 (q, $J = 7.1$ Hz, 2 H), 3.63 - 3.50 (m, 4 H), 2.64 (t, $J = 6.7$ Hz, 2 H), 2.58 (t, $J = 6.7$ Hz, 2 H), 1.21 (t, $J = 7.1$ Hz, 3 H); MS (ES+) m/z 360.1 $[\text{M}+\text{H}]^+$. The signals arising from one of the NH and the CO₂H protons could not be observed, either because of exchange on the NMR timescale, or masking by the water peak (3.33 - 3.27 ppm).

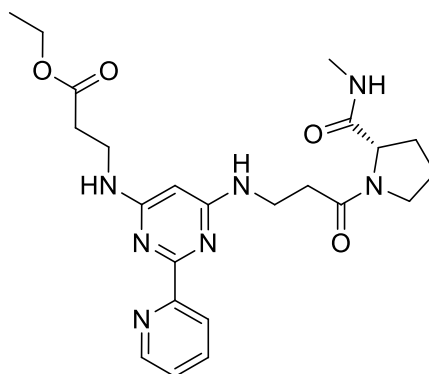
Ethyl 3-(((6-((3-(methylamino)-3-oxopropyl)amino)-2-(pyridin-2-yl)pyrimidin-4-yl)amino)propanoate **392a**



HATU (53.3 mg, 0.14 mmol) and methylamine (0.18 mL, 0.35 mmol) were added to a solution of **391** (42 mg, 0.12 mmol) in DMF (4 mL). After stirring at rt for 4 h and left ageing without stirring for 16 h, HATU (26.7 mg, 0.07 mmol) and methylamine (0.06 mL, 0.12 mmol) were added. After stirring at rt for 3 h, the reaction was concentrated under reduced pressure. The residue was loaded onto a SNAP silica cartridge (10 g), partially purified by automated chromatography (SP4), using a 0 - 10% gradient of methanolic ammonia (2N) in DCM (10 CV). The appropriate fractions were combined and concentrated under reduced pressure to give **392a** (43 mg, 99%) as a yellow oil.

^1H NMR (400 MHz, DMSO- d_6) δ 12.89 - 12.76 (br. s, 1 H), 8.74 (d, $J = 4.3$ Hz, 1 H), 8.31 (d, $J = 7.8$ Hz, 1 H), 8.07 - 7.99 (br. s, 1 H), 7.88 (d, $J = 4.3$ Hz, 1 H), 7.64 - 7.57 (br. s, 1 H), 5.66 - 5.60 (br. s, 1 H), 4.09 (q, $J = 7.2$ Hz, 2 H), 3.62 - 3.45 (m, 4 H), 2.65 (t, $J = 6.7$ Hz, 2 H), 2.60 (d, $J = 4.5$ Hz, 3 H), 2.41 (t, $J = 6.7$ Hz, 2 H), 1.19 (t, $J = 7.2$ Hz, 3 H); MS (ES+) m/z 373.1 $[\text{M}+\text{H}]^+$. The signal arising from the NH proton could not be observed, either because of exchange on the NMR timescale, or masking by the water peak (3.33 - 3.27 ppm).

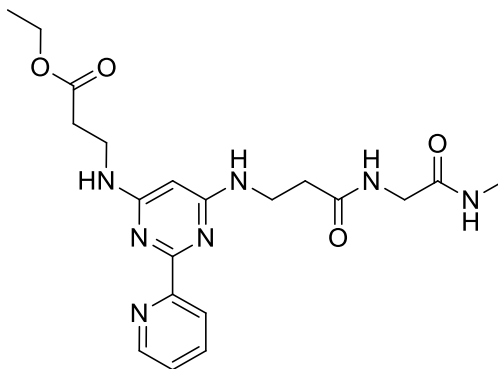
(S)-Ethyl 3-(((6-((3-(2-(methylcarbamoyl)pyrrolidin-1-yl)-3-oxopropyl)amino)-2-(pyridin-2-yl)pyrimidin-4-yl)amino)propanoate **392b**



HATU (53.3 mg, 0.14 mmol) and DIPEA (0.05 mL, 0.26 mmol) were added to a solution of 3-(((6-((3-ethoxy-3-oxopropyl)amino)-2-(pyridin-2-yl)pyrimidin-4-yl)amino)propanoic acid (42 mg, 0.12 mmol) in DMF (5 mL). After stirring at for 30 min of (S)-N-methylpyrrolidine-2-carboxamide hydrochloride (23.1 mg, 0.14 mmol) was added. After stirring at for 3 h, the reaction mixture was concentrated under reduced pressure. The residue was loaded onto a SNAP silica cartridge (10 g), partially purified by automated chromatography (SP4), using a 0 - 8% gradient of methanolic ammonia (2M) in DCM (15 CV). The appropriate fractions were combined and concentrated under reduced pressure to give crude **392b** (47 mg) as a colourless oil.

MS (ES+) m/z 470.3 [M+H]⁺.

Ethyl 3-((6-((3-((2-(methylamino)-2-oxoethyl)amino)-3-oxopropyl)amino)-2-(pyridin-2-yl)pyrimidin-4-yl)amino)propanoate 392c

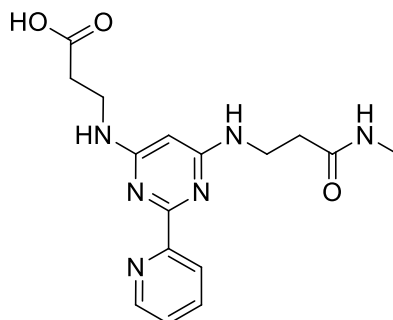


Was prepared as for **392b** from HATU (53.3 mg, 0.14 mmol), DIPEA (0.05 mL, 0.26 mmol), 3-((6-((3-ethoxy-3-oxopropyl) amino)-2-(pyridin-2-yl) pyrimidin-4-yl)amino) propanoic acid (42 mg, 0.12 mmol) and 2-amino-N-methylacetamide hydrochloride (18 mg, 0.14 mmol).

The usual purification afforded **392c** (32 mg, 63%) as a brown solid.

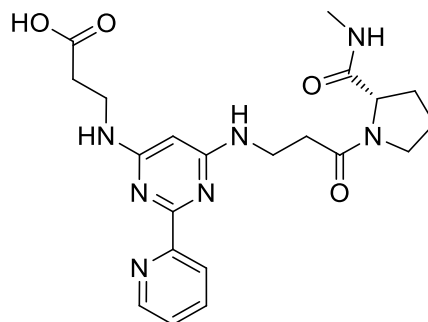
¹H NMR (400 MHz, DMSO-d₆) δ 8.65 - 8.61 (m, 1 H), 8.25 - 8.20 (m, 2 H), 7.87 (td, *J* = 7.6, ⁴*J* = 1.8 Hz, 1 H), 7.70 (d, *J* = 4.3 Hz, 1 H), 7.42 (ddd, *J* = 7.6, 4.3, ⁴*J* = 1.1 Hz, 1 H), 6.80 - 6.75 (m, 1 H), 6.74 - 6.78 (br. s, 1 H), 5.44 (s, 1 H), 4.07 (q, *J* = 7.1 Hz, 2 H), 3.66 (d, *J* = 5.8 Hz, 2 H), 3.55 - 3.42 (m, 4 H), 2.66 - 2.56 (m, 5 H), 2.46 (t, *J* = 6.9 Hz, 2 H), 1.18 (t, *J* = 7.1 Hz, 3 H); MS (ES+) *m/z* 430.2 [M+H]⁺.

3-((6-((3-(Methylamino)-3-oxopropyl)amino)-2-(pyridin-2-yl)pyrimidin-4-yl)amino)propanoic acid 393a



Was prepared as for **332b** from **392a** (43 mg, 0.12 mmol) and lithium hydroxide monohydrate (7.3 mg, 0.17 mmol). The usual purification afforded **393a** (24 mg, 60%) as an orange solid.

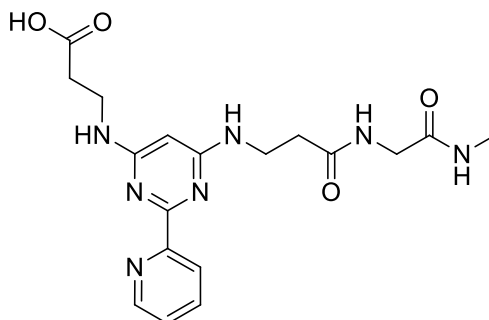
$^1\text{H NMR}$ (400 MHz, DMSO-d_6) δ 8.64 (d, $J = 3.8$ Hz, 1 H), 8.21 (d, $J = 7.8$ Hz, 1 H), 7.84 (td, $J = 7.7$, $^4J = 1.8$ Hz, 1 H), 7.71 - 7.63 (br. s, 1 H), 7.41 - 7.36 (m, 1 H), 6.41 (t, $J = 5.5$ Hz, 1 H), 5.47 (s, 1 H), 3.52 - 3.45 (m, 4 H), 2.61 (d, $J = 4.5$ Hz, 3 H), 2.55 - 2.48 (m, 2 H), 2.39 (t, $J = 6.9$ Hz, 2 H); MS (ES+) m/z 345.1 $[\text{M}+\text{H}]^+$. The signals arising from the CO_2H and one of the NH protons could not be observed, either because of exchange on the NMR timescale, or masking by the water peak (3.76 - 2.89 ppm). Spectrum recorded at 353 K.

(S)-3-((6-((3-(2-(Methylcarbamoyl)pyrrolidin-1-yl)-3-oxopropyl)amino)-2-(pyridin-2-yl)pyrimidin-4-yl)amino)propanoic acid 393b

Was prepared as for **332b** from **392b** (45.2 mg, 0.1 mmol) and lithium hydroxide monohydrate (6.1 mg, 0.14 mmol). The usual purification afforded **393b** (25 mg, 48% over 2 steps) as a pink solid.

^1H NMR (600 MHz, DMSO- d_6) δ 8.63 (d, $J = 2.9$ Hz, 1 H), 8.20 (d, $J = 7.7$ Hz, 1 H), 7.90 - 7.82 (m, 1 H), 7.70 (d, $J = 4.4$ Hz, 1 H), 7.44 - 7.37 (m, 1 H), 6.77 - 6.67 (br. s, 1 H), 6.67 - 6.59 (br. s, 1 H), 5.43 (s, 0.67 H, major rotamer), 5.41 (s, 0.33 H, minor rotamer), 4.37 (dd, $J = 8.4, 2.6$ Hz, 0.33 H, minor rotamer), 4.23 (dd, $J = 8.4, 2.6$ Hz, 0.67 H, major rotamer), 3.61 - 3.36 (m, 5 H), 2.63 - 2.52 (m, 5 H), 2.48 - 2.43 (m, 2 H), 2.17 - 1.71 (m, 4 H); ^{13}C NMR (126 MHz, DMSO- d_6) δ 173.6 (br.), 172.1, 169.8, 163.0 (br.), 162.0, 156.3, 148.9, 136.5, 136.4, 124.0, 122.9, 80.5 (br.), 59.5, 46.8, 37.1 (br.), 34.6 (br.), 31.6, 29.5, 25.6, 24.1, 22.3; IR (cm^{-1}) 3680, 2971 (br.), 1585, 1055; HRMS (TOF): $M + H$ calcd for $\text{C}_{21}\text{H}_{28}\text{N}_7\text{O}_4$ 442.2197, found 442.2194; mp = 153.7 °C. The signals arising from the CO_2H proton could not be observed, either because of exchange on the NMR timescale, or masking by the water peak (3.60 - 3.11 ppm). The α_D was not recorded.

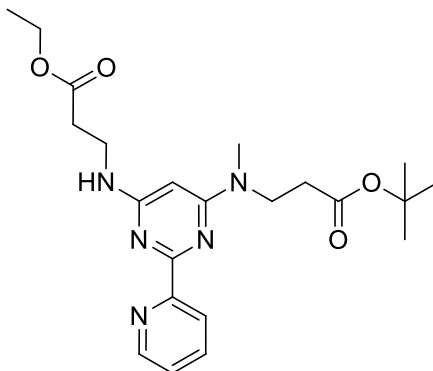
3-((6-((3-((2-(Methylamino)-2-oxoethyl)amino)-3-oxopropyl)amino)-2-(pyridin-2-yl)pyrimidin-4-yl)amino)propanoic acid 393c



Was prepared as for **332b** from **392c** (28.6 mg, 0.07 mmol) and lithium hydroxide monohydrate (4.2 mg, 0.10 mmol). The usual purification afforded **393c** (16 mg, 61%) as a yellow solid.

$^1\text{H NMR}$ (400 MHz, DMSO-d_6) δ 8.64 - 8.60 (m, 1 H), 8.21 (d, $J = 7.8$ Hz, 1 H), 8.13 - 8.06 (br. s, 1 H), 7.84 (td, $J = 7.6$, $^4J = 1.9$ Hz, 1 H), 7.57 - 7.49 (br. s, 1 H), 7.38 (ddd, $J = 7.6$, 4.8, $^4J = 1.1$ Hz, 1 H), 6.44 (t, $J = 5.8$ Hz, 1 H), 5.50 (s, 1 H), 3.68 (d, $J = 5.8$ Hz, 2 H), 3.55 - 3.45 (m, 4 H), 2.60 (d, $J = 4.5$ Hz, 3 H), 2.56 - 2.44 (m, 4 H); MS (ES⁺) m/z 402.1 $[\text{M}+\text{H}]^+$. The signals arising from the CO_2H and one of the NH protons could not be observed, either because of exchange on the NMR timescale, or masking by the water peak (3.57 - 3.03 ppm). Spectrum recorded at 353 K.

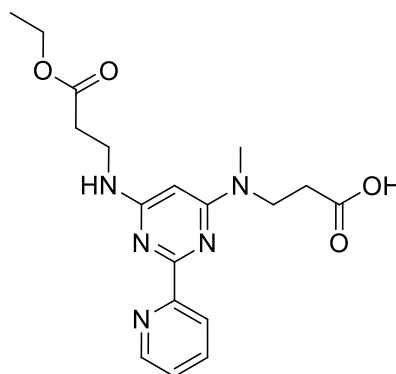
Tert-butyl 3-(((6-((3-ethoxy-3-oxopropyl)amino)-2-(pyridin-2-yl)pyrimidin-4-yl)(methyl)amino)propanoate **395**



Was prepared as for **208** from **313** (420 mg, 1.37 mmol), *tert*-butyl 3-(methylamino)propanoate (218 mg, 1.37 mmol) and DIPEA (0.24 mL, 1.37 mmol). The usual purification afforded **395** (319 mg, 54%) as a brown oil.

^1H NMR (400 MHz, DMSO- d_6) δ 8.65 (d, $J = 4.5$ Hz, 1 H), 8.23 (d, $J = 7.9$ Hz, 1 H), 7.86 (td, $J = 7.9$, $^4J = 1.8$ Hz, 1 H), 7.44 - 7.39 (m, 1 H), 6.81 (t, $J = 5.7$ Hz, 1 H), 5.51 (s, 1 H), 4.07 (q, $J = 7.2$ Hz, 2 H), 3.82 (s, 2 H), 3.58 - 3.51 (br. s, 2 H), 2.99 (s, 3 H), 2.60 (t, $J = 6.8$ Hz, 2 H), 2.57 - 2.50 (m, 2 H), 1.36 (s, 9 H), 1.18 (t, $J = 7.2$ Hz, 3 H); MS (ES+) m/z 430.2 $[\text{M}+\text{H}]^+$.

3-((6-((3-Ethoxy-3-oxopropyl)amino)-2-(pyridin-2-yl)pyrimidin-4-yl)(methyl)amino)propanoic acid 396

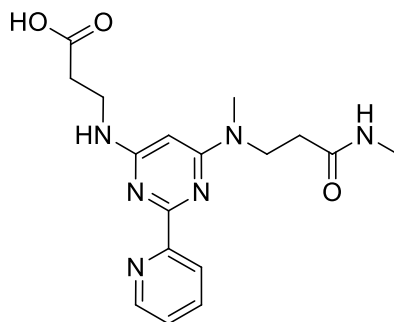


Was prepared as for **391** from **395** (319 mg, 0.74 mmol) and TFA (1.14 mL, 14.85 mmol).

The usual purification afforded **396** (237 mg, 85%) as a yellow solid.

$^1\text{H NMR}$ (400 MHz, DMSO- d_6) δ 8.65 (d, $J = 3.8$ Hz, 1 H), 8.23 (d, $J = 7.8$ Hz, 1 H), 7.87 (td, $J = 7.8$, $^4J = 1.8$ Hz, 1 H), 7.41 (ddd, $J = 7.8$, 4.8, $^4J = 1.8$ Hz, 1 H), 6.79 (t, $J = 5.6$ Hz, 1 H), 5.52 (s, 1 H), 4.07 (q, $J = 7.1$ Hz, 2 H), 3.74 (t, $J = 7.2$ Hz, 2 H), 3.54 (d, $J = 6.5$ Hz, 2 H), 3.01 (s, 3 H), 2.60 (t, $J = 6.5$ Hz, 2 H), 2.43 (t, $J = 7.2$ Hz, 2 H), 1.18 (t, $J = 7.1$ Hz, 3 H); MS (ES+) m/z 374.1 $[\text{M}+\text{H}]^+$. The signal arising from the CO_2H proton could not be observed, either because of exchange on the NMR timescale, or masking by the water peak (3.52 - 3.14 ppm).

3-((6-(Methyl(3-(methylamino)-3-oxopropyl)amino)-2-(pyridin-2-yl)pyrimidin-4-yl)amino)propanoic acid **398**



A solution of **396** (60 mg, 0.16 mmol) in DCM (5 mL) was evacuated and filled with N₂ 3 times. Oxalyl chloride (0.03 mL, 0.32 mmol) was added dropwise, followed by DMF (10.2 μL, 0.13 mmol). After stirring at rt for 2 h under N₂, the reaction mixture was concentrated under reduced pressure. The residue was taken up in DCM (5 mL), methylamine (0.09 mL, 0.18 mmol) and DIPEA (0.06 mL, 0.32 mmol) were added. Fuming was observed when adding DIPEA. After stirring at rt for 36 h under N₂, the reaction mixture was concentrated under reduced pressure. The residue was loaded onto a SNAP silica cartridge (25 g), partially purified by automated chromatography (SP4), using a 0 - 10% gradient of methanolic ammonia (2N) in DCM. The appropriate fractions were combined and concentrated under reduced pressure to give crude ester **397** (36 mg).

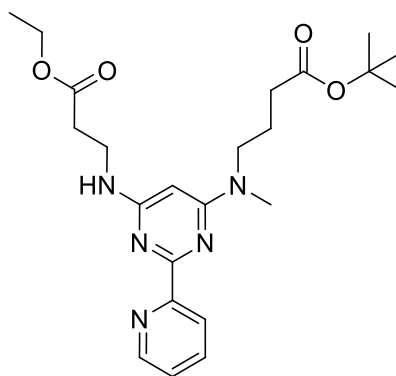
MS (ES+) m/z 387.2 [M+H]⁺.

The ester **397** (36 mg) was taken up in aqueous THF (3.5 mL of a 6:1 mixture), lithium hydroxide monohydrate (5.9 mg, 0.14 mmol) was added. After stirring at rt for 1 h, the reaction mixture was concentrated under reduced pressure. The residue was purified by MDAP on a Waters Xbridge C18 column using ammonium bicarbonate (10 mM in methanol, adjusted to pH 10 with ammonia). The appropriate fractions were combined and concentrated under reduced pressure to give **398** (7 mg, 12% from **396**) as a yellow solid.

¹H NMR (400 MHz, DMSO-d₆) δ 8.66 (d, J = 4.0 Hz, 1 H), 8.26 (d, J = 7.6 Hz, 1 H), 8.04

(d, $J = 3.8$ Hz, 1 H), 7.87 (td, $J = 7.6$, $^4J = 1.8$ Hz, 1 H), 7.42 (dd, $J = 7.6$, 4.8 Hz, 1 H), 6.80 - 6.71 (br. s, 1 H), 5.52 (s, 1 H), 3.76 (t, $J = 6.9$ Hz, 2 H), 3.51 - 3.53 (br. s, 2 H), 2.98 (s, 3 H), 2.56 (d, $J = 4.5$ Hz, 3 H), 2.45 (t, $J = 6.9$ Hz, 2 H), 2.37 (t, $J = 6.9$ Hz, 2 H); MS (ES+) m/z 359.2 $[M+H]^+$. The signal arising from the CO₂H proton could not be observed, either because of exchange on the NMR timescale, or masking by the water peak (3.95 - 3.39 ppm).

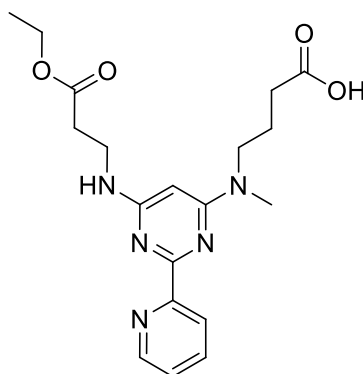
***Tert*-butyl 4-((6-((3-ethoxy-3-oxopropyl)amino)-2-(pyridin-2-yl)pyrimidin-4-yl)(methyl)amino)butanoate 400**



Was prepared as for **208** from **313** (100 mg, 0.33 mmol), *tert*-butyl 4-(methylamino)butanoate hydrochloride **399** (103 mg, 0.49 mmol) and DIPEA (0.17 mL, 0.98 mmol). The usual purification afforded **400** (59 mg, 41%) as a brown oil.

¹H NMR (400 MHz, DMSO-*d*₆) δ 8.65 (d, $J = 4.8$ Hz, 1 H), 8.23 (d, $J = 7.7$ Hz, 1 H), 7.86 (td, $J = 7.7$, $^4J = 1.8$ Hz, 1 H), 7.41 (dd, $J = 7.7$, 4.9 Hz, 1 H), 6.76 (t, $J = 5.7$ Hz, 1 H), 5.51 (s, 1 H), 4.07 (q, $J = 7.1$ Hz, 2 H), 3.61 - 3.50 (m, 4 H), 2.99 (s, 3 H), 2.61 (t, $J = 6.8$ Hz, 2 H), 2.23 (t, $J = 7.2$ Hz, 2 H), 1.83 - 1.74 (m, 2 H), 1.37 (s, 9 H), 1.18 (t, $J = 7.1$ Hz, 3 H); MS (ES+) m/z 444.3 $[M+H]^+$.

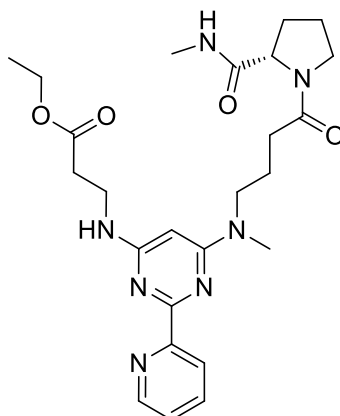
4-((6-((3-Ethoxy-3-oxopropyl)amino)-2-(pyridin-2-yl)pyrimidin-4-yl)(methyl)amino)butanoic acid **401**



TFA (0.05 mL, 0.64 mmol) was added to a solution of *tert*-butyl 4-((6-((3-ethoxy-3-oxopropyl)amino)-2-(pyridin-2-yl)pyrimidin-4-yl)(methyl)amino)butanoate (57 mg, 0.13 mmol) in DCM (3 mL). After stirring at rt for 4 days, TFA (0.050 mL, 0.64 mmol) was added. After stirring at rt for 5h, TFA (0.1 mL, 1.29 mmol) was added to the reaction mixture which was left standing without stirring for 18h. The reaction mixture was concentrated under reduced pressure and the residue was purified by MDAP on a Waters Xbridge C18 column using ammonium bicarbonate (10 mM in methanol, adjusted to pH 10 with ammonia). The appropriate fractions were combined and concentrated under reduced pressure to give **401** (20 mg, 40%) as a brown oil.

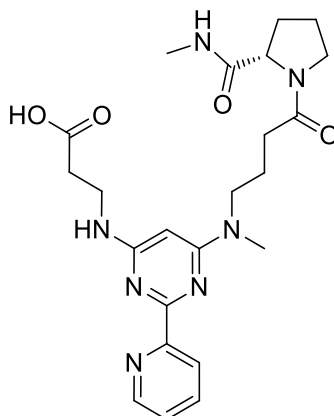
^1H NMR (400 MHz, DMSO- d_6) δ 8.65 (d, $J = 4.5$ Hz, 1 H), 8.24 (d, $J = 7.6$ Hz, 1 H), 7.86 (td, $J = 7.6$, $^4J = 1.6$ Hz, 1 H), 7.41 (dd, $J = 7.6$, 5.2 Hz, 1 H), 6.76 (t, $J = 5.7$ Hz, 1 H), 5.53 (s, 1 H), 4.07 (q, $J = 7.1$ Hz, 2 H), 3.61 - 3.49 (m, 4 H), 3.01 (s, 3 H), 2.61 (t, $J = 6.8$ Hz, 2 H), 2.23 (t, $J = 7.3$ Hz, 2 H), 1.86 - 1.75 (m, 2 H), 1.18 (t, $J = 7.1$ Hz, 3 H). The signal arising from the CO_2H proton could not be observed, either because of exchange on the NMR timescale, or masking by the water peak (3.43 - 3.05 ppm).

(S)-Ethyl 3-((6-(methyl(4-(2-(methylcarbamoyl)pyrrolidin-1-yl)-4-oxobutyl)amino)-2-(pyridin-2-yl)pyrimidin-4-yl)amino)propanoate **402**



Was prepared as for **392b** from HATU (23.6 mg, 0.062 mmol), DIPEA (22 μ L, 0.124 mmol) **401** (20 mg, 0.052 mmol) and (S)-N-methylpyrrolidine-2-carboxamide hydrochloride (10.2 mg, 0.062 mmol). The usual purification afforded crude **402** (35 mg) as a brown oil.
MS (ES+) m/z 498.3 [M+H]⁺.

(S)-3-((6-(methyl(4-(2-(methylcarbamoyl)pyrrolidin-1-yl)-4-oxobutyl)amino)-2-(pyridin-2-yl)pyrimidin-4-yl)amino)propanoic acid **403**



Was prepared as for **332b** from **402** (33 mg, 0.07 mmol) and lithium hydroxide monohydrate (2.8 mg, 0.7 mmol). The usual purification afforded crude **403** (35 mg, 63%) as a yellow oil.
LC-MS analysis showed product MS (ES+) m/z 470.3 [M+H]⁺.

¹H NMR (400 MHz, DMSO-d₆) δ 8.65 (d, J = 4.8 Hz, 1 H), 8.24 (d, J = 7.8 Hz, 1 H), 7.87

CONFIDENTIAL – DO NOT COPY

(dt, $J = 7.8, 1.8$ Hz, 1 H), 7.71 (d, $J = 4.7$ Hz, 1 H), 7.47 - 7.37 (m, 1 H), 6.71 (br. s, 1 H),
5.53 (s, 1 H), 4.28 - 4.14 (m, 1 H), 3.85 - 3.26 (m, 9 H), 2.54 (d, $J = 4.7$ Hz, 3 H), 2.42 (m, 2
H), 2.31 (t, $J = 6.9$ Hz, 2 H), 1.89 - 1.64 (m, 6 H)

V Appendices

Appendix 1 Matrix of pairwise identities for several JmjC containing proteins

Enzyme	JMJD2A	JMJD2B	JMJD2C	JMJD2D	JMJD2E	JARID1A	JARID1B	UTX	JMJD3	JHDM1D	PHF8	PHF2	JMJD6	JMJD5
JMJD2A	100	82.63	84.43	74.25	74.25	39.52	40.72	16.46	15.82	13.82	11.18	11.18	13.58	9.63
JMJD2B		100	87.43	77.84	75.45	36.53	37.13	17.09	17.09	12.5	11.18	10.53	12.96	10.37
JMJD2C			100	75.45	74.25	36.53	37.13	15.19	15.19	13.82	13.16	11.84	12.96	9.63
JMJD2D				100	93.41	42.51	38.92	17.72	15.82	11.84	11.18	11.18	13.58	9.63
JMJD2E					100	42.51	38.92	17.72	16.46	11.84	11.18	11.18	12.96	9.63
JARID1A						100	87.43	19.62	17.09	11.84	10.53	11.18	15.43	8.15
JARID1B							100	19.62	17.72	13.16	11.84	11.18	14.81	8.15
UTX								100	79.11	9.21	11.18	9.21	13.29	13.33
JMJD3									100	9.21	9.87	7.89	10.76	11.11
JHDM1D										100	75	65.13	19.74	11.85
PHF8											100	70.39	19.08	11.85
PHF2												100	17.11	11.11
JMJD6													100	16.3
JMJD5														100
JMJD7														
JMJD4														
JMJD8														
EGLN1														

Matrix of pairwise identities for several JMJC proteins.

Green = 70-100%: closely related JMJC domains

Yellow = 30-70%: clearly related JMJC domains

Orange = 20-30%: borderline relationship

Red = <20%: poor relationship.

Appendix 2

The JmjD3 RapidFire™ and MALDI-TOF mass spectrometry assays both monitor demethylation of a histone H3 peptide containing tri-methylated K27, by recombinant Jumonji D3 family demethylase enzyme. Disappearance of the trimethylated peptide substrate and formation of the dimethylated product are both monitored by mass spectrometry. The JmjD3 TR-FRET assays are based on competition between H3K27Me1 reaction product and an H3K27Me1 ULight tracer complex for binding to a specific Europium labelled antibody. The H3K27Me1-ULight tracer complex is formed by the tight interaction between Biotin-H3K27Me1 and streptavidin labelled with ULight. When the ULight tracer is antibody bound, excitation of the Eu-chelate at 340 nm results in energy transfer to the ULight molecules and emission at 665 nm. JmjD3 inhibitors reduce the levels of H3K27Me1 reaction product available to compete for binding and therefore result in increased TR-FRET signal.

Materials: Ascorbic acid, α -ketoglutarate, DMSO, 4-(2-hydroxyethyl)-1-piperazineethanesulfonic acid (Hepes), 3-[(3-cholamidopropyl)dimethylammonio]-1-propanesulfonate (CHAPS) and bovine serum albumin (BSA) were purchased from Sigma-Aldrich (Gillingham, Dorset, UK). TFA was from Applied Biosystems (Warrington, UK). Acetonitrile and ammonium iron(II) sulphate were purchased from Fisher Scientific (Loughborough, UK). H3K27-Me3 peptides were synthesized and HPLC-purified to >95% purity by Cambridge Research Biochemicals (Cambridge, UK). Biotinylated-H3K27Me1 was purchased from Millipore (Billerica, MA, USA) and biotinylated in house. Europium labelled Anti-monomethyl-Histone H3 (Lys27) antibody (Eu-Ab) was purchased from Millipore (Billerica, MA, USA) and labelled with Europium by PerkinElmer (Waltham, MA,

USA) .LANCE® Ultra ULight™-Streptavidin and LANCE® detection buffer were both purchased from PerkinElmer (Waltham, MA, USA).

Expression and purification of human Jmjd3: Jmjd3 DNA encoding the catalytic domain (residues 1141–1682), and lacking residues 1637-1675 (a splice variant deletion; GenBank BC009994) was amplified by PCR to add an N-terminal Flag tag and cloned into the pFB-HTb vector (Invitrogen) using BamHI and XhoI restriction sites, which resulted in a protein with an N-terminal 6His tag followed by a TEV-protease cleavage site and Flag tag. pFB1-HTb-Flag-Jmjd3 1141-1682 (del 1637-1675) was transposed into the baculovirus genome using the BAC-to-BAC technology (Invitrogen). Bacmid DNA was transfected into *Spodoptera frugiperda* (Sf9) cells using Cellfectin II (Invitrogen), and expression was performed at a 1 L scale in Excel 420 media (SAFC Biosciences). The culture, at a cell concentration of 3.8x10⁶ cells/ml, was infected with P1 recombinant Baculovirus at a nominal multiplicity of infection of 3 and incubated for 48 h. The cells were removed from the media by centrifugation at 2500 g for 20 min, and the cell pellet was frozen for subsequent purification. The pellet from the Baculovirus culture was resuspended in buffer A (20 mM Tris pH 8.5, 300 mM NaCl, 10% glycerol, 1uL/mL Protease Inhibitor Cocktail Set III (Calbiochem 539134)). Cells were lysed by Dounce Homogenisation, on ice, and centrifuged at 100,000 x g for 90 min at 4 °C. The 100,000 x g supernatant was applied to a HisTRAP HP Column (GE Healthcare 17-5248-02). The column was washed with ten CV of buffer A, followed by ten CV of buffer A containing 20 mM imidazole. Bound protein was eluted from the column using a linear gradient of 20-250 mM imidazole over twenty CV. The Jmjd3 protein was eluted between 100 mM and 200 mM imidazole. Eluted Jmjd3 protein from the HisTRAP column was concentrated fourfold (Amicon Ultrafree-15 30 kDa, Millipore UFC903024) and loaded onto a HiLoad 26/20 Superdex 200 prep grade size exclusion column (GE Healthcare 17-1069-01), equilibrated with buffer B (20 mM Tris pH

8.0, 150 mM NaCl, 5% glycerol, 0.5 mM TCEP, 2 mM α -ketoglutaric acid sodium salt (Sigma K1875) and 10 μ M $\text{Fe}(\text{NH}_4)_2(\text{SO}_4)_2$. Fractions containing JmjD3 were pooled and concentrated (Ultrafree-15 30 kDa). Protein identity was confirmed by peptide mass fingerprinting and predicted molecular weight confirmed by mass spectrometry.

Preparation of compound screening plates: For dose-response curves, 3-fold serial dilutions were prepared from 10 mM compound solutions in DMSO across 384 well HiBase plates (Greiner Bio-one, Stonehouse, UK). 100 nL of this dilution series was transferred into 384 well V base assay plates (RapidFire and MALDI assays) or 384 well low volume black plates (TR-FRET assays) (both Greiner Bio-one, Stonehouse, UK) giving a concentration range between 100 μ M and 1.7 nM. Columns 6 and 18 of the assay plates were reserved for the high and low controls, respectively. The high controls had 100 nL of DMSO, but no compound, while the low controls also had 100 nL of DMSO but either the enzyme was acid-inactivated by pretreatment with 0.5% (v/v) TFA (MALDI and RapidFire assays), or buffer was added in place of JmjD3 enzyme (TR-FRET assays). Compounds and DMSO were dispensed using the Echo™ acoustic dispenser (Labcyte Inc, Sunnyvale, CA, USA).

RapidFire™ mass spectrometry assay: Assays were performed by initially dispensing 5 μ L of a 2 \times solution containing 0.3 μ M JmjD3, 0.5 mg/mL BSA and 200 μ M CHAPS in 50 mM Hepes pH 7.0 into the 384-well plates containing 100 nL compound. Plates were allowed to incubate for 10 min at ambient temperature before reactions were initiated by the addition of 5 μ L of a 2 \times substrate solution containing 100 μ M ascorbate, 100 μ M Fe^{2+} , 20 μ M α -ketoglutarate, and 60 μ M H3K27(me3) peptide also in 50 mM Hepes pH 7.0. Plates were centrifuged at 1000 rpm for 1 min and the reactions incubated at room temperature for 6 min, before being quenched by the addition of 30 μ L of a 0.5% (w/v) TFA solution. For the enzyme-inactivated control wells in column 18, the TFA solution was dispensed prior to

addition of the enzyme solution. Plates were centrifuged at 1000 rpm for 5 min before analysis. All solutions were dispensed using a Multidrop Combi™ dispenser (Thermo Fisher Scientific, Waltham, MA, USA). Assay plates were transferred onto a RapidFire200 integrated autosampler/solid phase extraction (SPE) system (Agilent Technologies Inc., Wakefield, MA, USA) coupled to an API4000 triple quadrupole mass spectrometer (Applied Biosystems, Concord, Ontario, Canada). Solvent A was water containing 0.01% (v/v) TFA and 0.09% (v/v) formic acid. Solvent B was acetonitrile/water (8:2, v/v) containing 0.01% (v/v) TFA and 0.09% (v/v) formic acid. Samples were aspirated under vacuum directly from 384-well assay plates for 500 ms. The sample was then loaded onto a C4 SPE cartridge to remove non-volatile buffer salts, using solvent A at a flow rate of 1.5 mL/min for 3 s. The retained analytes were eluted to the mass spectrometer by washing the cartridge with solvent B at 1.25 mL/min for 3 s. The cartridge was re-equilibrated with solvent A for 500 ms at 1.5 mL/min. The entire sampling cycle was approximately 7 seconds per well, enabling analysis of a 384 well plate in approximately 45 minutes. The mass spectrometer was operated in positive electrospray MRM mode. MRM transitions (Q1/Q3) for each species were as follows. H3K27Me3: 418.3/515.0; H3K27Me2: 414.8/519.7.

A dwell time of 50 ms was used for all of the MRM transitions. The mass spectrometer was operated with a spray voltage of 3500 V and at a source temperature of 650 °C. The peaks detected by mass spectrometry were approximately 1.2 s wide at half-height and they were integrated and processed using the RapidFire™ peak integration software.

TR-FRET Assay: Initially 2.5 uL of a substrate solution consisting of 10 μM H3K27Me3, 25 μM α-ketoglutaric acid and 60 nM biotinylated H3K27Me1 in a buffer of 50 mM Hepes, 100 mM NaCl, 20 μM (NH₄)₂Fe(SO₄)₂, 1 mM Ascorbic acid, and 0.1 mM CHAPS pH 7.5 was added to all wells of compound plates. 2.5 μL enzyme solution consisting of 700 nM JmjD3 in buffer was then added to all wells except column 18 of the plate. 2.5 uL of buffer

alone was added to column 18 to act as the low control. Plates were incubated at room temperature for 50 minutes before the addition of 2.5 μL of detection solution consisting of 0.5 nM Europium anti-H3K27Me1 Ab, 1 nM ULight-Stv and 0.825x Lance Buffer in a buffer of 50 mM Hepes, 100 mM NaCl, 0.012% Tween 20 pH 7.5. All solutions were dispensed using a Multidrop Combi™ dispenser (Thermo Fisher Scientific, Waltham, MA, USA). Concentrations quoted are final assay concentrations. Plates were incubated at room temperature for a further 30 minutes before being transferred to the EnVision plate reader (PerkinElmer, Waltham, MA, USA) for analysis, with laser excitation at 320 nm and following donor and acceptor emission at 615 and 665 nm respectively.

MALDI-TOF Assay: Assays were performed by initially dispensing 5 μL of a 2 \times solution containing 0.6 μM JmjD3 and 200 μM CHAPS in a buffer of 150 mM NaCl, 20 mM Tris-HCl pH 8.0. Plates were allowed to incubate for 15 min at ambient temperature before reactions were initiated by the addition of 5 μL of a 2 \times substrate solution containing 4 mM ascorbate, 100 μM Fe^{2+} , 70 μM α -ketoglutarate and 30 μM H3K27Me3 peptide in a buffer of 100 mM Hepes. Plates were centrifuged at 1000 rpm for 1 min and the reactions incubated at room temperature for 9 min, before being quenched by the addition of 10 μL of a 1% (w/v) TFA solution. For the enzyme-inactivated control wells in column 18, the TFA solution was dispensed prior to addition of the enzyme solution. Samples were then further diluted by the addition of 20 μL of 10% acetonitrile solution and centrifuged for a further 1 minute. During this time a separate dilution plate was prepared by dispensing 100 μL of 5% acetonitrile into all wells of a 384 well black hibase plate (Greiner Bio-one, Stonehouse, UK). All solutions were dispensed using a Multidrop Combi™ dispenser (Thermo Fisher Scientific, Waltham, MA, USA). Using a Biomek FX (**Beckman Coulter, IA, USA**), 2 μL of assay reaction was removed from the assay plate and added to the dilution plate to give a further 1:50 dilution of the sample. 1 μL of this diluted sample was then transferred using the Biomek FX from the

dilution plate onto a Pre-Spotted AnchorChip MALDI target (PAC 384 HCCA) (Bruker Daltonics, Bremen, Germany). Once dry, the target was washed by manually dipping into a solution of 10mM ammonium phosphate/ 0.1% TFA and allowed to dry, before transferring to the mass spectrometer for analysis. Matrix-assisted laser-desorption/ionization time-of-flight mass spectra were collected on an Ultraflex III mass spectrometer (Bruker Daltonics, Bremen, Germany) in reflectron mode. Data were analysed in FlexAnalysis used the SNAP algorithm and automatically extracted from each sample. The laser was set to Fuzzy control using a random walk raster with 5 X 120 shots. The fuzzy method power range was 28%-45%.

Data analysis: Data were analyzed using the ActivityBase Suite (ID Business Solutions Ltd, Surrey, UK). For the mass spectrometry (RapidFire and MALDI) assays, the extent of enzymatic turnover of the tri-methylated substrate to di-methylated product was expressed as percent conversion as shown in Eq. (1):

$$\% \text{ Conversion} = 100 \times \text{Me}_2 / (\text{Me}_2 + \text{Me}_3) \quad (1)$$

where Me₂ and Me₃ represent the integrated peak areas of the di- and trimethylated peptides. Data were then fitted to Eq. (2) to determine IC₅₀ values

$$\% \text{ Inhibition} = (a - d) / [1 + ([I] / \text{IC}_{50})^h] + d \quad (2)$$

where a is the uninhibited value, d is the fully inhibited value, [I] is the inhibitor concentration, IC₅₀ is [I] that gives $\frac{1}{2} \times (a - d)$, and h is the Hill slope.

For the TR-FRET assay, data were expressed as a ratio of emission counts at 615 nM and 665 nM and then fitted to equation 2.

EGLN3 HTRF assay

Materials: Eu-streptavidin chelate was purchased from Perkin Elmer. TCEP HCl was purchased from Pierce. KCl was purchased from JT Baker. CHAPS, BSA, ascorbic acid, FeCl₂, HEPES free acid and α -ketoglutarate were all purchased from Sigma Aldrich.

Preparation of compound screening plates: For dose-response curves, 3-fold serial dilutions were prepared from 10 mM compound solutions in DMSO across across 384 well HiBase plates (Greiner Bio-one, Stonehouse, UK). 100 nL of this dilution series was transferred into black, low volume 384 well assay plates (Nunc International, Rochester, NY, USA). Columns 6 and 18 of the assay plates were reserved for the high and low controls, respectively. The high controls contained 100 nL of DMSO, but no compound, while the low controls contained 100nl of 10mM GSK1002043A in DMSO. Compounds and DMSO were dispensed using the Echo™ acoustic dispenser (Labcyte Inc, Sunnyvale, CA, USA).

EGLN3 HTRF assay: This assay utilised TR-FRET to measure hydroxylation of the cy-5 labelled C-terminal oxygen dependent domain (Cy5 CODD) of the substrate, Hif2A by EGLN3. Hydroxylation of Cy5 CODD induced binding of biotin labelled VBC complex to the Cy5 CODD. Addition of Europium-streptavidin chelate brought the Cy5 label and the Europium label into close proximity (as streptavidin and biotin are binding partners) under conditions where Cy5 CODD had been hydroxlyated. This proximity resulted in Fourier resonance energy transfer (FRET) between the Europium and the Cy5. Assays were performed by preparing a 2 x stock of enzyme mix, containing working concentrations of 0.3 mM CHAPS, 0.2 mg/ml BSA, 1mM TCEP, 0.4mM ascorbic acid, 1.25 ug/ml FeCl₂, 4nM EGLN3, diluted in assay buffer (50mM HEPES free acid and 50 mM KCl, in distilled water, pH'd to 7.5 with NaOH). 5ul/well 2x enzyme mix was added to each well of the compound plates using a Multidrop combi (Thermo Fisher Scientific, Waltham, MA, USA). Plates were then centrifuged at 500rpm for 30 seconds, then incubated, stacked at room temperature

for 30 minutes. Meanwhile, 2 x substrate mix was prepared, containing working concentrations of 0.3 mM CHAPS, 25 nM VBC, 1ug/ml Europium-streptavidin, 50 nM Cy5 CODD and 20 nM α -ketoglutarate, diluted in assay buffer. At the end of the 30 minute incubation, 5ul/well 2 x substrate mix was added to each well of the plates, using a Multidrop Combi (Thermo Fisher Scientific, Waltham, MA, USA). Plates were centrifuged at 500 rpm for 30 seconds, and then incubated, stacked at room temperature for 40 minutes. Plates were then read on a Viewlux plate reader (Perkin Elmer, Waltham, MA, USA). Excitation wavelength was 360 nm and Cy5 emission was at 660 nm, while Eu emission was at 610 nm.

Data analysis

Data were analysed using the ActivityBase Suite (ID Business Solutions Ltd, Surrey, UK). Data was ratioed by dividing the Cy 5 emission by the Eu emission, then normalised such that 100% inhibition was represented by the column 18 low control wells and 0% inhibition was represented by the column 6 high control wells. A four parameter curve fit of the following form was then applied.

Oxidative stability assay

Assay run by Matthew Lochansky.

Materials: Coularray and Coularray 12 Cell Detector were purchased from Thermo Scientific. NH_4Oac , MeOH, DMSO, Acetaminophen and Phenacetin were purchased from Sigma Aldrich.

Sample preparation: Dilute the sample with DMSO to 1 mM final concentration. 10 μL of a 10 mM sample requires 90 μL of DMSO.

Chromatographic set up:

A = H₂O + 100 mM NH₄OAc

B = MeOH + 100 mM NH₄OAc

Column: Phenomenex Kinetex C18, 50 x 2.1 mm, 1.7 μm

Initial Conditions - 1% B. Hold for 0.5 min

Linear Gradient - 0.5 to 2 min from 1% B to 99% B

Hold at 99% B for 1 min.

Flow Rate: 0.5 mL/min

Injection Volume: 1μL (sample concentration should be ~1mM)

Quality control: A 50:50 mixture of 1 mM solutions of Acetaminophen and Phenacetin are used to control the quality of the system. The mixture is analyzed the same way as other samples. The Acetaminophen peak should elute at 1.03 min and the Phenacetin at 1.5 min.

Acetaminophen should exhibit a E⁰ of 300 mV +/- 50 mV.

Phenacetin should exhibit an E⁰ of 825 mV +/- 50 mV.

A sample must have an acceptable quality control before and after the analysis to be considered acceptable. Quality control should be run no less frequently than once every 192 samples.

A blank sample (typically MeOH) can also be run with the quality control to establish a background for subtraction purposes.

Cell set up: The system contains 12 electrochemical cells. The analyte flows through the cells, in series, from cell 1 through 12.

Cell 1: 0 mV

Cell 2: 120 mV

Cell 3: 240 mV

Cell 4: 360 mV

Cell 5: 480 mV

Cell 6: 600 mV

Cell 7: 720 mV

Cell 8: 840 mV

Cell 9: 960 mV

Cell 10: 1080 mV

Cell 11: 1200 mV

Cell 12: 1320 mV

Each cell collects data corresponding to the current generated as electrons are removed from the analyte in the oxidative process.

The signal from cell 1 may be replaced with an analog input for UV data. Should a molecule not be oxidized in any cell, the UV data is used to ensure a sufficient amount of compound was injected to expect a response.

Data analysis: Data first integrated using the Coularray software. The software will do background subtraction and baseline filtering to allow for minimal extraneous peaks to be integrated. Then, the chromatogram showing current versus time for each cell is integrated with the peak given a value corresponding to the current generated (area under the curve).

The individual cells are looked at collectively by time window to determine the various oxidative transitions each analyte has undergone. The software processes this and assigns each transition its own cumulative current. This data is then exported into a tab delimited text file using the export option in the software. The data is fed into MS Excel where a

custom written macro will analyze the data and report E^0 for the lowest energy transition for the largest peak in the chromatogram.

Acceptance and rejection criteria:

- If the sample is detected by both UV and electrochemical cells, the standard potential value is reported as calculated by the excel macro.
- For samples with UV response but no electrochemical response, data is reported as a value greater than cell 11's value, i.e. > 1000 mV.
- In the case of no UV signal but a clear electrochemical signal, further evaluation will occur. If molecule lacks a chromophore, electrochemical response will be recorded as calculated by the excel macro. Otherwise, follow up through another analytical method is required. If no verification possible, no result will be recorded.
- In the case of no UV signal nor electrochemical response, no result will be returned unless it can be verified the expected material is definitely present through an alternative analytical method.

Appendix 3

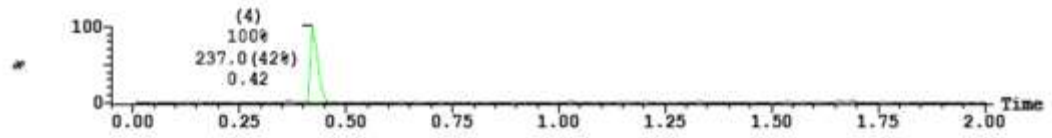
INSTRUMENT: GREEN Page 1
 Sample: 2 Vial: 1:37 LNB ref: N14399-23-M1
 File: L5100940-2 Date: 26-Jan-2010 Time: 11:10:04
 Submitter: Hawa X Diallo (hd35835) Method: E:\gsk.PRO\Acq~2min_For.olp Comment:

Printed: Tue Jan 26 11:15:21 2010

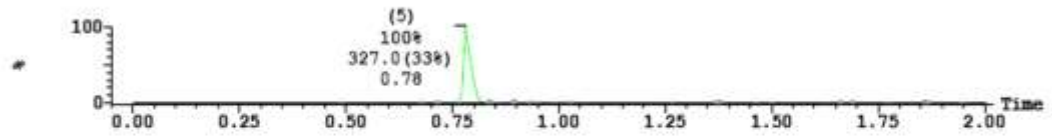
Sample Report:

Sample: 2

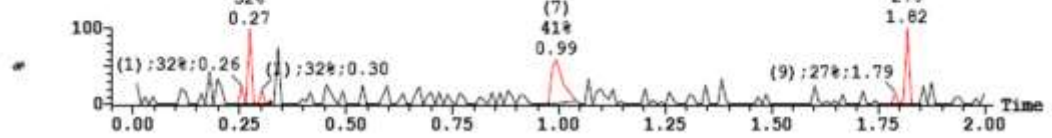
1: MS ES+ : 238 5.0e+006



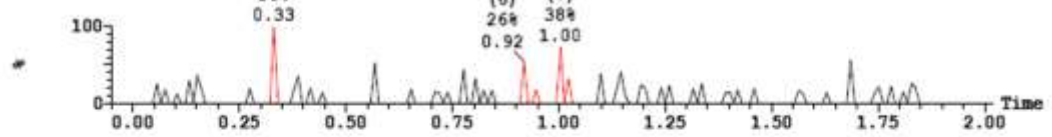
1: MS ES+ : 328 1.5e+006



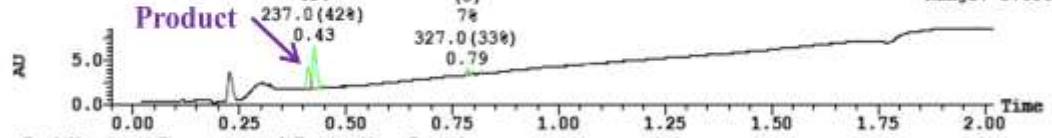
2: MS ES- : 282 2.7e+004



2: MS ES- : 372 9.2e+003



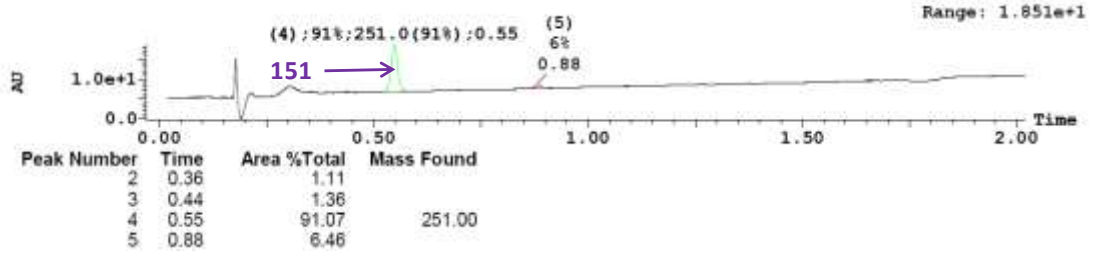
3: UV Detector: TIC 8.697
Range: 8.686



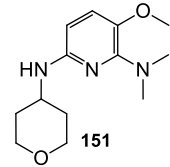
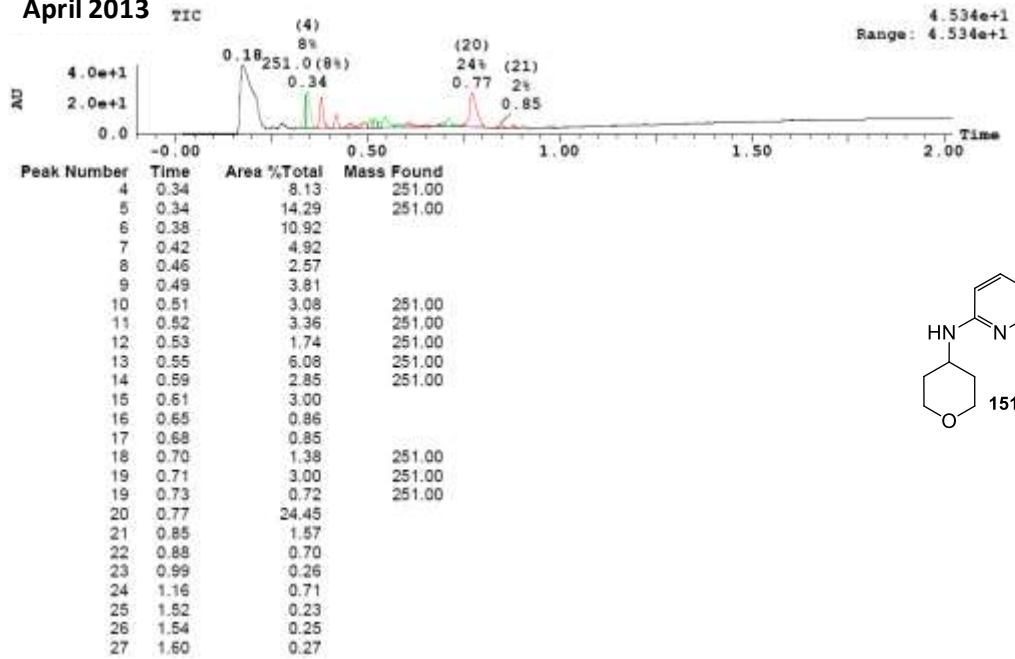
Peak Number	Time	Area %Total	Mass Found
3	0.41	28.56	237.00
4	0.43	62.67	237.00
5	0.79	6.90	327.00
8	1.06	1.87	

Appendix 4

December 2009



April 2013



Appendix 5

Bis-aminopyridyl series investigation on Sci-Finder.²¹³

A sub-structure search was carried out for analogues of **421** (Figure 97), and no molecules were found.

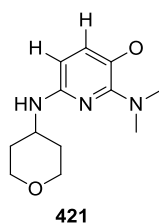


Figure 97.

A sub-structure search was carried out for analogues of **422** (Figure 98); the exact molecule was found, but there was neither literature reference nor experimental data available for it, and the molecule cannot be bought.

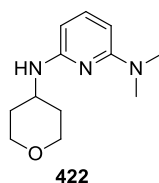


Figure 98.

A sub-structure search was carried out for analogues of **423** (Figure 99) which resulted in 907 molecules being found.

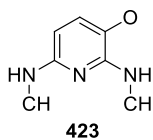


Figure 99.

The closest analogues (Figure 100) had neither literature reference nor experimental data available. These molecules are offered by two companies, Milestone Pharmtech¹³⁰ and FCH group.¹³¹ However, Milestone Pharmtech had discontinued these compounds and FCH group could supply these molecules in seven to eight weeks.

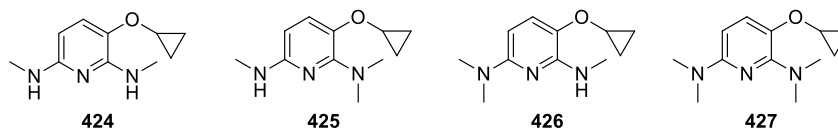


Figure 100.

Another analogue **428** (Figure 101) was described in a Japanese patent covering the synthesis of PGD2 receptor antagonist. The patent could not be read as it was written in Japanese.

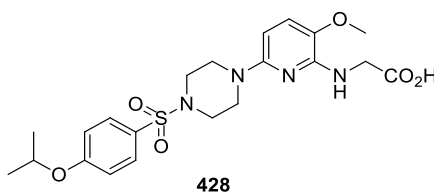


Figure 101.

The remainder of the 902 molecules had one of the nitrogen atoms attached to a carbonyl group as in an amide, carbamate or urea bond, and the other N attached to an alkyl, aryl or carbonyl group.

A sub-structure search was carried out for analogues of **429** (Figure 102) which resulted in 634 molecules being found.

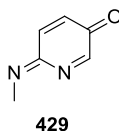


Figure 102.

There were two close analogues (Figure 103)

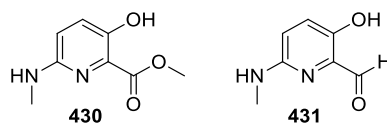


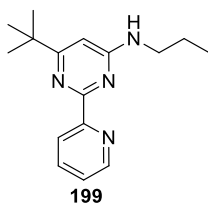
Figure 103.

Compound **430** had neither literature reference nor experimental data, and compound **431** was described in a patent covering synthesis of herbicides.²¹⁴

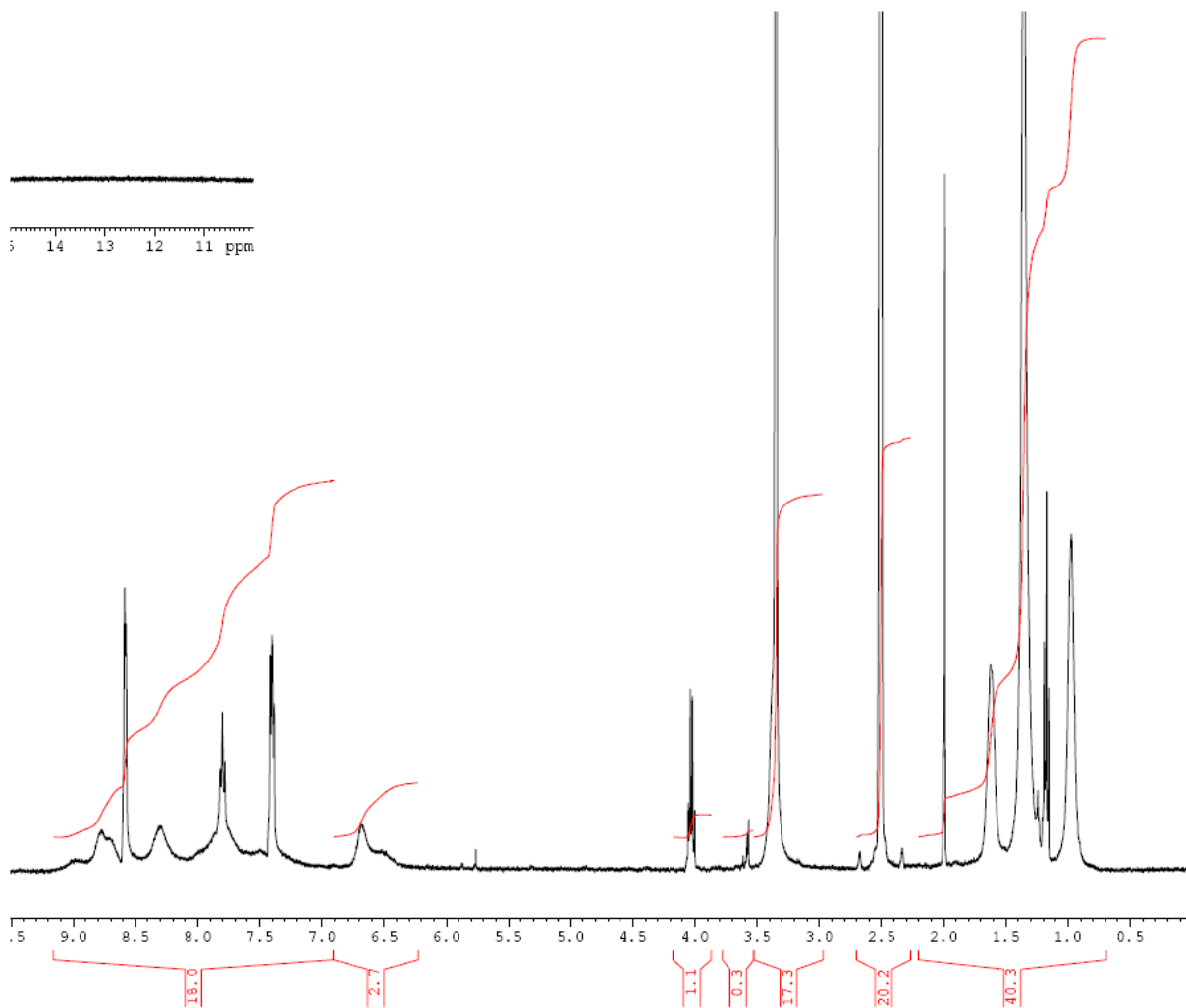
The remaining of the 632 compounds contained [6,6], [6,5] systems such as naphthyridines, quinolines, imidazo-pyridines or had the N attached to any aryl or carbonyl group.

The range of precedents for **421** and **422** is surprisingly limited. These are small molecules, and their absence in any numbers from the literature would not be inconsistent with some intrinsic instability.

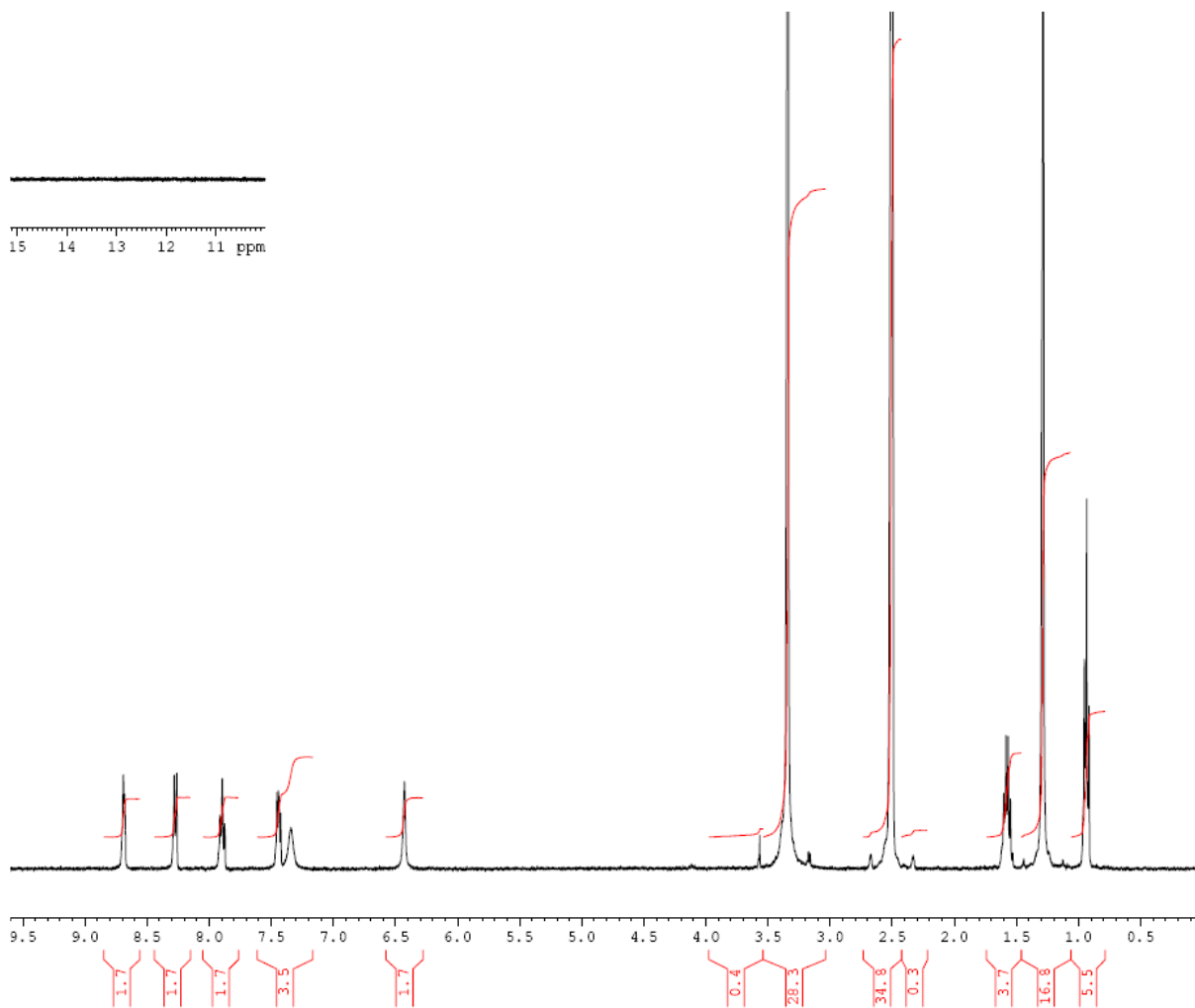
Appendix 6



NMR before MDAP purification.



NMR after MDAP purification.



Appendix 7

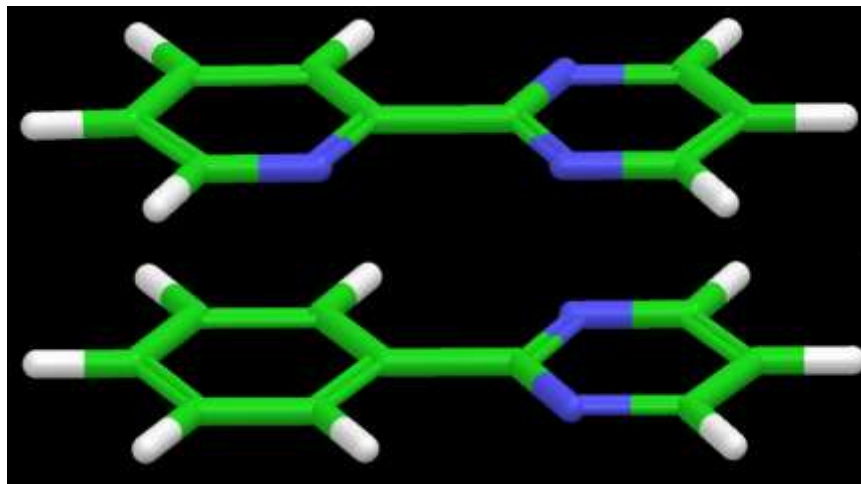


Figure 45. Pyridyl-pyrimidine (top structure) and phenyl-pyrimidine (bottom structure) in their minimal energy conformations.

Minimisation done by R. Sheppard.

Package used: Maestro version 9.1.107. Potential: force field: OPLS-2005; solvent: water; electrostatic treatment: constant dielectric; dielectric constant: 1.0; charges from: force field; cut-off: extended. Minimisation: method: PRCG; maximum iterations: 5000; converge on: gradient; convergence threshold: 0.05. Conformer search: perform automatic set up; method: mixed torsion/ low-mode sampling; max number of steps: 1000; use 100 steps per rotatable bond; number of structures to save for each search: 0; energy window for saving structures: $21\text{kJ}\cdot\text{mol}^{-1}$. Eliminate redundant conformers using maximum atom deviation cut-off: 0.5Å; probability of a torsion rotation/ molecule translation: 0.5; minimum distance for low-mode move: 3.0; maximum distance for low-mode move: 6.0.

Appendix 8

Dockings carried out by Pamela Thomas.

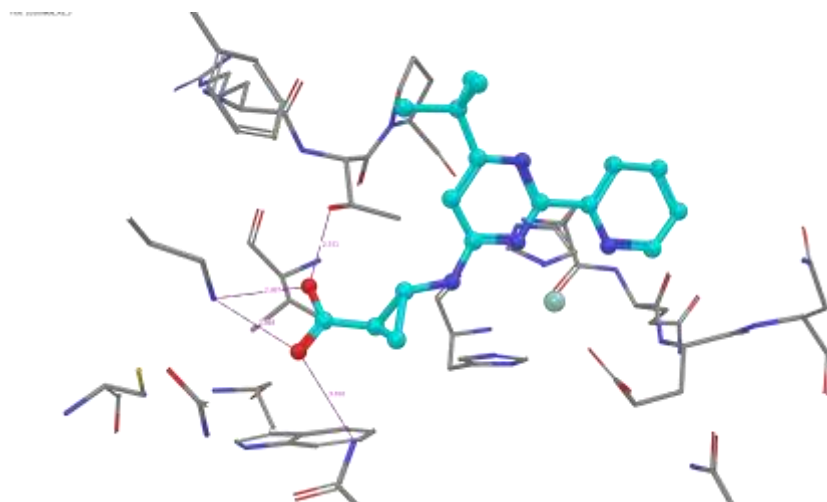


Figure 55. Docking of *trans*-cyclopropyl ring linked **296**. Glide docking score -9.16.

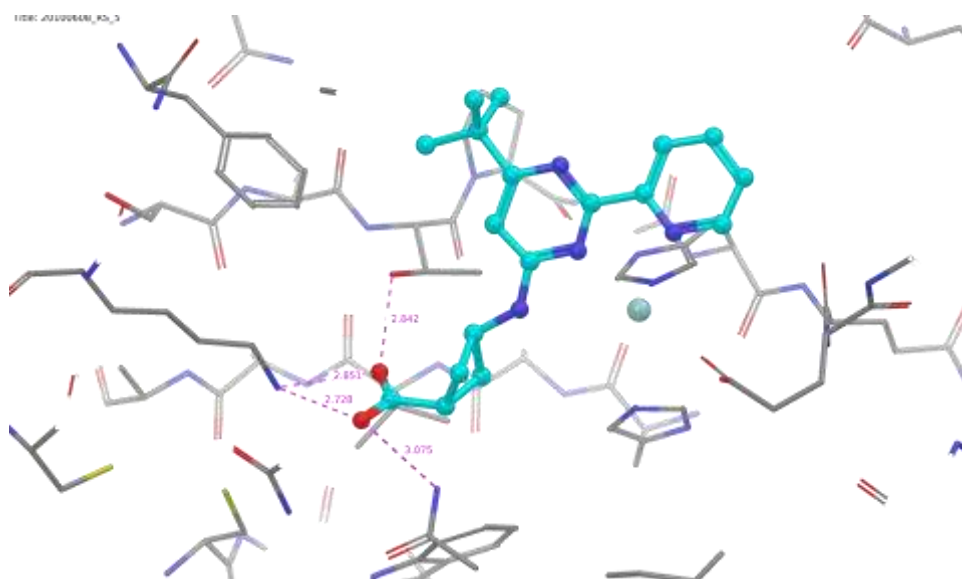


Figure 56. Docking of *trans*-cyclobutyl ring linked **291**. Glide docking score -8.84.

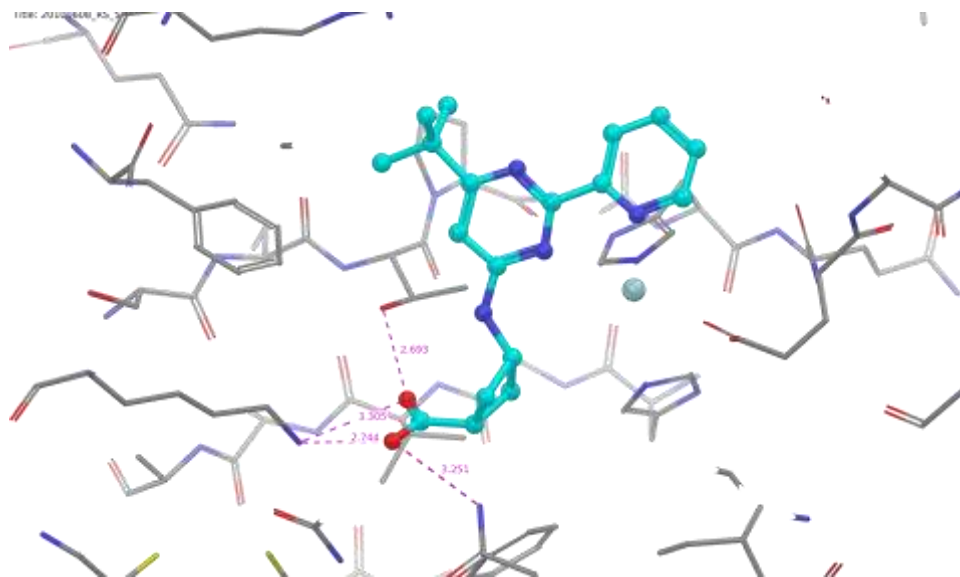


Figure 57. Docking of *cis*-cyclobutyl ring linked **292**. Glide docking score -8.12.

Docking carried out using Glide in Maestro (v9.1)

The docking calculations used 3 hydrogen bonding constraints which are:

- Asn 1400 constrained to hydrogen bond to a hydrogen bond acceptor in the ligand;
- Lys 1381 constrained to hydrogen bond to a hydrogen bond acceptor in the ligand;
- Thr 1387 constrained to hydrogen bond to a hydrogen bond acceptor in the ligand.

When applied, these three constraints cause the carboxylate moiety of the ligand to bind to these three residues (as is seen in X-ray structures).

Also waters bound to the metal and occupying two other sites (carboxylate site and adjacent to Arg1247) were included in the calculation with all other water molecules removed. The metal binding waters are left in order to obtain the correct co-ordination of the ligand and metal as established in X-ray structures. The carboxylate site water prevents ligands binding too deeply into the carboxylate pocket and the water close to Arg1247 was left in to encourage ligand binding in the most likely orientation in this pocket.

Appendix 9

Dockings carried out by Pamela Thomas.

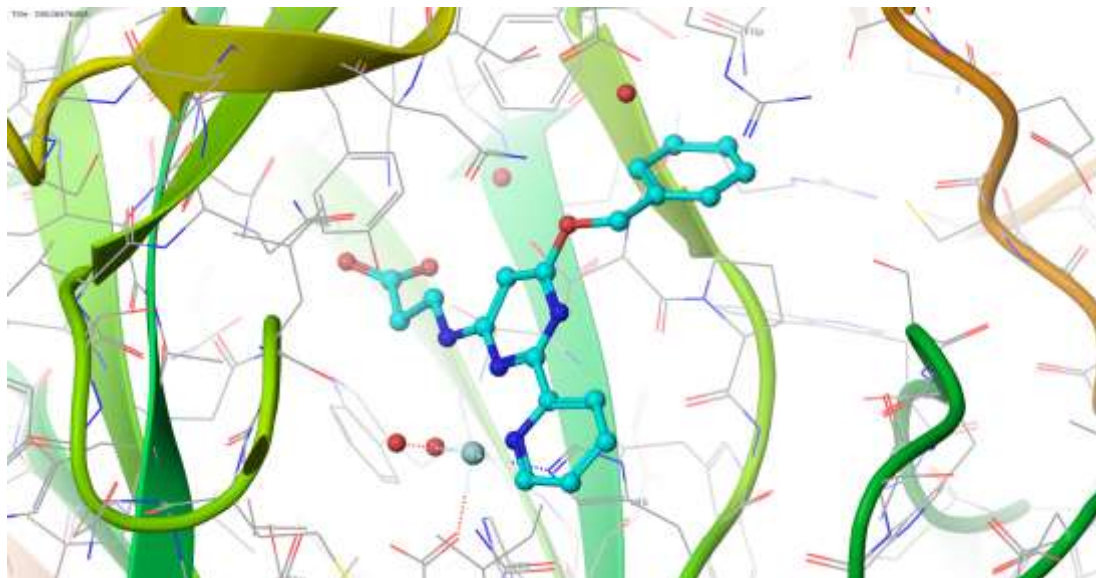


Figure 73. Docking of *O*-benzyl **337** in JmjD3 active site.

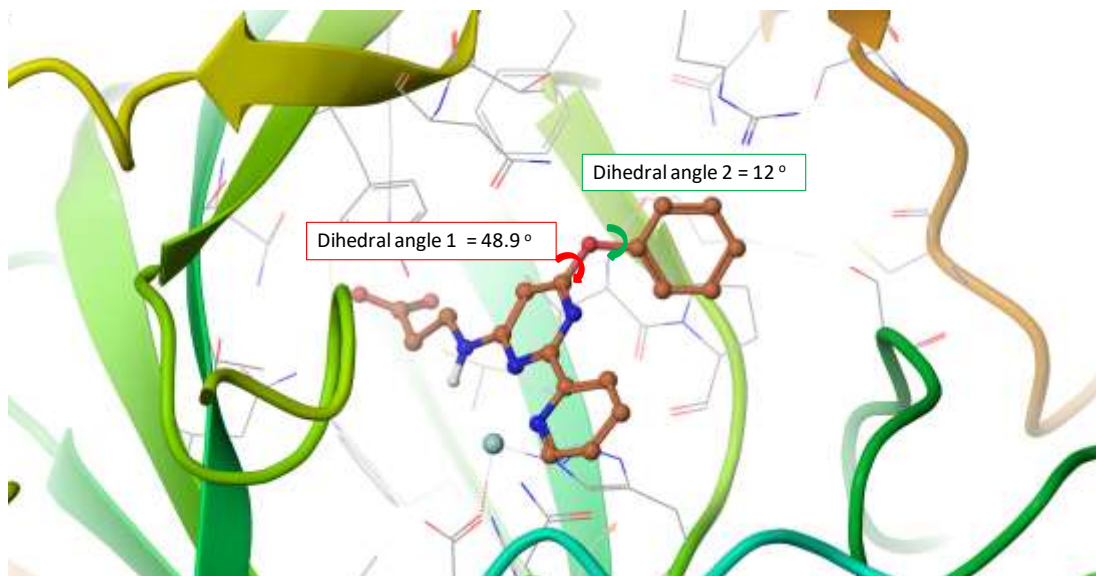


Figure 76. Docking of *O*-phenyl **346** in JmjD3 active site.

Docking carried out using Glide in Maestro (v9.3.515).

The docking calculations used 3 hydrogen bonding constraints which are:

CONFIDENTIAL – DO NOT COPY

- Asn 1400 constrained to hydrogen bond to a hydrogen bond acceptor in the ligand;
- Lys 1381 constrained to hydrogen bond to a hydrogen bond acceptor in the ligand;
- Thr 1387 constrained to hydrogen bond to a hydrogen bond acceptor in the ligand.

When applied, these three constraints cause the carboxylate moiety of the ligand to bind to these three residues (as is seen in X-ray structures).

Also waters bound to the metal and occupying two other sites (carboxylate site and adjacent to Arg1247) were included in the calculation with all other water molecules removed. The metal binding waters are left in order to obtain the correct co-ordination of the ligand and metal as established in X-ray structures. The carboxylate site water prevents ligands binding too deeply into the carboxylate pocket and the water close to Arg1247 was left in to encourage ligand binding in the most likely orientation in this pocket.

Appendix 10

Chemoproteomics: work carried out by colleagues at Cellzome.

Cell culture. HL-60 and HEK293 cells were purchased from ATCC. HL-60 were grown in IMDM medium (Invitrogen, Carlsbad, CA, USA) supplemented with 20% fetal calf serum (PAA Laboratories, Pasching, Austria). HEK-293 cells were grown in 15 cm diameter plates to subconfluency in DMEM (Invitrogen) supplemented with 10% Foetal Bovine Serum. Cells are harvested by scrapping and washed once in 1 x PBS.

Preparation of cell fractions. Nuclear extract was produced from fresh HL-60 cells grown at 5.0×10^6 cells/mL using a cytostat sonoperfused bioreactor. Cells were collected by centrifugation, washed with PBS and resuspended in hypotonic buffer A (10 mM Tris-Cl, pH 7.4, 1.5 mM MgCl₂, 10 mM KCl, 25 mM NaF, 1 mM Na₃VO₄, and 1 Roche protease inhibitor tablet per 25 mL). After ca.3 min the swollen cells were again spun down and resuspended in buffer A and homogenized with 10 strokes using a Dounce homogenizer. Nuclei were collected by centrifugation for 10 min at 3300 rpm, washed with buffer A and homogenized in one volume of extraction buffer B (50 mM Tris-Cl, pH 7.4, 1.5 mM MgCl₂, 20 % glycerol, 420 mM NaCl, 25 mM NaF, 1 mM Na₃VO₄, 400 Units/ml DNase I, and 1 Roche protease inhibitor tablet per 25 mL). Extraction was allowed to proceed under agitation for 30 min at 4 °C before the extract was clarified by centrifugation at 13000 g. The extract was diluted 3:1 in buffer D (50 mM Tris-Cl, pH 7.4 (RT), 1.5 mM MgCl₂, 25 mM NaF, 1 mM Na₃VO₄, 0.6% NP40, and Roche protease inhibitors), centrifuged again, and aliquots were snap frozen in liquid nitrogen and stored at -80 °C. HEK293 cells were transfected with constructs expressing N-terminally Flag tagged full length UTX and/or JmjD3 under the control of CMV promoter by Calcium phosphate precipitation. 48 h after transfection cells were collected and homogenized at 4 °C in extraction buffer (50 mM

TRIS/HCl, 5% Glycerol, 1.5 mM MgCl₂, 150 mM NaCl, 1 mM Na₃VO₄ with 0.8% NP40 and Roche protease inhibitors). Detergent was then diluted in same buffer down to 0.4%. Extract was ultracentrifuged (145,000 g), supernatant snap frozen in liquid nitrogen and stored at -80 °C. 200 μM sodium-L-ascorbate and 10 μM FeCl₂ were added prior to use.

Compound profiling. Kinobeads experiments and immobilization of GSK-J3 to sepharose were performed as described.²¹⁵ 20 μL of GSK-J3 beads were incubated at 4 °C for 1 h with 1 mL aliquots of cell extract (5 mg/mL), which had been preincubated with inhibitor or vehicle alone, on an end-over-end shaker. Beads were transferred to disposable columns, washed with lysis buffer and eluted with 50 μL 2x SDS sample buffer. Proteins were alkylated with 200 mg/mL iodoacetamide, separated on 4–12% NuPAGE gels (Invitrogen), and stained with colloidal Coomassie. For Western blot, proteins were transferred to PVDF membranes and JmjD3 was detected using JmjD3 antibody HPA037988 (Sigma).

Mass Spectrometry. Procedures were essentially as previously reported.²⁰³ Gels were cut into slices across the entire separation range and subjected to in-gel digestion. Peptide extracts from vehicle treated samples were labeled with TMT reagent 131 (Thermo-Fisher Scientific), and combined with extracts from compound-treated samples labeled with TMT reagents 126-130, fractionated using reversed phase chromatography at pH 11, dried and acidified prior to LC-MS/MS analysis using a nano-LC system (Eksigent 1D+) coupled to Orbitrap mass spectrometers (Thermo-Fisher Scientific). Data dependent tandem mass spectra were generated for up to six peptide precursors using a targeted data acquisition approach.²¹⁶

Peptide and protein identification and quantification. Mascot™ 2.0 (Matrix Science) was used for protein identification using 10 ppm mass tolerance for peptide precursors and

0.8 Da (CID) tolerance for fragment ions. The search data base consisted of a customized version of the IPI protein sequence database combined with a decoy version of this database. We accepted protein identifications as follows: i) For single spectrum to sequence assignments, we required this assignment to be the best match and a minimum Mascot score of 31 and a 10x difference of this assignment over the next best assignment. Based on these criteria, the decoy search results indicated <1% false discovery rate (FDR); ii) For multiple spectrum to sequence assignments and using the same parameters, the decoy search results indicate <0.1% false discovery rate. For protein quantification a minimum of 2 sequence assignments matching to unique peptides was required. FDR for quantified proteins was <<0.1%.

Appendix 11

Experiments run by biologist colleagues at GSK.

Cell isolation and culture: Healthy donor blood was sourced ethically and collected and used in accordance with the terms of the informed consents and under Hertfordshire Research Ethics Committee approval. Blood from rheumatoid arthritis patients was obtained under the NHS ethical permission COREC06/Q1606/139 ("Immune function in inflammatory arthritis") and informed consent was obtained from all patients. Peripheral blood mononuclear cells (PBMCs) were prepared from 200 mL heparinized blood, which was diluted 1:1 in PBS (w/o calcium and magnesium, Invitrogen), and layered in 30 mL aliquots over 20 mL Ficoll-Paque Plus (Amersham Biosciences) in 50 mL Falcon tubes. Following centrifugation at 400xg, rt for 20 min with the brake off, the Buffy coat formed at the interface was transferred to fresh 50 mL tubes, diluted in PBS, centrifuged at 400xg, rt for 10 min and supernatant was removed. PBMCs were then resuspended in 3 mL 4 °C Miltenyi buffer with 0.5% BSA (Miltenyi Biotec) containing 300 µL human CD14 MicroBeads (Miltenyi Biotec), and incubated at 4 °C for 15-25 min. Following this incubation, samples were washed and cells were resuspended in 4 mL 4 °C Miltenyi buffer. Subsequently, 4 LS Separation columns (Miltenyi Biotec) were placed in a magnetic holder and calibrated with 3 mL Miltenyi buffer. The cell suspension was then divided onto these columns after which columns were washed with 3x3 mL 4 °C Miltenyi buffer. Bound CD14+ cells were subsequently eluted by removing columns from their magnetic holder, placing them over a 15 mL Falcon tube, and plunging 5 mL Miltenyi buffer through the columns using a supplied syringe barrel (Miltenyi Biotec). Eluted cell suspensions were spun down at 400xg, rt for 10 min, resuspended in 2 mL culture medium (RPMI 1640 medium (Invitrogen) supplemented with 2 mM L-glutamine (Invitrogen), 100 units/mL penicillin (Invitrogen) and 100 µg/mL streptomycin (Invitrogen)) with 5% foetal bovine serum (FBS,

heat-inactivated, Invitrogen) and counted using a haemocytometer, after which culture medium was added to a final concentration of 1×10^6 cells/mL. CD14⁺ monocyte suspensions were seeded into three 24-well plates (Corning) at 1×10^6 cells/well and incubated in culture medium containing 5% FBS and 5 ng/mL hrGM-CSF (R&D Systems) at 37 °C in a humidified atmosphere with 5% CO₂ for 5 days. Cell viability was checked using the WST-1 assay (Roche 11644807001), according to the manufacturer's instructions.

Determination of intercellular compound concentrations: Diluted whole macrophage lysate and supernatant samples (25 µL) were extracted with 300 µL of 5% acetonitrile (aq) containing Reserpine at 175 ng/mL as the internal standard. All samples were shaken for 10 min on a vortex mixer then centrifuged for 10 min at 1600 g. An aliquot of the resulting supernatant was analysed by reverse phase LC-MS/MS using a heat assisted electrospray interface in positive ion mode. The instrument was an AB Sciex API 4000 triple quadrupole Mass spectrometer coupled to a PAL CTC auto sampler and Jasco XTC pumps. Nominal MRM transitions for analytes were 418.4 to 330.1 for **419**, 390.3 to 330.1 for **420**, 390.1 to 104.9 for **332b**, 418.2 to 104.8 for **331b** and 609.3 to 195 for Reserpine. MRM methods were ran over a 1.4 min gradient running from 5% ACN + 0.1 % formic acid (aq) to 95% ACN + 0.1 % formic acid (aq) up to 1 minute held for 0.25 minutes and returning to the starting conditions over 0.05 minutes. Samples were assayed against calibration standards prepared in relevant control buffer over the range 1 to 10000 ng/mL, and the lower limit of quantification ranged from 1 to 10 ng/mL and the upper limit of quantification ranged from 2000 to 10000 ng/mL for analytes.

RNA extraction: Cell lysates were generated by addition of 100 µL trizol (Invitrogen #15596-026) per 10^6 cells after removal of culture media. Trizol cell lysates were stored at -80 °C for subsequent RNA extraction with the Qiagen RNeasy kit (Qiagen #74104). For

extraction, Trizol samples were thawed and mixed well with 1/5th volume of chloroform on a shaker at 650 rpm for 5 min at rt. The mixed samples were centrifuged at 16,000g for 3 min. The supernatant (clear aqueous phase) was carefully transferred to a clean tube on ice. An equal volume of 70% ethanol was added and mixed by pipetting. The samples were immediately applied to a Qiagen RNeasy mini-column and centrifuged for 30 seconds at 9,000xg. Eluates were reloaded on the columns and centrifuged again for 30 seconds at 9,000xg. 600 μ L of buffer RW1 was added to each RNeasy column and centrifuged as above. The flow-through was discarded. A DNase-1 stock solution was prepared from the Qiagen RNase-free DNase Set (Cat. 79254; 1500U; 50 reactions). The solid DNase (1500 Kunitz units) was dissolved in 550 μ L of RNase-free water provided in the kit. Then for each column 10 μ L of DNase-1 stock solution was added to 70 μ L of buffer RDD from the kit and mixed gently. 80 μ L of DNase-1/RDD buffer was pipetted onto the centre of each mini-column and incubated at rt for 15 min. 600 μ L of buffer RW1 was added to each RNeasy column and centrifuged for 30 seconds at 9,000xg. 500 μ L of buffer RPE was pipetted onto the column and centrifuged for 30 seconds at 9,000xg. The flow-through was discarded. 500 μ L of buffer RPE was pipette onto the column and centrifuged for 2 min at 16,000xg, the flow-through was discarded and the tubes dry spun for 1 min at 16,000xg. The RNeasy columns were transferred to new 1.5 mL collection tubes and 35 μ L of RNase-free water was pipetted directly onto the centre of the silica-gel membrane. Tubes were centrifuged for 1 min at 100xg then for 1 min at 16,000xg. The flow-through was re-applied to the column for 1 min at 100xg followed by 1 min at 16,000xg to elute. After changing the orientation of the columns they were re- centrifuged for 1 min at 16,000xg to fully elute. RNA was quantified using a Nanodrop spectrophotometer (Thermo) according to the manufacturer's instructions. Samples were stored at -80 °C.

Reverse Transcription and RT2 Profiler Array PCR: Reverse transcription was performed with the RT2 First Strand Kit (Qiagen #330401) according to the manufacturer's instructions with 400 ng of RNA per sample, in a maximum of 8 μL . The difference in volume was made up with RNase-free water. A preliminary genomic elimination step was performed by the addition of 2 μL of GE buffer per sample and incubation at 42 °C for 5 min. This was followed by a reverse transcription reaction, in which 4 μL of 5X BC3 buffer, 1 μL P2 buffer, 2 μL RE3 buffer and 3 μL RNase-free water were added to each genomic DNA-free RNA sample. This was incubated at 42 °C for 15 min, and then 95 °C for 5 min on a thermal cycler, then put on ice for at least 1 min. 91 μL of RNase-free water was then added to each sample and mixed gently by pipetting up and down. 102 μL of this cDNA was then added to a PCR premix of 448 μL of RNase-free water and 550 μL of RT2 SYBR GreenROX qPCR Mastermix (Qiagen #330401). The complete PCR mix was then vortexed briefly and aliquoted out onto the Human Common Cytokine RT2 Profiler PCR Array plate (Qiagen PAHS-021E-4) at 10 μL per well. The plate was centrifuged at 524xg for 5 min, then loaded onto an ABI7900HT (Applied Biosystems) with the following cycling conditions: 1 hot start cycle at 95 °C for 10 min; 40 PCR cycles of 95 °C for 15 seconds, and 60 °C for 1 min; then 1 thermal denaturation cycle of 95 °C for 15 seconds (ramp rate 100%), 60 °C for 15 seconds (ramp rate 100%), and 95 °C for 15 seconds (ramp rate 2%).

Statistical analysis (Array Studio V5.0): The raw CT data was normalised to GAPDH and then converted to copy number assuming an assay efficiency of 95%. Genes that were not detectable in all four treatment groups were omitted from further analysis. Fold changes and corresponding *P*-values were obtained by fitting a linear model to the normalised copy number for each gene that accounted for both a donor and treatment effect. The differences between donors were removed from the normalised copy number data and then a hierarchical

clustering was performed using Pearson's correlation as a distance measure and an average linkage method. The analyses were performed in Array Studio version 5.

ELISA: Macrophages were stimulated with 10 ng/mL LPS (O111:B4) for 6 h, after which supernatants were collected and TNF and IL-10 ELISAs (MesoScale Discovery) were carried out according to the manufacturer's instructions.

Western blotting: Macrophages were stimulated with 10 ng/mL LPS (O111:B4) for 30 min, after which the cells were lysed in Cell Lysis Buffer (CST 9803 [20 mM Tris-HCl (pH 7.5), 150 mM NaCl, 1 mM Na₂EDTA, 1 mM EGTA, 1% Triton, 2.5 mM sodium pyrophosphate, 1 mM β -glycerophosphate, 1 mM Na₃VO₄, 1 μ g/mL leupeptin], with additional protease inhibitors [Roche 11 206 893 001] added). Protein content was determined using a Bradford protein assay kit (Bio-Rad 500-0007), and 20 μ g of each sample was diluted in Western LDS loading buffer (Invitrogen NP0008, containing NuPAGE sample reducing agent (Invitrogen NP0004)), and heated at 70 °C for 10 min. Samples were quickly cooled, spun down and subjected to SDS-polyacrylamide gel electrophoresis under reducing conditions on a NuPAGE Novex 3-8% Tris-Acetate gel (1.5 mm, 10 well, Invitrogen EA0375) in NuPAGE Tris-Acetate SDS running buffer (Invitrogen LA0041). In addition, a 10 μ L sample of a pre-stained protein marker (Invitrogen, SeeBlue Plus2 LC5925) was loaded. Gels were run at 200 V (constant) for ca 45 min. Gels were equilibrated in equilibration buffer (NuPAGE Transfer Buffer [Invitrogen NP0006] (@2X), containing 10% methanol) for 20 min at rt, with gentle agitation. Proteins were electrophoretically transferred for 8 min onto polyvinylidene difluoride (PVDF) membrane using Invitrogen's iBlot transfer system according to the manufacturer's instructions. Blots were blocked for 3 h at 4 °C in 3% BSA in PBS containing 0.1% Tween 20 (PBS-T), after which I κ B- α (CST 9242) or histone 3 (Abnova ab1791) antibodies were added to the blocking buffer for overnight incubation at 4

°C. After thorough (4x) washing in PBS-T, the blots were incubated for 1 h at 4 °C with HRP-conjugated donkey anti-rabbit IgG (Abcam 16284) diluted 1:5000 in blocking buffer. After thorough (4x) washing in PBS-T, hybridised bands were visualized using the SuperSignal West Femto chemiluminescence system (Pierce 34096) and a chemiluminescence imager (Fuji LAS3000).

Transfection: Based on a previous study in our lab (published as patent WO/2011/051264), in which four different siRNA sequences per target were tested in a primary human macrophage screen, two siRNA motifs per target were pre-selected for the current work (Qiagen; scrambled #1027281, JmjD3 Hs_JMJD3_2 [SI00449827] and Hs_JMJD3_6 [SI04133836], UTX Hs_UTX_8 [SI04306743] and Hs_UTX_9 [SI04314303]). These were prepared at 200 nM (10x final concentration), in Optimem media (Gibco, Invitrogen), in a 96-well plate and stored at -20 °C. Immediately before transfection, the diluted siRNA motifs were thawed at 37 °C and 10 µL from motif was mixed with 10 µL Gemini transfection reagent (GSK300062; diluted in Optimem to 100 µg/mL). Mixtures were left to complex for 20-30 min before 80 µL/well of macrophage culture media (see above, 5% FCS RPMI) was added. 95 µL/well of media was removed from the cells, and replaced with diluted complex. The plates were sealed with gas permeable sealers and incubated for 48 h. For compound studies, siRNA motifs Hs_JMJD3_6 and Hs_UTX_8 were used. After transfection, media were removed and cells were treated with compounds and/or LPS (E.coli O111:B4 at 10 ng/mL) as required.

Chromatin immunoprecipitation (ChIP): Macrophages were fixed by adding Fix solution (10% formaldehyde, 0.1 M NaCl, 1 mM EGTA, 0.5 mM EGTA, 10 mM Tris-HCL pH8 in water) to cells in media. Fixation was performed at rt for 30 min and stopped by the addition of glycine to a final concentration of 0.125 M. The adherent cells were harvested by scraping

and collected by centrifugation and washed in cold PBS, and then resuspended in lysis solution (0.25% Triton X-100, 0.5% NP-40, 10 mM EDTA, 0.5 mM EGTA, 10 mM Tris HCL pH8, in water with Proteinase Inhibitor Cocktail (P.I.C. Roche) and incubated on ice for 10 min. The cell contents were retrieved by centrifugation and resuspended in post-lysis buffer (0.5 M NaCl, 1 mM EDTA, 0.5 mM EGTA, 10 mM Tris-HCL pH 8, in water with P.I.C.) and incubation 10 min at rt. Cell nuclei were collected by centrifugation and resuspended in sonic buffer (1 mM EDTA, 0.5 mM EGTA, 10 mM Tris-HCL pH8, in water with P.I.C.). Samples were sonicated on ice with an Ultrasonics Sonicator for ten 20 second pulses to leave an average fragment length of approximately 1000 base pairs. The fragments were collected by centrifugation and pre-cleared using ssDNA- beads (protein A sepharose beads CL4B, Amersham, that had been cleared with salmon sperm DNA) and left on rotation at rt for 3-4 h. The supernatants were harvested and the formaldehyde-crosslinked protein-DNA complexes were precipitated overnight at by incubation at 4 °C with the desired antibody or with rabbit immunoglobulin (Ab37415, Abcam Ltd, UK). The ChIP antibodies used were anti-RNA polymerase II (05-952 Millipore), anti-trimethyl-Histone H3K27 (07-449 Millipore) and Histone H3 antibody (Ab1791, Abcam Ltd, UK). The samples were then incubated with ssDNA-beads to harvest the antibodies (and chromatin bound to them). Samples were left on rotation for 3-4 h at 4 °C. Beads were washed seven times using RIPA wash buffer (1% Triton X-100, 0.1% Na-deoxycholate, 0.1% SDS, 500 nM NaCl, in water) and resuspended in 100 µL nuclease free water. After this, 5 µL of 10% SDS and 1 µL proteinase K (20 mg/µL) were added to the samples with beads and 10 µL and 2 µL (respectively) added to the inputs. Samples were incubated overnight at 59-62 °C to reverse formaldehyde cross-linking and the precipitated DNA fragments were isolated using a ChIP DNA Clean and Concentrator kit (Zymo Research) and were amplified using DNA was quantified by quantitative real time RT-PCR performed in duplicate on an ABI PRISM 7900HT Sequence Detection System with bespoke primer and probe sets.

Quantitative real-time PCR: Macrophages were lysed with Trizol and RNA was prepared with an RNeasy Plus kit (Qiagen) and was reverse transcribed with the SuperScript III First-Strand Synthesis system (Invitrogen). Quantitative real time RT-PCR was performed in duplicate on an ABI PRISM 7900HT Sequence Detection System with bespoke primer and probe sets. Results were normalised to the abundance of B-Actin and UBB.

Immunofluorescence: 8000 HeLa cells were seeded in DMEM media supplemented with 10% FBS and penicillin/streptomycin, after which cells were transiently transfected with Flag-tagged JMJD3. 0 μ M, 25 μ M and 50 μ M of compounds were added after 4 h. After 24 h incubation, cells were fixed and permeabilised. All cells were stained with anti-Flag mouse monoclonal antibody (Sigma F1804), rabbit anti-H3K27me3 (Millipore 07-449) and DAPI for DNA. Alexa488 conjugated rabbit and Alex594 conjugated mouse secondary antibodies were used to fluorescently label the H3K27me3 and Flag tag. Image analysis was performed using CellProfiler (citation). Transfected cells were identified as cells with Flag tag immunofluorescence higher than 500 intensity units.

Appendix 12

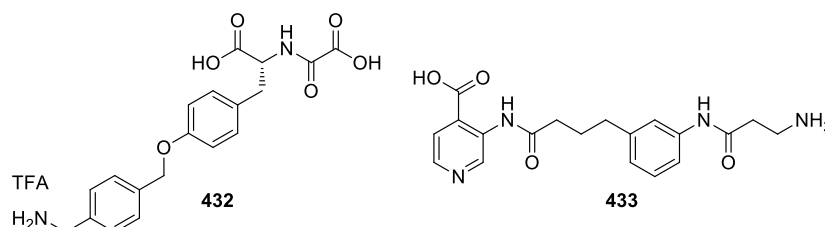
Experiments run by colleagues at Cellzome.

Cell culture. HEK-293 cells (ATCC) were grown in 15 cm diameter plates to subconfluency in DMEM medium (Invitrogen, 41965-039) supplemented with 10% foetal calf serum (FCS). For JmjD3 expression, cells at 60% subconfluency were transfected with pCDNA3.1 vector expressing Flag-JMJD3(1142-1642) using the calcium phosphate precipitation technique.²¹⁷ For one 15 cm diameter plate, 25 µg of plasmid was mixed with 250 µl of 2.5 M CaCl₂ and 975 µl of water. 1,250 µl of 2x BBS solution (50 mM BES (N-N-Bis (2-hydroxyethyl)-2-amino-ethanesulfonic acid), 280 mM NaCl, 1.5 mM Na₂HPO₄ pH 6.95) was added dropwise to the solution with gentle mixing. After 10 min the solution was added dropwise to the cell culture plate. The next day, medium was changed and the following day cells were harvested by scrapping and washed once in 1 x PBS. HUT-78 (ATCC) were grown in spinner flasks in IMDM medium supplemented with 20% FCS up to a cell concentration of 1x10⁶ cells/mL. Cells were harvested by centrifugation and washed once with 1 x PBS buffer.

Cell lysates. All steps were performed at 4 °C. HEK-293 total lysate: frozen cell pellets were homogenized in lysis buffer (50 mM Tris-HCl, 0.8% Igepal-CA630, 5% glycerol, 150 mM NaCl, 1.5 mM MgCl₂, 25 mM NaF, 1 mM sodium vanadate, 1 mM DTT, pH 7.5). One complete EDTA-free protease inhibitor tablet (Roche) per 25 mL was added. The sample was dispersed using a Dounce homogenizer, kept rotating for 30 min and spun for 10 min at 20,000 g. The supernatant was spun again for 1 h at 145,000 g. The protein concentration was determined by Bradford assay (BioRad), and aliquots were snap frozen in liquid nitrogen and stored at –80 °C. HUT-78 nuclear extract: frozen cell pellets were homogenized in 4 volumes of hypotonic buffer (10 mM TRIS-Cl, pH 7.4, 1.5 mM MgCl₂, 10 mM KCl, 25 mM NaF, 1 mM Na₃VO₄) supplemented with EDTA-free protease inhibitor tablet (Roche, 1

tablet per 25 mL) and centrifuged for 5 minutes at 20,000 g. Pellet was re-suspended in 2 volumes of hypotonic buffer and sample was dispersed using a Dounce homogenizer, kept rotating for 30 min and spun for 10 min at 20,000 g. The pelleted nuclei were washed in 3 volumes of hypotonic buffer and centrifuged for 15 minutes at 20,000 g. The pellet was re-suspended in 1 volume of extraction buffer (50 mM TRIS-Cl, pH 7.4, 1.5 mM MgCl₂, 20 % glycerol, 420 mM NaCl, 25 mM NaF, 1 mM Na₃VO₄, 400 units/mL of DNase I (Sigma), and protease inhibitors (1 tablet for 25 mL)) and then homogenized using a Dounce homogenizer, kept rotating for 30 min and spun for 30 min at 20,000 g. The supernatant was diluted in dilution buffer (1.8 mL buffer per 1 mL supernatant; 50 mM TRIS-Cl, pH 7.4, 1.5 mM MgCl₂, 25 mM NaF, 1 mM Na₃VO₄, 0.6 % Igepal CA-630 (Sigma, I3021) and protease inhibitors (1 tablet for 25 mL)). After 10 min incubation on ice, the lysate was centrifuged for 1 h at 145,000 g. The protein concentration was determined by Bradford assay (BioRad), and aliquots were snap frozen in liquid nitrogen and stored at -80 °C.

Probe matrix preparation:



Compounds **432** and **433** were coupled via their NH₂ group to NHS-activated Sepharose 4 Fast Flow beads (Amersham Biosciences) that have been previously equilibrated with anhydrous DMSO; 1 mL of settled beads was placed in a 15 mL Falcon tube, compound stock solution (100 mM in DMSO) was added (final concentration 1 μmol/mL beads) in presence of 15 μL of triethylamine. Derivatized beads were incubated over night at room

temperature in darkness on an end-over-end shaker. Coupling efficiency was determined by HPLC. Non-reacted NHS-groups were blocked by incubation with aminoethanol at room temperature on the end-over-end shaker over night. Beads were washed with 10 mL of DMSO and were stored in *isopropanol* at -20 °C. These beads were used as the affinity matrix and were washed three times with 5 – 10 volumes of DP buffer, collected by centrifugation 1 min at 311 x g in the Heraeus centrifuge and finally re-suspended in DP buffer to prepare a 5% beads slurry.

Proteomics-based inhibitor profiling. HEK-293 (expressing JmjD3) and HUT-78 lysates were thawed and mixed 1/1 to a final protein concentration of 5 mg/mL. Final buffer composition was 50 mM TRIS pH 7.4, 5% Glycerol, 150 mM NaCl, 25 mM NaF, 1.5 mM MgCl₂, 0.4% Igepal CA-630, 200 μM sodium-L-ascorbate, 10 μM FeCl₂ and protease inhibitors (1 tablet for 25 mL lysate). The supernatant was spun for 20 min at 145,000 g prior to use. Affinity profiling assays were carried out as described previously with minor modifications.²¹⁵ Derivatized sepharose beads (35 μL beads per sample) were equilibrated in lysis buffer and incubated with 1 mL (5 mg protein) cell lysate, which had been preincubated with test compound **332b** or vehicle for 45 min, on an end-over-end shaker for 1 h. Incubation was done at 4 °C for all compounds. Beads were transferred to disposable columns (MoBiTec), washed with lysis buffer containing 0.2% Igepal CA-630 and eluted with 50 μL 2× SDS sample buffer. Proteins were alkylated with 200 mg/mL iodoacetamide for 30 min, separated on 4–12% NuPAGE (Invitrogen), and stained with colloidal Coomassie.

Sample preparation for MS analysis. Gels were cut into slices and subjected to in-gel digestion.²¹⁵ For acquisition of dose-response inhibitor data in one single multiplexed run, TMT (Thermo-Fisher Scientific) tags were used. Peptide extracts were labeled with TMT in 90 mM triethylammoniumbicarbonate, pH 8.53. After quenching of the reaction with

glycine, labeled extracts were combined. For compound profiling experiments, extracts from vehicle-treated samples were labeled with TMT reagent 131, and combined with extracts from compound-treated samples labeled with TMT reagents 126–130, fractionated using reversed-phase chromatography at pH 12, dried and acidified before LC-MS/MS analysis.

LC-MS/MS analysis. Samples were dried *in vacuo* and resuspended in 0.1% formic acid in water and aliquots of the sample were injected into a nano-LC system (Eksigent 1D+) coupled to LTQ-Orbitrap mass spectrometers (Thermo-Finnigan). Peptides were trapped on a custom 4 cm x 200 μ M reversed-phase column (Reprosil) and separated on custom 50 cm \times 100 μ M (internal diameter) reversed-phase columns (Reprosil) at 40 °C. Gradient elution was performed from 2% acetonitrile to 40% acetonitrile in 0.1% formic acid over 2 h. The Orbitrap Velos instrument was operated with XCalibur 2.1 software. Intact peptides were detected in the Orbitrap at 30,000 resolution. Internal calibration was performed using the ion signal from $(\text{Si}(\text{CH}_3)_2\text{O})_6\text{H}^+$ at m/z 445.120025.²¹⁸ Data-dependent tandem mass spectra were generated for up to four peptide precursors using a combined CID/HCD approach or using HCD at a resolution of 7,500 for histone modification data.²¹⁹ For CID, up to 3,000 ions (Orbitrap Velos) were accumulated in the ion trap within a maximum ion accumulation time of 200 msec. For HCD, target ion settings were 25,000 (Orbitrap Velos), respectively.

Peptide and protein identification. Mascot 2.0 (Matrix Science) was used for protein identification using 10 p.p.m. mass tolerance for peptide precursors and 0.8 Da (CID) or 20 mDa (HCD) tolerance for fragment ions. Carbamidomethylation of cysteine residues and iTRAQ/TMT modification of lysine residues were set as fixed modifications and S,T,Y phosphorylation, methionine oxidation, N-terminal acetylation of proteins and TMT modification of peptide N termini were set as variable modifications. The search database consisted of a customized version of the International Protein Index database combined with a decoy version of this database created using a script supplied by Matrix Science. Unless

stated otherwise, we accepted protein identifications as follows: (i) for single spectrum to sequence assignments, we required this assignment to be the best match and a minimum Mascot score of 31 and a 10× difference of this assignment over the next best assignment. Based on these criteria, the decoy search results indicated <1% false-discovery rate (FDR); (ii) for multiple spectrum to sequence assignments and using the same parameters, the decoy search results indicate <0.1% FDR. For protein quantification a minimum of two sequence assignments matching to unique peptides was required. FDR for quantified proteins was <<0.1%. For analysis of histone peptides additional variable modifications considered were acetylation of lysine, mono- di- and trimethylation of lysine, mono- and dimethylation of arginine. Localization of post-translational modifications on histone peptides was validated by remapping the de-isotoped and de-convoluted tandem MS spectra to b and y ions expected from the peptide hit within 20 p.p.m. mass accuracy. Only spectrum to sequence matches for which fragment ions support localization on only one amino acid and that yielded an H score > 6 indicating 99% confidence were considered for further analysis.^{216,220} For identification of peptides with acetylated lysine the presence of the 126.0913 immonium ion was required.

Peptide and protein quantification. Centroided iTRAQ/TMT reporter ion signals were computed by the XCalibur software operating and extracted from MS data files using customized scripts. Only peptides unique for identified proteins were used for relative protein quantification. Further, quantification spectra matching to unique peptide assignment were filtered according to the following criteria: mascot ion score > 15, signal to background ratio of the precursor ion > 4, signal to interference > 0.5.²¹⁶ Reporter ion intensities were multiplied with the ion accumulation time yielding an area value proportional to the number of reporter ions present in the mass analyzer. For compound competition binding experiments, fold-changes are reported based on reporter ion areas in comparison to vehicle

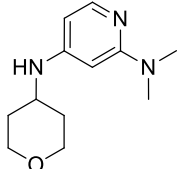
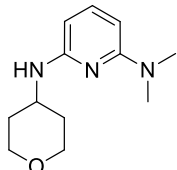
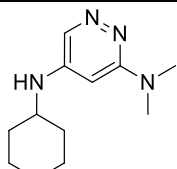
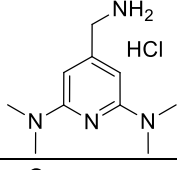
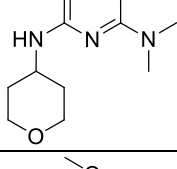
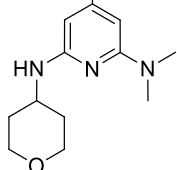
control and were calculated using sum-based bootstrap algorithm. Fold-changes were corrected for isotope purity as described and adjusted for interference caused by co-eluting nearly isobaric peaks as estimated by the signal-to-interference measure.²¹⁶ Fractional abundance was calculated by the reporter ion response in condition i divided by the summed reporter ion response across all conditions:

$$FA(i) = \frac{A(i)}{\sum_{j=1}^n A(j)}$$

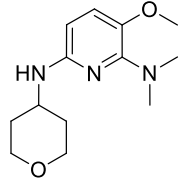
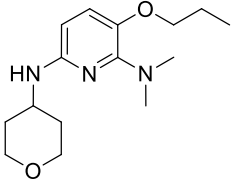
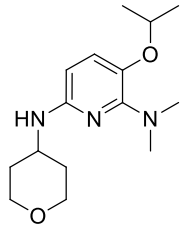
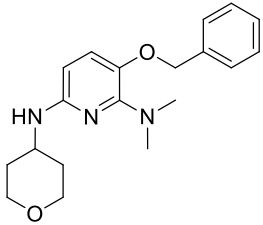
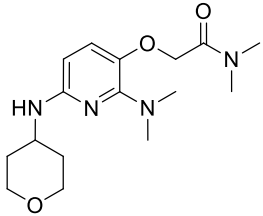
Dose-response curves were fitted using R (<http://www.r-project.org/>) and the drc package (<http://www.bioassay.dk>), as described previously.²¹⁵ IC₅₀ values were confirmed in replicate experiments using targeted data acquisition for a subset of proteins.²¹⁶

Appendix 13

All final compounds tested in biochemical assays had their purity assessed by NMR and LC-MS. The following Table includes all final compounds with $pIC_{50} \geq 5$ and some examples with $pIC_{50} < 5$ with their respective purities assessed by LC-MS.

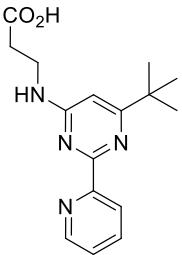
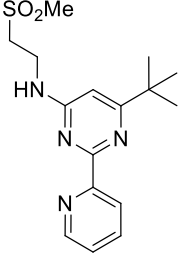
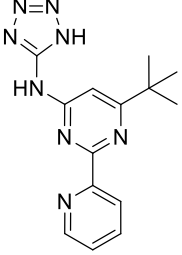
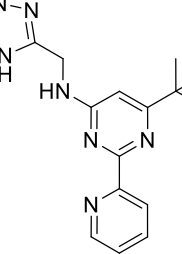
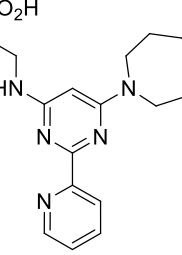
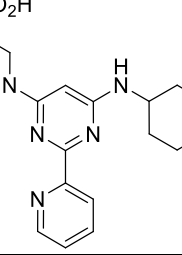
Structure	Compound	Biochemical assay pIC_{50}	LCMS method	Retention Time	Purity (%)
	127	< 4.0 ^a	Formic	0.47	100
	132	5.0 ^a	TFA	0.53	99
	137	< 4.0 ^a	High pH	0.61	100
	143	5.4 ^a	Formic	0.36	99
	153	5.6 ^a	Formic	0.55	91
	156	5.8 ^a	Formic	0.58	100

^a TR-FRET assay.

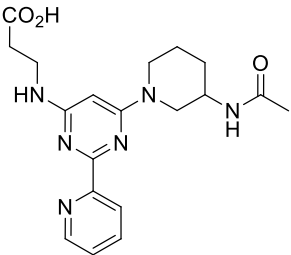
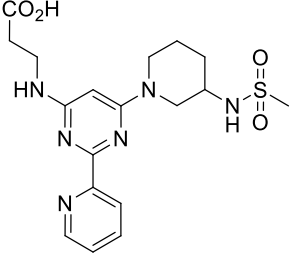
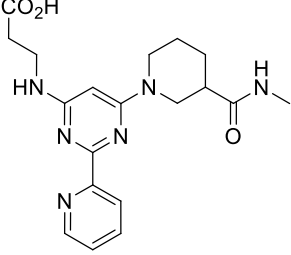
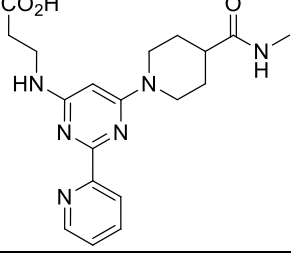
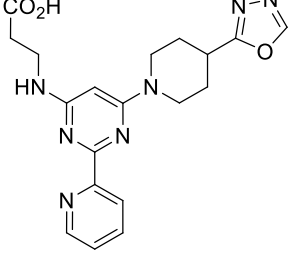
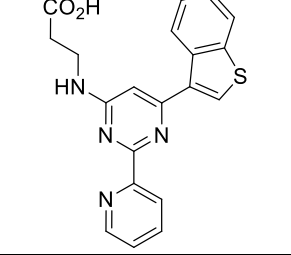
Structure	Compound	Biochemical assay pIC ₅₀	LCMS method	Retention Time	Purity (%)
	151	5.7 ^a	Formic	0.51	96
	147b	4.8 ^a	Formic	0.65	100
	147c	5.3 ^a	Formic	0.67	100
	147a	5.5 ^a	Formic	0.78	100
	159	6.6 ^a	Formic	0.5	100

^a TR-FRET assay.

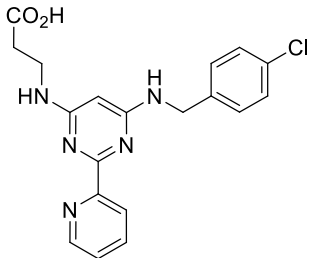
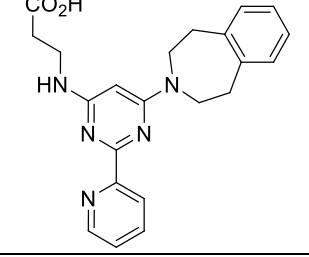
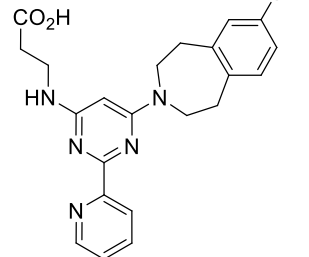
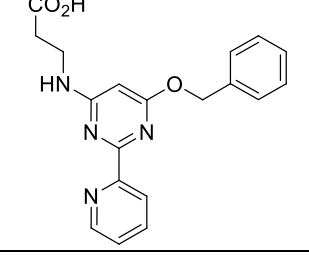
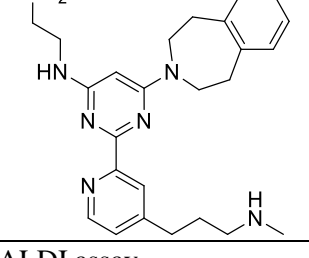
CONFIDENTIAL – DO NOT COPY

Structure	Compound	Biochemical assay pIC ₅₀	LCMS method	Retention Time	Purity (%)
	11	5.0 ^b	Formic	0.63	100
	223	< 4.0 ^b	Formic	0.62	100
	224	< 4.0 ^b	Formic	0.83	100
	225	< 4.0 ^b	Formic	0.65	100
	329a	5.1 ^b	Formic	0.81	100
	329b	< 4.0 (n = 1) 4 (n = 1) ^b	Formic	0.75	100

^b MALDI assay.

Structure	Compound	Biochemical assay pIC ₅₀	LCMS method	Retention Time	Purity (%)
	321a	5.0 ^b	Formic	0.54	100
	321b	4.8 ^b	Formic	0.56	100
	324	5.1 ^b	Formic	0.55	100
	327a	5.0 ^b	Formic	0.52	100
	327b	5.0 ^b	Formic	0.58	100
	314	5.1 ^b	Formic	0.79	100

^b MALDI assay.

Structure	Compound	Biochemical assay pIC ₅₀	LCMS method	Retention Time	Purity (%)
	332a	5.3 ^b	Formic	0.82	98.5
	332b	5.6 ^b	Formic	0.88	100
	332c	6.0 ^b	Formic	0.72	100
	337	5.8 ^b	Formic	0.72	100
	332b	5.6 ^c	High pH	0.71	98

^b MALDI assay.

^c RapidFire assay.

-
- ¹ Hansen, J. C.; Turgeon, C. L. *Chromatin Protocols*, Ed. Becker, P. B., Human Press, Totowa NJ, **1999**, 119, 127-141 (permission granted).
- ² Kouzarides T. *Cell* **2007**, 128, 693-705.
- ³ Qiu J. *Nature* **2006**, 441, 143-145 (permission granted).
- ⁴ Kron K. J.; Liu, L.; Pethe, V. V.; Demetrashvili, N.; Nesbitt, M. E.; Trachtenberg, J.; Ozcelik, H.; Fleshner, N. E.; Briollais, L.; Van Der Kwast, T. H.; Bapat, B. *Lab. Invest.* **2010**, 90, 1060-1067.
- ⁵ Jenuwein, T.; Allis, C. D. *Science* **2001**, 293, 1074-1080 (permission granted).
- ⁶ Di Lorenzo, A.; Bedford, M. T. *FEBS (Fed. Eur. Biochem. Soc.) Lett.* **2011**, 585, 2024-2031.
- ⁷ Bedford, M. T.; Clarke, S. G. *Mol. Cell* **2009**, 33, 1-13.
- ⁸ Wooster, P. M. *Ann. Rep. Med. Chem.* **2010**, 45, 245-259.
- ⁹ Frye, S. V.; Heightman, T.; Jin J. *Ann. Rep. Med. Chem.* **2010**, 45, 329-343.
- ¹⁰ Zhang, X.; Bruice, T. C. *Biochemistry* **2008**, 47, 6671-6677.
- ¹¹ Taverna, S. D.; Li, H.; Ruthenburg, A. J.; Allis, C. D.; Patel, D. J. *Nat. Struct. Mol. Biol.* **2007**, 14, 1025-1040.
- ¹² Yun, M.; Wu, J.; Workman, J. L.; Li, B. *Cell. Res.* **2011**, 21, 564-578.
- ¹³ Hughes, R. M.; Wiggins, K. R.; Khorasanizadeh, S.; Waters, M. L. *PNAS* **2007**, 104, 11184-11188.
- ¹⁴ Shi, Y.; Lan, F.; Matson, C.; Mulligan, P.; Whetstine, J. R.; Cole, P. A.; Casero, R. A.; Shi, Y. *Cell* **2004**, 119, 941-953.
- ¹⁵ Zheng Y. G.; Wu J.; Chen Z.; Goodman M. *Med. Res. Rev.* **2008**, 28, 645-687.
- ¹⁶ Description obtained from structural classification of proteins (SCOP) database: <http://scop.mrc-lmb.cam.ac.uk/scop/>.
- ¹⁷ Stavropoulos, P.; Blobel, G.; Hoelz, A. *Nat. Struct. Mol. Biol.* **2006**, 13, 626-632 (permission granted).
- ¹⁸ Chen, Y.; Yang, Y.; Wang, F.; Wan, K.; Yamane, K.; Zhang, Y.; Lei, M. *PNAS* **2006**, 103, 13956-13961.
- ¹⁹ Chen, Z.; Zang, J.; Whetstine, J.; Hong, X.; Davrazou, F.; Kutateladze, T. G.; Simpson, M.; Mao, Q.; Pan, C.; Dai, S.; Hagman, J.; Hansen, K.; Shi, Y.; Zhang, G. *Cell* **2006**, 125, 691-702.
- ²⁰ Anand, R.; Marmorstein, R. *J. Biol. Chem.* **2007**, 282, 35425-35429.
- ²¹ Lora, J. M.; Wilson, D. M.; Lee, K.; Larminie, C. G. *Drug Discov Today Technol.* **2010**, 7, 67-75.
- ²² Cole P. A. *Nat. Chem. Bio.* **2008**, 4, 590-597.
- ²³ Keppeler B. R.; Archer T. K. *Expert Opin. Ther. Targets* **2008**, 12, 1301-1312.
- ²⁴ Klose, R. J.; Kallin, E. M.; Zhang, Y. *Nat. Rev. Gen.* **2006**, 7, 715-727.
- ²⁵ Phylogenetic tree put together by computational chemists, GSK.
- ²⁶ De Santa, F.; Totaro, M. G.; Prosperini, E.; Notarbartolo, S.; Testa, G.; Natoli, G. *Cell*, **2007**, 130, 1083-1094.
- ²⁷ De Santa, F.; Narang V.; Yap, Z. H.; Tusi, B. K.; Burgold, T.; Austenaa, L.; Bucci, G.; Caganova, M.; Notarbartolo, S.; Casola, S.; Testa, G.; Sung, W. K.; Wei, C. L.; Natoli, G. *EMBO* **2009**, 28, 3341-3352 (permission granted).
- ²⁸ Heightman T. D. *Expert Opin. Ther. Targets* **2011**, 15, 729-740.
- ²⁹ Kim, H.; Bae, S. *Am. J. Transl. Res.* **2011**, 3, 166-179.
- ³⁰ Chowdhury, R.; Yeoh, K. K.; Tian, Y. M.; Hillringhaus, L.; Bagg, E. A.; Rose, N. R.; Leung, I. K.; Li, X. S.; Woon, E. C.; Yang, M.; McDonough, M. A.; King, O. N.; Clifton, I. J.; Klose, R. J.; Claridge, T. D.; Ratcliffe, P. J.; Schofield, C. J.; Kawamura, A. *EMBO Rep.* **2011**, 12, 463-469 (permission granted).
- ³¹ Cloos, P. A. C.; Christensen, J.; Agger, K.; Maiolica, A.; Rappsilber, J.; Antal, T.; Hansen, K. H.; Helin, K. *Nature* **2006**, 442, 307-311 (permission granted).
- ³² Rose, N. R.; Woon, E. C. Y.; Kingham, G. L.; King, O. N. F.; Mecinovic, J.; Clifton, I. J.; Ng, S. S.; Talib-Hardy, J.; Oppermann, U.; McDonough, M. A.; Schofield, C. J. *J. Med. Chem.* **2010**, 53, 1810-1818 (permission granted).
- ³³ Rose, N. R.; Ng, S. S.; Mecinovic, J.; Lienard, B. M. R.; Bello, S. H.; Sun, Z.; McDonough, M. A.; Oppermann, U.; Schofield, C. J. *J. Med. Chem.* **2008**, 51, 7053-7056 (permission granted).
- ³⁴ Chang, K.; King, O. N. F.; Tumber, A.; Woon, E. C. Y.; Heightman, T. D.; McDonough, M. A.; Schofield, C. J.; Rose, N. R. *ChemMedChem* **2011**, 6, 759-764 (permission granted).

- ³⁵ King, O. N. F.; Li, X. S.; Sakurai, M.; Kawamura, A.; Rose, N. R.; Ng, S. S.; Quinn, A. M.; Rai, G.; Mott, B. T.; Beswick, P.; Klose, R. J.; Oppermann, U.; Jadhav, A.; Heightman, T. D.; Maloney, D. J.; Schofield, C. J.; Simeonov, A. *PLoS ONE* **2010**, *5*, e15535 (permission granted).
- ³⁶ Ng, S. S.; Kavanagh, K. L.; McDonough, M. A.; Butler, D.; Pilka, E. S.; Lienard, B. M. R.; Bray, J. E.; Savitsky, P.; Gileadi, O.; Von Delft, F.; Rose, N. R.; Offer, J.; Scheinost, J. C.; Borowski, T.; Sundstrom, M.; Schofield, C. J.; Oppermann, U. *Nature* **2007**, *448*, 87-91 (permission granted).
- ³⁷ Thallammer, A.; Mecinovic, J.; Loenarz, C.; Tumber, A.; Rose, N. R.; Heightman, T. D.; Schofield, C. J. *Org. Biomol. Chem.* **2011**, *9*, 127-135.
- ³⁸ Assay set up by Sinah, Y., GSK, AESOP AP11368v1.
- ³⁹ Yu, V.; Fisch, T.; Long, A. M.; Tang, J.; Lee, J. H.; Hierl, M.; Chen, H.; Yakowec, P.; Schwandner, R.; Emkey, R. *J. Biomol. Screen.* **2012**, *17*, 27-38.
- ⁴⁰ Assay set up by Sinah, Y., GSK, AESOP AP11369v1.
- ⁴¹ Assay set up by Sinah, Y.; Calvo-Vicente, D.; Gordon, L., GSK, AESOP AP11368v1.
- ⁴² Assay set up by Leveridge, M. V.; Freeman, N.; Hutchinson, S. E., GSK, AESOP AP11434v1.
- ⁴³ Assay set up by Leveridge, M. V.; Gordon, L.; Hutchinson, S. E., GSK, AESOP AP12416v1.
- ⁴⁴ Hutchinson, S. E.; Leveridge, M. V.; Heathcote, P. F.; Williams, L.; Gee, M.; Munoz-Muriedas, J.; Leavens, B.; Shillings, A.; Jones, E.; Homes, P.; Baddeley, S.; Chung, C.; Bridges, A.; Argyrou, A. *J. Biomol. Screen.* **2012**, *17*, 39-48.
- ⁴⁵ Assay set up by Haslam, C.; Emmons, A.; Jepras, R.; Mellor, G.; Taylor, J., GSK, AESOP AP10680v5.
- ⁴⁶ Mulji, A.; Haslam, C.; Brown, F.; Randle, R.; Karamshi, B.; Smith, J.; Eagle, R.; Munoz-Muriedas, J.; Taylor, J.; Sheikh, A.; Bridges, A.; Gill, K.; Jepras, R.; Smees, P.; Barker, M.; Woodrow, M.; Liddle, J.; Thomas, P.; Jones, E.; Gordon, L.; Tanner, R.; Leveridge, M.; Hutchinson, S.; Martin, M.; Brown, M.; Kruidenier, L.; Katso, R. *J. Biomol. Screen.* **2012**, *17*, 108-120.
- ⁴⁷ Rishton, G. M. *DDT*, **1997**, *2*, 382-384.
- ⁴⁸ Feng, B. Y.; Shelat, A.; Doman, T. N.; Guy, R. K.; Shoichet, B. K. *Nat. Chem. Biol.* **2005**, *1*, 146-148.
- ⁴⁹ Baell, J. B.; Holloway, G. A. *J. Med. Chem.* **2010**, *53*, 2719-2740.
- ⁵⁰ Lor, L. A.; Schneck, J.; McNulty, D. E.; Diaz, E.; Brandt, M.; Thrall, S. H.; Schwartz, B. *J. Biomol. Screen.* **2007**, *12*, 881-890.
- ⁵¹ Johnston, P. A. *Curr. Opin. Chem. Biol.* **2011**, *15*, 174-182.
- ⁵² Pourbaix, M. *Atlas of Electrochemical Equilibria in Aqueous Solutions*, NACE, Houston and Cebalcor, Brussels, **1966**.
- ⁵³ Communication with Matthew Lochansky, GSK.
- ⁵⁴ Abad-Zapatero C.; Metz T. J. *Drug Discovery Today* **2005**, *10*, 464-469.
- ⁵⁵ Hann, M. M. *Med. Chem. Commun.* **2011**, *2*, 349-355.
- ⁵⁶ Leeson, P. D.; Springthorpe, B. *Nat. Rev. Drug Discov.* **2007**, *6*, 881-890.
- ⁵⁷ J. Seal, T. Hayhow, E. Kiss and H. Diallo, unpublished results, GSK.
- ⁵⁸ King, A. O.; Okukado, N.; Negishi, E. *J. Chem. Soc., Chem. Commun.* **1977**, *19*, 683-684.
- ⁵⁹ Negishi, E.; King, A. O.; Okukado, N. *J. Org. Chem.* **1977**, *42*, 1821-1823.
- ⁶⁰ Negishi, E.; Van Horn, D. E. *J. Am. Chem. Soc.* **1977**, *99*, 3168-3170.
- ⁶¹ King, A. O.; Negishi, E.; Villani, F. J. Jr.; Silveira, A. Jr. *J. Org. Chem.* **1978**, *43*, 358-360.
- ⁶² Negishi, E.; Okukado, N.; King, A. O.; Van Horn, D. E.; Spiegel, B. I. *J. Am. Chem. Soc.* **1978**, *100*, 2254-2256.
- ⁶³ Baba, S.; Negishi, E. *J. Am. Chem. Soc.* **1976**, *98*, 6729-6731.
- ⁶⁴ Negishi, E. in *Handbook of Organopalladium Chemistry for Organic Synthesis*, Ed. Negishi, E., Wiley, New York, **2002**, 229-247.
- ⁶⁵ Rillat, I.; Jackson, R. F. W. *J. Org. Chem.* **2008**, *73*, 8694-8704.
- ⁶⁶ Frankland, E. *Justus Liebigs Ann. Chem.* **1849**, *71*, 213-216.
- ⁶⁷ Frankland, E. *Justus Liebigs Ann. Chem.* **1853**, *85*, 329-373.
- ⁶⁸ Coleridge, B. M.; Bello, C. S.; Ellenbeger, D. H.; Leitner, A. *Tetrahedron Lett.* **2010**, *51*, 357-359.
- ⁶⁹ Knochel, P.; Leuser, H.; Gong, L.; Perrone, S.; Kneisel, F. in *The Chemistry of Organozinc Compounds*; Ed. Rappoport, Z. and Marek, I., Wiley, Chichester, **2007**, ch. 8.
- ⁷⁰ Parham, W. E.; Bradsher, C. K. *Acc. Chem. Res.* **1982**, *15*, 300-305.
- ⁷¹ Cameron, J. F.; Frechet, J. M. J. *J. Am. Chem. Soc.* **1991**, *113*, 4303-4313.

- ⁷² Tucker, C. E.; Majid, T. N.; Knochel, P. *J. Am. Chem. Soc.* **1992**, *114*, 3983-3985.
- ⁷³ Rieke, R. D. *Science* **1989**, *246*, 1260-1264.
- ⁷⁴ Rieke, R. D.; Hanson, M. V. *Tetrahedron* **1997**, *53*, 1925-1956.
- ⁷⁵ <http://www.riekemetals.com>, accessed on the 22nd of July 2013.
- ⁷⁶ Huo, S. *Org. Lett.* **2003**, *5*, 423-425.
- ⁷⁷ Mulvey, R. E. *Acc. Chem. Res.* **2009**, *42*, 743-755.
- ⁷⁸ Knochel, P.; Dong, Z.; Closoki, G. C.; Wunderlich, S. F.; Unsinn, A.; Li, J. *Chem. Eur. J.* **2009**, *15*, 457-468.
- ⁷⁹ Bresser, T.; Knochel, P. *Angew. Chem., Int. Ed.* **2011**, *50*, 1914-1917.
- ⁸⁰ Andrikopoulos, P. C.; Armstrong, D. R.; Barley, H. R. L.; Clegg, W.; Dale, S. H.; Hevia, E.; Honeyman, G. W.; Kennedy, A. R.; Mulvey, R. E. *J. Am. Chem. Soc.* **2005**, *127*, 6184-6185.
- ⁸¹ Clegg, W.; Dale, S. H.; Hevia, E.; Honeyman, G. W.; Mulvey, R. E. *Angew. Chem., Int. Ed.* **2006**, *45*, 2370-2374.
- ⁸² Conway, B.; Hevia, E.; Kennedy, A. R.; Mulvey, R. E. *Chem. Commun.* **2007**, 2864-2866.
- ⁸³ Armstrong, D. R.; Clegg, W.; Dale, S. H.; Hevia, E.; Hogg, L. M.; Honeyman, G. W.; Mulvey, R. E. *Angew. Chem., Int. Ed.* **2006**, *45*, 3775-3778.
- ⁸⁴ Armstrong, D. R.; Garcia-Alvarez, J.; Graham, D. V.; Hevia, E.; Honeyman, G. W.; Kennedy, A. R.; Mulvey, R. E. *Chem. Eur. J.* **2009**, *15*, 3800-3807.
- ⁸⁵ Kurti, L.; Czako, B. in *Strategic Applications of Named Reactions in Organic Synthesis*, Ed. Elsevier, Burlington, **2005**, 448.
- ⁸⁶ Hayashi, T.; Konishi, M.; Kobori, Y.; Kumada, M.; Higuchi, T.; Hirotsu, K. *J. Am. Chem. Soc.* **1984**, *106*, 158-163.
- ⁸⁷ Casares, J. A.; Espinet, P.; Fuentes, B.; Salas, G. *J. Am. Chem. Soc.* **2007**, *129*, 3508-3509.
- ⁸⁸ Fuentes, B.; Garcia-Melchor, M.; Lledos, A.; Maseras, F.; Casares, J. A.; Ujaque, G.; Espinet, P. *Chem. Eur. J.* **2010**, *16*, 8596-8599.
- ⁸⁹ Hartwig, J. F. *Inorg. Chem.* **2007**, *46*, 1936-1947.
- ⁹⁰ Rudolph, A.; Lautens, M. *Ang. Chem. Int. Ed.* **2009**, *48*, 2656-2670.
- ⁹¹ Han, C.; Buchwald, S. L. *J. Am. Chem. Soc.* **2009**, *131*, 7532-7533.
- ⁹² Çalimsiz, S.; Organ, M. G. *Chem. Commun.* **2011**, *47*, 5181-5183.
- ⁹³ Crabtree, R. H. In *Organometallic chemistry of the transition metals*, Ed. John Wiley & Sons, 5th ed., **2009**, 315.
- ⁹⁴ Gusev, D. G. *Organometallics* **2009**, *28*, 6458-6461.
- ⁹⁵ Dias, P. B.; Piedale, M. E. M.; Simões, J. A. M. *Coord. Chem. Rev.* **1994**, *135-136*, 737.
- ⁹⁶ Scott, N. M.; Nolan, S. P. *Eur. J. Inorg. Chem.* **2005**, *2005*, 1815-1828.
- ⁹⁷ Hu, X.; Castro-Rodriguez, I.; Olsen, K.; Meyer, K. *Organometallics* **2004**, *23*, 755-764.
- ⁹⁸ Tolman, C. A. *Chem. Rev.* **1977**, *77*, 313-348.
- ⁹⁹ Clavier, H.; Nolan, S. P. *Chem. Commun.* **2010**, *46*, 841-861.
- ¹⁰⁰ Hillier, A. C.; Sommer, W. J.; Yong, B. S.; Petersen, J. L.; Cavallo, L.; Nolan, S. P. *Organometallics* **2003**, *22*, 4322-4326.
- ¹⁰¹ Altenhoff, G.; Goddard, R.; Lehmann, C. W.; Glorius, F. *Angew. Chem. Int. Ed.* **2003**, *42*, 3690-3693.
- ¹⁰² Organ, M. G.; Chass, G. A.; Fang, D.; Hopkinson, A. C.; Valente, C. *Synthesis* **2008**, 2776-2797.
- ¹⁰³ Crabtree, R. H. *J. Organomet. Chem.* **2005**, *690*, 5451-5457.
- ¹⁰⁴ Love, J. A.; Morgan, J. P.; Trnka, T. M.; Grubbs, R. G. *Angew. Chem. Int. Ed.* **2002**, *41*, 4035-4037.
- ¹⁰⁵ Chass, G. A.; O'Brien, C. J.; Hadei, N.; Kantchev, E. A. B.; Mu, W.; Fang, D.; Hopkinson, A. C.; Csizmadia, I. G.; Organ, M. G. *Chem. Eur. J.* **2009**, *15*, 4281-4288.
- ¹⁰⁶ Kienle, M.; Knochel, P. *Org. Lett.* **2010**, *12*, 2702-2705.
- ¹⁰⁷ Manolikakes, G.; Knochel, P. *Angew. Chem. Int. Ed.* **2009**, *48*, 205-209.
- ¹⁰⁸ Kramer, A. V.; Labinger, J. A.; Bradley, J. S.; Osborn, J. A. *J. Am. Chem. Soc.* **1974**, *96*, 7145-7147.
- ¹⁰⁹ Kramer, A. V.; Osborn, J. A. *J. Am. Chem. Soc.* **1974**, *96*, 7832-7833.
- ¹¹⁰ Elson, I. H.; Morrell, D. G.; Kochi, J. K. *J. Organomet. Chem.* **1975**, *84*, C7-C10.
- ¹¹¹ Hegedus, L. S.; Thompson, D. H. P. *J. Am. Chem. Soc.* **1985**, *107*, 5663-5669.

- ¹¹² Achonduh, G. T.; Hadei, N.; Valente, C.; Avola, S.; O'Brien, C. J.; Organ, M. G. *Chem. Commun.* **2010**, *46*, 4109-4111.
- ¹¹³ Jin, L.; Liu, J.; Liu, C.; Hu, F.; Lan, Y.; Batsanov, A. S.; Howard, J. A. K.; Marder, T. B.; Lei, A. *J. Am. Chem. Soc.* **2009**, *131*, 16656-16657.
- ¹¹⁴ Hevia, E.; Chua, J. Z.; Garcia-Alvarez, P.; Kennedy, A. R.; McCall, M. D. *PNAS* **2010**, *107*, 5294-5299.
- ¹¹⁵ Jana, R.; Pathak, T. P.; Sigman, M. S. *Chem. Rev.* **2011**, *111*, 1417-1492.
- ¹¹⁶ Ku, Y.; Grieme, T.; Raje, P.; Sharma, P.; Morton, H.; Rozema, M.; King, S. *J. Org. Chem.* **2003**, *68*, 3238-3240.
- ¹¹⁷ Manley, P.; Acemoglu, M.; Marterer, W.; Pachinger, W. *Org. Proc. Res. Dev.* **2003**, *7*, 436-445.
- ¹¹⁸ Oswald, C. L.; Carrillo-Marquez, T.; Caggiano, L.; Jackson, R. F. W. *Tetrahedron* **2008**, *64*, 681-687.
- ¹¹⁹ Dai, C.; Fu, G. C. *J. Am. Chem. Soc.* **2001**, *123*, 2719-2724.
- ¹²⁰ Luo, Y. *Handbook of Bond Dissociation Energies in Organic Compounds*, Ed. CRC Press, **2003**.
- ¹²¹ Organ, M. G.; Avola, S.; Dubovyk, I.; Hadei, N.; Kantchev, E. A. B.; O'Brien, C. J.; Valente, C. *Chem. Eur. J.* **2006**, *12*, 4749-4755.
- ¹²² Çalimsiz, S.; Sayah, M.; Mallik, D.; Organ, M. G.; *Angew. Chem. Int. Ed.* **2010**, *49*, 2014-2017.
- ¹²³ Valente, C.; Belowich, M. E.; Hadei, N.; Organ, M. G. *Eur. J. Org. Chem.* **2010**, 4343-4354.
- ¹²⁴ Totsuka, Y.; Takamura-Enya, T.; Nishiagaki, R.; Sugimura, T.; Wakabayashi, K. *J. Chromatogr. B* **2004**, *802*, 135-141.
- ¹²⁵ De Angelis, M.; Katzenellenbogen, J. A. *Bioorg. Med. Chem. Lett.* **2004**, *14*, 5835-5839.
- ¹²⁶ J. Seal, unpublished results, GSK.
- ¹²⁷ *US. Pat.*, 839641P, **2006**.
- ¹²⁸ J. Seal, T. Hayhow, E. Kiss and H. Diallo, unpublished results, GSK.
- ¹²⁹ Sanjay, K. M.; Lawrence Q., Jr. *Inorg. Chem.* **1997**, *36*, 5424-5425.
- ¹³⁰ <http://www.milestonepharmtech.com>.
- ¹³¹ <http://www.fchgroup.net>.
- ¹³² Young, R. J.; Green, D. V. S.; Luscombe, C. N.; Hill, A. P. *Drug Discov. Today* **2010**, *15*, 648-655.
- ¹³³ Bioduro is an outsourcing company which produce building blocks and final compounds following chemistry routes designed by GSK chemists.
- ¹³⁴ Zuo, L.; Yao, S.; Wang, W.; Duan, W. *Tetrahedron Lett.* **2008**, *49*, 4054-4056.
- ¹³⁵ Hintermann L.; Xiao, L.; Labonne, A. *Angew. Chem. Int. Ed.* **2008**, *47*, 8246-8250.
- ¹³⁶ Dr J. Liddle, GSK, confirmed that the presence of broad signals in an NMR spectrum is characteristic of the presence of paramagnetic metal in the sample being analysed.
- ¹³⁷ Kaes, C.; Katz, A.; Hosseini, M. W. *Chem. Rev.* **2000**, *100*, 3553-3590.
- ¹³⁸ Compound synthesised by M. J. Daubney, GSK.
- ¹³⁹ Sekirnik, R.; Rose, N. R.; Mecinovic, J.; Schofield, C. J. *Metallomics*, **2010**, *2*, 397-399.
- ¹⁴⁰ Compound **237** synthesised by Dr S. Atkinson, GSK.
- ¹⁴¹ Mao, C.; Hauser, C. R.; Miles, M. L. *J. Am. Chem. Soc.* **1967**, *89*, 5303-5304.
- ¹⁴² Weiler, L.; Huckin, S. N. *J. Am. Chem. Soc.* **1974**, *96*, 1082-1087.
- ¹⁴³ Pendarvis, R. O.; Hampton, K. G. *J. Org. Chem.* **1974**, *39*, 2289-2291.
- ¹⁴⁴ Doherty, A. M.; Ley, S. V.; Lygo, B.; Williams, D. J. *J. Chem. Soc., Perkin Trans. I* **1984**, 1371-1377.
- ¹⁴⁵ Gupta, A.; Beazley, G.; Lee, J.; Berube, G. *Synth. Commun.* **2007**, *37*, 2031-2037.
- ¹⁴⁶ Zhang, Y.; Jiao, J.; Flowers, R. A. *J. Org. Chem.* **2006**, *71*, 4516-4520.
- ¹⁴⁷ Ghosh, S. K.; Buchanan, G. S.; Long, Q. A.; Wei, Y.; Al-Rashid, Z. F.; Sklenicka, H. M.; Hsung, R. P. *Tetrahedron* **2008**, *64*, 883-893.
- ¹⁴⁸ Private communication with Dr S. Atkinson and R. Sheppard, GSK. It was thought that DMPU would break up the lithium aggregates and by doing so would facilitate the formation of the dianion.
- ¹⁴⁹ Lee, C.-C.; Zhou X.; Liu, X.; Li, W. *Org. Lett.* **2010**, *12*, 548-551.
- ¹⁵⁰ Use of calcium hydride advised by Dr S. Atkinson, GSK, in private communication.
- ¹⁵¹ Sci-finder search on formation of pyrimidine ring from nitrogen containing 6-membered ring amidine and diketone.

- ¹⁵² Kitbunnadaj, R.; Zuiderveld, O. P.; Christophe, B.; Hulscher, S.; Menge, W. M. P. B.; Gelens, E.; Snip, E.; Bakker, R. A.; Celanire, S.; Gillard, M.; Talaga, P.; Timmerman, H.; Leurs, R. *J. Med. Chem.* **2004**, *47*, 2414-2417.
- ¹⁵³ Ohno, H.; Okumura, M.; Maeda, S.; Iwasaki, H.; Wakayama, R.; Tanaka, T. *J. Org. Chem.* **2003**, *68*, 7722-7732.
- ¹⁵⁴ Kruidenier, L.; Chung, C.; Cheng, Z.; Liddle, L.; Che, K.; Joberty, G.; Bantscheff, M.; Bountra, C.; Bridges, A.; Diallo, H.; Eberhard, D.; Hutchinson, S.; Jones, E.; Katso, R.; Leveridge, M.; Mander, P. K.; Mosley, J.; Ramirez-Molina, C.; Schofield, C. J.; Sheppard, R. J.; Smith, J.; Swales, C.; Tanner, R.; Thomas, P.; Tumber, A.; Drewes, G.; Oppermann, U.; Patel, D. J.; Lee, K.; Wilson, D. M.; *Nature*, **2012**, *488*, 404-408.
- ¹⁵⁵ *US. Pat.* 20090062263A1, **2009**.
- ¹⁵⁶ *WO* 2002002513, **2002**.
- ¹⁵⁷ Seebach, D.; Amstutz, R.; Laube, T.; Schweiser, W. B.; Dunitz, J. D. *J. Am. Chem. Soc.* **1985**, *107*, 5403-5409.
- ¹⁵⁸ Haner, R.; Seebach, D.; Laube, T. *J. Am. Chem. Soc.* **1985**, *107*, 5396-5403.
- ¹⁵⁹ Cheng, H.; Chong, Y.; Hwang, I.; Tavassoli, A.; Zhang, Y.; Wilson, I. A.; Benkovic, S. J.; Boger, D. L. *Bioorg. Med. Chem.* **2005**, *13*, 3577-3585.
- ¹⁶⁰ Lemoine, R. C.; Peterson, A. C.; Setti, L.; Wanner, J.; Jekle, A.; Heilek, G.; DeRosier, A.; Ji, C.; Berry, P.; Rotstein, B. *Bioorg. Med. Chem. Lett.* **2010**, *20*, 704-708.
- ¹⁶¹ De Meijere, A. *Angew. Chem., Int. Ed.* **1979**, *18*, 809-886.
- ¹⁶² Godier-Marc, E.; Aitken, D. J.; Husson, H. *Tetrahedron Lett.* **1997**, *38*, 4065-4068.
- ¹⁶³ Intermediate synthesised by M. J. Daubney, GSK.
- ¹⁶⁴ Ferrari, C.; Predieri, G.; Tiripiccio, A. *Chem. Mater.* **1992**, *4*, 243-245.
- ¹⁶⁵ Liu, P.; Pu, Q.; Su, Z. *Analyst*, **2000**, *125*, 147-150.
- ¹⁶⁶ <http://www.silicycle.com>, accessed on the 22nd of July 2013.
- ¹⁶⁷ M. Campbell, GSK, unpublished results.
- ¹⁶⁸ Intermediate synthesised by C. Douault, GSK.
- ¹⁶⁹ Intermediate synthesised by R. Sheppard, GSK.
- ¹⁷⁰ Compounds synthesised by C. Douault and M. Perryman, GSK.
- ¹⁷¹ Radinove, R.; Haimova, M.; Simova, S.; Simova, E. *Liebigs Ann. Chem.* **1988**, *1988*, 231-234.
- ¹⁷² White, J. D.; Hansen, J. D. *J. Org. Chem.* **2005**, *70*, 1963-1977.
- ¹⁷³ Analysis carried out in CCDC on the 18th of Decmeber 2013.
- ¹⁷⁴ Li, C.; Benet, L. Z.; Grillo, M. P. *Chem. Res. Toxicol.* **2002**, *5*, 1309-1317.
- ¹⁷⁵ Meanwell, N. A. *J. Med. Chem.* **2011**, *54*, 2529-2591.
- ¹⁷⁶ Hadden, M.; Goodman, A.; Guo, C.; Guzzo, P. R.; Henderson, A. J.; Pattamana, K.; Ruenz, M.; Sargent, B. J.; Swenson, B.; Yet, L.; Liu, J.; He, S.; Sebhat, I. K.; Lin, L. S.; Tamvakopoulos, C.; Peng, Q.; Kan, Y.; Palyha, O.; Kelly, T. M.; Guan, X.; Metzger, J. M.; Reitman, M. L.; Nargund, R. P. *Bioorg. Med. Chem. Lett.* **2010**, *20*, 2912-2915.
- ¹⁷⁷ Aberg, V.; Das, P.; Chorell, E.; Hedenstrom, M.; Pinkner, J. S.; Hultgren, S. J.; Almqvist, F. *Bioorg. Med. Chem. Lett.* **2008**, *18*, 3536-3540.
- ¹⁷⁸ Herr, R. J. *Bioorg. Med. Chem.* **2002**, *10*, 3379-3393.
- ¹⁷⁹ Carini, D. J.; Duncia, J. V.; Aldrich, P. E.; Chui, A. T.; Johnson, A. L.; Pierce, M. E.; Price, W. A.; Santella, J. B., III; Wells, G. J.; Wexler, R. R.; Wong, P. C.; Yoo, S.-E.; Timmermans, P. B. M. W. *M. J. Med. Chem.* **1991**, *34*, 2525-2547.
- ¹⁸⁰ Khan, A. R.; Parrish, J. C.; Fraser, M. E.; Smith, W. W.; Barlett, P. A.; James, M. N. G. *Biochemistry* **1998**, *37*, 16839-16845.
- ¹⁸¹ Compound synthesised by P. Boissarie, GSK.
- ¹⁸² Compound synthesised by M. Campbell, GSK.
- ¹⁸³ Chan, A. W. E.; Laskowski, R. A.; Selwood, D. A. *J. Med. Chem.* **2010**, *53*, 3086-3094.
- ¹⁸⁴ Biggadike, K.; Bledsoe, R. K.; Coe, D. M.; Cooper, T. W. J.; House, D.; Iannone, M. A.; Macdonald, S. J. F.; Madauss, K. P.; McLay, I. M.; Shipley, T. J.; Taylor, S. J.; Tran, T. B.; Uings, I. J.; Weller, V.; Williams, S. P. *PNAS* **2009**, *106*, 18114-18119.
- ¹⁸⁵ Dougherty, D. A. *Science* **1996**, *271*, 163-168.
- ¹⁸⁶ Sunner, J.; Nishizawa, K.; Kebarle, P. *J. Phys. Chem.* **1981**, *85*, 1814-1820.
- ¹⁸⁷ Guo, B. C.; Purnell, J. W.; Castleman Jr., A. W. *Chem. Phys. Lett.* **1990**, *168*, 155-160.

- ¹⁸⁸ Deakyne, C. A.; Meot-Ner, M. *J. Am. Chem. Soc.* **1985**, *107*, 474-479.
- ¹⁸⁹ Meot-Ner, M.; Deakyne, C. A. *J. Am. Chem. Soc.* **1985**, *107*, 469-474.
- ¹⁹⁰ Burley, S. K.; Petsko, G. A. *FEBS Lett.* **1986**, *203*, 139-143.
- ¹⁹¹ Gallivan, J. P.; Dougherty, D. A. *Proc. Natl. Acad. Sci. U.S.A.* **1999**, *96*, 9459-9464.
- ¹⁹² Dougherty, D. A.; Ma, J. C. *Chem. Rev.* **1997**, *97*, 1303-1324.
- ¹⁹³ Flocco, M. M.; Mowbray, S. L. *J. Mol. Biol.* **1994**, *235*, 709-717.
- ¹⁹⁴ Nandi, C. L.; Singh, J.; Thornton, J. M. *Protein Eng.* **1993**, *6*, 247-259.
- ¹⁹⁵ Sörme, P.; Arnoux, P.; Kahl-Knutsson, B.; Leffler, H.; Rini, J. M.; Nilsson, U. J. *J. Am. Chem. Soc.* **2005**, *127*, 1737-1743.
- ¹⁹⁶ Rensing, S.; Arendt, M.; Springer, A.; Grawe, T.; Schrader, T. *J. Org. Chem.* **2001**, *66*, 5814-5821.
- ¹⁹⁷ Compound synthesised by J. Cuff, GSK.
- ¹⁹⁸ Compound synthesised by J. Cuff, GSK.
- ¹⁹⁹ Crowley, P. B.; Golovin, A. *Proteins: Struc., Func., Bioinf.* **2005**, *59*, 231-239.
- ²⁰⁰ Angle measured by Pamela Thomas.
- ²⁰¹ Gallivan, J. P.; Dougherty, D. A. *J. Am. Chem. Soc.* **2000**, *122*, 870-874.
- ²⁰² Luo, X.; Liu, Y.; Kubicek, S.; Myllyharju, J.; Tumber, A.; Ng, S.; Che, K. H.; Podoll, J.; Heightman, T. D.; Oppermann, U.; Schreiber, S. L.; Wang, X. *J. Am. Chem. Soc.* **2011**, *133*, 9451-9456.
- ²⁰³ Bantscheff, M.; Hopf, C.; Savitski, M. M.; Dittmann, A.; Grandi, P.; Michon, A.; Schlegl, J.; Abraham, Y.; Becher, I.; Bergamini, G.; Boesche, M.; Delling, M.; Dümpelfeld, B.; Eberhard, D.; Huthmacher, C.; Mathieson, T.; PoECKel, D.; Reader, V.; Strunk, K.; Sweetman, G.; Kruse, U.; Neubauer, G.; Ramsden, N. G.; Drewes, G. *Nat. Biotechnol.* **2011**, *29*, 255-265.
- ²⁰⁴ Gagna, C. E.; Winokur, D.; Lambert, W. C. *Cell Biology International* **2004**, *28*, 755-764.
- ²⁰⁵ Sengoku, T.; Yokoyama, S. *Genes Dev.* **2011**, *25*, 2266-2276.
- ²⁰⁶ Niesen, F. H.; Berglund, H.; Vedadi, M. *Nat. Protoc.*, **2007**, *2*, 2212-2221.
- ²⁰⁷ Pedersen, M. T.; Helin, K. *Trends in Cell Biology*, **2010**, *20*, 662-671.
- ²⁰⁸ Cuperly, D.; Gros, P.; Fort, Y. *J. Org. Chem.*, **2002**, *67*, 238-241.
- ²⁰⁹ Schlosser, M.; Bobbio, C.; Rausis, T. *J. Org. Chem.* **2005**, *70*, 2494-2502.
- ²¹⁰ Cheung, C. W.; Surry, D. S.; Buchwald, S. L. *Org. Lett.* **2013**, *15*, 3734-3737.
- ²¹¹ Van De Sande, M.; Gais, Ha. *Chem. Eur. J.* **2007**, *13*, 1784 - 1795.
- ²¹² Bode, R. H.; Bol, J. E.; Driessen, W. L.; Hulsbergen, F. B.; Reedijk, J.; Spek, A. L. *Inorg. Chem.* **1999**, *38*, 1239-1243.
- ²¹³ Sci-Finder searches carried out on the 6th of May 2014.
- ²¹⁴ US. Pat., 5403816, **1995**.
- ²¹⁵ Bantscheff, M.; Eberhard, D.; Abraham, Y.; Bastuck, S.; Boesche, M.; Hobson, S.; Mathieson, T.; Perrin, J.; Raida, M.; Rau, C.; Reader, V.; Sweetman, G.; Bauer, A.; Bouwmeester, T.; Hopf, C.; Kruse, U.; Neubauer, G.; Ramsden, N. G.; Rick, J.; Kuster, B.; Drewes, G. *Nat. Biotechnol.* **2007**, *25*, 1035-1044.
- ²¹⁶ Savitski, M. M.; Fisher, F.; Mathieson, T.; Sweetman, G.; Lang, M.; Bantscheff, M. *J. Am. Soc. Mass Spectrom.*, **2010**, *21*, 1668-1679.
- ²¹⁷ Graham, F. L.; Van Der Eb, A. J. *Virology*, **1973**, *52*, 456-467.
- ²¹⁸ Olsen, J. V.; De Godoy, L. M. F. Li, G.; Macek, B.; Mortensen, P.; Pesch, R.; Makarov, A.; Lange, O.; Horning, S.; Mann, M. *Mol. Cell. Proteomics*, 2005, *4*, 2010-2021.
- ²¹⁹ Köcher, T.; Pichler, P.; Schutzbier, M.; Stingl, C.; Kaul, A.; Teucher, N.; Hasenfuss, G.; Penninger, J. M.; Mechtler, K. *J. Proteome Res.*, **2009**, *8*, 4743-4752.
- ²²⁰ Savitski, M. M.; Mathieson, T.; Becher, I.; Bantscheff, M. *J. Proteome Res.*, **2010**, *9*, 5511-5516.